

AFFDL-TR-74-129

Volume I

AD-A021700

BE 65
FIBEC OFFICE FILE
COPY

**CRACK GROWTH ANALYSIS FOR
ARBITRARY SPECTRUM LOADING
Volume I - Results and Discussion**

*GRUMMAN AEROSPACE CORPORATION
BETHPAGE, NEW YORK*

*DEL WEST ASSOCIATES, INC.
WOODLAND HILLS, CALIFORNIA*

OCTOBER 1974

FINAL REPORT: JUNE 1972 - OCTOBER 1974
TECHNICAL REPORT AFFDL-TR-74-129
Volume I

Approved for public release; distribution unlimited

AIR FORCE FLIGHT DYNAMICS LABORATORY
Air Force Systems Command
Wright-Patterson Air Force Base, Ohio 45433

Best Available Copy


20060921245

NOTICE

When Government drawings, specifications, or other data are used for any purpose other than in connection with a definitely related Government procurement operation, the United States Government thereby incurs no responsibility nor any obligation whatsoever; and the fact that the Government may have formulated, furnished, or in any way supplied the said drawings, specifications, or other data, is not to be regarded by implication or otherwise as in any manner licensing the holder or any other person or corporation, or conveying any rights or permission to manufacture, use, or sell any patented invention that may in any way be related thereto.

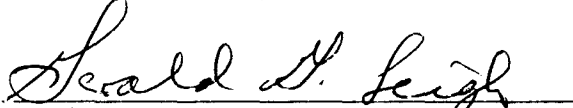


ROBERT M. ENCLE
Project Engineer
Fatigue, Fracture & Reliability Gp



ROBERT M. BADER, Chief
Structural Integrity Branch
Structures Division

FOR THE COMMANDER



GERALD G. LEIGH, Lt Col, USAF
Chief, Structures Division

This report has been reviewed by the Information Office (OI) and is releasable to the National Technical Information Service (NTIS). At NTIS it will be available to the general public, including foreign nations.

Copies of this report should not be returned unless return is required by security considerations, contractual obligations, or notice on a specific document.

UNCLASSIFIED

SECURITY CLASSIFICATION OF THIS PAGE (When Data Entered)

REPORT DOCUMENTATION PAGE		READ INSTRUCTIONS BEFORE COMPLETING FORM
1. REPORT NUMBER AFFDL-TR-74-129	2. GOVT ACCESSION NO.	3. RECIPIENT'S CATALOG NUMBER
4. TITLE (and Subtitle) CRACK GROWTH ANALYSIS FOR ARBITRARY SPECTRUM LOADING VOLUME I - RESULTS AND DISCUSSION		5. TYPE OF REPORT & PERIOD COVERED FINAL TECHNICAL REPORT JUNE 1972 - OCTOBER 1974
		6. PERFORMING ORG. REPORT NUMBER
7. AUTHOR(s) P.D. BELL, M. CREAGER		8. CONTRACT OR GRANT NUMBER(s) F33615-72-C-1744
9. PERFORMING ORGANIZATION NAME AND ADDRESS GRUMMAN AEROSPACE CORPORATION BETHPAGE, NEW YORK 11714		10. PROGRAM ELEMENT, PROJECT, TASK AREA & WORK UNIT NUMBERS
11. CONTROLLING OFFICE NAME AND ADDRESS AIR FORCE FLIGHT DYNAMICS LABORATORY WRIGHT-PATTERSON AIR FORCE BASE DAYTON, OHIO 45433		12. REPORT DATE OCTOBER 1974
		13. NUMBER OF PAGES
14. MONITORING AGENCY NAME & ADDRESS (if different from Controlling Office) SAME		15. SECURITY CLASS. (of this report) UNCLASSIFIED
		15a. DECLASSIFICATION/DOWNGRADING SCHEDULE
16. DISTRIBUTION STATEMENT (of this Report) APPROVED FOR PUBLIC RELEASE; DISTRIBUTION UNLIMITED		
17. DISTRIBUTION STATEMENT (of the abstract entered in Block 20, if different from Report)		
18. SUPPLEMENTARY NOTES		
19. KEY WORDS (Continue on reverse side if necessary and identify by block number) <div style="display: flex; justify-content: space-between;"> <div> CRACK CLOSURE CRACK GROWTH INTERACTION MATHEMATICAL MODEL OVERLOADS </div> <div> SPECTRUM LOADS 2219-T851 ALUMINUM Ti 6Al-4V TITANIUM </div> </div>		
20. ABSTRACT (Continue on reverse side if necessary and identify by block number) <p>THIS COMBINED ANALYTICAL AND EXPERIMENTAL STUDY WAS UNDERTAKEN TO INVESTIGATE FATIGUE CRACK GROWTH INTERACTION EFFECTS AND TO EITHER MODIFY EXISTING CRACK GROWTH RETARDATION MODELS OR TO DEVELOP NEW MODELS. A TEST PROGRAM WAS CONDUCTED ON 2219-T851 ALUMINUM AND ON Ti 6Al-4V TITANIUM CENTER CRACKED PANEL AND COMPACT TENSION SPECIMENS. A VARIETY OF LOADING CONDITIONS, INCLUDING CONSTANT AMPLITUDE, SINGLE AND MULTIPLE OVERLOADS, SINGLE AND MULTIPLE PERIODIC OVERLOADS, SIMPLIFIED</p> <p style="text-align: right;">(CONTINUED ON NEXT PAGE)</p>		

DD FORM 1 JAN 73 1473

EDITION OF 1 NOV 65 IS OBSOLETE

UNCLASSIFIED

SECURITY CLASSIFICATION OF THIS PAGE (When Data Entered)

UNCLASSIFIED

SECURITY CLASSIFICATION OF THIS PAGE(When Data Entered)

BLOCK PROGRAMS, COMPRESSION, TENSION-COMPRESSION AND COMPRESSION-TENSION SEQUENCES, WAS INVESTIGATED. LOADING VARIABLES INCLUDED THE RELATIVE MAGNITUDES OF OVERLOADS AND BASELINE LOADS, FREQUENCY OF OCCURRENCE OF SINGLE AND MULTIPLE PERIODIC OVERLOADS, RELATIVE MAGNITUDE OF COMPRESSION SPIKE LOADS AND STRESS RATIO. SIMPLIFIED BLOCK PROGRAM LOAD VARIABLES INCLUDED ORGANIZING THE LOAD LAYERS AS LOW-TO-HIGH, HIGH-TO-LOW OR RANDOMIZED LOADS, AND THE INTRODUCTION OF EITHER A SINGLE OVERLOAD CYCLE TO EACH BLOCK OR AN OCCASSIONAL UNDERLOAD. TWO MULTI-LAYER FIGHTER SPECTRUM TESTS WERE INCLUDED. IT WAS CONCLUDED THAT THE CRACK CLOSURE CONCEPT COULD BE USED TO EXPLAIN A VARIETY OF CRACK GROWTH INTERACTION EFFECTS. AN EMPIRICAL MATHEMATICAL MODEL USING THIS CONCEPT WAS DEVELOPED AND SHOWN TO YIELD REASONABLY ACCURATE PREDICTIONS OF CRACK GROWTH BEHAVIOR FOR MANY LOADING SEQUENCES. THIS MODEL WAS INTEGRATED INTO THE CRACKS II DIGITAL COMPUTER PROGRAM.

UNCLASSIFIED

SECURITY CLASSIFICATION OF THIS PAGE(When Data Entered)

FOREWORD

This report describes an investigation of fatigue crack growth interaction effects in airframe structural materials performed by the Grumman Aerospace Corporation from June 2, 1972 through October 2, 1974 under Air Force Contract F33615-72-C-1744. A portion of the analytical and experimental effort was subcontracted to Del Research Corporation and to Del West Associates, Inc.

The work was sponsored under Project 486U, "The Advanced Metallic Structures - Advanced Development Program" (AMS-ADP), Task 486U02, "Applied Fracture Mechanics" Air Force Flight Dynamics Laboratory (AFFDL) with Mr. Robert M. Engle (AFFDL/FBE) as project engineer.

The program was conducted by structural mechanics personnel of the Grumman Aerospace Corporation under the supervision of F. Berger, Manager, Advanced Development Systems Engineering. The Project Engineer was A. Wolfman. The principal investigator was P. D. Bell and program test engineering and coordination was provided by S. Hoops. Technical and experimental support was provided by Drs. P. Paris and R. Bucci and program support was provided by D. Schmidt of Del Research Associates. Dr. M. Creager provided technical and experimental support and W. Renslen provided program support for Del West Associates, Inc.

This report was submitted by the authors on October 1, 1974.

A second volume, containing all raw data generated under this program, is available upon request. Send requests to:

AFFDL/FBE
Attn: R. M. Engle
Wright-Patterson AFB, OH 45433

CONTENTS

	Page
SUMMARY	xiii
1. INTRODUCTION	1
2. MATERIALS AND PROCEDURES	3
2.1 Material Selection	3
2.2 Testing Procedures	3
2.3 Specimen Geometry	4
2.4 Crack Closure Measurements	5
3. RESULTS AND DISCUSSION OF TEST DATA	10
3.1 Constant Amplitude Test Results	10
3.1.1 Aluminum	11
3.1.2 Titanium	12
3.2 Single Overload Test Results	14
3.2.1 Aluminum	15
3.2.2 Titanium	26
3.2.3 Interactions of Overloads	28
3.3 Multiple Overload Test Results	29
3.3.1 Aluminum	29
3.3.2 Titanium	32
3.4 Variable Amplitude Test Results	34
3.5 Effects of Underloads and Compression Spikes	35
3.6 Miscellaneous Test Results	39
3.6.1 Stable Tear	39
3.6.2 Thickness Effects	41
3.6.3 Tensile Tests	42
3.7 Summary of Test Results	43
4. MATHEMATICAL MODELING	45
4.1 Crack Closure Model	46
4.1.1 Concepts	46
4.1.2 Application to Model	50
4.1.3 Results and Discussion	70
4.1.4 Logic Diagram	79
4.1.5 Basic Data Requirements	80
4.2 Residual Force Model	83
4.1.1 Concepts	83
4.1.2 Application to Model	83
4.1.3 Results and Discussion	88
5. SUGGESTIONS FOR FUTURE EFFORTS	94
6. OBSERVATIONS AND CONCLUSIONS	96
7. REFERENCES	98

CONTENTS (Cont)

	Page
FIGURES FOR MAIN TEXT	100
TABLES FOR MAIN TEXT	247
APPENDIX A - EQUATIONS	262
APPENDIX B - COMPUTER PROGRAM	265
FIGURES FOR APPENDIX B	269
TABLES FOR APPENDIX B	270
APPENDIX C - STRESS INTENSITY FACTOR FOR CTB SPECIMEN	278
FIGURE FOR APPENDIX C	279

LIST OF SYMBOLS

- a - Crack length for compact tension specimens; half-crack length for center cracked panel specimens (inch)
- a_o - Crack length at which an overload(s) was applied (inch)
- a_p - Crack length which defines the extent of the material elastic-plastic interface.
- a_r - Difference between crack length and reversed plastic zone radius, $a-r_y$ (inch)
- a_s - Crack length at start of current cyclic loading (inch)
- a_t - Incremental crack front tunneling (inch)
- Δa - Crack growth increment (inch)
- Δa^* - Crack length over which transient crack growth conditions exist (inch)
- B - Empirical exponent in decreasing closure equation, also designation for one block (cyclic loads within one block are repeated)
- b - Dimension along crack (inch)
- C - Empirical crack growth coefficient
- C' - Empirical crack growth coefficient
- C_f - Crack closure factor, ratio of K_c to K_{max} (or K), or S_c to S_{max} (or S), or P_c to P_{max} (or P)
- C'_f - Modified crack closure factor
- C_{f_o} - Crack closure factor at $R = \text{zero}$
- C_p - Empirical parameter used in Wheeler retardation model

CCP	- Center cracked panel specimen
CTA	- Compact tension specimen, ASTM geometric proportions
CTB	- Compact tension specimen, modified geometric proportions
COD	- Crack opening displacement (inch)
C_1, C_2	- Constants for crack closure instrumentation
c	- Surface crack half-length, dimension along crack (inch)
d	- Dimension from crack tip to closure gage (inch)
$\frac{da}{dN}$	- Crack growth rate (inch/cycle)
$\frac{da}{dB}$	- Crack growth per block (inch/block)
f_n	- Normalized crack growth rate, ratio of measured crack growth rate to calculated constant amplitude crack growth rate
K	- Stress intensity ($\text{ksi}\sqrt{\text{inch}}$)
K_c	- Stress intensity calculated using the stress or load at which crack closure occurs ($\text{ksi}\sqrt{\text{inch}}$)
K_{cr}	- Critical stress intensity ($\text{ksi}\sqrt{\text{inch}}$)
K_{max}	- Maximum stress intensity ($\text{ksi}\sqrt{\text{inch}}$)
$K_{max_{OL}}$	- Maximum stress intensity caused by an overload ($\text{ksi}\sqrt{\text{inch}}$)
$K_{min_{OL}}$	- Minimum stress intensity caused by an overload ($\text{ksi}\sqrt{\text{inch}}$)
K_{min}	- Minimum stress intensity ($\text{ksi}\sqrt{\text{inch}}$)
K_r	- Residual stress intensity ($\text{ksi}\sqrt{\text{inch}}$)
K_{st}	- Stress intensity at which stable tear reaches measurable proportions ($\text{ksi}\sqrt{\text{inch}}$)

ΔK	- Stress intensity range, $K_{\max} - K_{\min}$ (ksi $\sqrt{\text{inch}}$)
ΔK_b	- Stress intensity range for baseline loading (ksi $\sqrt{\text{inch}}$)
ΔK_{eff}	- Effective stress intensity range, $K_{\max} - K_c$ or $K_{\max_{\text{OL}}} - K_c$ (ksi $\sqrt{\text{inch}}$)
$\Delta K_{\text{eff}_{\text{th}}}$	- Effective stress intensity range threshold, $K_{\max} - K_c$ (ksi $\sqrt{\text{inch}}$)
ΔK_{th}	- Stress intensity range threshold at which the crack growth rate is apparently zero (ksi $\sqrt{\text{inch}}$)
ΔK_{th_0}	- ΔK_{th} at $R = \text{zero}$ (ksi $\sqrt{\text{inch}}$)
m	- Empirical exponent used in Wheeler retardation model
N	- Cycles of load
n	- Empirical crack growth exponent
n'	- Modified empirical crack growth exponent
N_D	- Number of delay cycles
N_O	- Cycle count at which an overload(s) was applied
N_{OL}	- Number of overload cycles
N_{sat}	- Number of overload cycles required to produce stabilized closure and, subsequently, maximize retardation
ΔN	- Cyclic increment
ΔN_s	- Number of load cycles since load change
O/L	- Overload ratio, ratio of P_{OL} to P (or P_{OL} to P_{\max}), or S_{OL} to S (or S_{OL} to S_{\max})
P	- Applied load, also maximum applied baseline load (lb)
P_c	- Load at which crack closure occurs (lb)

P_{\max}	- Maximum applied baseline load (lb)
P_{\min}	- Minimum applied baseline load (lb)
P_{OL}	- Overload, maximum applied load (lb)
p	- Empirical exponent in crack closure equation
q	- Empirical crack growth constant
R	- Stress or load ratio, S_{\min}/S_{\max} or P_{\min}/P_{\max}
\bar{R}	- Stress ratio equal to either the applied stress ratio or the stress ratio cutoff value, R_{co} , whichever is less
R_c	- Ratio of closure stress or load after a few overload cycles to the previous (baseline) closure stress or load
R_{co}	- Stress ratio cutoff value above which crack growth rates are not stress ratio dependent
r_y	- Reversed plastic zone radius (inch)
S	- Applied stress, also maximum applied baseline stress (ksi)
S_{ap}	- Stress required to extend plastic zone from current crack length to elastic-plastic interface (ksi)
S_c	- Stress at which crack closure occurs (ksi)
S'_c	- Modified crack closure stress (ksi)
S_{\max}	- Maximum applied baseline stress (ksi)
$S_{\max_{eff}}$	- Effective maximum stress (ksi)
S_{\min}	- Minimum applied baseline stress (ksi)
$S_{\min_{eff}}$	- Effective minimum stress (ksi)

S_{OL}	- Overload, maximum applied stress (ksi)
S_p	- Subscript p indicates previous stress or load (max, min, c, etc.)
S_r	- Residual stress (ksi)
S_{red}	- Reduced stress, $S_{ap} - S_{max}$, (ksi)
ΔS_{eff}	- Effective stress range, $S_{max_{eff}} - S_{min_{eff}}$ or S_{max} (or S) - S_c , (ksi)
t	- Specimen thickness (inch)
U	- $(1 - C_f)/(1 - R)$
V_d	- Displacement voltage from strain gages (volts)
V_l	- Load voltage from load cell (volts)
W	- Total width of panel specimens; dimension from load line to extreme fiber for compact tension specimens (inch)
α	- Relates residual stress to applied stress, $\alpha = S_r/S$
β	- Plastic zone coefficient
γ	- Ratio of closure stress after a few overload cycles to the stabilized closure stress after many overload cycles
Γ	- Denominator in residual force model equation
μ	- Prefix, micro (10^{-6})
ρ	- Plastic zone radius (inch)
σ_y	- Material yield stress (ksi)

SUMMARY

This program is one in a series of research and development programs undertaken by the United States Air Force to develop methods and data needed for design against fracture in military aircraft. This combined analytical and experimental program was directed to an investigation of fatigue crack growth interaction effects under arbitrary spectrum loading conditions.

The test program consisted of approximately 160 specimens almost equally divided between 2219-T851 aluminum and Ti 6Al-4V mill-annealed titanium alloys. Compact tension and center-cracked panel specimens were employed. All tests were performed under ambient laboratory conditions. The test program included constant amplitude, single and multiple overload, compression spike, tension/compression, compression/tension and simplified block loading sequences.

The results of the experimental program were used to review existing crack-growth prediction models and finally to develop a new crack-growth prediction model which was based on the crack closure concept. The resultant crack closure model predicts the crack growth during more complex loading sequences than existing models. It considers negative stress ratios, number of overload effects, and the effects of compression spikes with and without or preceding or following a tensile spike or multiple overloads.

1 - INTRODUCTION

New fracture control and damage tolerance criteria (Reference 1 for example) are being developed and implemented to reduce the risk of the loss of military aircraft due to the existence of crack-like defects in the airframe structure. These defects can occur through material processing or fabrication techniques in a typical airframe component. As a result, the criteria specify that flaws be assumed to exist in critical structural locations and, further, that a component be designed in such a way that its life expectancy meets or exceeds the specified life for the aircraft or inspection interval before the flaw grows to critical dimensions. A necessary element in this concept is an analytical method of determining the sub-critical crack growth caused by a typical aircraft load spectrum.

This program was initiated by the United States Air Force to modify existing models or develop a new model to provide improved predictive capability for the growth of cracks subjected to arbitrary load spectra. An experimental program was conducted to obtain detailed information regarding the behavior of cracks subjected to discrete and simplified variable-amplitude loads. The materials tested were 2219-T851 aluminum and Ti 6Al-4V mill-annealed titanium alloys, both typical aircraft structural materials. With few exceptions, all tests were performed on 1/4 in.-thick specimens of three geometries. The loadings employed ranged from constant amplitude to four-level block spectrum loading, and included compression loads. Crack closure measurements using three different techniques were obtained during many tests. Crack growth data were obtained during all tests. The frequency of observation varied, depending on the type of test conducted.

The analytical portion of the program consisted of two basic parts. The first centered around the reduction and analysis of the crack growth data. Crack closure data were investigated to a lesser extent. The second part consisted of reviewing existing crack growth prediction models with an eye toward their improvement, and the development of new models. The final mathematical model was based on the crack closure concept.

Preliminary investigations indicated that the crack closure concept could be used to explain a variety of crack growth interaction effects, including retardation and acceleration and the effect of different numbers of tensile overloads or compression loads on subsequent crack growth rates. Therefore, the mathematical modeling effort in this program was directed principally toward models which employed variations in crack closure to produce effective stress ranges. The effective stress ranges were then used to calculate modified crack growth rates.

It was further thought that since crack closure is a physical phenomenon, insight could be gained through direct measurement of crack closure during crack growth interaction tests. The testing portion of this program revealed that it was quite difficult to obtain quantitative values of crack closure during the transient crack growth caused by load perturbations. However, qualitative trends could be observed. The problems encountered in measuring crack closure are described in Sections 2 and 3 of this report.

Even though experimental difficulties were encountered, a model based on crack closure behavior was developed that was found to predict a variety of crack growth interaction effects quite well. The development of this model and some results obtained by its application are described in Section 4 of this report.

2 - MATERIAL AND PROCEDURES

2.1 MATERIAL SELECTION

The selection of the two alloys for flaw growth characterization was based on the potential widespread utilization of the results from this program. The materials selected were 2219-T851 aluminum and Ti 6Al-4V mill-annealed titanium alloys. The crack growth data for these two materials, and the use of that data in the development of crack growth interaction models, was expected to afford greater confidence in the utility of the results. That is, a designer employing either material in a new design would have confidence that the crack life predictions obtained from the model would be reliable for these two materials.

Each material was obtained in plate form from one material heat. This was done to minimize the scatter which might be expected when comparing the crack growth data from two different material heats. The aluminum plates were nominally 5/8 inch thick while the titanium was nominally 3/4 inch thick. Since a limited thickness effect investigation was included in the program, all plates were mill polished from the as-received thickness to the required specimen thickness. In this way, the material homogeneity was maintained and the polishing process introduced minimal surface residual stresses.

2.2 TESTING PROCEDURES

Fatigue crack growth tests were performed using a variety of closed-loop servo-hydraulic testing machines. Different machines, which will not be listed here, were employed for economy in testing the various geometries and because the testing was performed in three different laboratories. One machine utilized a computer control, while others employed paper tape control to perform the two-, three- and four-level block loading tests.

Crack growth measurements were obtained optically from the surface of the specimens. In many cases, the surface crack lengths were measured on both sides of the specimen. The optical instruments were matched to the type of test performed so that low-power instruments were used where gross values of crack length increments (>0.030 inch) were required whereas high-powered instruments were used at the other extreme. These latter instruments provided the capability of directly reading the crack length to 0.001 inch.

Testing frequency varied according to the machine, material and specimen geometry. In most cases, the cyclic frequency exceeded 1 Hz. All tests were performed in a laboratory environment at ambient temperature and relative humidity. The exception was that one compact tension specimen of each material was tested under constant amplitude loading conditions in a 95% relative humidity environment at various cyclic frequencies. The results from

these tests compared favorably with those from the laboratory air environment and are reported in Section 3 of this report.

The ambient temperature ranged from 65 to 75 degrees F while the relative humidity had a considerably larger range. Relative humidity measurements are reported on the data sheets included in Volume II.

Crack closure measurements were performed using two different techniques. The procedures and equipment are reported in Subsection 2.4.

Material tensile properties were obtained from six aluminum tensile specimens. For two thicknesses (1/4 inch and 3/4 inch), four titanium tensile specimens each were used to obtain tensile properties for the titanium. All tensile specimens were oriented in the longitudinal grain direction and were selected randomly from the plates. The machine employed was a Riehle FH 60 Universal Testing machine and the extensometer was a DN-20 with a 2 in. gage length. The material tensile properties are presented in Subsection 3.5.3.

All specimens were precracked at load levels selected to provide a minimum amount of interaction with the test loads, or fast crack initiation, or at the load level used for the test. All precracking loads are specified in Volume II of this report.

2.3 SPECIMEN GEOMETRY

Three different basic specimen geometries were employed for this program. These were the center cracked panel shown in Figure 1 and the two varieties of compact tension specimen shown in Figure 2.

The center cracked panel (CCP) specimens were of nominally constant geometry with a thickness of .25 in. and a width of six inches in the test section. Crack starter notches were electro-discharge machined into one surface of the specimens at the longitudinal and lateral centerlines. The starter notches were of constant radius approximately 0.025 inch deep, 0.10 inch long on the surface and 0.010 inch wide. Some of the panels were loaded in compression. To prevent column buckling, the panels were enclosed in a stabilizing fixture which was separated from the specimen by Teflon liners. One specimen was fitted with strain gages to ensure that the stabilizing fixture did not pick up load through friction.

The compact tension specimens were of two geometries. Those tested by the Del organizations were of the standard ASTM geometry except that the thickness relationship specified for plane strain conditions was not retained. These specimens are defined as CTA specimens in Figure 2. Almost all were fabricated with dimension $W = 2.5$ inches. A few were fabricated with $W = 2.2$ inches to economize on material so that the material heat would be constant.

The compact tension specimens tested by Grumman were modified from the ASTM proportions and are defined as CTB specimens in Figure 2. The basic difference was that the height of these specimens was increased to provide clearance for the Amsler "Movomatic" displacement gage (described in Subsection 2.4). The stress intensity solution for the CTB geometry is presented in Appendix C.

All specimens were oriented with the load line parallel to the rolling (longitudinal grain) direction so that the crack grew normal to the rolling direction.

Compact tension specimen identification numbers consist of a pair of letters and two numerical pairs: (ie. AD-25-32 or TG-25-12). The first letter designates the material (A=2219-T851 aluminum, T=Ti 6Al-4V titanium) while the second letter indicates the testing laboratory (G=Grumman, D=Del Research or Del West). The specimens with a D designation were all of ASTM standard geometry (CTA) while those with a G were non-standard (CTB) or center-cracked panels. The first pair of numbers represents the nominal material thickness in hundredths of an inch while the second pair is the specimen sequence number. A few compact tension specimens had duplicate sequence numbers, so the lower case letter a was added following the sequence number.

In the case of center-cracked panel specimens, the system is the same except that a P is appended (ie. AG-25-12P).

2.4 CRACK CLOSURE MEASUREMENTS

Preliminary analyses and the work reported by a number of authors indicated that variations in crack closure might be used to describe a variety of crack growth interaction effects. Because of this, crack closure measurements were obtained during many specimen tests. The objectives were to quantify the crack closure level as a function of stress ratio during steady-state constant-amplitude conditions, and to define how the closure level varied during transient conditions such as during the application of overloads and while the crack was propagating subsequent to the application of one or more overloads. Measurements were also obtained during loading sequences in which the maximum load was held constant and the minimum load was varied. In a few cases, the minimum load was allowed to go into compression. Closure measurements were also obtained during simplified block-loading sequences.

Although some authors have observed differences in the magnitudes of the opening and closure loads, no significant differences were observed during this program. As a result, the terms opening and closure are used interchangeably and are considered to be the same value of load or stress.

Two different methods were employed to measure crack closure. The first employed strain gages mounted across the crack tip, while the second employed a mechanical displacement gage similarly located. These techniques will be described below.

The principal conclusion drawn from this investigation was that meaningful quantitative values of closure could be obtained only during steady-state conditions. These were either constant-amplitude loading or periodic block-loading situations. In the case of periodic loading, the closure level generally did not vary significantly within a block of loads and, as such, approached steady-state conditions. Even for steady-state conditions, however, significant amounts of scatter were encountered. Generally, for a given specimen and gage location, the results were repeatable. However, if the gage was moved or if a different gage were employed, repeatability deteriorated. The final conclusion drawn from these results was that quantitative closure measurements, useful for modeling purposes, could not be obtained using the methods described below. However, the data obtained did prove useful from a qualitative standpoint and provided justification for many of the assumptions made during the modeling effort.

Crack closure measurements made at Del Research and at Del West utilized a technique developed by R. Schmidt (Ref 2) to measure crack closure. The objective of the closure measurement was to monitor the relationship between applied loads and the local crack displacements, and to note the load level in this relationship where it becomes non-linear (See Figure 3). Schmidt utilized an electrical resistance strain gage bonded to the specimen at its ends only to measure local displacements, as shown in Figure 4, rather than a mechanical device. In order to bond the gage only at its ends, a piece of cellophane tape was placed beneath the gage along the projected crack path prior to mounting. Micro-measurement EA-13-Z30DS-120 gages were used for most tests in this program.

Note that it is not necessary to calibrate either the load or gage output. The applied loads are known and the dimensions along the ordinate are proportional to the applied loads. Therefore, the maximum and minimum applied loads define the upper and lower extremes of the trace and intermediate values may be scaled. The strain gage output is proportional to the local displacements and the onset of non-linearity in the load-displacement record can be observed. Since the absolute magnitudes of strain were not required, the gages were not calibrated.

The determination of the exact load value at the onset of non-linearity is somewhat subjective. This of course is equally true when similar measurements are made with other displacement measuring devices. Personnel at Del Research made the observation that sensitivity of the opening load measurement could be increased if the linear contribution to the displacement were subtracted. That is, rather than having a test output of load voltage (V_1) versus displacement voltage (V_d), electronics were placed in the instrumentation line which produced an output record of V_1 versus $(C_1V_d - C_2V_1)$ where C_1 and C_2 are constants that were set during the test. By changing C_1 and C_2 , a variety of outputs are possible (See Figure 5). This has been referred to as a cancellation technique. When this method is used, the opening load determination is less ambiguous than it is in the corresponding load-displacement plot.

Even with this additional technique, closure load determinations must still be classified as a difficult experimental procedure. There are many reasons for this. Outstanding among them is the fact that any test which requires the determination of a non-linear point requires an arbitrary definition of where that occurs. Determination of the proportional limit is an example of this. The fact that the linear part of interest extends to the upper portion of the load-displacement record, rather than to the origin, only compounds the difficulty. It was found during many of the tests that the load-displacement record consisted of three, rather than two, linear portions as shown in Figure 6. The two discontinuities are referred to as the lower and upper bumps respectively. The significance of these two discontinuities will be discussed below.

The closure load measurement is most successful when the closure level is stable and a number of similar output records are available to be interpreted simultaneously. That is, it is far easier to measure the closure load for constant amplitude loading than it is for tests in which there are overloads and transient closure load behavior. In fact, the more transient the crack growth and closure behavior is, the more difficult it is to interpret closure load records. This can be seen in Figures 7 through 9.

Figure 7a shows a plot of crack length vs cycles for a titanium compact tension specimen subjected to essentially constant amplitude loading. Figure 7b presents the applied maximum and minimum loads and the measured opening loads. The data points are taken as the upper tangent point of the load-displacement (eg. Figure 3) or load-voltage plots. Based on the results from Gage No. 2, the closure level appears to have stabilized at about 250 lb prior to the first load change at 810,000 cycles. Then, subsequent to about 820,000 cycles, the closure level is stabilized at about 350 lb. In these two regions, where stabilized crack growth existed, meaningful quantitative values can be obtained. However, during the transient period subsequent to the load change (810,000 cycles to 820,000 cycles), the closure behavior is not well defined.

Figure 8 presents similar results for a titanium specimen subjected to a multiple overload (step) test where the overloads are 1.5 times the baseline loading. Here, (Figure 8b) a differentiation can be made between the previously described upper and lower bumps. Prior to the first series of overloads ($N_{OL} = 1019$), there is only one non-linear point (bump) on the trace and the closure load is approximately 250 lb. When the overloads are applied, two bumps were readily apparent. The upper one reaches a value of approximately 670 lb while the lower one reaches a value of approximately 350 lb. Subsequent to the application of the overloads, both values decay to about 300 and 125 lb respectively. Experience has shown that the lower value (125 lb) is far too low to represent a true closure level. The higher value (300 lb) is 40% of the maximum applied load and experience also indicates that this is a typical value for the closure level at this applied stress ratio of 0.05. (The stress ratio, R , is P_{min}/P_{max} .) This indicates that the upper bump is the significant closure variable. The steady-state closure level before the overloads is about one third of the maximum applied load, while

afterward it is about 40% of the maximum. Using the maximum value (40%), the stabilized closure load during the application of the overloads should not exceed 450 lb ($.40 \times 1125$ lb). However, it can be seen that, for both loading sequences, the upper bump value easily exceeds 600 lb. Even on an expanded scale, it was very difficult to define how the closure level increased during the application of the overloads because of extensive scatter. Subsequent to the overloads, the closure level returned to a stable value in an orderly fashion. However, lacking end point values which are considered valid, it is difficult to have much confidence in any expression fitted to the data.

Figure 9 presents crack length and closure load data vs cycles for a titanium specimen subjected to single discrete overloads which were 1.25 times the baseline loading. The closure load data (Figures 9b and 9d) are typical examples of "good" data taken during this type of test. Referring to Figure 9b, the steady-state closure load prior to the overload application is approximately 315 lb or about 45% of the maximum applied load. (This value appears to be slightly high based on other results.) Subsequent to the application of the single overload, two bumps were readily apparent on the load-voltage records. The lower bump would indicate a significant decrease in the closure level, while the upper bump generally describes an increased closure level. It will be shown later that increased closure results in retarded (reduced) crack growth rates. Therefore, the upper bump again seems to best fit our concept of how the closure level should behave. A close examination of these data indicates that the closure level (upper bump) first decreases slightly and then increases to a maximum, thereafter decaying to a steady-state level. The initial decrease would result in slightly accelerated (increased) crack growth rates immediately after the overload. However, it can be seen that the minimum value immediately after the overload is approximately the same as the stabilized value at the right-hand end of the data. This stabilized value (approximately 265 lb) is 38% of the maximum applied baseline load (700 lb) and agrees closely with the steady-state values obtained from Figure 8b. Thus, the initial value of closure before the overload is probably incorrect. Assuming that the closure level prior to the overload is about 265 lb, a general behavior can be defined: the closure level first increases to a value of perhaps 370 lb (42% of the overload) and then it decays. Here again, it would be difficult to reach any but the grossest conclusions as to how the closure level actually varies. Figure 9d verifies this. The data shown there possess extensive scatter and defy any attempt to quantify the results. Here, even qualitative conclusions are difficult to reach.

Figure 10 presents similar data for an aluminum specimen subjected to single discrete overloads. Although the closure measurements obtained from aluminum specimen tests exhibited less scatter and the variations in closure were more uniform than their titanium counterparts, the results were still impossible to quantify.

Many more difficulties were encountered in the closure measurements of titanium than those of aluminum. This could be attributed to two major sources: the basic scatter in the material's response to load, and to the fact that pin bearing friction problems arose in some of the tests. The increased

loads in the titanium and its tendency to gall at the loading pin interfaces were thought to be responsible for the latter problem.

Crack closure measurements made at Grumman utilized an Amsler "Movomatic" model DBM 233 displacement gage. This instrument has an accuracy of $\pm 1\%$ of full scale and can measure displacements on the order of 10^{-5} meters. The output from this instrument, along with a load signal, were put into an X-Y recorder to obtain traces of load vs displacement typified by Figure 3.

Adaptors, developed to fit the instrument, allowed a minimum gage length of approximately 0.060 inch. An additional mechanism was devised to accurately place the gage across the crack on the specimen.

The results using this gage were mixed. Whenever constant amplitude loading was employed, the results, obtained by interpreting the load-displacement traces, were repeatable. When the gage was relocated on the same or on a different specimen, the closure level exhibited some scatter. It was difficult to pick out the upper "bump" described earlier and, as a result, closure variations during transient crack growth conditions could not be defined using this technique.

Based on the results obtained in this program, the state-of-the-art closure measurement capability is not sufficiently accurate to obtain the precise closure values required for modeling purposes. However, the advantages of a crack closure-based model outweigh the experimental difficulties which were encountered. Further, it will be shown in Section 4 that simplified assumptions of crack closure behavior can be used to yield reasonably good crack growth predictions for a variety of loading sequences.

3 - RESULTS AND DISCUSSION OF TEST DATA

The test plan was developed to provide insight into the fatigue crack growth behavior for constant- and variable-amplitude loading. Two materials (Ti 6Al-4V titanium and 2219-T851 aluminum alloys) were tested under similar conditions where possible, in order to determine whether or not differences in material behavior exist from the standpoint of load interaction effects.

The test program was generalized in order to provide an evaluation capability for existing crack growth retardation models as well as for any new modeling efforts. Crack growth measurements were taken over small increments of crack growth (or small cyclic increments) before, during and after load changes. This was done in an effort to discern all interactions which might exist. When the crack growth was stabilized (i.e., constant amplitude growth without previous load history effects) the crack growth increments were increased. Many of the specimens were fitted with the Amsler "Movomatic" gage or with strain gages so that load-displacement traces could be obtained. These load-displacement traces were then used to obtain measured values of crack closure and opening. Here again, the crack closure measurements were made frequently near load change locations and less frequently after stabilized conditions were attained.

Revisions in the original test plan were necessary since, originally, compact tension specimens were to be used for certain load sequences involving compression loads. During the course of the test program, it was revealed that the compact tension specimen does not provide accurate data during the application of compression loads. Based on these results, the test program was modified so that compression load sequences were applied only to center cracked panels. Some earlier tests had already been performed on compact tension specimens (ref. Tables 8a and 8b) and are reported here, although little analysis of the results was performed.

3.1 CONSTANT AMPLITUDE TEST RESULTS

Constant amplitude fatigue crack growth tests were performed to characterize the steady-state crack growth behavior of the two materials. Table 1 shows the constant amplitude test plan for both materials.

It was known (Reference 3) that varying the stress ratio has a strong effect on crack growth rates. The stress ratio, R , is defined as the ratio of the minimum applied stress or load to the maximum applied stress or load.) A variety of stress ratios, including $R = -1$, were tested. Since it was desired to obtain da/dN data over the range 10^{-7} to 10^{-4} inch/cycle, the allowable stress (or load) ranges were limited. Initially, it was desired to investigate whether or not a stress level effect existed during constant

amplitude loading. A stress level effect on crack growth rates is defined as: for constant values of stress ratio and stress intensity range, the crack growth rate is a function of the maximum applied stress. For the limited stress ranges tested, no stress level effect on crack growth rates was observed for either material.

Three different specimen geometries (CCP, CTA and CTB) were used for each material to obtain da/dN data to insure that specimen configuration was not a factor in determining crack growth rates. Crack growth rate data was not obtained at each stress ratio investigated using each of the specimen types. Based on the test results, specimen geometry did not influence the crack growth rate data except for negative values of stress ratio. In the latter case, it was found that the compact tension specimen produced erroneous results when subjected to compression loads.

3.1.1 2219-T851 Aluminum Results

Figures 11a through 11d show crack growth rate, da/dN , plotted against applied stress intensity range, ΔK , for the 2219-T851 aluminum for a variety of stress ratios. The figures show that as the stress ratio, R , is increased, the crack growth rate increases for the same value of ΔK . This is true up to a stress ratio of approximately 0.5, a value determined analytically. For stress ratios greater than this value, there appears to be no further layering.

The data were fitted to a modified Elber equation of the form:

$$\frac{da}{dN} = C [(1 + q\bar{R}) \Delta K]^n \quad (1)$$

A least squares procedure was used to fit the data to Equation 1. The stress ratio cutoff value, R_{co} , above which no further layering occurred was determined analytically by varying the value of R_{co} , such that for $R \leq R_{co}$, $\bar{R} = R$, but for $R > R_{co}$, $\bar{R} = R_{co}$. The parameter q was considered to be an empirical constant. However, independent studies on a variety of materials have indicated that it generally ranges between .6 and .8, suggesting that q may have a physical significance. The parameters q and R_{co} were varied systematically and, for each pair a least squares analysis was performed for C and n . The total error was determined for each set of four parameters. The least total error produced:

$$C = 1.96 \times 10^{-9}$$

$$n = 3.34$$

$$q = 0.6$$

$$R_{co} = 0.5$$

so that:

$$\frac{da}{dN} = 1.96 \times 10^{-9} [(1 + .6R) \Delta K]^{3.34} \quad 0 \leq R \leq 0.5 \quad (1a)$$

$$\frac{da}{dN} = 1.96 \times 10^{-9} [1.3 \Delta K]^{3.34} \quad R \geq .5 \quad (1b)$$

The test data for $R = -1$ were not included in the least squares analysis.

Figure 12 presents da/dN vs. ΔK data for 2219-T851 aluminum specimens subjected to stress ratios of -1 . For reference, Equation 1a is shown for the case of $R = 0$. Two CTB specimens were subjected to a fully reversed loading of 500 lb and one CTB specimen was subjected to a fully reversed loading of 700 lb. In all cases of R less than 0, the stress intensity range was calculated using $K_{min} = 0$. It can be seen from Figure 12 that there is a layering of the data for these specimens such that the specimens subjected to 500 lb produce slower growth than the specimen subjected to 700 lb at the same value of ΔK . At the same time, the slope of the three sets of data is nominally 2.49 while the overall slope of the positive stress ratio data is 3.34. The test data for a center cracked panel is shown to lie parallel to the positive stress ratio data and agrees both in terms of the nominal slope and the crack growth rate at a given ΔK . Data presented in other references (e.g. Ref 3) indicate that this latter behavior is typical for some aluminum alloys. Although only one test with a negative stress ratio was performed on a center cracked panel, it is felt that the result was valid. The ΔK for the CCP (AG-25-7P) data was calculated using $K_{min} = 0$, such that $\Delta K = K_{max}$ to produce:

$$\frac{da}{dN} = 2.60 \times 10^{-9} (K_{max})^{3.34} \quad (2)$$

One CTB specimen (AF-50-01) which was 1/2 inch thick was tested at a stress ratio of 0.05 to obtain an indication of whether or not thickness was a factor for the aluminum. These data nominally exhibit the same da/dN vs. ΔK behavior as the 1/4 inch data, as shown by Figure 13.

One 2219-T851 aluminum specimen was tested in 95% relative humidity with cyclic frequencies ranging from 1/2 to 10 Hz to insure that the results obtained by testing in laboratory air at various cyclic frequencies were not sensitive to humidity variations. The data from this test are presented in Figure 14 and compared to Equation 1a. These results show that the aluminum is not sensitive to variations in relative humidity or cyclic frequency.

3.1.2 Ti-6Al-4V Titanium Test Results

Figures 15a through 15e show da/dN plotted against ΔK for the Ti-6Al-4V titanium alloy material. The figures show that, as the stress ratio increases, da/dN increases for constant ΔK . In the case of the titanium, there is no apparent cutoff of this stress ratio effect up to the maximum tested value of $R = 0.7$.

The positive stress ratio data were fitted to the modified Elber equation (Eq 1) using the same procedures as for the 2219-T851 aluminum to produce:

$$C = 5.90 \times 10^{-10}$$

$$n = 3.08$$

$$q = 0.7$$

$$R_{co} > 0.7$$

so that

$$\frac{da}{dN} = 5.90 \times 10^{-10} [(1 + 0.7R) \Delta K]^{3.08} \text{ for } 0 \leq R \leq .7 \quad (1c)$$

Since Equation 1c was fitted to data for the range specified ($0 \leq R \leq .7$), its validity is undefined for $R > 0.7$.

For the $R = -1$ data,

$$\frac{da}{dN} = 1.11 \times 10^{-9} (K_{max})^{3.08} \quad (3)$$

In Equation 3, $K_{min} = 0$ such the $\Delta K = K_{max}$.

One CTB specimen (TG-75-01) which was 3/4 inch thick was tested under constant amplitude conditions to obtain an indication of the effect of thickness. Figure 16 presents the limited test data obtained and compares them to scatter bands taken from the 1/4 inch data (Figures 15a and 15c). Although the slopes of the data in Figure 16 tend to be greater than the equivalent 1/4 inch data, the bulk of the 3/4 inch data lie within the 1/4 inch material scatterbands. Based on the limited data available, no definite conclusions can be drawn regarding the effect of thickness on crack growth rates in titanium.

The titanium data exhibits an apparent threshold effect for low values of ΔK . At a value of da/dN of approximately 10^{-6} inch/cycle, the slope of the data in Figure 15a becomes much higher than that of the data above 10^{-6} inch/cycle. This effect was not accounted for in developing Equation 1c.

Figure 17 presents da/dN vs. ΔK for all data with a stress ratio of 0.05. Equation 1c is shown along with a scatter band which encompasses all

but the most widely scattered data. At a given value of ΔK , the upper bound of the scatter band is approximately twice the mean behavior (Eq 1c) while the lower bound is approximately one half of the mean behavior. Therefore, if Equation 1c were used to calculate the life of a titanium constant amplitude test specimen, the results could be from one half to two times the test life. The magnitude of this scatter is much greater than the equivalent aluminum results.

One CTA titanium specimen was tested under constant amplitude conditions with a relative humidity of 95% and cyclic frequencies ranging from 1/2 to 25 Hz. These results, shown in Figure 18, indicate that the specimen tested under these conditions produced nominally the same crack growth behavior as those specimens tested in laboratory air.

3.2 SINGLE OVERLOAD TEST RESULTS

The effects on subsequent crack growth of single overloads were examined. The test matrix was developed in order to examine three possible situations for both materials investigated. The first was to determine the effect on subsequent crack growth rates of the application of a single overload. In this case, the crack was propagated under constant amplitude loading conditions, a single overload cycle was applied, and the crack was then cycled under constant amplitude loading until stabilized crack growth behavior was regained.

In the second case, two single overloads were applied in such a manner that the second overload was applied while the crack was still growing under the influence of the first overload. In the case of the titanium specimens, the affected length, Δa^* , caused by the overload, was extremely small (on the order of .001 to .010 inch) and this condition of interaction could not be achieved. (The dimension Δa^* is that crack growth increment subsequent to overload(s) during which the crack growth is influenced by the application of the overload(s).)

The third situation investigated represented, in a simplified manner, the behavior seen in typical aircraft spectra. Here, single overload cycles were applied at various frequencies of occurrence (i.e., repeated applications of 1 cycle of overload followed by N cycles of baseline loading).

For the three situations investigated, up to four overload ratios, O/L, were used. The overload ratio, O/L, is defined as the overload stress (or load) divided by the maximum baseline stress (S_{OL}/S) or load (P_{OL}/P). For the 2219-T851 aluminum, nominal values of O/L = 1.25, 1.5, 1.8 and 2.1 were used. Values of 1.25, 1.5 and 1.8 were used for the Ti 6Al-4V titanium. Table 2 presents the test matrix for all single overload tests performed on both materials.

Crack growth measurements were obtained during all sequences. For many tests, these data were obtained over very small crack growth increments (e.g., .001 to .002 inch). In addition, crack closure measurements were obtained during many of the tests.

Because the mathematical model developed during the program is based on crack closure, many references to closure behavior will be found during the ensuing discussion. In many cases, it is a convenient way to visualize physically why crack growth interaction effects take place.

3.2.1 2219-T851 Aluminum Test Results

Single Overloads - The objectives of these tests were to obtain detailed crack growth and crack closure measurements during and subsequent to the application of single overloads, and to quantitatively define the effects of those overloads on subsequent crack growth behavior. The data were analyzed by plotting crack length, a , vs. N and the normalized crack growth rate, f_n , vs. crack growth increment after each overload for various overload ratios. The normalized crack growth rate is defined as the ratio of the measured crack growth rate to the calculated constant amplitude rate under the current loading. The calculated constant amplitude rate neglects any effects of load interaction. Each specimen tested was subjected to from three to about ten overload sequences (referred to as events). Only a few pertinent events are presented here.

Figures 19 through 26 present overall a vs. N data for several specimens subjected to discrete overload applications. Data of this type proved to be of little value for analysis purposes. However, detailed a vs. ΔN_s plots (ΔN_s is the number of cycles since the overload) such as those shown in Figures 27 through 30 were more useful. The figures present data and two or more calculated constant amplitude crack growth curves for specimens subjected to three different overload ratios (1.5, 1.8 and 2.1). (The overload ratio is the ratio of the overload stress or load to the maximum baseline stress or load.) The constant amplitude curves were introduced as an aid in analyzing the data to determine the number of delay cycles and the crack growth increment where unretarded (constant amplitude) crack growth conditions were re-established. Figure 27, for example, shows two calculated constant amplitude curves. The curve on the left represents the expected crack growth behavior in the absence of the overload. The curve on the right is identical to the first except that it has been translated to the right by approximately 3600 cycles so that it provides a reasonable approximation to the stabilized crack growth behavior when the crack length is greater than about 0.51 inch. The number of cycles between the two curves (in this case 3600) is defined as the number of delay cycles, N_D .

When this method was used, the crack length and value of N_D at which the retarded crack growth returned to constant amplitude behavior could be determined and it eliminated the scatter encountered when other methods were

used. As a further convenience, the calculated plane strain and plane stress plastic zone radii caused by the maximum overload stress intensity are also shown. It appears that the plane strain plastic zone is in best agreement with the data.

Figure 28 presents similar data for specimen AG-25-2P which was subjected to single discrete overloads where the overload ratio was 1.5. This particular figure (event) exhibits extensive scatter. However, the overload stress intensity for this event is almost identical to the preceding case and is therefore useful in the following discussion. The effects of the scatter can be reduced by applying the same approach as for the previous case. Here, however, three constant amplitude curves have been constructed and it can be seen that the central curve best fits the overall crack growth behavior for the crack lengths exceeding the plastic zone radii. Even though the data points oscillate about the central curve, it is reasonable to assume that the nominal crack growth behavior is best described by the central curve.

The values of N_D for the four conditions shown (Figures 27 through 30) are plotted against the baseline stress intensity range, the maximum overload stress intensity, and the overload ratio, in Figure 31. In the central figure, there are two pairs of data at approximately equal values of K_{maxOL} . It would seem that this parameter would have a significant effect on the number of delay cycles, but it can be seen that no consistent trend exists. The overload ratio best correlates the data. The right-hand figure shows a consistent trend of increasing N_D with increasing overload ratio. It can also be seen that at an overload ratio of approximately 1.4, N_D equals zero. This result differs from the expected result. For example, Reference 4 indicates significant delays (large values of N_D) for 2024-T3 subjected to an overload ratio of 1.5. Similarly, Reference 5 shows large values of N_D for two successive overload applications at an overload ratio of 1.5 in 7075-T6511 aluminum alloy.

The minimum effective overload ratio value of 1.4 determined in this program is supported by the results of Figure 32. This figure presents a portion of the data of Figure 19 on an expanded scale. The calculated constant amplitude behavior is also shown. For the two events shown, where the overload ratio was 1.25, the overloads have negligible effect on the overall crack growth. Referring again to Figure 31, it can be seen that the number of delay cycles increases quite rapidly with increasing overload ratio. The limited data here indicate that an overload ratio of, for example, 2.5 would produce such a large value of N_D as to constitute crack arrest. Additional testing would be required to demonstrate whether or not this conclusion is valid.

The number of delay cycles also depends on the crack length at which each overload is applied. Specimen AG-25-2P (reference Figure 28) was subjected to eight overload sequences. These results are presented in Table 3. It can be seen that, as the crack length at which the overloads were applied increased, there was an orderly increase in the number of delay cycles. The

first case (Table 3) indicates that the crack propagated more quickly after the overload application than it might have without the overload, as evidenced by the negative value of N_D . This result is probably due to data scatter. The last three events occurred when the overload stress intensity was close to or exceeded the stable tear threshold, K_{st} . (The stable tear threshold is defined in Subsection 3.6.1 as the stress intensity above which stable tear reaches measurable proportions.) The value for aluminum was estimated to be 30 ksi $\sqrt{\text{in.}}$. Because of the potential for stable tear, the last three values of N_D in Table 3 may be invalid.

It can be concluded that the number of delay cycles is an increasing function of the crack length at which a single overload cycle is applied and of the overload ratio. Overload ratios less than approximately 1.5 produce essentially no retardation while an overload ratio greater than 2.1 is required to cause crack arrest. For this method of analysis, the plane strain plastic zone radius caused by the overload stress intensity provided the best description of the overload-affected crack length. It is shown in Section 4 that, from a modeling standpoint, the use of the plane stress plastic zone provides a good fit to the data. This apparent contradiction will be discussed further there. Upon reviewing all of the a vs. N and a vs. ΔN_s curves presented here, it was concluded that the crack growth exhibited immediate retardation subsequent to the application of a single discrete overload. No delayed retardation is apparent.

Another approach used to evaluate the crack growth data subsequent to the application of a discrete overload was to analyze the detail crack growth rates. It was found to be very difficult to quantitatively characterize the crack growth behavior on this basis for two principal reasons. First, the crack growth increment over which the transient phenomenon occurs is very small for the 2219-T851 aluminum and even smaller for the Ti 6Al-4V titanium. Secondly, the data, when viewed in this manner, exhibits extensive scatter. This can be seen from the typical test results presented in Figures 33 through 36.

These data are for a series of three nominally identical tests for a single overload ($O/L = 1.25$), applied to an aluminum specimen. Figure 33 is simply a plot of crack length versus the number of cycles since the overload. Figures 34 through 36 are various attempts at analyzing the data. The first was a simple plot of $\Delta a/\Delta N$ as a function of growth since the overload for each increment of growth recorded. As can be seen in Figure 34, a pattern is observed but a quantitative description of the behavior is impossible. Note that the isolation of a single test might cause the observer to describe "delayed retardation", "initial acceleration", etc. When viewed as a whole, the three data sets do not allow the observer to draw any quantitative conclusions and reduces one's confidence in qualitative descriptions as well. The instantaneous rate data is simply not reproducible.

In an attempt to clarify the situation, a plot of total average growth rate since the overload versus crack growth since the overload, $a - a_0/N - N_0$ vs. $a - a_0$, was made. (See Figure 35). As can be seen in the figure, a large amount of scatter was present for the initial period of growth in this data reduction as well. However, after about .008 inches of growth, the averages stabilize and in fact are ordered by increasing values of stress intensity factor (absolute crack length). Since our crack growth measurements are far more accurate than the scatter in the earlier portion of Figure 35, we believe Figure 35 implies that crack growth under nominally identical conditions is only reproducible in an average sense over distances on the order of .008 inch. For other test conditions (e.g. different stress intensities or materials), the actual number may be somewhat different. It is believed that this occurs because of material inhomogeneity, oscillation of crack growth on either side of the crack, tunneling, minor load variations, etc. No experimental technique is known which will eliminate this problem.

In light of the above result, rates averaged over each .008 inches were plotted for these same data. (See Figure 36). Although this decreases the scatter as compared to Figure 34, which is essentially rates averaged over .002, we feel that quantitative evaluations are still not possible.

Delayed Retardation - The above discussion and figures clearly illustrate that the crack propagation data "immediately" after an overload cannot be established with any meaningful degree of accuracy. To define "immediately", we use a set of typical curves showing da/dN versus the number of cycles since the overload (Figure 37). Figure 37a is taken from Reference 5. Figure 37b is a replot of the same data on a linear scale. Data obtained during this program were not used for this example because they cannot be represented meaningfully by such a plot. Although it is not clear from the referenced paper, the data shown seems to be taken from an average of ten striation measurements. This data is similar to curves presented in many other papers. It is to be emphasized that in all of these papers, this curve is presented as a schematic or a representation of one data set. Apparently, all these authors are concerned with phenomenological descriptions and not predictions, thus reproducibility of data and its use in a prediction scheme were not of concern.

Returning to the definition of "immediately", the portion of Figure 37b prior to the ordered return to constant amplitude rate is the immediate region for which instantaneous rates cannot be accurately observed, measured and used in a predictive model. A distinction between instantaneous rate and average rate must be made. This is because, in the previous discussion, it was shown that the average rate after some initial period was reproducible.

As mentioned previously, the lack of reproducibility in instantaneous rate is not due to measurement limitations but seems to be due to the basic variability of the material and its reaction over small distances. Also

involved are interactions with tunneling and growth oscillations on either side of the crack. The fact that the crack growth rate data immediately after an overload is not available presents a significant problem. How could a model be developed using this data to predict growth under general-spectrum loading? One solution would be to show that this information is not necessary and that only the average value is of interest. This is, in fact, believed to be the case. It should be noted that if a material does not behave reproducibly, except in an average sense, then only two possibilities exist: 1) only that average can possibly be of importance, or 2) no predictions can be made, even by using data from a test which is identical to the case which is to be predicted.

Referring again to Figure 37b, note that if the return from a minimum rate could be classified as a transient phenomenon, the period of delay in rate should be classified as a highly transient phenomenon and it would appear that it would be unlikely to be of importance. This variation in the closure stress intensity, K_c , that would produce the variation in crack growth rates shown in Figure 37b is depicted schematically in Figure 38a. The closure stress intensity, K_c , is calculated using the stress at which crack closure occurs and the appropriate crack length. When an overload occurs, it sets up the potential variation in K_c shown in Figure 38b. Note that by utilizing the variation of K_c with growth since the overload, rather than Figure 37b, one can consider the many levels of loads which may occur and still determine how the retardation is affected. That is, one is not confined to considering constant amplitude loading after the overload. An overload is now defined as a load that interrupts the potential variation in K_c . First, assume that an overload does not occur until K_c has almost returned to its minimum value. Obviously, the initial highly transient phase does not contribute significantly to the overall growth for this loading case. If this closure behavior is typical of a particular spectrum, then any representation of the highly transient region (including ignoring it), will produce essentially the same crack growth prediction.

This result is shown in Figure 39. The crack length vs. cycles curves were calculated by numerically integrating the solid curve in Figure 37a to produce the solid curve in Figure 39. The dashed curve (Figure 39) excludes the highly transient portion of Figure 37a. In this case, the crack growth rate was assumed to be described by the dashed line in Figure 37a. Figure 39 shows that, at the extent of the data (1000 cycles), the error in crack length introduced by simply excluding the highly transient behavior is less than 2 percent. By using a slightly higher curve than the assumed (dashed) curve in Figure 37a, the life, calculated without the highly transient behavior, could be made to agree almost exactly with the life resulting from the calculation which includes the highly transient behavior. It is apparent that the highly transient behavior can be neglected if an average crack growth rate behavior is assumed, and further, that the minimum average assumed rate will not be substantially different from the observed minimum rate.

Now assume that an overload occurs at some point in the variation right after the highly transient period. If this is typical of the spectrum under consideration, then the early highly transient portion could have some impact on the growth, but only the average of this transient period can be of importance. That is, any model that produces the same average rate in the highly transient period will predict the overall growth.

Lastly, assume that an overload occurs in the middle of the highly transient period. Note that the crack growth since the previous overload in this case will be very small. In fact, it will be much smaller than the overload-affected crack length (plastic zone size). If this is typical of a spectrum under consideration, then the behavior should essentially reproduce the behavior during the periodic load tests in our test program, in which there was little growth between overloads. In these tests it was observed that the closure load remained constant for all loads in the sequence.

Thus, if additional overloads often interrupt the highly transient period, the highly transient portion is eliminated. If the transient behavior is interrupted only occasionally, the contribution of this portion of the spectrum will not affect the life significantly, just as it did not during the first case considered. It has therefore been demonstrated that the only description of the highly transient period after an overload that is needed is the average growth rate. In fact, this is only necessary for the particular case of an additional overload being applied immediately after the highly transient phase of a preceding overload.

Single Periodic Overload Test Results - A distinction was made between those tests which are periodic in nature and those tests which are not periodic in nature. The reason for this is that, as a general rule, those tests which are periodic display little transient behavior (i.e., highly changing rates). Of course, in the extreme, if the periodicity is large enough, a periodic overload test will look exactly like a single isolated overload test. However, most of the tests run were not of this nature. It would be expected that modeling of both the periodic and isolated single overload tests would be done in exactly the same manner. However, when reviewing the data, different approaches should be used depending on whether or not transient behavior is present.

In many of the periodic overload tests the closure loads remain approximately constant. (This will be discussed in greater depth in a subsequent portion of the text.) This fact makes the plotting of periodic overload data in other manners more appropriate. For example, one can consider da/dN vs. ΔK_b for a particular periodic overload test and thereby obtain information on the effective closure level for that test. As will be seen in the bulk of the tests, the conditions under which these various plotting techniques may be of value can be readily established.

Figures 40a and 40b are typical closure measurement records taken from a test for which the overload factor, O/L , was 1.8 times the base loading and a single overload was applied every 1000 cycles. The data of Figures 40a and 40b were produced with different strain gages and the crack lengths for each differed by about 0.2 inch.

Figure 40a includes many closure measurements. Although it appears that the closure load decreases as more low cycles are applied, the drop is not very significant. In fact, the closure load (actually opening load) made during the application of the overload (which is the 1001st load) indicates that this apparent trend may not be real at all. When Figure 40 is considered, it appears that a constant closure is probably the best interpretation of what is occurring. The average closure load in a given test sequence is plotted in Figure 41 for the entire test duration. It can be seen that an average value of 400 lb for the entire test is a reasonable estimate.

The fact that, for periodic overload tests, the closure load is essentially constant is not entirely unexpected. A constant closure level under certain periodic overload conditions is consistent with our concepts of closure. It was pointed out in Section 2.4 that the application of periodic overloads could be treated as an essentially steady-state condition. This can be explained by the following. Consider the material in the crack tip vicinity at a time immediately after a single overload within the periodic sequence. If the subsequent low loads extend the crack by a small amount relative to the affected length due to the overload, then each succeeding overload influences material that has already seen a large number of previous overloads. Thus, each additional single overload causes little change in the material state in the crack tip vicinity (which has experienced many prior overloads) and therefore little change in the closure level will be brought about by that particular load.

The closure load then may be expected to be comparable to the closure load associated with a very large number of overloads prior to applying any low loads at all. Thus, we reach two conclusions about this particular type of periodic overload test. The first conclusion is that the closure level remains essentially constant throughout the test. The second, is that the closure level which occurs is the same as that which would occur due to a large number of overloads. It will be seen that these conclusions can be shown to be true from the data gathered, and that they can be very useful in designing experiments which yield fundamental information about closure levels. It is important to note that the constant closure approximation will only be true when the nature of the periodicity is such that there is only a little growth between overloads. By little growth we of course mean a small amount of growth compared to the affected length (plastic zone) due to the overload.

Utilizing the fact that the closure load remains constant during certain periodic overload tests, it is possible to describe a technique to generate "closure data" (i.e., K_c/K_{max}), indirectly using crack growth data in

lieu of actual closure measurements. The technique uses the results of a constant amplitude test (Test 1) and a periodic overload test (Test 2). The number of cycles between overloads in Test 2 must be sufficiently small so that there is little growth between overloads. In addition, the magnitude and number of overloads must be sufficiently small so that virtually all of the crack growth can be attributed to the low loads. No restriction on the number of overloads for each periodic sequence is necessary. A better description will be obtained by considering actual data.

An example of a spectrum that would in most cases meet these requirements would be a periodic sequence of two loads, one cycle of the first at a level 1.8 times that of the baseline load, followed by 1000 baseline loads. The technique depends on the following assumptions concerning such a periodic overload test.

- The closure level remained constant. That is, it did not change as the crack grew and it was the same for each cycle in the spectrum.
- The closure load was a function of the overload only, and was predictable from constant amplitude closure measurements at the same stress ratio as the overload.
- Crack growth rates were predictable from the closure load and constant amplitude rate data.

These conclusions suggest the following procedure for determining closure loads, without actually making closure measurements. For simplicity, we will consider $R = 0$ first.

Figure 42 is an example of the results obtained for the test described above. Test 1 is a constant amplitude loading in which the stress intensity cycles between zero and K_1 . In Test 2, the baseline stress intensity cycles between zero and K_2 . At regular cyclic intervals, an overload is applied to produce K_{OL} such that $K_{OL} = K_2 \cdot O/L$, where O/L is the overload ratio. Consider points on the Test 1 and Test 2 curves, which represent the same crack growth rate. The stress intensity factor at these rates will be K_1 and K_2 respectively. The effective stress intensity ranges are:

$$\Delta K_{eff1} = K_1 - K_{c1} = K_1 - K_1 \cdot C_{f0} \quad (4)$$

$$\Delta K_{eff2} = K_2 - K_{c2} = K_2 - K_{OL} \cdot C_f = K_2 - K_2 \cdot C_{f0} \cdot O/L \quad (5)$$

where C_{f0} is the closure factor for $R = 0$. The closure factor is the ratio of the stress intensity (or load) at which the crack closes to the maximum stress intensity (or load.) Note that since the stress ratios are the same for these tests (they are both $R = 0$), the value of the stress intensity at

the point where the crack closes, K_c , is found by multiplying the same closure factor, C_{f_o} , by each of the peak stress intensities (K_1 and $O/L \cdot K_2$ respectively).

In order for the rates to be equal, the effective stress intensities must be equal:

$$\Delta K_{eff1} = \Delta K_{eff2}$$

$$K_1 - K_1 \cdot C_{f_o} = K_2 - K_2 \cdot C_{f_o} \cdot O/L$$

$$C_{f_o} = \frac{K_2 - K_1}{K_2 \cdot O/L - K_1} \quad (6)$$

Similarly, $C_f = K_c/K_{max}$ could be found for any value of R simply by having $R_1 = P_{min1}/P_{max1}$ for Test 1 and $R_2 = P_{min2}/(O/L \cdot P_{max2})$ for Test 2, both equal to R .

The general result for C_f as a function of R is:

$$C_f(R) = (K_{max2} - K_{max1}) / (O/L \cdot K_{max2} - K_{max1})$$

where

$$R = P_{min1}/P_{max1} = P_{min2}/(O/L \cdot P_{max2}) \quad (7)$$

Once C_f at some value of R was known, it would only be necessary to run constant amplitude tests at the stress ratios of interest. (Overload tests at each R value would not be needed.) For example, assume that the value of C_{f1} at a particular R was developed as described above and a constant amplitude test at another stress ratio was run. Call this Test 3. The test results might be as in Figure 43. Since, at constant fatigue crack propagation rates the effective K 's must be the same:

$$K_{\max_3} - C_{f_3} K_{\max_3} = K_{\max_1} - C_{f_1} K_{\max_1}$$

$$C_{f_3} = (K_{\max_3} - K_{\max_1} + C_{f_1} K_{\max_1}) / K_{\max_3}$$

$$C_{f_3} = 1 - (1 - C_{f_1}) (K_{\max_1} / K_{\max_3})$$

where

$$K_{\max_3} = \Delta K_3 / (1 - R_3) \quad (8)$$

Here, K_{\max} is the maximum applied stress intensity for either Test 1 or Test 3. (K_{\max_1} was previously referred to as K_1). Using the relationship of Equation 4, it is possible to construct the fatigue crack propagation curve at $R = R_{co}$. Recall that the cutoff stress ratio, R_{co} , is that stress ratio above which no layering of crack growth rates occurs. For 2219-T851 aluminum, R_{co} was found to be 0.5 while, for Ti 6Al-4V titanium, no cutoff value was observed up to the maximum stress ratio tested (0.7). The fatigue crack propagation rate curve at $R = R_{co}$ is the maximum extent of fatigue crack propagation rates (with respect to ΔK). No stress ratio effect on crack growth rates is observed for $R > R_{co}$.

If the closure factor, C_f , properly accounts for stress ratio effects, then the calculated effective stress intensity range, ΔK_{eff} , is independent of stress ratio. That is, if data are plotted as da/dN vs. ΔK_{eff} , all of the data would fall along the same line regardless of the stress ratio at which it was generated. From Equation 4:

$$\Delta K_{eff} = (1 - C_{f_1}) K_{\max_1} = \frac{1 - C_{f_1}}{1 - R_1} \Delta K_1 \quad (9)$$

Once C_{f_1} has been determined, the data may be replotted on a ΔK_{eff} basis.

This corresponds to a horizontal shift on a log-log plot as shown in Figure 44. Since this line represents the behavior of all data (including those where $R > R_{co}$), it also represents the extreme crack growth rate curve. That is, on a rate vs. ΔK_{eff} basis, no data points would be expected to fall above this curve. It should be noted, however, that the value of R_{co} cannot be determined by this method, since the extreme rate curve, properly constructed, is independent of stress ratio.

It has been previously reported (Ref 6) that the crack growth stress intensity threshold is dependent on the stress ratio. Equation 9 predicts threshold behavior which agrees conceptually with existing data on fatigue crack propagation thresholds. Replacing stress intensities in Equation 9 with threshold stress intensities:

$$\Delta K_{eff_{th}} = \frac{\Delta K_{th}}{1-R} (1 - C_f) \quad (9a)$$

At $R = 0$,

$$\Delta K_{eff_{th}} = \Delta K_{th_o} (1 - C_{f_o}) \quad (9b)$$

where ΔK_{th_o} is the applied stress intensity range threshold at $R = 0$. As described earlier, $\Delta K_{eff_{th}}$ is a constant if C_f properly describes the crack closure behavior. Therefore, we can write

$$\frac{\Delta K_{th}}{1-R} (1 - C_f) = \Delta K_{th_o} (1 - C_{f_o}) \quad (10)$$

or:

$$\Delta K_{th} = \Delta K_{th_o} \left(\frac{1 - C_{f_o}}{1 - C_f} \right) (1 - R) \quad (10a)$$

so that the threshold value for any value of R is given in terms of the threshold value at $R = 0$ for all values of $R < R_{co}$. For $R > R_{co}$, $\Delta K_{th} = \Delta K_{eff_{th}}$. These results are shown schematically in Figure 45.

These techniques will now be considered utilizing actual test data. Figure 46 is a plot of da/dN vs. ΔK_b for two periodic overload tests. In each case, a straight line has been drawn which represents the predominant mass of data over the range of 10^{-6} to 10^{-5} inch/cycle. Both of these tests were run at $R = .05$. The above analysis can be modified to give an expression for C_f . In this case:

$$C_{f_{.05}} = \frac{\Delta K_2 - \Delta K_1}{(O/L)_2 \Delta K_2 - (O/L)_1 \Delta K_1}$$

Choosing 3×10^{-6} as the crack growth rate for calculating the ΔK 's, $\Delta K_1 = 8.7$, $\Delta K_2 = 12.6$ and $C_{f.05} = .33$. This value is within the range of measured values of C_f at $R = 0.05$ for the 2219-T851 aluminum data obtained during this program. Measured values of C_f ranged from 0.28 to 0.55, as shown in Figure 100.

3.2.2 Ti6Al-4V Titanium Test Results

Like the aluminum tests, the objectives of these tests were to obtain detailed crack growth and crack closure measurements during and subsequent to the application of overloads. The titanium test data were more difficult to analyze than the aluminum data. This was principally due to the data scatter which seems to be inherent in the titanium material. This will become apparent after reviewing some of the data presented here.

Single Discrete Overloads - These tests were performed in the same manner as the equivalent aluminum tests. Subsequent to the application of an overload, the behavior of the crack growth on the specimen surfaces was somewhat erratic. Figures 47 and 48 present overall a vs. N curves for titanium CTB specimens subjected to overloads with O/L values of 1.5 and 1.8 respectively. Again, this type of data plot is not useful as an analytical tool. Figures 49a through 49f show detail plots of a vs. ΔN_s for the 18 overload sequences in Figures 47 and 48.

Several observations can be made. The crack growth behavior subsequent to each overload typically exhibits an initial slow rate which eventually becomes approximately equal to the constant amplitude rate. Of the 18 sequences presented, only three exhibit delayed retardation. During the stabilized crack growth portion, the rates are nominally constant amplitude rates. Attempts to plot the normalized crack growth rate function, the ratio of measured to calculated constant amplitude crack growth rates, f_n , were fruitless. This is because, although the general growth behavior is uniform, the calculated rates exhibit excessive scatter. The general trend of the data indicate that, as the stress intensity increases (crack length increases) the number of delay cycles decreases. This is in direct contrast to the aluminum results. Delay cycles vs. the stress intensity caused by the overload, $K_{max_{OL}}$, and vs. the difference between the overload stress intensity and the baseline stress intensity, K_{max} , are presented in Figure 50. It can be seen that delay cycles decrease as stress intensity increases, but that neither of the parameters correlates the data. The plane stress plastic zone radius caused by the overload is shown for each sequence (Figure 49). For the cases where the cracks are relatively short, these values are quite small. The plane stress radii nominally describe the point where the crack growth rates are stabilized. It is interesting to note that, for all of the sequences, plane strain conditions predominate but that a plane stress plastic zone best describes the crack length affected by the overload. Pertinent data for all 18 overload sequences are presented in Table 4.

The stress intensity at which stable tear begins is given in Sub-section 3.5 as $72 \text{ ksi } \sqrt{\text{in.}}$. Only the last two events listed in Table 4 exceed this value. Even so, the behavior of these data appears reasonable when compared with the other data.

Single Periodic Overloads - Six titanium compact tension specimens were subjected to single periodic overloads. Three specimens were subjected to overload ratios of 1.8 and the balance to overload ratios of 1.25. The crack length vs. cycles results for these tests are presented in Figures 51 and 52. Figure 51 shows that, for $O/L = 1.8$, when the frequency of occurrence of the overload is increased from one application for every 1000 low-load cycles to one application for every 500 low-load cycles, the life of the specimen is approximately halved. This implies that the overloads contribute significantly to the crack growth behavior. Conversely, for $O/L = 1.25$ (Figure 52), when the frequency of occurrence is halved, there is no significant change in the life of the specimens. (In this case, the lives seem to be slightly longer.) These test results indicate that the effects of the overloads are independent of frequency of occurrence or do not affect the crack growth rates at all.

Figure 53 shows that the overloads ($O/L = 1.25$) have negligible effect on crack growth rates. In this figure, the average crack growth rate (including the growth due to overloads) is plotted against the stress intensity range for the baseline loading. The crack growth rates obtained from equation 1c for the baseline loading are also shown. Although the actual rates are slightly lower than those obtained from Equation 1c, the differences are generally quite small. For the range of data shown in Figure 53, and using a frequency of occurrence of 50 cycles, the crack growth between the overloads ranges from about 10% of the plane strain plastic zone radius produced by the overloads at the low end of the data to about 25% at the high end. The overloads should have the greatest influence on the average crack growth rates when the growth between overloads is the smallest (at the low end of the data.) However, it can be seen that this is where the data most closely agrees with Equation 1c. The conclusion obtained here is that when the overload ratio is 1.25 and the frequency of occurrence exceeds 50 cycles, the overloads have negligible effect on crack growth rates.

Figures 54 and 55 show that this is not the case when the overload ratio is 1.8. There, the average crack growth rate is plotted against ΔK_b and ΔK_{OL} respectively. It can be seen that the measured crack growth rates are always less than those calculated from Equation 1c. Referring to Figure 54, the actual rates range from about one third to about two thirds of the calculated rates. Interestingly, these figures show that the absolute value of the overload is more significant than the frequency of occurrence of the overload. For example, in Figure 54, the data for the two specimens where the overload is 1440 lb are closely grouped even though the frequency of occurrence of the overloads differs by a factor of two. Where the overloads are 1870 lb, the crack growth rates are measurably lower.

Using the method described for the aluminum data in Subsection 3.2.1 to determine the crack closure factor (Eq 7) at a crack growth rate of 4×10^{-6} inch/cycle, the following results are obtained. For the cases where $P_{OL} = 1440$ lb and 1870 lb, $C_f = .28$ and $.38$ respectively. The value of $.28$ is low for this material, but the value of $.38$ agrees closely with the value obtained in Subsection 2.4. The difference ($.28 - .38$) is explained by the amount of crack growth relative to the plastic zone radius. For $P_{OL} = 1440$ lb, the average growth between overloads is 29% ($N = 500$) and 57% ($N = 1000$) of the plane strain plastic zone produced by the overloads. As described in Subsection 3.2.1, the growth between overloads must be small relative to the affected crack length for the values of C_f obtained in this manner to be valid. For P_{OL} equal to 1870 lb, the growth between overloads is less than 20% of the plane strain plastic zone radius. In this case, the calculated value of C_f is expected to be more accurate.

3.2.3 Interactions of Single Overloads

The effect of single overload interactions, where additional overloads are applied before the effect of a previous overload has died out, has been investigated in two different ways. First, a number of the periodic overload tests were single periodic overload tests in which a specific overload was repeatedly applied after a particular number of lower loads had been applied. These tests are discussed in other sections of this report. One of the important conclusions reached from these tests was that, if the number of low loads between overloads is sufficiently small, the closure load is the same as if a large number of overloads had been applied and the closure load is stable.

The second approach was to utilize tests in which another overload was applied while the crack tip was still in the vicinity of the original overload. Figures 56a and 56b are crack length vs. cycle plots for one of these tests. Figure 56a shows an event in which a single overload was applied. Figure 56b shows five additional events. In three of the events shown in Figure 56b, a second overload was applied after the crack grew 0.006 inch from its length at the time of the first overload application. The remaining two events had the second overload applied after 0.010 inch of growth.

In viewing Figure 56, it is difficult to draw any quantitative conclusions about the effect of the second overload. It is originally expected that closure load measurements of these tests would prove informative but, as discussed in other sections, closure load measurements after single overloads cannot be made effectively. Figures 57a, b and c present crack growth rate data for the events shown in Figure 56b in which the overloads were separated by 0.006 inch. In two of these figures (57b and c) the second overload seems to have perturbed the crack growth rate pattern. However, for the reasons discussed in Subsection 3.2.1 concerning data scatter, quantitative use of this information is difficult. A similar test which shows the same trends is shown in Figure 58.

Figure 59 shows a test result for a test in which a slightly different approach was tried. First, a single overload was applied and crack length vs. cycle data was collected (circles). The baseline loading had a stress ratio of 0.7 and the overload factor was 1.25. This was followed by a load sequence in which an overload was applied every 2000 cycles (squares). Two thousand cycles were chosen since it appeared that after 2000 cycles, the crack would penetrate well into the plastic zone produced by the overload. Finally, just the low loads were applied and the crack growth rate was allowed to return to its constant amplitude value (triangles). Once again quantitative conclusions are difficult to reach, but it appears that no retardation occurs for the single overload, while the repeated overload causes significant retardation (a crack growth rate reduction of 40%).

Titanium data were not included in this section since the affected crack length is too small to be observed and plotted. It appears that interaction effects must be evaluated by an inverse approach. That is, the data generated should be used to check a hypothesized model, rather than be quantitatively evaluated.

3.3 MULTIPLE OVERLOAD TEST RESULTS

3.3.1 2219-T851 Aluminum

The effects of multiple overloads on subsequent crack growth were examined. The test matrix was developed in order to examine three possible situations for both materials investigated. The first was to determine the effect on subsequent crack growth rates of the application of many overloads. Here, many means that enough overloads are applied so that stabilized crack growth conditions exist during the overload applications. The second was to determine the effect on subsequent crack growth of the application of a few overload cycles. Finally, tests which were essentially two-level block loading were performed.

For the three situations investigated, up to three different overload ratios were used for each of the two materials. In most cases, the stress ratios for the two stress (load) levels were maintained at or near zero. In some of the sequences, the minimum stresses (loads) were not necessarily close to zero and/or equal for both stress levels. Table 5 presents the test matrix for all multiple overload tests performed on both materials.

In this section, crack closure behavior has been utilized to explain certain observed behavior.

Stabilized Overloads - A number of tests consisting of many overload cycles followed by many low level loads were run. The number of loads at each level was large enough so that stability was reached within that portion of the load sequence. That is, each of the steps in the two step load sequence contained sufficient cycles so that the crack growth rates reflected constant amplitude loading conditions.

The primary purpose of these tests was to investigate the transient conditions during the low load sequence as the crack growth rate varied from fully retarded to unretarded (constant amplitude). This transient behavior was far less difficult to observe than was the transient behavior in a single overload test. Typical test results for the 2219-T851 aluminum are shown in Figure 60. Once the load has dropped, the variation in rate is monotonic. This is not always the behavior with single overload tests. (See Subsection 3.2.) The highly transient behavior described in Subsection 3.2 does not occur because the large number of overloads has caused a stable closure value to be produced. Thus the monotonic variation in rate is simply a manifestation of the monotonic variation in closure level, from a value associated with the high load to a value associated with the low load. This can clearly be seen in Figure 61, which represents the results of a test in which the baseline loading was at a stress ratio, R , of .5. In Figure 61a, the entire a vs. N plot is shown. Figures 61b and c focus attention on a single event in that test. Figure 61b presents the crack length record for that event and Figure 61c presents the applied loads and closure load measurements for that event. The upper and lower bumps called out in Figure 61c are described in the section on closure measurements. We associate closure with the upper bump only. Thus Figure 61c shows that the closure load rises during the initial portion of the overload sequence, stabilizes, and then drops monotonically during the low-load sequence to a stable level associated with that low-loading condition.

Note that, for the closure load to return to a low value, the number of cycles and the change in crack length since the overload is significantly larger than any comparable measurement on the a vs. N plot (Fig. 61b). The number of cycles to return to the lower closure value is approximately 25,000 (362,000 - 333,000) and the corresponding change in crack length is .085 inches (1.29 - 1.205). However, from the a vs. N plot, there is a sharp change in rate to an apparently unretarded condition at a crack length change of about .007 inches and a cycle count of about 15,000. Although the data taken after the overload in this test is a little too sparse to construct detailed crack growth rate plots in the vicinity of the overload, other tests indicate that a plot of da/dN versus Δa since the overload would yield an estimate for the duration of the effect of the overload of .003 to .020 inch for this case. An example of this is given in Figure 62a and b in which the estimates of this critical length would be .004 and .012 respectively. Thus we see that the determination of the duration of the overload effect (Δa^*) is dependent on the method used to determine it.

Note that the manner in which the closure load returns to its constant amplitude value in Figure 61c is quite complex. Therefore any model that represents this closure variation in a simple fashion (such as a linear or parabolic variation with Δa) will only be an approximation of the behavior shown in Figure 61c. Thus for a model to be meaningful as a predictive tool, it will be necessary to choose Δa^* in a manner compatible with the assumed

variation of the closure load, and in such a way as to yield a match in data and predictions. The proper method, as far as a predictive model is concerned, is to use a value of Δa^* which, in conjunction with the variation in closure load assumed, yields the correct average rates in the transient region and thus a good life prediction.

The parameter Δa^* is not simply a single value but varies with the parameters of the test. Many previous investigators have assumed that Δa^* is proportional (or equal) to the plastic zone radius as determined from the maximum value of the overload. That is, it is assumed that $\Delta a^* \approx \frac{1}{2\pi} \left(\frac{K_{\max OL}}{\sigma_y} \right)^2$. However, arguments based on the fact that residual compressive stresses play an important role in crack growth interactions would indicate that an appropriate range of stress intensity might be the correct variable.

In order to ascertain the correct variable, data for measured Δa^* values was gathered and compared to plastic zone radius calculations using a variety of stress intensity variables. These variables are shown schematically in Figure 63. In that figure the solid lines represent stress intensities caused by applied loads and the dotted lines represent stress intensities calculated using the closure loads. In Figure 63a, the three possible pertinent variables for a two-level test with the same minimum stress intensity in each are indicated.

In Figure 63b, two additional possible controlling variables are indicated for those tests in which the minimum stress intensity is different for each loading sequence. One of the additional variables ($K_{\max OL} - K_{\min}$) arises simply because of the presence of the second minimum load. The other additional variable indicated in Figure 63b occurs because the closure load, and therefore K_c , variation might follow the pattern established by the dotted line marked II. For that possibility, the final effective range in stress intensity for the overload is determined by $K_{\min}/K_{\max OL}$ rather than $K_{\min OL}/K_{\max OL}$. That is, the reduction to a lower minimum load is effective immediately. There is evidence of this behavior in other phases of the program (see Section 4).

The five possible combinations of pertinent variables and the resulting plastic zone equations are given in Table 6. Table 7 presents a compilation of data and analysis from eleven different events. Overload ratios were 1.5 and 1.8, stress ratios for the low loads were .05 and .5, and constant-minimum and different-minimum loads for the overloads and base loads were used. Measured values of Δa^* were determined from Δa versus N plots such as Figure 62a. A plastic zone radius size, $\rho = \frac{1}{2\pi} \left(\frac{K}{\sigma_y} \right)^2$, was calculated with each of the trial variable stress intensities substituted for K . The parameter $.25\rho$ is listed in three of the cases, simply to maintain all the scales

used for plotting at about the same value. Plotting the measured Δa^* versus a plastic zone calculation containing the correct variable should produce a straight line dependence of Δa^* with ρ_y .

The data from Table 7 are plotted in Figures 64 through 68. In Figures 65 and 66, two distinct trends are present, indicating that ΔK_{OL} and $(K_{max_{OL}} - K_{cI})$ are not appropriate stress intensity variables for determining Δa^* . An examination of the basic data used for these two figures indicates that the steeper sloping line segment is associated with tests with different minimum loadings for the two load sequences. In addition, we note in Figure 66 that there appears to be a tendency toward two distinct lines, and that the steeper line is associated with high stress ratio tests. The remaining two plots (Figures 64 and 68) both indicate an approximately linear variation between the calculated and measured values. However, it appears that the plot using $(K_{max_{OL}} - K_{cII})$ (Figure 68) has the least scatter. The reason for the difficulty in clearly discerning which of these two variables, $(K_{max_{OL}} - K_{cII})$ or $K_{max_{OL}}$, is more important is that the range of $(K_{max_{OL}} - K_{cII})$ was only .4 to .6 times K_{max} for all the tests considered. In Subsection 4.1, it will be shown that the use of $K_{max_{OL}}$ in calculating the affected crack length (plastic zone) is straightforward and provides a good fit to the data for the mathematical model developed under this program.

3.3.2 Ti 6Al-4V Titanium

As in most of the tests run in this program, it was more difficult to analyze the multiple overload titanium test results than it was to analyze the aluminum test results. This is due to the apparent increase in data scatter in titanium, the significantly smaller plastic zone sizes in titanium as compared to the aluminum, and the increased difficulties with the closure measurements as described in Subsection 2.4. It was therefore necessary to rely heavily on information from the aluminum tests during the development of the predictive model.

This is a reasonable approach and is supported by data typified in Figure 69. Figure 69a is a crack length vs. cycle plot for a two-level test with a baseline stress ratio equal to 0.5, an overload factor of 1.5 and equal minimum stresses in both segments of the load sequence. Two distinct events are shown. Figure 69b presents the applied loads and the measured closure loads for this test. Note that, after the overloads were applied, closure load monotonically decreases from a high value associated with the overload to a lower value associated with the baseline loading. This type of response is identical to that which was observed for similar tests in aluminum. (See Fig. 61c.) However, the details of the manner in which the closure level returns to the lower level are quite different for the two events shown. This implies that attempts to model the closure variation using actual closure data would be quite difficult.

Although significant crack growth retardation is apparent in both the crack length vs. cycle plot and, indirectly, in the closure measurements, the distance over which the retardation is effective is quite small. This will be even more apparent in subsequent figures. Note that the closure loads measured before the overloads appear to be higher than the steady state response after the overloads. It is felt that this is simply a manifestation of problems in measuring closure and not indicative of any real material response.

Some of the problems encountered with closure measurements in the titanium can be seen in Figure 70. Figure 70a shows the crack length vs. cycles plot for a two-level titanium test, Figure 70b is a similar plot of a single event in that test, and Figure 70c shows the applied loads and measured closure loads for that test. Retardation is seen in the crack length vs. cycles plots. However, there is too much scatter in the closure measurements to arrive at any quantitative interpretations. Note that, even prior to the overload, there is considerable scatter in the closure load measurement. In terms of the maximum load, this scatter is not excessive ($\sim 15\%$) but, in terms of the closure load itself, the scatter of approximately 30% causes an enormous problem of interpretation.

Figure 71 presents detailed plots of crack length vs. cycles for a single test specimen. The baseline loading had a stress ratio of .05, the overload factor was 1.5 and different numbers of overloads were applied for each of the eight events. The figures show the growth after each set of overloads. The large number of events in a single test is possible because of the small interaction distance after an overload for the titanium material. Significant increases in the amount of retardation still occurred as the number of overload cycles was increased past fifty. Note, however, that we cannot really see a retarded growth, but that what we see in these plots is a "delay." This is almost certainly a result of the measuring scale not being sufficiently fine. For example, had the scale for the aluminum data been sufficiently gross, all we would have seen would have been a "delay" as well. Thus it is impossible to measure Δa^* as was done for the aluminum data. As a result, conclusions reached regarding appropriate stress intensity variables to control Δa^* on the basis of aluminum data have to be assumed to be valid for titanium as well.

Figures 72a through 72h show sequences similar to those of Figure 71. However, these data are for a test in which the baseline loading had a stress ratio of 0.3 and the number of overloads applied decreased as the crack grew longer, rather than increased as was the case in the previously discussed test. Here again, it can be seen that there is more retardation with 50 overload cycles than with 20 but, in addition, a value of Δa^* could be discerned with the larger number of overloads. That is, there does seem to be an identifiable location where there is a significant change in crack growth rate. That this point is discernible in this test may be attributed to the fact that the maximum overloads are approximately 40% higher than in the previous test.

As an additional point, the fact that a value of Δa^* is discernible in the tests with a large number of overloads opens the question of whether increasing the number of overload cycles affects the degree of retardation or the duration of retardation.

Since the overloads are approximately 40% greater in magnitude for the data of Figure 72 than for Figure 71, the overload plastic zone would be approximately doubled. Therefore, larger values of Δa^* are to be expected. However, a casual inspection of the data reveals even larger values of Δa^* than those which were expected. The implication is that Δa^* increases as the number of overloads increases. In this case, the duration of retardation would be a function of the number of overload cycles. The material cyclic strain hardening or softening characteristics might also contribute to this effect. It seems more likely, however, that the degree of retardation might be altered by additional overloads. It will be shown in Section 4 that when Δa^* is assumed to be the plastic zone created by the overload(s), regardless of the number of overloads, it yields a generally good definition of the interacted crack length. Based on this assumption it follows that the number of overloads controls the degree, but not the duration, of retardation.

Because of the difficulties associated with the analysis of the titanium test results, the modeling approaches used for aluminum were applied to the titanium test results. The model was verified by comparing the gross behavior of the titanium test results to the results predicted by the model. This procedure is discussed in Section 4. Generally, this approach produced satisfactory correlation.

3.4 VARIABLE AMPLITUDE TESTS

Variable amplitude tests were performed on specimens fabricated from both materials. These tests utilized block program loadings with variations. The blocks were composed of three or four layers, and were arranged in high-low, low-high and randomized sequences, with all of the minimum loads equal to or nearly zero. Each loading block was identical to the others in a given test. Variations on the basic loadings included maintaining all of the minimum loads at some elevated (greater than zero) value with occasional excursions to zero load.

One center cracked panel specimen of each material was subjected to a fighter spectrum as defined in Table 5 of Reference 7. The limit stresses of 30.9 ksi for 2219-T851 aluminum and 61.9 ksi for Ti 6Al-4V titanium shown there were also employed in this program.

These tests were performed as an aid in the verification of the mathematical model developed during this program. As a result, very little analysis of the data was performed.

Table 8 presents the test matrix while Table 9 presents the spectra employed for these tests.

3.5 EFFECTS OF UNDERLOAD AND COMPRESSION SPIKES

A few specimens were tested to obtain some understanding of the effect of underload or compression spikes. An underload is defined as a reduction in the minimum load (or stress) such that its minimum value is greater than, or equal to, zero (tensile). The test program included compression (underload) spikes only, tensile overloads followed by compression (underload) spikes and, to a limited extent, tensile overloads preceded by a compression (underload) spike. Table 10 presents the loading conditions employed.

Underloads - The test plan originally included some compact tension specimen tests to investigate the effect of compressive loads on crack growth behavior. However, preliminary tests and some reflection indicated that the results might be difficult to interpret. It can be seen that, for any specimen configuration, once the crack surfaces are in contact, a cracked specimen behaves like an uncracked specimen and the important load parameter is the stress, not the stress intensity factor. The load at which the entire crack is closed will be a complex function of specimen geometry and crack length. No method currently exists to determine the load at which the entire crack closes. In the case of the compact tension specimen, there is a tendency for the crack tip to open when compression loads are applied. This is especially true for long cracks (large values of a/W). In this case, proper characterization of crack growth phenomena in terms of either stress or stress intensity is currently beyond the state-of-the-art.

As a result, an alternate test procedure was adopted. The new tests were performed using a baseline loading with a stress ratio greater than zero so that the minimum applied load was significantly greater than zero. Then, occasional or multiple excursions to approximately zero load (referred to as underloads) were applied. It was felt that, in tests of this nature, the underload(s) would have the same general effect on subsequent crack growth during the baseline loading as a compression load(s) might have if the specimen had been a center-cracked panel. For example, an underload with $R = .05$ should have the same qualitative effect on tests with a baseline $R = .5$ as compressive loads have on tests run with a baseline $R = .05$. Since the major portion of the crack surfaces are not in contact during these tests, interpretation of the test data in terms of stress intensities is considered to be rational.

Six specimens, three each of titanium and aluminum, were tested in this manner. All six specimens had a baseline loading with $R = .5$. Two each of the aluminum and titanium specimens had additional single cycles of loading with an underload of zero and an overload ratio of 1.5 superimposed on the baseline loading. However, the order of loading (underload-overload or overload-underload) was modified for different specimens. The aluminum test results are shown in Figures 73 and 74. As noted earlier, a single overload cycle with an overload ratio of 1.5 does not cause very much retardation in 2219-T851 aluminum. One could argue that there was retardation in the test

in which the underload preceded the overload and that there was no retardation when the underload followed the overload, but the differences are not significant. The titanium test results shown in Figures 75 and 76 are slightly more conclusive. This is due to the fact that single overloads with overload ratios at 1.5 do cause some retardation in titanium. There appears to be some retardation in the test in which the underload follows the overload, but it is certainly quite small. However, the test for which the underload precedes the overload shows significant retardation.

The remaining specimens in this series were used to investigate the effect on subsequent crack growth of a large number of overloads followed by a single underload cycle. The test results for the titanium specimen are shown in Figure 77 and those for the aluminum specimen are shown in Figure 78. In both these figures, little if any retardation is evident.

In addition to these tests, a single underload cycle was applied during the constant amplitude loading of one of the specimens (AD-25-117). It was felt that the drop in load could have decreased the closure level and thereby caused a short period of crack acceleration. As can be seen in Figure 79, no significant acceleration occurred.

Although, only a limited number of underload tests were run, these tests indicate that:

- A single underload can change the closure load sufficiently to remove the effects of previous overloads.
- Although a single underload may reduce the closure load, subsequent constant amplitude cycling causes the closure load to recover rapidly enough to eliminate any significant acceleration.

If these observations are extended to compression, we may conclude that compression excursions reduce or eliminate retardation, but do not cause significant acceleration.

Compression Spikes - Center-cracked panel specimens, suitably stabilized against column buckling, were subjected to compression, tension-compression and compression-tension loading sequences. Results from 2219-T851 aluminum tests indicate that the application of a single isolated compression spike has virtually no effect on subsequent crack growth behavior. This conclusion is substantiated by the test results shown in Figures 80a through 80c and 81. There, crack length is plotted against ΔN_s (the number of cycles since the compression spike) for compression spikes ranging from one half to two times the maximum baseline tension loading. In addition, the crack length vs. ΔN_s curve, calculated using constant amplitude growth rates and neglecting any effect of the compression spike, is plotted for each case. In Figures 80a through 80c, there is a tendency for the calculated lives to be slightly longer than the actual lives. In Figure 81 however, the opposite result can

be observed. Based on the results of these tests, it was concluded that the compression spikes had negligible effect on subsequent crack growth in the aluminum.

Figure 82 presents similar results for a titanium panel subjected to occasional compression spikes. These results seem to indicate that the compression spikes produce subsequent crack growth rates which are greater than constant amplitude rates. In some cases there is an initial perturbation of the data immediately following the application of the compression spike and the rates are higher than the constant amplitude calculations. The two cases shown on the left side of Figure 82 show this most prominently. However, after a crack extension of about 0.05 inch (for these two cases), the crack growth behavior appears to stabilize. The rates in these apparently-stabilized regions are still measurably greater than the calculated values. This tendency indicates that some scatter may be present in the constant amplitude crack growth behavior for this specimen. The data shown in the right side of Figure 82 lie somewhat closer to the calculated curves, but still exhibit shorter lives than the constant amplitude calculations. Based on the results from these two figures, the compression spikes seem to produce somewhat faster subsequent crack growth rates in the titanium material, but the data are insufficient to reach any quantitative conclusions.

Tension-Compression Spike Sequences - Figures 83a through 83c present a vs. ΔN_s data for aluminum specimens subjected to tension spikes followed immediately by compression spikes. A calculated constant amplitude crack growth curve which neglects any effects of the tension or compression spikes is also shown for each case. The first two cases (Fig. 83a) resulted from the application of tension-compression spike sequences where the magnitude of both spikes was 1.5 times the baseline loading. It can be seen that the actual crack growth rates are much lower than the calculated rates. These results imply that the tensile spike causes a retarding effect on subsequent crack growth rates and that the compression spike does not appear to offset the effects of the tensile spike. It was concluded in Subsection 3.2.1, however, that a single overload, where the overload ratio was 1.5, produced very little retarding effect on subsequent crack growth rates for the 2219-T851 aluminum material. The decreased rates shown in Figure 83a are therefore attributed to scatter and these results are inconclusive. The results shown in Figure 83b and 83c are only slightly more conclusive. There, the tensile overload ratios were 1.5 and 2.1 and the compression spikes ranged from 0.5 to 3 times the baseline tensile loading. For the cases where the tensile overload is 9 ksi (overload ratio = 1.5), the data lie close to the calculated constant amplitude curves.

If the compression spikes had not been included, the tensile overload would be expected to cause very little effect on subsequent crack growth behavior. The compression spikes by themselves have been shown to produce essentially no effect on the subsequent rates for this material. Therefore,

it can be concluded that the combination of tensile overloads followed by compression spikes have, for the overload ratio of 1.5, very little effect on subsequent crack growth behavior.

For the three cases where the tensile overloads are 12.6 ksi (overload ratio = 2.1), there is a consistent trend such that the actual lives are always greater than the calculated constant-amplitude lives. These results indicate that the tensile overloads have caused some subsequent retardation. The number of delay cycles are approximately 9,000, 7,000 and 11,000 for the cases where the compression spikes are 3, 12 and 18 ksi respectively. Insufficient data were gathered for single overload spikes alone (where the overload ratio was 2.1) to quantify the number of delay cycles. It is therefore impossible to say how much the subsequent compression spikes influenced these results.

It is interesting to note that the number of delay cycles are approximately the same for all three cases and that the stress intensity for the longest crack length, when the spikes are applied (1.205 inches), was only 17% greater than that for the shortest crack length (0.88 inch). It can be expected that if no subsequent compression spikes had been applied, the number of delay cycles would be approximately the same since K is nominally constant. The introduction of the compression spikes did not cause any significant variation in the number of delay cycles. It can therefore be concluded that the subsequent compression spikes either: 1) do not alter the effects on subsequent crack growth rates of the tensile overload, or 2) any modification of the tensile overload effects is independent of the magnitude of the compression spikes, at least for the ranges considered here. It will be shown in Subsection 4.1.3 that, for these three cases for this specimen (AG-15-10P), the conclusion that the compression spikes have negligible effect is correct.

The data for a similar test, performed on a titanium specimen, are presented in Figure 84. In addition to tension-compression sequences, some compression-tension sequences were also applied to the specimen. The tensile overloads were always 1.5 times the maximum baseline loading and the compression spikes were either 0.5 or 1.5 times the maximum baseline loading. For the Ti6Al-4V material, single overload spikes having an overload ratio of 1.5 do cause some subsequent crack growth retardation. For three of the four cases, where the compression spike precedes the tensile spike, some initial retardation is present. (The first data point after $\Delta N_S = 0$ shows a crack length which is equal to or only slightly larger than the value at $\Delta N_S = 0$.) However, the subsequent stabilized crack growth rates are always greater than the calculated constant amplitude rates, so quantification of the number of delay cycles is impossible. In three of the four cases where the compression spike was applied after the tensile spike, the first data point after $\Delta N_S = 0$ shows that the crack length is greater than the value at $\Delta N_S = 0$. These results indicate that, for the titanium, the application of the compression spikes tends to negate the retarding effects of the tensile overloads. Again, no quantitative conclusions are possible.

It can be concluded that, generally, the application of compression spikes, either alone or following a tensile overload, have very little influence on the subsequent crack growth behavior in 2219-T851 aluminum. For the Ti6Al-4V titanium material, compression spikes seem to accelerate subsequent crack growth. When compression spikes are applied prior to a tensile overload, the results were inconclusive, but where they were applied subsequent to a tensile overload, they tend to negate the effect of the overload on subsequent crack growth rates.

3.6 MISCELLANEOUS TEST RESULTS

3.6.1 Stable Tear

Some of the aluminum specimens tested at high K levels exhibited slow stable tear. This is the phenomenon which occurs when the stress intensity under monotonically increasing tensile loading approaches the critical stress intensity of the material, thereby causing a significant amount of crack extension. In order to quantify this stable tear, a crack growth resistance test was performed on a 2219-T851 aluminum compact tension specimen. This test was performed by measuring the crack opening displacement (COD) under monotonically increasing load until the load vs. COD trace became nonlinear. The specimen was then unloaded sufficiently to produce a new, linear, load vs. COD trace. The load was again increased monotonically until some further non-linearity occurred and the process was repeated. Figure 85 shows the procedure schematically. Each of the linear unloading traces was used to determine the crack length and maximum stress intensity at each point where the linear unloading lines intercepted the overall load-displacement curve. In this manner, plasticity effects were excluded and crack extension was the only significant variable. Since the material thickness was nominally the same for most aluminum specimens, it is not considered to be a variable here.

It should be noted that the initial crack length prior to running the test was measured on the surface of the specimen and was assumed to be straight and normal to the surface. Subsequent calculations, based on COD measurements by necessity, used the same assumptions. In reality, some curvature of the crack front was present, although no effort was made to include this curvature in the stress intensity calculations. The results are plotted in Figure 86 as K_{\max} vs. incremental crack extension, Δa , measured from the initial crack length. The total crack length was calculated from the COD measurements. The results were extrapolated to an intercept value of approximately 30 ksi $\sqrt{\text{in}}$ for Δa equal to zero. This value of K is defined as the threshold for stable tear, K_{st} . Since failure occurs at the point where the applied stress intensity curve is tangent to the resistance curve (see Reference 8,) the upper bound or maximum value of the apparent critical stress intensity, K_{cr} , is 57.5 ksi $\sqrt{\text{in}}$.

The results of this test indicate that whenever the stress intensity exceeds $30 \text{ ksi } \sqrt{\text{in}}$ (K_{St}) for this aluminum, some stable tear could be expected to occur. In some cases of single overload applications, the peak stress intensity during the overload exceeded K_{St} .

Specimen AG-25-6P, a center cracked panel, was subjected to several single overload applications of 21 ksi with a baseline stress range of 10.0 to 0.5 ksi. In all cases, the stress intensity during the overload exceeded K_{St} . A visual examination of the fracture surface revealed that, during the overload, the crack growth along the center line of the specimen exceeded the growth on the surface of the specimen. The internal growth is referred to as tunneling and is shown schematically in Figure 87. For the cases of long cracks (K_{maxOL} approaching K_{Cr}), this difference was relatively large. The tunneling, defined as a_t , was measured for five events, using an optical comparator. The values obtained from both crack tips were averaged and are presented in Table 11. Values of a_t , taken from the resistance curve (Figure 86) for each value of K_{maxOL} , are also presented and agree closely with the measured values.

Figure 88 shows a vs. N after one overload application on specimen AG-25-6P. The data points representing surface measurements are almost flat from the point of application of the overload up to about 329,000 cycles, indicating that there is almost no surface growth during this period. At about 329,000 cycles, a sudden jump in the surface length occurs which is followed by a monotonically increasing a vs. N curve.

The stress intensity during the overload was $36.3 \text{ ksi } \sqrt{\text{in}}$. at a half crack surface length of 0.852 inch. From the crack growth resistance curve (Fig. 86) the expected stable tear is 0.008 inch. It was assumed that the crack front increased by this amount at the centerline of the specimen thickness during the application of the overload, to a half crack length of 0.860 inch. The dashed curve in Figure 88 indicates the assumed behavior of the crack tip at the centerline of the specimen thickness. At 329,000 cycles, after the jump in length, the surface length agrees closely with the assumed centerline crack length.

Figure 89 presents the normalized crack growth factor vs. crack growth increment subsequent to the overload, for the data of Figure 88. The normalized crack growth factor, f_n , is the measured crack growth rate divided by the calculated constant amplitude crack growth rate. When interpreted literally, the data exhibits an unusual sinusoidal behavior. The dashed line, however, indicates schematically how the crack growth at the centerline of the crack tip might vary. The crack growth and rate data were of no value for analysis purposes until after the surface lengths agreed with the internal lengths. Prior to this point, the apparent surface crack growth rate was zero.

These large crack extensions were generally accompanied by extensive plasticity near the crack tip. The extent of plasticity was observed to be considerably greater than values obtained from the Irwin plastic zone expression (Reference 9). It was apparent upon reviewing data such as this that it would be very difficult to define the actual, nominal crack tip growth behavior.

A crack growth resistance test was also performed on a Ti6Al-4V specimen. The results, shown in Figure 90, indicate that K_{st} is approximately 72 ksi $\sqrt{\text{in.}}$ (extrapolated) and that the upper bound or maximum value of K_{cr} is about 81 ksi $\sqrt{\text{in.}}$. Only a few events involved stress intensities in excess of 72 ksi $\sqrt{\text{in.}}$, so stable tear was not a problem for the titanium.

3.6.2 Thickness Effects

Although a detailed evaluation of the effects of thickness variation on fatigue crack growth retardation is beyond the scope of the present study, a few tests of .75 inch thick Ti 6Al-4V titanium were run for comparison with the .25 inch thick material used in the bulk of the program.

The results of the first test on .75 inch (instead of .25 inch) material are shown in Figure 91, along with test results from a .25 inch specimen. Both specimens were sized identically (except for thickness) and the applied loads were scaled by the thickness. In each test a periodic series of 100 overloads followed by 1000 low loads was applied. Care was taken to start the loading sequence at about the same location in each specimen.

As can be seen, the two test results match quite well. The lower rate at the longer crack lengths in the thin specimens can be explained in terms of decreased environmental susceptibility in plane stress. This same trend has been observed in constant amplitude test results of other investigators. In fact, this test is very similar to constant amplitude testing in many ways. It is essentially a steady-state test in which the closure load remains constant throughout the test. This constant-closure phenomenon was demonstrated for this type of periodic loading early in the program. Thus, the fact that the thickness does not significantly affect the retarded crack growth is not surprising in light of the general lack of a thickness effect for constant amplitude loadings. From this test result one might hastily (and apparently incorrectly) conclude that the thickness does not affect the closure loads. Actually, a proper conclusion is only that the stable or quasi-stable closure levels do not depend on thickness. Obviously, in constant amplitude loading, the closure level reached and maintained corresponds to the stable level reached after a large number (>100) of loads are applied. Since the crack tip does not grow significantly (\sim plastic zone radius) between overloads in the test shown in Figure 91, the (quasi-stable) closure level reached also corresponds to the level reached after a large

number of loads are applied. The results shown here simply support the results of constant amplitude loading which indicate that the closure level is not a function of thickness. The effect of isolated overloads, however, does appear to vary significantly with thickness.

This can be seen in Figure 92, where two corresponding tests of .25 and .75 inch thick material are compared. The test specimens were not identical. However, each individual loading sequence was initiated at nominally matching stress intensity factors. This was accomplished by choosing appropriate crack lengths for each loading sequence in the .75 inch specimen. The surprising observation of the comparison in Figure 92 is that there is more (or at least longer periods of) retardation in the thick specimens than in the thin. This result is exactly the opposite of what was anticipated.

To confirm the results of the previous test and to remove the confounding effects of varying the number of overloads, the test of specimen TD-25-106, in which single 1.8 overloads were applied, was reproduced on a thick specimen. Once again the test specimens were different but the stress intensities at each overload were matched. As can be seen in Figures 93 through 96, the conclusion is the same; the thick specimen shows more pronounced retardation than does the thin specimen.

In each of these figures, a $\log a$ vs. N for a particular overload in the .75 inch material has been plotted along with the data from the test of TD-25-106. It is important to note that although the retardation in the thick and thin specimens is different, the rates in each thickness match once a constant amplitude rate is attained. This can be seen by the matching of the slopes of a $\log a$ vs. N . It confirms our previous conclusions and the fact that the test is being run properly.

Since constant amplitude testing and Figure 91 imply that the saturation closure levels are invariant with thickness, and since Figure 92 contains load sequences that have as many as 2000 overloads and still show a variation in retardation (or at least a variation in the return to baseline) with thickness, one must conclude that the closure stress variation as the crack grows must be different in the thick and thin sheets. It is not yet clear whether the resumption of the constant amplitude (saturation) closure level occurs at the same Δa^* or at a different Δa^* . However, it is important to note that, at least for those cases where the number of overloads is large, the initial closure load must be the same. Obviously, the other end point, the constant amplitude closure level, must also be the same.

3.6.3 Tensile Tests

Tensile tests to obtain material mechanical properties were conducted using the equipment described in Section 2. The results are self-explanatory and are presented in Table 12.

3.7 SUMMARY OF TEST RESULTS

Under constant amplitude conditions, crack growth rates are functions of both stress intensity range and stress ratio for both materials. The stress ratio cutoff was 0.5 for 2219-T851 aluminum while no cutoff was observed for R up to 0.7 for Ti6Al-4V titanium. No effect of stress or load level on crack growth rates was observed for either material over the ranges tested. At the same values of stress intensity range and stress ratio, the aluminum crack growth rates were approximately three times those for the titanium. All three basic specimen geometries yielded comparable crack growth rates although the compact tension specimen yielded erroneous results for negative stress ratios.

Single overload cycles less than, or equal to, 1.5 times the baseline loading have negligible effect on subsequent crack growth rates for 2219-T851 aluminum. The same is true for overloads equal to 1.25 times the baseline loading in Ti 6Al-4V titanium. At a given overload ratio and baseline stress ratio, delay cycles increase as a function of crack length and therefore, stress intensity for aluminum. For titanium, the opposite result was observed. For the methods used to analyze the data subsequent to a single cycle overload, the affected crack length was approximately equal to the plane strain plastic zone for aluminum and to the plane stress plastic zone for titanium. Delayed retardation was not evident in either material.

Single periodic overload tests can be employed to obtain an approximate value of the closure factor. These data can be used in conjunction with constant amplitude data to obtain the extreme crack growth rate curve, which is independent of stress ratio effects.

In tests where a single overload cycle was applied before the effect of a previous overload had disappeared, the results were inconclusive. For this type of test, the aluminum exhibited extensive scatter and the titanium was impossible to analyze due to the extremely small affected crack lengths.

Where multiple overloads are applied, the degree of retardation of subsequent crack growth increases as the number of consecutive overload cycles increases, up to a limiting number of overload cycles. Beyond that limit, the addition of overload cycles produces no additional retardation. The duration of retardation subsequent to one or more overloads appears to be independent of the number of overloads. The duration of retardation (affected crack length) is a function of the plastic zone caused by either the maximum amplitude of the overload or by the difference between the maximum amplitude of the overload and the closure level. Closure data were easier to read for multiple overload conditions than for single overload conditions, but still possessed considerable scatter.

Single underload or compression spikes, either applied alone or preceding or following a single tensile overload cycle, had very little influence on subsequent crack growth for 2219-T851 aluminum. However, a single underload negated the retarding effects of multiple preceding tensile overloads. In the Ti 6Al-4V titanium material, single underload or compression spikes caused slightly accelerated subsequent crack growth rates. The effect of a single underload or compression spike which preceded a tensile overload cycle had little effect on the retardation caused by the tensile overload. When a single underload or compression spike followed one or more tensile overloads, it significantly reduced the retarding effect on subsequent crack growth of the overload(s).

Measurable stable tear began at a stress intensity level of about 30 ksi $\sqrt{\text{in.}}$ for 2219-T851 aluminum and at about 72 ksi $\sqrt{\text{in.}}$ for Ti 6Al-4V titanium. Stable tear tends to manifest itself as internal tunneling with, in many instances, negligible surface growth. The limiting values of critical stress intensity for the 1/4 inch materials are 57.5 ksi $\sqrt{\text{in.}}$ for aluminum and 81 ksi $\sqrt{\text{in.}}$ for titanium.

Varying the material thickness does not appear to affect stabilized crack growth behavior for either material, but may influence transient behavior.

4 - MATHEMATICAL MODELING

Several mathematical models have been developed in an attempt to describe crack growth interaction effects. Perhaps the most widely known are the Wheeler model (Ref. 10) and the Effective Stress Retardation model developed by Willenborg, et. al. (Ref. 11). Both of these models modify the crack growth rates subsequent to overload(s) in order to account for retardation. The Wheeler model modifies the crack growth rate such that the retarded crack growth rate is equal to the unretarded crack growth rate times a parameter C_p :

$$\left(\frac{da}{dN}\right)_{\text{ret}} = \left(\frac{da}{dN}\right)_{\text{CA}} C_p \quad (11)$$

where

$$C_p = \left(\frac{\rho}{a_p - a}\right)^m \quad \text{for } a + \rho < a_p \quad (12)$$

$$\text{and } C_p = 1. \quad \text{for } a + \rho \geq a_p \quad (13)$$

Here, ρ is the plastic zone radius caused by the current loading at the current crack length a . The parameter a_p represents the farthest extent of the elastic-plastic interface caused by a previous overload. The empirical exponent m is determined from spectrum test data by trial and error. It was intended that m be a material constant and, once determined, be spectrum independent. However, several investigators (i.e., References 5 and 7) and results of work on this contract have shown that m is spectrum dependent.

The Effective Stress model accounts for interaction effects by modifying the applied stress range to an effective stress range:

$$\Delta S_{\text{eff}} = S_{\text{max}_{\text{eff}}} - S_{\text{min}_{\text{eff}}} \quad (14)$$

where

$$S_{\text{max}_{\text{eff}}} = S_{\text{max}} - S_{\text{red}} \quad (14a)$$

and

$$S_{\min_{\text{eff}}} = S_{\min} - S_{\text{red}} \quad (14b)$$

where

$$S_{\text{red}} = S_{\text{ap}} - S_{\text{max}} \quad (14c)$$

The magnitude of S_{ap} is that stress required to set the plastic zone caused by S_{ap} (acting on the current crack length, a) equal to the elastic-plastic interface, a_p , caused by a previous high load. Both ΔS_{eff} and $S_{\min_{\text{eff}}}$ are constrained to be \geq zero.

In some loading sequences, this retardation model predicts the crack growth under spectrum loading fairly well. However, Figure 97 shows a typical case where the prediction is very unconservative. An additional shortcoming of this model is that an overload will cause crack arrest for the subsequent loading if the subsequent loading is equal to or less than half the magnitude of the overload ($O/L = 2$). This has been demonstrated to be incorrect (Ref. 5). A modification to the model, developed by Gallagher (Ref. 12), makes the overload factor, O/L , a variable. This has been shown to produce improved predictions.

The greatest shortcoming of both of these models (Wheeler and Effective Stress) is that they do not differentiate between the effect on subsequent crack growth of single and multiple overloads. As described in Section 3 of this report and by others (References 5, 13 and 14), this effect can be significant.

4.1 CRACK CLOSURE MODEL

Elber (Ref. 15) demonstrated the phenomenon of crack closure and suggested that variations of the crack closure stress might be responsible for or help to explain crack growth interaction effects. Based on this premise, a mathematical model, using crack closure as a basis, has been developed. The model uses the variations in crack closure to predict crack growth interaction effects during spectral loading.

4.1.1 Crack Closure Concepts

Elber (Ref. 15) showed that cracks subjected to tension-tension loading open and close when the remotely-applied stress is some value greater than zero. This effect is shown schematically in Figure 98. Assuming that crack growth (extension) occurs during the increasing tensile portion of a cyclic loading sequence as proposed by Elber, the pertinent stresses involved in the growth process should be the crack opening and maximum stresses. It has been shown

(References 15 and 16) that the crack opening stress differs from the crack closure stress, but for the purposes of this discussion they will be considered to be equal and will be referred to as the closure stress.

Referring again to Figure 98, the effective stress range, ΔS_{eff} , is equal to the difference between the maximum stress, S_{max} , and the closure stress S_c :

$$\Delta S_{\text{eff}} = S_{\text{max}} - S_c \quad (15)$$

Defining the closure factor, C_f , as:

$$C_f = \frac{S_c}{S_{\text{max}}} \quad (16)$$

Equation (15) becomes:

$$\Delta S_{\text{eff}} = S_{\text{max}} (1 - C_f) \quad (15a)$$

Elber proposed indirectly that C_f is a function of stress ratio, R , through his equation:

$$U = \frac{S_{\text{max}} - S_{\text{op}}}{S_{\text{max}} - S_{\text{min}}} \quad (17)$$

where S_{op} is the crack opening stress, called S_c here. Therefore,

$$U = \frac{1 - C_f}{1 - R} \quad (17a)$$

which, according to Elber

$$= .5 + .4R \quad (17b)$$

for 2024-T3 aluminum. Therefore:

$$C_f = 1 - (.5 + .4R) (1 - R) \quad (17c)$$

Equation (17c) can be inserted into Equation (15a) to produce:

$$\Delta S_{eff} = S_{max} \left[(.5 + .4R) (1 - R) \right] \quad (15b)$$

which can be generalized to:

$$\Delta S_{eff} = S_{max} \cdot \alpha \left[(1 + qR) (1 - R) \right] \quad (15c)$$

When Equation (15c) is inserted into a Paris-type crack growth equation, it is referred to as the Elber growth equation (reference subsection 3.1):

$$\frac{da}{dN} = C \left[S_{max} (1 + qR) (1 - R) \sqrt{\pi a} \right]^n \quad (15d)$$

for the case of a through crack in an infinite sheet. This geometry has been assumed for convenience, but it should be noted that $S \sqrt{\pi a}$ times an appropriate stress intensity magnification factor may be used in any of these equations for other geometric configurations.

For the purposes of this model, a Paris-type growth equation was employed:

$$\frac{da}{dN} = C \Delta K^n \quad (18)$$

$$= C \left[S_{max} (1 - R) \sqrt{\pi a} \right]^n \quad (18a)$$

Elber also showed that

$$\frac{da}{dN} = C' \left[(S_{max} - S_c) \sqrt{\pi a} \right]^n \quad (18b)$$

For constant amplitude crack growth conditions, equations (18a) and (18b) must be equivalent so that:

$$C \left[S_{\max} (1 - R) \sqrt{\pi a} \right]^n = C' \left[S_{\max} (1 - C_f) \sqrt{\pi a} \right]^n \quad (18c)$$

or:

$$C' = C \left[\frac{1 - R}{1 - C_f} \right]^n \quad (18d)$$

For the case of $R = 0$,

$$C' = C \left[\frac{1}{1 - C_{f_0}} \right]^n \quad (18e)$$

where C_{f_0} is the closure factor at $R = \text{zero}$. Equation (18b) then becomes:

$$\frac{da}{dN} = C \left[\frac{S_{\max} - S_c}{(1 - C_{f_0})} \sqrt{\pi a} \right]^n \quad (19)$$

The coefficient C and exponent n have the same values that would be determined by using the Paris expression (Equation (18)) to fit crack growth rate data plotted against the actual applied stress intensity range.

Equation (19) is the basis for all crack growth calculations performed by the model. Elber showed that S_c was a function of S_{\max} and R during steady-state (constant amplitude) crack growth. If S_c in Equation (19) is defined as a function of stress ratio, then Equation (19) will predict the effect of stress ratio on crack growth rates. (It should be noted that the results of this investigation indicate that the closure stress is a function of stress ratio only and does not appear to be stress-level dependent. That is, the closure stress is always some percent of the maximum load, depending on what R is, and does not depend on the absolute magnitude of the maximum load.) Further, if S_c is defined as a function of the previous load history, then

Equation (19) will predict crack growth interaction effects. It remains then, to define S_c as a function of stress ratio and previous load history, and any other pertinent parameters, so that Equation (19) will properly predict crack growth rates for any conditions. The determination of the generalized behavior of S_c as a function of load history is the subject of the following section.

4.1.2 Application of Crack Closure to Mathematical Model

The discussion of the crack closure model centers around the results for the 2219-T851 aluminum test data obtained during this program. This was done for convenience since the aluminum test data was more convenient to analyze and revealed information not readily available from the titanium test data, particularly in the definition of affected lengths (plastic zones) and the crack growth within the affected lengths.

After the model had been developed for the aluminum data, the necessary parameters were determined for the titanium data, and the model was used to verify that it properly predicted the crack growth behavior of the titanium data. In general, the latter is true and is an indication that the model employs the basic concepts necessary for general predictive work.

In the past, it has been suggested that many parameters influence crack growth interactions. The most significant parameters were determined from the test data as far as possible. In some areas, quantitative values were not divulged by the data and a certain amount of intuition was employed. In all cases, the model was verified by comparing predicted a vs N curves with the test data. The most significant parameters found during this program were:

- Effect of R on constant amplitude crack growth
- Effect of maximum overload stress, S_{OL} , on subsequent retarded growth
- Effect of previous minimum stress relative to current minimum stress on subsequent growth
- Effect of number of overload cycles, N_{OL} on subsequent retarded growth
- Effect of compression on both constant amplitude and variable amplitude growth.

Constant Amplitude Crack Growth - The crack growth rate equation for 2219-T851 aluminum was given as

$$\frac{da}{dN} = 1.96 \times 10^{-9} \left[(1 + .6R) \Delta K \right]^{3.34} \quad \text{for } 0 \leq R \leq 0.5 \quad (1a)$$

Equation (19) with $C = 1.96 \times 10^{-9}$ and $n = 3.34$ is

$$\frac{da}{dN} = 1.96 \times 10^{-9} \left[\frac{S_{\max} - S_c}{1 - C_{f_o}} \sqrt{\pi a} \right]^{3.34} \quad (19)$$

As a convenience, taking $K_{\max} = S_{\max} \sqrt{\pi a}$ and $K_c = S_c \sqrt{\pi a}$,

$$\frac{da}{dN} = 1.96 \times 10^{-9} \left[\frac{K_{\max} - K_c}{1 - C_{f_o}} \right]^{3.34} \quad (19a)$$

Equations (1a) and (19a) are equivalent under the same conditions so that:

$$\frac{K_c}{K_{\max}} = C_f = 1 - (1 - C_{f_o}) (1 + .6R) (1 - R) \quad (20)$$

Equation (20) is plotted against stress ratio in Figure 99 for the case of $C_{f_o} = 0.23$. This value of C_{f_o} was selected so that at $R = R_{co} = 0.5$ (from subsection 3.1.1) in Equation (20), the effective stress range is equal to the applied stress range. The difference between $C_f = 1$ and Equation (20), multiplied by K_{\max} is the effective stress intensity range ΔK_{eff} . The dashed line on the right represents R , so that the difference between $C_f = 1$ and R multiplied by K_{\max} is the applied stress intensity range, ΔK . It can be seen that Equation (20) crosses the R curve at a value of $R = 0.5$. The figure indicates that for $R < 0.5$, the closure stress intensity, K_c , is higher than the minimum stress intensity, K_{\min} , and $\Delta K_{\text{eff}} = K_{\max} - K_c$. For $R > 0.5$, K_c is less than K_{\min} so that, physically, $\Delta K_{\text{eff}} = \Delta K$ ($K_c = K_{\min}$) at $R = 0.5$ and stress ratio layering stops at that value of R .

Figure 100 presents Equation (20) using $C_{f_o} = 0.23$, replotted with measured crack closure values. It can be seen that the calculated values of C_f lie along the lower edge of the scatterband of the data and indicate that the calculated value of C_{f_o} (0.23) is too low.

Figure 100 also shows Equation (20) plotted with $C_{f_o} = 0.40$. It will be shown later that this value provides a better fit to the variable amplitude data from a predictive standpoint and here, in the figure, fits the measured closure values quite well except for $R > 0.4$. It is apparent that the form of Equation (20) is incorrect. Further, Figure 100 shows that, for values of R less than $-1/3$, C_f increases; an undesirable behavior.

Another form for C_f was developed, specifically to describe the crack growth behavior for negative values of R while at the same time providing reasonable correlation for positive stress ratios. For a stress ratio of -1 ,

$$\frac{da}{dN} = 2.6 \times 10^{-9} (K_{max})^{3.34} \quad (R = -1) \quad (2)$$

and for $R = 0$, Equation (1a) becomes

$$\frac{da}{dN} = 1.96 \times 10^{-9} (K_{max})^{3.34} \quad (R = 0) \quad (1a)$$

so that

$$\frac{\left(\frac{da}{dN}\right)_{R = -1}}{\left(\frac{da}{dN}\right)_{R = 0}} = \frac{2.60}{1.96} = 1.327$$

Similarly, taking the ratio of the crack growth rates, but using the form of Equation (19):

$$\frac{\left(\frac{da}{dN}\right)_{R = -1}}{\left(\frac{da}{dN}\right)_{R = 0}} = \frac{\left[\frac{K_{max} - K_c}{1 - C_{f_o}} \right]_{R = -1}^{3.34}}{\left[\frac{K_{max} - K_c}{1 - C_{f_o}} \right]_{R = 0}^{3.34}}$$

Since K_{\max} was defined to be the same as ΔK at $R = 0$ and $R = -1$

$$\frac{\left(\frac{da}{dN}\right)_{R=-1}}{\left(\frac{da}{dN}\right)_{R=0}} = \left\{ \frac{1 - C_{f-1}}{1 - C_{f0}} \right\}^{3.34} = 1.327$$

$$C_{f-1} = 1 - 1.088(1 - C_{f0})$$

and

$$= 0.347 \text{ for } C_{f0} = 0.4$$

In a similar manner, the C_f at a positive stress ratio may be obtained. For $R = 0.5$, $C_{f.5} = 0.789$. These values of C_f vs. R were fitted to an equation of the form:

$$C_f = C_{f-1} + (C_{f0} - C_{f-1})(1 + R)^p \quad (21)$$

where

$$C_{f-1} = 0.347$$

$$C_{f0} = 0.40$$

$$p = 3.93$$

and plotted in Figure 10la. It can be seen that Equation (21) agrees closely with Equation (19) in the region $0 < R < 0.5$. Equation (21) was used to define C_f as a function of R and the resulting closure stress intensities were used

in Equation (19a) to calculate crack growth rates. These rates are compared in Table 13 with those of Equations 1a and 2, which were generated independent from crack closure considerations.

The table shows that the crack growth rates calculated from Equations (19a) and (21) are always less than 5% greater than those obtained from Equations 1a, 1b and 2 up to a stress ratio of 0.6. The maximum error of 5% is well within the accuracy of the crack growth rate data. As a result, Equation (21) was used to define crack closure as a function of R, so that the effects of negative stress ratios and compression stresses are accounted for.

For Ti 6Al-4V titanium, the parameters for Equation (21) were determined to be:

$$C_{f-1} = 0.332$$

$$C_{f_0} = 0.40$$

$$p = 3.33$$

Equation 21 is shown in Figure 101b for the titanium material.

A comparison of crack growth rates as a function of R is shown in Table 14 for Ti 6Al-4V titanium. It can be seen that, for $R > 0$, the crack growth rates calculated from Equations (19a) and (27) are within 2% of the values obtained from Equation 1c. For $R = -1$, the values from Equations (19a) and (21) are about 25% less than the value from Equation 3. Since only one titanium specimen was tested to obtain the $R = -1$ data, the parameters for Equation (21) were selected to provide a good fit to the $R > 0$ data.

High-Low Loading Sequence - The high-low loading is the sequence most frequently analyzed by investigators. Following is a description of how the crack growth data during the low portion of a high-low loading sequence can be used to determine the closure factor at $R = 0$, (C_{f_0}) as well as the affected

crack length over which retarded crack growth occurs. Figure 102 shows the case for many cycles of high stress, S_1 , followed by a lower stress, S_2 . For convenience, the stress ratio for both stresses is taken as zero. It is well known that, initially, the crack growth during the lower loading, S_2 , is retarded.

The crack closure model assumes that the closure stress, S_c , varies as shown. Immediately prior to the change in stress, the closure level is the stabilized level, S_{c_1} , associated with S_1 , and varies as shown through some affected length, ρ , to the stabilized value, S_{c_2} , associated with level S_2 . The expression defining the variation is given by:

$$S_c = S_{c_1} - (S_{c_1} - S_{c_2}) \left(\frac{\Delta a}{\rho} \right)^B \quad \text{for } 0 \leq \Delta a \leq \rho \quad (22)$$

where

S_c = Generalized closure stress

Δa = Crack growth since the stress change at a_o

ρ = Plastic zone radius caused by S_1 at a_o

B = Empirical exponent

By definition, $S_{c_1} > S_{c_2}$. It will be shown that the crack growth rate following the load change is immediately retarded. Delayed retardation does not occur.

Previously, it was stated that a value of $C_{f_o} = 0.4$ provided a good fit to the variable amplitude aluminum data. This value can be verified and in addition, the parameters ρ and B may also be calculated. Figure 103 shows schematically how the crack growth rate varies as a function of Δa subsequent to the load change. Immediately after the load change, the rate is $(da/dN)_1$.

This value is used in Equation (19) while at the same time setting $S_{max} = S_2$, $S_c = S_{c_1}$ and $a = a_o$. For $R = 0$, $S_{c_1} = S_1 C_{f_o}$, so that:

$$\left(\frac{da}{dN} \right)_1 = c \left[\left(\frac{S_2 - S_1 C_{f_o}}{1 - C_{f_o}} \right) \sqrt{\pi a_o} \right]^n \quad (23)$$

which can be solved for C_{f_o} since all other parameters are known. This was the procedure used to obtain C_{f_o} from test data for several high-low loading sequences.

Returning to Figure 103, the affected length ρ can be determined by inspection. Finally, at some intermediate value of Δa , say $\Delta a/\rho = 0.5$ arbitrarily, the crack growth rate $(da/dN)_2$ may again be inserted into Equation (19), this time using the previously determined value of C_{f_o} . Again,

$S_{max} = S_2$ but $a = a_o + \rho/2$, so that

$$\left(\frac{da}{dN}\right)_2 = c \left[\left(\frac{S_2 - S_c}{1 - C_{f_o}} \right) \sqrt{\pi (a_o + \rho/2)} \right]^n \quad (24)$$

The value of S_c obtained from Equation (24) is inserted into Equation (22) with $\Delta a/\rho = 0.5$ to obtain B. A single high-low test sequence, therefore, can be used to obtain C_{f_o} , ρ and B, but the results from several test sequences are recommended in order to be reasonably certain that the parameters obtained are correct.

In many cases, the measured crack growth rates subsequent to a load change are not well behaved and may demonstrate considerable scatter. Measurements may not have been taken sufficiently close together during this transient period so that a curve, such as that plotted in Figure 103 can be developed. This situation did occur during the test program and an alternate technique was developed to obtain the three parameters C_{f_o} , ρ and B.

The approach involved assuming values for the three parameters. From these, Equation (22) was used to determine S_c as a function of Δa . This result was used in Equation (19) which was numerically integrated to produce an a vs. ΔN_s curve. The three parameters were varied and the predicted and measured a vs. ΔN_s curves were compared until agreement was obtained. This technique is effective as long as at least one data point falls within the affected length, ρ .

A logical sequence for determining C_{f_o} , ρ and B is shown in Figure 104.

First, assume reasonable values of ρ and B (say plane stress plastic zone and unity) and vary C_{f_o} until the initial slope of the a vs. ΔN_s curve (immediately

following the load change) matches the data. Then the affected length, ρ , is altered until the crack length when unretarded crack growth resumes agrees with the data. As a rule, this crack length can be determined by plotting constant amplitude crack growth on the apparent steady-state growth for the data and estimating the point where the calculated and measured curves diverge as shown in Figure 104. Finally, the parameter B is varied until the number of delay cycles agrees with the data.

For the 2219-T851 aluminum alloy, the values of the parameters obtained were:

$$C_{f_o} = 0.4$$

$$\rho \approx \text{plane stress plastic zone radius} \left(\frac{1}{2\pi} \right) \left(\frac{K_{ol}}{\sigma_y} \right)^2$$

$$B \approx 1$$

It was shown in subsection 3.2.1 of this report that, for a different analytical technique, a plane strain plastic zone provided a good fit to the aluminum data. However, when using the assumed closure variation outlined above, it was found that the plane stress plastic zone provided the best fit. This is probably due to the manner in which the closure level is assumed to vary. When the closure stress approaches the stabilized closure level, the crack growth rate is nearly constant amplitude and the resultant crack length vs cycles curve is almost the same as its constant amplitude counterpart. In this case, the bulk of the retarded crack growth occurs over the first portion of the affected crack length which, for the cases shown, approximates the plane strain plastic zone.

Figures 105 through 107 present a vs. ΔN_s test data and predictions for several cases. The results verify that the parameters obtained reasonably represent the material.

The Ti 6Al-4V titanium test data were considerably more difficult to analyze. As discussed in Section 3 of this report, the only significant, measureable parameter was the number of delay cycles, N_D . It was therefore assumed that the values of C_{f_o} , ρ and B were identical to those for aluminum (ρ = plane stress plastic zone). Figures 108 through 110 show a vs ΔN_s data and predictions for several titanium test specimens. The results again indicate that the parameters are reasonably representative of the data.

For materials such as the titanium investigated here, and others having fairly high yield strengths, the affected lengths are generally quite small. It is necessary to obtain very accurate a vs N data subsequent to the load change. However, if a sufficient number of less-accurately measured cases are

available, representing different stress intensities at the overload obtained for different stress combinations and crack lengths, it is possible to obtain reasonable values of C_f , ρ and B through a process of trial and error.

Initially it was specified that the stress ratios for the two stresses in the high-low sequence be zero. The procedure described above may be applied to cases where $R > 0$ except that, to simplify the analysis, the minimum stress should be the same for both maximum stresses. This requirement will become clear in the discussion regarding the effect of minimum stress variations on closure level. In addition, the minimum stresses should in no case exceed, and preferably be much lower than, the closure stress expected for either the high or low stresses in the sequence. If the closure stress is less than the applied minimum stress, S_{min} , then, no interaction should occur. There is some disagreement as to whether this premise is correct or not (eg. Ref. 17), but it has been assumed to be true here.

Effect of Minimum Stress on Closure - Tests have shown that the two loading sequences shown in Figure 111 produce the same crack life subsequent to the load change. This result is shown schematically in the lower portion of the figure. Tests of this type were not run during this program. However, an indirect proof follows. It has already been shown that closure is a function of stress ratio (ref. Equation 21) and, therefore, the stabilized value for the high stress in sequence B must be higher than the equivalent value in sequence A. The explanation for similar crack growth behavior subsequent to the load change is that the closure stress in sequence B quickly changes to approximately the same value as in sequence A. The key parameter in this sudden fluctuation is the minimum stress.

Figure 112 shows actual crack closure (load vs. COD) curves for an aluminum specimen subjected to an initial stress ratio of 0.5 and subsequently to a stress ratio of 0.05. Because the maximum and minimum applied loads are known and the ordinate is linear, any value of load on the curves may be obtained. Further, the displacements need not be calibrated since they are proportional to the local displacements near the crack tip and, as such, any non-linearities on the load-displacement curve represent equivalent crack tip displacement non-linearities. The arrows parallel to the upper portion of the curves indicate the loading phase (loading up or unloading) and the arrows approximately normal to the traces represent the estimated crack closure (and opening) levels. In all cases, the maximum applied load was the same (6 ksi). Apparent differences in maximum load and load ranges were caused by adjusting the plotter controls.

During cycles 0 and 1, the closure stress is stable and slightly higher than the minimum stress. During the unloading portion of cycle 2, the closure level remains the same. Loading up from the new minimum stress ($R = .05$), the crack opening stress is seen to be significantly lower than its preceding closure value. After an additional cycle, the level is again reduced and by cycle 4 has apparently stabilized at a value of about 1.2 ksi (20% of the 6 ksi maximum). Although this value (20%) is somewhat lower than for

other typical data with $R = 0.05$, the significant item here is that the closure stress was reduced considerably and restabilized in only two cycles.

Figure 113 presents similar data. The initial stress ratio is 0.7 and no crack closure (or opening) is apparent during cycles 1 through 3. While unloading during cycle 4, the crack is seen to close at about 55% of the maximum load. During reloading, the crack opening stress occurs at a very low value and is seen to stabilize at that value (cycles 5 and 6). In this case, the crack was quite long so that considerable plasticity existed. The absolute values of the closure levels again appear low, but the significant aspect is that only one cycle of the new low-load was required to stabilize the closure level. The crack closure behavior shown in the two figures supports the results shown in Figure 111.

The crack closure model assumes that step-wise changes in closure level such as those described above occur during the first load cycle during which the minimum stress decreases. This causes a step-wise change in the crack closure stress as shown in Figure 114 for the loading sequence shown. Prior to the load change, the closure factor, C_f , is calculated using Equation (21) where $R = S_{\min_1}/S_1$ and $S_{c_1} = S_1 \cdot C_f$. Immediately after the application of the new, lower minimum stress, S_{\min_2} , the closure factor, C'_f , is calculated from Equation (21) using $R = S_{\min_2}/S_1$ and $S'_{c_1} = S_1 \cdot C'_f$. Starting from this value, the closure stress varies as described by Equation (22). For the loading sequences in Figure 111, it can be seen that the calculated values of S'_{c_1} for sequence B, and S_{c_1} for sequence A, are identical. The subsequent closure variation is therefore identical and the calculated (and observed) crack growth behavior should be the same. This premise is verified indirectly by the results shown in Figures 115 and 116. These figures present a vs. ΔN_s data for compact tension specimens subjected to a constant maximum load of 951 lb. In Figure 115, the previous stress ratio was 0.7 ($P_{\min} = 666$ lb). At $\Delta N_s = 0$, the minimum cyclic load was reduced to zero. A constant-amplitude calculation for the crack growth under $P = 951$ lb. and $R = 0$. agrees closely with the data. From equation (21), the closure factor, C_f , is .77 for $R = 0.7$ and 0.4 for $R = 0$. The corresponding closure loads are 732 lb. and 384 lb., a significant difference. If the 732 lb. closure load were initially effective, the a vs ΔN_s data would not agree with the calculated constant amplitude crack growth behavior.

In Figure 116, the maximum load was again held constant at 951 lb. and the previous (prior to $\Delta N_s = 0$) stress ratio was 0.5. At $\Delta N_s = 0$, the stress

ratio was reduced to 0.3. The corresponding closure loads are 578 lb. and 472 lb. Again, the previous high closure load did not affect the crack growth for $R = 0.3$, since the calculated constant amplitude growth agrees closely with the data.

The crack closure model performs this minimum-stress adjustment regardless of the relationship between S_1 and S_2 (i.e., even for the case where $S_2 > S_1$.) The only criterion is the relationship between the minimum stresses.

Because of the manner in which the minimum-stress adjustment is performed, a single cycle of reduced minimum stress has the effect of immediately reducing the closure level, and affecting the subsequent crack growth. This concept is easily extended to handle compression spikes and will be discussed subsequently. It will be shown later that for certain materials, the impact of this reduction is not very significant.

Effect of Single and Multiple Overloads on Subsequent Crack Growth -
It has been shown by several investigators (References 14 and 18) that a single overload cycle, superposed on constant amplitude cyclic loading, produces a lesser degree of subsequent retardation than several overload cycles. None of the currently existing models (References 10 and 11) differentiates between the number of overload cycles. They assume that the crack growth subsequent to any number of overloads is always fully retarded. A method to account for the number of overloads effect has been developed for the crack closure model.

In general, one overload cycle produces some subsequent retardation, two overload cycles produce more, and so on. There appears to be a limit to the amount of retardation which can be attained for a given material (References 4, 14 and 16). Figure 117 shows schematically how the closure stress might vary during a low-high loading sequence. Prior to the load change, the closure stress is that stabilized value, S_{c1} , associated with the initial loading, S_1 . Subsequent to the load change to S_2 , the closure stress increases to the stabilized value, S_{c2} , associated with stress level S_2 . Data gathered prior to and during this program indicates that the closure level varies as a function of the number of cycles, N_{OL} , of the overload stress level, S_2 . The number of overload cycles at which no further increase in closure level occurs is defined as N_{sat} . If no overloads are applied, the closure stress does not change and crack growth during subsequent cycling at S_1 would be unretarded. If $N_{OL} \geq N_{sat}$, the retardation of the crack growth during subsequent cycling at S_1 would be maximized. Intermediate values of N_{OL} ($0 < N_{OL} < N_{sat}$) would produce intermediate values of retardation. Figure 118 presents this effect schematically.

Some of the data gathered during this program indicated that the overload ratio, O/L , must attain some minimum value before the overload stress has any apparent effect on subsequent crack growth. (The overload ratio, O/L , was defined earlier as the ratio of the overload stress to the baseline stress, S_{OL}/S .) For example, Figures 119 through 123 present a vs N data for specimens subjected to single discrete overloads where the overload ratio was 1.25, 1.4 and 1.5. Calculated constant amplitude growth curves (neglecting any growth or retardation due to the overloads) are also shown. It can be seen that the calculated curves agree very closely with the data. This indicates that overloads with O/L values ≤ 1.5 have negligible effect on the crack growth behavior. Therefore, the closure stress is unaffected for $1.0 < O/L \leq 1.5$.

Figure 124 presents the ratio, R_c (the calculated closure stress after one overload cycle over the initial closure stress), vs the overload factor, O/L , for data gathered during several single overload events. The closure stress immediately after the overload, S_{c1} , was calculated by assuming different values of S_{c1} and comparing predicted a vs ΔN_s curves with the data. Equation (21) with the values of C_{f0} , ρ and B for aluminum was used to define the variation of S_c and Equation (19) was numerically integrated to obtain a vs ΔN_s . The values in parentheses represent the number of events analyzed to produce the plotted value. The diagonal, dashed line represents the case where the closure stress equals the stabilized value. If the calculated points fell along this line it would mean that there is no difference between one and many overloads. It can be seen, however, that almost all of the values lie below the line. It can also be seen that R_c is equal to 1 up to an overload ratio of approximately 1.5. This means that after one overload cycle, for $O/L \leq 1.5$, the closure stress does not increase.

At $O/L = 1.8$, there is considerable scatter in the calculated results ($1.2 < R_c < 1.8$). These points were re-plotted in Figure 125 along with calculated values of R_c for values of $N_{OL} > 1$. (Other data points for $N_{OL} = 50$ to 2000 cycles produced values of $R_c = 1.8$ but are not shown here.) The number of overload cycles that causes saturation, N_{sat} , is apparently between 10 and 20. The trend of the data based on $N_{OL} > 1$ indicates that the value of R_c at $N_{OL} = 1$ should be about 1.4. Since it was desired to produce a conservative prediction based on these data, a value of 1.2 was selected. This means that the closure stress after $N_{OL} = 1$ is $2/3$ ($1.2/1.8$) of the stabilized value and is conservative since the calculated closure stress is less than the actual closure stress. The calculated subsequent retardation will therefore be less than the actual retardation.

The parameter γ is defined as:

$$\gamma = \frac{\text{Closure stress after } N_{OL}}{\text{Closure stress after } N_{sat}} \quad (25)$$

and is a function of the number of overload cycles, N_{OL} . For $N_{OL} = 1$, $\gamma = 2/3$ and for $N_{OL} \geq N_{sat}$, $\gamma = 1$. It was assumed, therefore, that the closure stress after $N_{OL} = 1$ was $2/3$ of the stabilized closure stress regardless of the overload ratio. This assumption is shown as the solid line in Figure 124. The dashed line represents the closure levels for $N_{OL} \geq N_{sat}$. In no case, however, can R_c be less than unity since the closure stress would not be expected to decrease after an overload(s) has been applied.

The data of Figure 124 are replotted in Figure 126 as γ vs N_{OL} for all values where $O/L \geq 1.5$. The value of γ was assumed to vary linearly as:

$$\gamma = \gamma_1 + (1 - \gamma_1) \cdot \left(\frac{N_{OL} - 1}{N_{sat} - 1} \right) \quad (26)$$

For 2219-T851 aluminum:

$$\gamma_1 = 2/3 \text{ so that: } \gamma = 2/3 + 1/3 \left(\frac{N_{OL} - 1}{N_{sat} - 1} \right) \quad (26a)$$

The value of N_{sat} was selected (somewhat arbitrarily) as 13, but is substantiated by the results of Ref. 18. There, the authors indicated that for 7075-T6 aluminum, when $N_{OL} = 10$, the delay (retardation) was nearly maximized. In all probability, the expression used here for γ as a linear function of N_{OL} is incorrect (and unnatural). It is suspected that γ should approach a value of 1 asymptotically. An insufficient number of values of N_{OL} were investigated to test this assumption and the crack closure model assumes the linear function to be correct.

Titanium specimens subjected to single overloads with overload ratios of 1.25, 1.5 and 1.8 were tested. Where the overload ratio was 1.25, the overload had little or no effect on subsequent crack growth. Unlike the aluminum, the titanium overload ratios of 1.5 did produce measurable crack growth retardation.

Results similar to the aluminum results were obtained although considerable scatter in the calculated values of γ was encountered. These results are presented in Figure 127. For the titanium, the parameters selected were:

$$\gamma_1 = .80$$

$$N_{sat} = 100$$

This value for N_{sat} is supported by Wei (Ref. 14) who measured delay cycles as a function of the number of applied overloads for Ti 6Al-4V titanium. He found that the number of delay cycles was maximized after approximately 100 overload cycles under constant stress intensity conditions.

It is worth noting that the evaluation of γ is based on data obtained predominately at stress ratios which were nominally zero. It is probable that the variation of closure load with the number of overloads is significantly different at higher values of R . This conclusion can be reached by considering probable causes of the variation in closure with the number of overloads and some of the data presented in this program.

Previous investigators (Ref. 19, for example) have attributed the variation in retardation to the fact that, with increasing numbers of overloads, the crack propagates further into the overload plastic zone before the return to constant amplitude loading. That this is not the governing phenomenon is demonstrated by the low values of N_{sat} found in this program (particularly in aluminum), during the application of which a crack would propagate through a very small percentage of the plastic zone. Additionally, the titanium, which has a much smaller plastic zone than the aluminum, required a much larger number of cycles to reach saturation even though the overall range of crack growth rates investigated was nominally the same.

The number of cycles required for saturation is of the same order of magnitude as the number of cycles required to reach stability in a cyclic stress-strain test. This is what one might expect if saturation was reached after the local crack-tip residual stress pattern stabilized in a similar manner. If this is indeed the governing phenomenon (and certainly local cyclic stress-strain behavior should play some role), then a significant variation in saturation cycles with stress ratio is to be expected. Consider a test being run at a high R value such that the closure load caused by an overload is below the minimum baseline load. Subsequent cycling would produce totally linear load-displacement records, the local stress-strain behavior would be essentially elastic, and no further changes in residual stress patterns would occur. Therefore, at high R values, the number of cycles to saturation would be one. The important point in this argument is that the closure load is below the minimum applied load. Thus, the amount of "crushing" or closing

below the closure level may control the number of cycles it takes to achieve stability in the residual stress pattern and, therefore, to reach closure saturation. A measure of the "crushing" might be the difference between C_f and R as shown schematically in Figure 128.

The data of subsection 3.5 tends to support this conclusion. Consider for example Figure 76. Retardation is obviously present. However, the model presently proposed predicts a closure level of 832 lbs. due to the basic constant amplitude loading and a closure load of 762 lbs. due to the single overload application. Therefore, the model would predict no retardation. The low closure load is due to the fact that, after the first cycle, only 2/3 of the overload saturation closure level is reached. At the other extreme, assume that the saturation level is reached for this R value (1/3 for the overload) so that a closure load of 1069 lbs. is obtained. Then significant retardation would be predicted. A more reasonable assumption might be a linear variation in γ with $(C_f - R)$. This would produce a closure load of 912 lbs.

Presently, there is insufficient data to determine whether or not these hypotheses concerning the variation of the saturation behavior with stress ratio are valid.

Effect of Compression Loading on Closure - In the preceding discussion, it was shown that a single cycle of reduced minimum stress is treated as producing an immediate reduction in the closure stress. This concept can be extended to the case where the minimum stress is negative (compression). Figure 101 shows that, as the stress ratio is reduced below zero, the closure factor decreases slowly. This implies that for both 2219-T851 aluminum, and Ti 6Al-4V titanium, the application of compression stresses is only slightly more damaging than the application of minimum stresses which are equal to zero. This is also apparent from the constant amplitude data, where the crack growth rate for $R = -1$ is only 33% faster than for $R = 0$ at a given ΔK (Equations 1a and 2).

The crack closure model treats the cases of negative (compression) loads as an extension of the minimum stress adjustment. Figure 129 shows schematically how the closure stress varies for the case of a high-low loading sequence where the minimum stress of the low portion of the sequence, S_{\min_2} , is negative (compression). Before the load change, the closure stress, S_{c_1} , is the stabilized value associated with the initial (high) stresses, S_1 and S_{\min_1} . Immediately after the load change, a new closure stress, $S'_{c_1} = S_1 \cdot C_f$, is calculated. Equation (21) is used to determine C_f and R is taken as S_{\min_2}/S_1 . The closure stress, S_c , then varies from S'_{c_1} to S_{c_2} as described by Equation (22).

Effect of Compression Spikes on Subsequent Crack Growth - Compression spikes and underloads are treated by the model in the same manner as constant amplitude and step-wise loadings. Underloads are defined as single cycle excursions of the minimum stress to lower tensile values, where the nominal stress ratio is greater than zero. These loading sequences are shown schematically in Figures 130 and 131. Prior to the application of the spike load, the closure level is the stabilized value, S_c , associated with the applied stresses S_1 and S_{min_1} . Immediately after the application of the spike loads, a new, lower closure stress, S'_c , is calculated from Equation (21) using $R = S_2/S_1$. The closure level then returns to the stabilized level S_c in the same manner as described under the heading "Increasing and Decreasing Closure Level" below.

For load sequences such as those described, and particularly during spectrum loading, it is common to calculate modified stress ratios based on preceding maximum stresses and current minimum stresses which are much less than -1. Actual values of $R < -1$ might also be encountered. Data were not obtained for $R < -1$ under constant amplitude loading conditions. Therefore the closure behavior, either measured or calculated from crack growth rate data for large negative R values, is unknown. Based on the behavior of C_f in Figure 101, it appears that the closure level asymptotically approaches some minimum value as R becomes more negative. The model therefore treats values of $R < -1$ as $R = -1$ until additional data for $R < -1$ is obtained.

Increasing and Decreasing Closure Level - It is necessary to define whether the closure level is increasing or decreasing during variable amplitude loading. The current closure stress is that value which exists prior to a load change. It may be modified by overload or minimum stress considerations immediately after the application of the new loadings. The expected closure stress is the stabilized value associated with the new loading.

If the current closure stress is greater than the expected value, a decreasing closure situation exists and the behavior of the closure stress is defined by Equation (22). Generally, for this condition, the drop in closure level requires many applications of the new loading to propagate the crack through the affected length established by the previous loading. Conversely, when the closure level is increasing (current closure stress is less than the expected closure stress), Equation (26) applies, and it takes very few cycles of the new loading to regain a stabilized closure value. In the latter case, about 13 cycles are required for the 2219-T851 aluminum and approximately 100 cycles for the Ti 6Al-4V titanium to attain stability.

Variable Amplitude Loading - Previous discussions have described how the model treats crack closure during constant amplitude and discrete load change sequences. During variable amplitude loading sequences, load changes occur much too frequently for stabilized conditions to occur between the load changes. Typically, several (or many) transient conditions overlap. The following discussion describes how the model treats these conditions.

Figure 132a presents schematically how the closure level varies for the case of increased maximum load when the minimum load is held constant. Prior to the load change, S_c is stabilized at S_{c1} . After the first cycle of S_2 , S_c is $S_{c2} \cdot \gamma$ from Equation (26). In this case, $S_{c2} \cdot \gamma > S_{c1}$. Thereafter, S_c increases to S_{c2} by Equation (26). The number of cycles of S_2 required to reach S_{c2} is N_{sat} .

Figure 132b shows a similar case, except that immediately after the load change, $S_{c2} \cdot \gamma$ is less than S_{c1} . In this case, the value of N_{OL} in Equation (26) is replaced by the value N'_{OL} and γ is replaced by S_{c1}/S_{c2} :

$$\frac{S_{c1}}{S_{c2}} = \gamma_1 + (1 - \gamma_1) \left(\frac{N'_{OL} - 1}{N_{sat} - 1} \right) \quad (26c)$$

The value of N'_{OL} obtained from Equation (26c) is the apparent number of overload cycles (cycles of S_2 in this case) which have already been applied to the crack. Cycles of S_2 are then counted starting at N'_{OL} rather than zero, and Equation (27) is used to calculate the closure behavior starting at N'_{OL} . It can be seen that, for $S_{c1} > \gamma S_{c2}$, the number of overload cycles required to reach S_{c2} is always less than N_{sat} . In the limit, when $S_{c1} = S_{c2}$, the number of overload cycles is zero and is physically consistent.

Figure 133 presents two variations of the cases previously discussed. In Figure 133a, the maximum stress is held constant while the minimum stress is increased. This case is handled in the same manner as those presented in Figure 132. The number of cycles to achieve stability is $< N_{sat}$. In Figure 133b, the maximum and minimum stresses change as shown. Immediately after the load change, the minimum stress adjustment is employed to reduce the closure stress to S'_{c2} . Equation (26) is used to determine if a subsequent adjustment upward to S''_{c2} is required. If so, the closure stress then varies over N_{sat} cycles to S_{c2} (solid line). If not, the closure stress varies to S_{c2} along the dashed (alternative) line. In the latter case, N_{OL} can be less than or equal to N_{sat} depending on the relative values of S'_{c2} and S_{c2} (alternative).

The preceding discussion covered typical cases of increasing closure. All cases of increasing closure are treated in the same manner. The extension of these cases to variable amplitude loading is fairly simple and requires only the use of Equation (26c) to adjust the cycle count for use in Equation (26). In all cases, for $S_{c_2} > S_{c_1}$, or $S_{c_2} > S'_{c_2}$, the closure condition is defined as increasing.

The treatment for decreasing closure is more complex for two reasons. First, many of the potential interaction situations were not investigated during the test program. Even those cases which were investigated were difficult to analyze directly because of the limited amount of crack growth during a given load level and because of the small affected lengths. For example, it is difficult to apply several load sequences within a given affected crack length (which may be of the order of 0.020 inch) and to optically measure transient crack growth behavior during each of the load sequences to obtain meaningful data. As described earlier, the crack growth subsequent to the load change was not well behaved, even for cases of discrete load changes. Secondly, from a modeling standpoint, a complex load history requires a complex book-keeping capability. The question of the significance of some previous load sequence also arises. For these reasons, only those parameters deemed to have the greatest influence on crack growth retardation are tracked by the model. These are:

- ρ - affected crack length over which transient behavior occurs
- a - current crack length
- a_o - crack length at which ρ was generated
- a_p - $a_o + \rho$, elastic-plastic interface
- a_s - crack length at start of current loading
- S_{min_p} - previous, smallest minimum stress which was applied while $a_o < a < a_p$
- S - current maximum stress
- S_{min} - current minimum stress
- S_{c_1} - existing closure stress
- S_{c_2} - expected stabilized closure stress for S and S_{min}

The affected length, ρ , shown in Figure 134, is generated by some previous maximum load, S_p , applied at a_o and assumed to be proportional to the Irwin plastic zone radius:

$$\rho = \beta \cdot \left(\frac{S_p \sqrt{\pi a_o}}{\sigma_y} \right)^2 \quad (27)$$

where σ_y is the material yield stress. The coefficient β is assumed to be a variable and can be the plane strain value $\left(\frac{1}{4\sqrt{2\pi}} \right)$, the plane stress value $\frac{1}{2\pi}$ or any other value which was determined to fit the data as described previously. As long as the crack tip, a , is within the affected length ($a_o < a < a_p$), transient conditions exist. For a less than a_o (not possible) or greater than a_p , stabilized steady-state conditions exist. If, during the application of a given load level, a equals or exceeds a_p , stabilized conditions prevail throughout the balance of that level. The extent of the elastic-plastic interface, a_p , is updated (using S in Equation (27)) at the beginning and at the end of each load level as required. Whenever a_p is updated, S_p is set equal to S . For the following discussion, it is assumed that the crack tip is always within the affected length.

The crack length at the start of the current loading, a_s , is used in Equation (22) to define the downward movement of the closure level. The pertinent geometry is shown in Figure (134) and Equation (22) becomes:

$$S_c = S_{c_1} - \left(S_{c_1} - S_{c_2} \right) \left(\frac{a - a_s}{a_p - a_s} \right)^B \quad (22a)$$

The previous, least minimum stress, S_{\min_p} , is tracked for use in the minimum stress adjustment. Whenever a new minimum stress, S_{\min} , which is lower than S_{\min_p} , is encountered, the minimum stress adjustment is applied to calculate a modified value of S_{c_1} . The effective stress is S_{\min}/S_p for use in Equation (23). In certain instances, the modified value of S_{c_1} exceeds the

original value of S_{c1} . In this case, the original value of S_{c1} is retained. Finally, S_{\min_p} is set equal to S_{\min} .

The expected stabilized closure stress, S_{c2} , is the endpoint closure stress in Equation (22) or (22a) when $a \geq a_p$.

Figure 135 presents schematically the treatment of three potential situations for a three level descending load sequence. The minimum stress is taken as zero for all load levels. In Figure 135a, there are a sufficient number of cycles of S_2 and S_3 to propagate the crack through the affected lengths ρ_1 and ρ_2 respectively. The subscripts of ρ are associated with the stresses which created each ρ (i.e. ρ_1 was caused by S_1). The appropriate parameters are inserted into Equation (22a) and the closure behavior within each affected length is defined. (The exponent B in Equations (22) and (22a) has been depicted as unity in all figures for convenience.)

Figure 135b shows the next higher level of complexity which can occur. Here, an insufficient number of cycles of S_2 are applied to grow the crack through a_{p1} . The closure level has declined to a value S'_{c2} where ($S_{c1} > S'_{c2} > S_{c2}$). In addition $a_{p2} < a_{p1}$ so Equation (22a), for the closure variation during S_3 , becomes:

$$S_c = S'_{c2} - (S'_{c2} - S_{c3}) \left(\frac{a - a_{s3}}{a_{p1} - a_{s3}} \right)^B \quad \text{for } a_{s3} < a < a_{p1}$$

Figure 135c presents a similar case except that $a_{p2} > a_{p1}$. Now Equation (22a) becomes:

$$S_c = S'_{c2} - (S'_{c2} - S_{c3}) \left(\frac{a - a_{s3}}{a_{p2} - a_{s3}} \right)^B \quad \text{for } a_{s3} < a < a_{p2}$$

to define the closure variation during the application of S_3 . The location of a_0 , originally equal to a_{s_2} , is now advanced to be equal to a_{s_3} or the crack length from which the new elastic-plastic interface is measured. In addition, the value of S_p originally equal to S_1 is updated to S_2 .

In all three figures, when the loading S_3 is completed, steady-state conditions exist and every parameter would be updated based on S_3 . The extension of these rules for more complex loadings follows logically.

Figure 136 presents cases where the maximum and/or the minimum stresses vary. In the first case, (Figure 136a), the maximum stress is held constant and the minimum stress decreases in steps. For this type of load sequence, only the minimum stress adjustment is employed at each load change to calculate a step-wise change in the closure level. Interestingly, this type of loading sequence has no interactions and the crack growth during each part is solely constant amplitude in nature.

Figure 136b presents two sequences, the first requiring a minimum stress adjustment and the second a simple application of Equation (22a).

A slightly more complex situation is depicted in Figure 136c. At the point where S_2 begins, the minimum stress also changes to S_{\min_2} . First, the minimum stress adjustment is applied to calculate S'_{c_1} . In Equation (21), R is set equal to S_{\min_2}/S_1 to obtain C'_f and $S'_{c_1} = S_1 \cdot C'_f$. The closure level then varies through the affected length, ρ , caused by S_1 , to S_{c_2} by Equation (22a).

4.1.3 Results and Discussion

The proof of any model lies in its ability to predict the crack growth behavior of a specimen, or component, subjected to any arbitrary loading sequence. This section presents results obtained by the crack closure model for a variety of loading conditions. Almost all of the specimens and/or loading sequences were selected at random in an effort to be as objective as possible.

Constant Amplitude - Figures 137 through 143 compare constant amplitude predictions obtained by the model with test data. These results, obtained for various stress ratios for both aluminum and titanium, were used to verify that the closure equation (Equation 21) reasonably represents the material behavior. Figures 137 through 139 are for aluminum specimens subjected to stress ratios of .5, 0 and -1 respectively. The good correlation is typical of the aluminum behavior.

Figures 140 through 142 present the results for titanium specimens subjected to stress ratios of 0.5, 0.3 and 0.05 respectively. Here, the results are a little scattered. This was attributed to the basic material scatter as described in Subsection 3.1.2 of this report. These results all fall well within the scatterband described there.

The results presented in Figure 143 are in poorer agreement. The prediction and a calculation using Equation (3), for reference, began at a $\Delta K = 0.5$ inch ($\approx 774,000$ cycles). Equation (3) was fitted to this particular data (the only $R = -1$ titanium test) and is shown relative to the data in Figure 15e. There, it can be seen that for low values of ΔK , the data points exhibit somewhat faster growth than that of Equation (3). Since this is the crack length regime where most of the cycles are used, the slight over-prediction of total life is not unexpected.

The deviation between the prediction and the calculation using Equation (3) can be attributed to the fact that the closure equation, Equation 21, did not fit the rate data particularly well. This is shown in Table 14.

For $R = -1$, Equation (3) produced a crack growth rate of 5.5×10^{-7} inch/cycle at $\Delta K = 15$ ksi $\sqrt{\text{inch}}$. The closure equation, combined with the effective stress crack growth equation, Equation (19b), produced an equivalent value of 4.07×10^{-7} inch/cycle. This results in a predicted life which is about 35% greater than the life calculated from Equation 3.

These last results (Figure 143) indicate that either the data are incorrect (and that additional negative stress ratio tests should have been run for the titanium) or, more likely, that the closure equation is not general enough to properly represent different material behaviors.

Single Discrete Overloads - Figures 144 through 153 present data and predictions using the crack closure model for 2219-T851 aluminum and Ti 6Al-4V titanium. Results for overload ratios, O/L, of 1.25, 1.5 and 1.8 are shown for both materials. For aluminum with values of O/L = 1.25 and 1.5 (Figures 144 through 147), the model predictions are quite accurate. For an overload ratio of 1.8 the results are of mixed quality. In Figure 147, the predicted life is approximately 84% of the test life but, in Figure 148, the predicted life is only 60% of the test life. It should be noted that the predictions are conservative or only slightly unconservative for all of the cases shown.

The predictions obtained for titanium (Figures 149 through 153) are less accurate than those obtained for aluminum. For the lowest overload ratio (1.25), the predicted life is 12% greater than the actual life, as shown in Figure 149. Figures 150 and 151 present results for O/L = 1.5. For these two cases, the predicted lives are 17% less than and 25% greater than the test lives. At an overload ratio of 1.8, the model under-predicts the test lives consistently. For example, the predicted life is only 51% of the test life in Figure 152 and 47% of the test life in Figure 153.

For both materials, as the overload ratios increase, the ratio of the predicted life relative to the test life decreases. These results imply that there is an overload ratio effect, or a relationship between the overload stress (and/or baseline stress) to the material yield stress, or both, which has not been accounted for.

The number of overload ratios investigated was, of necessity, restricted. Perhaps higher values than those investigated would have proved to be more productive. At the same time, however, it was desired to gather crack growth rate data over specified rate ranges which restricted the magnitude of the overloads. Further, in the case of the aluminum, stable tear considerations placed an upper limit of 30 ksi $\sqrt{\text{in.}}$ on the maximum stress intensity caused by the overload. The investigation of higher overload ratios requires that smaller crack lengths be employed. In turn, the crack growth rates subsequent to overloads become very low. These result in long test times and, potentially, effective stress intensity ranges which are below the threshold for fatigue crack growth. Most of these comments would also apply to stress level investigations. In light of the above, it is felt that the results obtained thus far are acceptable, particularly since they are almost always conservative.

Single Periodic Overloads - The predictions obtained by the crack closure model for this type of loading are generally less accurate than those previously described. Figures 154 through 161 present test data and predictions obtained by the model for both materials. It can be seen that for 2219-T851 aluminum, except for the case shown in Figure 157, the model consistently overpredicts the test life. In some cases, the predicted life is many times the test life. These results are tabulated in Table 15 where the predictions were extended to larger values than those shown in the figures. Even so, for specimens AD-25-26 and -29, the prediction was terminated to reduce running time on the computer.

The over-predicted results for the aluminum can be traced to the manner in which the model treats overloads. Unless there are a sufficient number of low loads to cause the crack to escape the effect of the overload, the closure level continues to increase. This effect is shown schematically in Figure 132. Each time the overload is applied, the closure stress increases. During the application of the low loads, the closure stress decreases to some extent depending on how far the crack extends through the overload-affected length. If the closure stress has not decreased sufficiently when the overload is applied again, it then increases by Equation (26c). If the closure stress decreases enough, a quasi-stable situation develops where the closure stress oscillates about some average value. For the case of the aluminum, the crack lengths affected by the overload are quite large due to the relatively low material yield stress. If only a few cycles of low load are applied (as was the case here), the crack progresses only a small amount between overloads. Further, the aluminum has a value of N_{sat} equal to only 13 cycles. This means that less than 13 occurrences of the overload causes the closure level to attain a value which is essentially the stabilized value associated with the overload. Of course, during the application of the low loads, the crack propagated part of the way through the overload-affected length and the average closure level

was somewhere between the stabilized values for the overload and the low loads. For the first five cases shown in Table 15, the combination of overload ratio and/or few low-load cycles caused the calculated closure level to hover around a value which was close to the stabilized value for the overload. This resulted in a small effective stress range for the low-loads and a comensurate low crack growth rate. In the last case (Specimen AD-25-27), the overload ratio was low and the number of low-load cycles was sufficient to bring the average closure level into what is apparently the right range based on the good prediction.

The titanium predictions (Figures 158 through 161) are better than those for the aluminum. For cases where the overload ratio is 1.25 (Specimens TD-25-32, -39 and -31), the predictions are only slightly greater than the test values. For cases where the overload ratio is 1.8, the predictions are shorter than the test lives. These results for titanium are consistent with those discussed earlier for single discrete overloads. There, it was concluded that the effect of a single overload on subsequent crack growth, where the overload ratio was 1.8, was not strong enough. The closure level did not increase enough to produce sufficient subsequent retardation. It is apparent that the parameters for single overload applications in titanium have not been correctly defined.

Based on the aluminum results, it appears that the model requires additional work for the single periodic overload cases. However, there were an insufficient number of different overload ratios and applications of low loads to perform any meaningful effort.

Multiple Overloads - Multiple overloads fall into three basic categories. First is the case of many overloads applied ($N_{OL} > N_{sat}$). Second are situations where $1 < N_{OL} < N_{sat}$. Finally, there are multiple periodic overloads, which are essentially two-level block loading programs.

Several predictions using the crack closure model for situations where $N_{OL} > N_{sat}$ were presented in Figures 105 through 107 for 2219-T851 aluminum with overload ratios of 1.8, 1.6 and 1.5. Figures 108 through 110 presented similar results for titanium with O/L = 1.25, 1.5, 1.6 and 1.67. To complete the range of overload ratios, Figures 162 and 163 present test data and predictions using the crack closure model for 2219-T851 aluminum with O/L = 1.25 and 1.5 respectively. Similar results are shown in Figure 164 for titanium with O/L = 1.8. For all of the cases, the predictions agree very closely with the test data.

Figures 165 through 168 present similar data and predictions where the minimum load was maintained at a high level so that the stress ratio for the base loading was 0.50. The minimum load during the application of the overload sequences was maintained at the same level as the minimum load for the base loading. These predictions, most of which fit the data quite well, indicate that the model not only accounts for the retardation caused by the overloads,

but also properly accounts for the influence of stress ratio on closure level during load interaction situations. These results tend to indicate that the model can be applied to spectrum loading cases where stress ratios change with each stress level on a random basis.

The process of finding the number of overload cycles which cause saturation (the closure level attains the stabilized closure level for the overloads) is an iterative one. Further, the value of N_{sat} (described earlier) is markedly different for the two materials tested (i.e. $N_{sat} = 13$ for aluminum and 100 for titanium.) As a result, there were a limited number of test data gathered for the case where $1 < N_{OL} < N_{sat}$. Test results for all of the data obtained and predictions using the model are presented in Figures 169 through 171 for aluminum and 172 and 173 for titanium. It can be seen that the predictions follow the data very closely in all cases. These results indicate that the model properly accounts for the effect of the number of overloads on subsequent crack growth behavior, at least over the limited range of the data collected here.

Finally, tests were performed for the case of multiple overloads applied periodically, which is essentially a two-level block loading program. Test data and predictions from the crack closure model are presented in Figures 174 through 180 for aluminum and 181 through 187 for titanium. These tests were performed so that, for a given overload ratio, O/L, the relationship of the number of overload cycles to baseline cycles was varied. For example, in Figure 174, 100 overload cycles are followed by 1000 low-load cycles. In Figure 175, all values were multiplied by a factor of 5 so that 500 overload cycles were followed by 5000 low-load cycles. In Figure 176, the relationship of overload cycles to baseline cycles was changed from 1:10 to 1:5. In Figure 177, the loads were changed so that the stress ratio was 0.5 for the low-load cycles ($R = 0.05$ for all other cases). Figures 178 through 180 are similar to those of 174 through 176 except that the overload ratio is 1.8. For all cases, the predictions agree closely with the test data.

Test data and predictions for titanium subjected to similar multiple periodic overload sequences are presented in Figures 181 through 187. These tests are similar to those previously described for aluminum. In all cases, the predictions are accurate except for that in Figure 187. There, the stress ratio for the low loading was maintained at 0.7 and the predicted life is approximately 64% of the test life at a crack length of 1.4 inches. All predictions relative to the test data are, however, within the scatterband described in subsection 3.1.2 for this material.

Block Loading - A variety of tests were performed on both materials using three- and four-load level block loading. Test results and predictions for aluminum are shown in Figures 188 through 193. Figure 188 presents test data and a prediction by the model for a three-level high-low loading sequence. The predicted life is approximately 71% of the average of the two test lives at a crack length of 1.5 inches. Figure 189 presents similar results except

that the loading sequence is reversed to low-to-high. Again, the predicted life is about 71% of the test life at a value of $a = 1.5$ inches.

Block random loading was applied to the specimens shown in Figure 190. There, the load levels were maintained at the same values as for the low-high and high-low sequences. In those cases, a total of 6000 cycles was applied in each block.

For the randomized loading, each level was reduced by a factor of ten to a total of 600 cycles per block, for convenience in testing. These cycles were randomly ordered within the block, but each block was identical. In this case, the predicted life is about 53% greater than the average of the test lives at a crack length of 1.5 inches.

Figure 191 presents data and predictions for specimens subjected to low-high and high-low sequences, where the minimum load was maintained 500 lb. There, the stress ratio for the lowest load was 0.50 as compared to 0.05 for the previous cases. In addition, the load was reduced to zero at random intervals. This reduction is similar to a ground-air-ground loading cycle. The predictions neglect this zero load application and are based solely on the load values shown in the table in Figure 191. This was done as a convenience in making the predictions. However, it will be shown that the introduction of an occasional underload spike (or compression spike) has very little effect on specimen life. On this basis, the predictions which agree closely with the data are considered to be valid.

Figure 192 presents results for specimens subjected to the randomized spectrum. The single prediction nominally describes the average of the crack growth behavior for both specimens.

The results for the only four-level block loading test performed on aluminum are presented in Figure 193. The loads were identical to the values given in Figure 189 except that a single cycle of 1000 to 25 lb. was added to each block. The crack closure model predicts a life which is approximately 67% of the test life at $a = 1.5$ inches. At that crack length, the test life is 52 blocks which is identical to the life of Specimen AG-25-08 (Figure 189), where the initial crack length is nearly the same. The single cycle of 1000 lb. had negligible effect on the crack growth of Specimen AG-25-25 (Figure 193). The model predicts essentially the same result: 67% vs 71% of the test life at $a = 1.5$ inches.

The predictions obtained for titanium, using the model, are typically less accurate than those obtained for aluminum under nominally similar conditions. Figures 194 and 195 present data and predictions for specimens subjected to a three-level low-to-high block. The predictions are quite poor, yielding lives of 16% and 48% of the test values respectively. In Figure 196, a prediction is presented which is 51% of the average life for the two test specimens shown. There, the loading sequence was high-to-low. The low predictions in all three cases can be traced to the affected crack lengths caused by the higher loads. It is apparent that these values are too low, and that an

increase in their magnitudes would cause the average crack growth rates to decrease. Figure 197 presents a prediction and test values for specimens subjected to essentially the same loads as those in Figures 195 and 196. The differences are that the minimum load was not held constant in this case but was 10% of the maximum load in each level, and that the loads were applied in a randomized sequence, 600 total cycles to the block. There, the prediction is fairly good. In Figures 198 and 199, the load ranges were held constant, but the minimum load was increased to 400 lb. so that the stress ratio for the lowest loading was one-third. The loads were applied in ascending and descending order. The predictions are reasonably close to the data.

Figure 200 presents results for four-level block loading tests and predictions. Again, the model predicts short lives which are 42% and 55% of the test values for the high-low and low-high sequences respectively.

Typical Aircraft Spectra - Tests were performed on panel specimens to represent typical aircraft spectrum loading. The test results and predictions are presented in Figures 201 for aluminum and 202 for titanium. In this case, two predictions were made. The first neglected levels 63 and 64 of the spectrum, the first of which is applied once every six blocks and the second, once every eighteen blocks. The second prediction included the application of levels 63 and 64 once every block. The actual predicted life would lie somewhere between the two predictions. For the aluminum, the average of the two predictions is 58% greater than the test life at a half crack length of 0.7 inch. Again, the titanium prediction is short, the average being 42% of the test life at a half crack length of 0.9 inch.

Compression and Underload Spike Loads - One difficulty with currently-available models is that they do not accept compressive loads or stresses. Even for the case where the stress ratio for the base loading is greater than zero and a tensile overload is followed by a zero load (underload), these models neglect the underloads. The crack closure model accounts for these situations. However, all of the following examples are based on the crack closure data obtained from single tests at $R = -1$ for both materials. Considering this, the results obtained indicate that the concepts are basically sound.

Figures 203 and 204 present data and predictions for 2219-T851 panel specimens subjected to occasional compression spikes (single compression load cycles). In the first figure, the base stress range was 0.3 to 6 ksi tension. Compression spikes ranging from 3 to 12 ksi were applied in a quasi-random manner. The model overpredicts the test life by 20% at a half crack length of approximately 1.4 inches. It is interesting to note that a constant amplitude calculation for the base loading (6 ksi, $R = .05$) yields a life which is almost identical to the prediction. A similar calculation for $R = -1$ is also shown and yields about 85% of the test life at the same half crack length. The implication of these results is that the compression spikes have very little effect on the overall life. This is substantiated by the results shown in Figure 204 where, in this case, the model under-predicts the test life by about 18%. Although it is not shown, a constant amplitude calculation using

$S = 10$ ksi and $R = .05$ produces almost the same life as the prediction. The prediction errors of +20% and -18% are within normal data scatter.

The negligible effect of the compression spikes are caused by two separate effects. First, for a fully-reversed loading where $R = -1$ (or apparently for even lower values of R), the closure stress of Figure 101 does not decrease very much. At the base loading with $R = .05$, the closure level is about 41% of the maximum stress while, at $R = -1$, it is 34.7% of the maximum stress. In this case, the base closure stress is 4.1 ksi. After compression spike, it is 3.47 ksi and has only decreased by 10%. For values of R between -1 and zero, the difference is even smaller.

The second reason for the small effect of the compression spikes is that it takes about 13 cycles of the base loading for the closure level to regain its original value. These few cycles are an extremely small part of the overall life of the specimen.

Figure 205 presents similar test results and a prediction for a titanium specimen subjected to similar loading. At a half crack length of one inch, the model predicts a life which is 42% greater than the test life. In this case, it would appear that the compression spikes, ranging in value from $R = .5$ to $R = -2$, have some effect on the subsequent crack growth. This effect would be manifested in an increased crack growth rate subsequent to the application of a compression spike. However, Figure 206 indicates that this is not the case. There, crack length is plotted against cycles since the compression stress, ΔN_s . Data and constant amplitude calculations for 10 ksi and $R = .05$ are shown. It can be seen that the data do not generally exhibit a faster crack growth rate than normal immediately after the compression spike, but do exhibit a general, overall crack growth rate which is slightly faster than the calculated behavior. For example, starting at a half crack length of 0.5 inch, the data and calculated crack length differ by about 0.030 inch after 60,000 cycles. The average calculated crack growth rate is about 75% of the measured rate. These differences are cumulative, and account for most of the error in the prediction shown in Figure 205.

Figure 207 presents data for an aluminum specimen subjected to occasional tensile overload spikes followed by compression spikes. For the first three events, the tensile spike overload ratio is 1.5. It was shown earlier that, for aluminum, overloads of this magnitude have negligible effect on the subsequent crack growth. For the 4th, 5th and 6th events, the overload ratio is 2.1 for the tensile spikes. Overloads of this magnitude are expected to have a significant effect on subsequent crack growth rates. The data indicates that this is the case.

It is interesting to note that the compression spike did not reduce the retarding effect of the tensile overload for any of the nine events. This was verified by making another prediction which neglected all of the compression spikes. The result was identical to the prediction including those spikes. To understand the reason for this, follow the sequence of calculations

performed by the model for the 6th event where the tensile and compressive spikes are 12.6 and -18 ksi respectively.

- Prior to the spikes, the closure stress for 6 ksi, $R = .05$ is 2.47 ksi from Equations (16) and (21).
- Subsequent to the 12.6 ksi tensile spike where $R = .023$, the closure stress is 3.41 ksi by Equations (16), (21), (25) and (26a).
- For the compression spike, the minimum stress adjustment is used. The effective stress ratio is $-18/12.6 = -1.43$. As described earlier, this is treated as -1. From Equations (16) and (21) the closure stress would be 4.37 ksi. However, this value is greater than the existing value (3.41 ksi) and so that lower value is retained.

Therefore, the model predicts no effect of the compression spike, and this is substantiated by the data. In order for the compression spike to have any negating effect on the tensile spike, the tensile spike must be much larger, or be replaced by several spikes to achieve a higher closure stress. No tests of this type were performed, although data for similar tests, where the stress ratio for the base load was 0.5 and the compression spikes were replaced by underload spikes, were obtained. These will be discussed subsequently.

Figures 208 and 209 present data and predictions for aluminum specimens subjected to underload spikes followed by overload spikes, and overload/underload sequences respectively. The results are self-explanatory, the model predictions being within 17% of the test life in both cases.

Figure 210 presents data for the case discussed previously where multiple overloads are followed by an underload spike. Two predictions are shown. One includes the underload spikes following the overloads, and the other neglects them. The model differentiates between the two cases. Unfortunately, the data lies closer to the second prediction. These results are considered to be inconclusive and, in the absence of additional data, no firm conclusion on the effect of the underload spike can be reached.

One test was performed on a titanium panel specimen subjected to tension/compression and compression/tension sequences, the results of which are shown in Figure 211. It can be seen that the model overpredicts the test life by approximately 55% at a half crack length of about 1 inch. The model predicts that the compression spikes have no effect on a preceding tension spike (overload) by the procedure outlined earlier for aluminum. These results are also inconclusive since the closure function for negative stress ratios was defined by a single test. Further, the 55% error is within the scatter described in Section 3 of this report.

Titanium test results and predictions for specimens subjected to overload/underload, underload/overload, and multiple overloads followed by a single

underload, are presented in Figures 212 through 214. Like the aluminum results, the predictions agree closely with the data (greatest error 20 %) for all three cases.

Based on the results presented here, it is felt that the model accounts for compression and tension/compression interactions fairly well. This makes it possible to account for, rather than disregard, excursions to zero load and/or load reversals for typical aircraft spectra. It should be noted also that, in general, the application of occasional compression or underload spikes had little effect on the overall specimen life. Where they were preceded by a single overload cycle, they had minimal influence on aluminum, but did tend to offset the overload effects on titanium. Where an underload spike was preceded by multiple tensile overloads, it significantly reduced the retarding effects of the overloads in both materials.

It is suspected that compressive spikes, following single tensile overloads which are of sufficient magnitude, may negate at least partially the retarding effect of the overload. However, none of the specimens tested during this program had high enough single overloads to test this theory.

4.1.4 Crack Closure Model Logic Diagram

Figures 215 and 216 present the overall and detailed logic flow for the crack closure model. These charts are presented to provide additional clarification of the decision processes of the model. Certain functions are used in the charts and are described below. The significant equations are reproduced here for convenience.

$F(a)$ = Converts stress to stress intensity

$da/dN(\Delta K_{eff})$ = Crack growth rate based on ΔK_{eff} , Equation (19)

$C_f(R)$ = C_f as a function of R , Equation (21)

$Sc(\Delta a)$ = function for decreasing closure, Equation (22)

$\gamma(J)$ = function for increasing closure, Equation (26)

ρ = governing affected crack length

$$\frac{da}{dN} (\Delta K_{eff}) = C \left[\frac{(S_{max} - S_c) \cdot F(a)}{(1 - C_{f_0})} \right]^n \quad (19)$$

$$C_f(R) = C_{f_{-1}} + (C_{f_0} - C_{f_{-1}}) (1 + R)^p \quad (21)$$

$$S_c(\Delta a) = S_{c_1} - (S_{c_1} - S_{c_2}) \left(\frac{\Delta a}{\rho} \right)^B ; 0 \leq \Delta a \leq \rho \quad (22)$$

$$\gamma(J) = \gamma_1 + (1 - \gamma_1) \left(\frac{N_{OL} - 1}{N_{sat} - 1} \right) \quad (26)$$

$$\rho(S(\max)) = \frac{1}{2\pi} \left[\frac{F(a) \cdot S(\max)}{\sigma_y} \right]^2$$

The charts are self-explanatory and, coupled with the discussion in subsection 4.1.2 of this report, should allow convenient use of the model.

4.1.5 Basic Data Requirements

The crack closure model offers a greater sophistication and variety of loading options than currently available crack growth interaction mathematical models. As a result, the basic data required to use the model are more complex than for the other models. Additional data requirements center principally around the measurement of crack closure and the effects of number of overloads.

The crack closure model requires constant-amplitude crack growth rate data for at least three stress ratios. Two of these should be $R = -1$ and zero. The third stress ratio must be greater than zero, but less than the stress ratio cutoff value. If a value greater than the cutoff is used, an erroneous crack closure function will result. Unfortunately, there is no method of determining the cutoff value other than by obtaining crack growth rate data at various positive stress ratios and then comparing the results on a rate vs stress intensity range basis. Numerical procedures can be an aid in this effort. For example, Equation (1) can be used in conjunction with least squares and trial and error procedures to obtain q and R_{co} . Alternatively, the data can be plotted and the stress ratio cutoff value can be determined by inspection. The coefficient C and exponent n obtained from Equation (1) are used in Equation (19) to calculate crack growth rates.

The constant amplitude data are used as described in subsection 4.1.2 to obtain the closure Equation (21) as a function of the closure factors at $R = 0$ and -1 , (C_{f_0} and $C_{f_{-1}}$). There the crack growth rate data were used in

Equation (19a) to relate closure factors at stress ratios other than zero to the closure factor at R equal to zero. It should be noted that these data only relate the closure factors, and do not define their absolute values.

The magnitude of the closure factor at some stress ratio must be determined. A stress ratio of zero is suggested for convenience. However, as pointed out earlier, other values of stress ratio may be used with success except that R must be less than the cutoff value, R_{co} , to obtain a valid result.

The closure factor at the stress ratio selected may be measured using techniques similar to those described in subsection 2.4 of this report. It was pointed out there that experimentally-obtained values, based on the results of this program, generally exhibit considerable scatter. Comparatively small variations in the closure factor can produce large errors in predicted life, depending on the type of loading. As a result, an analytical method of determining the closure factor is suggested.

One method, outlined in Subsection 4.1.2, was used with success in this program. The technique employs Equation (22) and the numerical integration of Equation (19). The use of this technique requires the results from at least one test where the loading sequence is high-to-low. As described in Subsection 4.1.2, the method is iterative, but other useful data can be obtained. In addition to the closure factor, C_{f_o} , the affected crack length and the exponent B in Equation (22) can be obtained. Since these parameters are also required as input data, the proposed test serves a three-fold purpose.

Finally, data pertaining to the number of overloads must be obtained. As described in Subsection 4.1.2 (Effect of Single and Multiple Overloads on Subsequent Crack Growth), the crack closure model assumes that the closure stress varies linearly as a function of the number of overloads applied. The required input data are γ_1 and N_{sat} , which were described in relation to Equation (26). The parameter γ_1 is the effectiveness of a single overload cycle on increased closure level, while N_{sat} is the number of overload cycles required to achieve saturation.

These parameters are obtained from test results for different numbers of overload applications. Although the value of N_{sat} is generally unknown, the results from this program and other sources indicate that N_{sat} is from 10 to 20 cycles for aluminum alloys, and is approximately 100 for titanium. The test sequences shown in Figures 172 and 173, with the numbers of overloads altered to suit the material, provide a good range of values. The results from at least one single overload test are required to obtain γ_1 .

The analytical procedures used to obtain γ_1 and N_{sat} in this program are outlined below:

1. Obtain test data (a vs cycles) for different values of N_{OL} where the minimum stresses for both the overloads and baseline loading are zero or nearly zero.

2. Using the crack length vs cycles after the overload(s) and
3. The previously determined values of C_{f_o} , B and ρ ,
4. Let S_{c_1} in Equation (22) be an unknown.
5. Numerically integrate Equation (19) using different values of K_{c_1} (or S_{c_1}) until the calculated crack length vs cycles curve fits the data. Note that S_{c_1} must be greater than S_{c_2} in Equation (22).
6. Using the value of S_{c_1} obtained from a single discrete overload case, determine γ_1 from Equation (25), taking $N_{OL} = 1$. For the case where the minimum stresses are all zero, the closure stress after N_{sat} is C_{f_o} times the maximum overload stress.
7. The value of γ_1 must be greater than the reciprocal of the overload ratio, O/L . As mentioned earlier, unless the overload ratio for single overload application exceeds some minimum value, the overload has negligible effect on subsequent crack growth. The minimum values of O/L were found to be approximately 1.5 and 1.25 for 2219-T851 aluminum and Ti 6Al-4V titanium respectively. If γ_1 is approximately equal to the reciprocal of O/L , the test results are questionable and a larger overload ratio should be used.
8. The value of N_{sat} can be determined by plotting the ratio of S_{c_i} (or K_{c_i}) from Step 5 above to the stabilized closure stress for the overload against the number of applied overloads. This method is shown in Figures 126 and 127 where γ equals the ratio of the closure stress after N_{OL} overloads to the stabilized closure stress for the overloads. The value of N_{sat} is the value of N_{OL} for $\gamma = 1$.

To summarize, the data required as input for the crack closure model are:

- a. Crack growth rate data at three stress ratios. These yield the crack growth coefficient, C , and exponent, n .
- b. Closure factor at $R = \text{zero}$, C_{f_o}

- c. Closure factor at $R = -1$, C_{f-1} and exponent p (obtained from a. and b.).
- d. Affected crack length, ρ , and exponent, B , for use in Equation (22).
- e. Parameters γ_1 and N_{sat} for Equation (26).

4.2 RESIDUAL FORCE MODEL

4.2.1 Concepts

The effective stress range approach seems to be the most straightforward method of explaining crack growth interaction effects. For example, it was shown in Ref. 5 that the Wheeler Model (Ref. 10) can be related to the Effective Stress Retardation Model (Ref. 11). The Effective Stress Retardation Model can, in turn, be related to our crack closure model. Since all of these models can predict certain crack growth interaction effects, it was thought that a model based on the distribution of residual stresses left in the wake of a propagating crack could provide a basic understanding of the overall crack growth phenomenon. As a result, the Residual Force Model was developed. Although some analytical problems related to certain crack growth interaction effects were encountered, the basic concept is appealing since it may ultimately lead to a prediction model which is less empirical than those currently available. The development of the Residual Force Model and the results obtained using it are described below.

4.2.2 Application to Model

Elber (Ref. 15) proposed that the phenomenon of crack closure could be explained by the existence of residual tensile strains left in the wake of a propagating crack. These deformations cause interference along the fracture surface and, as the remotely applied stress, S , is reduced to zero, the crack closes at some positive stress. The stress distribution caused by the crack face interference tends to prop the crack open. Figure 217a shows this concept schematically. A crack of half length a_0 is subjected to a remote tensile stress, S , which causes a plastic zone of extent ρ_y . When the remote stress, S , is removed, a reverse plastic zone of extent, r_y , remains defining an area of compressive residual stresses. In Figure 217b, the crack has propagated to a new half length, a , and the crack tip is part way through the envelope of compressive residual stresses developed as the crack propagates. Figure 217c shows a residual stress distribution, S_r , which represents the integrated value of the residual forces existing from a_0^r to a . Extending this concept to the case where the crack has propagated a long distance, (Figure 217d), the crack is now subjected to the residual stress, S_r , along the entire length of its

faces. During the application of remote stress S , the crack tip stress intensity is composed of two parts:

$$K = S \sqrt{\pi a} \quad (28)$$

and

$$K_r = S_r \sqrt{\pi a} \quad (29)$$

For the case when $S > S_r$, the effective stress intensity is given by superposition as:

$$\Delta K_{\text{eff}} = (S - S_r) \sqrt{\pi a} \quad (30)$$

If the crack can propagate only when it is open, as proposed by Elber, then ΔK_{eff} is the stress intensity range which should be employed to compute crack growth.

In an effort to define the magnitude and extent of the residual stress, S_r , the following assumptions were made.

- S_r is proportional to S and may be proportional to S/σ_y where σ_y is the material tensile yield stress.
- S_r is related to the applied stress ratio, although no correlation has been found.
- The extent of S_r due to the application of one cycle of tensile loading is one quarter of the maximum plastic zone size, as suggested by Rice (Ref. 20) and is given by

$$r_y = \beta \left(\frac{K}{2\sigma_y} \right)^2 \quad (31)$$

where

$$\beta = \frac{1}{2\pi} \text{ for plane stress}$$

and

$$\beta = \frac{1}{6\pi} \text{ for plane strain}$$

Initially, it seemed that S_r should be equal to the material compression yield stress. However, a review of Equations (28) - (30) revealed that the crack could only be opened by the application of $S > \sigma_y$. Experience indicates that this is not the case and that S_r must therefore be something less than σ_y . It was decided that, since the value of S_r was not known, it would be taken as:

$$S_r = \alpha S \quad (32)$$

Further, initial analyses indicated that S_r should be proportional to the ratio of applied stress over the yield stress:

$$S_r = \alpha S \left(\frac{S}{\sigma_y} \right) \quad (33)$$

If the residual force proposition holds, then Equation (33) implies that all materials should show a stress level effect on crack growth rates, even during constant amplitude crack growth. Some materials strongly exhibit such an effect, while many materials do not. Because our interaction studies using the Residual Force Model have to date been limited to 2024-T3 which is an insensitive material, Equation (32) has been used.

An interesting effect produced by this model is that delayed retardation is predicted. It was found that the delay period depends on the number of overloads applied and that as the number of overloads increases to the saturation value, the delay period decreases to zero. In addition, the model predicts acceleration when changing from a low load to a high load. These results are included in the following discussion of the development of the working model.

Figure 218a shows a crack which has propagated to a half length, a_0 , under the influence of remote stress S_1 , which has caused the residual stress S_{r1} to be developed. At half length a_0 , a remote stress S_2 (where $S_2 > S_1$) has been applied and then removed. The plastic zone ρ caused by S_2 is shown, along with the reverse plastic zone r_y which exists when S_2 returns to zero. The crack then continues to propagate under the influence of S_1 .

Immediately after the application of S_2 , and neglecting any growth during the application of S_2 , the residual forces (stresses) acting behind the crack are those caused only by the application of S_1 , and the residual stress intensity is the same as for the constant-amplitude case for S_1 . However, as the crack begins to propagate into the reverse plastic zone caused by S_2 , the residual forces S_{r2} begins to act behind the crack tip, and an increase in K_r occurs. When the crack half length is, $a + r_y$, the influence of S_{r2} is most prominent and K_r is a maximum. As the crack continues to propagate, S_{r2} becomes remote from the crack tip so that its effect on K_r is reduced, and when the crack half length is large relative to $a + r_y$, the effect of S_{r2} on K_r approaches zero.

If a crack propagation law of the Paris type is used, so that:

$$\frac{da}{dN} = C(\Delta K_{eff})^n \quad (34)$$

$$\text{and} \quad \Delta K_{eff} = K - K_r \quad (35)$$

then ΔK_{eff} is smallest when the crack half length is $a + r_y$ and da/dN is the smallest at the same point. Therefore, the minimum crack growth rate occurs at a point r_y , from where the overload was applied and delayed retardation has been represented by the model. Figure 218b shows the resulting crack growth rate schematically.

To test this approach, an equation of the form

$$K_r = S_r \sqrt{\frac{a}{\pi}} \left[\sin^{-1}\left(\frac{c}{a}\right) - \sin^{-1}\left(\frac{b}{a}\right) - \sqrt{1 - \left(\frac{c}{a}\right)^2} + \sqrt{1 - \left(\frac{b}{a}\right)^2} \right]$$

was taken from Ref. 21. The force distribution for use in this expression is shown in Figure 219. The equation given in Ref. 21 has been multiplied by two to account for forces acting on both surfaces of the crack. At any crack length, a , it is a simple matter to sum the effects of the various residual stress distributions over the crack half length from zero to a , to obtain the total K_r .

One drawback of this approach, is that it predicts that an overload affects the residual stress intensity even after the crack has propagated several plastic zone sizes. Recent experimental investigations, including Ref. 4, indicate that this is not the case and that the effect of the overload should have been dissipated by the time the crack has propagated through a distance approximately equal to the plastic zone caused by the overload. In an effort to circumvent this drawback, it was decided to include only the effect of those residual stresses which extend back from the crack tip a distance equal to the distance from the crack tip to the elastic-plastic interface. This approach forces the residual stress intensity to return to a constant-amplitude value when the crack has propagated through one plastic zone. Although this assumption is open to question, some justification might be found in the fact that those forces closest to the crack tip have the most effect on crack tip behavior.

An equation for the effective stress intensity range, ΔK_{eff} , was finally formed as

$$\Delta K_{eff} = S \sqrt{\pi a} - \sum_{a - \rho_y}^a \left\{ S_{r_i} \sqrt{\frac{a}{\pi}} \left[\sin^{-1} \left(\frac{c_i}{a} \right) - \sin^{-1} \left(\frac{b_i}{a} \right) - \sqrt{1 - \left(\frac{c_i}{a} \right)^2} + \sqrt{1 - \left(\frac{b_i}{a} \right)^2} \right] \right\} \quad (36)$$

In order to relate ΔK_{eff} to the applied ΔK , it is necessary to introduce a modifying factor of the form

$$\Gamma = 1 - \frac{\alpha}{\pi} \left[\frac{\pi}{2} - \sin^{-1} \left(\frac{a - \rho_y}{a} \right) + \sqrt{1 - \left(\frac{a - \rho_y}{a} \right)^2} \right] \quad (36a)$$

as a denominator in the crack growth equation such that

$$\frac{da}{dN} = C \left(\frac{\Delta K_{eff}}{\Gamma} \right)^n$$

$$= C \left\{ \frac{S \sqrt{\pi a} - \sum_{a - \rho_y}^a \left\{ S_{r_i} \sqrt{\frac{a}{\pi}} \left[\sin^{-1} \left(\frac{c_i}{a} \right) - \sin^{-1} \left(\frac{b_i}{a} \right) - \sqrt{1 - \left(\frac{c_i}{a} \right)^2} + \sqrt{1 - \left(\frac{b_i}{a} \right)^2} \right] \right\}}{1 - \frac{\alpha}{\pi} \left[\frac{\pi}{2} - \sin^{-1} \left(\frac{a - \rho_y}{a} \right) + \sqrt{1 - \left(\frac{a - \rho_y}{a} \right)^2} \right]} \right\}^n \quad (37)$$

For the constant amplitude case, this equation reduces to:

$$\frac{da}{dn} = C \left\{ \frac{S \sqrt{\pi a} - S_r \sqrt{\frac{a}{\pi}} \left[\frac{\pi}{2} - \sin^{-1} \left(\frac{a - \rho_y}{a} \right) + 1 - \sqrt{\left(\frac{a - \rho_y}{a} \right)^2} \right]}{1 - \frac{\alpha}{\pi} \left[\frac{\pi}{2} - \sin^{-1} \left(\frac{a - \rho_y}{a} \right) + \sqrt{1 - \left(\frac{a - \rho_y}{a} \right)^2} \right]} \right\}^n \quad (38)$$

or

$$\frac{da}{dN} = C \left[S \sqrt{\pi a} \right]^n \quad (38a)$$

when

$$S_r = \alpha S$$

Obviously, these expressions do not account for stress ratio or stress level effects. However, it is felt that when an expression relating S_r to stress ratio and/or level is developed, it could be incorporated as a simple modification.

4.2.3 Results and Discussion

The model was tested using data which strongly exhibited delayed retardation. As stated earlier, this phenomenon was not strongly evident for the materials tested during this program. Therefore, data from the literature were employed.

Figure 220 shows data for 2024-T3 aluminum taken from Ref. 4 for several loading sequences, along with the predictions using this model. Certain liberties taken for convenience in the analysis procedure were:

- Test data were constant K; analysis was constant stress.
- Test specimens were compact tension; analysis assumes an infinite center cracked panel.

- Test stress ratios were .05 for $\Delta K = 15 \text{ ksi}\sqrt{\text{in.}}$ and .03 for $\Delta K = 22.5 \text{ ksi}\sqrt{\text{in.}}$; analysis assumes all stress ratios equal to zero.

In light of the limited change in crack length, it is felt that the influences of these modifications were minimal.

Figure 220 shows crack growth rate data vs crack growth increment after a load change for four different loading conditions:

- 1) Number of overload cycles equal to zero ($N_{OL} = 0$, constant amplitude)
- 2) $N_{OL} = 1$
- 3) $N_{OL} = 450$
- 4) $N_{OL} = 9000$

The dashed lines represent predictions for $N_{OL} = 1$ and ≥ 300 . The basic trend is evident and shows, for the case of $N_{OL} = 1$, a minimum crack growth rate when Δa is .08 inch. A comparison of the predicted and test curves indicates that the curve shapes and magnitudes agree fairly well. In the case of the Residual Force Model, when the limiting case of 300 or more overloads is applied, a crack growth rate is achieved which is much lower than the data suggests.

One characteristic of the Residual Force Model is that, as the number of overloads is increased, the initial crack growth rate is reduced, until saturation is reached, and then no further decrease in rate is observed regardless of the number of applied overloads. For the parameters α and β chosen for this analysis, saturation occurred after about 300 overloads had been applied. Referring to Figure 220, one can see that this is not consistent with the data, which indicate saturation sometime after 450 overloads.

A further difference is that the data indicate that a minimum crack growth rate always seems to occur at about the same Δa , while the model predicts less delay for more overloads, reaching a limit of no delay at saturation.

The irregularities which appear in the Residual Force Model curves are attributed to the selection of the dimension $a_p - a$ in Equations (36-38). In the computer program developed to generate these predictions, a_p was updated continuously so that when the plastic zone extent from S_1 exceeded that from S_2 , a discontinuity occurred.

Figure 221 shows a case from Ref. 4 where the crack growth rate vs distance after load change is plotted for a low-high loading. The plots begin at the change from $\Delta K = 15 \text{ ksi } \sqrt{\text{in.}}$ to $22.5 \text{ ksi } \sqrt{\text{in.}}$. Here, the predictions are based on the same values of α and β used for the delayed retardation cases. Prediction and test agree fairly well.

In order to extend the model to more complex loading cases, an integration scheme was introduced into the computer program. This method is similar to that suggested by T.R. Brussat (Ref. 22) and enables rapid calculation of crack growth for specimens subjected to block loading.

It is assumed that the crack growth per block, da/dB , can be related to the crack size, a , by the expression:

$$\frac{da}{dB} = C' a^{n'} \quad (39)$$

The two parameters, α and β , must be obtained prior to calculating a vs B . In its current stage of development, the model requires at least one spectrum test in addition to constant-amplitude data to evaluate α and β .

The evaluation can be made by comparing predicted and experimental crack growth curves under spectrum loading for various assumed values of α and β , and thereby determine the best-fit values of α and β . It is simpler, however, to compare predicted and experimental values of crack growth-rate at a few (at least two) crack lengths, for various assumed values of α and β , and determine the best-fit values of α and β in this way.

For example, the crack growth-rate data from a spectrum test are plotted as in Figure 222. By trial-and-error, values of α and β are determined which, when substituted into the Residual Force Model, result in calculated values of da/dB that lie close to the test data in the range of interest. (Two such points are shown by the dark triangles in Figure 222, corresponding to $\alpha = 2.6$ and $\beta = 0.1$.) These calculations require that test data describing the crack growth behavior of the material under constant amplitude loading also be available.

The simplifying assumption is then made that the crack growth-rate curve for the particular loading spectrum being considered can be approximated by a straight line (see Equation 39) drawn through the two calculated values of da/dB . The particular straight line shown in Figure 222 is defined by

$C' = 1.138 \times 10^{-3}$ and $n' = 2.263$ in Equation (39). This crack growth-rate equation is then easily integrated to give a crack growth equation (a vs B) which can be directly compared with the test curve.

Comparisons of predicted and experimental curves of a vs B are shown in Figure 223 for various loading spectra taken from Ref. 23. (The da/dB data in Figure 222 were obtained from the No.3 test curve in Figure 223.) For all cases of spectrum loading, the previously determined values of $\alpha = 2.6$ and $\beta = 0.1$ were assumed to apply. However, the calculated crack growth-rates are

different for the different loading spectra, so that the values of C' and n' in Equation (39) vary from spectrum to spectrum. These values are tabulated in Table 16. The crack growth curves calculated on the basis of these tabulated values of C' and n' are shown by the dashed lines in Figure 223. These calculated curves compare favorably with the test curves. Even better agreement might be possible if various additional factors were considered, such as finite-width corrections and non-linearity in the observed crack growth-rate behavior. With regard to the latter, efforts involving more sophisticated equations (in lieu of Equation 39) produced better approximations to the actual data in Figures 222 and 223, but all require the program to produce at least three values of $\frac{da}{dN}$. Many of the resulting expressions could not be integrated in a closed form. As a result, the program retained the simple form of Equation (39).

During an attempt to predict the data of Reference 24, it was found that the model would not produce sufficient retardation to fit the data. The reasons for this are outlined below.

The numerator of Equation (37) represents the effective stress intensity range ($\Delta K_{\text{eff}} = K_{\text{max}} - K_r$), while the denominator was introduced to normalize the total expression so that constant-amplitude conditions are represented when appropriate.

The variable S_{r_i} represents the residual stresses distributed behind the crack tip. The dimensions b_i and c_i define the limits of the distributions of S_{r_i} . The value of α may be varied to increase or decrease K_r . The residual stresses are summed over the distance $a - r_y$ to a , so that K_r may also be varied by varying the reversed plastic zone size r_y .

In general, increased retardation is obtained by increasing α while the duration of the retardation is controlled by r_y . However, the denominator of Equation (37) must always be greater than zero. As a result, it can be seen that α is limited by the reversed plastic zone size r_y , and must be less than some value, α_{max} , for a given value of r_y .

If

$$a_r = a - r_y, \quad (40)$$

then

$$\alpha_{\text{max}} \geq \frac{\pi}{\frac{\pi}{2} - \sin^{-1} \left(\frac{a_r}{a} \right) + \sqrt{1 - \left(\frac{a_r}{a} \right)^2}} \quad (41)$$

The value of α_{\max} ranges from 1.22 for $a_r/a = 0$ to ∞ for $a_r/a = 1$. Since the reversed plastic zone size is generally small relative to a , a_r/a is generally smaller than, but close to, unity. As a result, α_{\max} may usually be fairly large. However, the data of Reference 24 could not be fitted for $0 < \alpha \leq \alpha_{\max}$.

For cases where the crack growth rate is small, the effective stress intensity range should be small, and therefore α should be large. However, as α increases, the denominator of Equation (37) decreases, so that there may be a limit to the minimum value of Equation (37). In some cases, this minimum value may not be sufficiently small to yield the proper crack growth rates. The form of Equation (37) must therefore be modified.

A secondary constraint occurs due to the last term in the denominator of Equation (37):

$$\sqrt{1 - \left(\frac{a - r_y}{a}\right)^2} \quad (42)$$

For the simple case of a single cycle of overload, the reversed plastic zone radius, r_y , is set by the overload:

$$r_y = \beta \left(\frac{S_{OL} \sqrt{\pi a}}{\sigma_y} \right)^2 \quad (43)$$

Some data have indicated that the affected crack growth increment over which transient effects (crack growth rates higher or lower than normal) occur is not necessarily equal to the theoretical plastic zone radius. Because of this, the coefficient β in Equation (43) may be varied to match the observed affected length and r_y may be larger or smaller than the plane stress or plane strain plastic zones.

Substituting Equation (43) into (42):

$$\sqrt{1 - \left(\frac{a - r_y}{a}\right)^2} = \sqrt{1 - \left[\frac{a - \beta \left(\frac{S_{OL} \sqrt{\pi}}{\sigma_y} \right)^2 a}{a} \right]^2} \quad (42a)$$

The term

$$\frac{a - \beta \left(\frac{S_{OL}}{\sigma_y} \sqrt{\pi} \right)^2}{a}$$

should always be positive and less than 1, or:

$$0 < 1 - \beta \left(\frac{S_{OL}}{\sigma_y} \sqrt{\pi} \right)^2 < 1 \quad (44)$$

The second limit is trivial and requires that

$$\beta \left(\frac{S_{OL}}{\sigma_y} \right)^2 > 0 \quad (44a)$$

while the first term requires

$$\frac{S_{OL}}{\sigma_y} < \sqrt{\frac{1}{\pi\beta}} \quad (44b)$$

The relation between the plastic zone size coefficient, β , and S_{OL}/σ_y is generally not a significant constraint. For cases where the data indicate that the affected length for transient effects might be several times the theoretical plastic zone radius, Equation (44b) could be a too-restrictive constraint.

These constraints suggest that the form of Equation (37) is incorrect. Alternative forms were considered, but no definitive result was achieved. Further, this model, in its current form, cannot account for stress ratio or compressive load effects on subsequent crack growth. Finally, it is currently necessary to assume the magnitudes and distributions of the residual stresses. However, new developments in the field of finite element analysis of crack problems, notably References 16 and 25, indicate that these difficulties might be overcome analytically. The possibility of modifying the residual stresses, because of environmental variations like temperature cycles, appears attractive. With these considerations in mind, the Residual Force Model retains its basic appeal.

5 - SUGGESTIONS FOR FUTURE EFFORTS

A logical result of any program such as this is that new ideas are germinated. Such was the case for this program. It was found that there were certain bits of information which would have been desirable, but which were not included in the test program and which could not be deduced from the data available. In addition, there are programs which would be logical extensions of the work reported here. The following is a list of items which might be considered for inclusion of future Air Force developmental programs. The list is not arranged according to any priorities or our consideration of their importance.

- Investigation of thickness effects on crack growth interaction. This would consist of an analytical and experimental program to determine whether thickness affects plastic zone sizes as they are used for modeling purposes.
- Experimental program to determine the influence of the number of overloads on affected crack length and, if applicable, the extent of that influence.
- Experimental program to extend the validity of the Crack Closure Model to aircraft structural materials other than those tested under the current program. This would entail performing a specific set of tests to determine the factors required to use the model. Variable-amplitude tests might be included for verification purposes.
- Analytical and experimental program to extend the Crack Closure Model to other environments and loading regimes. These might include the effect of temperature cycles on crack growth retardation and the effect of delay time periods where, after an overload, the crack is maintained at zero or other loads for some specified period. This program might include some of the concepts of Reference 11.
- A program to obtain greater insight into the effects of compression loading under constant- and variable-amplitude loading conditions with the objective of updating the crack closure or other models.
- An analytical program to include crack growth under sustained loading in existing mathematical models.

- Further investigations into crack growth for the type of tests referred to as single periodic overloads. This type of loading was the only one to escape a reasonable prediction by the model. Logically, any insight obtained during such an investigation might reveal similar loading sequences which are not handled properly by the model.

6 - OBSERVATIONS AND CONCLUSIONS

This program has provided considerable insight into the phenomenon of crack growth during a variety of loading sequences. As a result, a variety of crack growth interaction effects can be predicted with reasonable confidence. Principal among these are the effects of compression, number of overloads, overload ratio and crack length affected by an overload or overloads. With the inclusion of the mathematical model developed during this program in the CRACKS 2 computer program, and through the distribution capability of AFFDL, it is felt that a large number of organizations will have access to a powerful predictive tool.

The following conclusions have been reached or verified and quantified as a direct result of investigations performed during this program:

- (1) A stress ratio effect on crack growth rate exists for both materials investigated.
- (2) Crack closure concepts explain a variety of crack growth interaction effects.
- (3) Crack closure levels can be obtained analytically through the use of crack growth rate data.
- (4) The number of overloads which causes maximum retardation is approximately 13 for 2219-T851 aluminum and approximately 100 for Ti 6Al-4V titanium.
- (5) The ratio of the crack closure level after one overload to the stabilized overload closure level is nominally 0.67 for aluminum and 0.8 for titanium.
- (6) During the application of a number of overloads, the increase in the closure level is proportional to the number of overloads applied, up to the saturation (stabilized) closure level for the overloads.
- (7) The crack length affected by the application of one or more overloads is proportional to the theoretical plastic zone radius of the overload.
- (8) The application of occasional compression or underloads has negligible effect on subsequent crack growth rates.

- (9) The application of a compression or underload spike preceding an overload has negligible effect on subsequent crack growth rates.
- (10) The application of a compression or underload spike following one or more overload applications may negate the effect of the overload on subsequent crack growth rates.
- (11) The application of a few cycles of load, where the new minimum load is less than the preceding minimum load, causes an almost immediate decrease in the crack closure level.
- (12) Under steady-state conditions, the ratio of the closure level to the maximum applied stress (or load) is a function of the steady-state stress ratio.
- (13) Crack growth retardation is the most significant interaction effect which occurs during variable amplitude loading.
- (14) Acceleration (faster than constant-amplitude growth) can be classified as a second-order effect.
- (15) The data obtained during this program did not reveal whether or not delayed retardation is a significant consideration for crack growth interaction effects.
- (16) Stable tear, which occurred during high K applications for 2219-T851 aluminum, masked some interaction effects based on surface measurements.
- (17) The stable tear threshold stress intensities were approximately $30 \text{ ksi}\sqrt{\text{in.}}$ and $72 \text{ ksi}\sqrt{\text{in.}}$ for aluminum and titanium respectively.
- (18) Neither the Wheeler nor Effective Stress Retardation models can account for several crack growth interaction effects.
- (19) The crack closure model developed during this program accounts for:
 - Effect of stress ratio, $R = S_{\text{min}}/S_{\text{max}}$, on constant amplitude crack growth.
 - Effect of maximum overload stress, S_{OL} , on subsequent retarded growth.
 - Effect of previous minimum stress relative to current minimum stress on subsequent growth.
 - Effect of number of overload cycles, N_{OL} on subsequent retarded growth
 - Effect of compression on both constant-amplitude and variable-amplitude growth.

7 - REFERENCES

1. "Military Specification, Airplane Damage Tolerance Requirements", MIL-A-83444 (USAF), 2 July 1974.
2. Roberts, R. and Schmidt, R.A., "Observations of Crack Closure", International Journal of Fracture Mechanics", Vol. 8, No. 4, 1972.
3. Hudson, C. Michael, "Effect of Stress Ratio on Fatigue-Crack Growth In 7075-T6 and 2024-T3 Aluminum-Alloy Specimens", NASA TN D-5390, August 1969.
4. Trebules, V.W., Roberts Jr., R., and Hertzberg, R.W., "Effect of Multiple Overloads in Fatigue Crack Propagation in 2024-T3 Aluminum Alloy," ASTM STP 536, July 1973.
5. Corbly, D.M. and Packman, P.F., "On the Influence of Single and Multiple Peak Overloads on Fatigue Crack Propagation In 7075-T6511 Aluminum," Journal of Engineering Fracture Mechanics, Vol. 5, 1973.
6. Schmidt, R.A. and Paris, P.C., "Threshold for Fatigue Crack Propagation and the Effects of Load Ratio and Frequency", ASTM STP 536, 1973.
7. Hall, L.R., Shah, R.C. and Engstrom, W.L., "Fracture and Fatigue Crack Growth Behavior of Surface Flaws and Flaws Originating at Fastener Holes," AFFDL-TR-74-47.
8. "Fracture Toughness Evaluation by R-Curve Methods", ASTM STP 527, 1973.
9. McClintock, F.A. and Irwin, G.R., "Plasticity Aspects of Fracture Mechanics," ASTM STP 381, 1964.
10. Wheeler, O.E., "Crack Growth Under Spectrum Loading," Report No. FZM-5602, General Dynamics Corporation, Fort Worth Division, June 1970.
11. Willenborg, J., Engle, R. and Wood, H.A., "A Crack Growth Retardation Model Using an Effective Stress Concept," Technical Memorandum 71-1FBR, Air Force Flight Dynamics Laboratory, WPAFB, January 1971.
12. Gallagher, J.P. and Hughes, T.F., "Influence of Yield Strength On Overload Affected Fatigue Crack Growth Behavior in 4340 Steel, AFFDL-TR-74-27, June 1974.
13. Jonas, O. and Wei, R.P., "An Exploratory Study of Delay in Fatigue Crack Growth," International Journal of Fracture Mechanics, Vol. 7, No. 1, March 1971.

14. Wei, R.P. and Shih, T.T., "Delay in Fatigue Crack Growth," Lehigh University Publication.
15. Elber, W., "The Significance of Fatigue Crack Closure," ASTM STP 486, 1971.
16. Newman Jr., J.C. and Armen Jr., H., "Elastic-Plastic Analysis of a Propagating Crack," Paper 74-366, AIAA/ASME/SAE 15th Structures, Structural Dynamics and Materials Conference, Las Vegas, Nevada, April 1974.
17. Shih, T.T. and Wei, R.P., "A Study of Crack Closure in Fatigue," NASA CR-2319.
18. Hudson, C. Michael and Raju, K.N., "Investigation of Fatigue Crack Growth Under Simple Variable-Amplitude Loading," NASA TN D-5702, March 1970.
19. von Euw, E.F.J., Hertzberg, R.W. and Roberts, R., "Delay Effects in Fatigue Crack Propagation", ASTM STP 513, 1972.
20. Rice, J.R., "Mechanics of Crack Tip Deformation and Extension by Fatigue", ASTM STP 415, 1966.
21. Paris, P.C. and Sih, G.C., "Stress Analysis of Cracks", ASTM STP 381, 1965.
22. Brussat, T.R., "Rapid Calculation of Fatigue Crack Growth by Integration", ASTM STP 559, 1974.
23. Porter, T.R., "Method of Analysis and Prediction for Variable Amplitude Fatigue Crack Growth", Engineering Fracture Mechanics, Vol. 4, No. 4, 1972.
24. Raju, "Effect of Exposure to Elevated Temperatures on Delay in Crack Growth due to a High Stress Cycle", International Journal of Fracture Mechanics, Vol. 8, 1972.
25. Newman, Jr., J.C., "Finite-Element Analysis of Fatigue Crack Propagation-Including the Effects of Crack Closure", Doctoral Thesis, Virginia Polytechnic Institute, 1974.

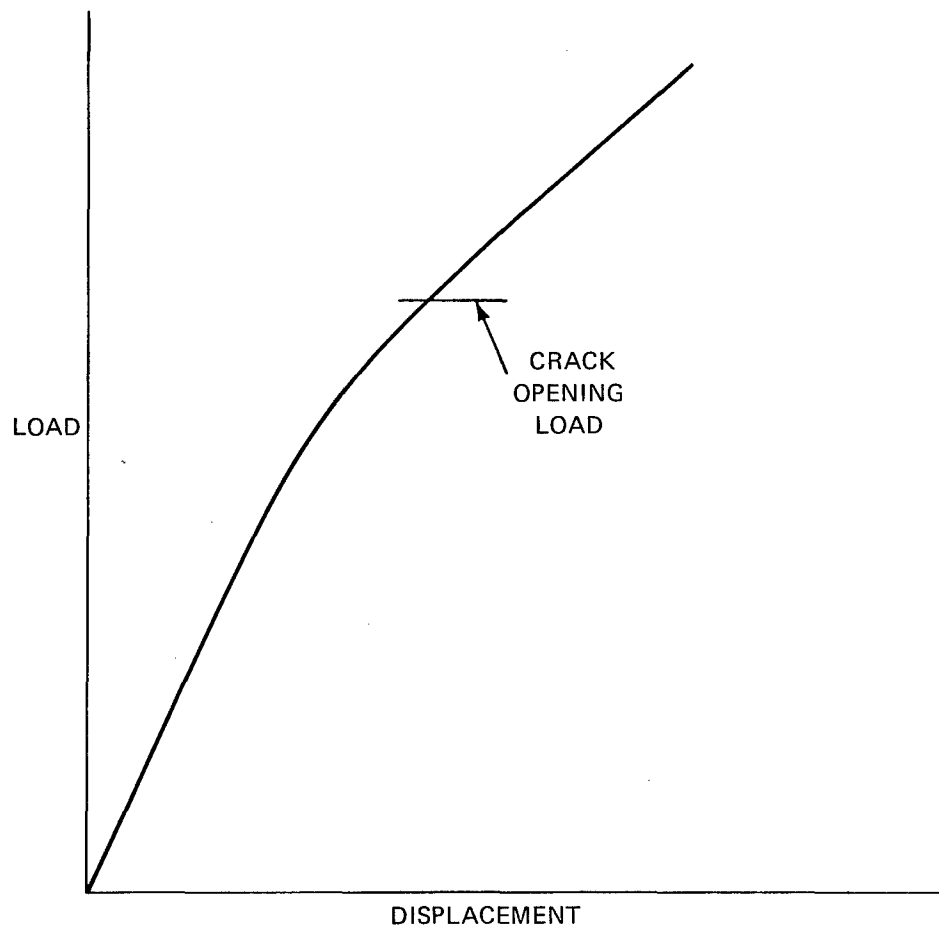


Fig. 3 Load vs Displacement Trace

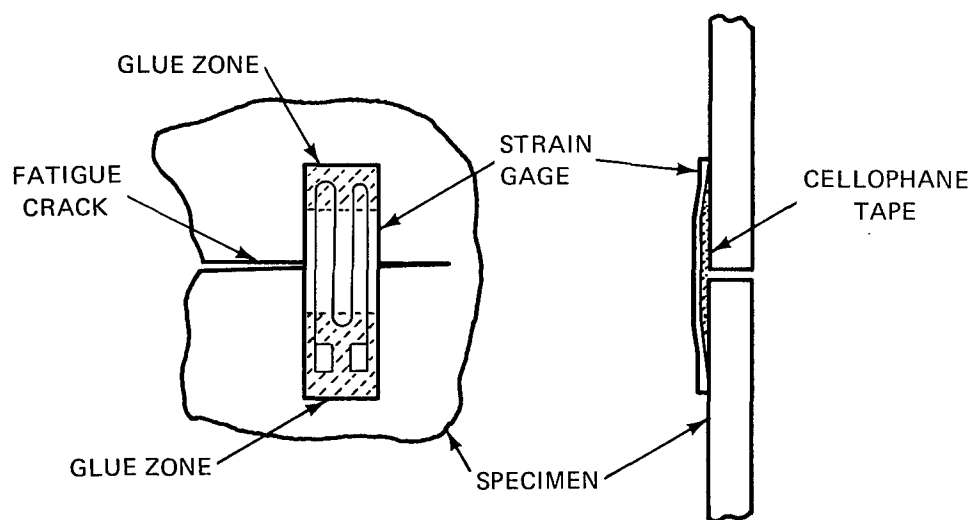


Fig. 4 Schmidt's Strain Gage Technique for Closure Measurements

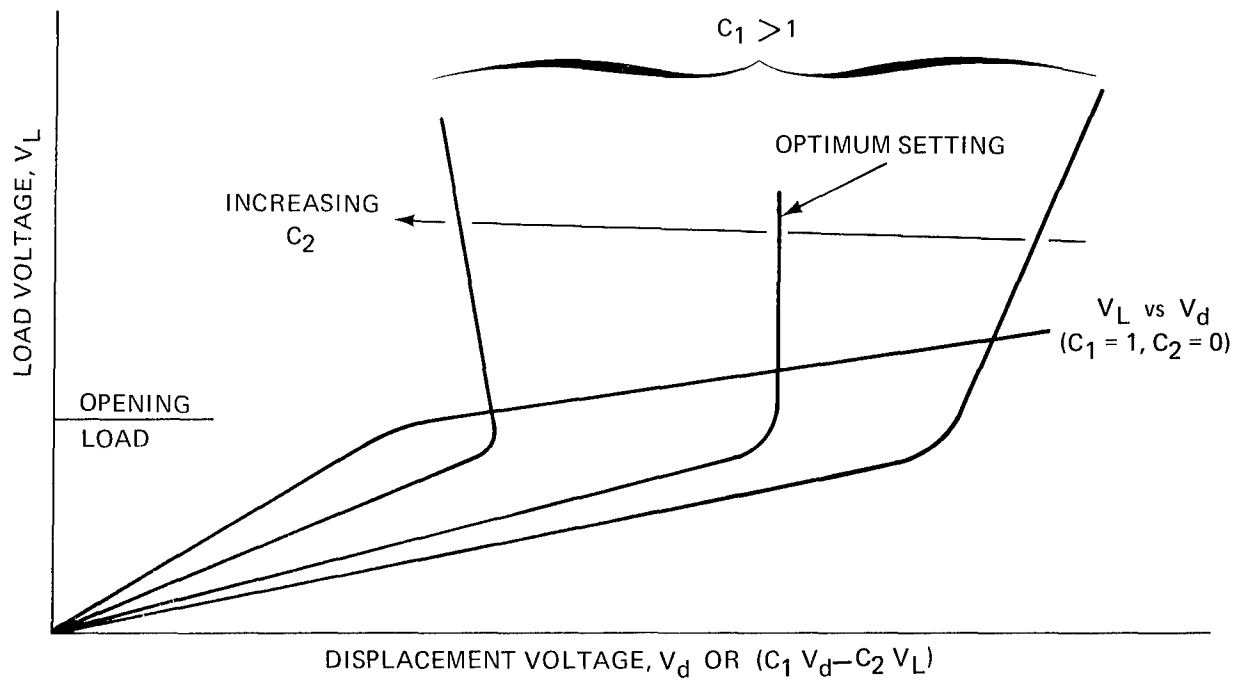


Fig. 5 Load vs Displacement Voltages

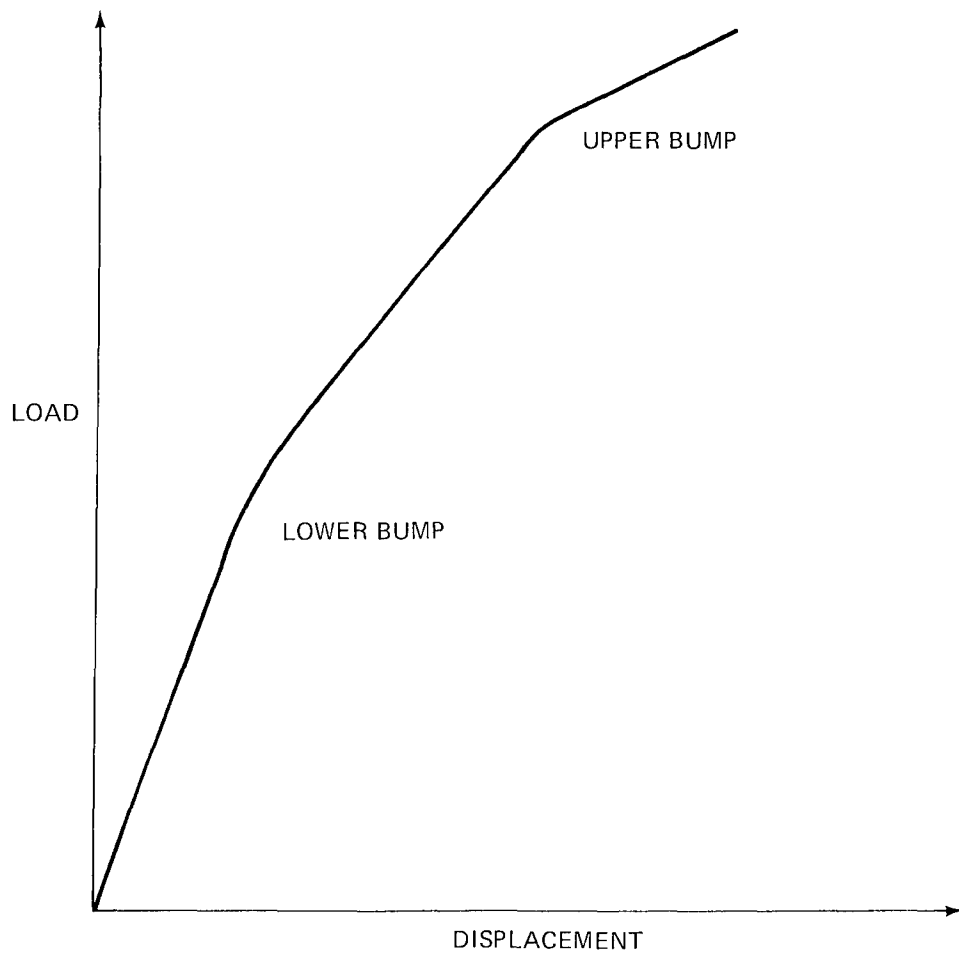
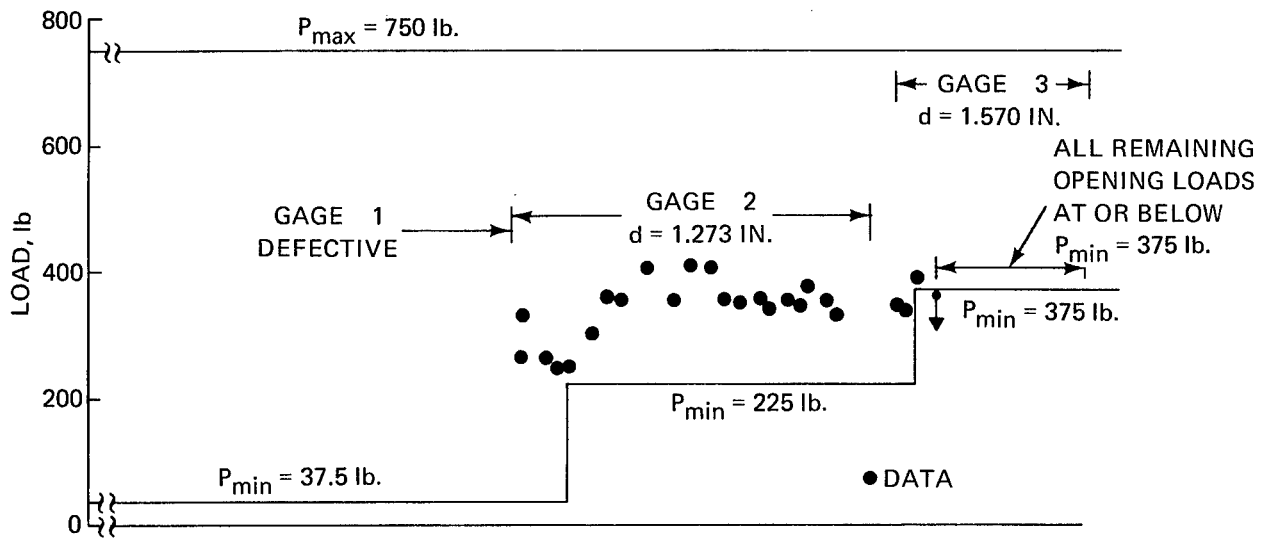
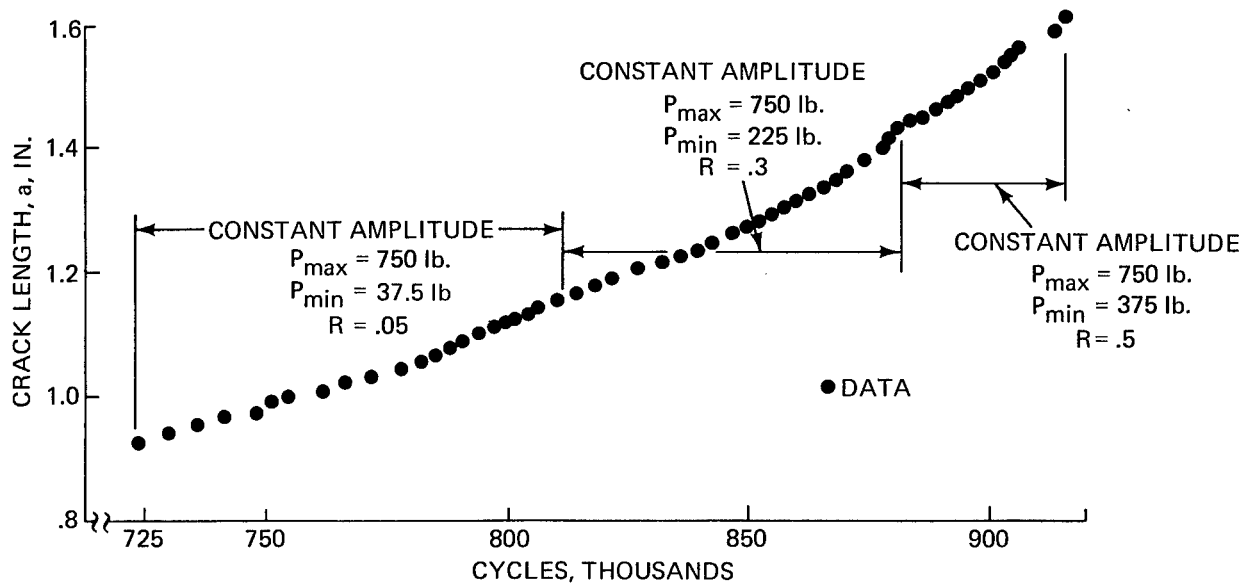


Fig. 6 Load vs. Displacement Trace

Ti-6Al-4V
SPECIMEN TD-25-25
CTA, W = 2.5 IN., t = .25 IN.

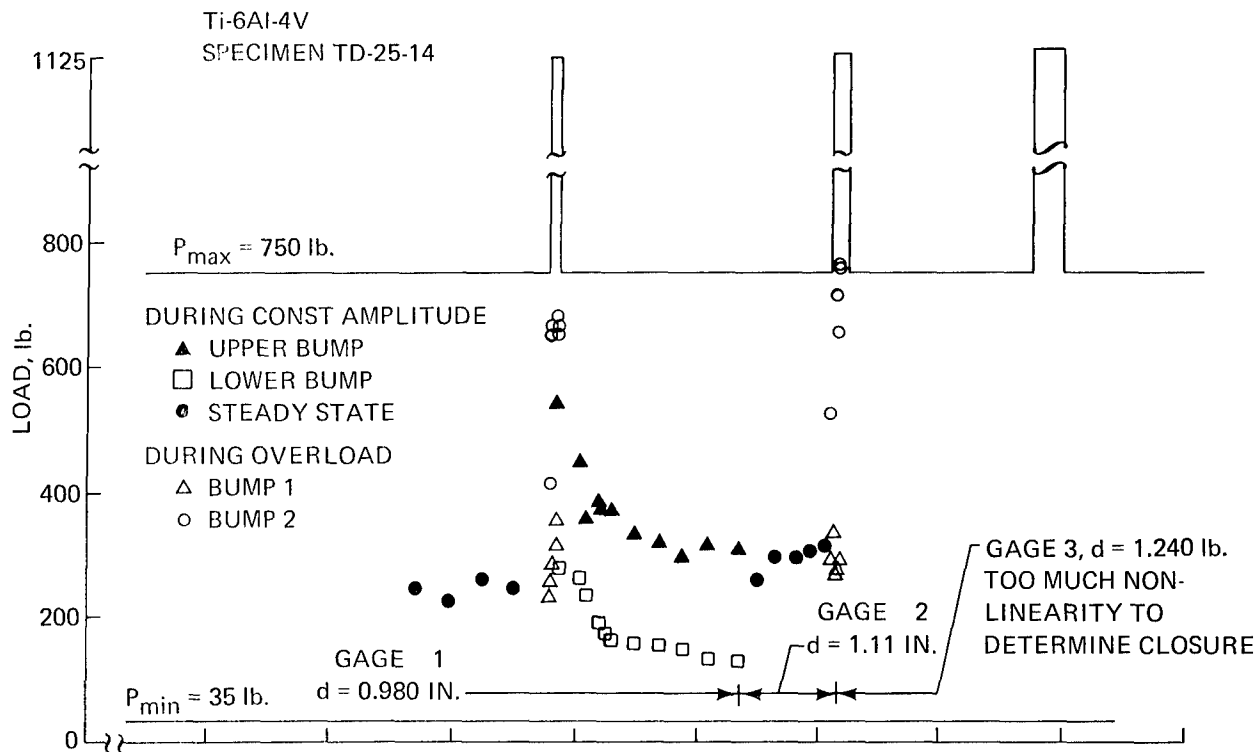


b) OPENING LOAD

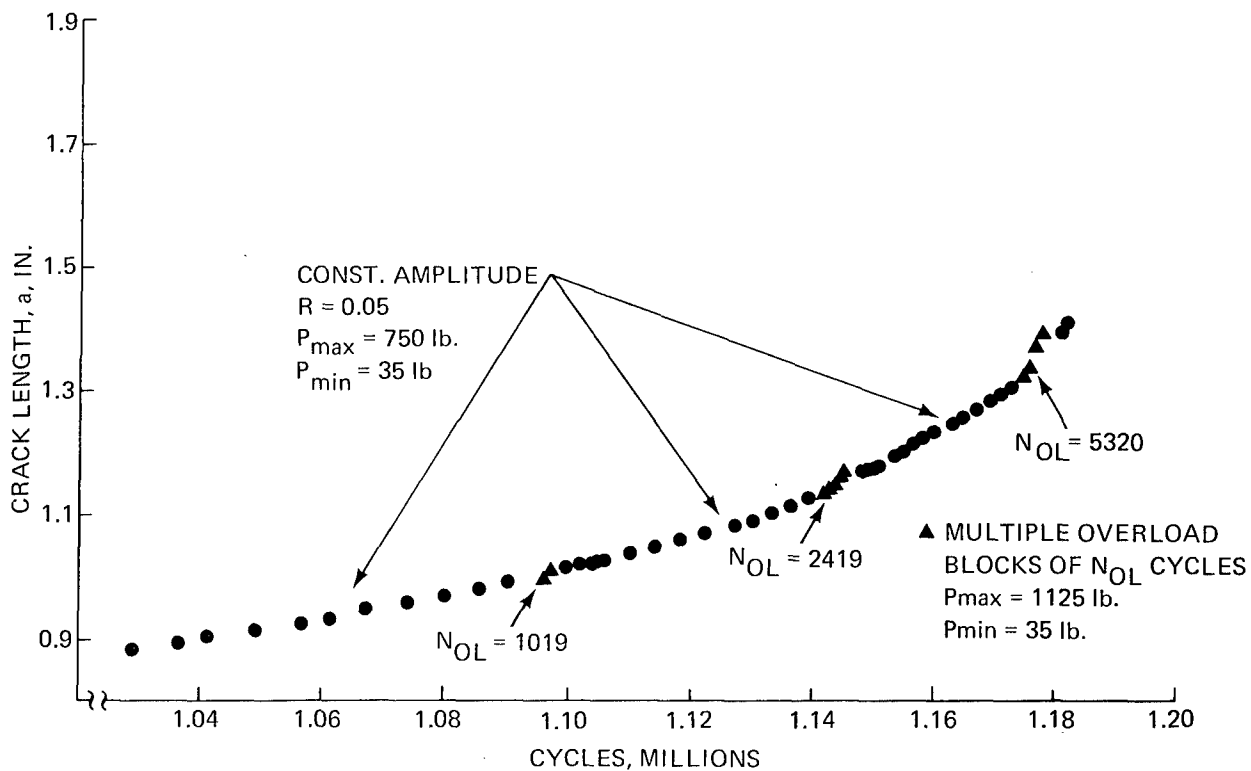


a) CRACK LENGTH

Fig. 7 Titanium Specimen with Constant Amplitude Loading

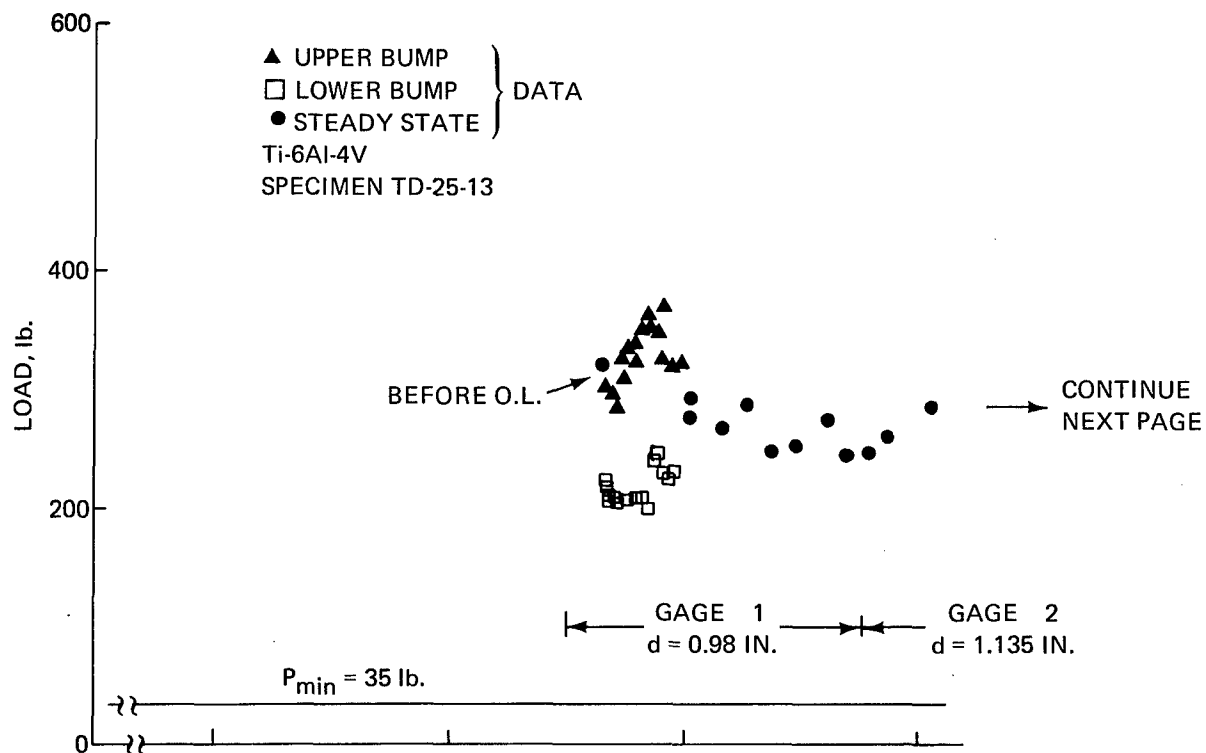


b) OPENING LOAD

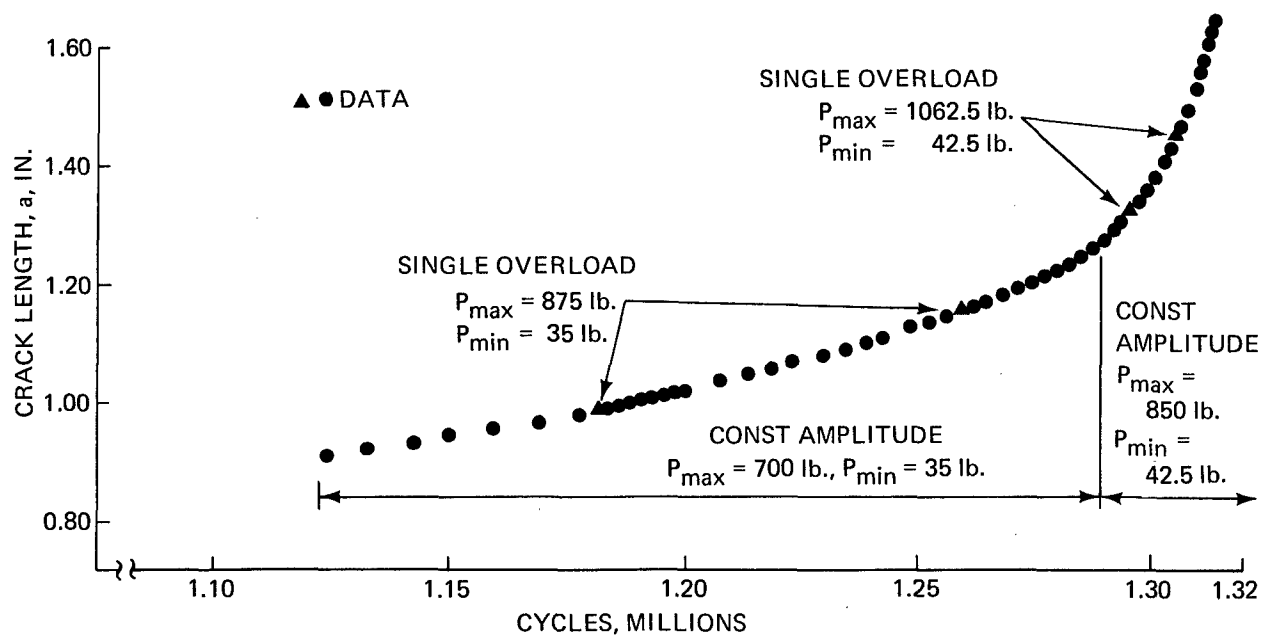


a) CRACK LENGTH

Fig. 8 Titanium Specimen with Multiple Overloads

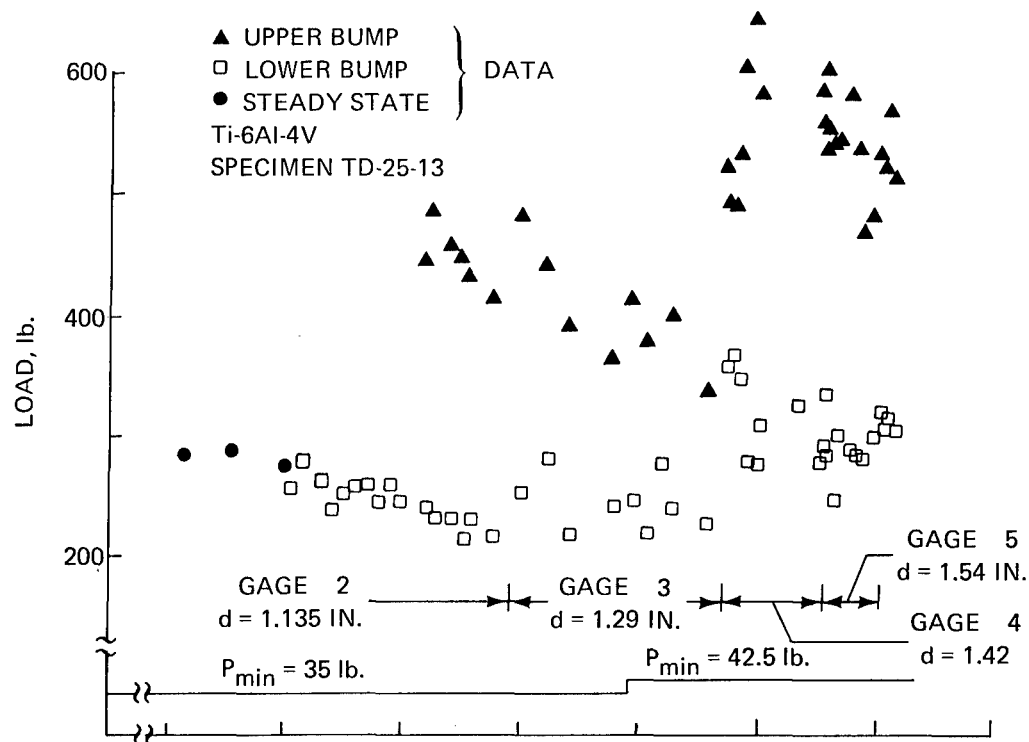


b) OPENING LOAD

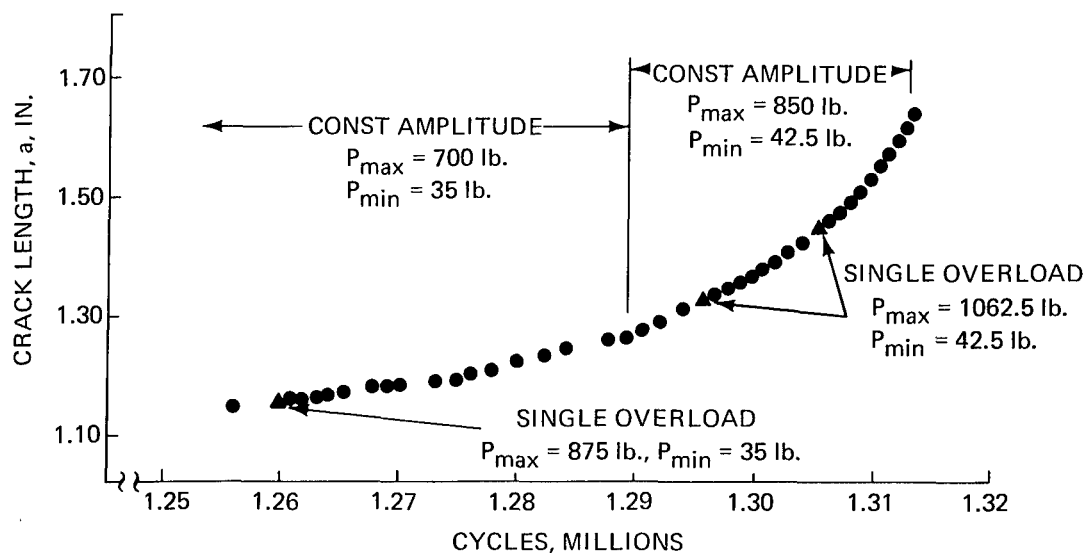


a) CRACK LENGTH

Fig. 9 Titanium Specimen with Single Overloads

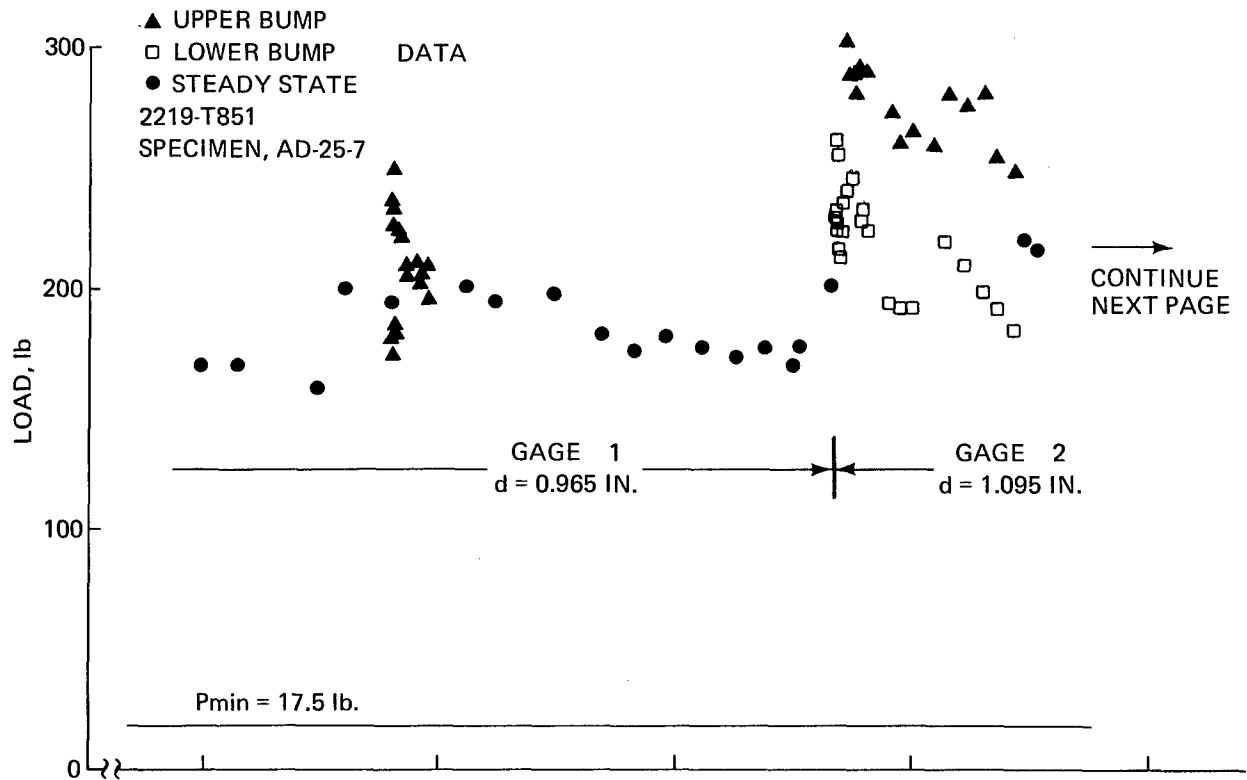


d) OPENING LOAD

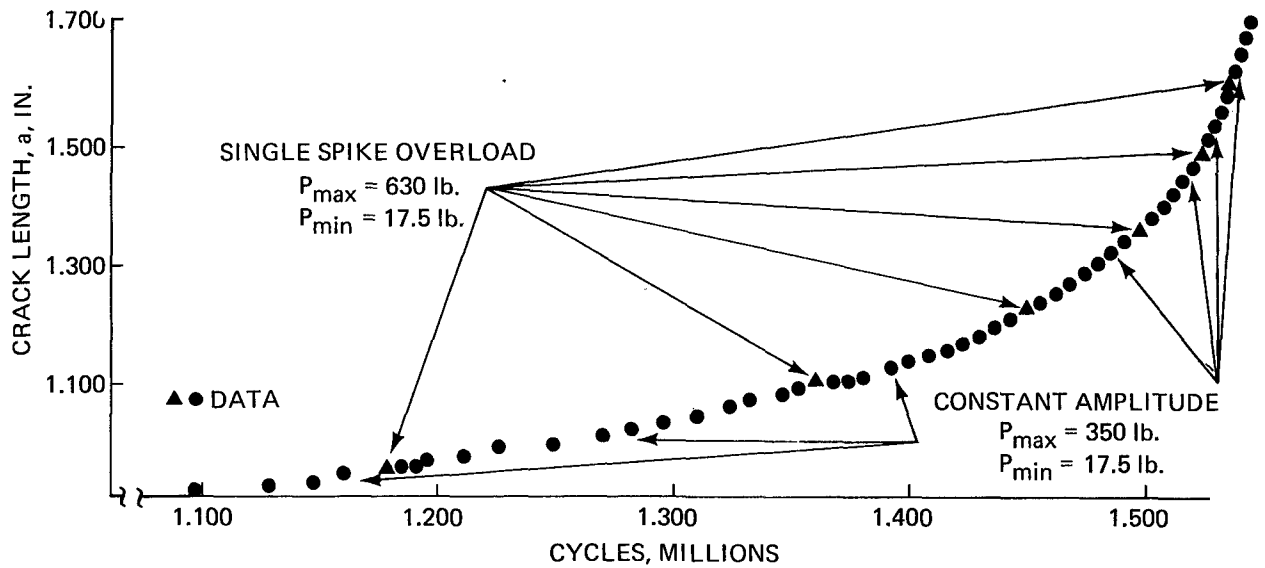


c) CRACK LENGTH

Fig. 9 (Cont'd)

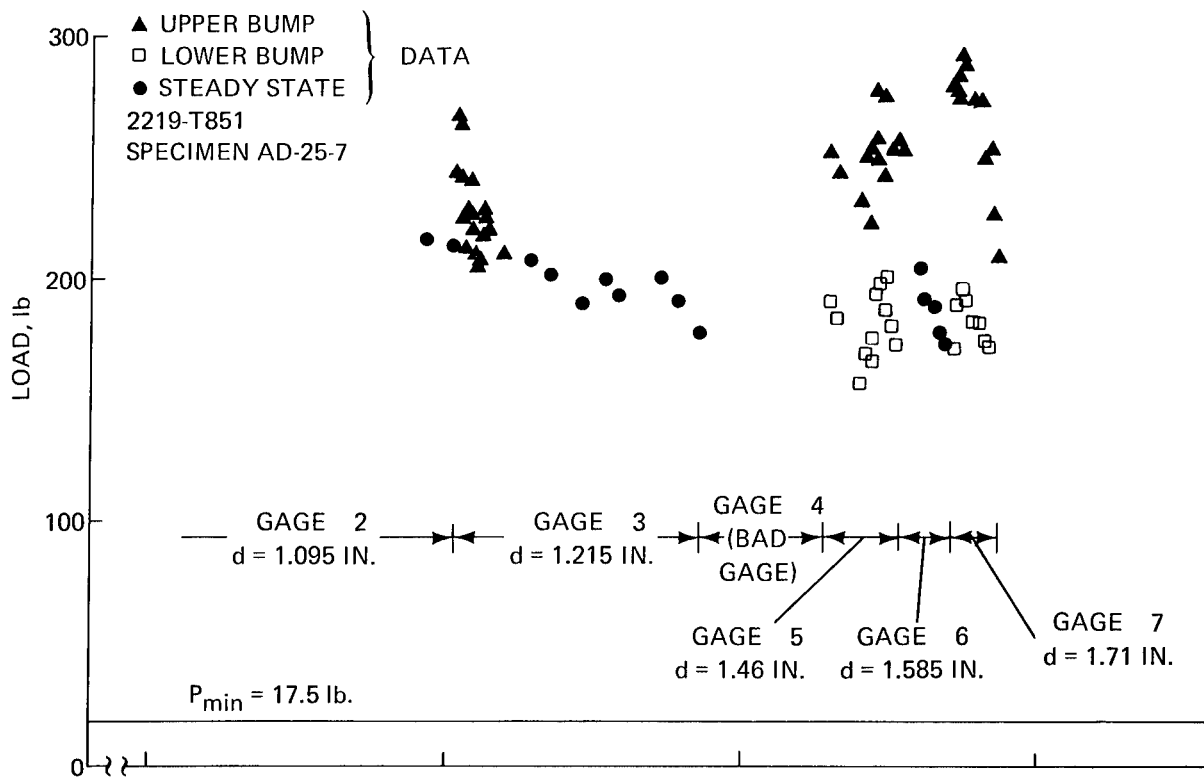


b) OPENING LOAD

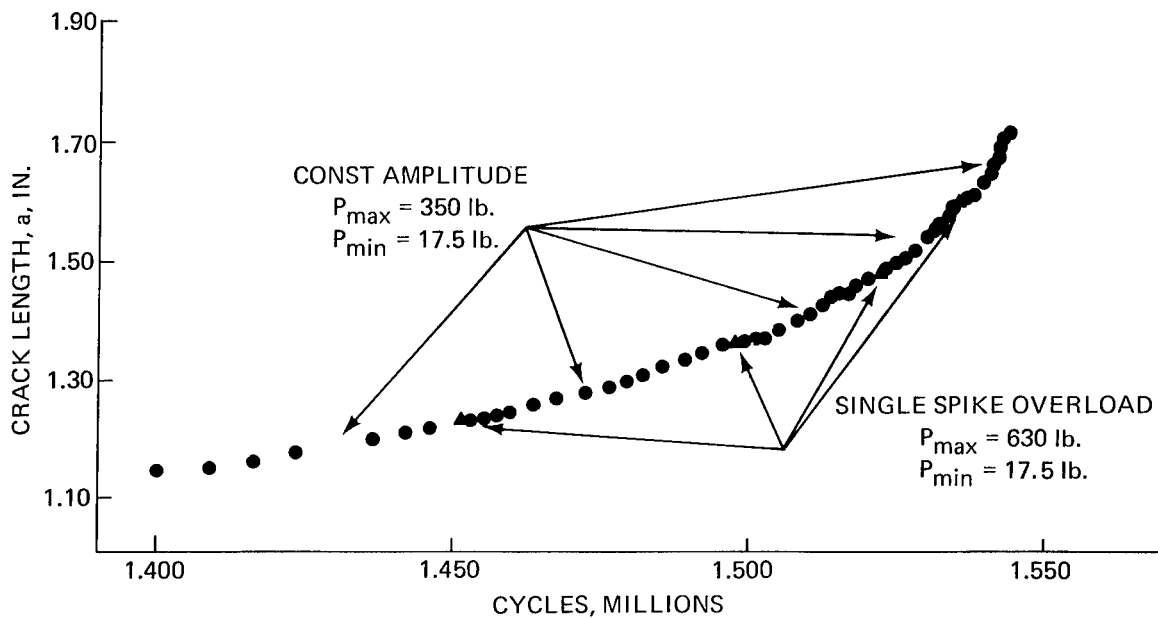


a) CRACK LENGTH

Fig. 10 Aluminum Specimen with Multiple Overloads



d) OPENING LOAD



c) CRACK LENGTH

Fig. 10 (Cont'd)

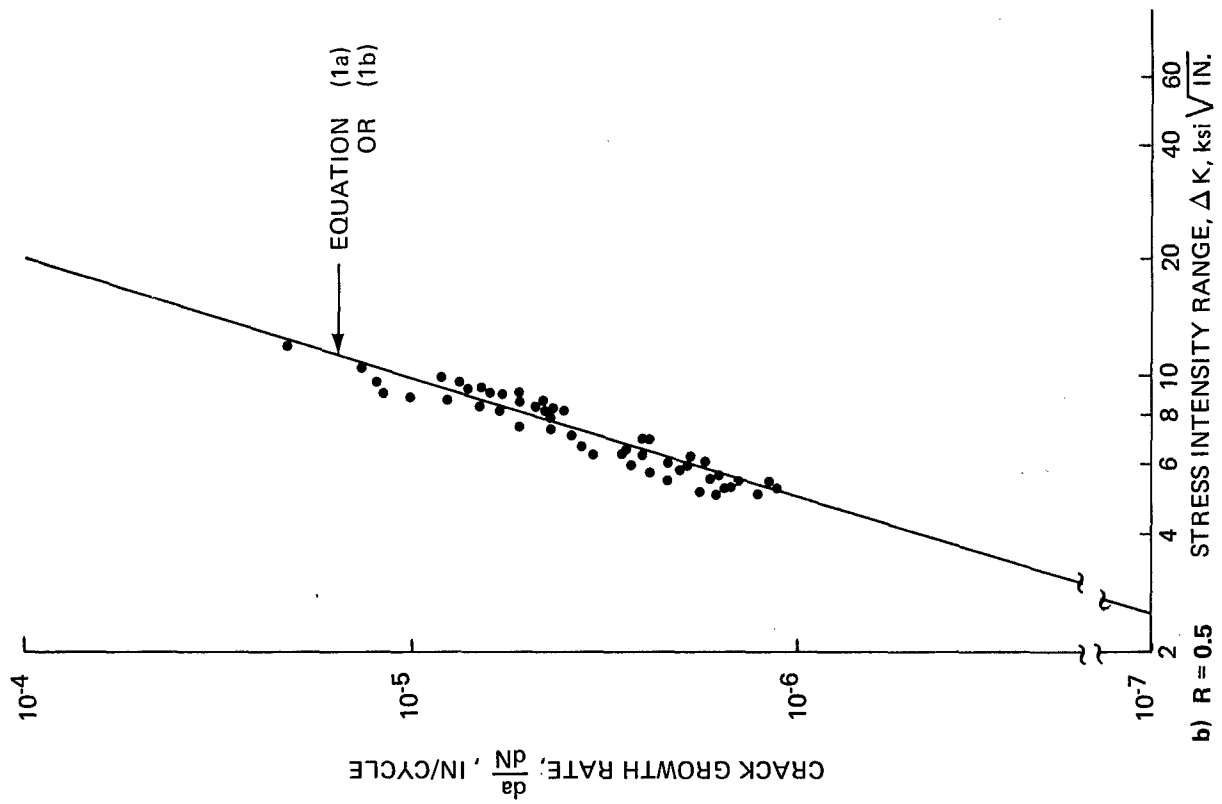
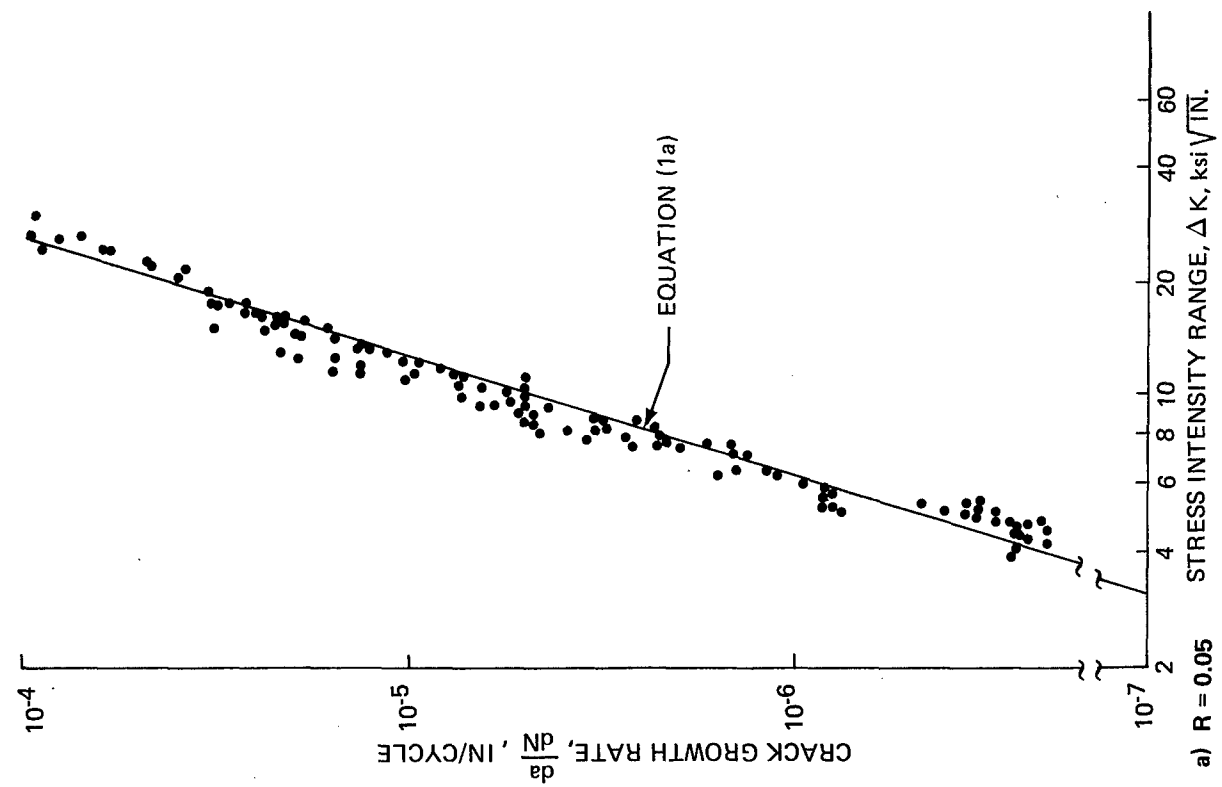


Fig. 11 da/dN vs ΔK for 2219-T851 Aluminum Constant Amplitude Tests

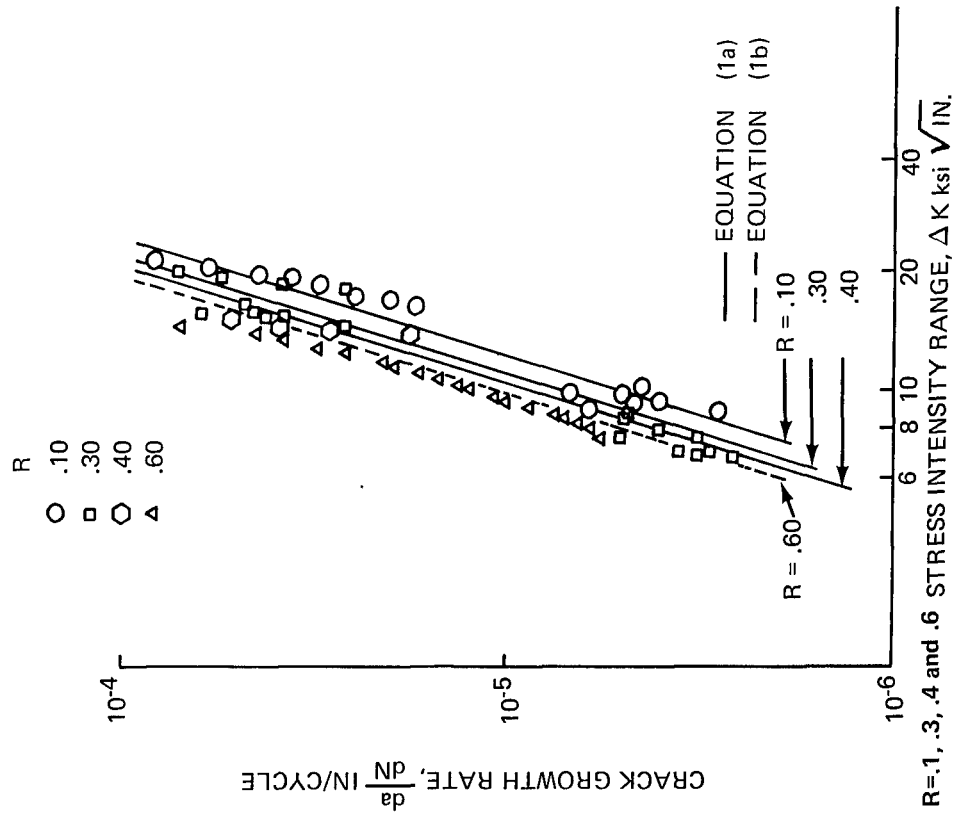
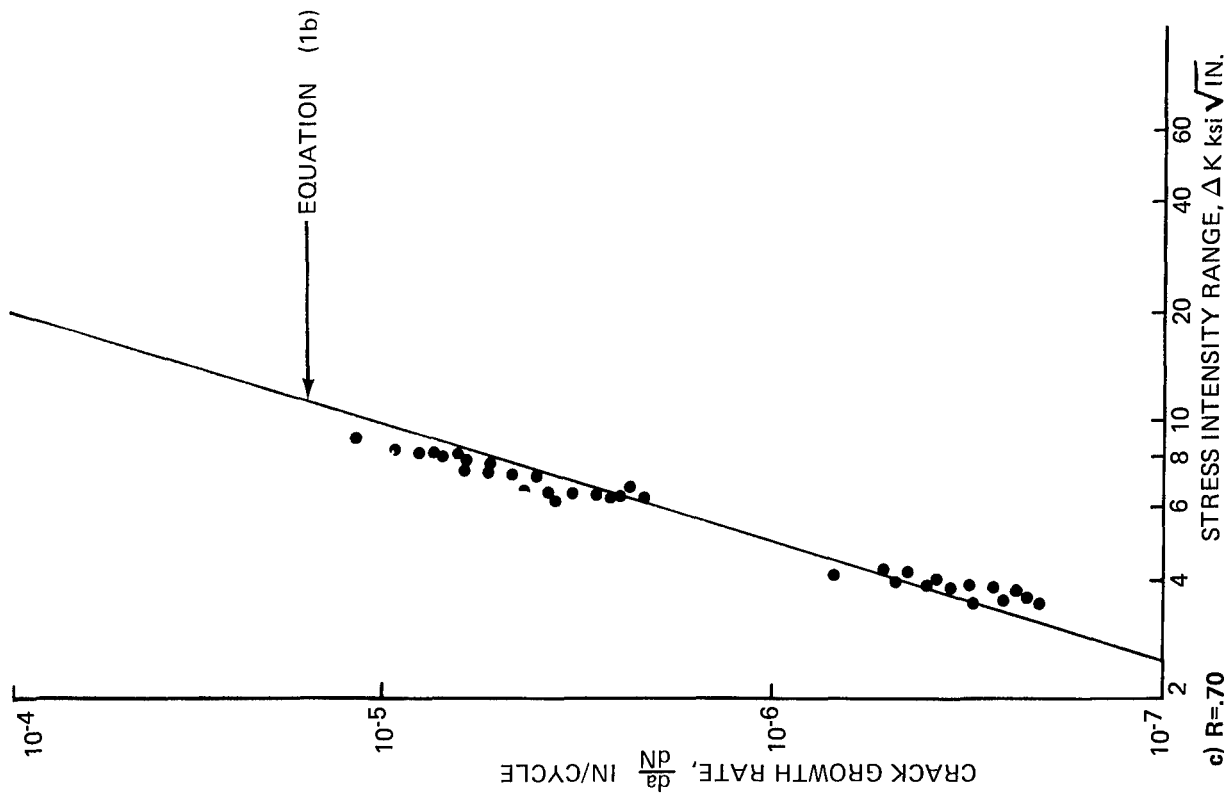


Fig. 11 (Continued)

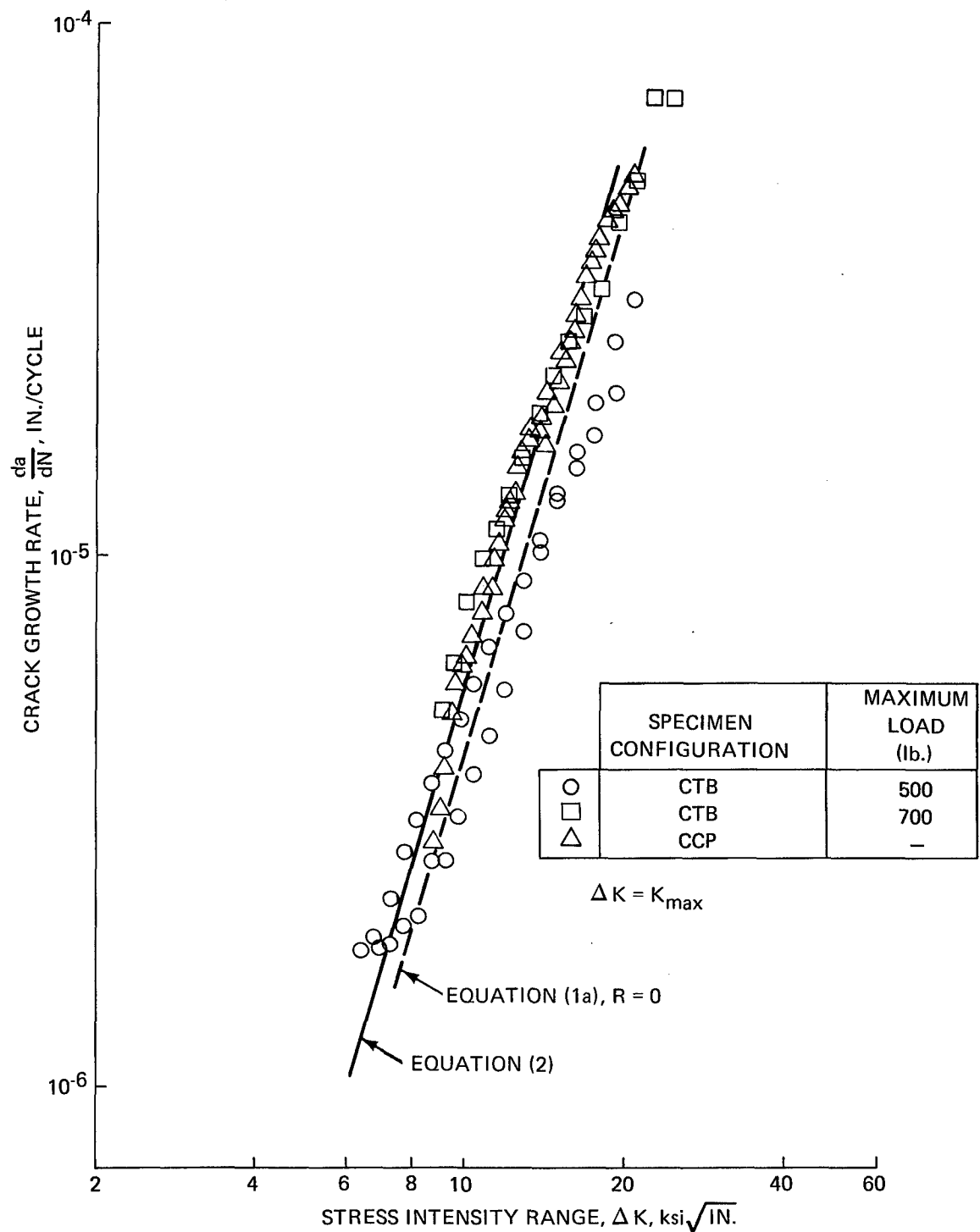


Fig. 12 da/dN vs ΔK for 2219-T851 Aluminum Constant Amplitude Tests; $R=-1$

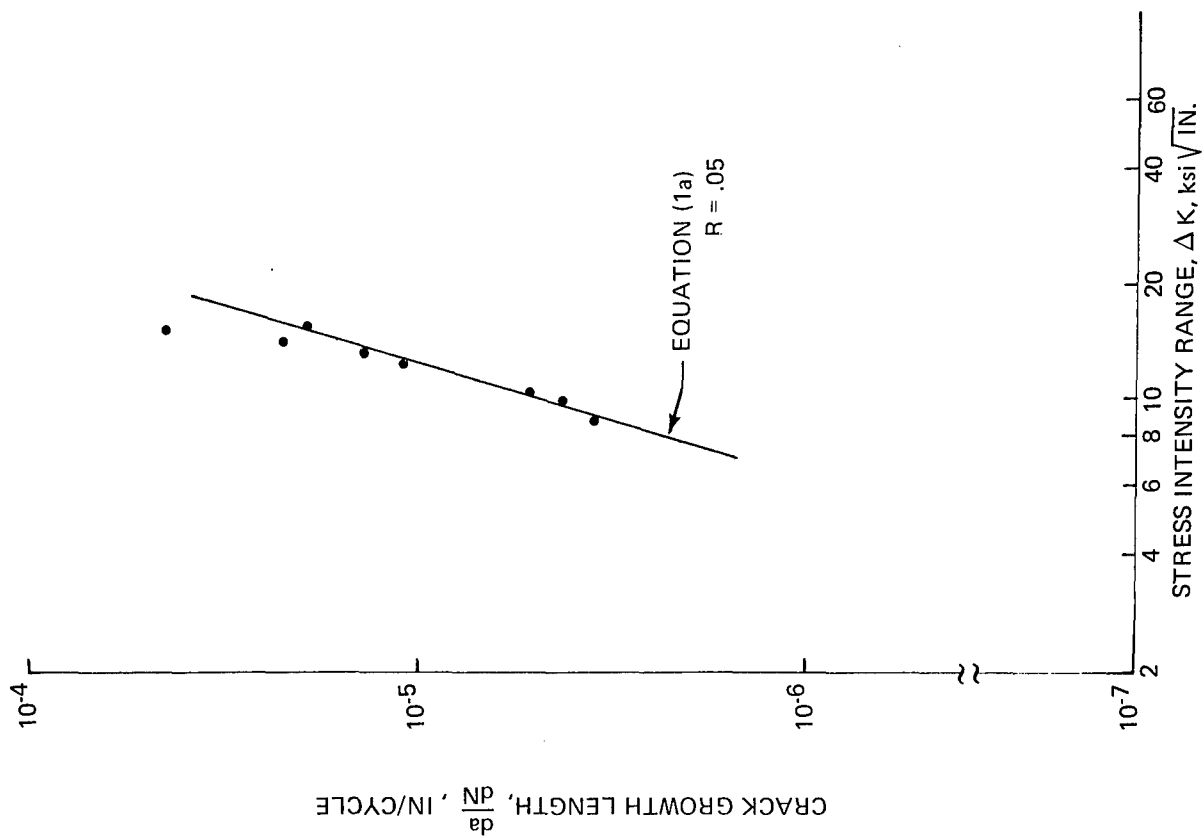


Fig. 13 da/dN vs ΔK for 2219-T851 Aluminum Constant Amplitude Tests; Thickness = .50 inch, $R = .05$

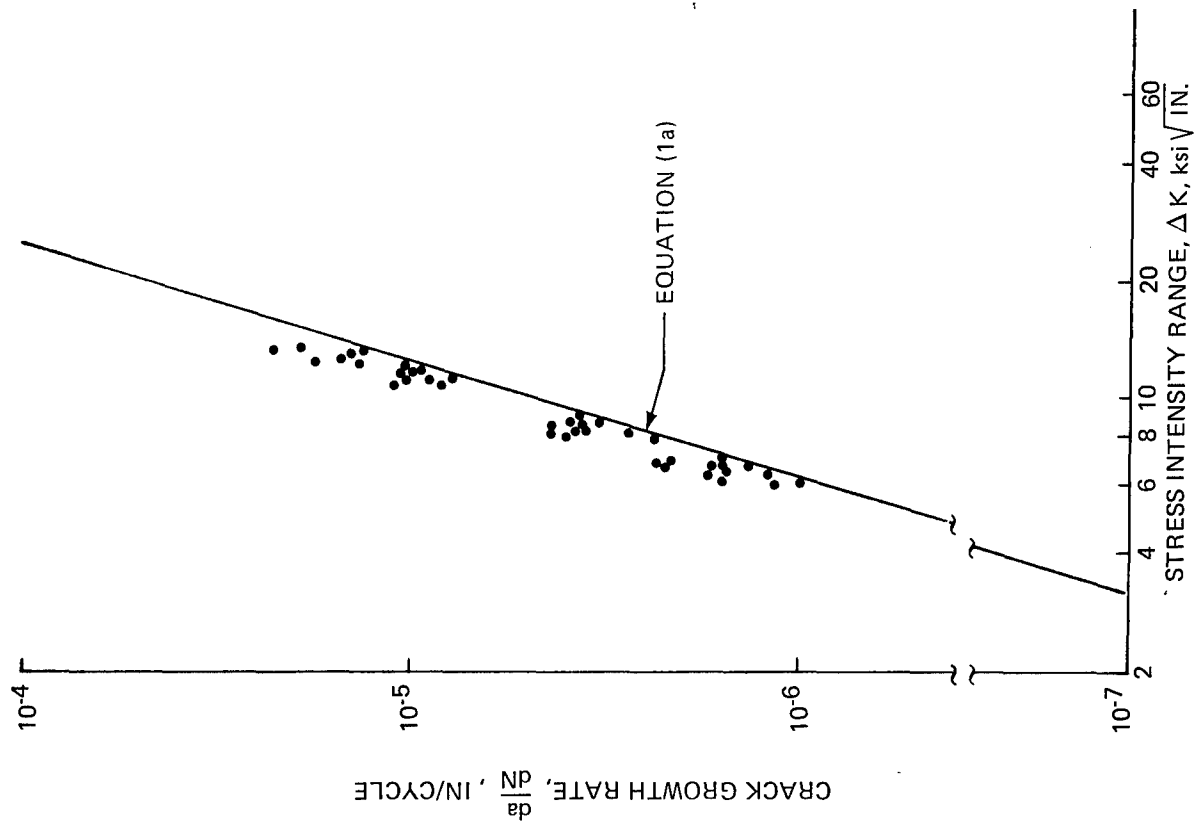
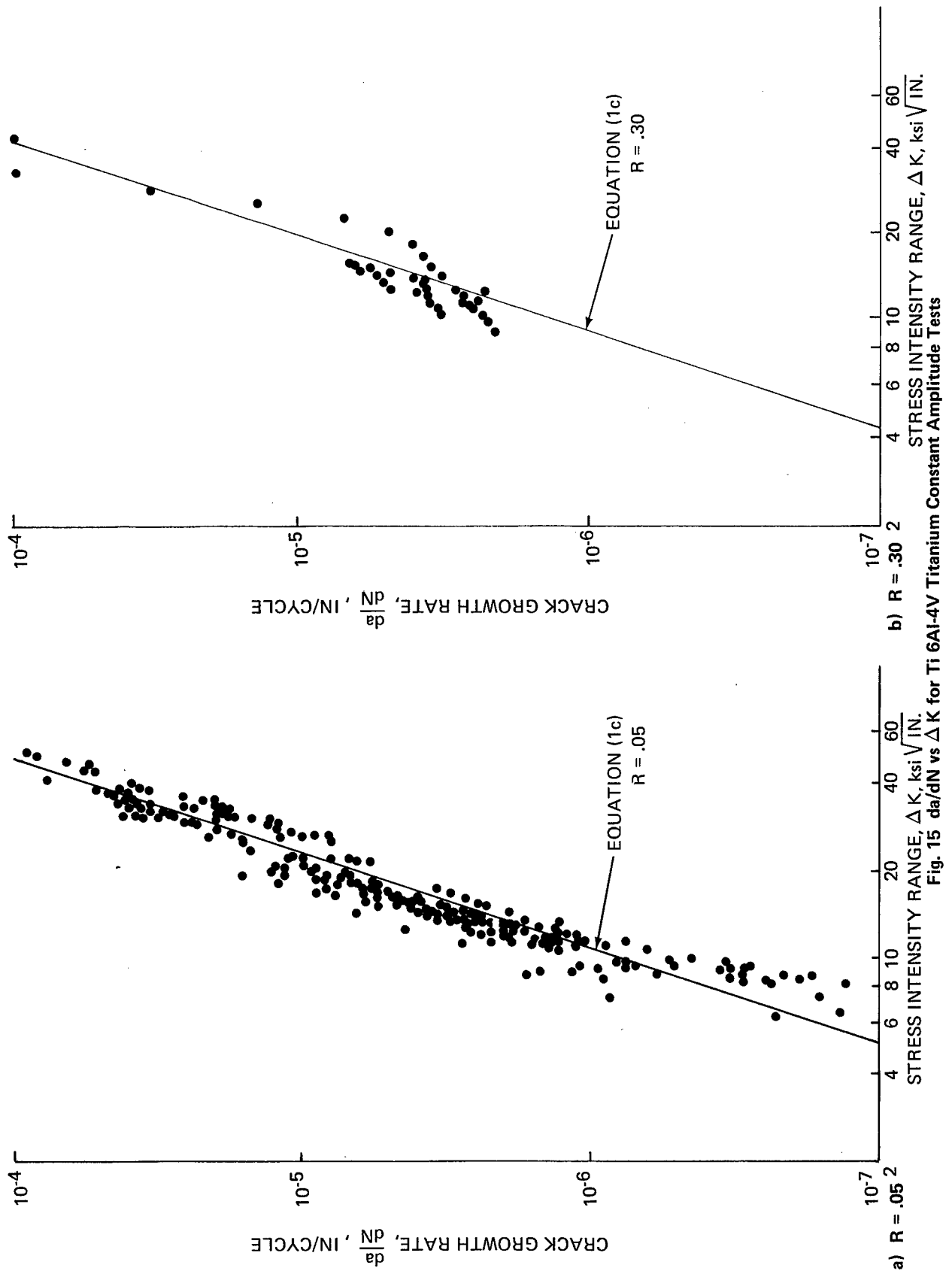


Fig. 14 da/dN vs ΔK for 2219-T851 Aluminum Constant Amplitude Tests; Relative Humidity = 95%, $R = .05$



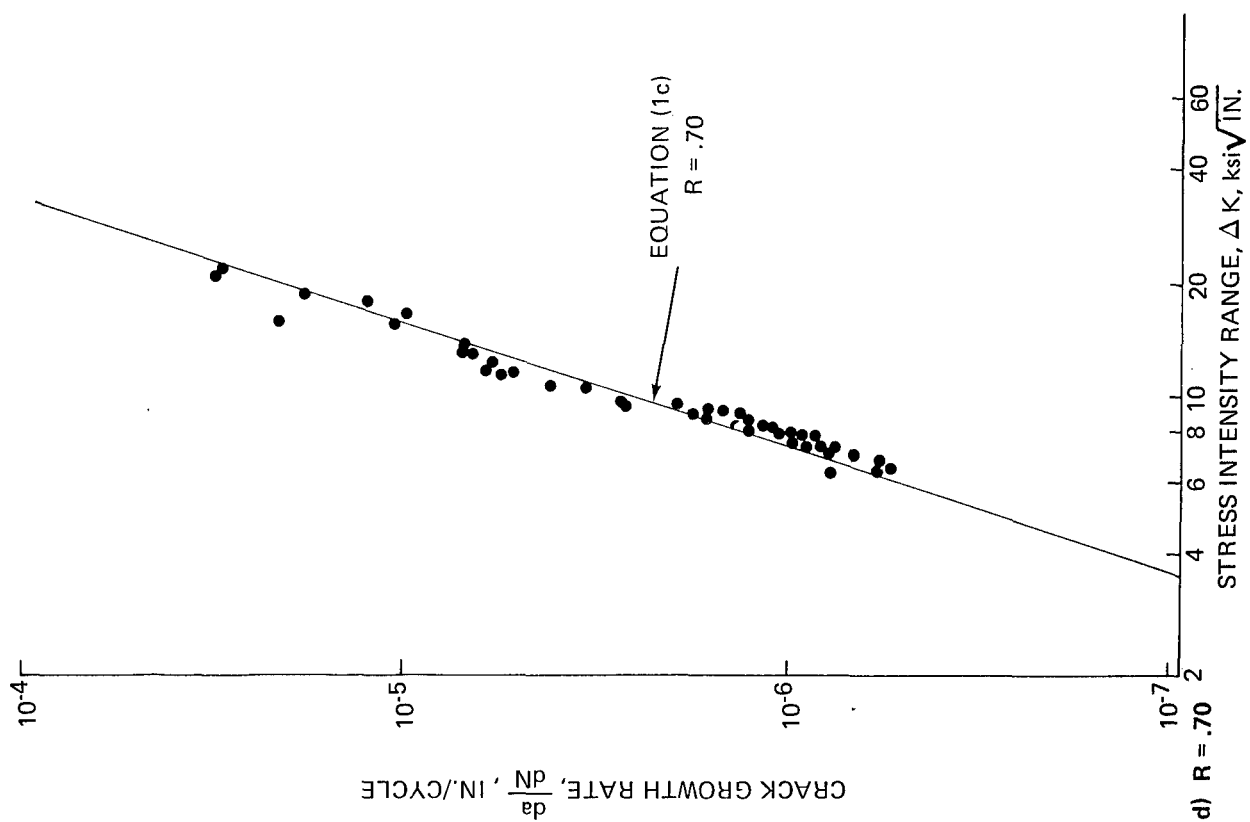
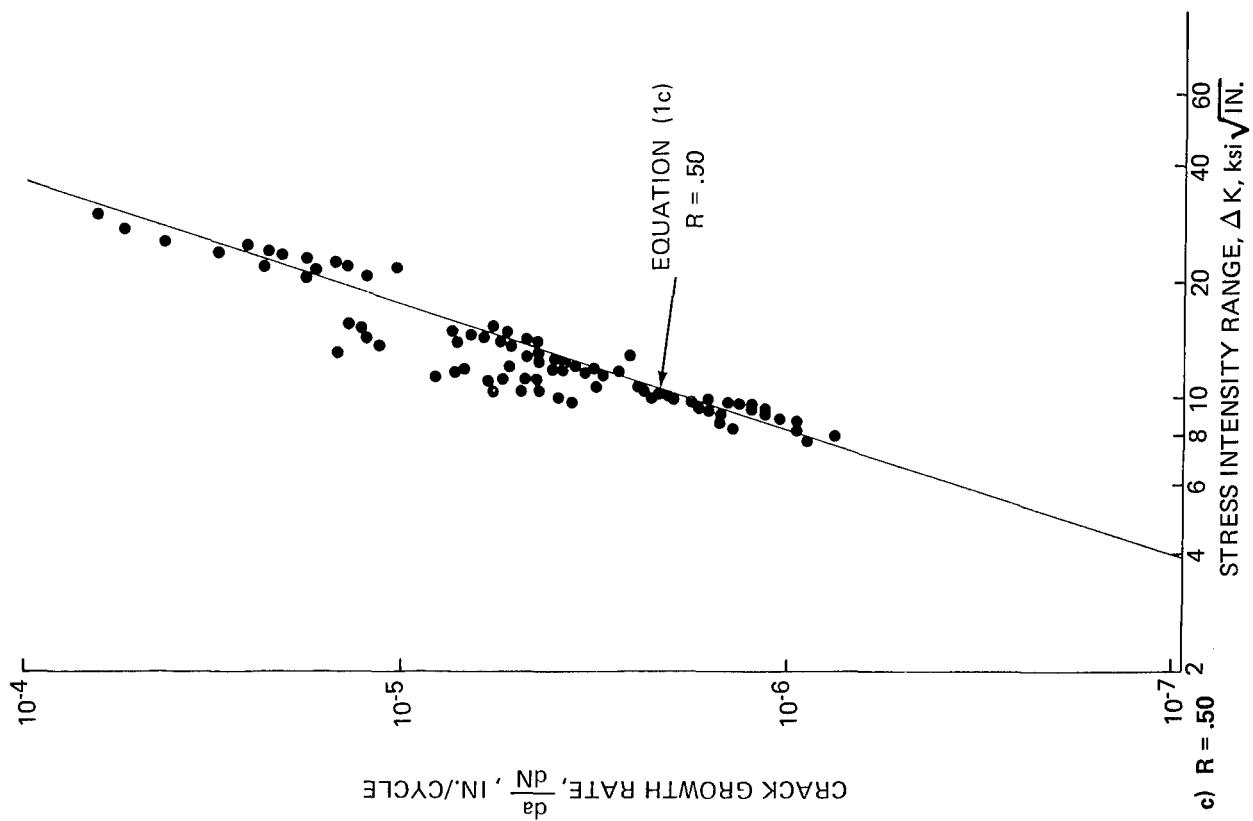
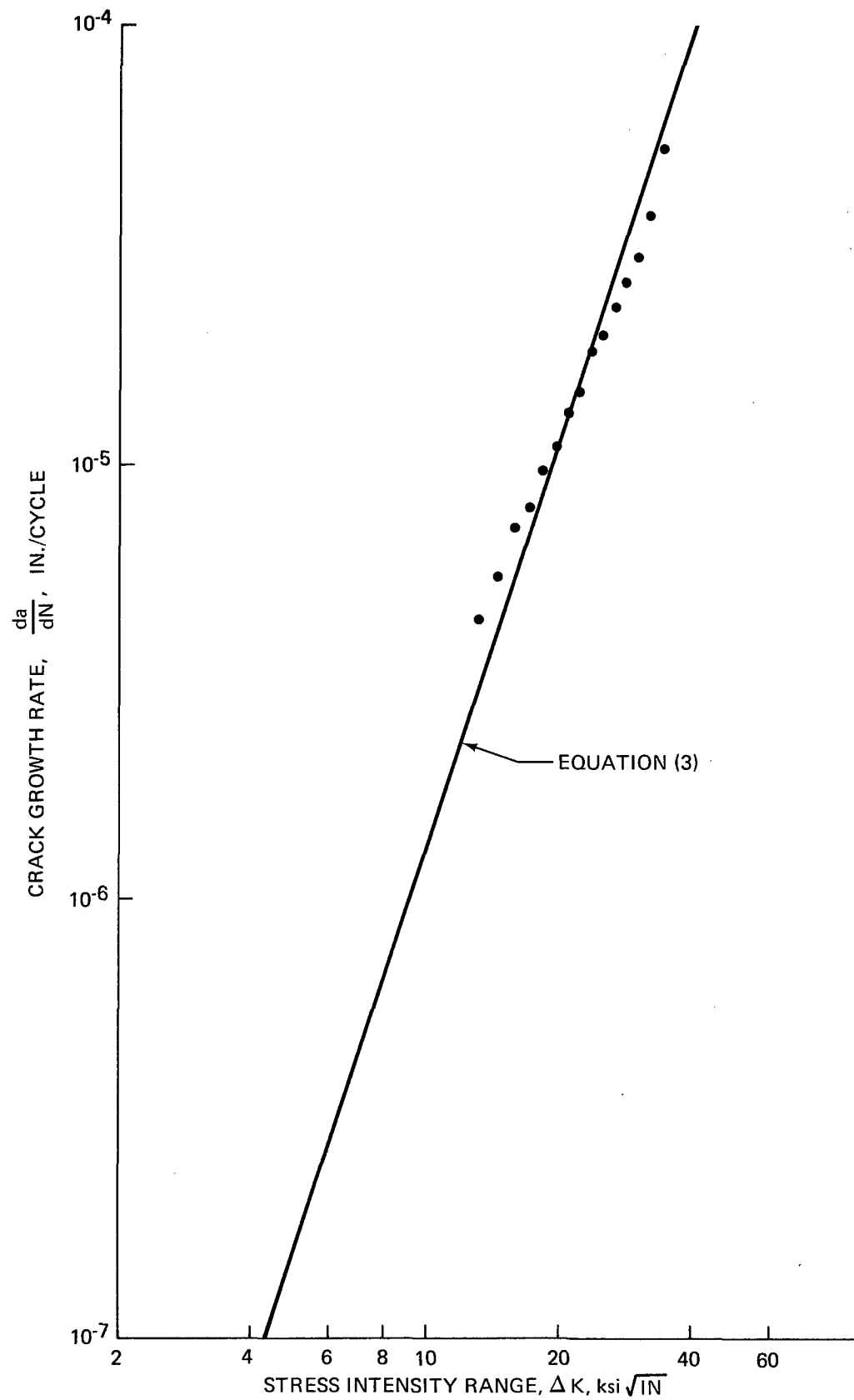


Fig. 15 (Continued)



e) $R = -1.0$, $\Delta K = K_{\max}$

Fig. 15 Concluded

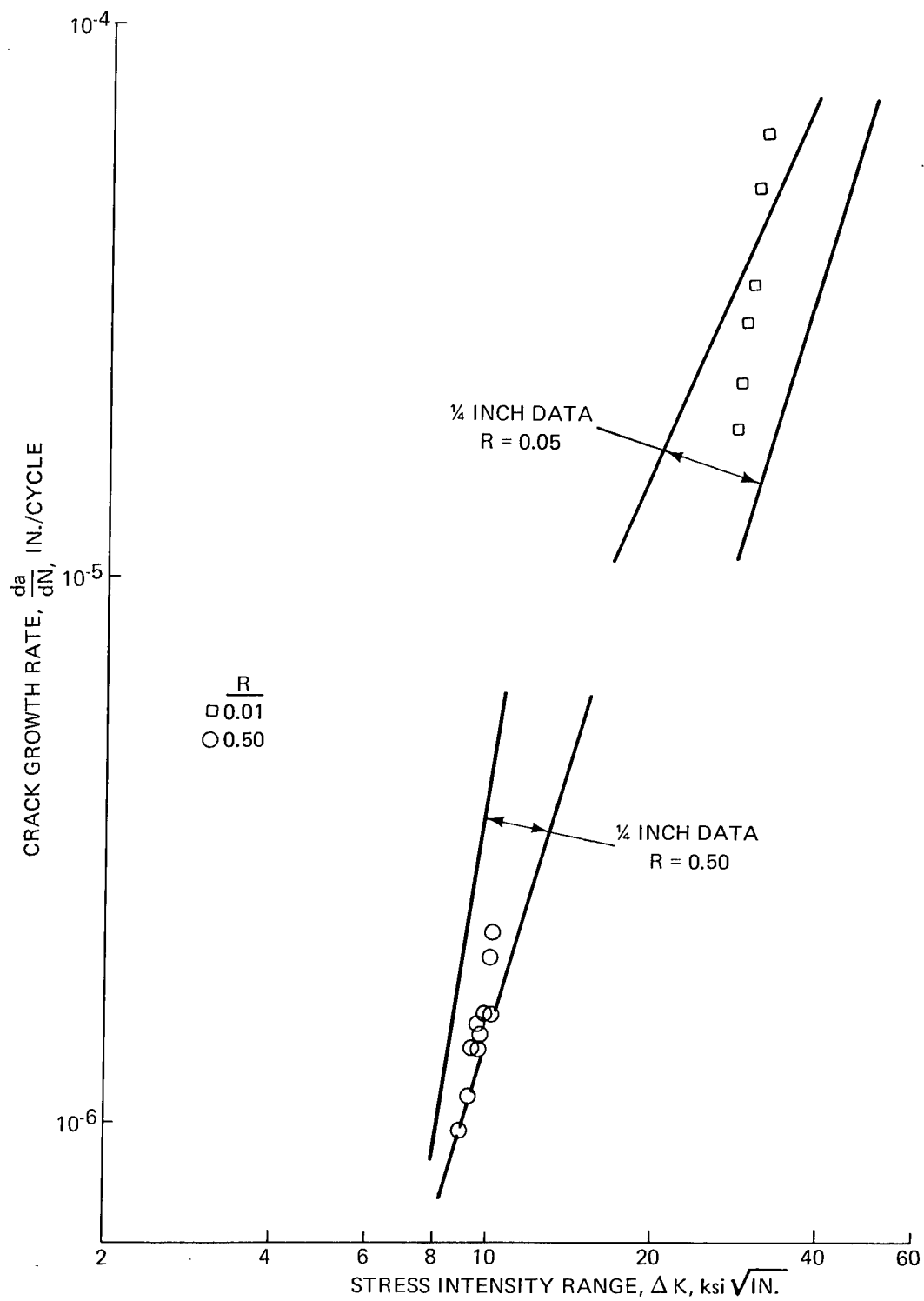


Fig. 16 da/dN vs ΔK for Ti 6Al-4V Titanium Constant Amplitude Tests;
 Thickness = .75 in., $R = .01$ and $.50$

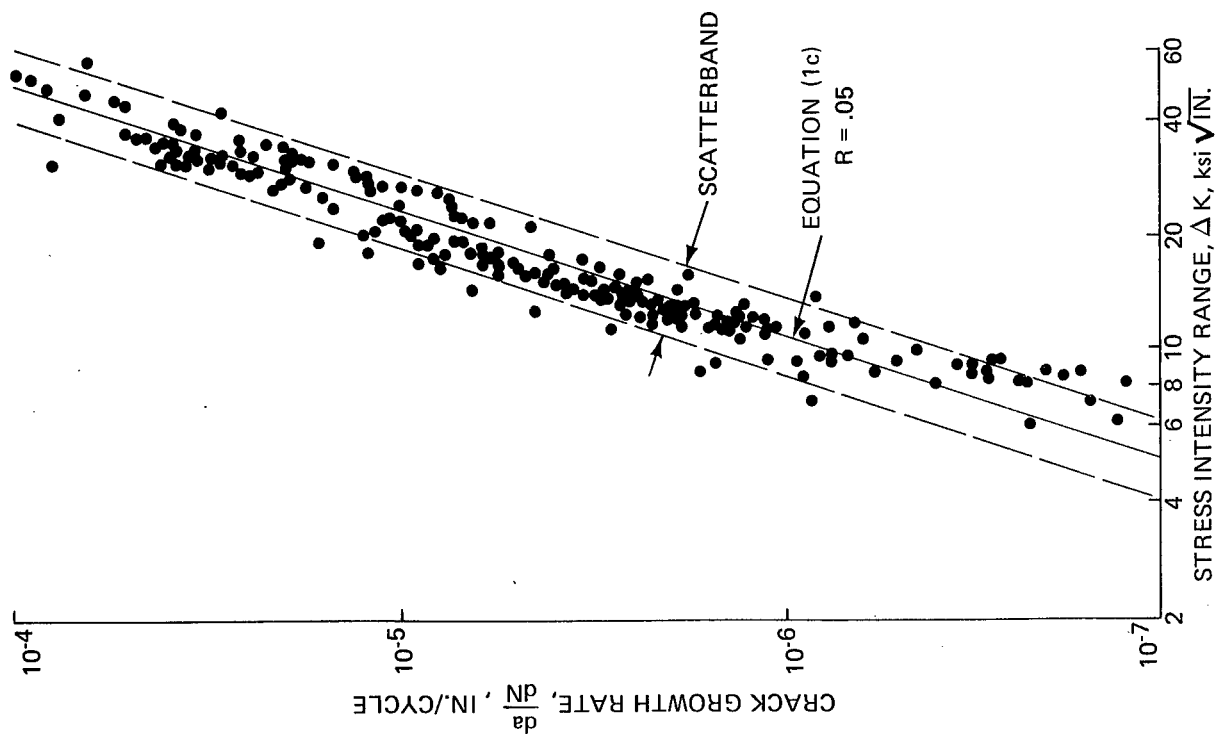


Fig. 17 Scatterband for Ti 6Al-4V Titanium for $R = .05$

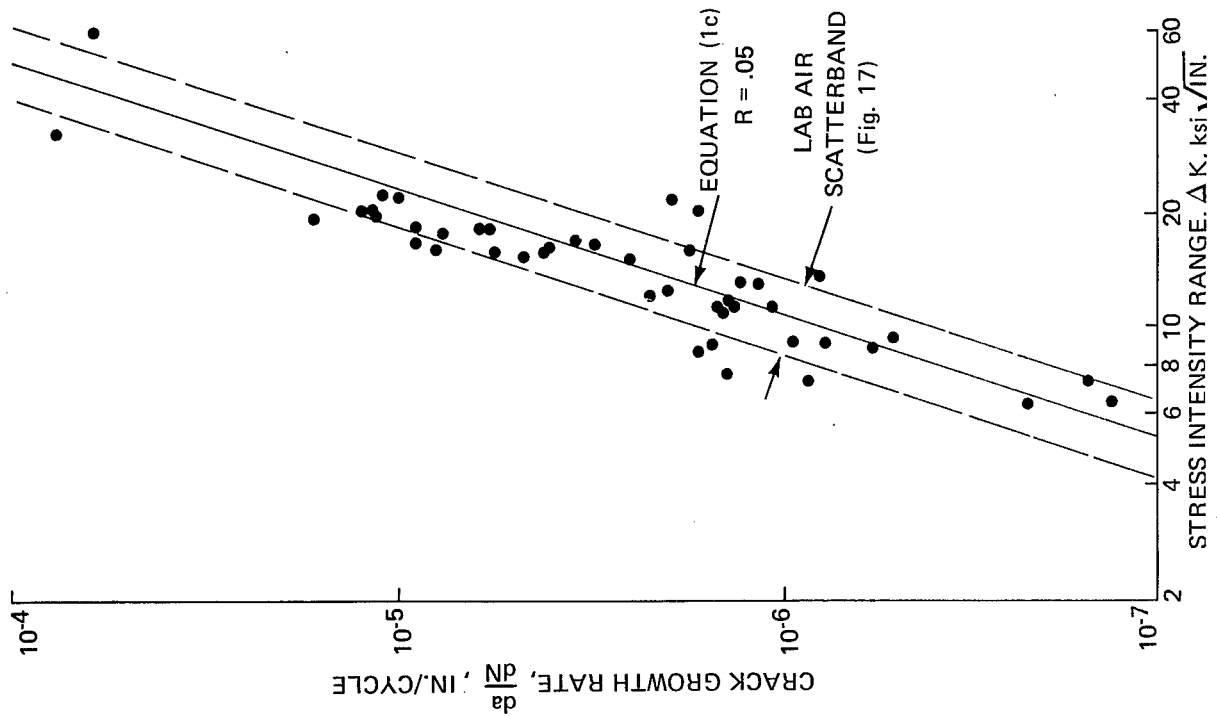


Fig. 18 da/dN vs ΔK for Ti 6Al-4V Titanium Constant Amplitude Tests; Relative Humidity = 95%, $R = .05$

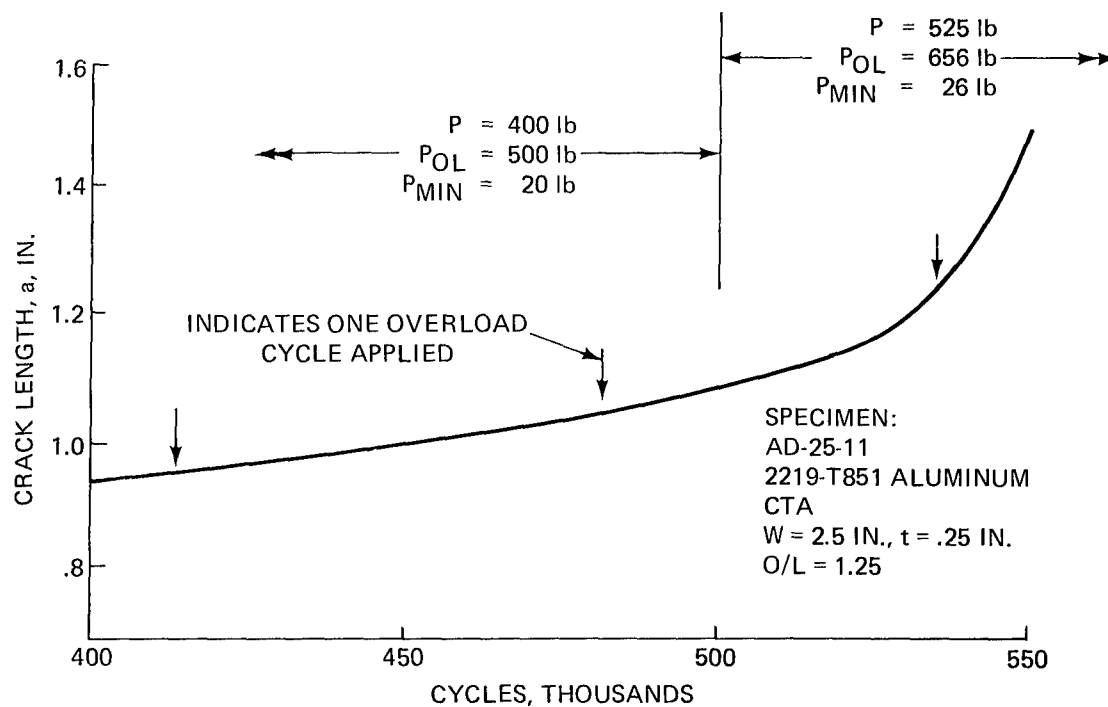


Fig. 19 Crack Length vs. Cycles for Overload Tests; O/L = 1.25, 2219-T851 Aluminum

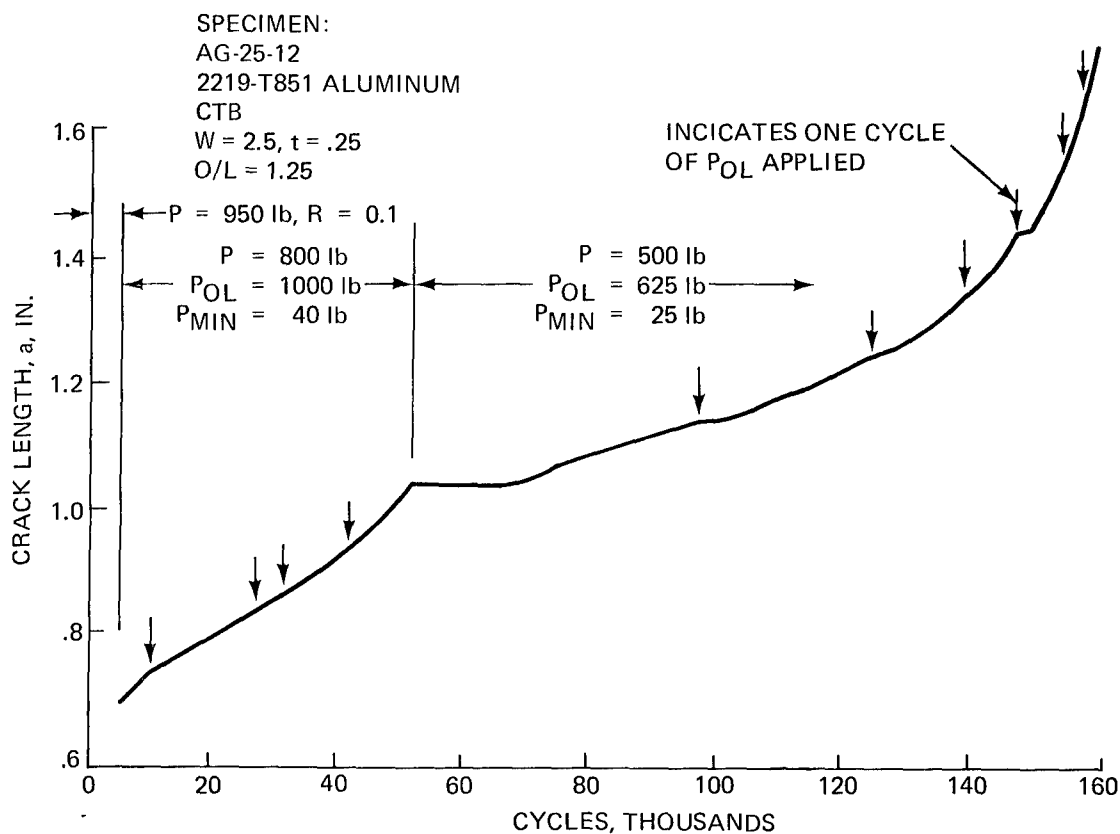


Fig. 20 Crack Length vs. Cycles for Overload Tests; O/L = 1.25, 2219-T851 Aluminum

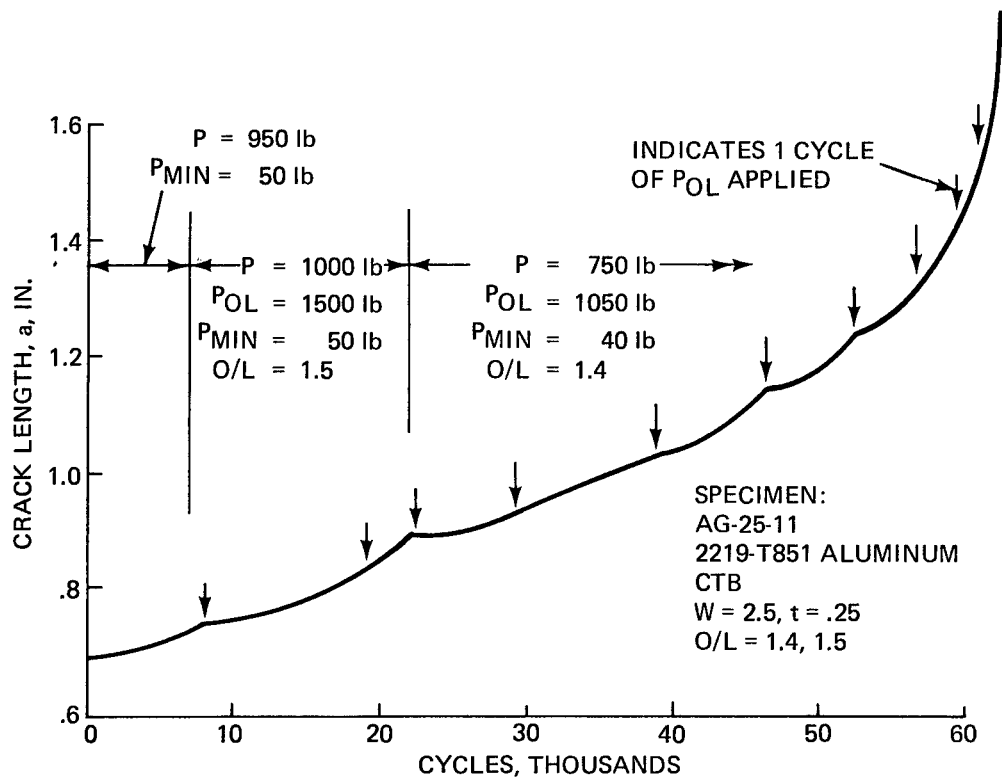


Fig. 21 Crack Length vs. Cycles for Overload Tests; O/L = 1.4 and 1.5, 2219-T851 Aluminum

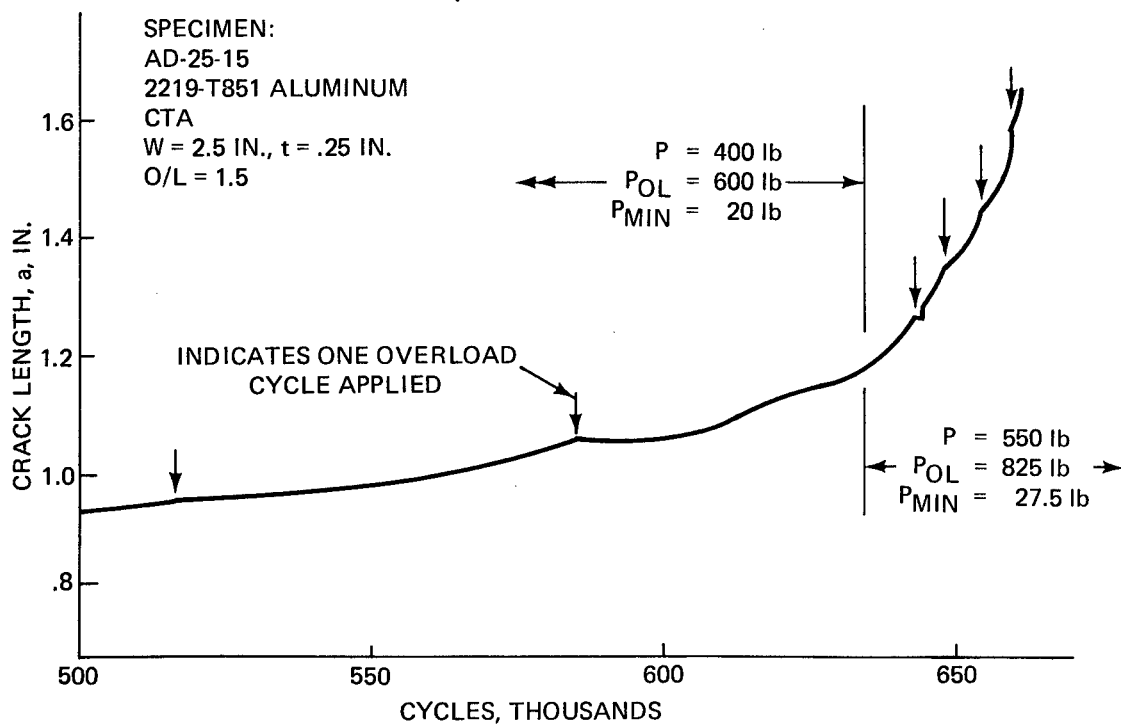


Fig. 22 Crack Length vs. Cycles for Overload Tests; O/L = 1.5, 2219-T851 Aluminum

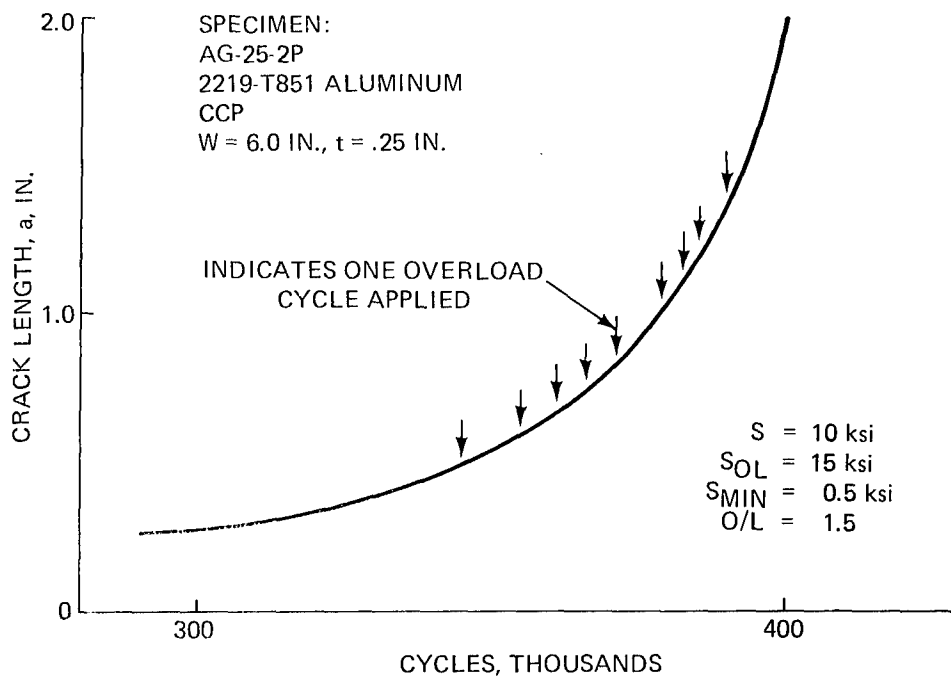


Fig. 23 Crack Length vs. Cycles for Overload Tests; O/L = 1.5, 2219-T851 Aluminum

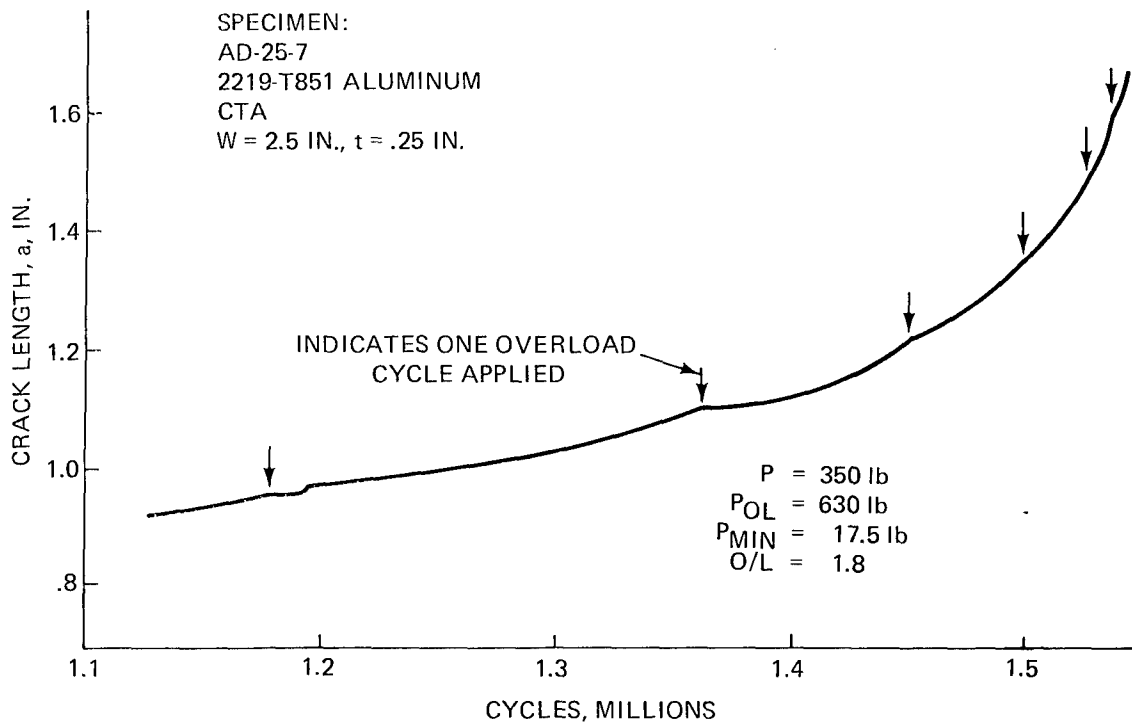


Fig. 24 Crack Length vs. Cycles for Overload Tests; O/L = 1.8, 2219-T851 Aluminum

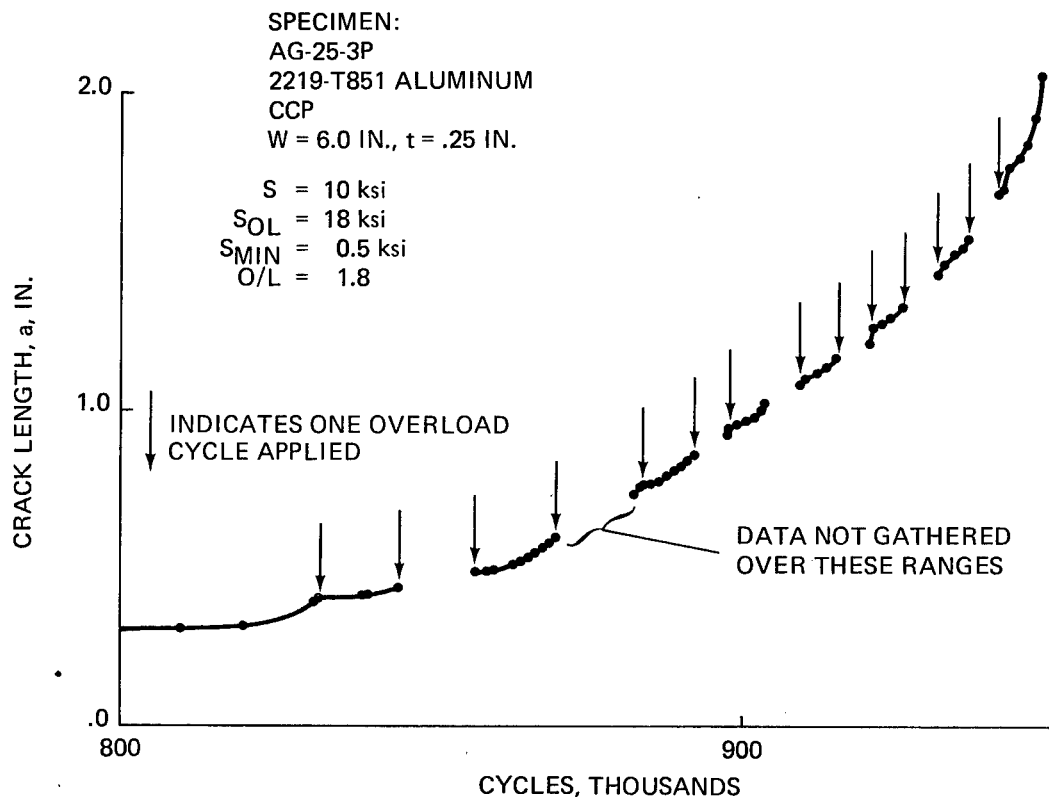


Fig. 25 Crack Length vs. Cycles for Overload Tests; O/L = 1.8, 2219-T851 Aluminum

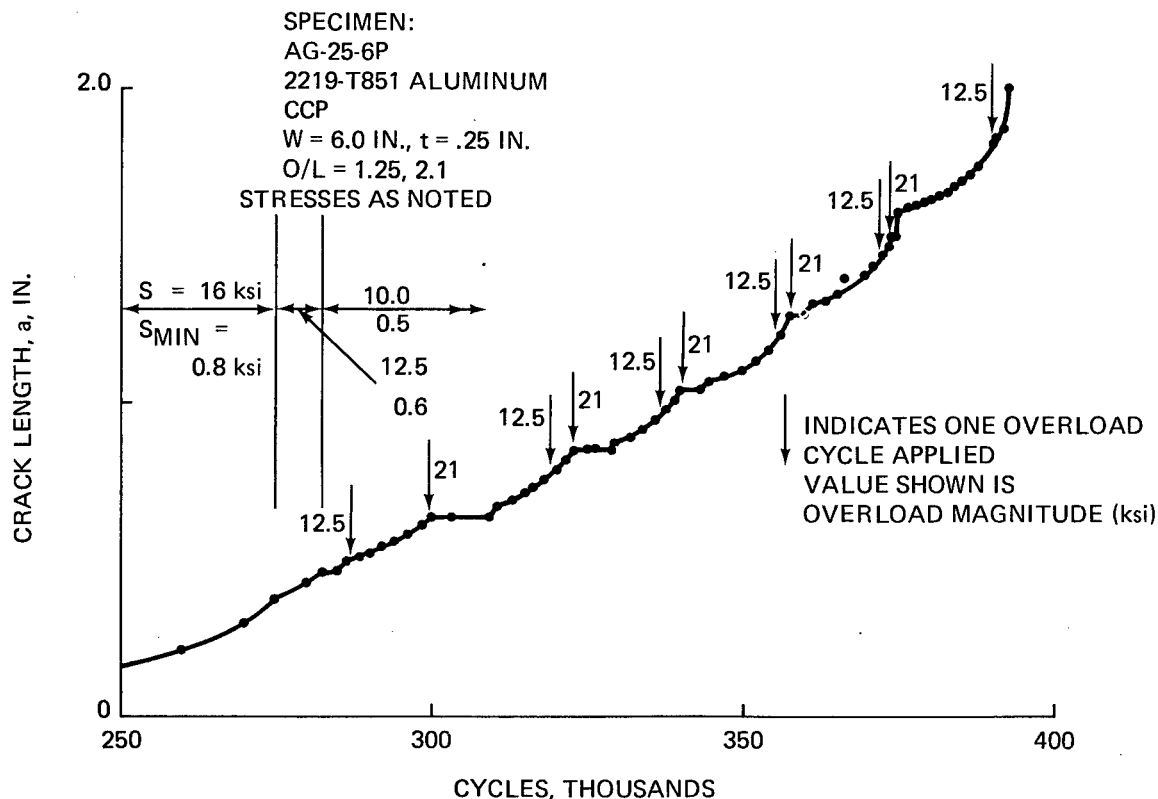


Fig. 26 Crack Length vs. Cycles for Overload Tests; O/L = 1.25 and 2.1, Aluminum

SPECIMEN:

AG-25-3P
2219-T851 ALUMINUM
CCP, W = 6.0 IN., t = .25 IN.

S = 10 ksi
SOL = 18 ksi
S_{min} = 0.5 ksi
K_{maxOL} = 22.4 ksi IN.
ΔK_b = 11.8 ksi IN.

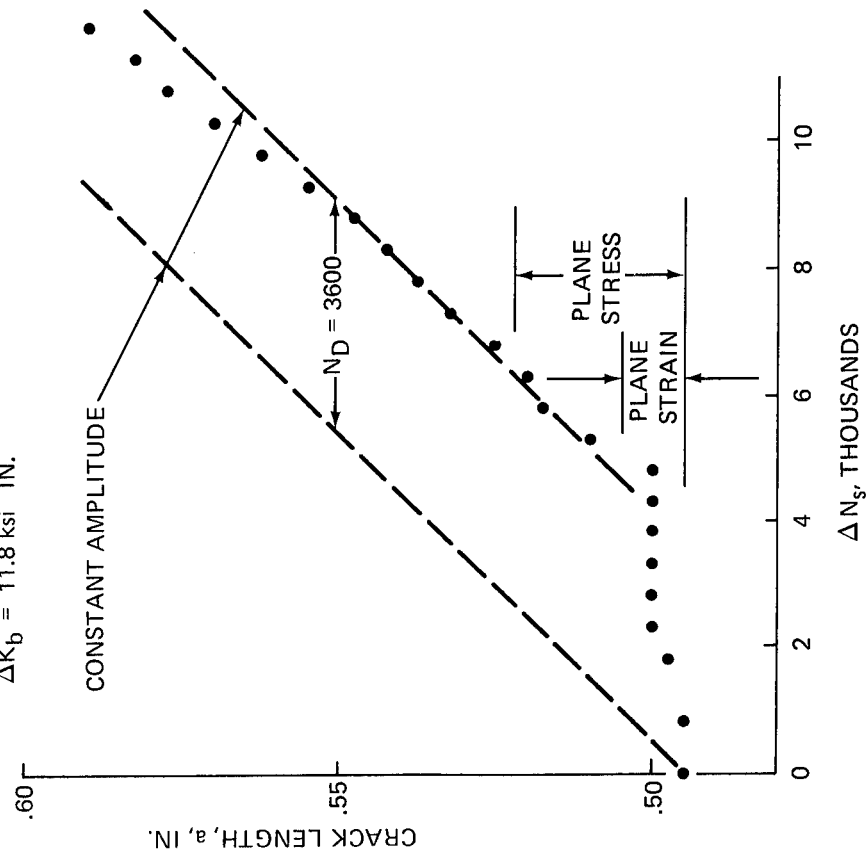


Fig. 27 a vs. ΔN_s for Overload Tests. O/L = 1.8, 2219-T851

SPECIMEN:

AG-25-2P
2219-T851 ALUMINUM
CCP, W = 6.0 IN., t = .25 IN.

S = 10 ksi
SOL = 15 ksi
S_{min} = 0.5 ksi
K_{maxOL} = 22.5 ksi IN.
ΔK_b = 14.3 ksi IN.

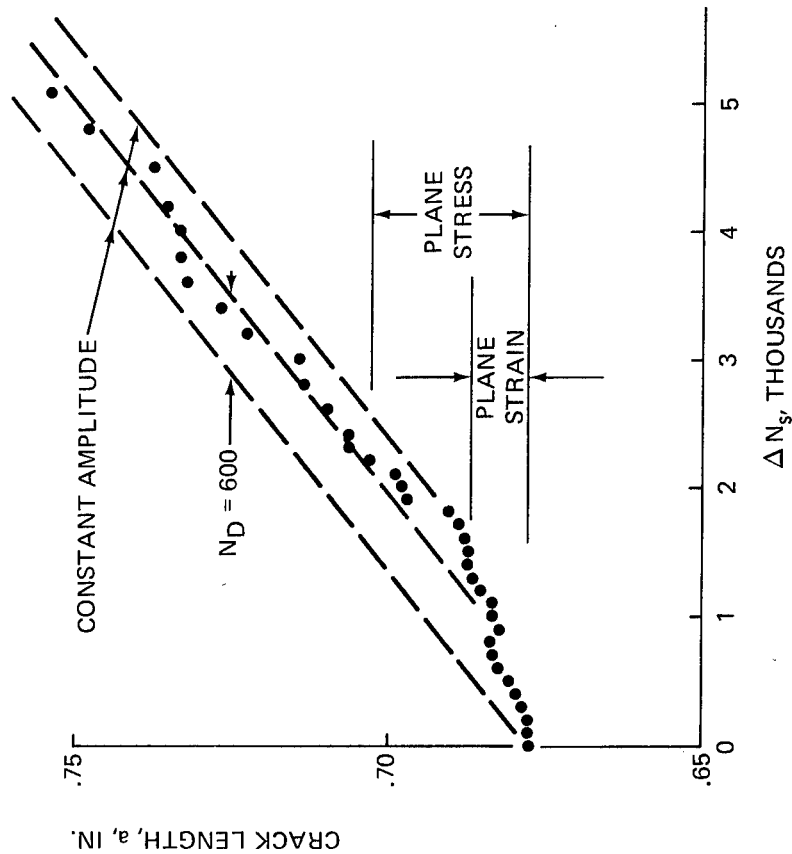


Fig. 28 a vs. ΔN_s for Overload Tests. O/L = 1.5, 2219-T851

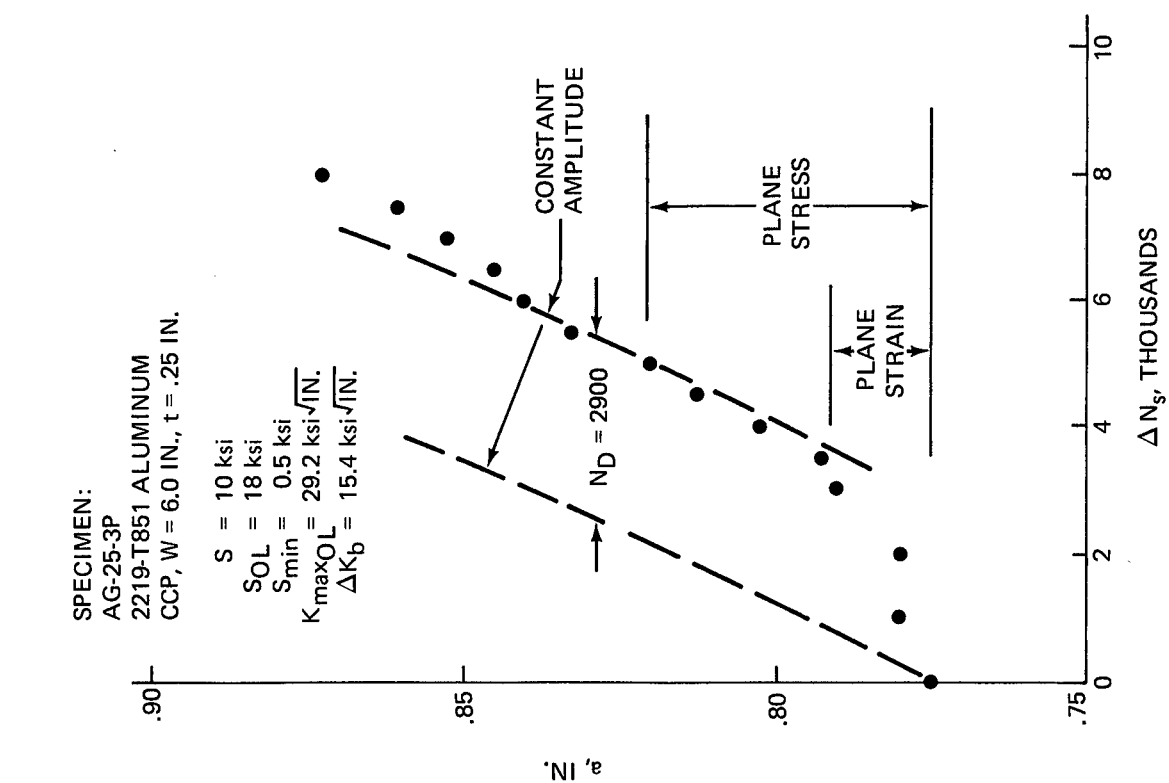


Fig. 29 a vs. ΔN_s for Overload Tests. O/L = 1.8, 2219-T851

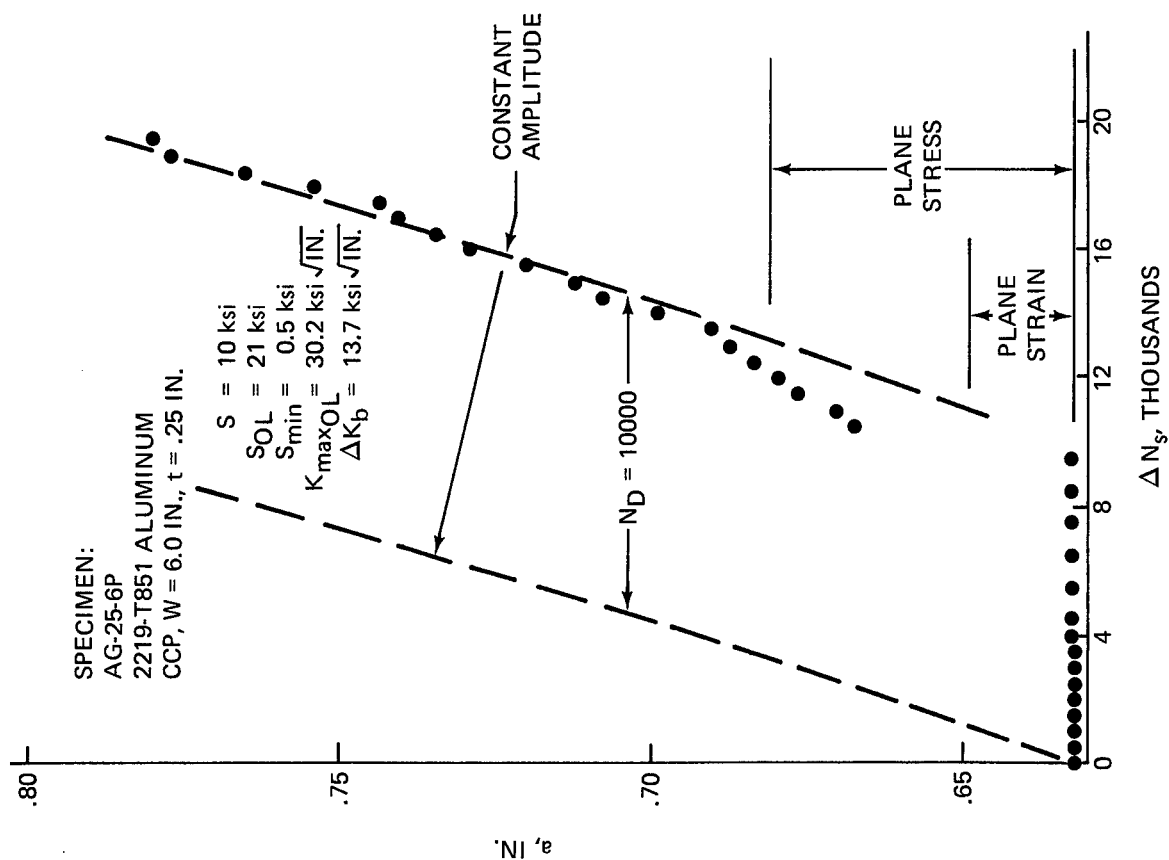


Fig. 30 a vs. ΔN_s for Overload Tests. O/L = 2.1, 2219-T851

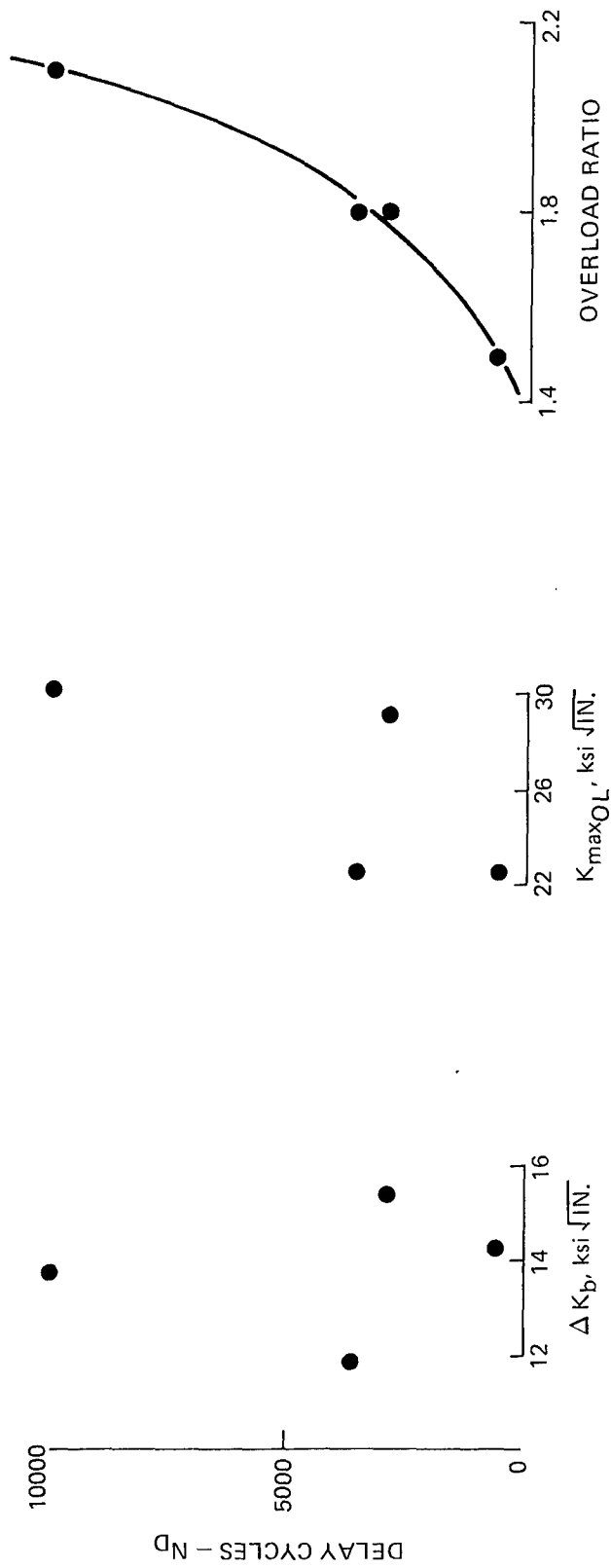


Fig. 31 Delay Cycles vs. Three Parameters

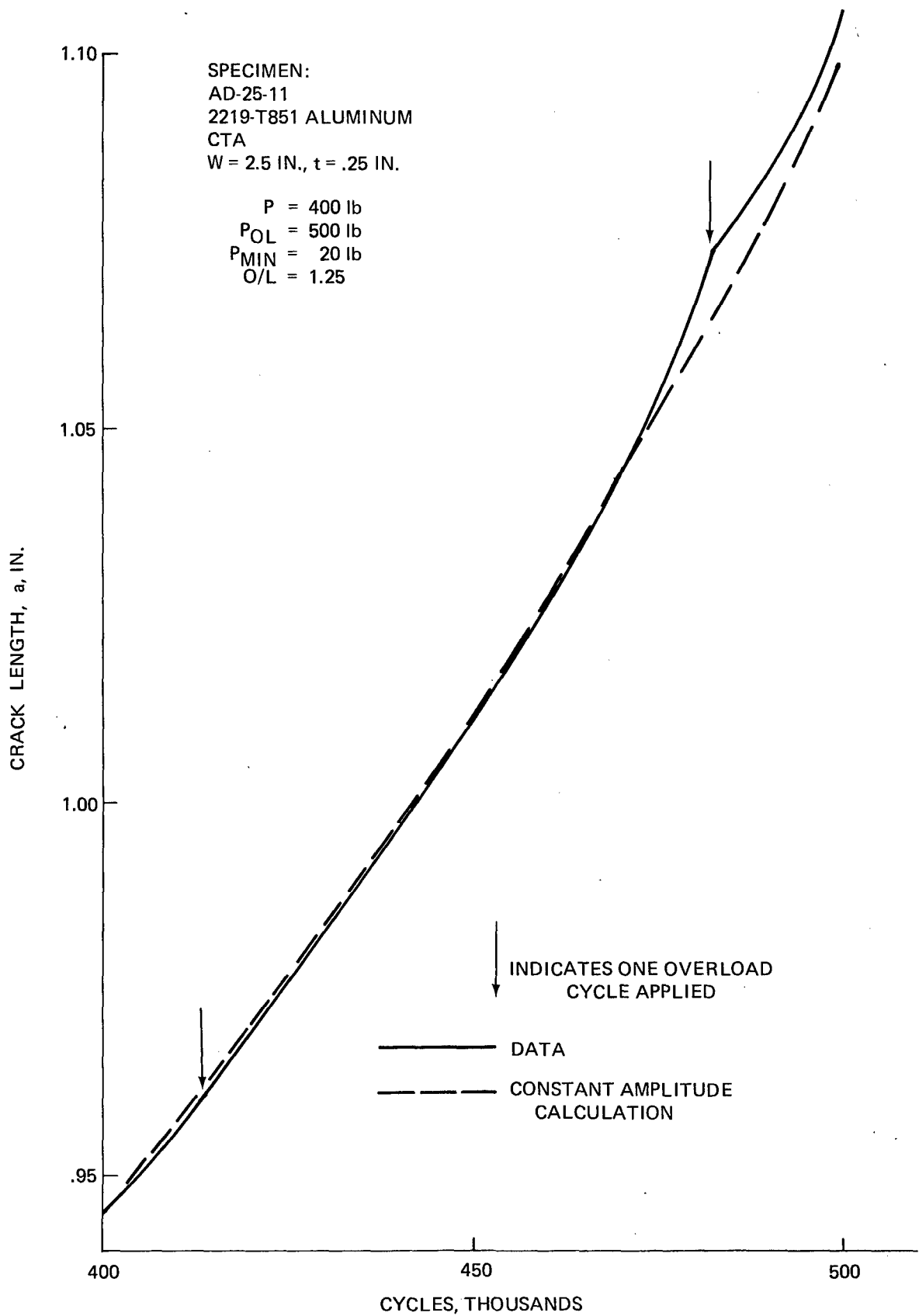


Fig. 32 Crack Length vs. Cycles for Overload Tests; O/L = 1.25, 2219-T851 Aluminum

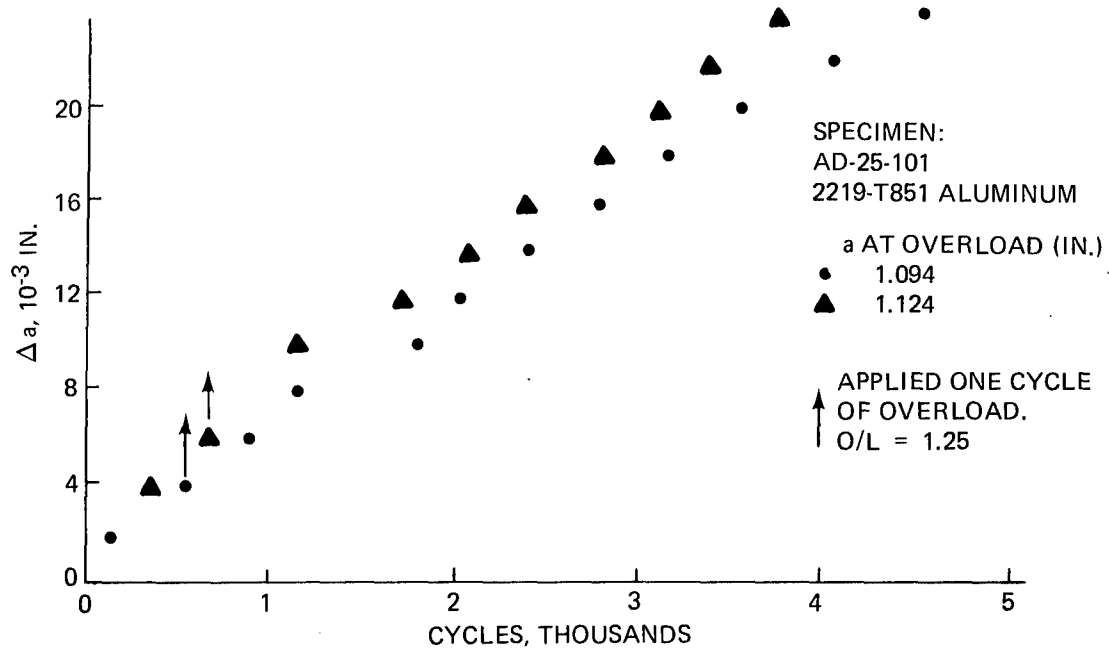


Fig. 33 Crack Length vs. Cycles, O/L = 1.25

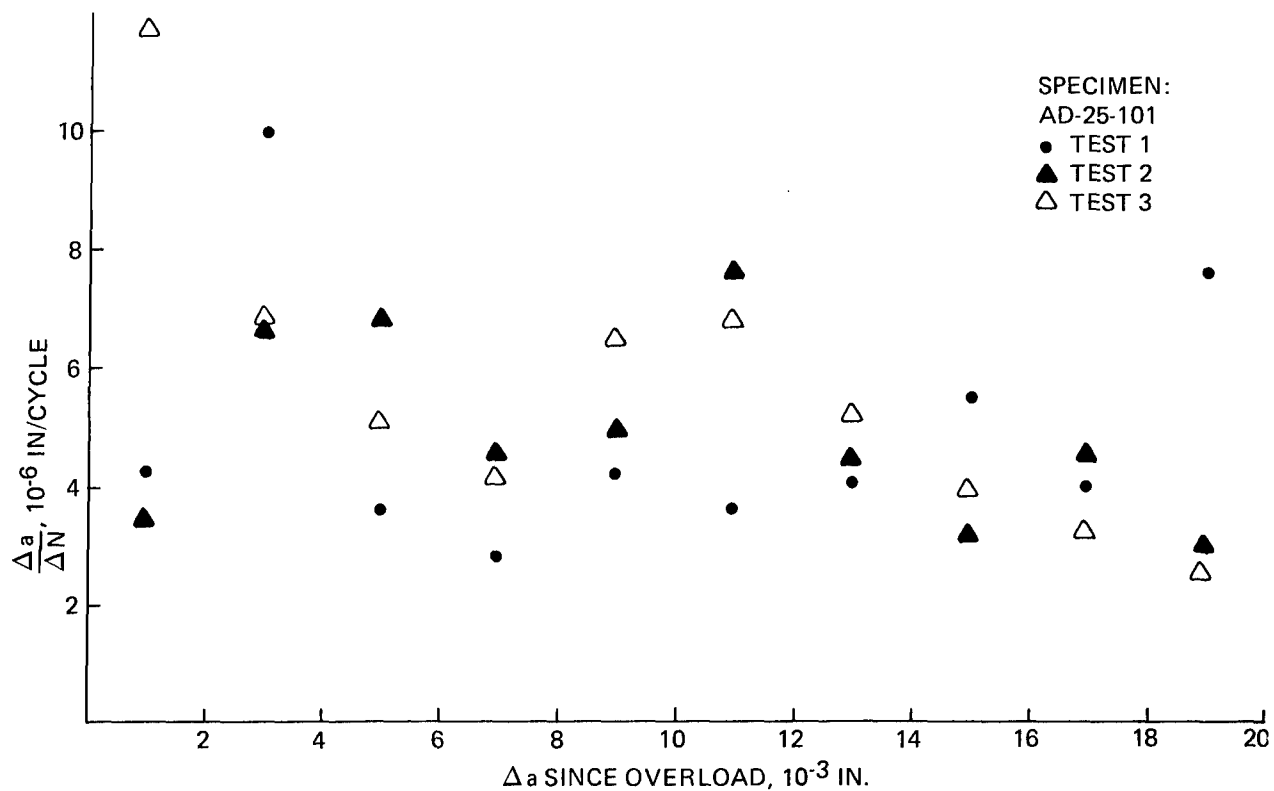


Fig. 34 Instantaneous $\Delta a/\Delta N$ vs. Δa after Overload

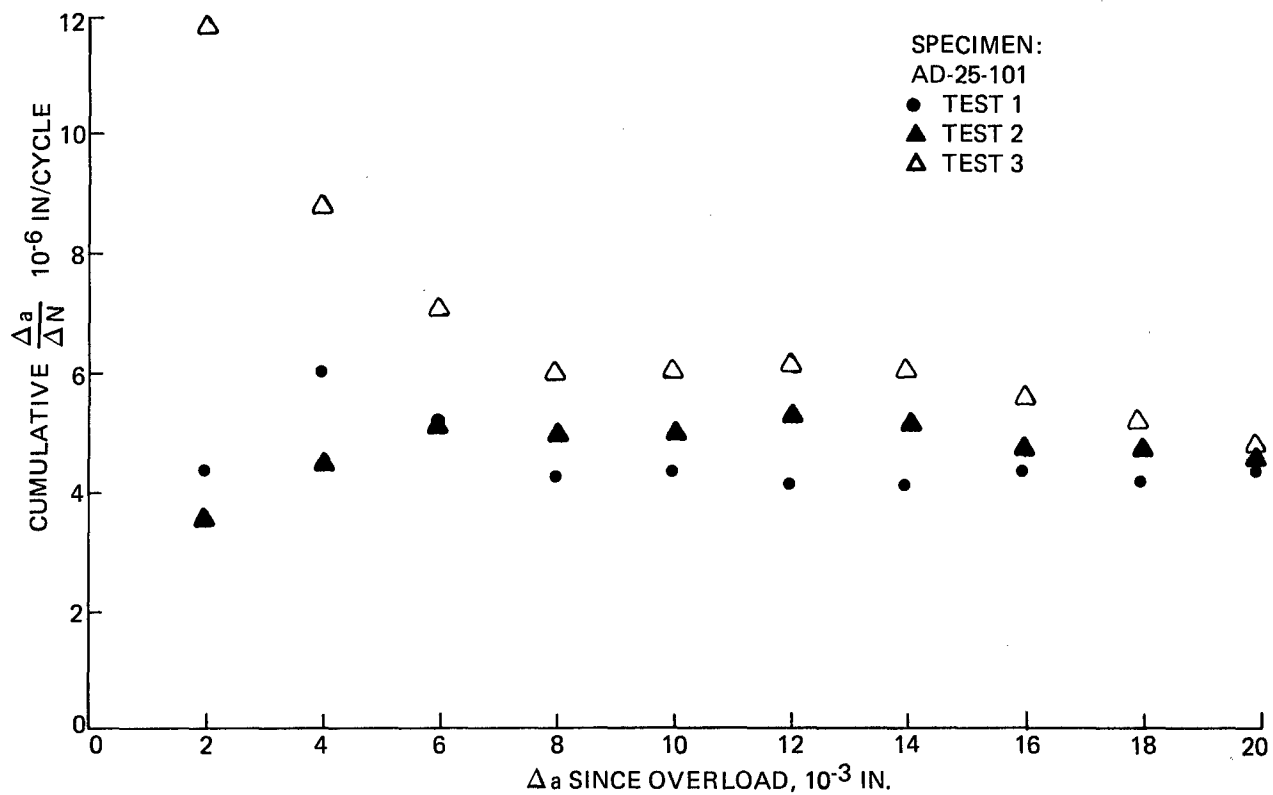


Fig. 35 Cumulative $\Delta a/\Delta N$ vs. Δa after Overload

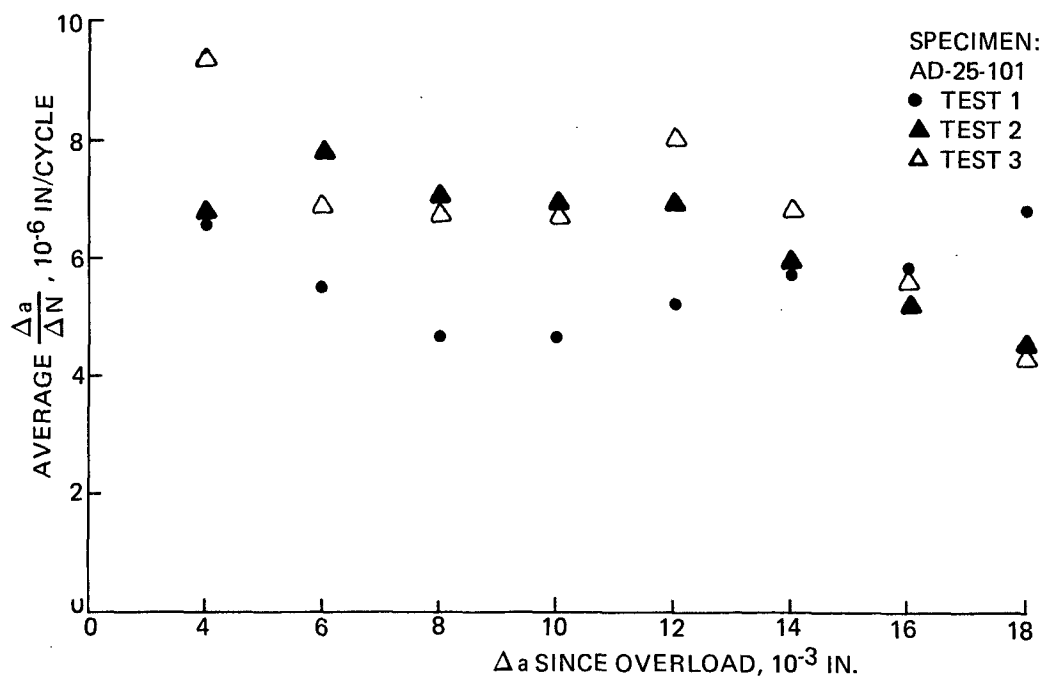
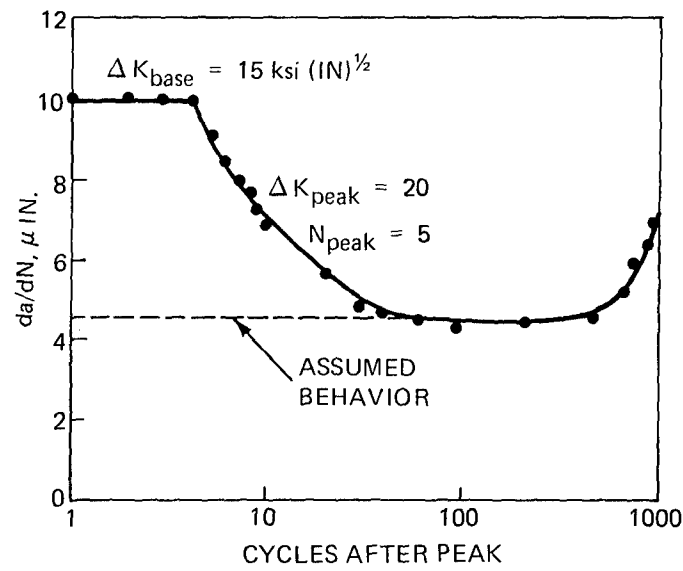
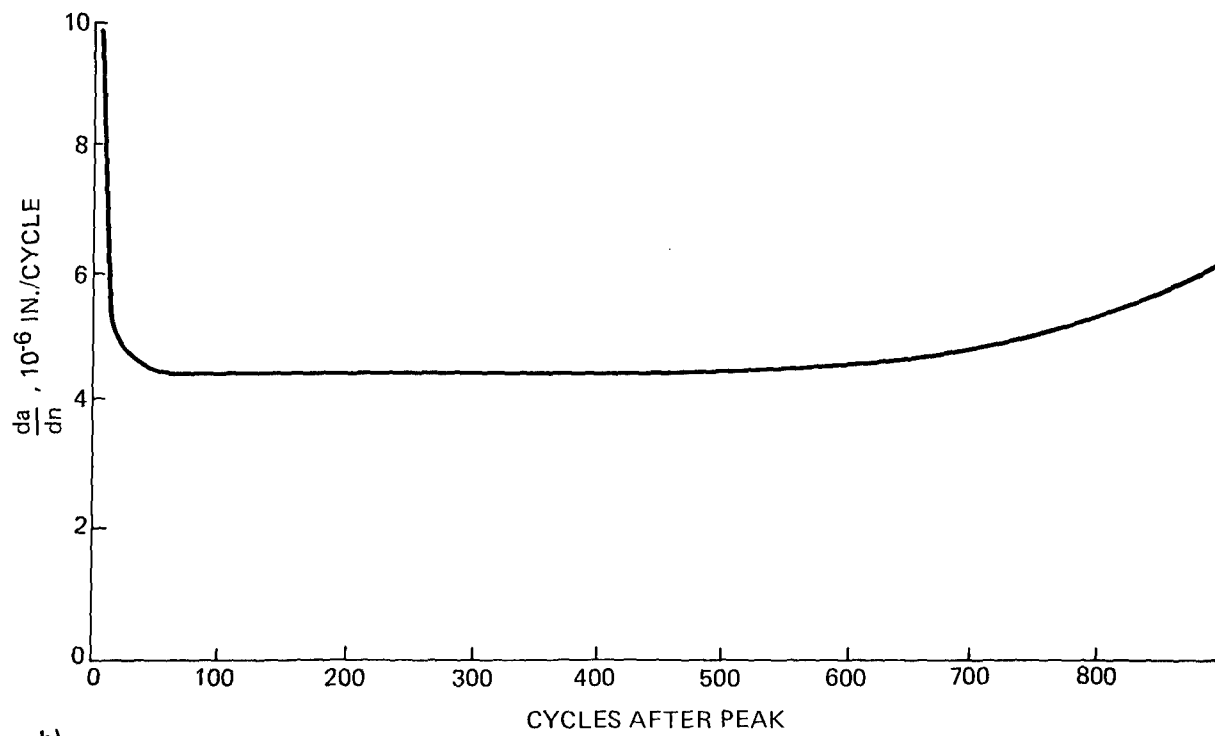


Fig. 36 Average $\Delta a/\Delta N$ vs. Δa after Overload



a)



b)

Fig. 37 "Typical" Crack Growth After An Overload

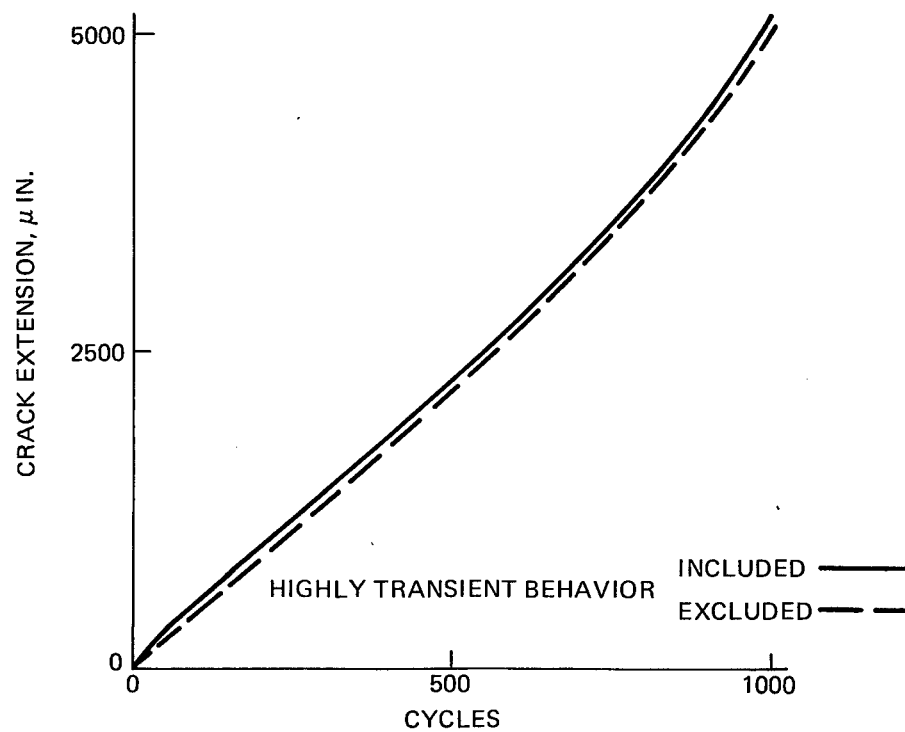
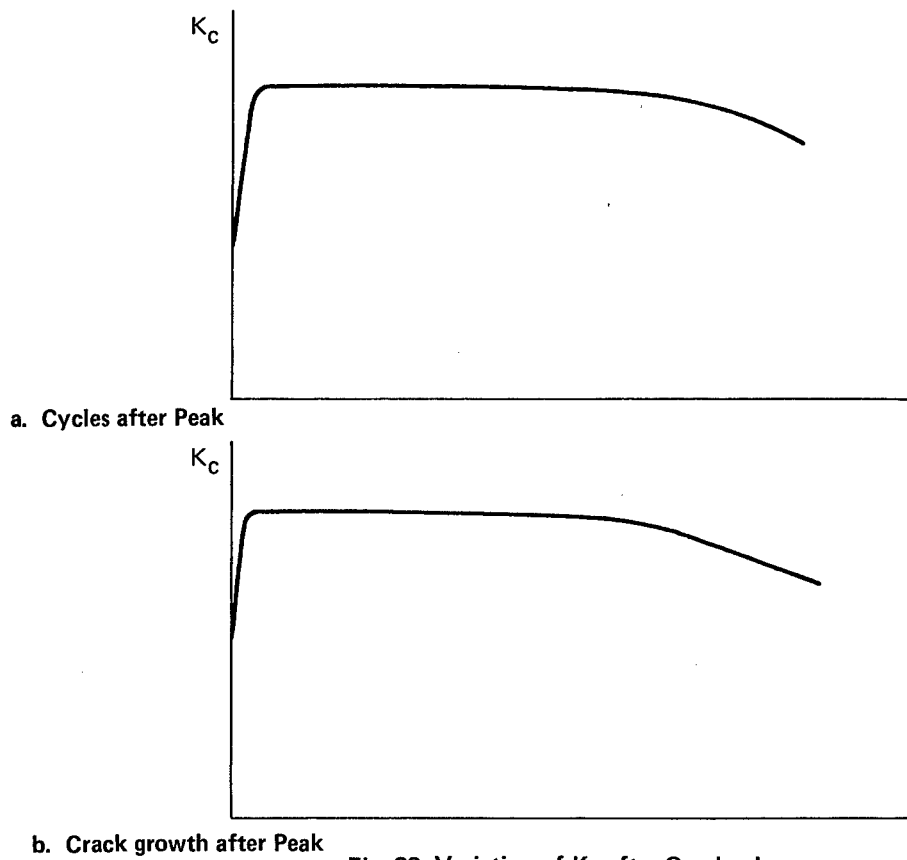


Fig. 39 Calculated Crack Growth With and Without Highly Transient Behavior

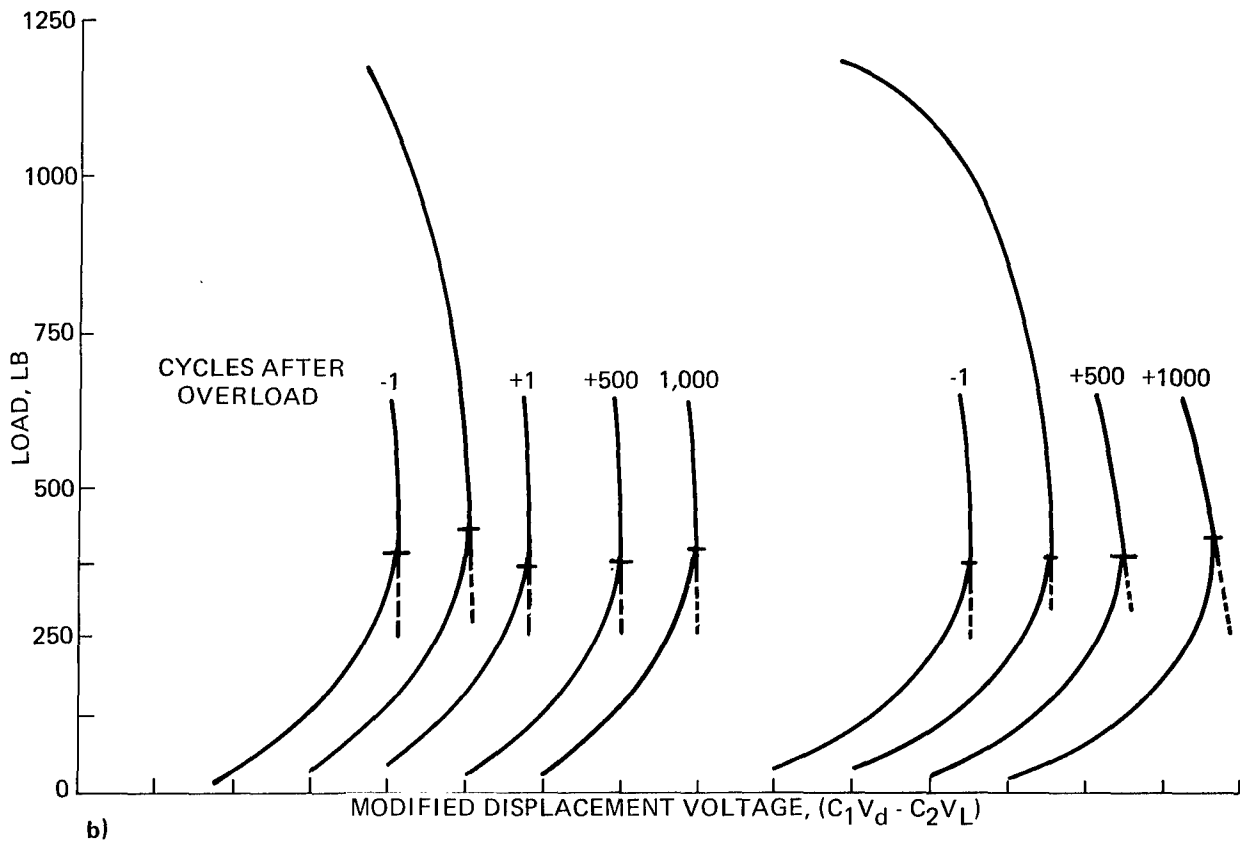
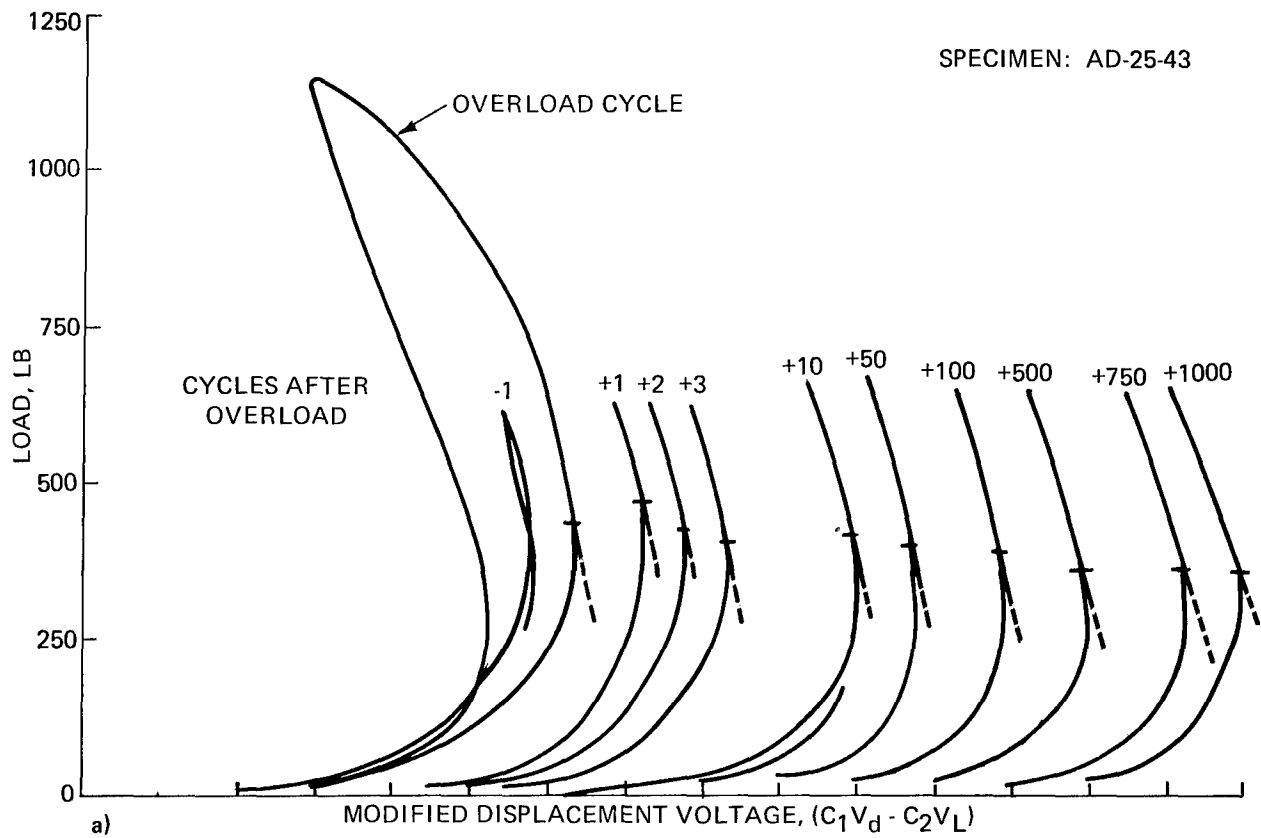


Fig. 40 Crack opening Traces, Periodic Overload

SPECIMEN AD-25-43
 2219-T851 ALUMINUM
 CTA, W = 2.5 IN., t = .25 IN.

P_{max} (lb)	P_{min} (lb)	CYCLES
1170	33	1
650	33	1000

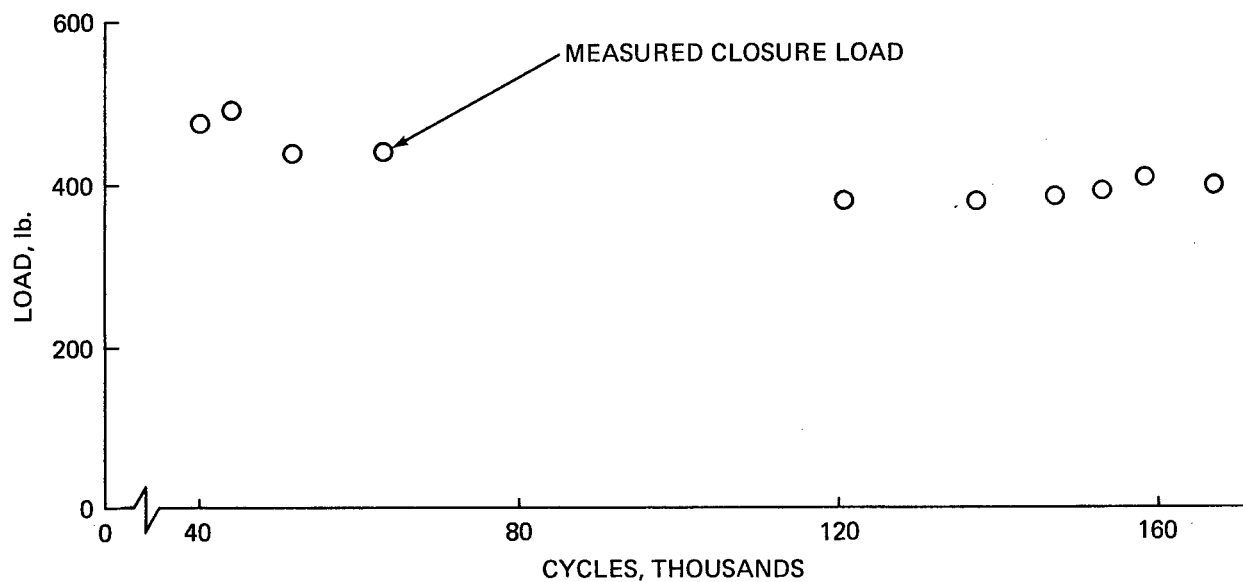


Fig. 41 Crack Opening Load vs Cycles, Periodic Overload

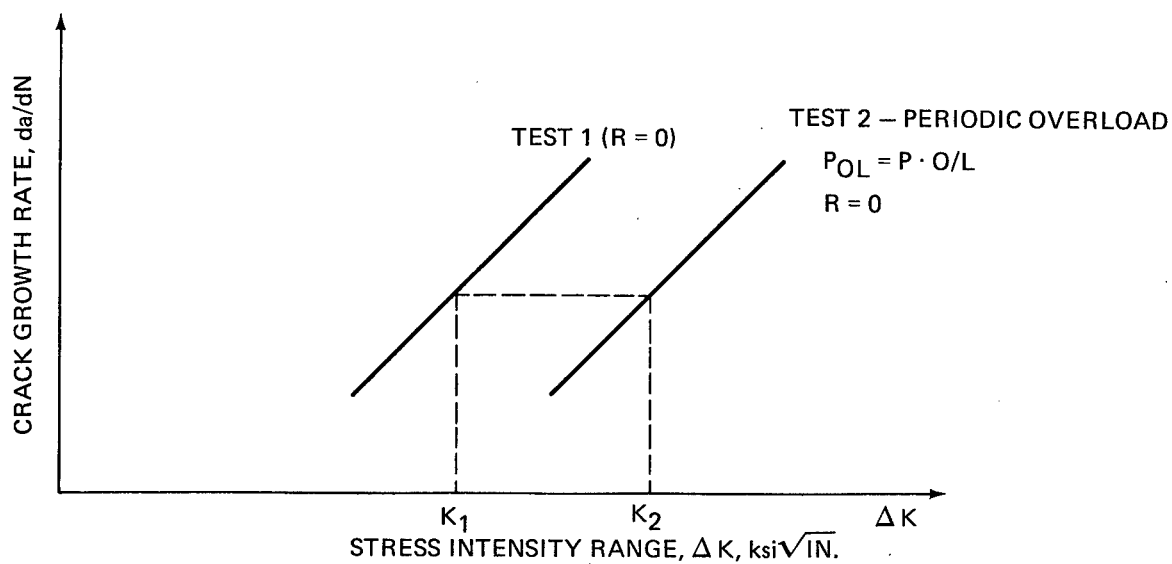


Fig. 42 Periodic Overload and Constant Amplitude Tests

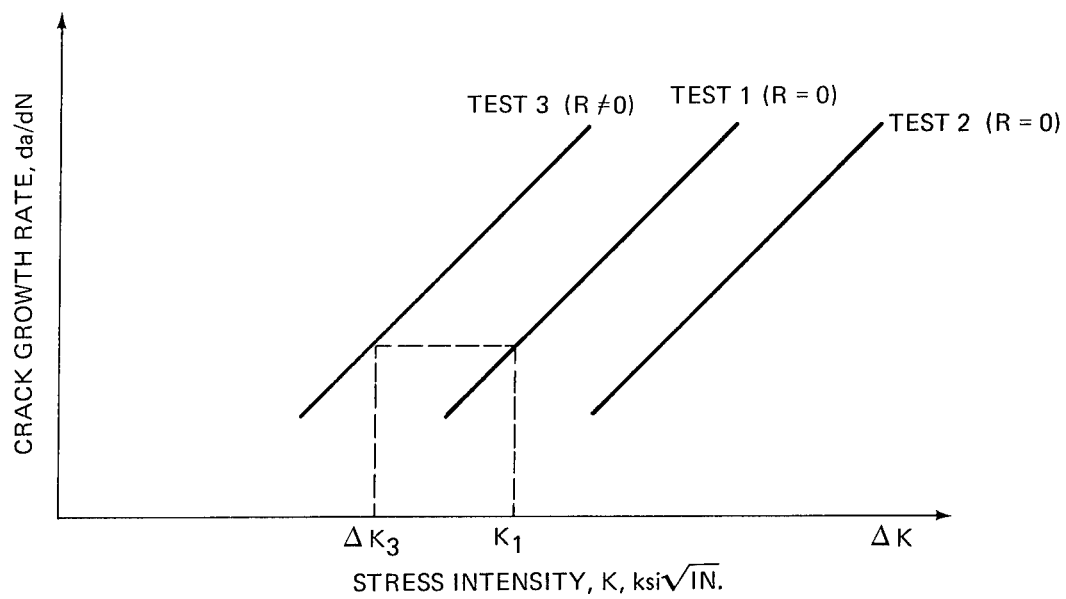


Fig. 43 Effect of Stress Ratio Changes

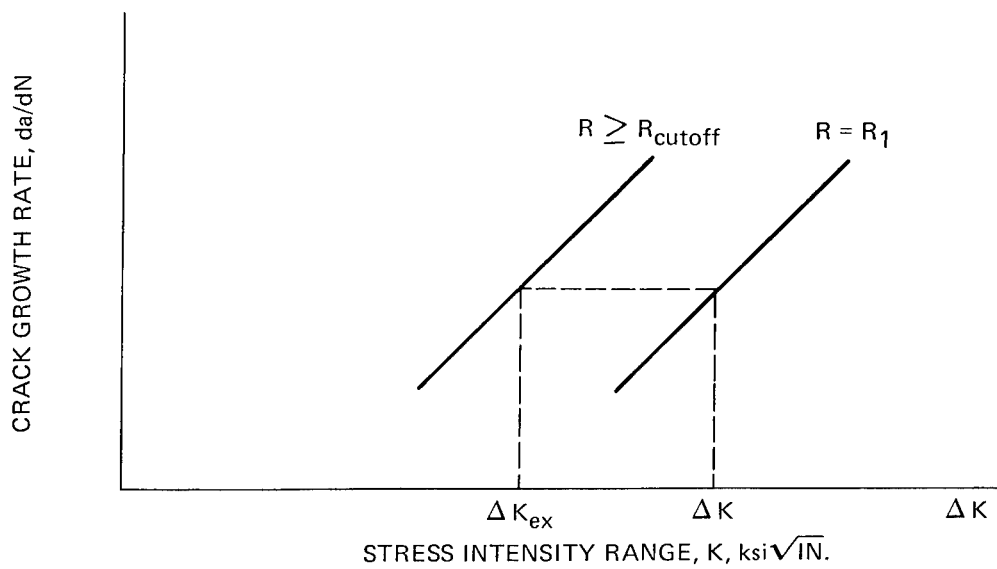


Fig. 44 Evaluation of Extreme Rate Curve

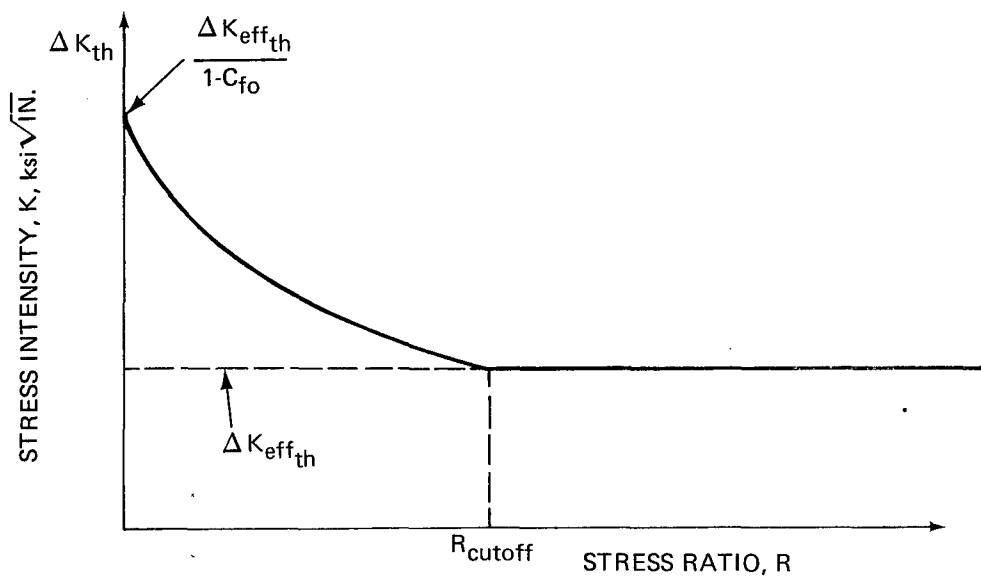


Fig. 45 Variation of ΔK_{th} with Stress Ratio

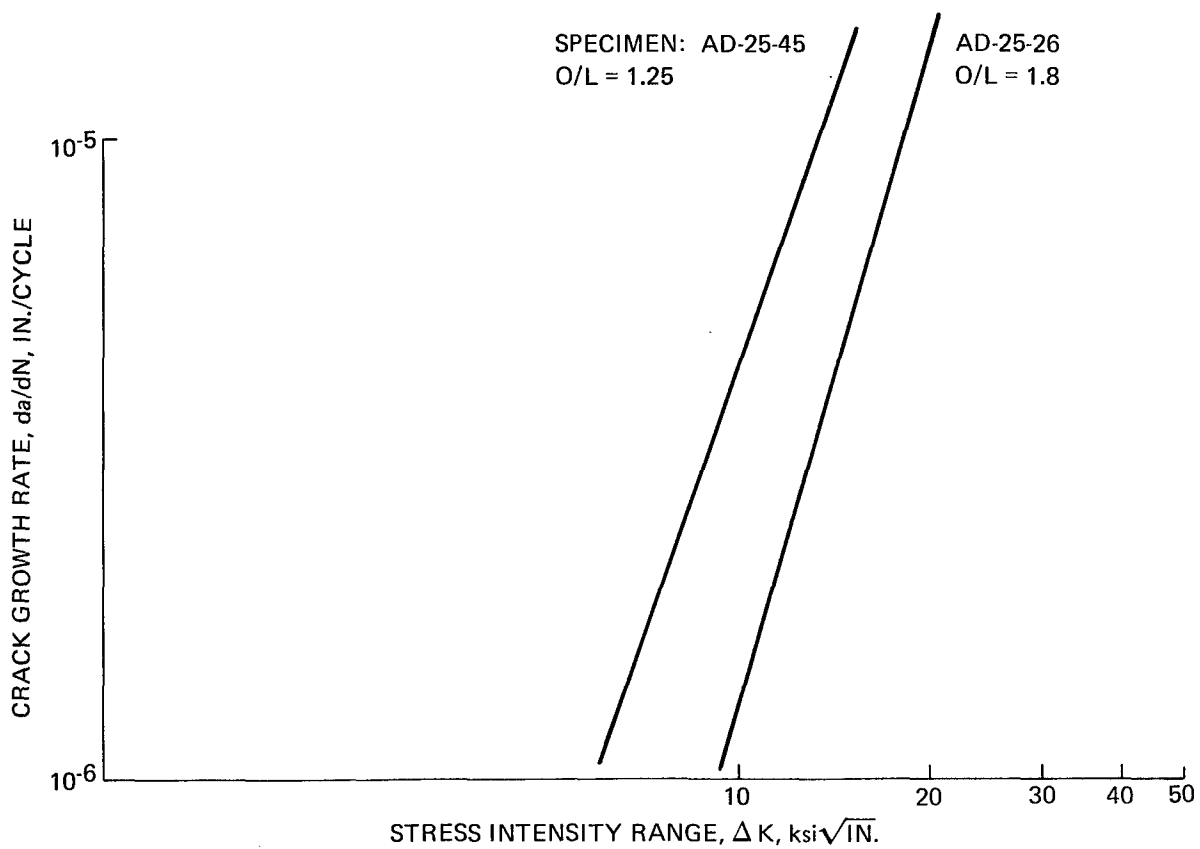


Fig. 46 Periodic Overload Test Comparison

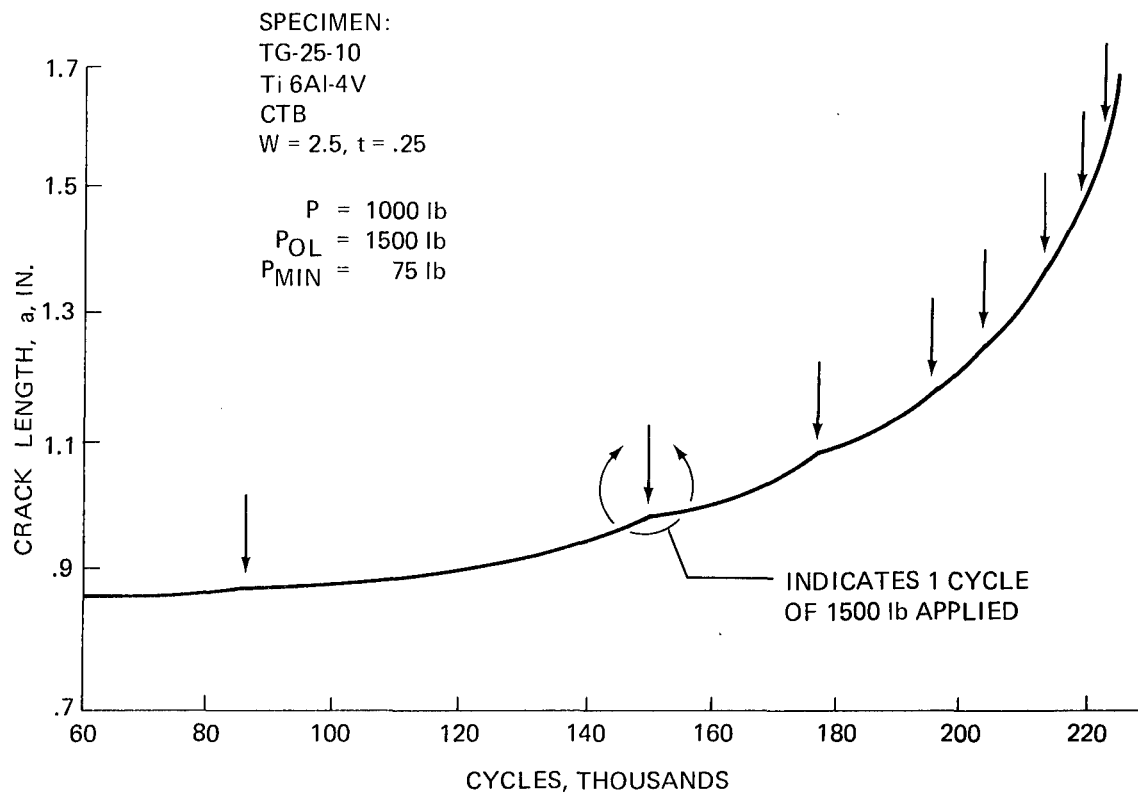


Fig. 47 Crack Length vs. Overloads for Single Overloads; O/L = 1.5, Ti 6Al-4V Titanium

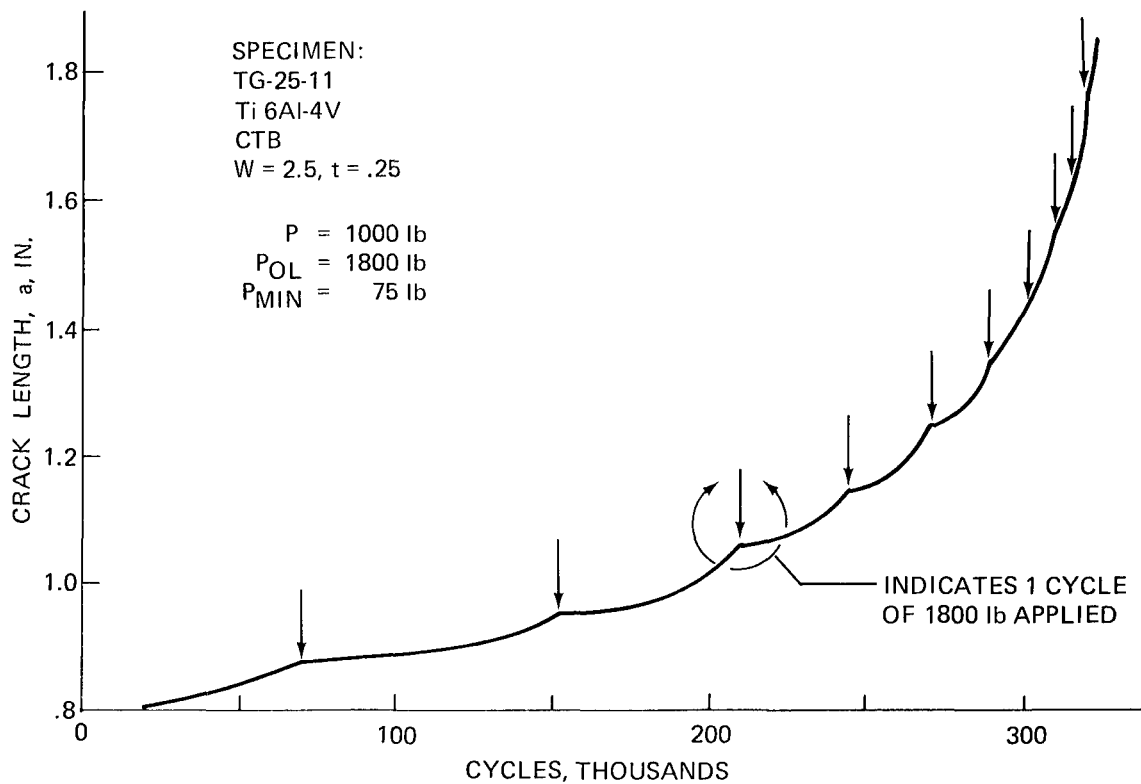


Fig. 48 Crack Length vs. Cycles for Single Overloads; O/L = 1.8, Ti 6Al-4V Titanium

SPECIMEN:
 TG-25-10
 Ti 6Al-4V
 CTB, W = 2.5 IN., t = .25 IN.

P = 1000 lb
 P_{OL} = 1500 lb
 P_{MIN} = 50 lb

• DATA
 --- CONSTANT AMPLITUDE CALCULATION
 ρ PLANE STRESS
 PLASTIC ZONE
 RADIUS

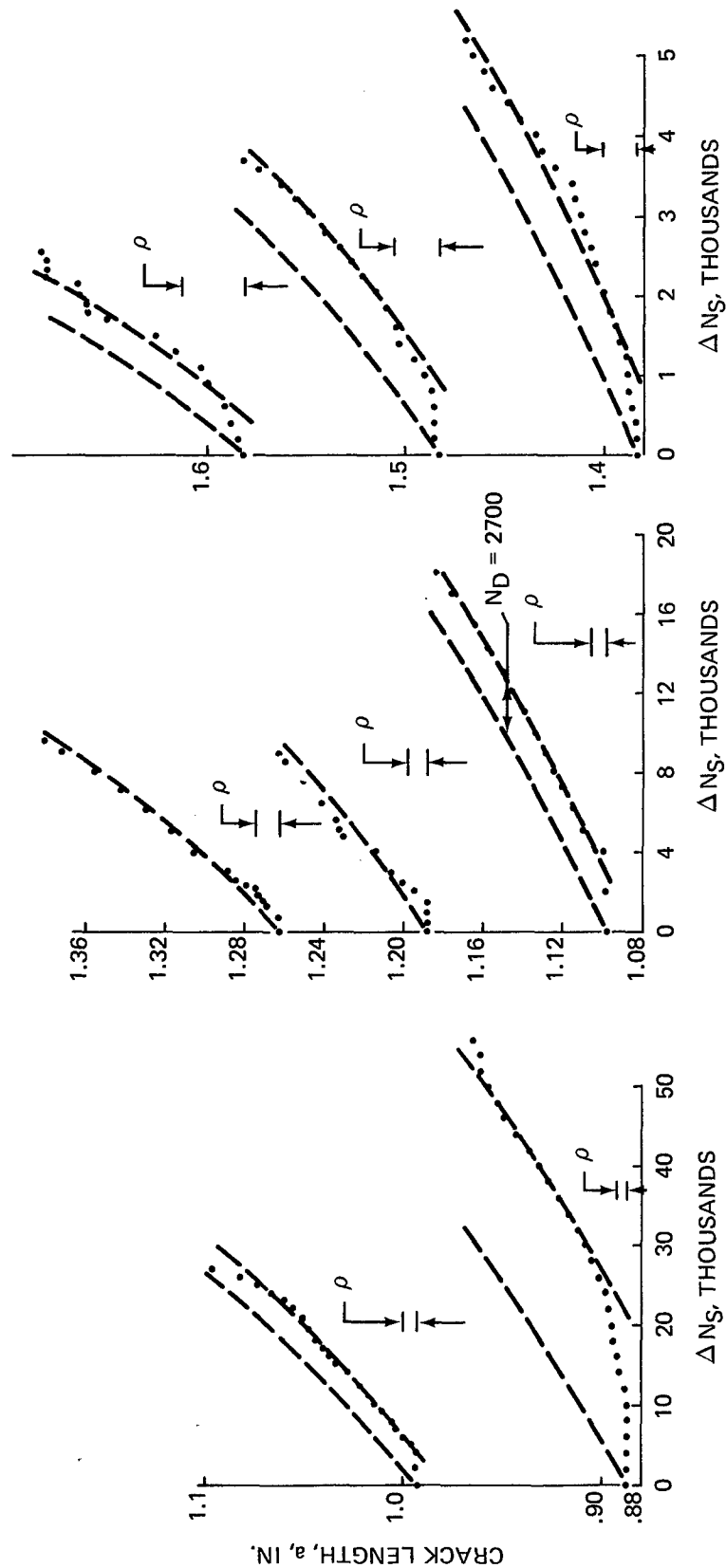


Fig. 49a Detailed Crack Length vs. ΔN_s for Single Overloads; O/L = 1.5, Ti 6Al-4V Titanium

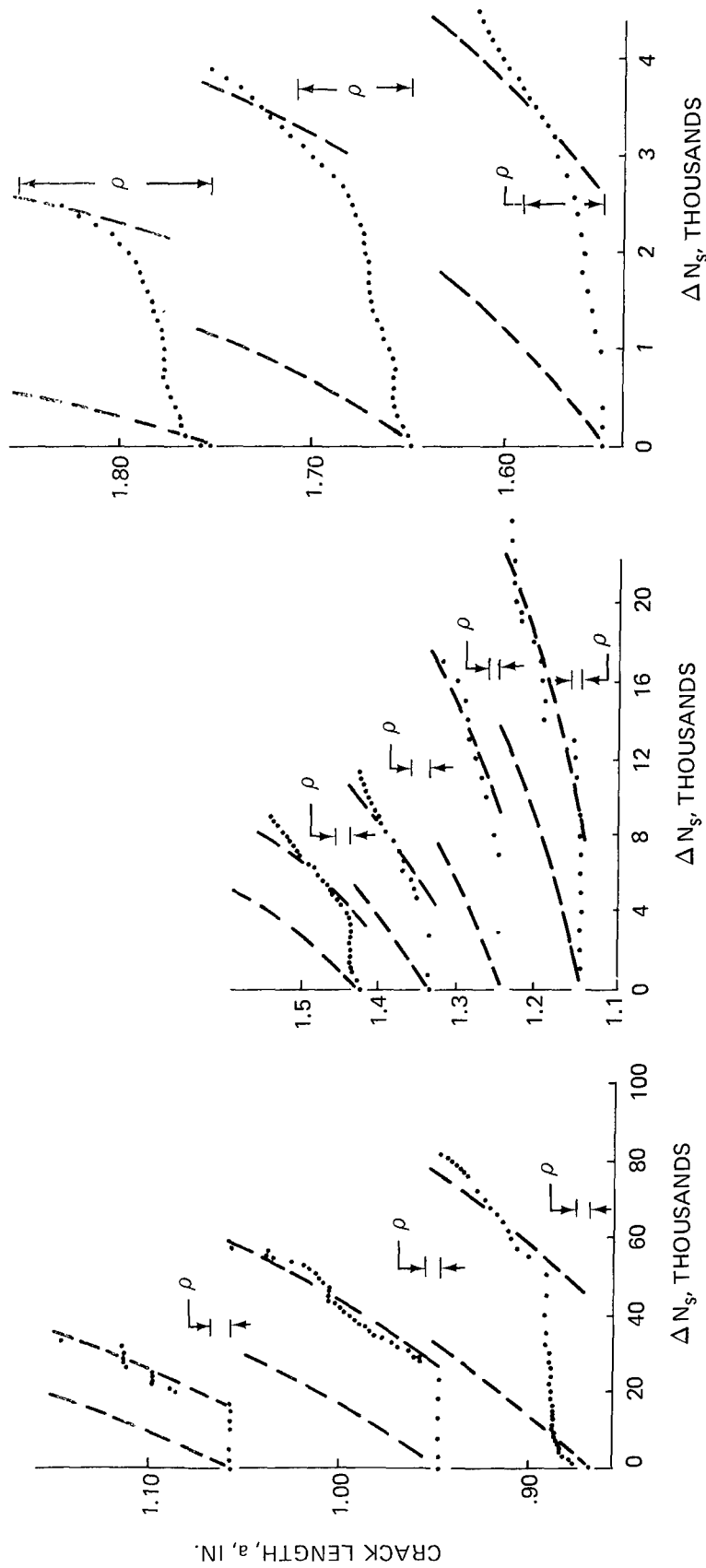
Fig. 49b

Fig. 49c

SPECIMEN:
TG-25-11
Ti 6Al-4V
CTB, W = 2.5 IN., t = .25 IN.

P = 1000 lb
POL = 1800 lb
P_{MIN} = 50 lb

• DATA
--- CONSTANT AMPLITUDE
ρ PLANE STRESS
PLASTIC ZONE
RADIUS



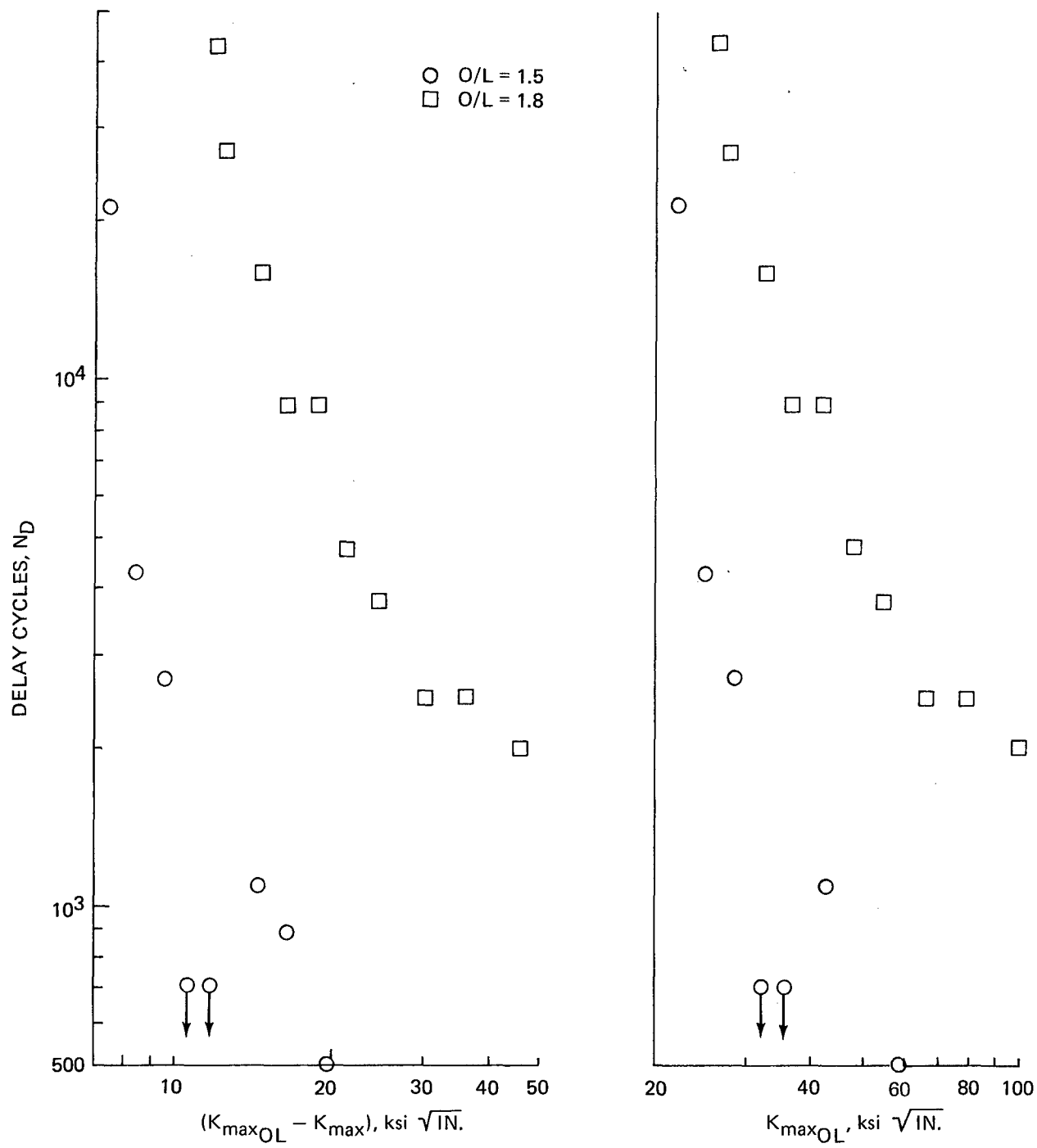


Fig. 50 Delay Cycles vs. $(K_{max_{OL}} - K_{max})$ and vs. $(K_{max_{OL}})$ for O/L = 1.5 and 1.8

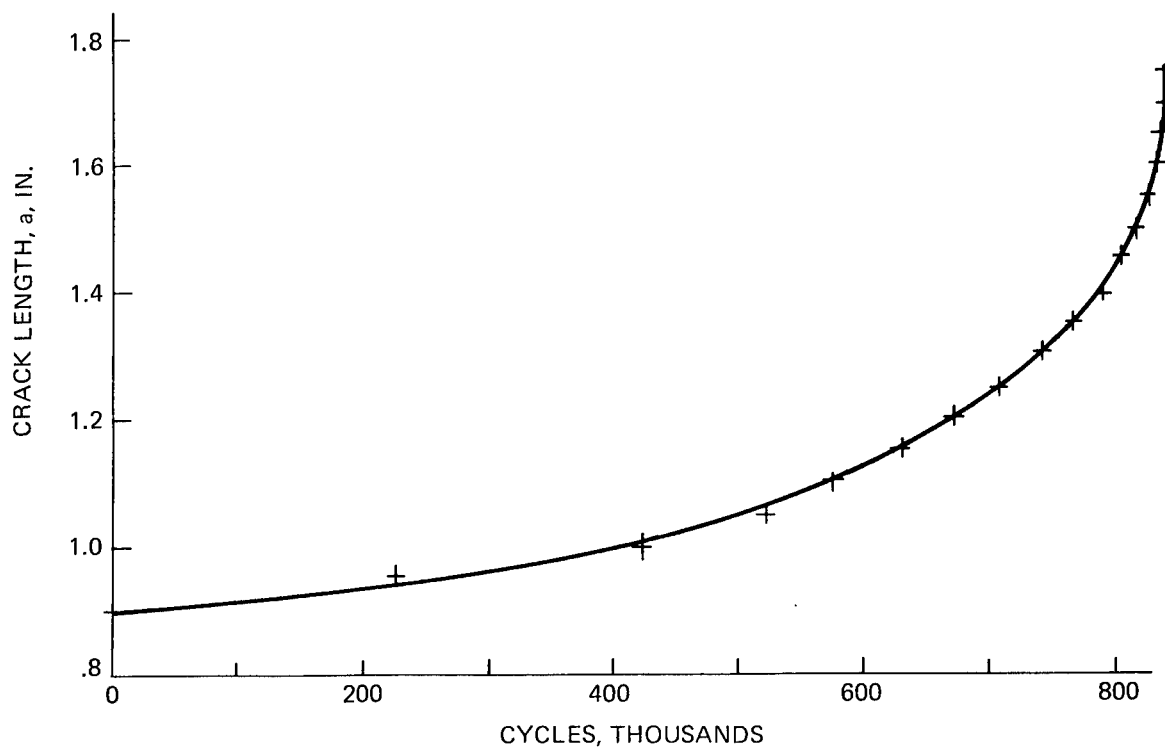
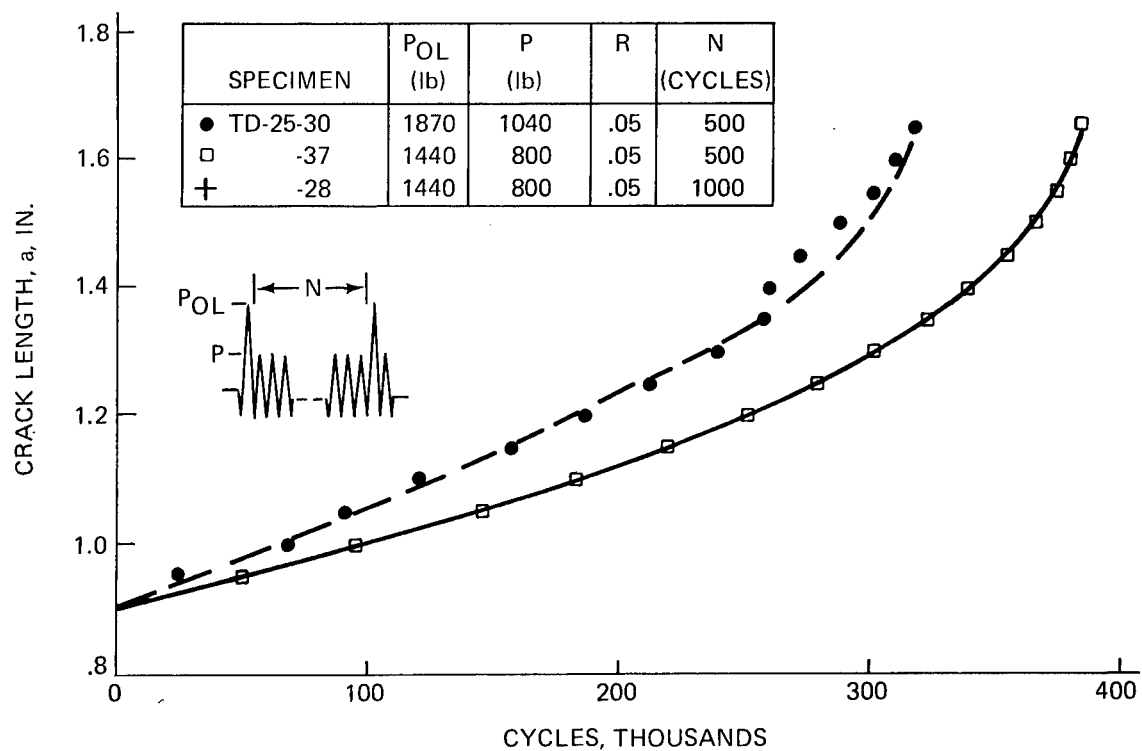


Fig. 51 Crack Length vs. Cycles for Single Periodic Overloads, O/L = 1.8, Titanium

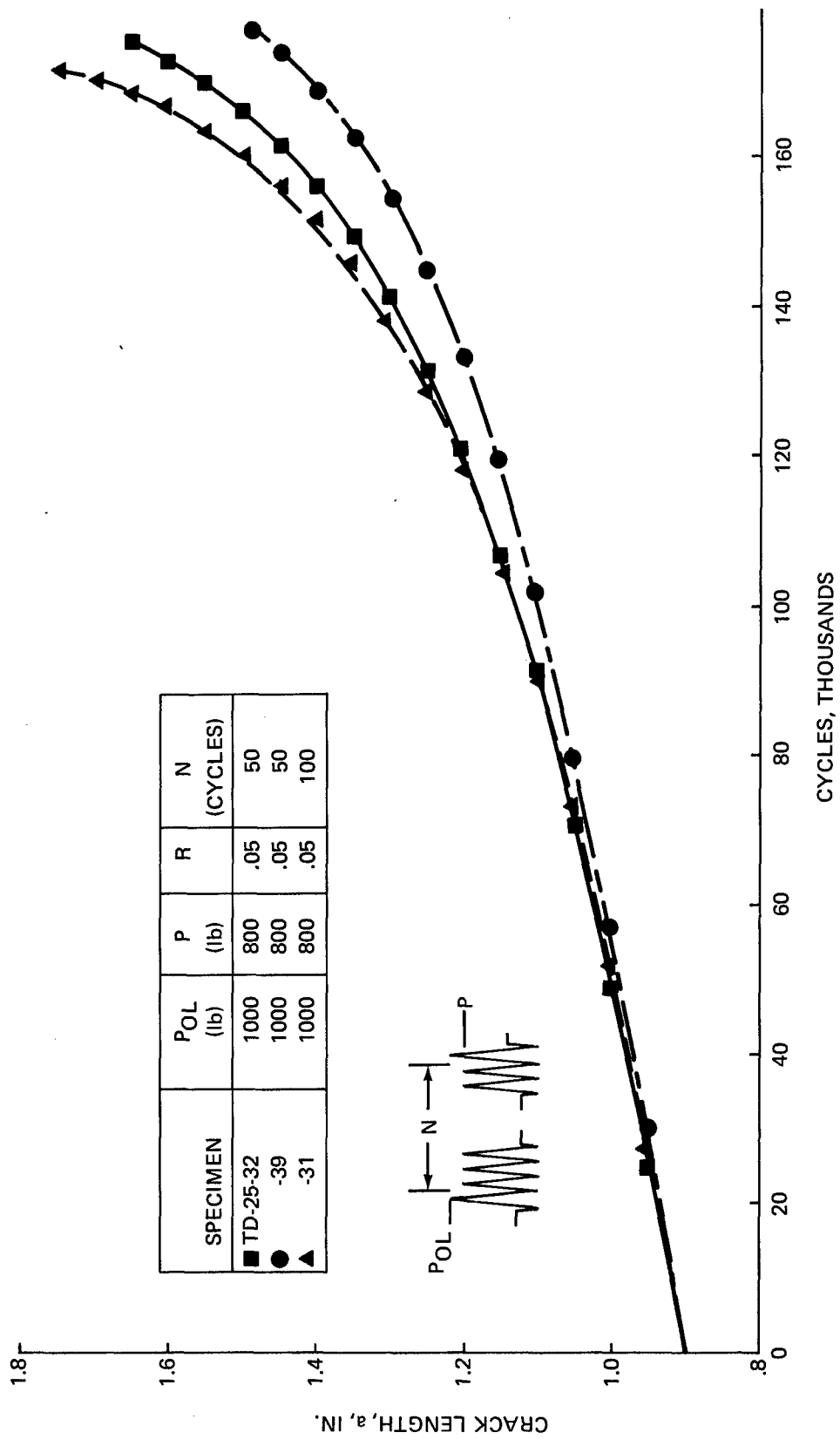


Fig. 52 Crack Length vs. Cycles for Single Periodic Overloads, $O/L = 1.25$ Titanium

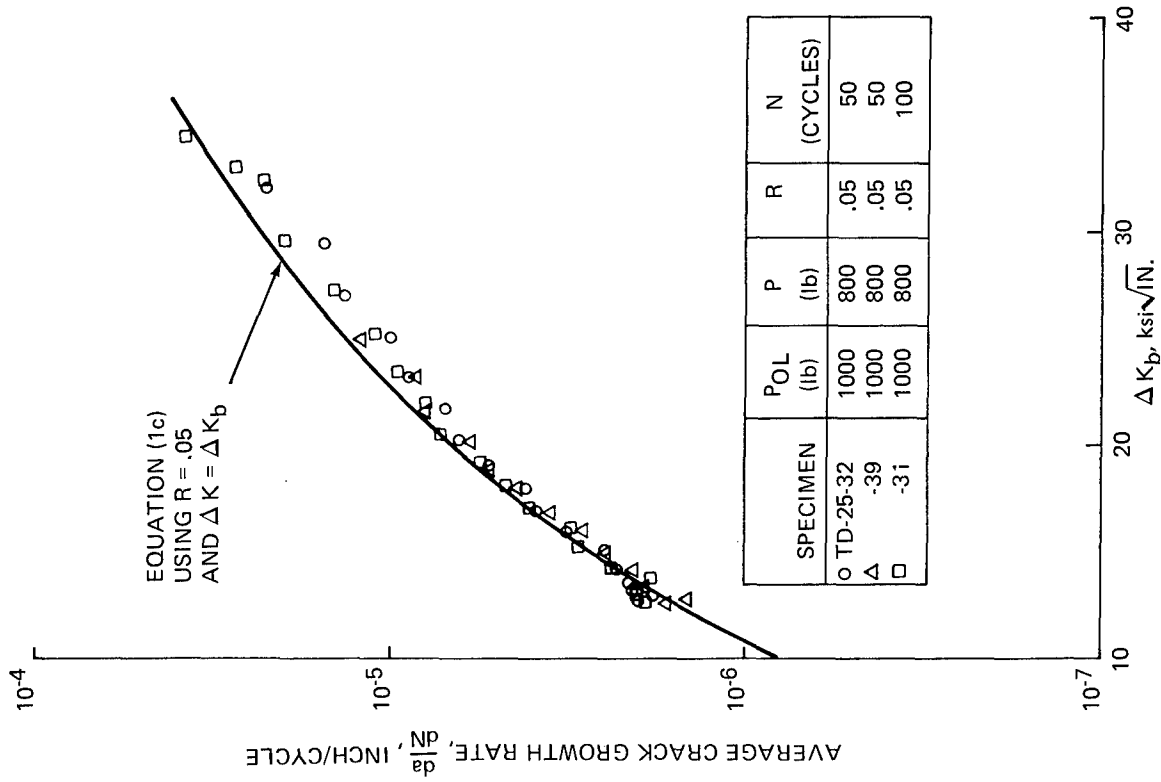


Fig. 53 $\frac{da}{dN}$ vs. ΔK_b for Single Periodic Overloads, $O/L = 1.25$, Titanium

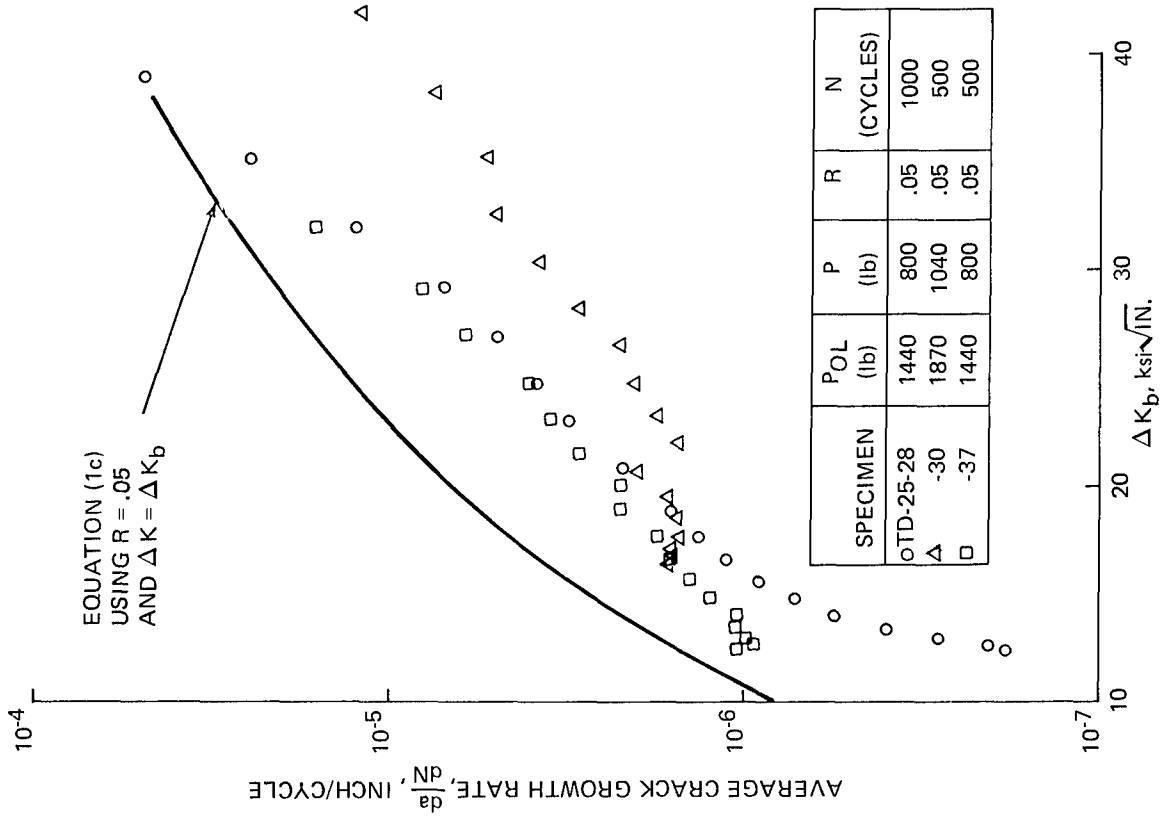


Fig. 54 $\frac{da}{dN}$ vs. ΔK_b for Single Periodic Overloads, $O/L = 1.8$, Titanium

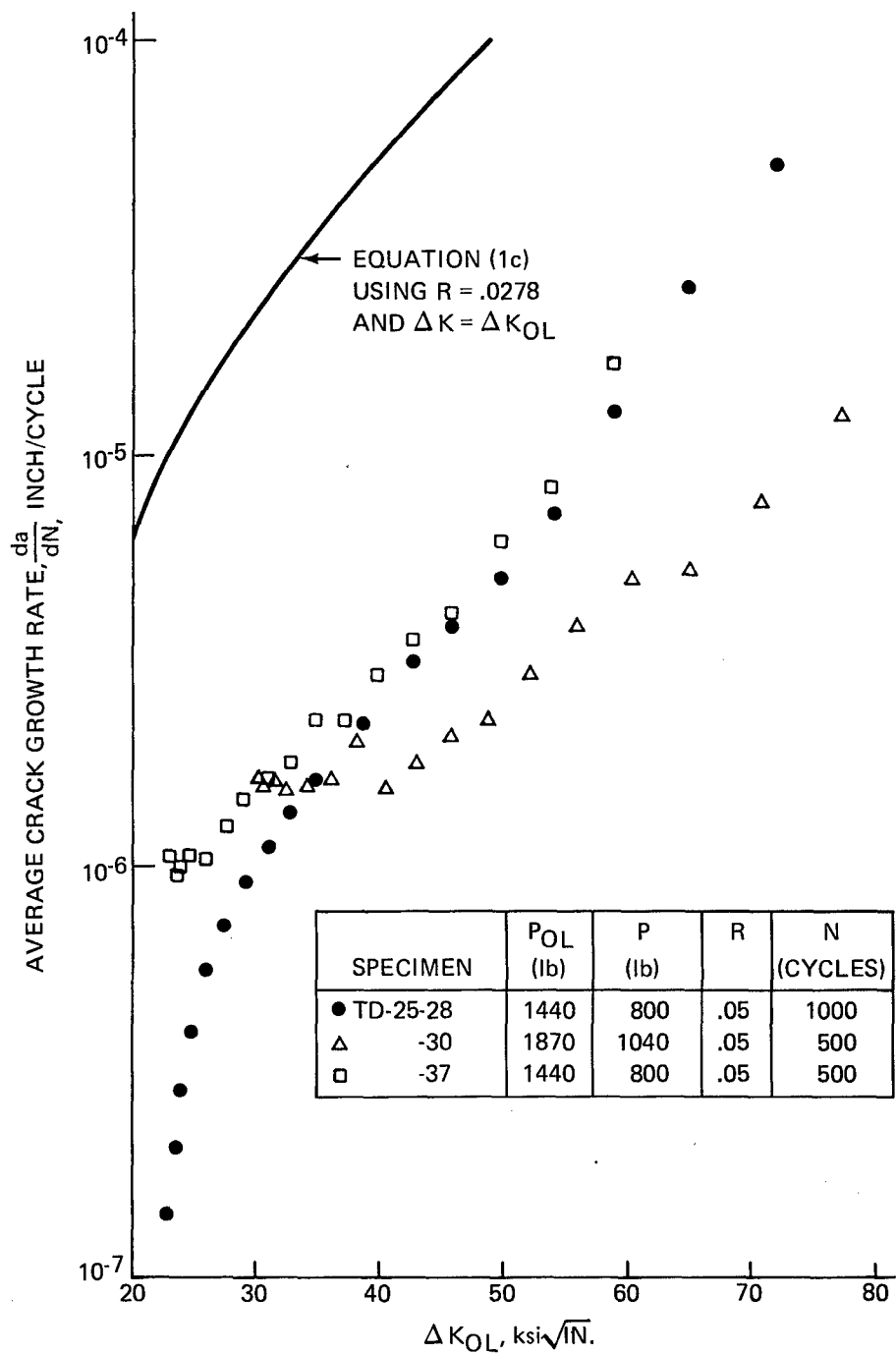
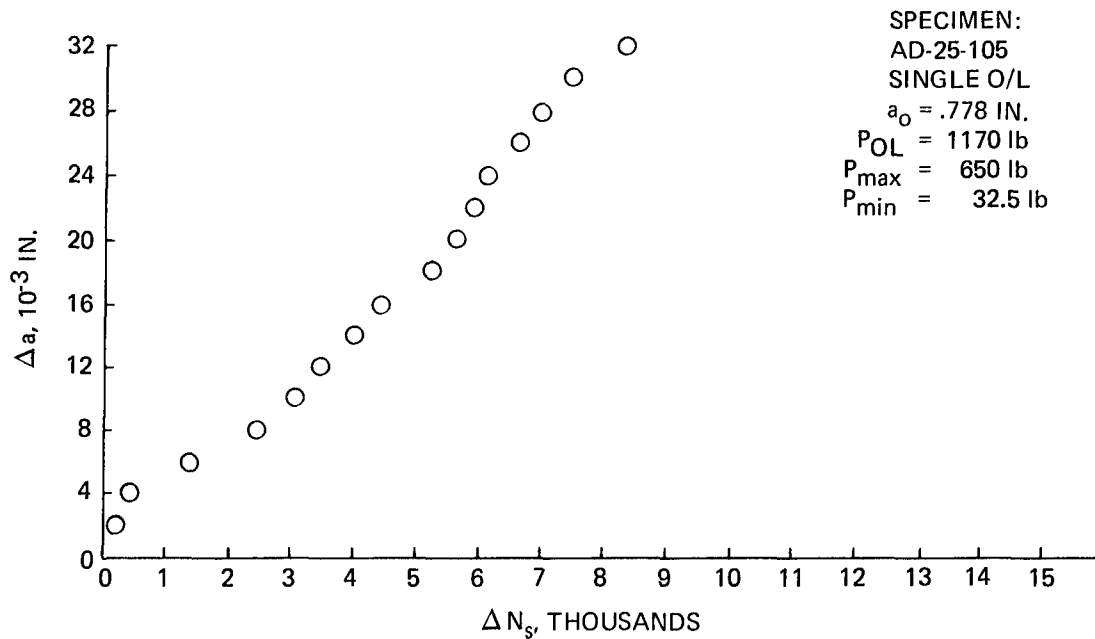
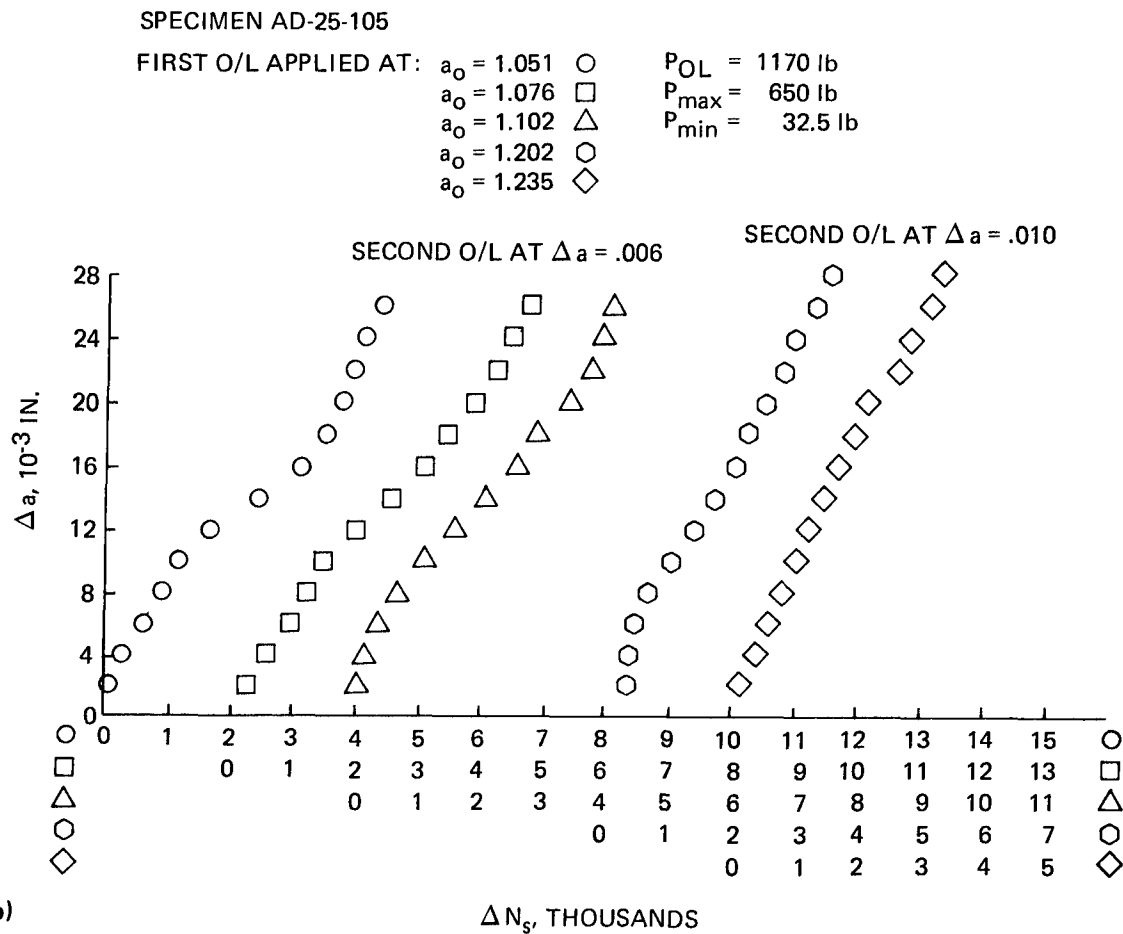


Fig. 55 $\frac{da}{dN}$ vs. ΔK_{OL} for Single Periodic Overloads, $O/L = 1.8$, Titanium



a)



b)

Fig. 56 Detailed Crack Growth vs. ΔN_s for Single Overload Interactions, 2219-T851

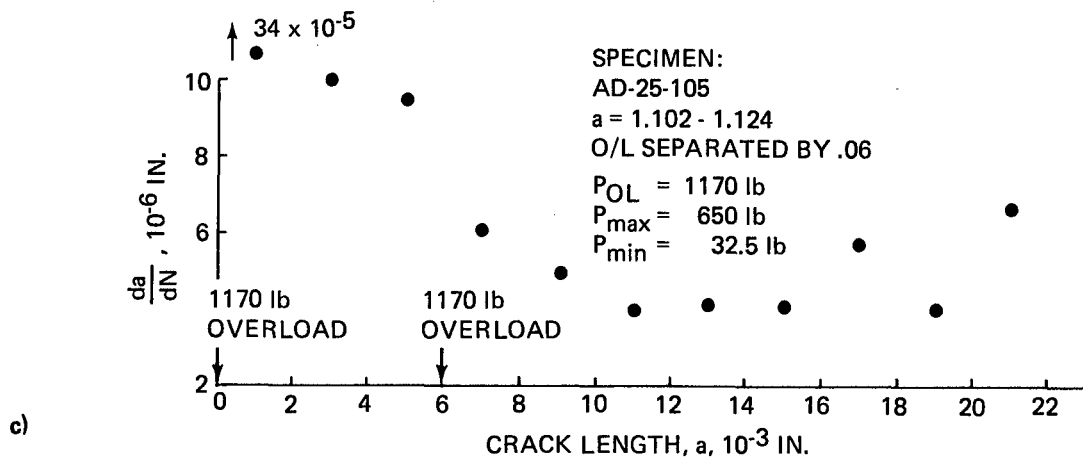
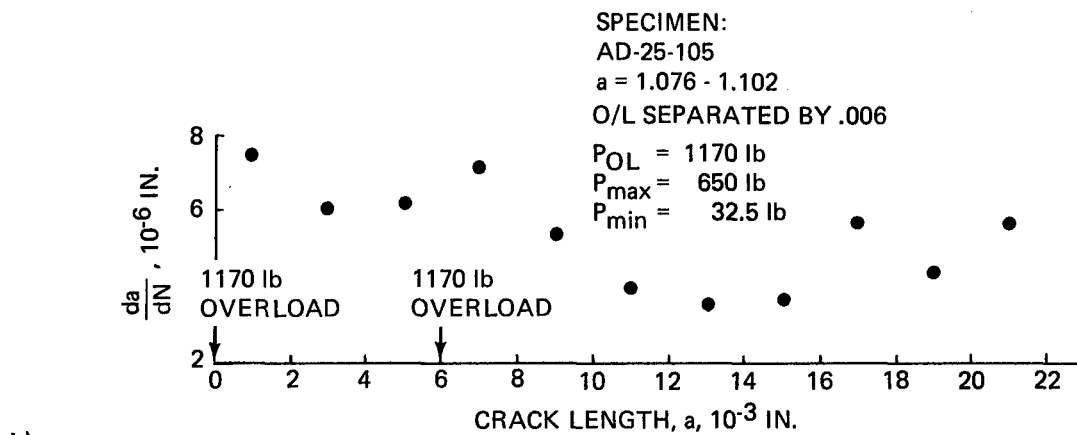
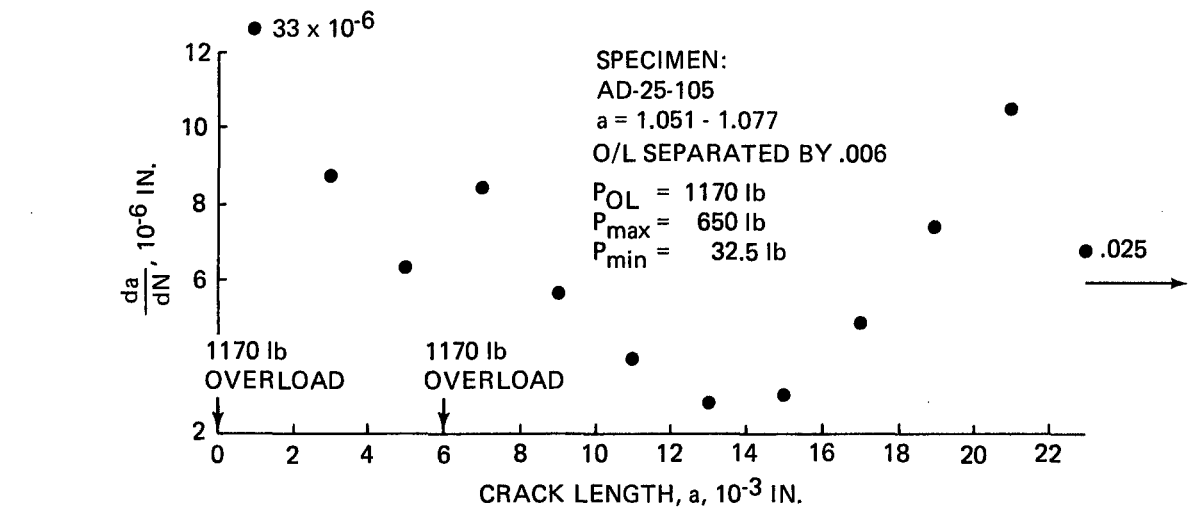


Fig. 57 Measured Crack Growth Rate vs. Crack Extension for Single Overload Interactions, 2219-T851

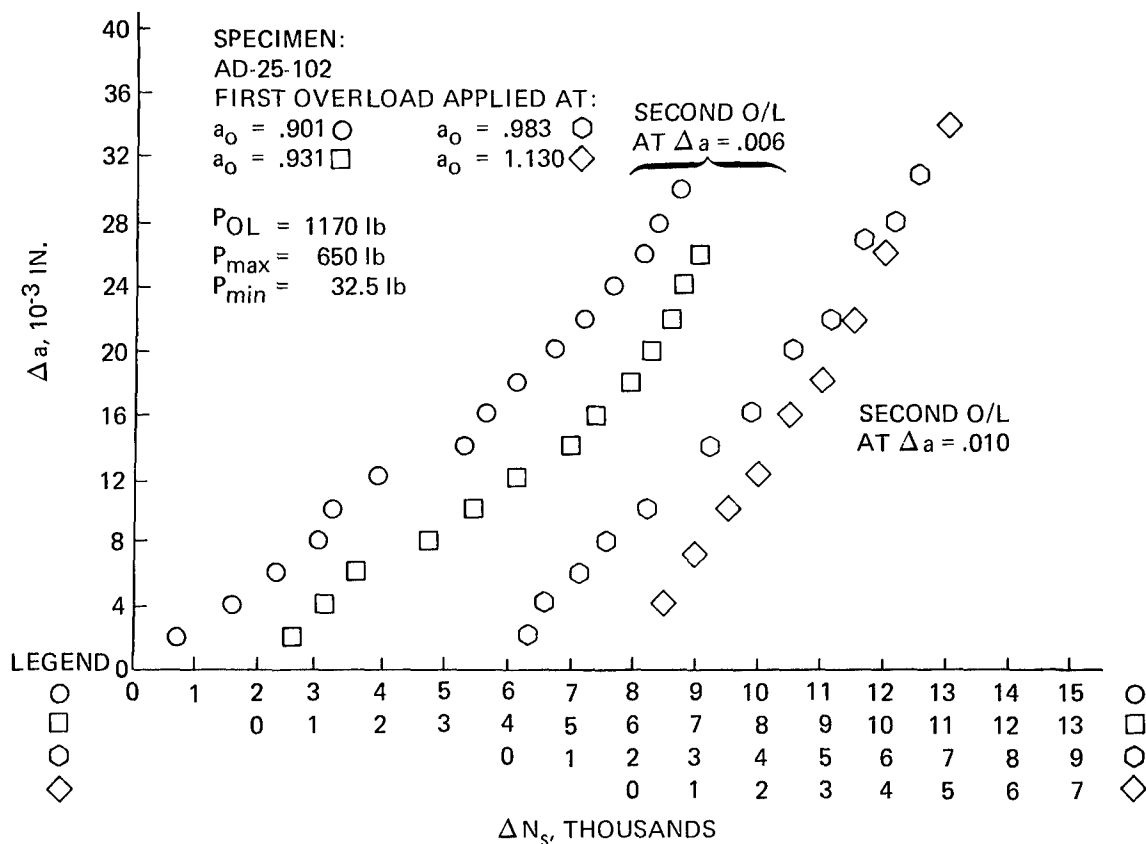


Fig. 58 Detailed Crack Growth vs. ΔN_s for Single Periodic Overloads, Aluminum

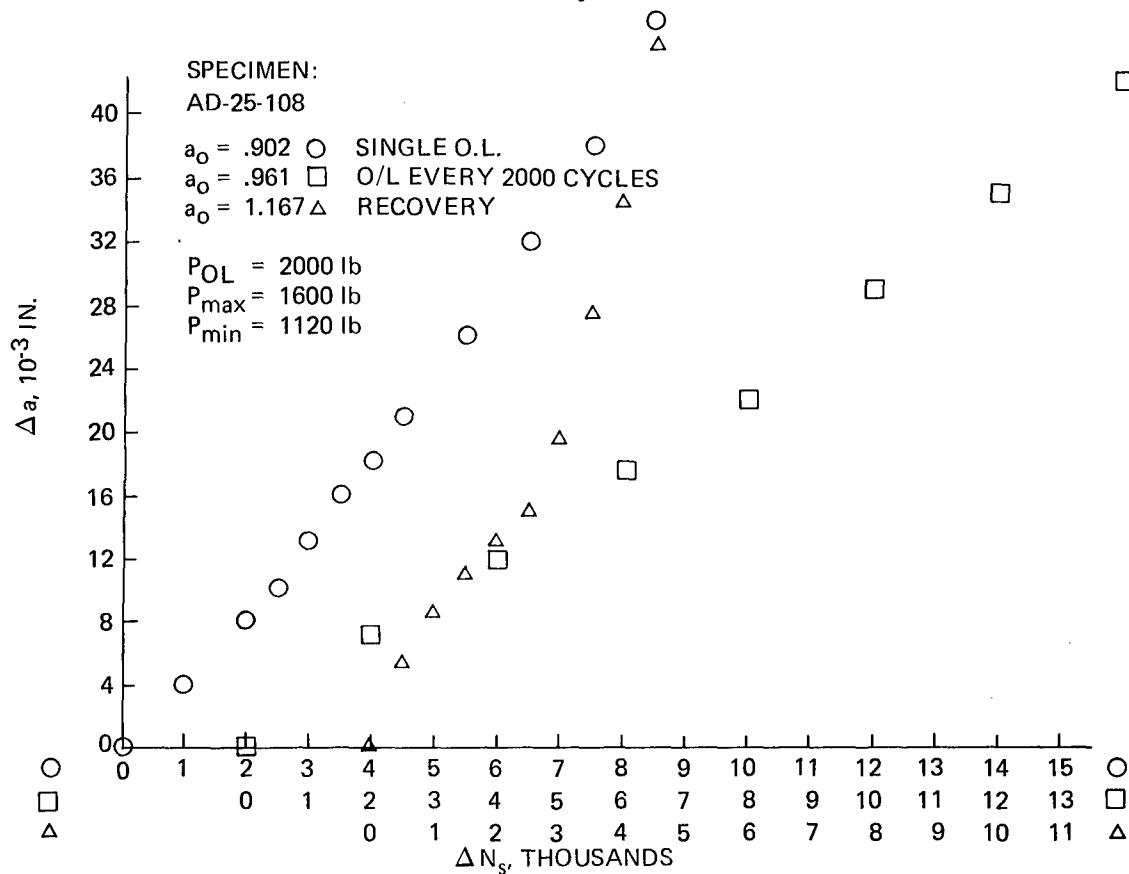


Fig. 59 Detailed Crack Growth vs. ΔN_s for Single Overload Interactions, Aluminum

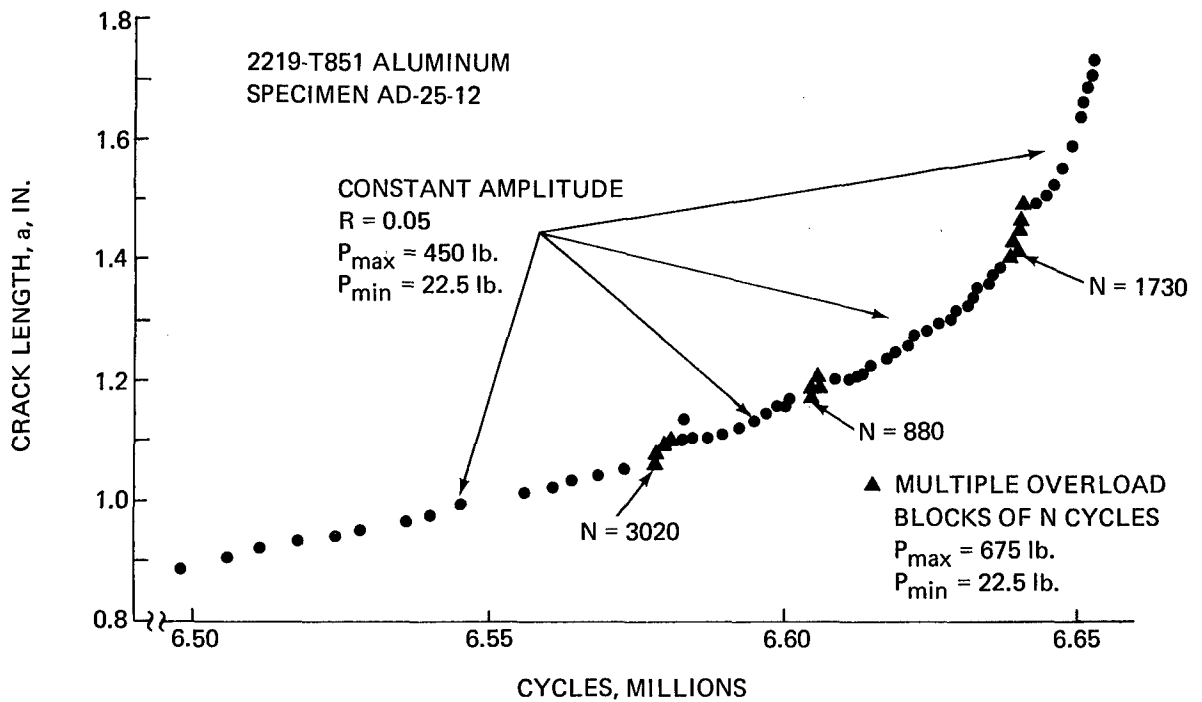
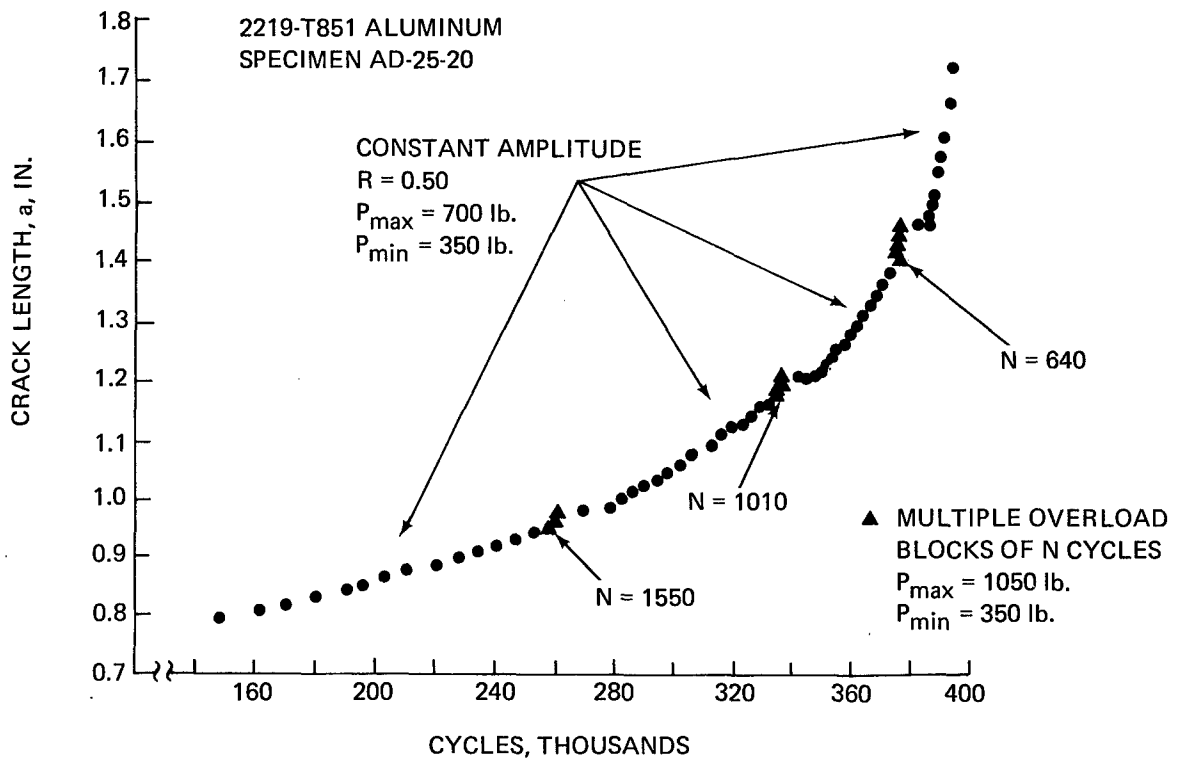
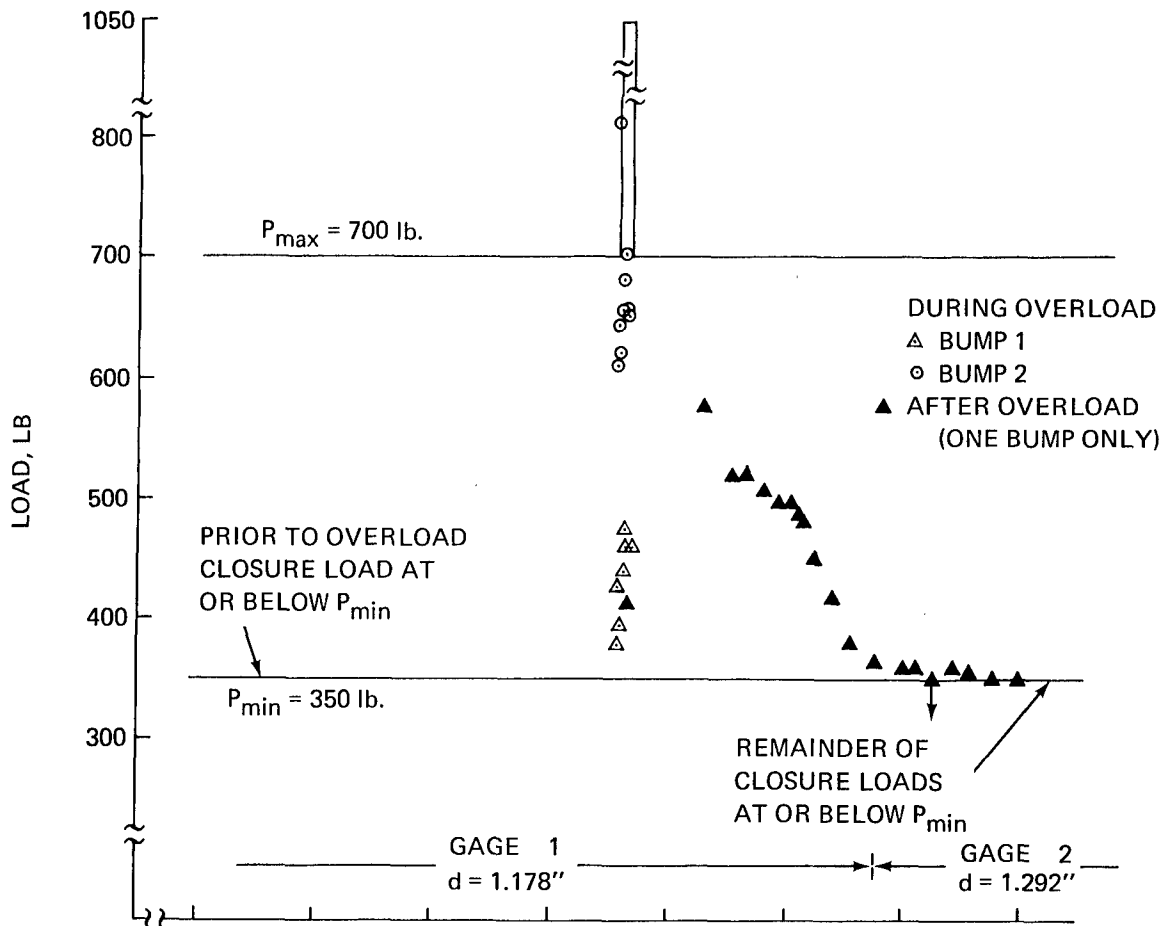


Fig. 60 Aluminum, a vs N for Multiple Overloads, $R = .05$

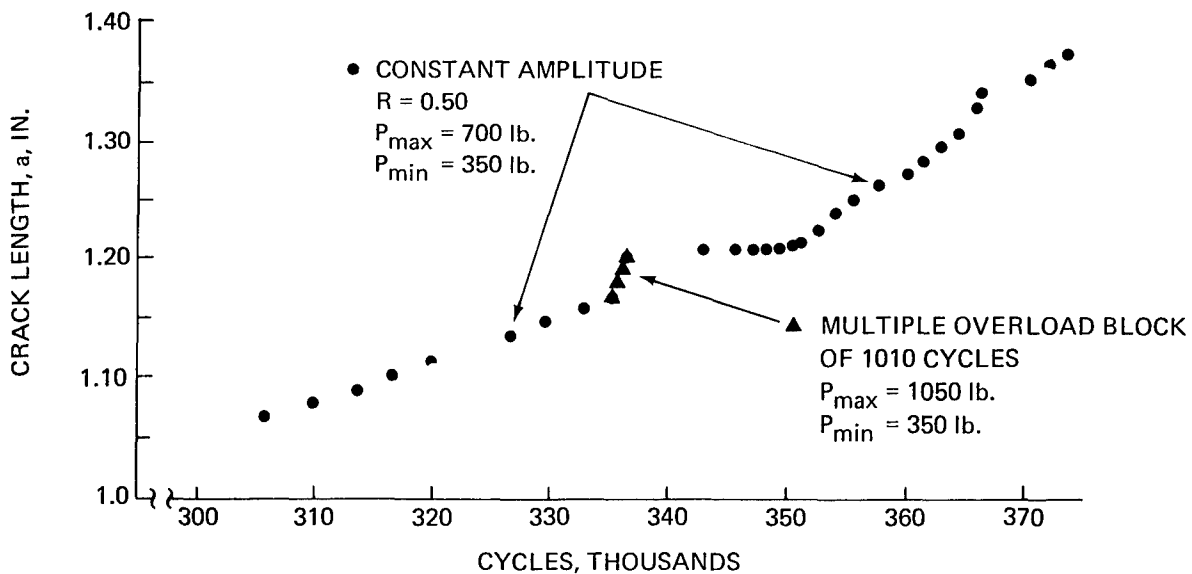


a) CRACK LENGTH

Fig. 61 Aluminum, a vs N for Multiple Overloads, $R = .50$



c) OPENING LOAD DETAIL
FOR ONE OVERLOAD BLOCK



b) CRACK LENGTH DETAIL FOR ONE OVERLOAD BLOCK

Fig. 61 (Continued)

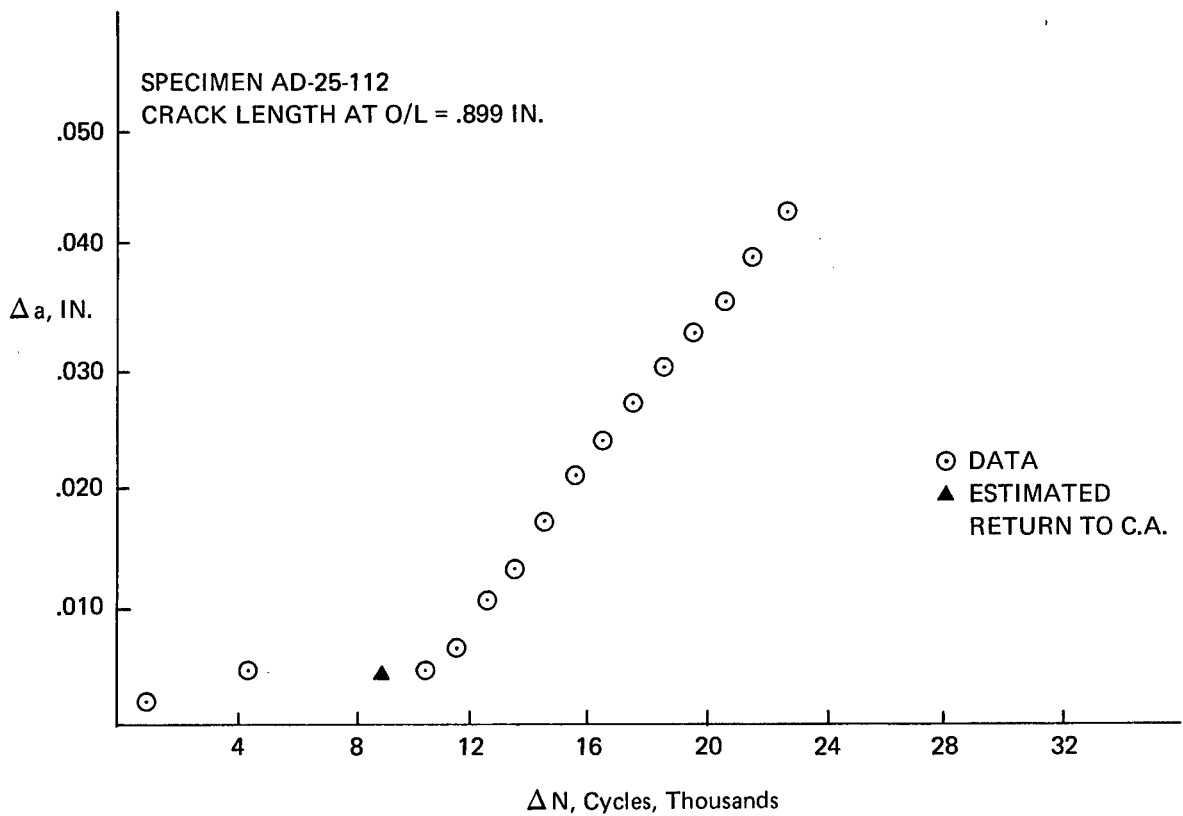


Fig. 62a Δa vs ΔN Since Multiple Overloads, Aluminum

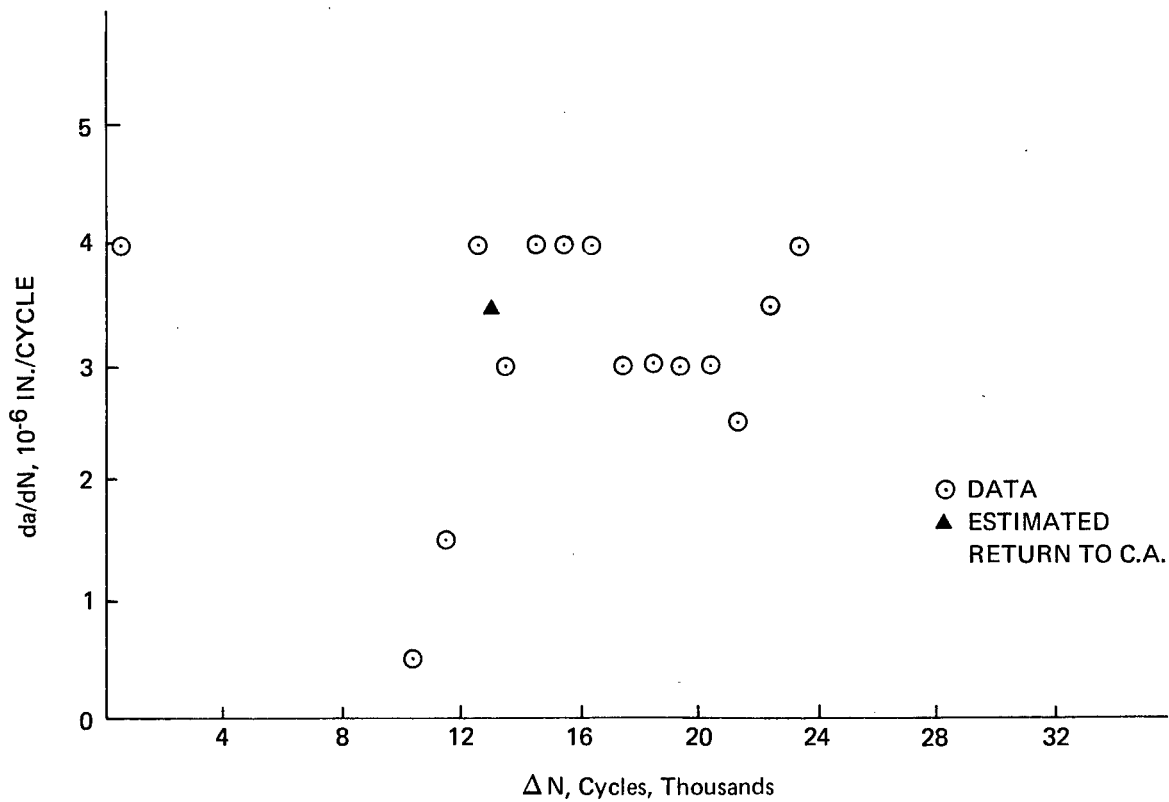


Fig. 62b $\frac{da}{dN}$ vs ΔN Since Multiple Overloads, Aluminum

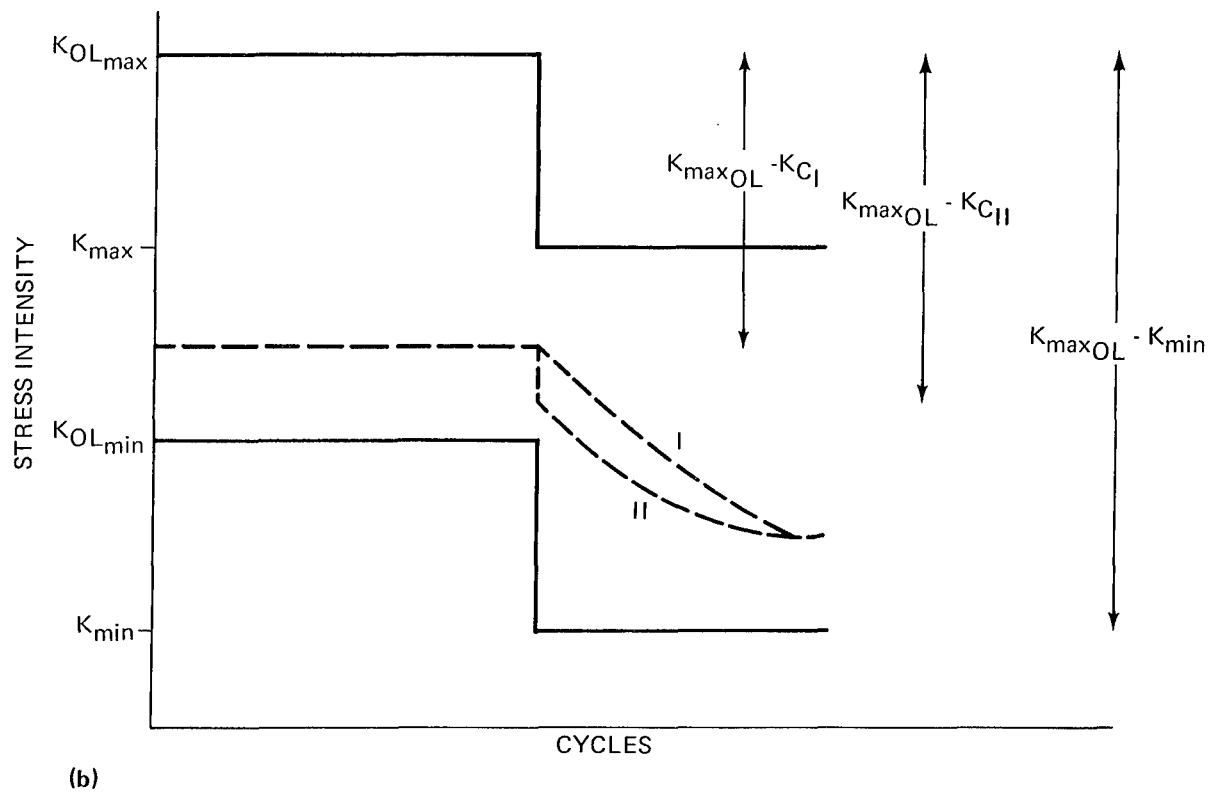
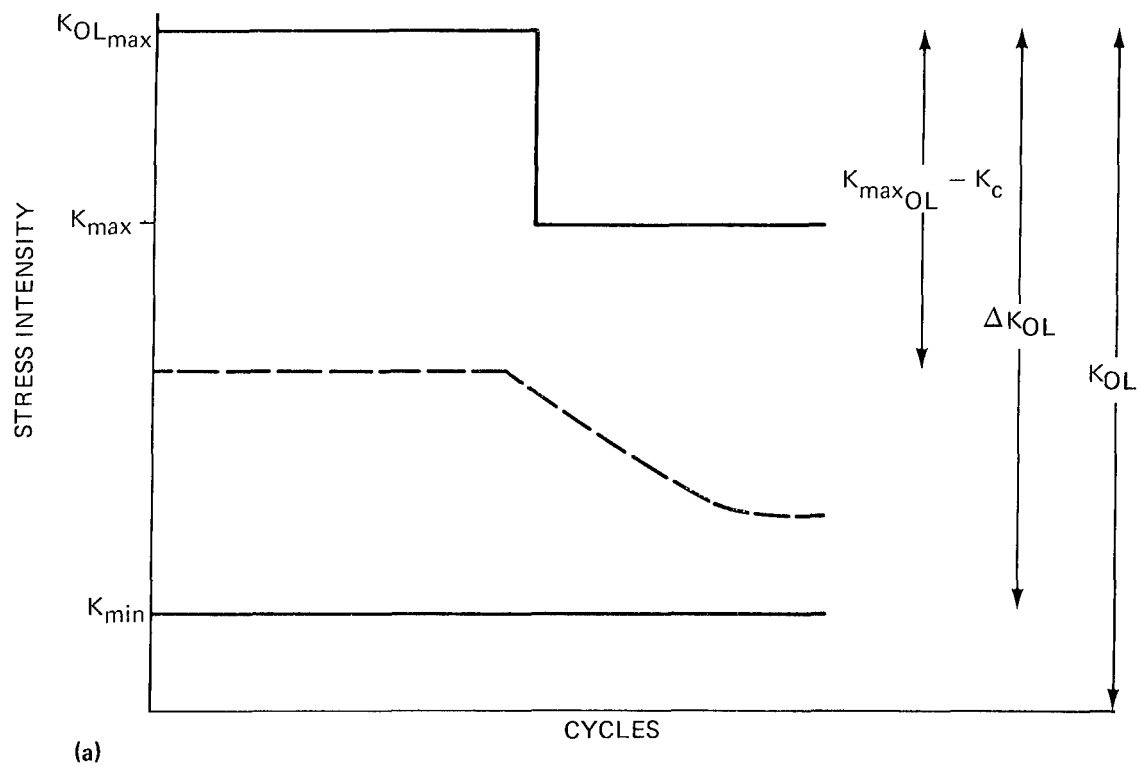


Fig. 63 Definition of Effective Stress Intensity Ranges

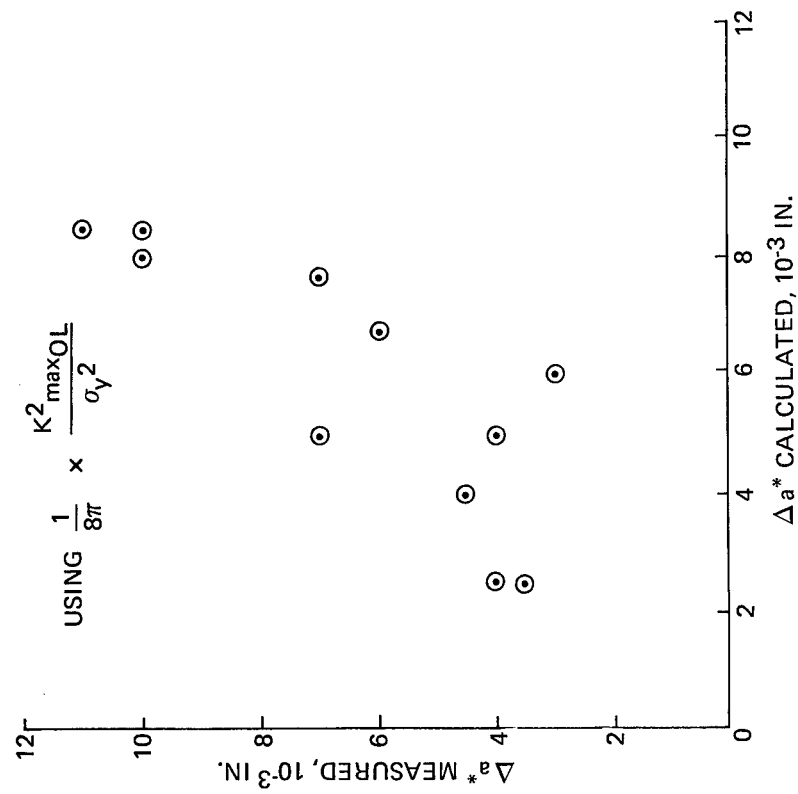


Fig. 64 Δa^* Measured vs Δa^* Calculated for $K_{\max OL}$

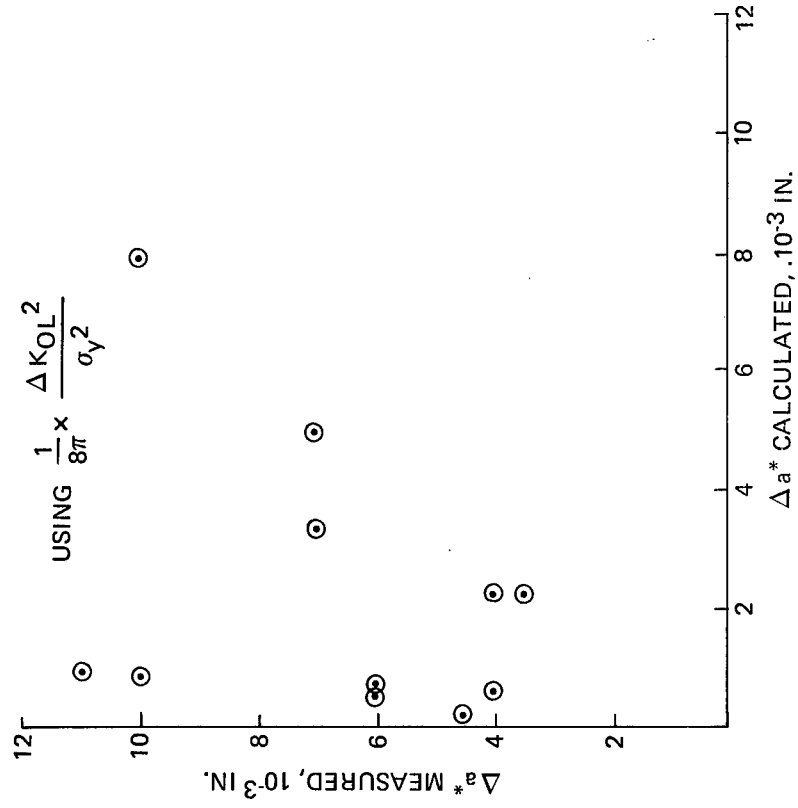


Fig. 65 Δa^* Measured vs Δa^* Calculated for ΔK_{OL}

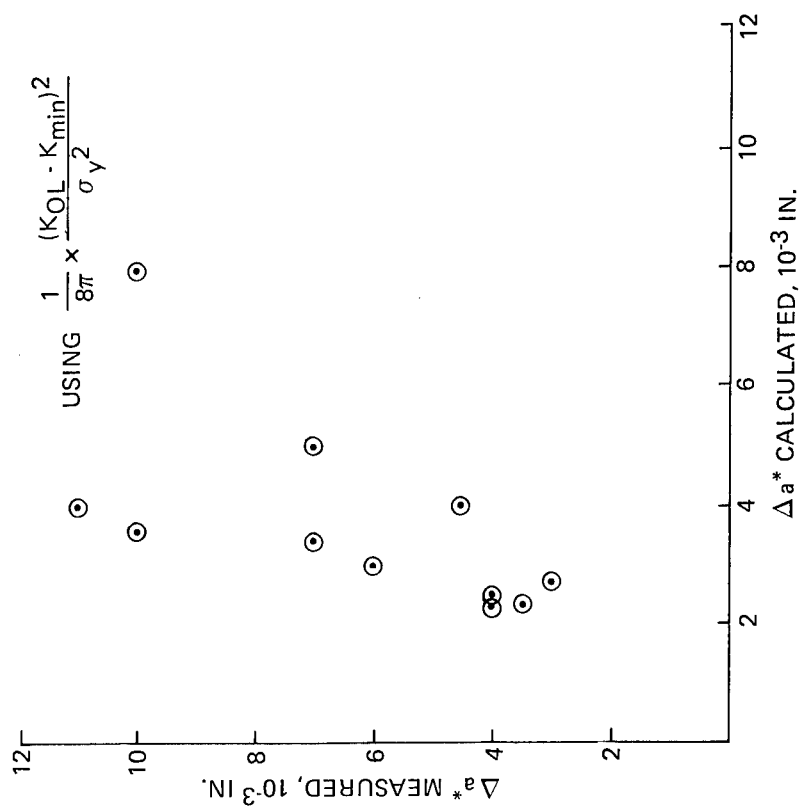


Fig. 66 Δa^* Measured vs Δa^* Calculated for $(K_{maxOL} - K_{min})$

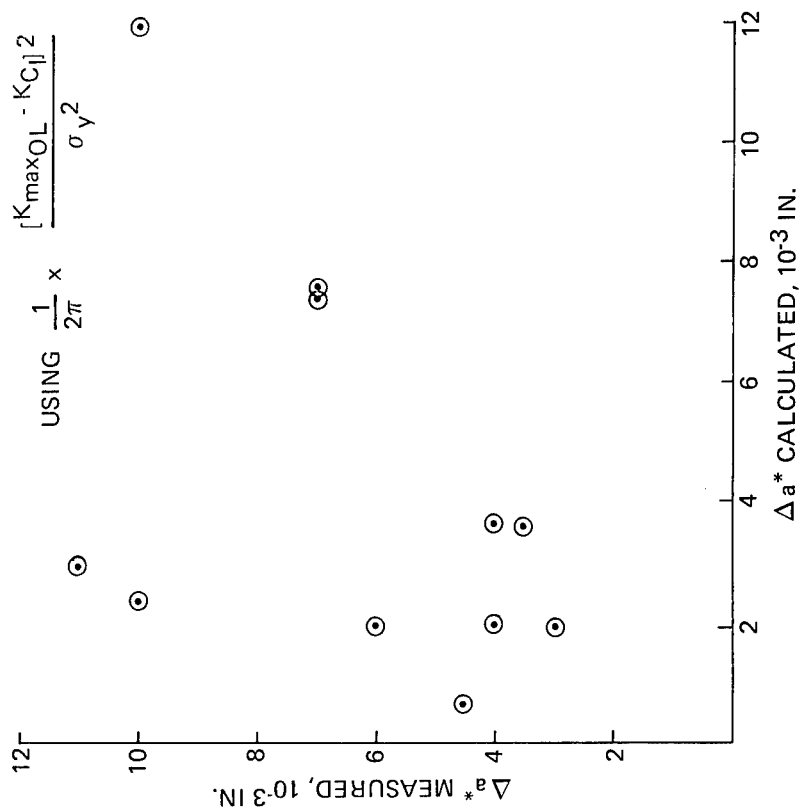


Fig. 67 Δa^* Measured vs Δa^* Calculated for $\Delta K_{eff} (R_{OL})$

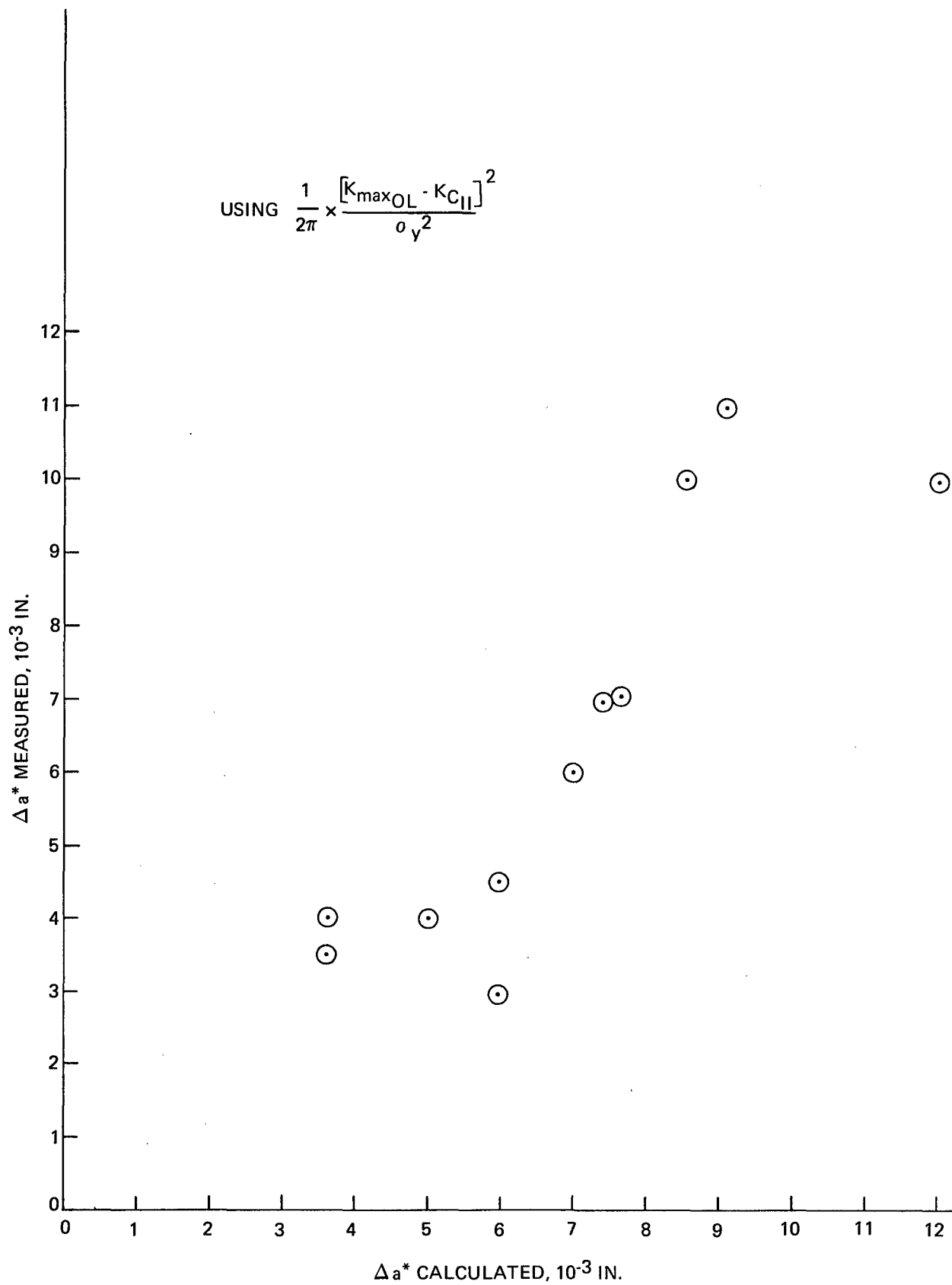


Fig. 68 Δa^* Measured vs Δa^* Calculated for $\Delta K_{\text{eff}} (R_{\min})$

TITANIUM SPECIMEN TD-25-21

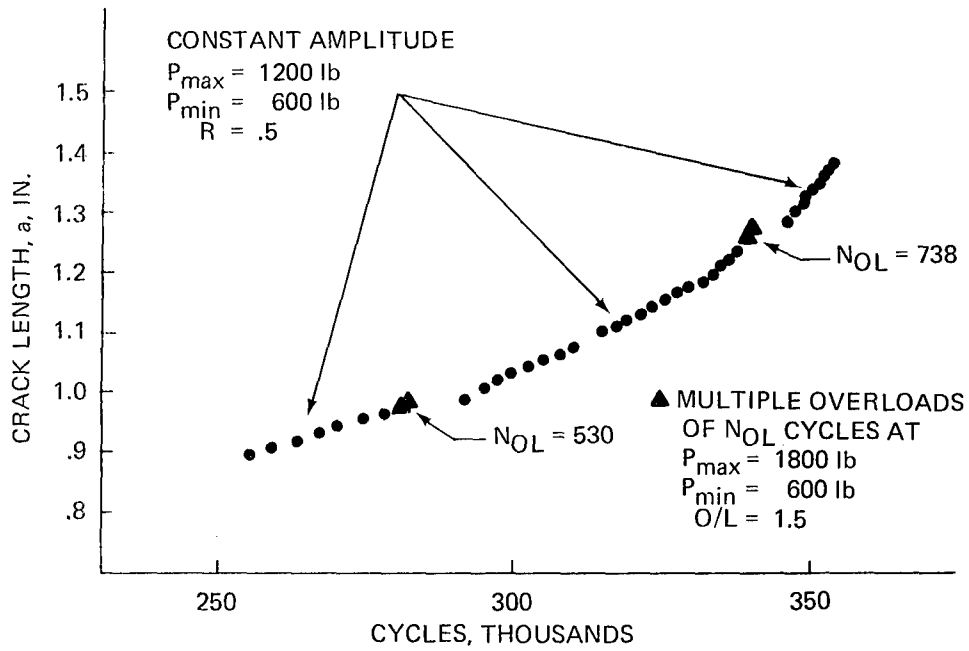


Fig. 69a Crack Length vs. Cycles for Multiple Overloads, $R = .50$, Titanium

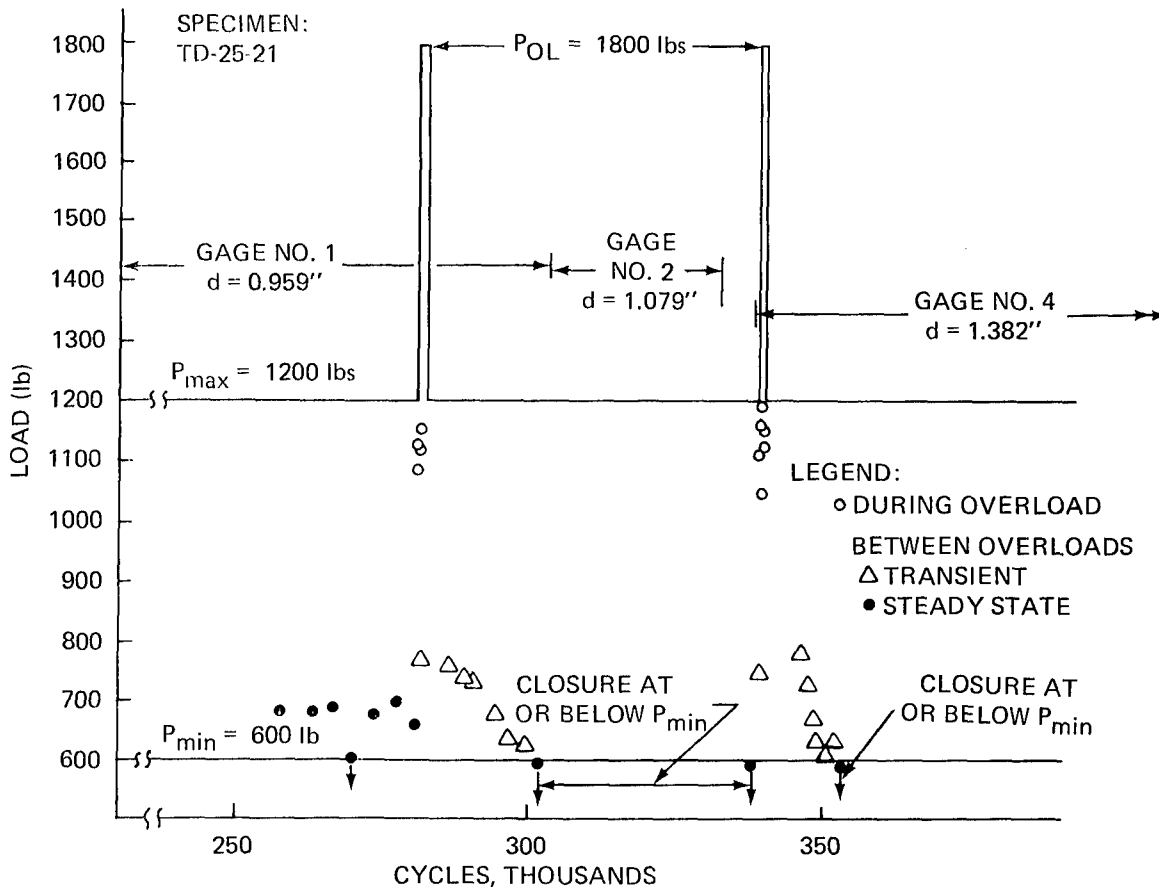


Fig. 69b Crack Opening Load vs. Cycles for Multiple Overloads, $R = .50$, Titanium

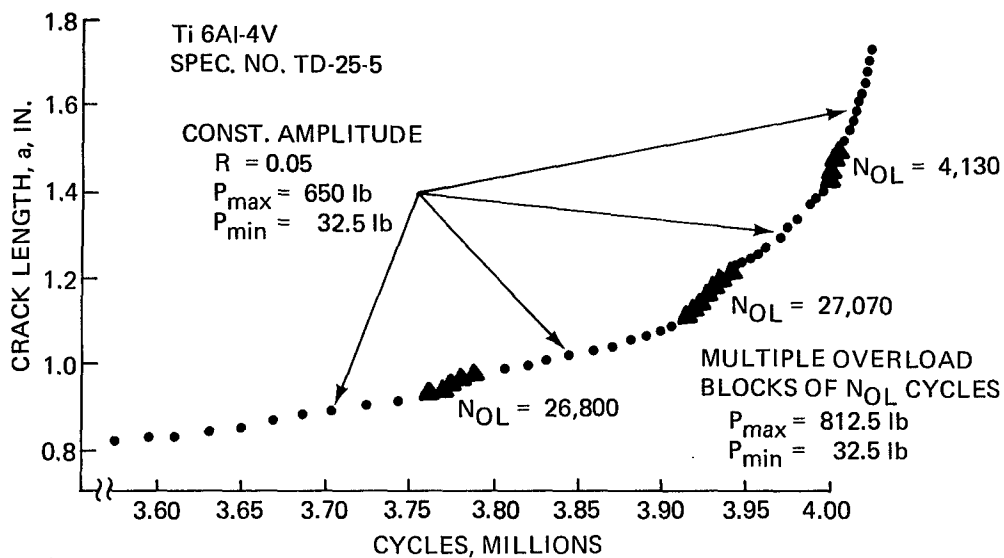


Fig. 70a Crack Length vs. Cycles, Multiple Overloads, $R = .05$, Titanium

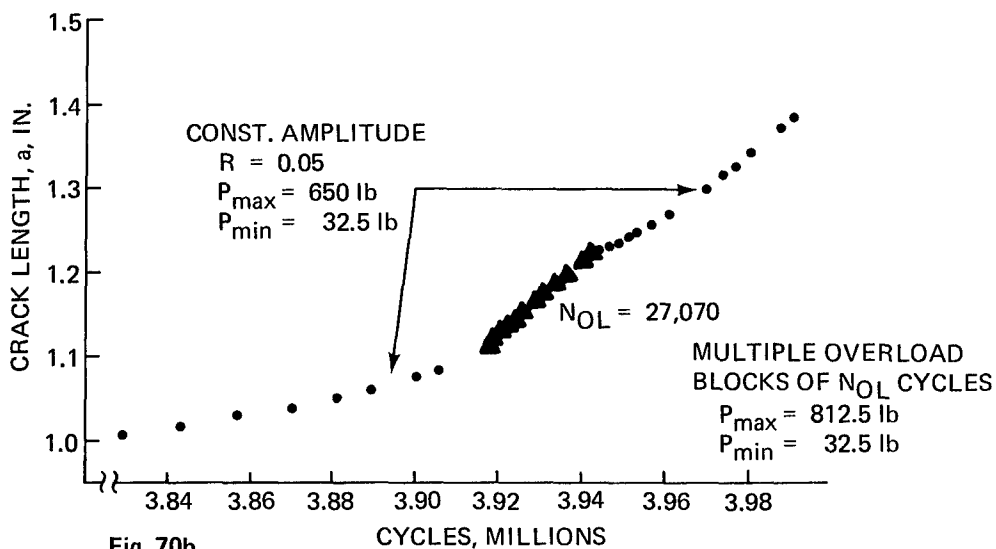


Fig. 70b

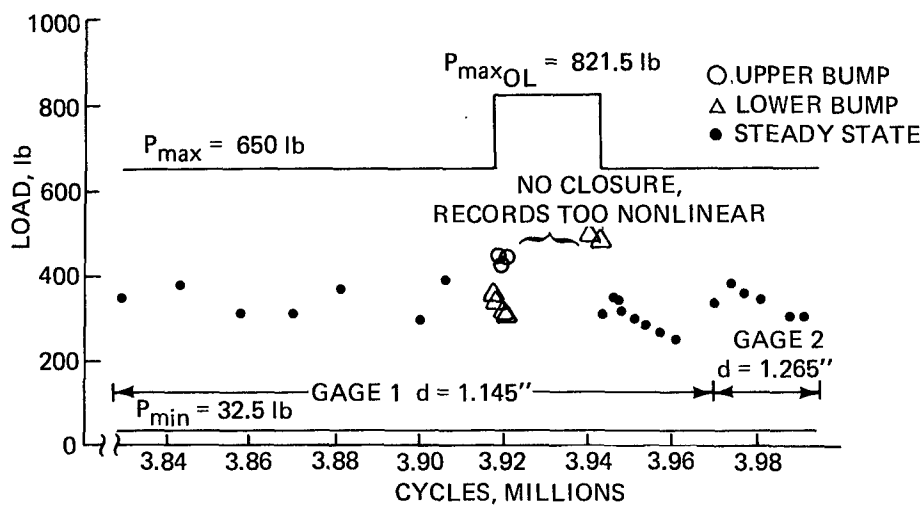


Fig. 70c

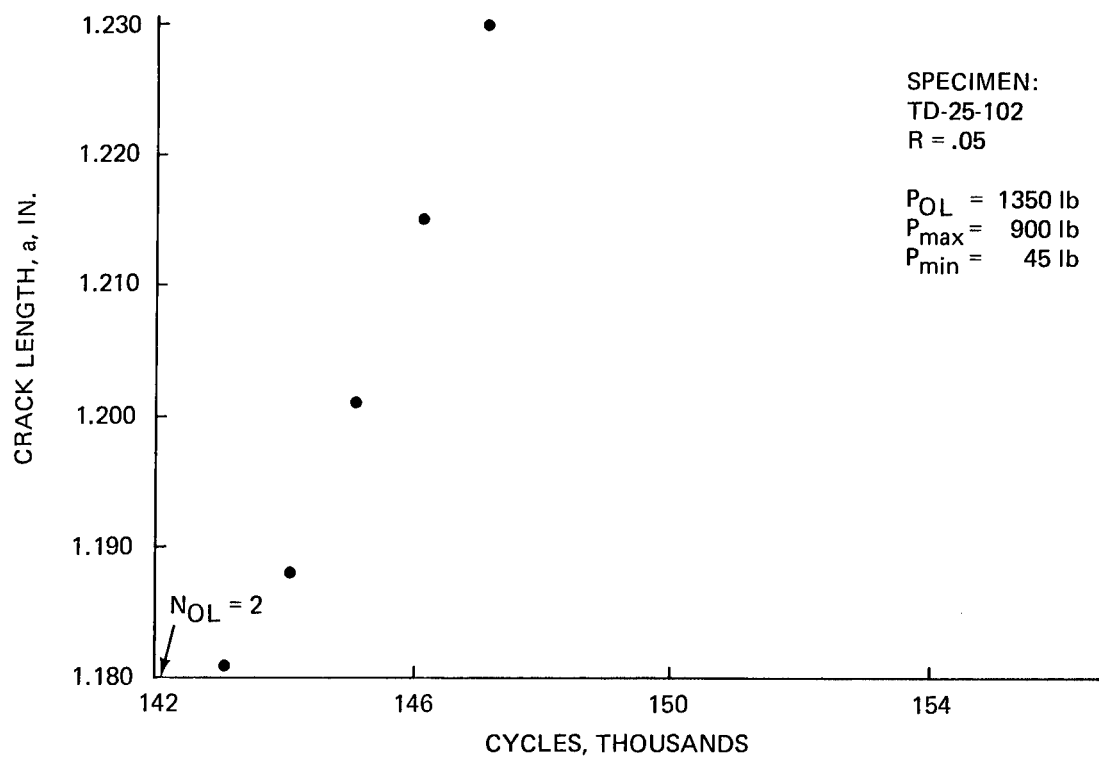


Fig. 71a Crack Length vs. Cycles for Multiple Overloads, $N_{OL} = 2$, Titanium

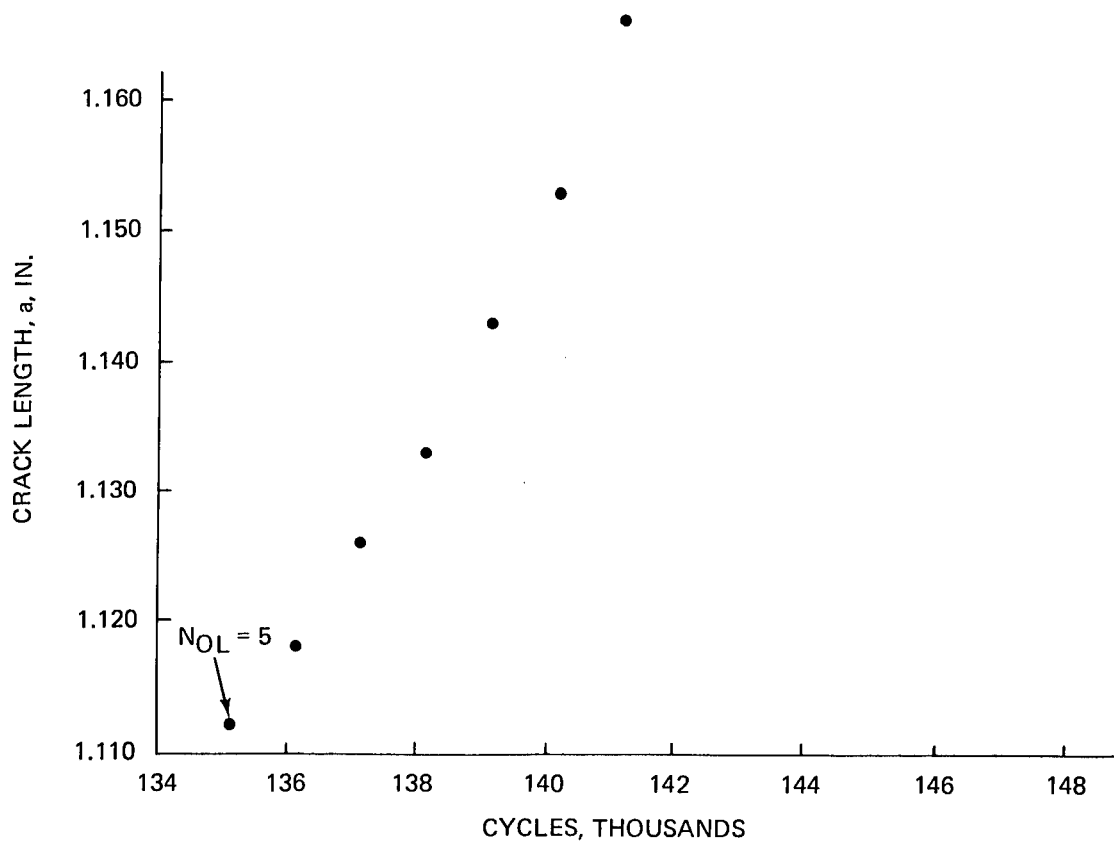


Fig. 71b $N_{OL} = 5$

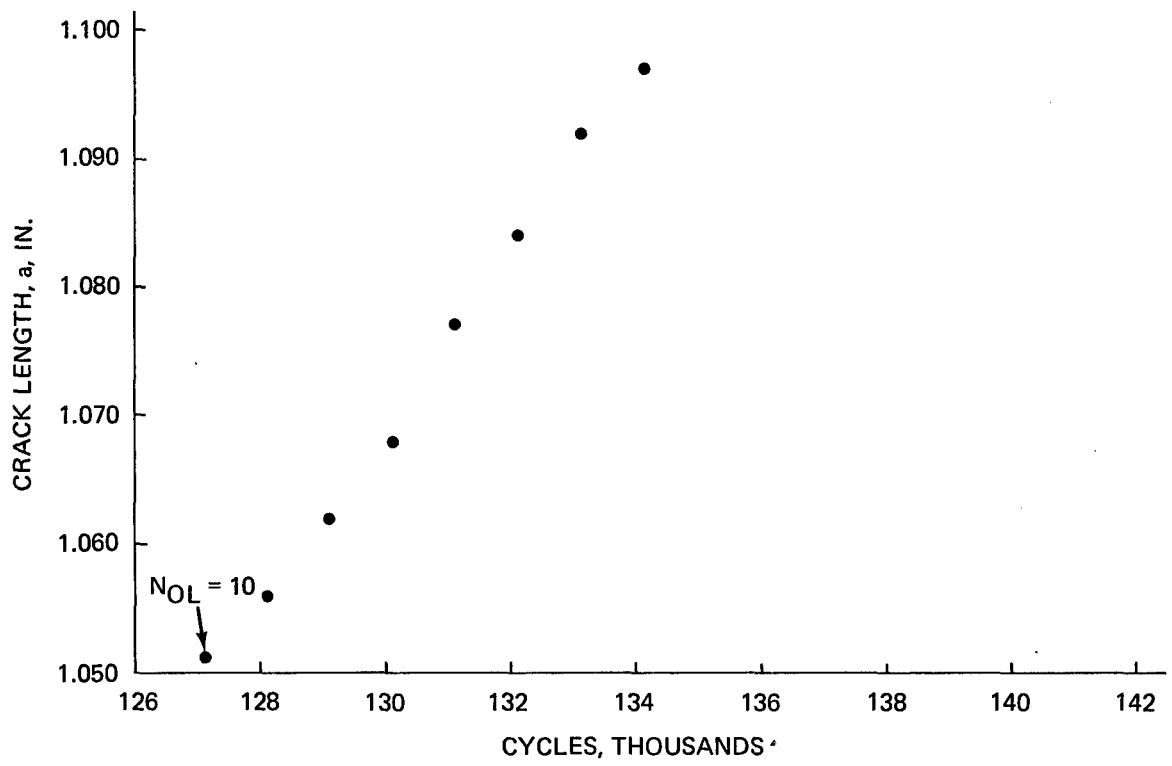


Fig. 71c $N_{OL} = 10$

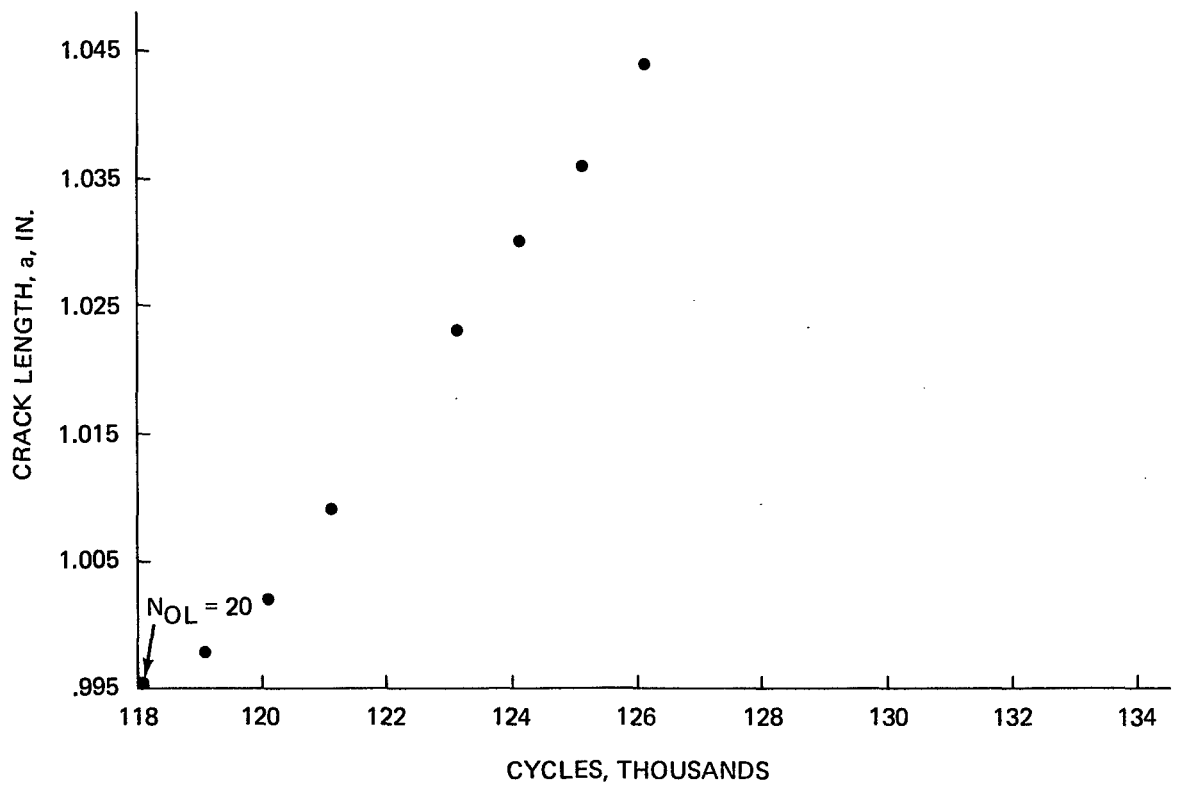


Fig. 71d $N_{OL} = 20$

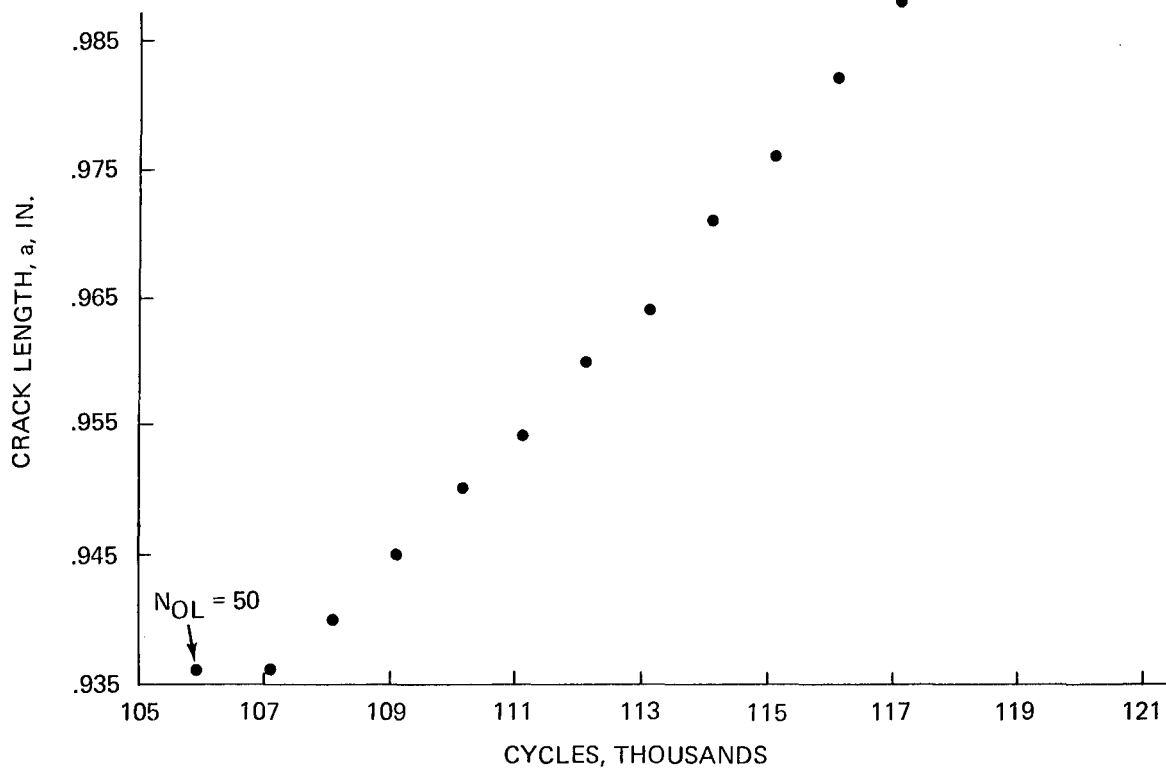


Fig. 71e $N_{OL} = 50$

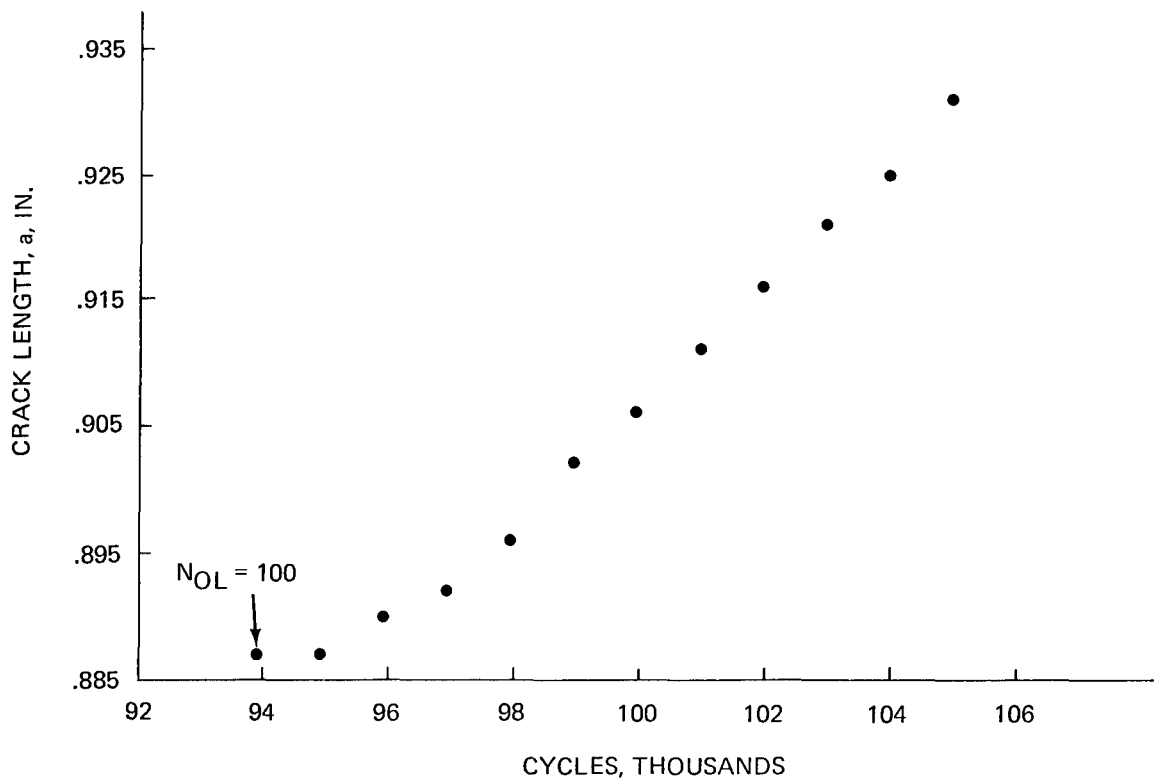


Fig. 71f $N_{OL} = 100$

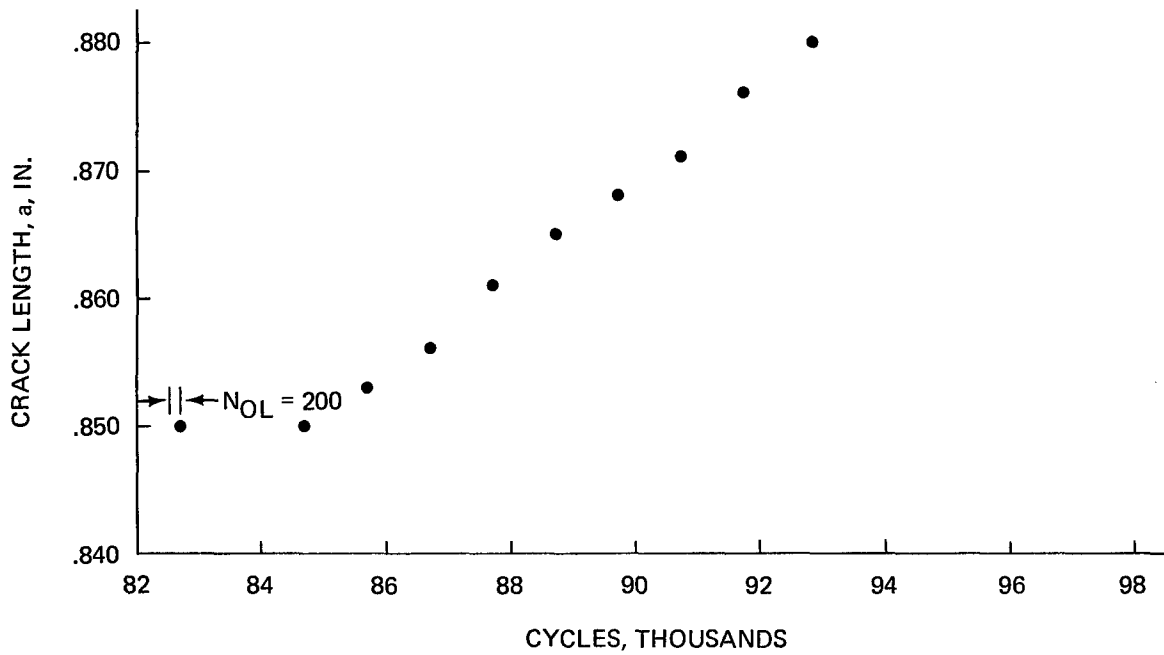


Fig. 71g $N_{OL} = 200$

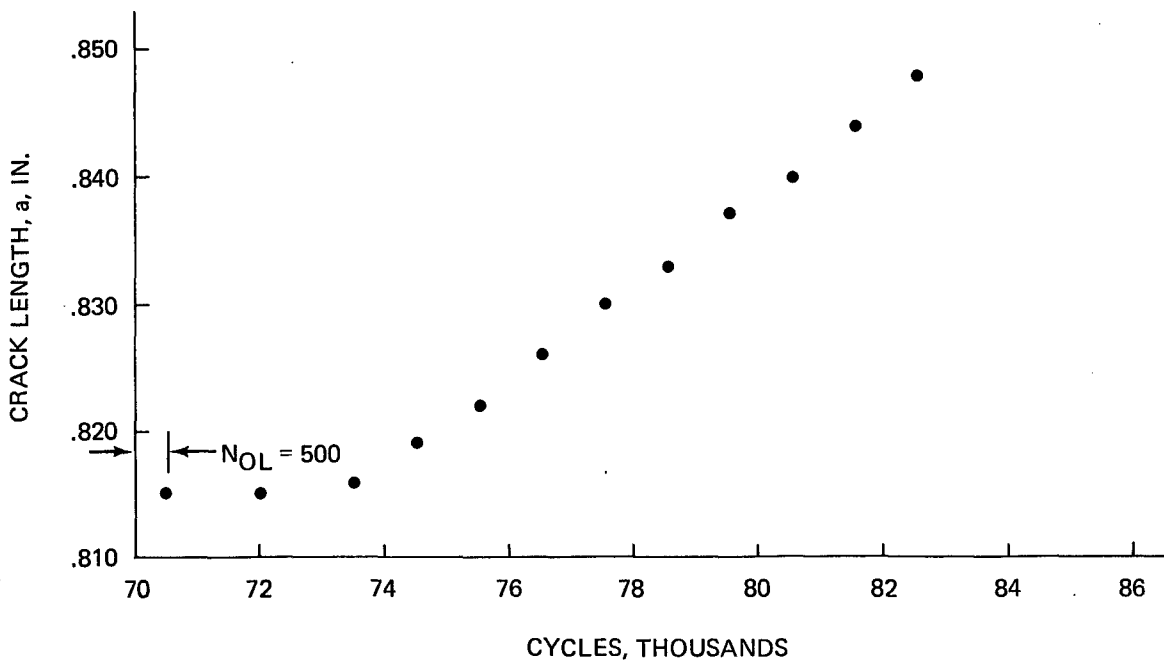


Fig. 71h $N_{OL} = 500$

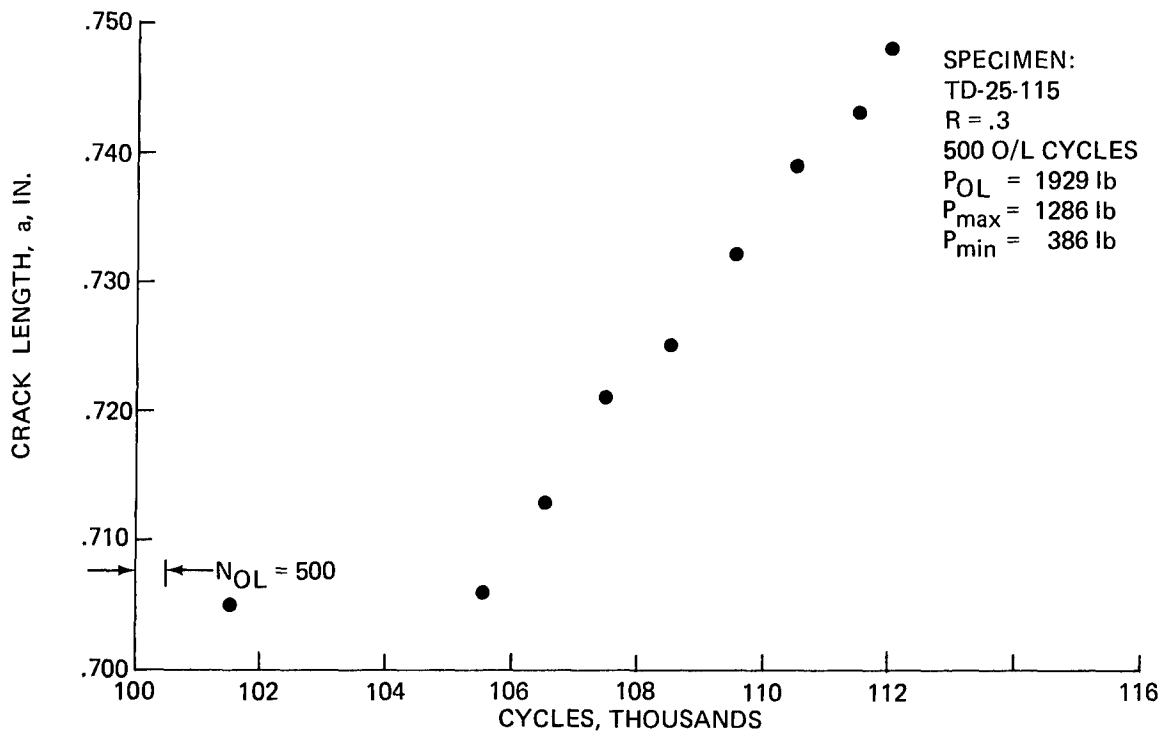


Fig. 72a Crack Length vs. Cycles for Multiple Overloads, N_{OL} = 500, Titanium

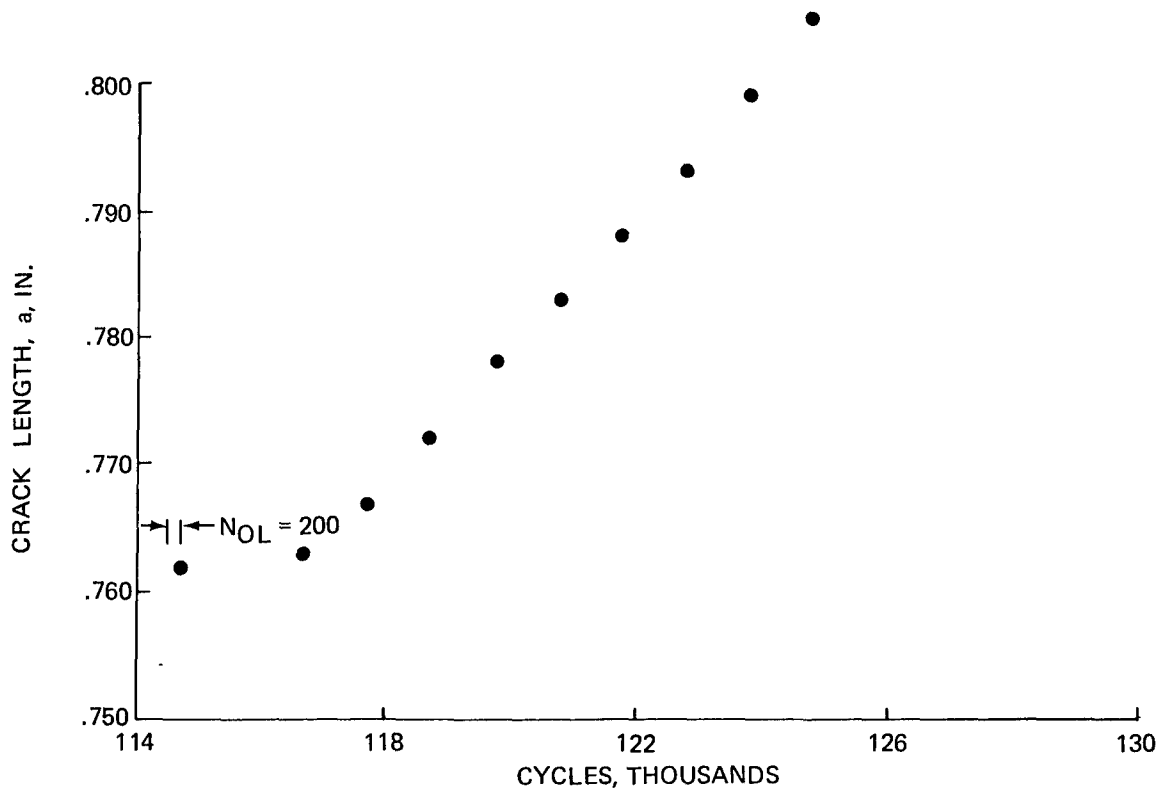


Fig. 72b N_{OL} = 200

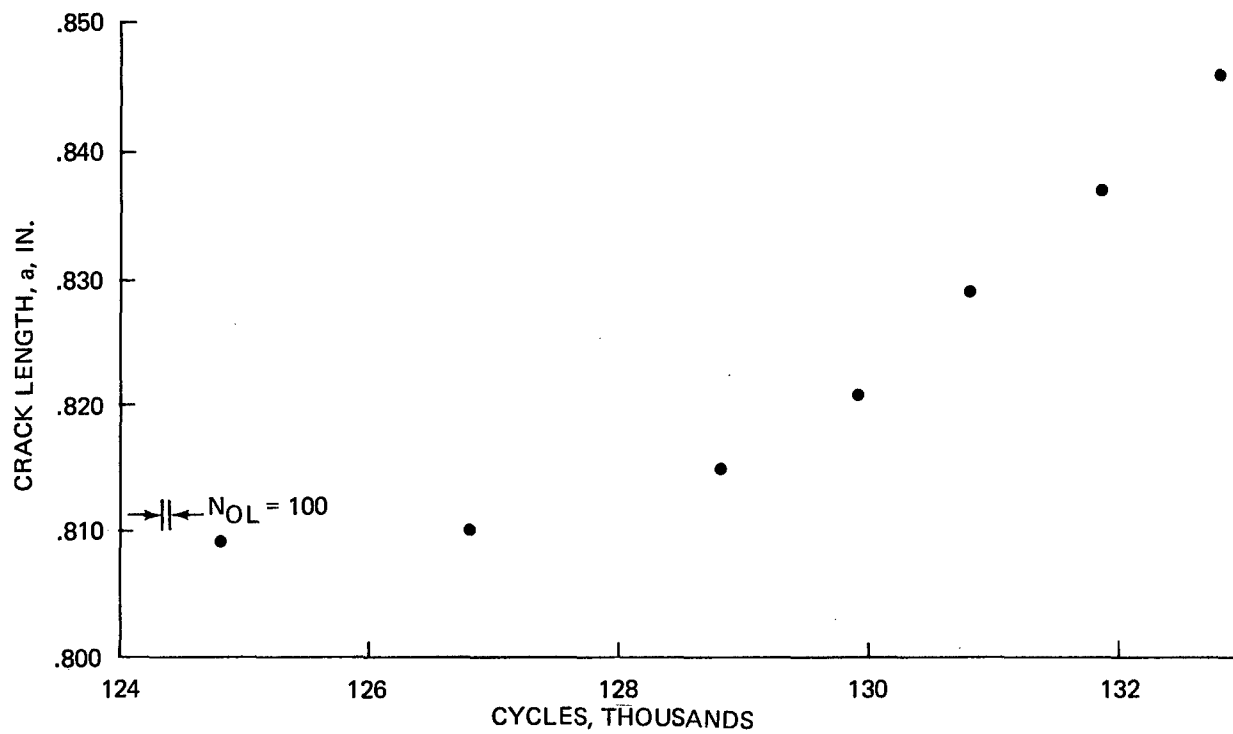


Fig. 72c $N_{OL} = 100$

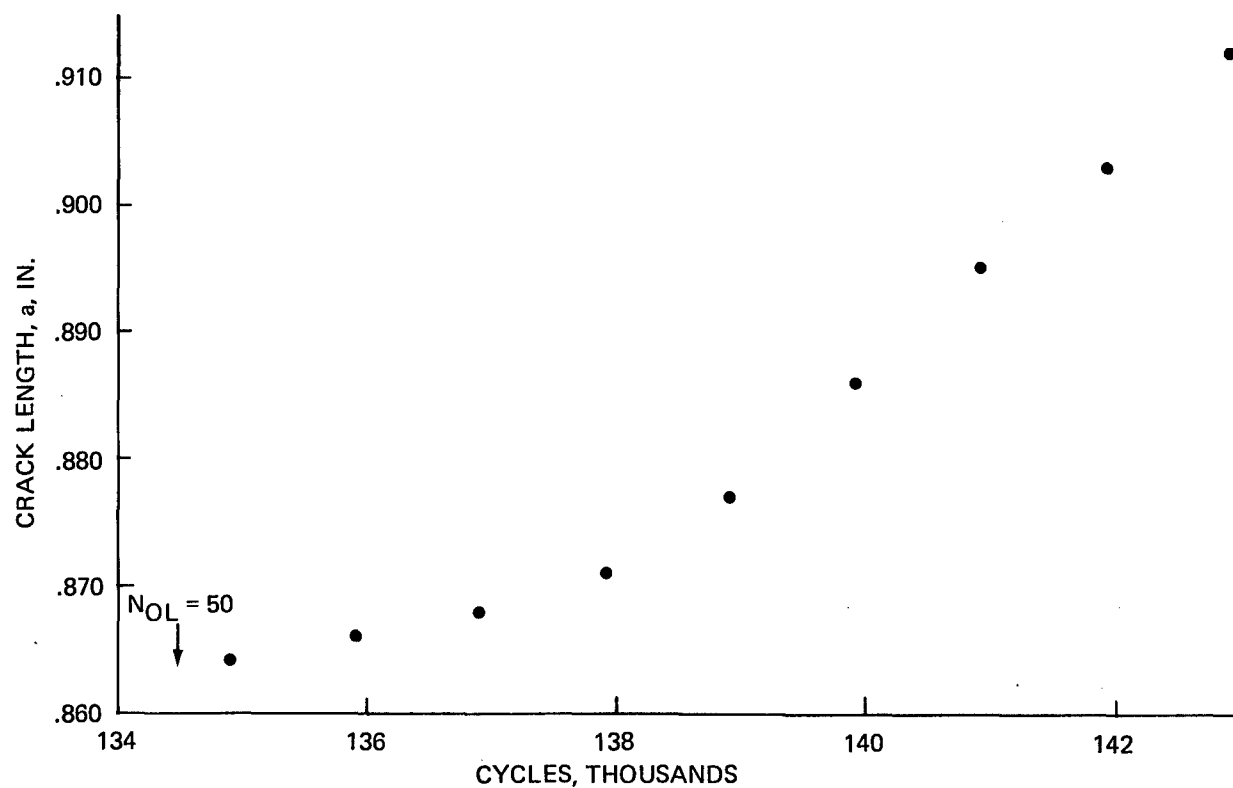


Fig. 72d $N_{OL} = 50$

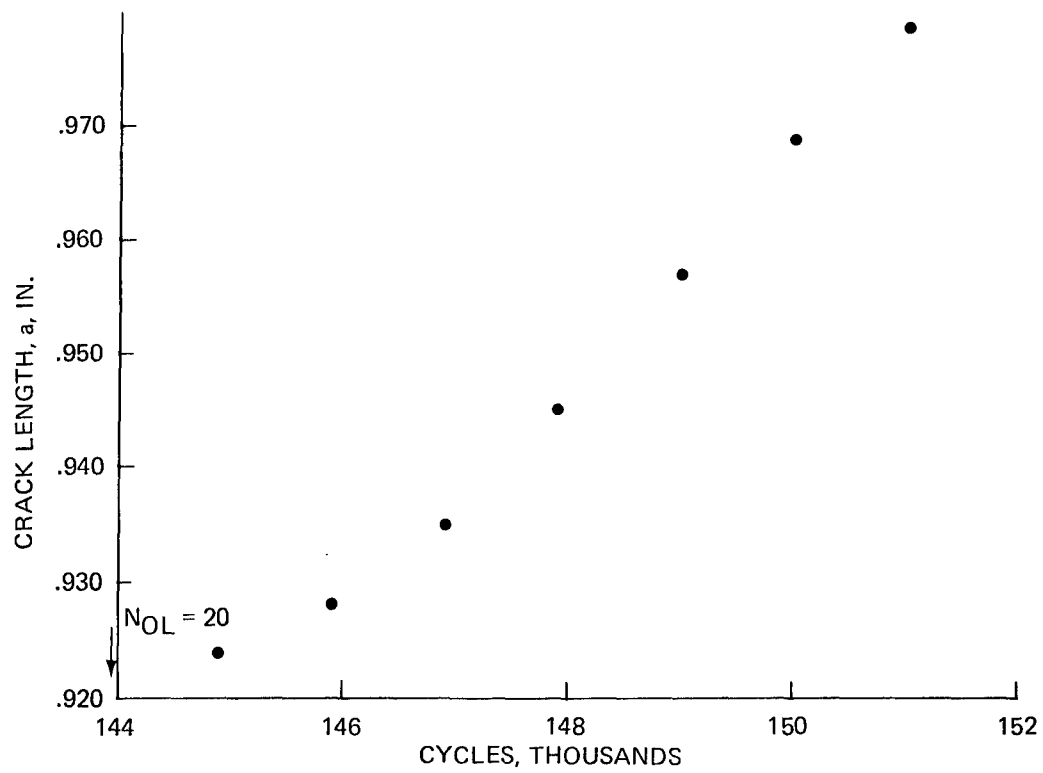


Fig. 72e NO_L = 20

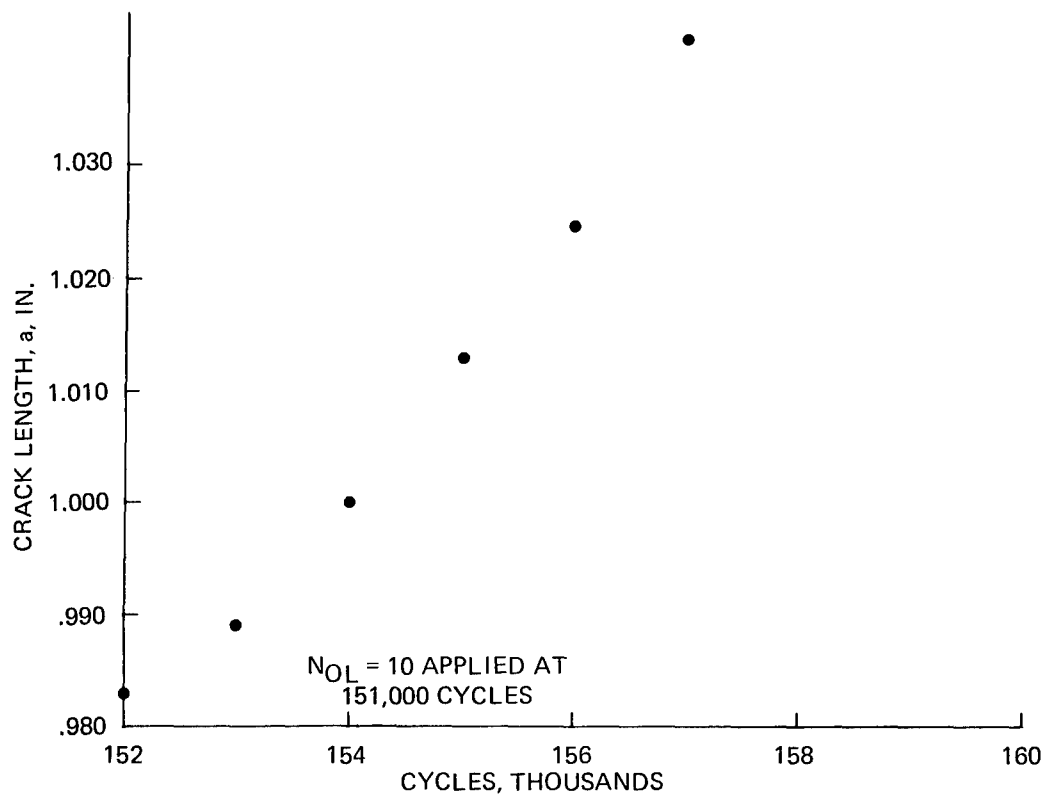
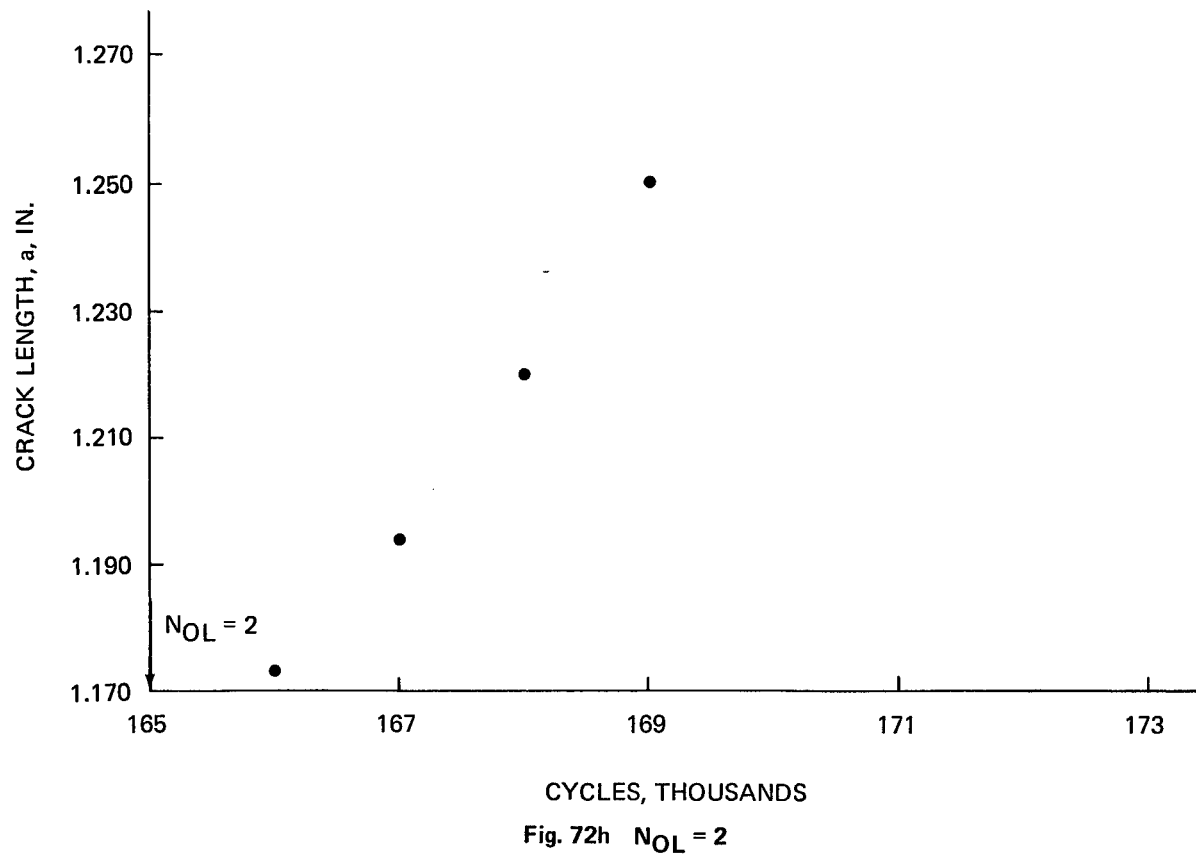
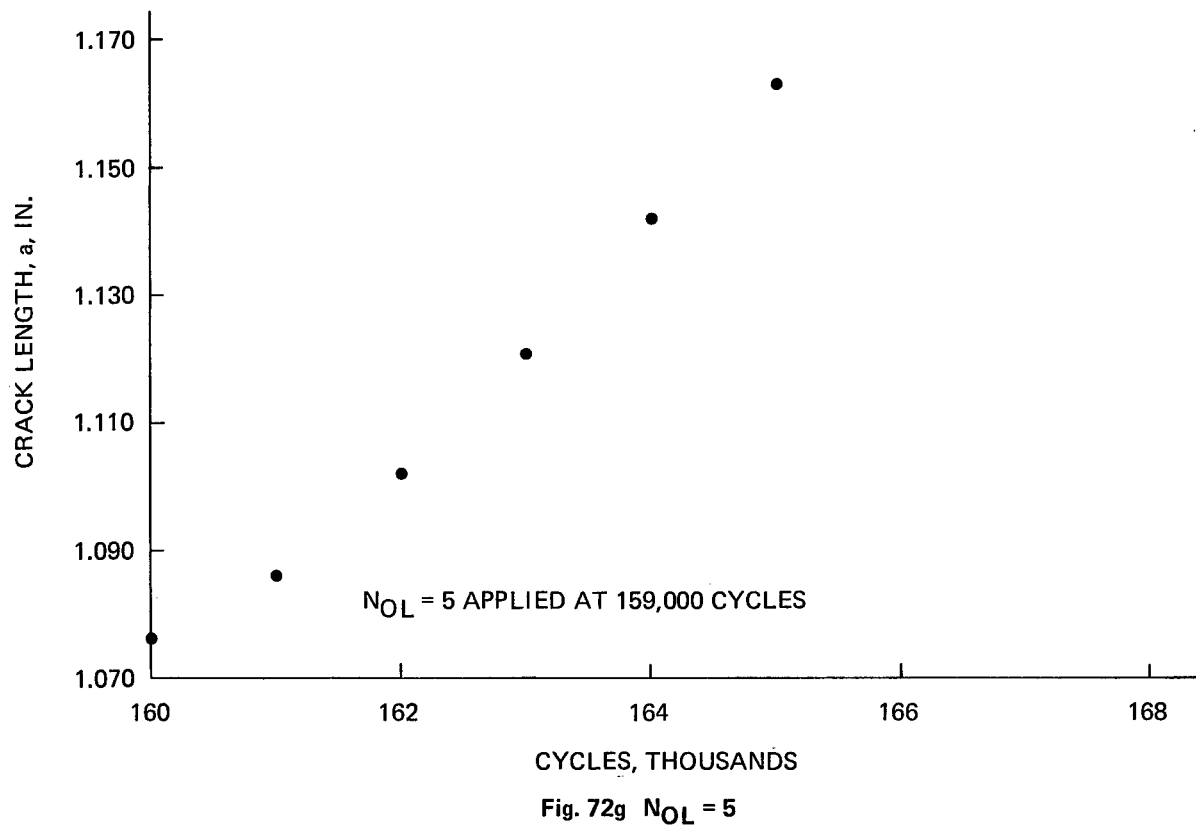


Fig. 72f NO_L = 10



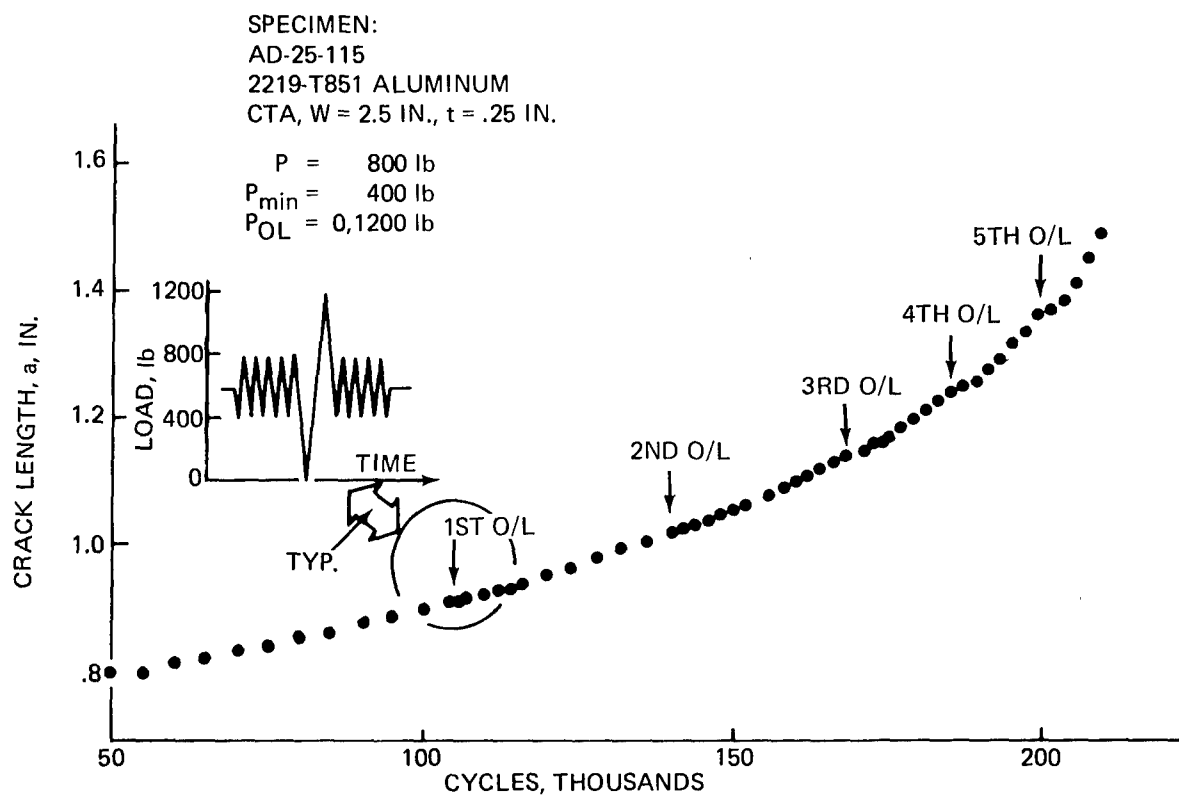


Fig. 73 Crack Length Data for Underload/Overload Spike Sequence, 2219-T851 Aluminum

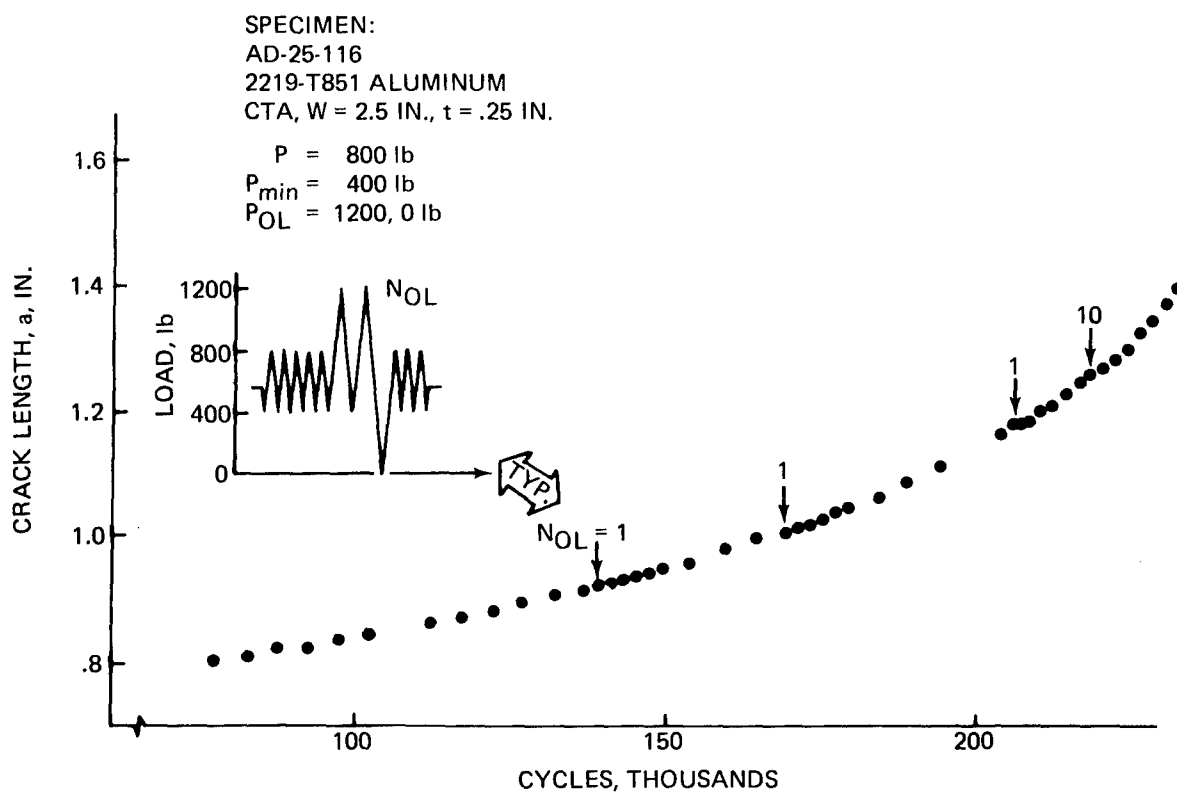


Fig. 74 Crack Length Data for Overload/Underload Spike Sequences, 2219-T851 Aluminum

SPECIMEN:
 TD-25-119
 Ti 6Al-4V TITANIUM
 CTA, W = 2.2 IN., t = .25 IN.

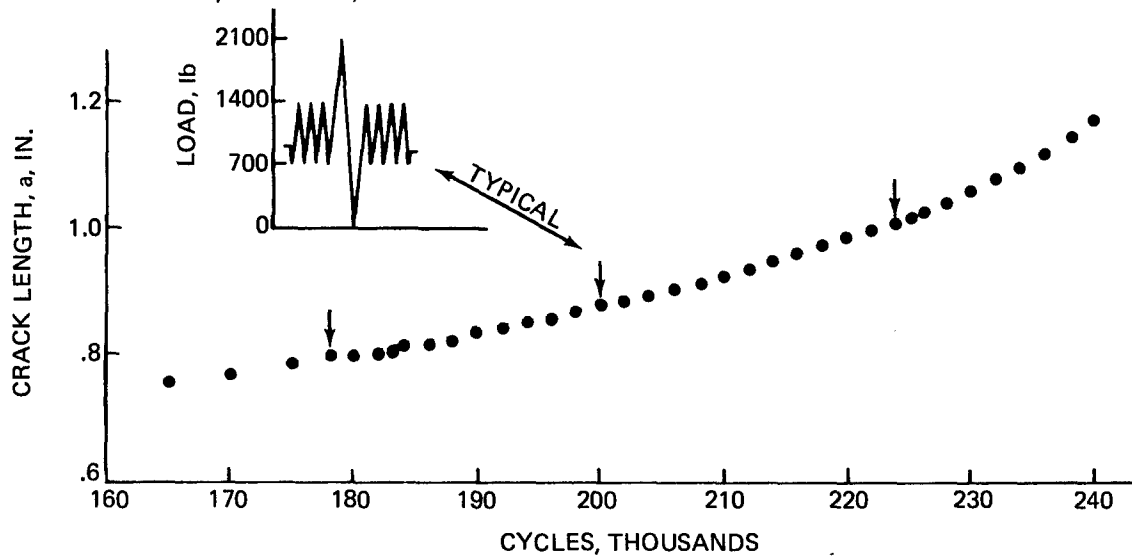


Fig. 75 Crack Length Data for Overload/Underload Spike Sequences, Ti 6Al-4V Titanium

SPECIMEN:
 TD-25-118
 Ti 6Al-4V TITANIUM
 CTA, W = 2.2 IN., t = .25 IN.

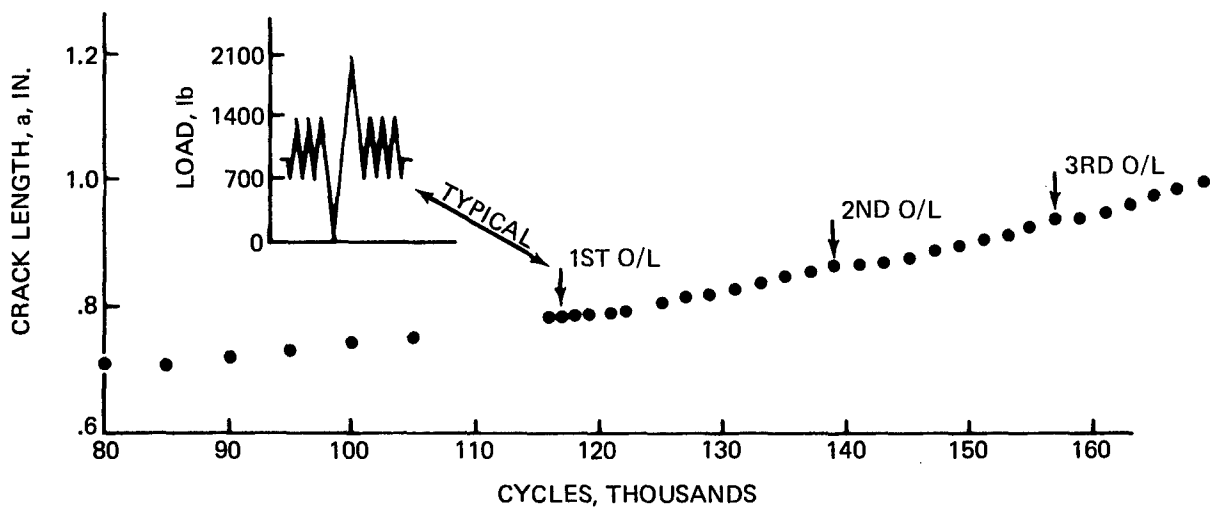


Fig. 76 Crack Length Data for Underload/Overload Spike Sequences, Ti 6Al-4V Titanium

SPECIMEN:
 TD-25-117
 Ti 6Al-4V TITANIUM
 CTA, W = 2.2 IN., t = .25 IN.

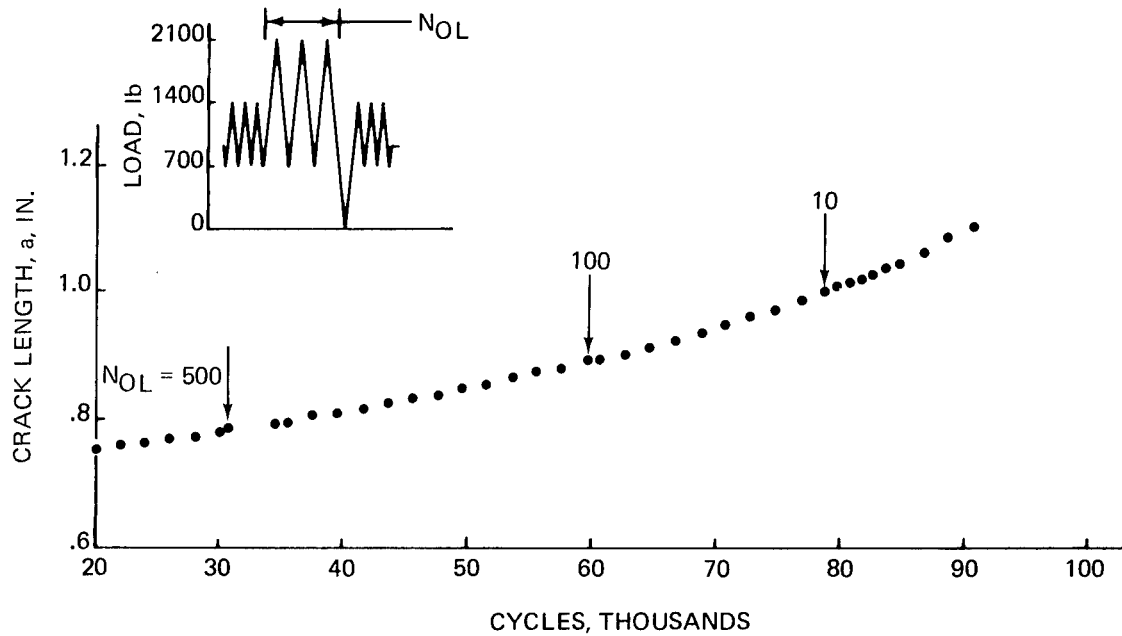


Fig. 77 Crack Length Data for Multiple Overload/Underload Spike Sequences, Ti 6Al-4V Titanium

SPECIMEN:
 AD-25-117
 2219-T851 ALUMINUM
 CTA, W = 2.5 IN., t = .25 IN.

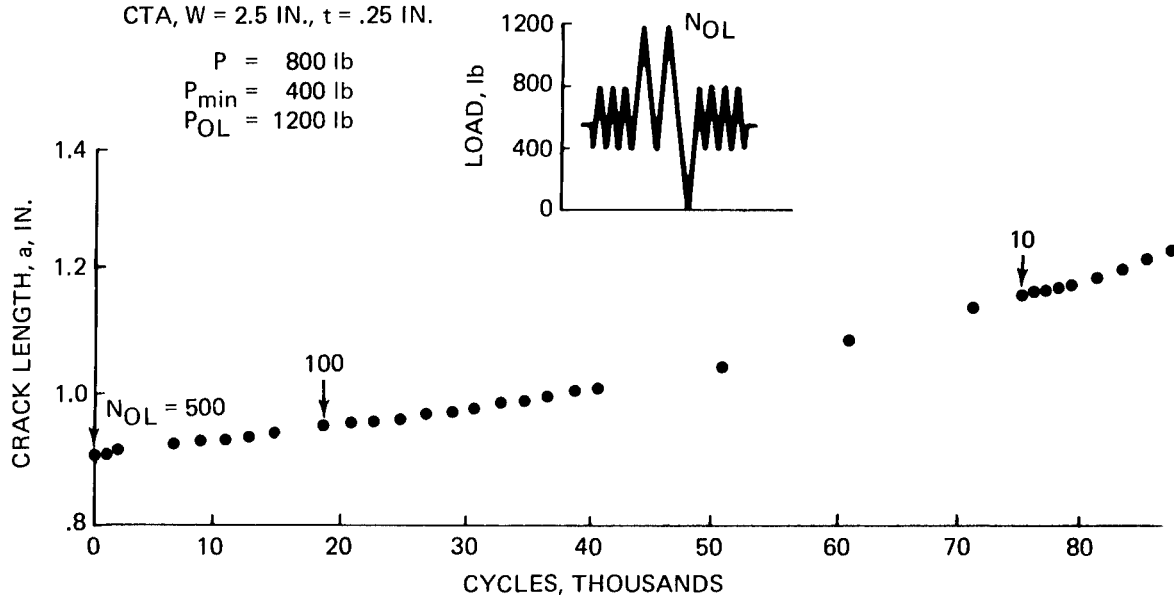


Fig. 78 Crack Length Data for Multiple Overload/Underload Spike Sequence, 2219-T851 Aluminum

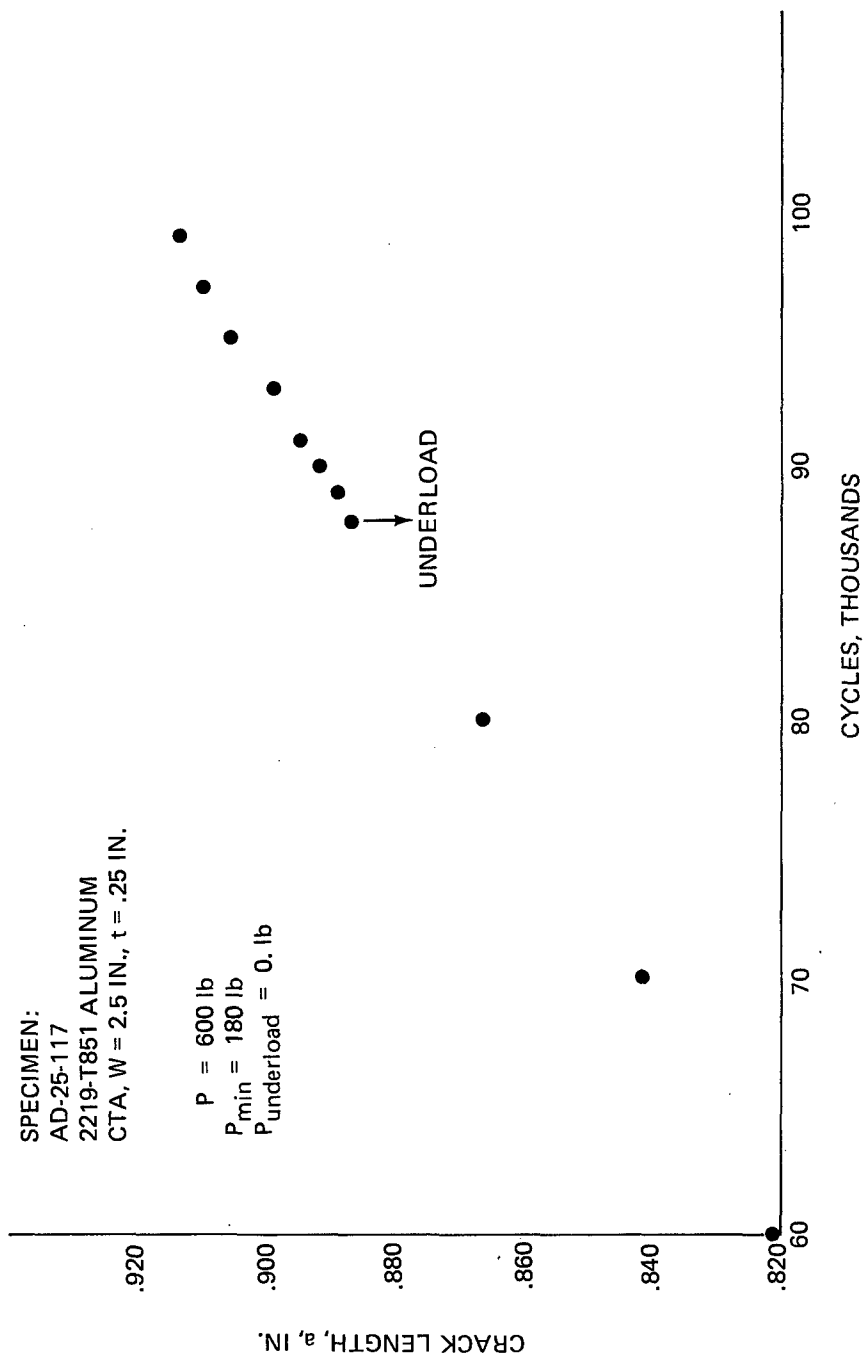


Fig. 79 Crack Length Data for Single Underload, 2219-T851 Aluminum

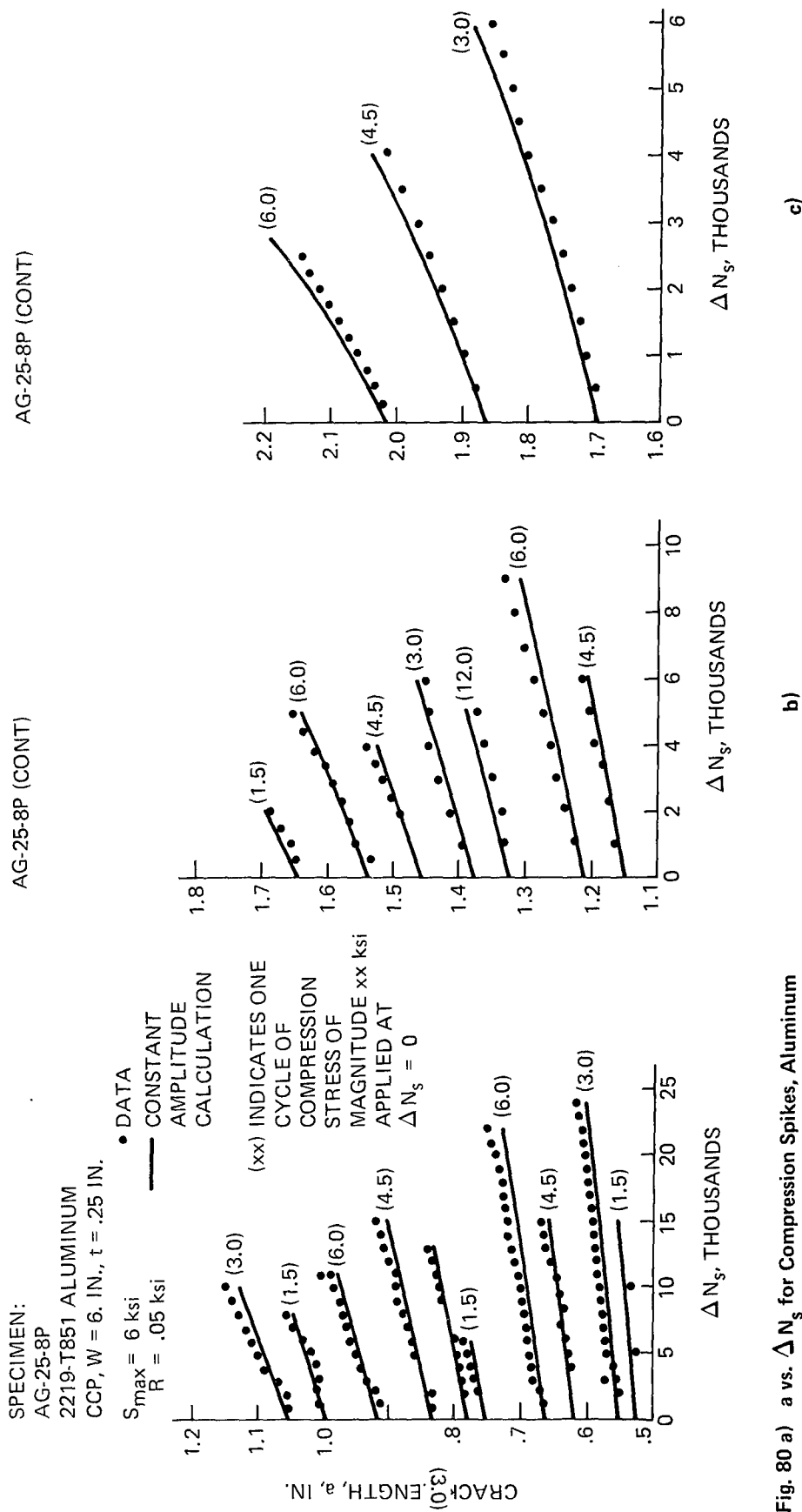


Fig. 80 a) a vs. ΔN_s for Compression Spikes, Aluminum

SPECIMEN:
 AG-25-9P
 2219-T851 ALUMINUM
 CCP, W = 6 IN., t = .25 IN.

$S_{\max} = 10$ ksi
 $R = 0.05$

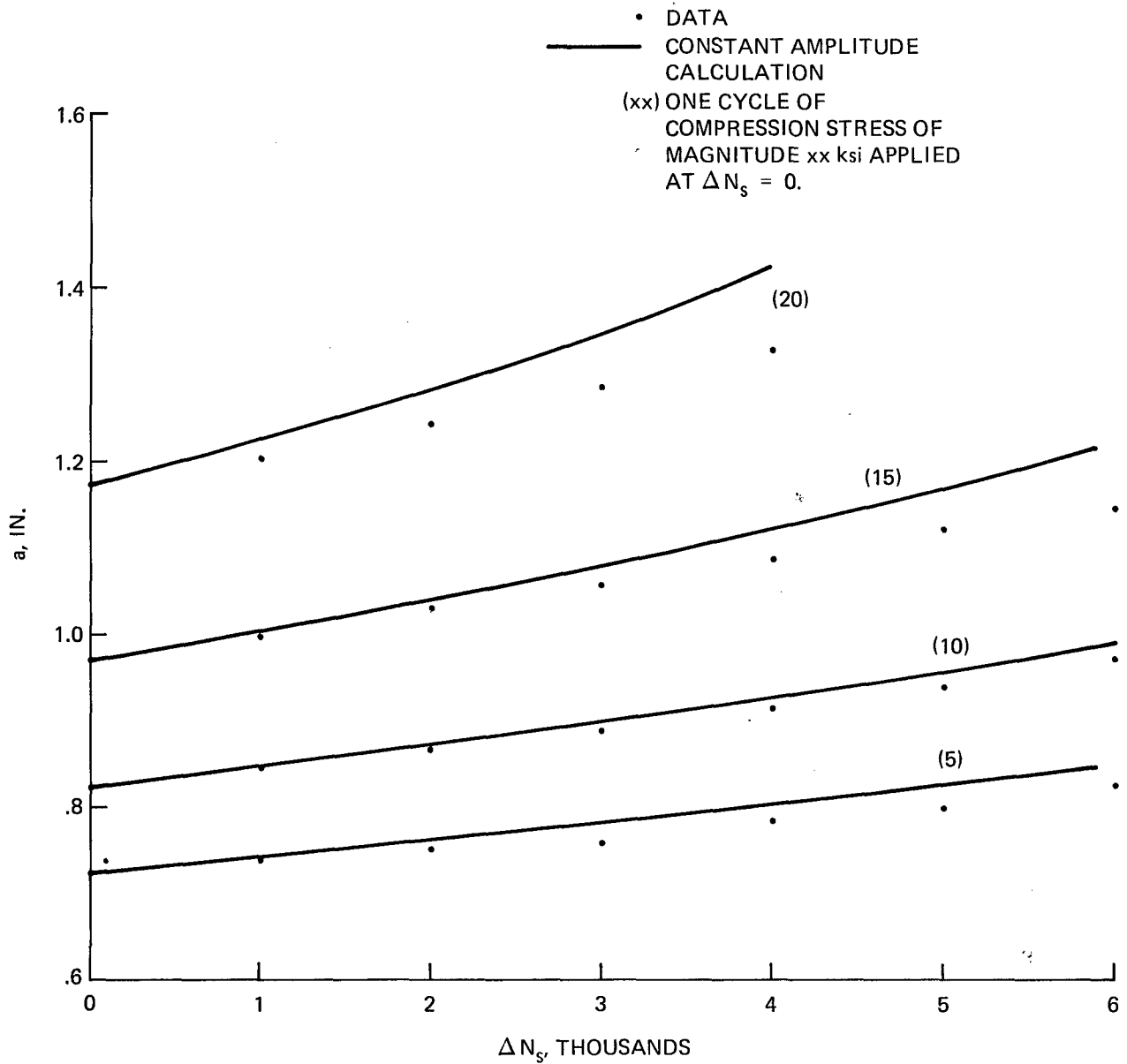
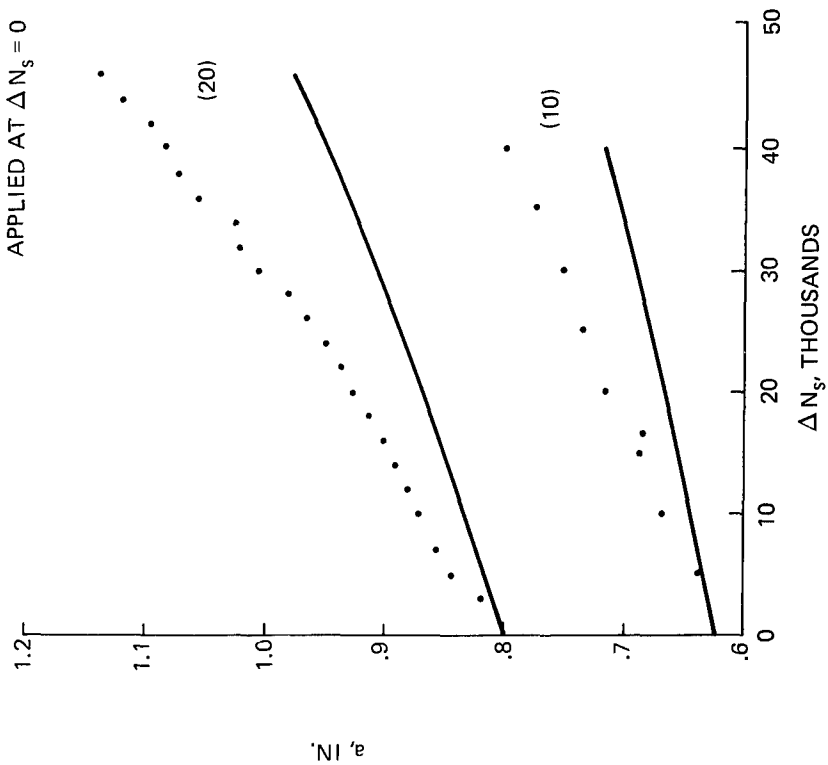


Fig. 81 a vs. ΔN_s for Compression Spikes, Aluminum

SPECIMEN:

TG-25-1P
Ti 6Al-4V TITANIUM
CCP, W = 6 IN., t = .252 IN.
 $S_{max} = 10$ ksi
 $R = .05$

• DATA
— CONSTANT AMPLITUDE
CALCULATION
(xx) ONE CYCLE OF
COMPRESSION STRESS
OF MAGNITUDE xx ksi
APPLIED AT $\Delta N_s = 0$



TG-25-1P (CONT)

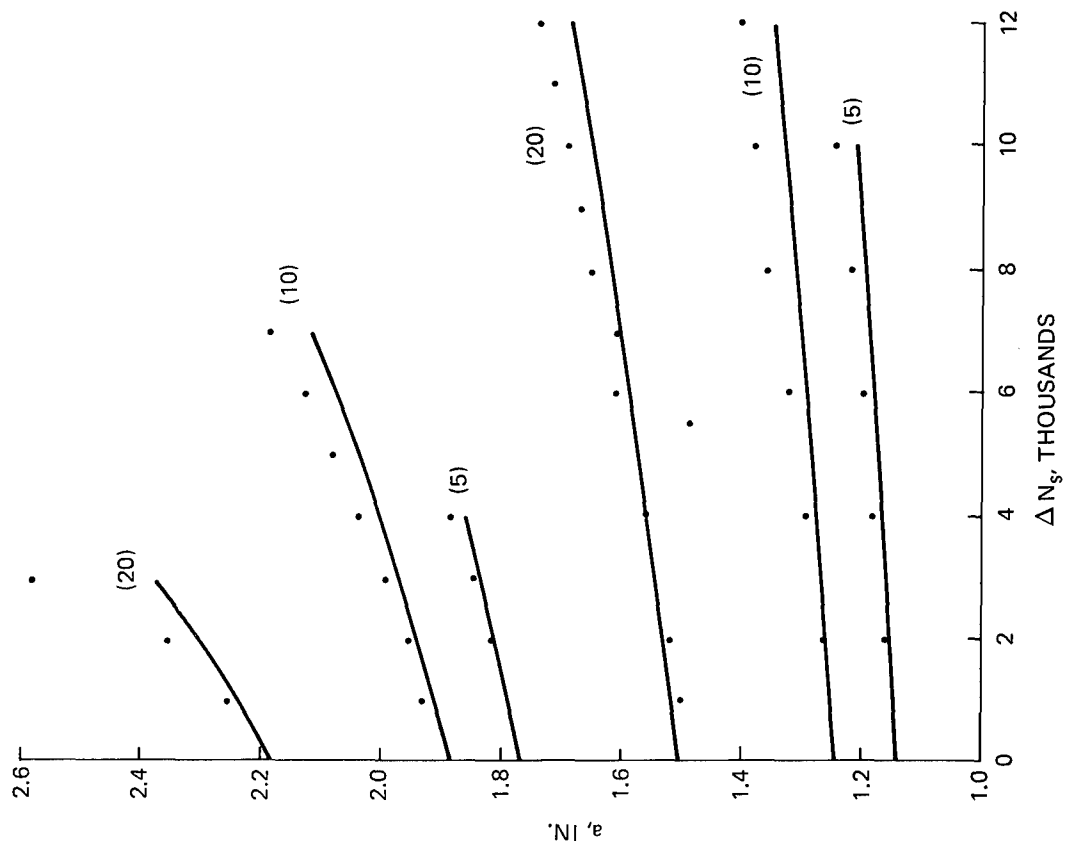


Fig. 82 a vs. ΔN_s for Compression Spikes, Titanium

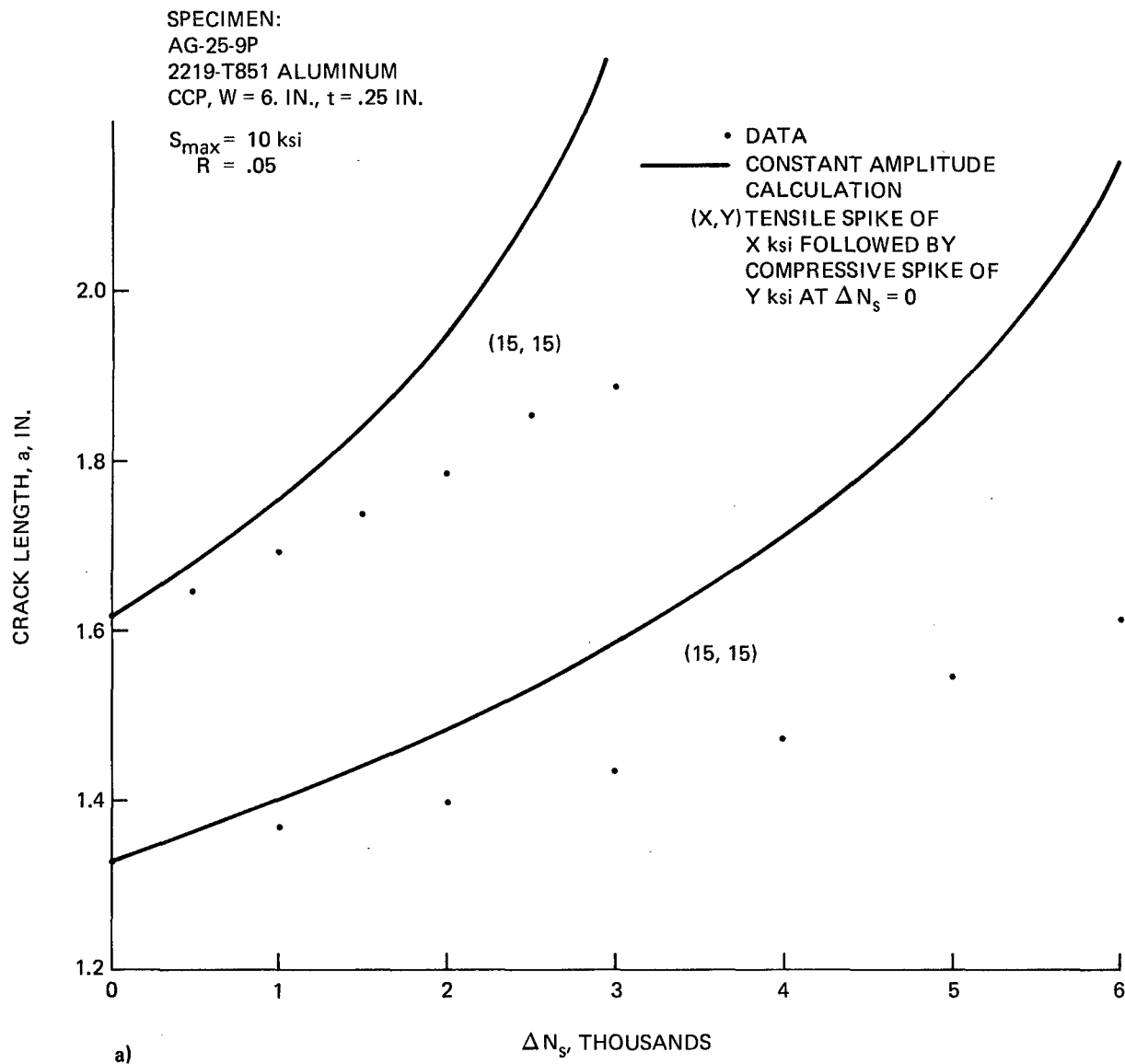


Fig. 83 a vs. ΔN_s for Tension/Compression Spike Sequences, Aluminum

SPECIMEN:
AG-25-10P
2219-T851 ALUMINUM
CCP, W = 6. IN., t = .25 IN.

$S_{max} = 6$ ksi
 $R = .05$

• DATA
— CONSTANT AMPLITUDE
CALCULATION

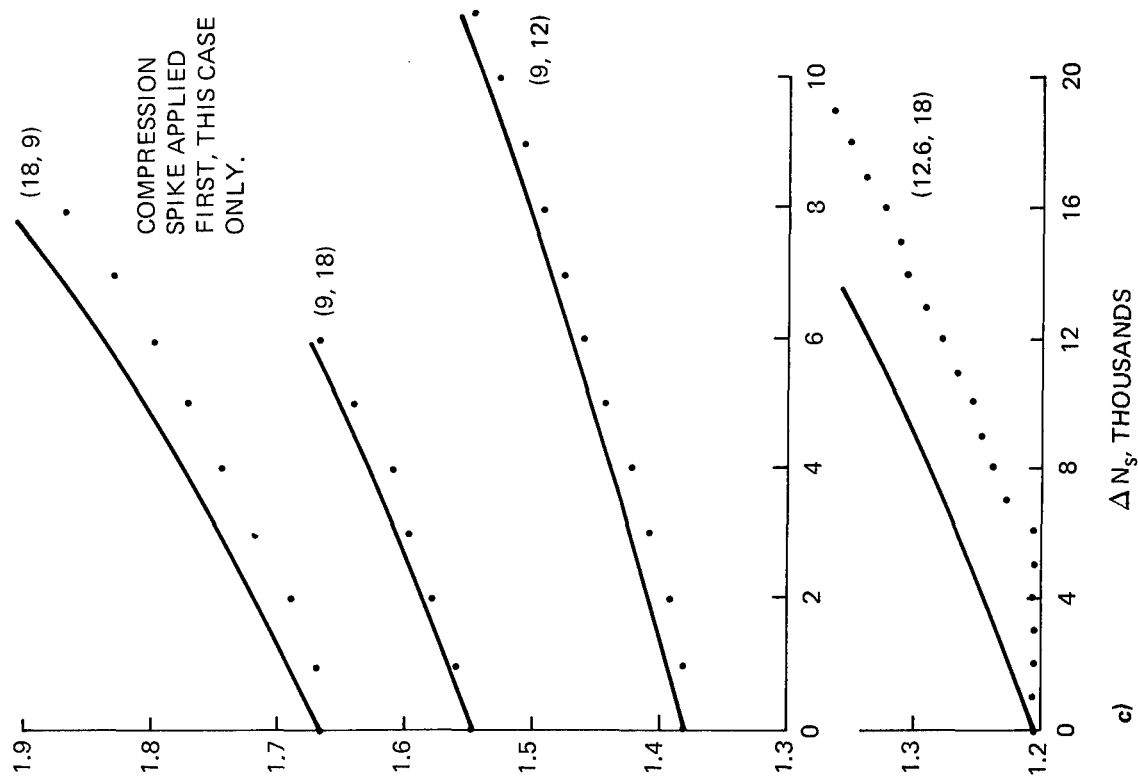
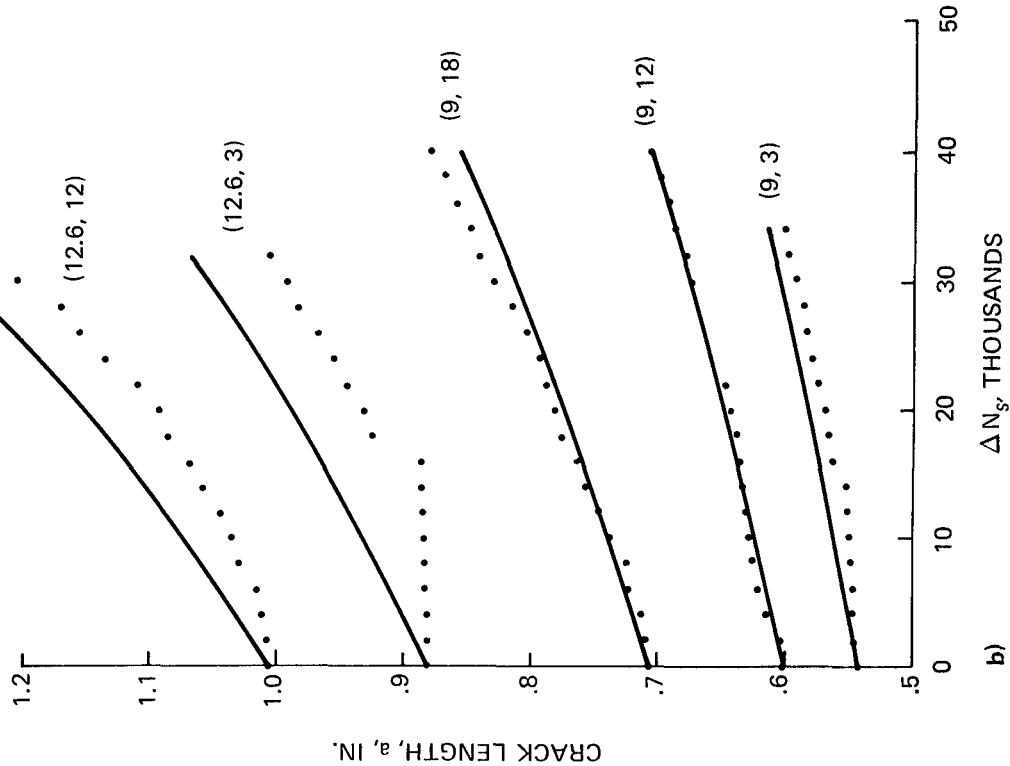


Fig. 83 (Cont)

SPECIMEN:
 TG-25-4P
 Ti 6Al-4V TITANIUM
 CCP, W = 6. IN., t = .25 IN.
 $S_{max} = 10$ ksi
 $R = .05$
 (X, Y) ONE CYCLE OF TENSION
 OF X ksi, FOLLOWED
 BY ONE CYCLE OF
 COMPRESSION OF
 Y ksi AT $\Delta N_s = 0$.
 + = TENSION
 - = COMPRESSION

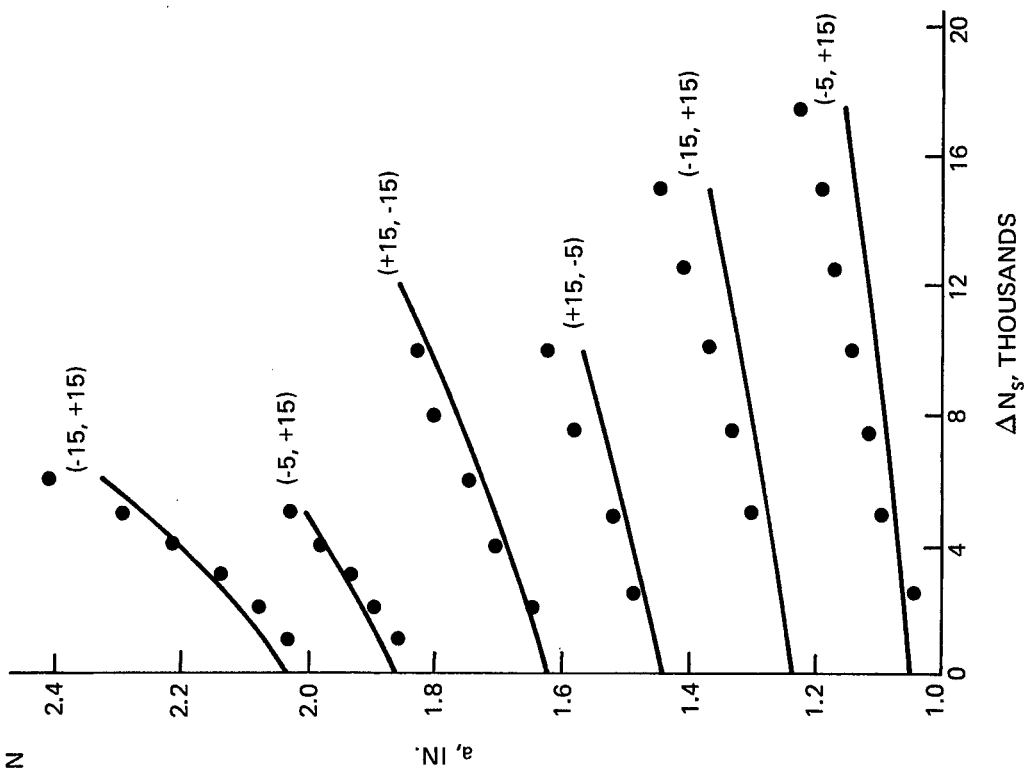
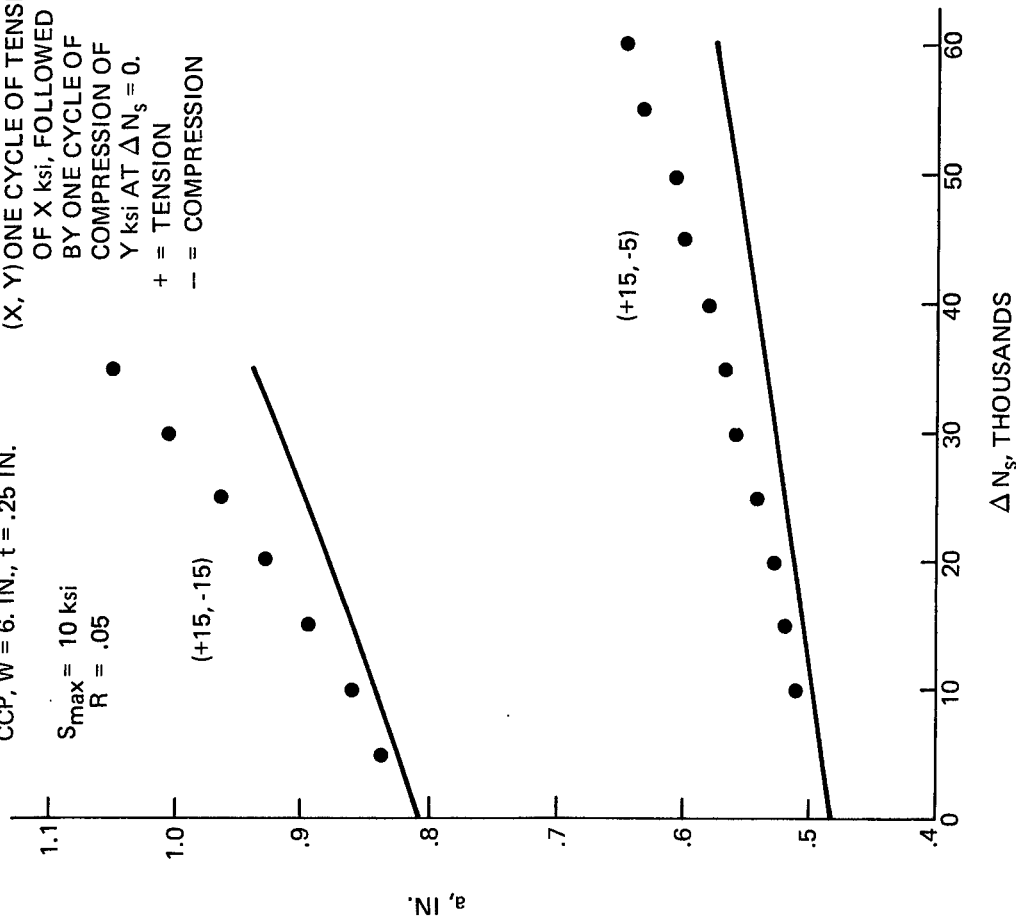


Fig. 84 a vs. ΔN_s after Tension/Compression and Compression/Tension Spikes, Titanium

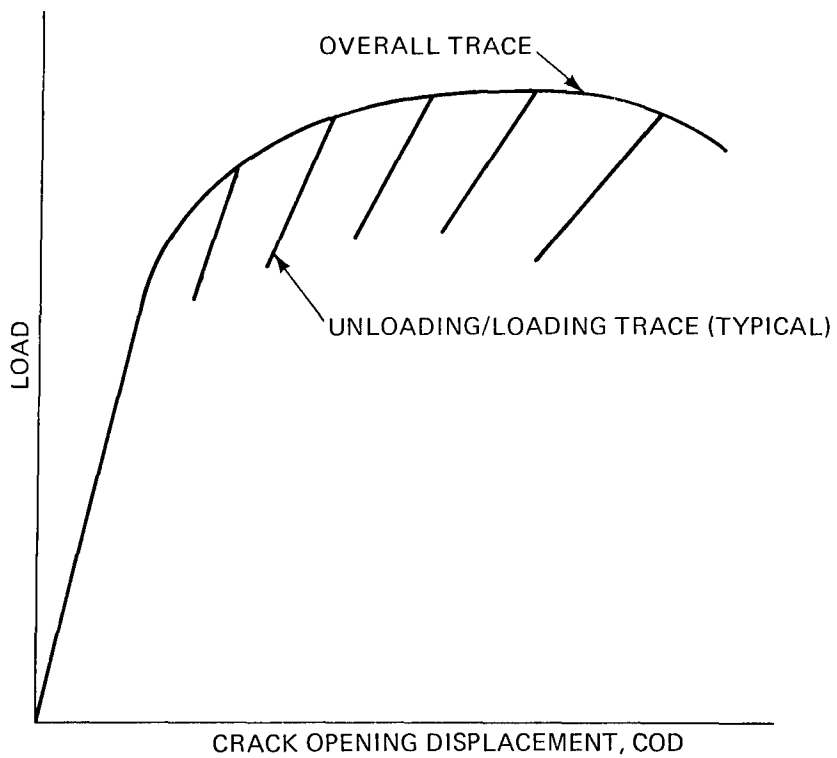


Fig. 85 Schematic of Crack Growth Resistance Test

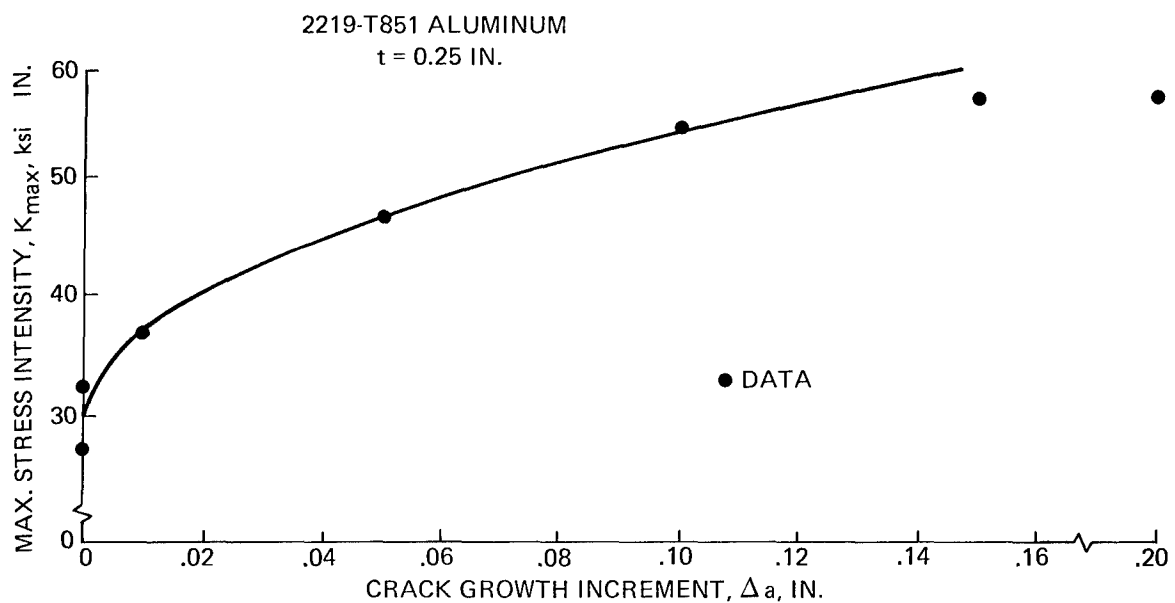


Fig. 86 Crack Growth Resistance Curve for 2219-T851 Aluminum

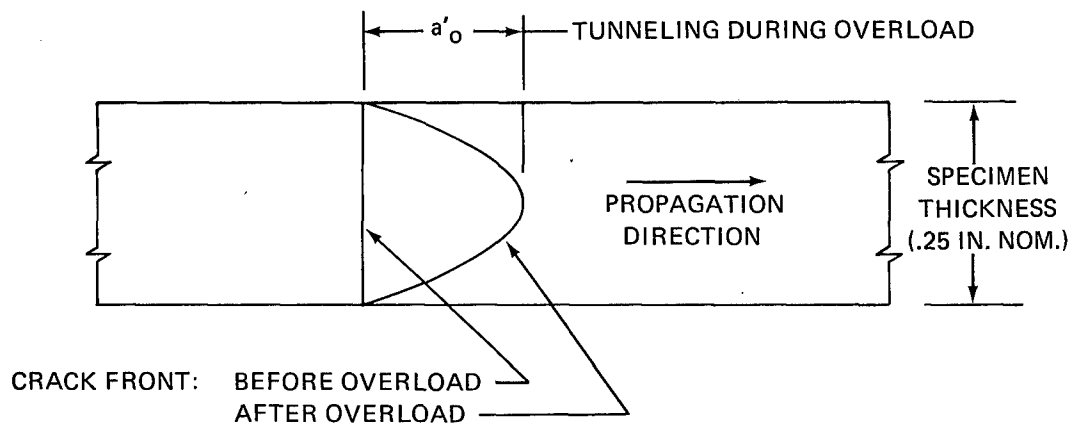


Fig. 87 Schematic of Crack Front Tunneling

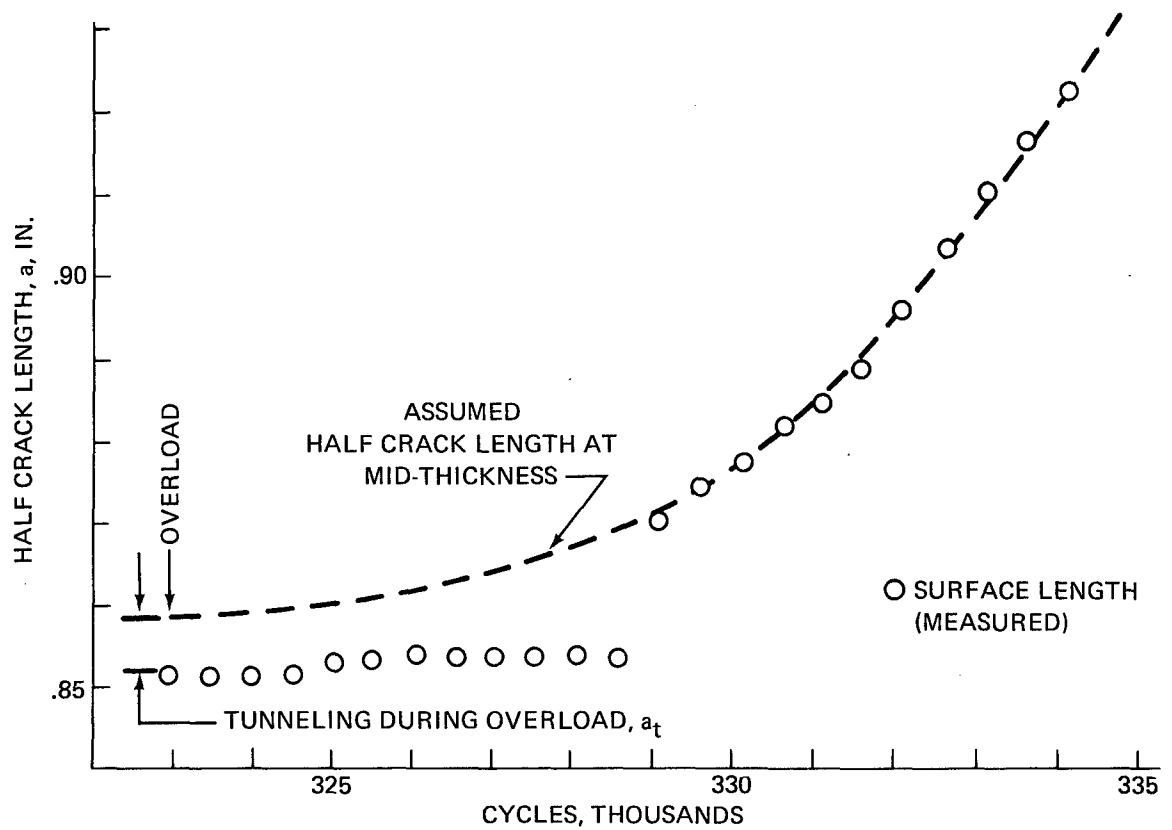


Fig. 88 Assumed Crack Front Behavior After Tunneling

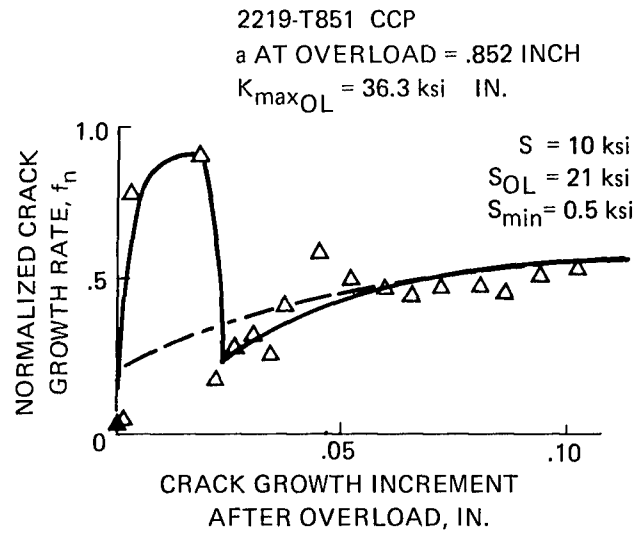


Fig. 89 Normalized Crack Growth Rate vs
 Crack Growth Increment After Overload

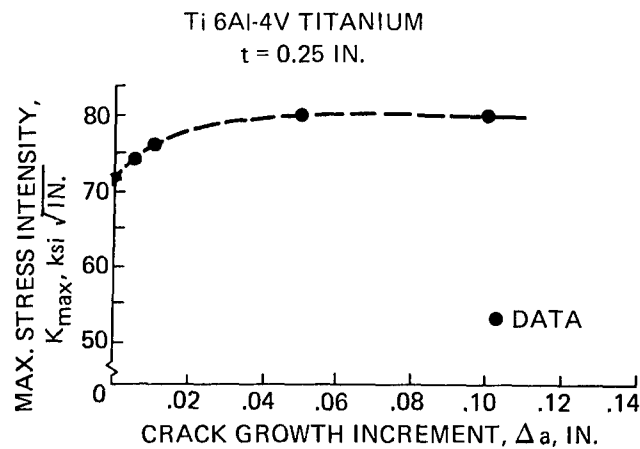


Fig. 90 Crack Growth Resistance Curve
 for Ti 6Al-4V Titanium

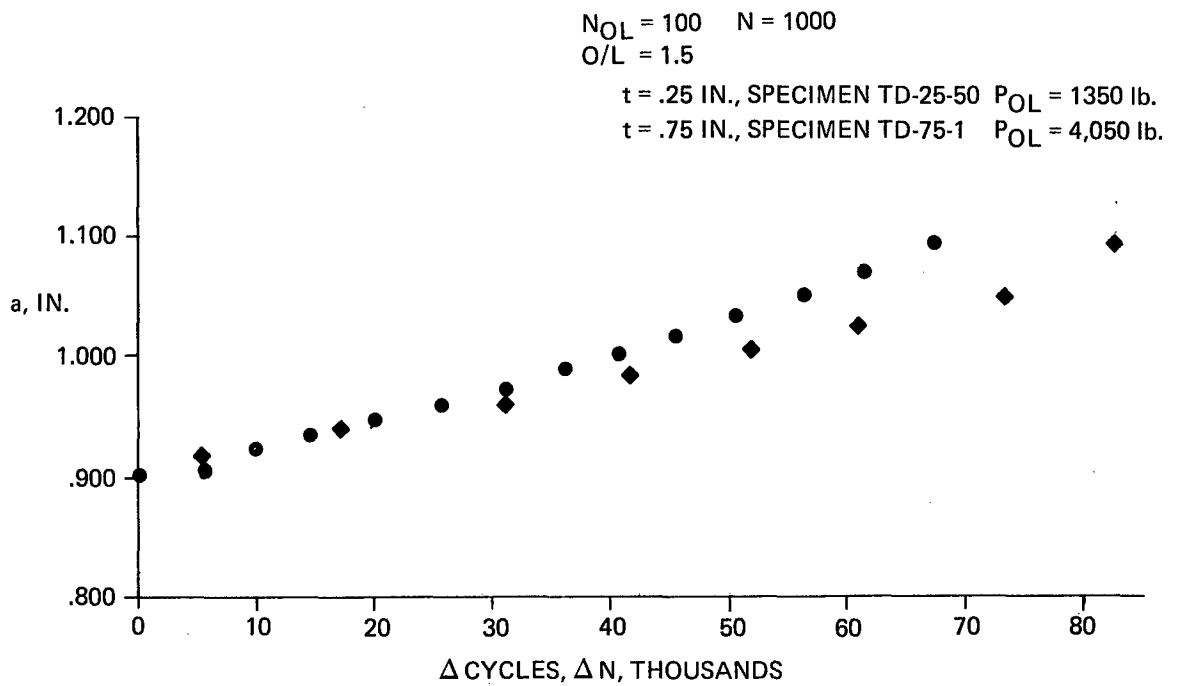


Fig. 91 a vs Δ N for Multiple Periodic Overloads for Two Thicknesses

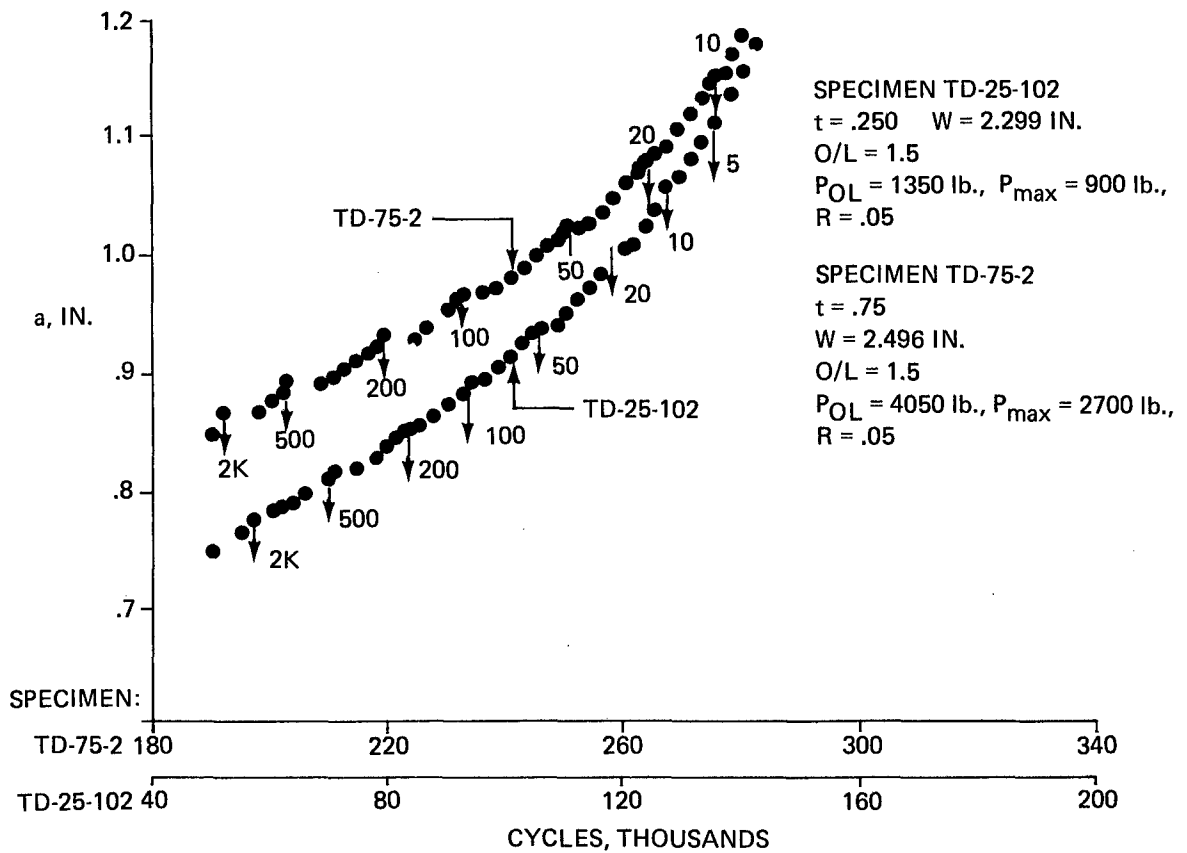


Fig. 92 Effect of Multiple Overloads for Two Thicknesses

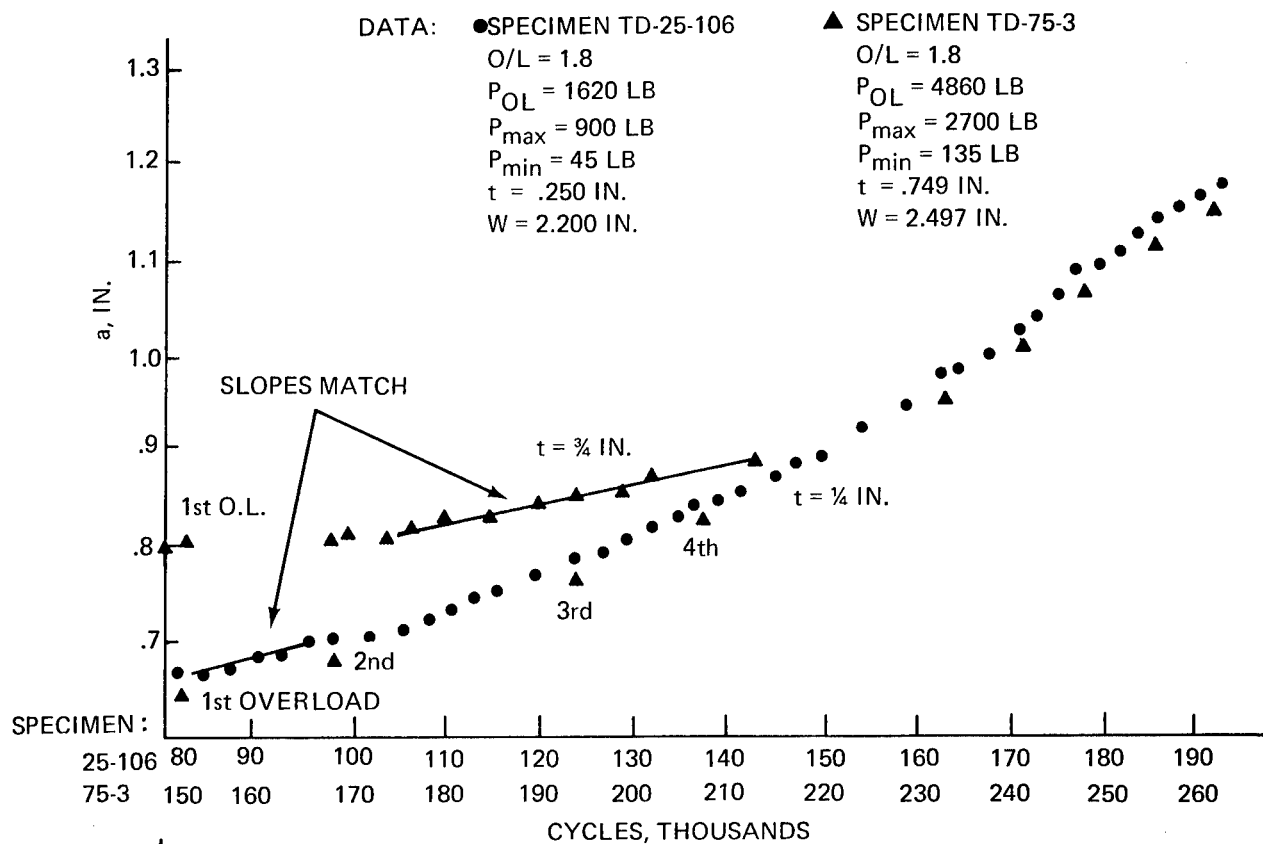


Fig. 93 Comparison of Crack Growth Rates for Two Thicknesses, 1st Overload

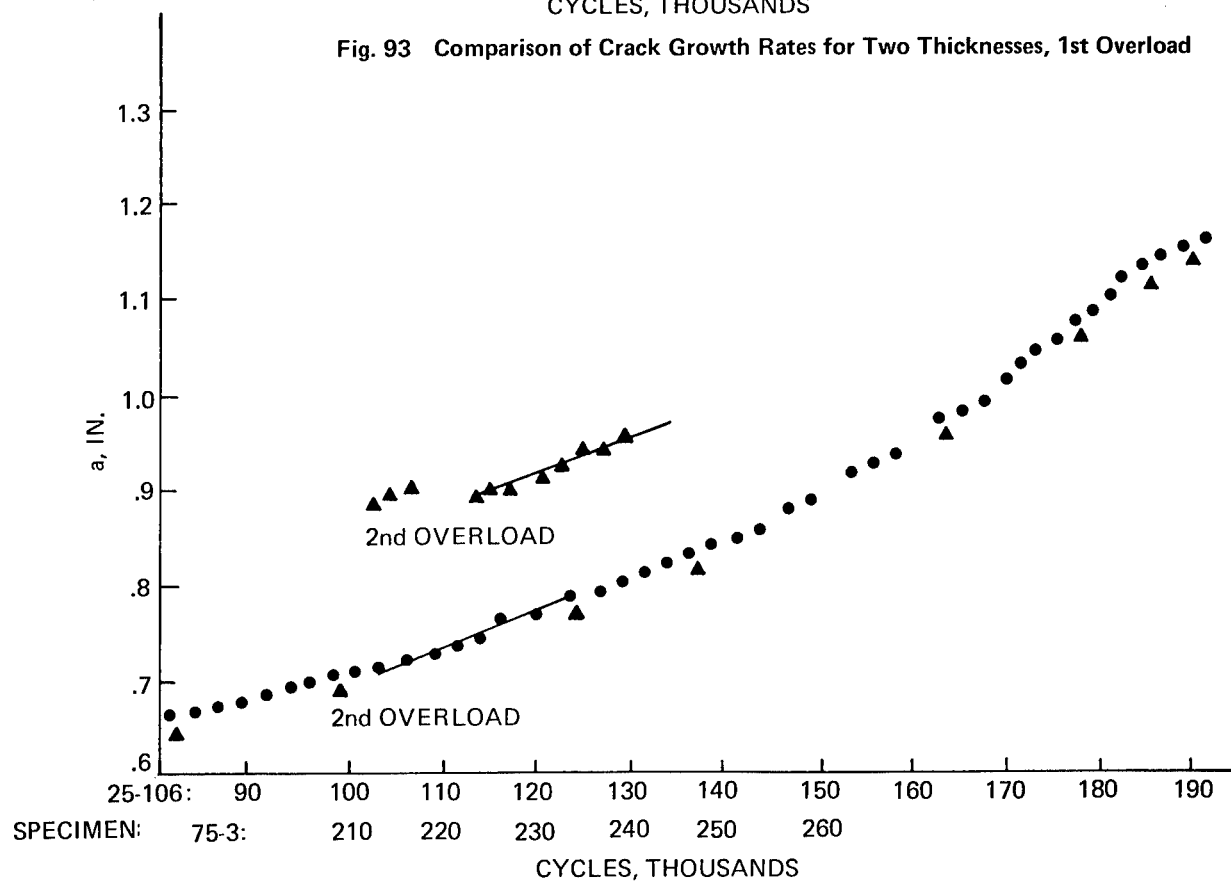


Fig. 94 (Continued Fig. 93 2nd Overload)

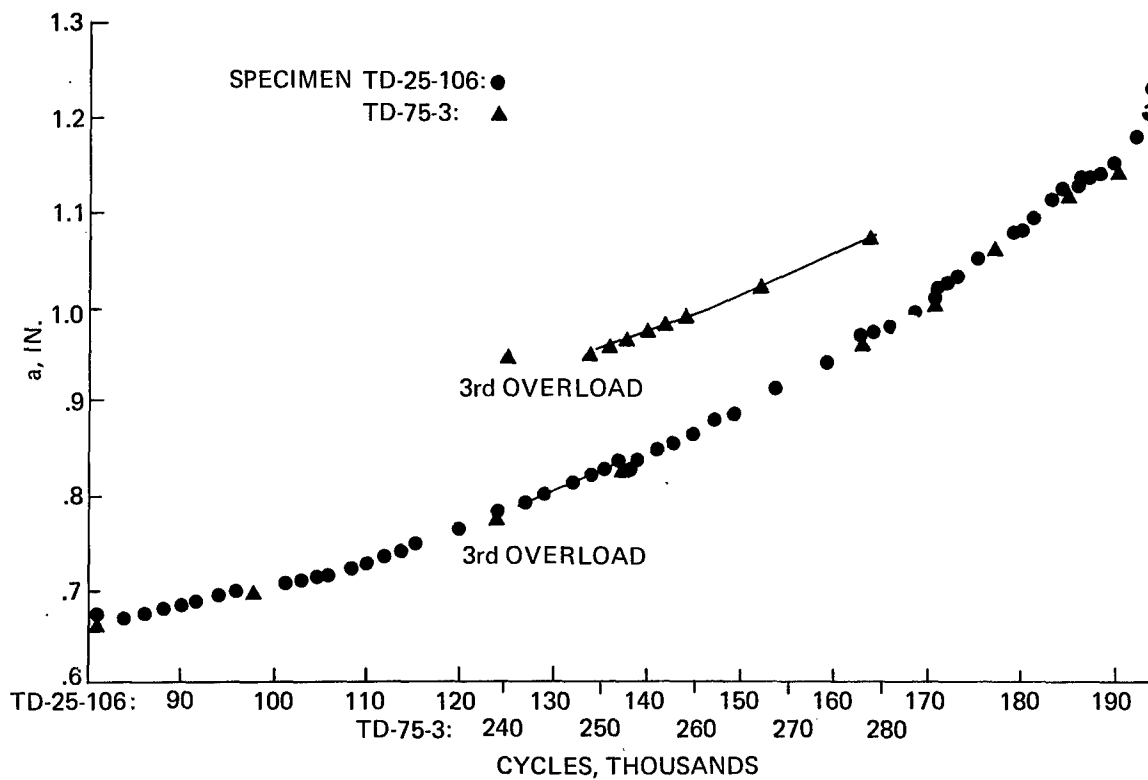


Fig. 95 (Continued from Fig. 94) 3rd Overload

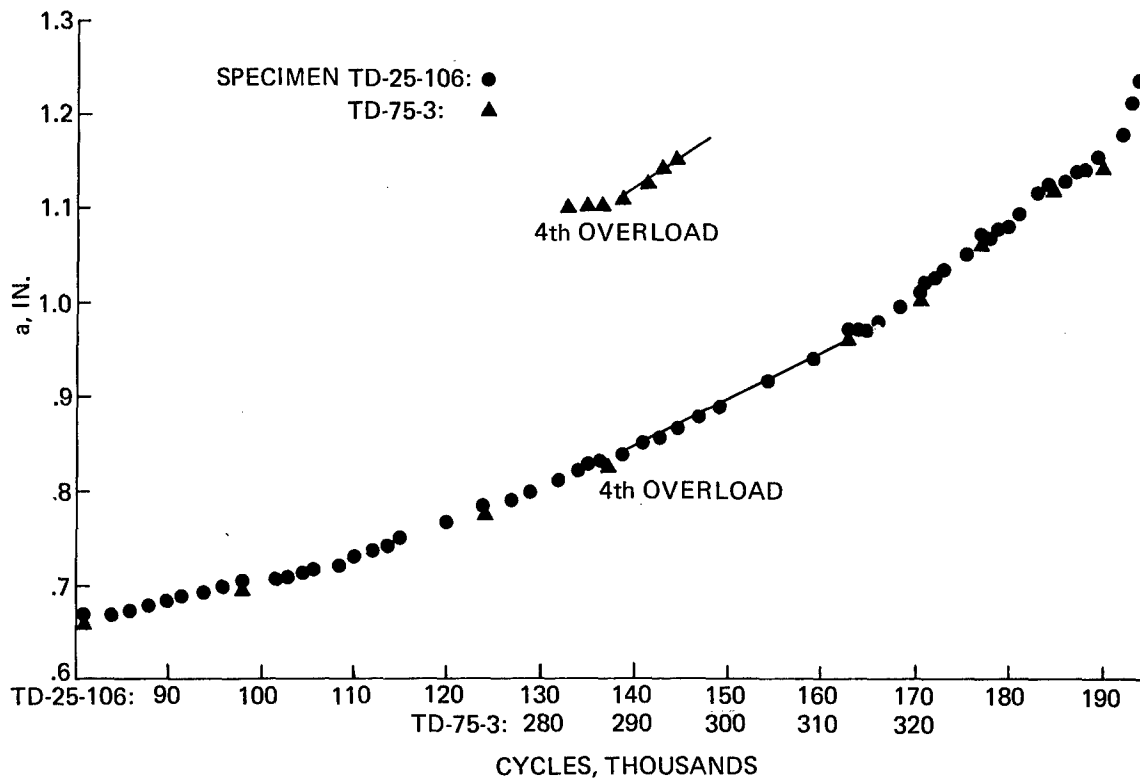


Fig. 96 (Continued from Fig. 95) 4th Overload

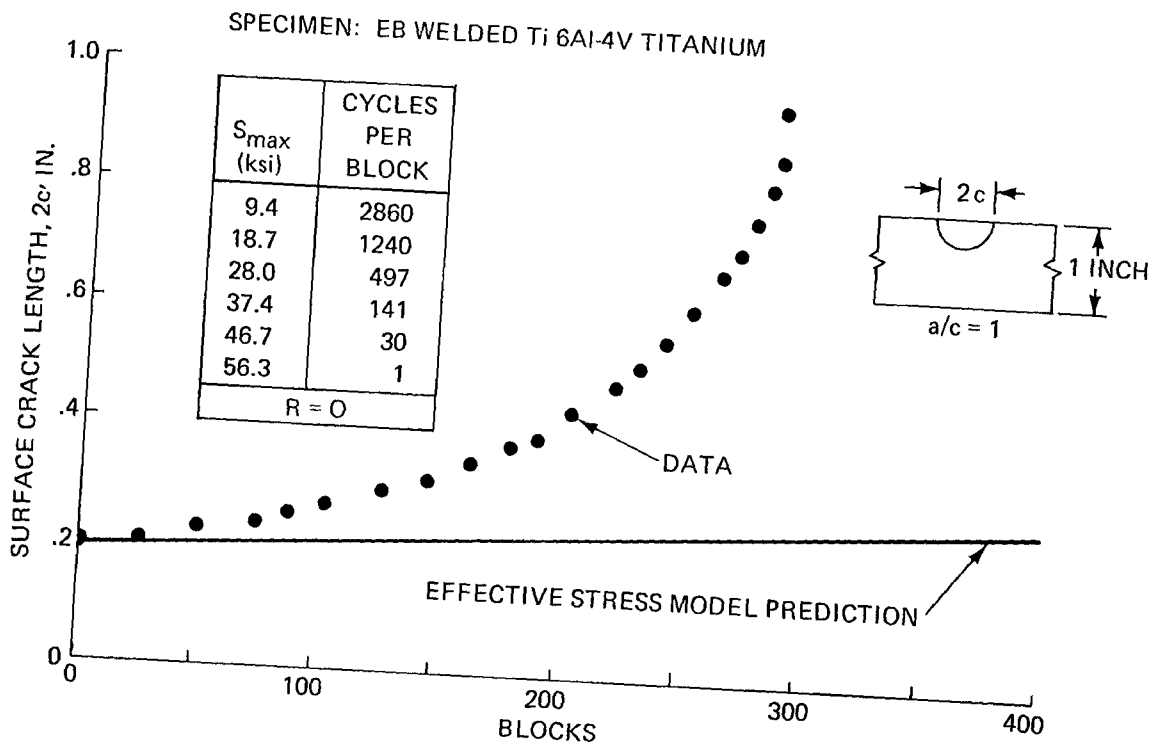


Fig. 97 Comparison of Data and Prediction Using Effective Stress Model

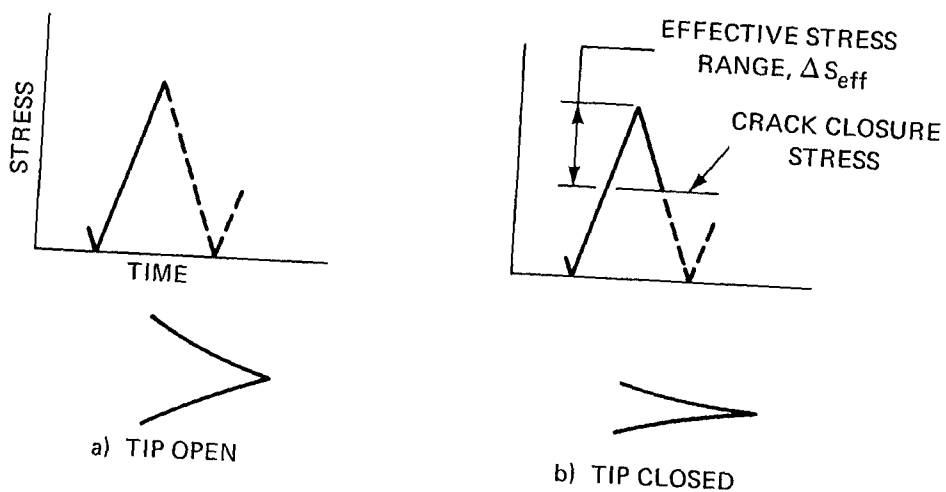


Fig. 98 Schematic of Crack Closure

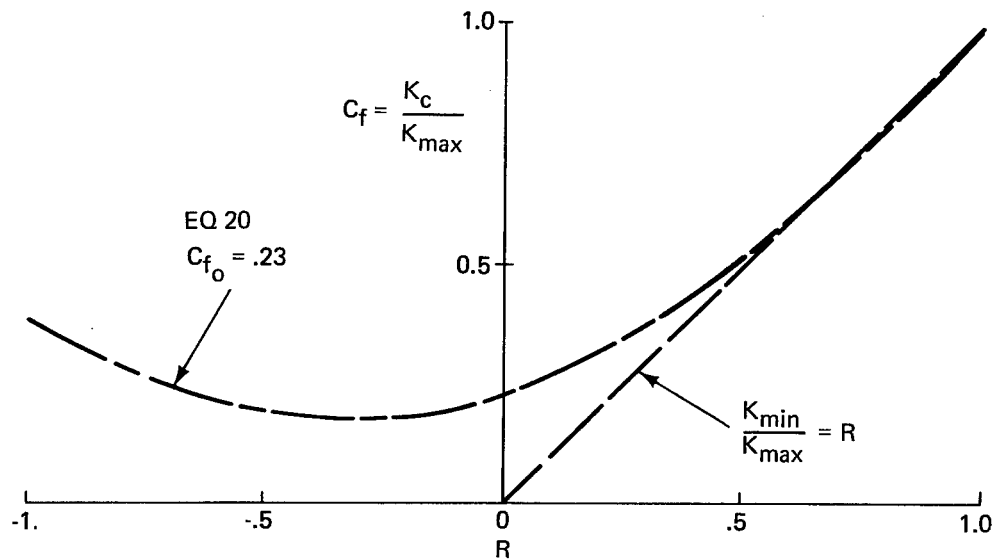


Fig. 99 Closure Factor vs R for 2219-T851 Aluminum

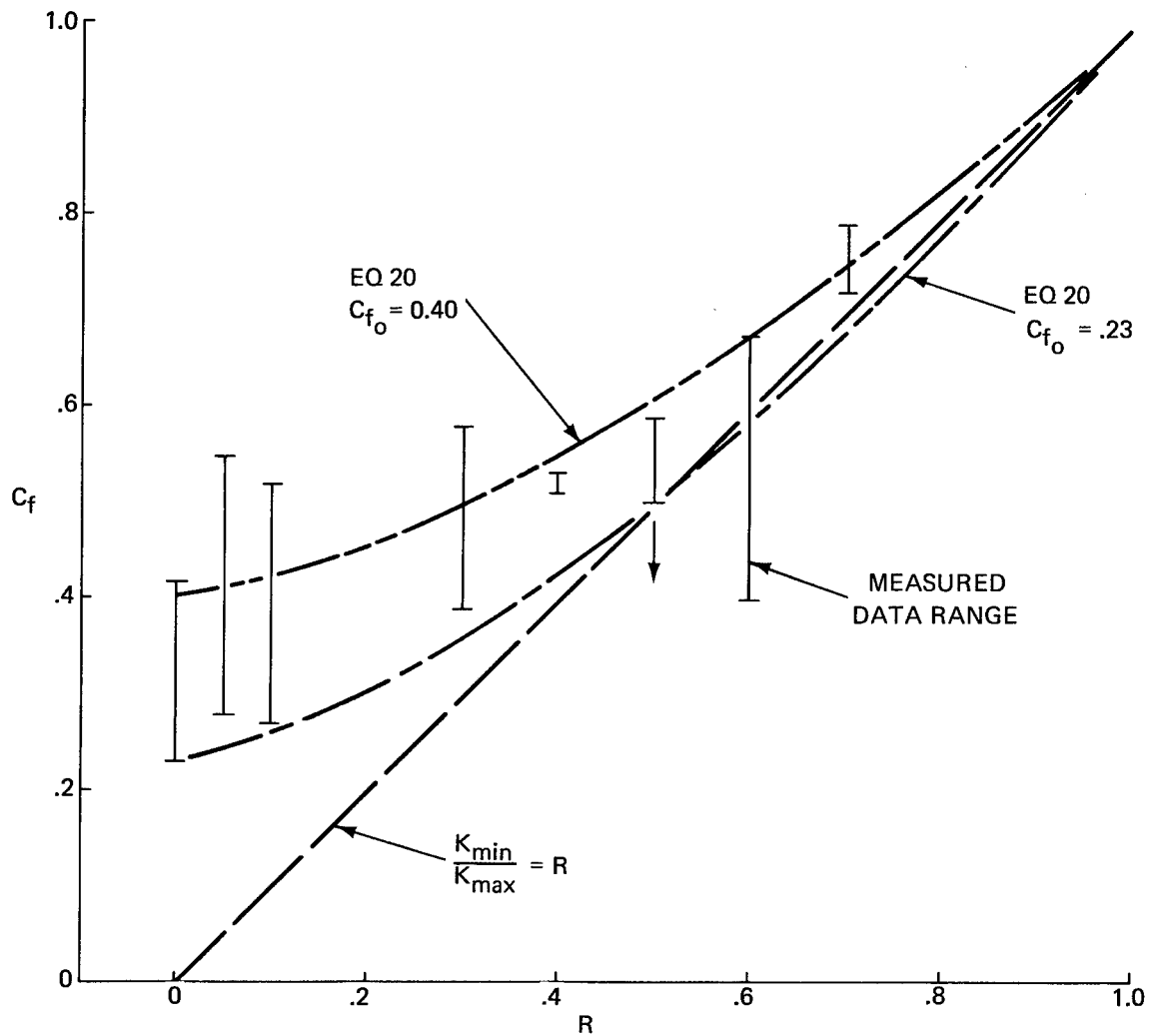
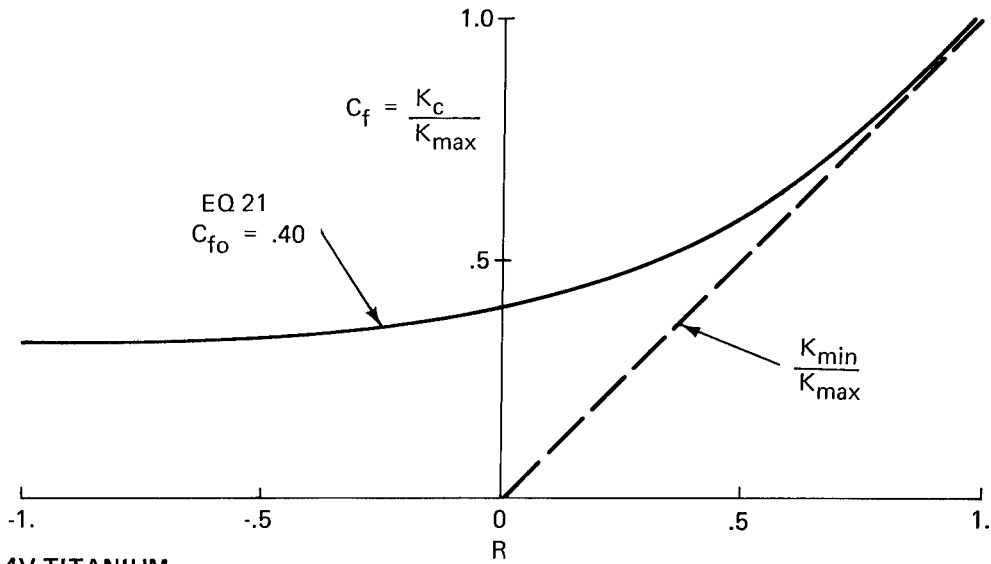
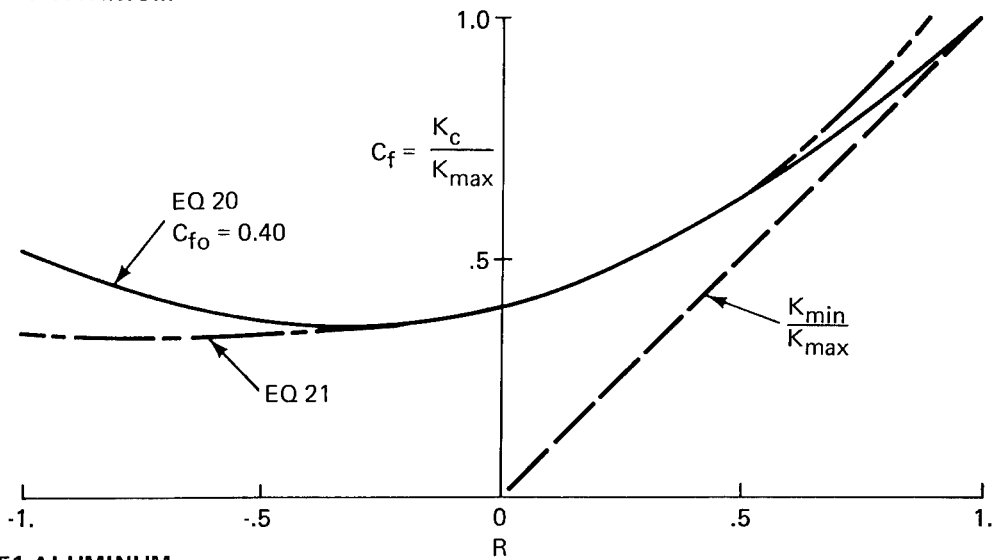


Fig. 100 Comparison of Closure Factor with Data for 2219-T851 Aluminum



b) TI-6AL-4V TITANIUM



a) 2219-T851 ALUMINUM

Fig. 101 Modified Closure Factor vs R

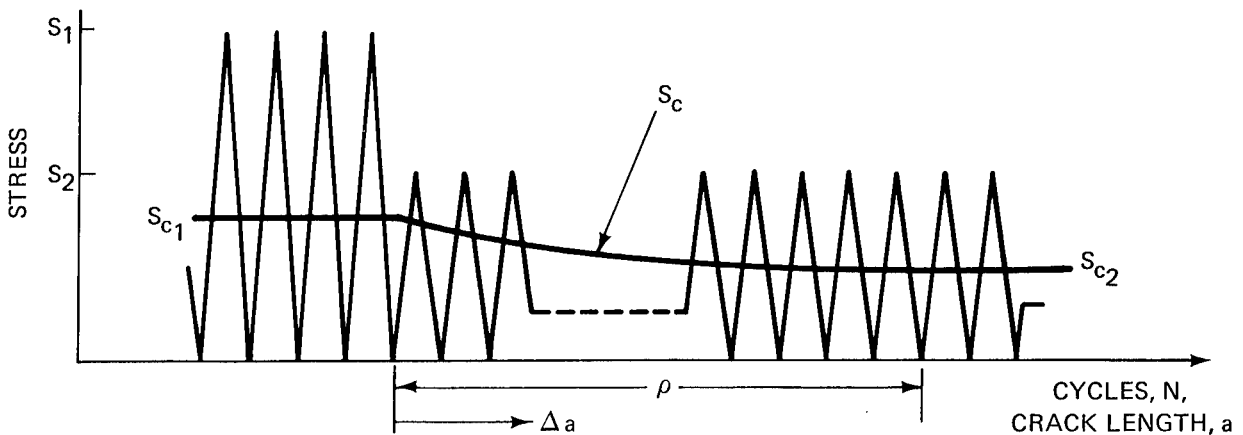


Fig. 102 Schematic of Closure Variation through Effected Length caused by Overload

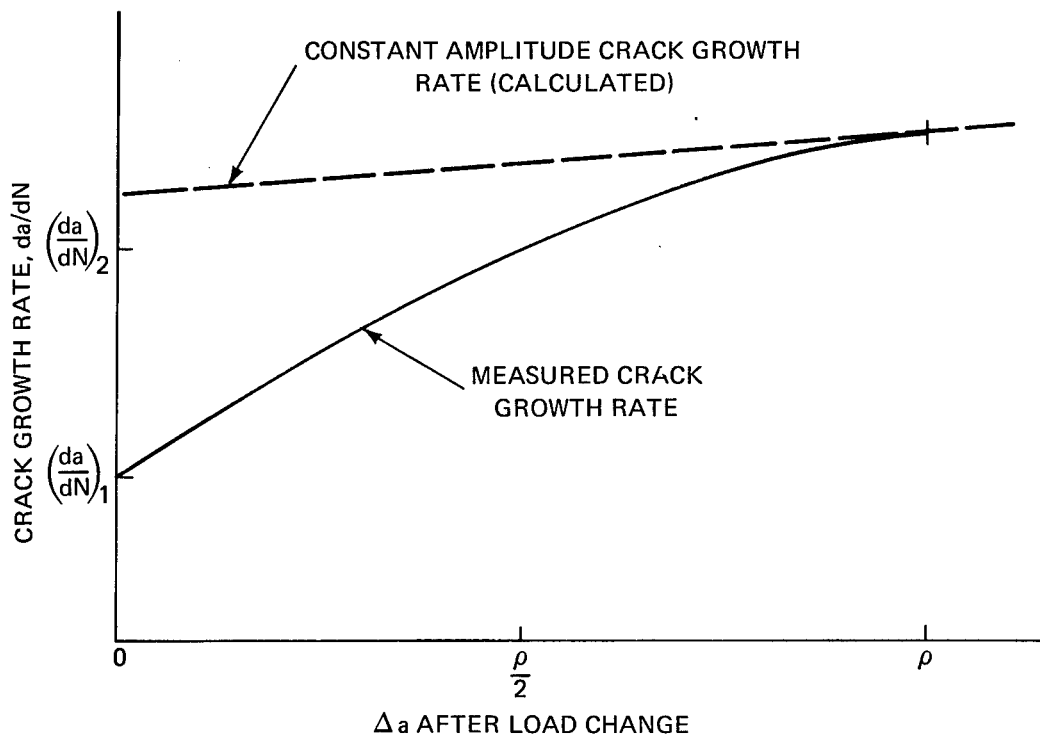


Fig. 103 Schematic of da/dN vs Δa After an Overload

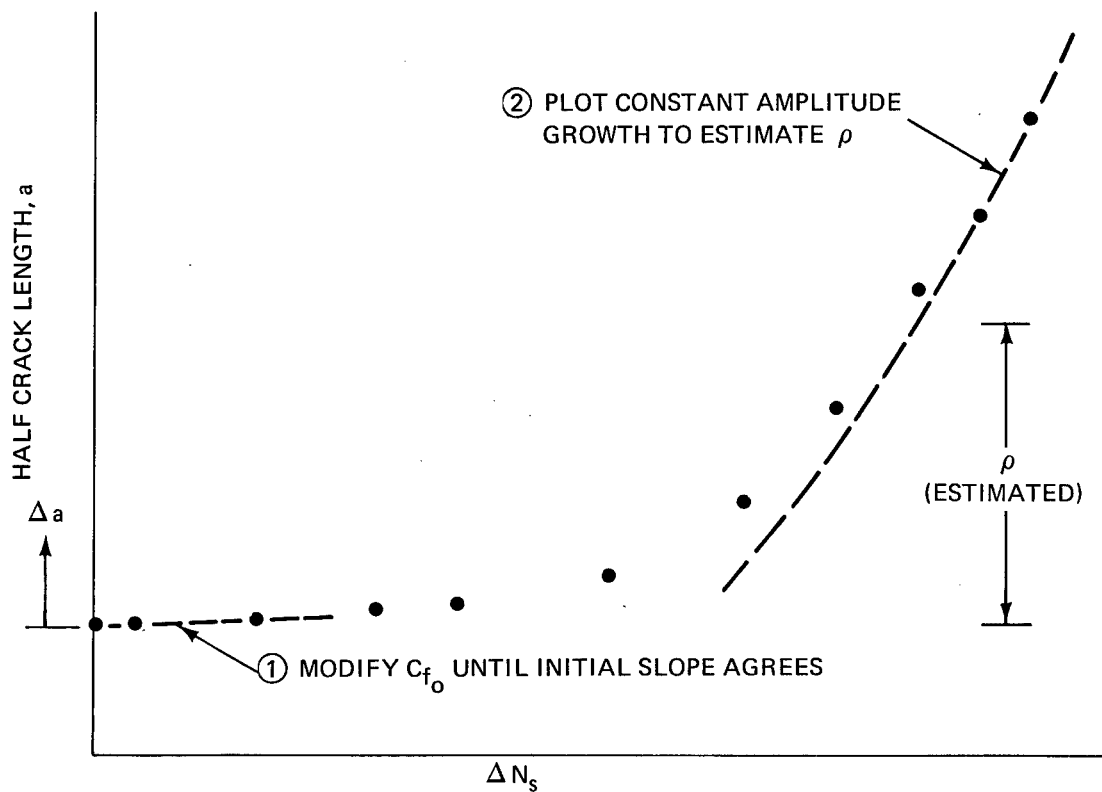


Fig. 104 Schematic of Iteration Procedure to Obtain C_{f0}

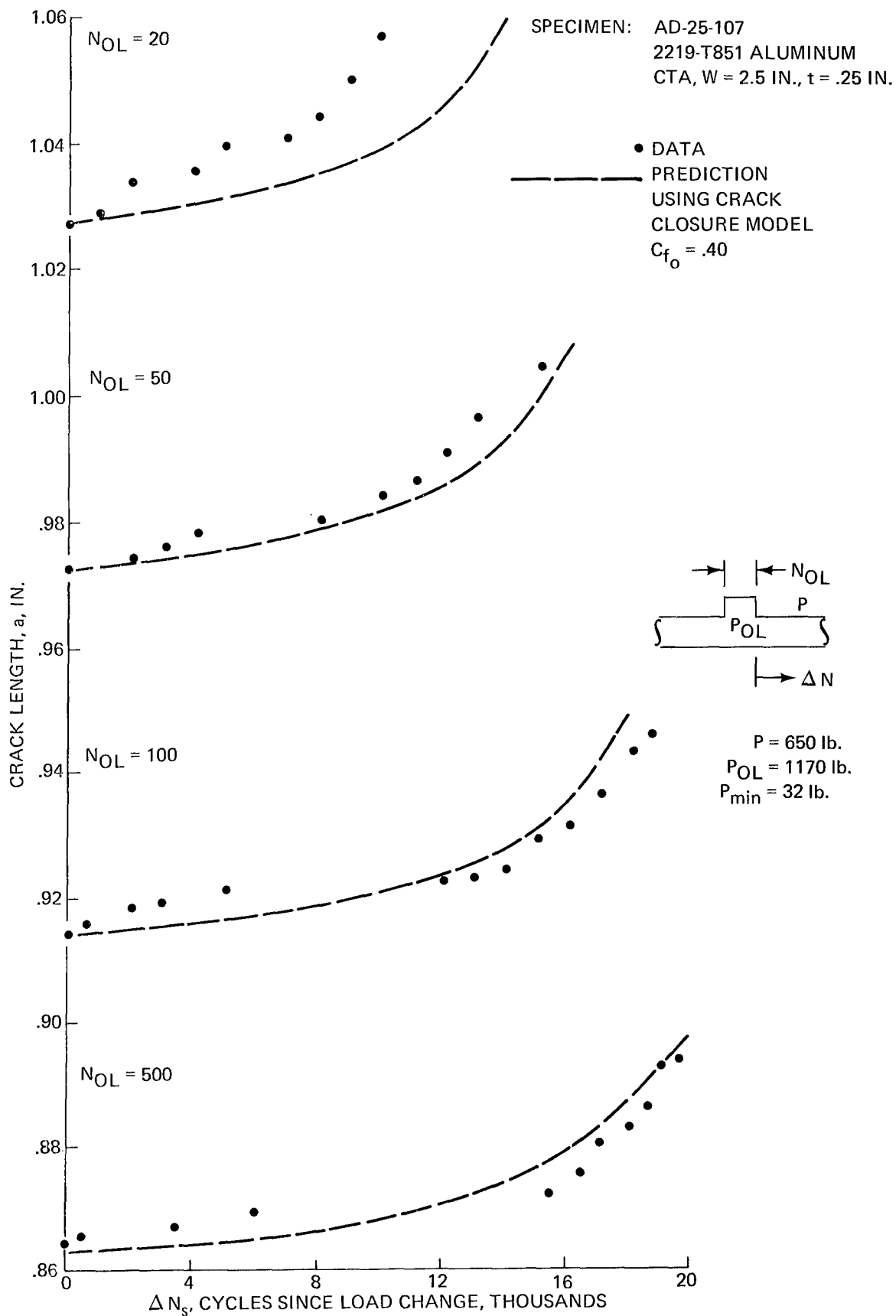


Fig. 105 Comparison of Predictions with Data for High-Low Sequence, 2219-T851 Aluminum, O/L = 1.8

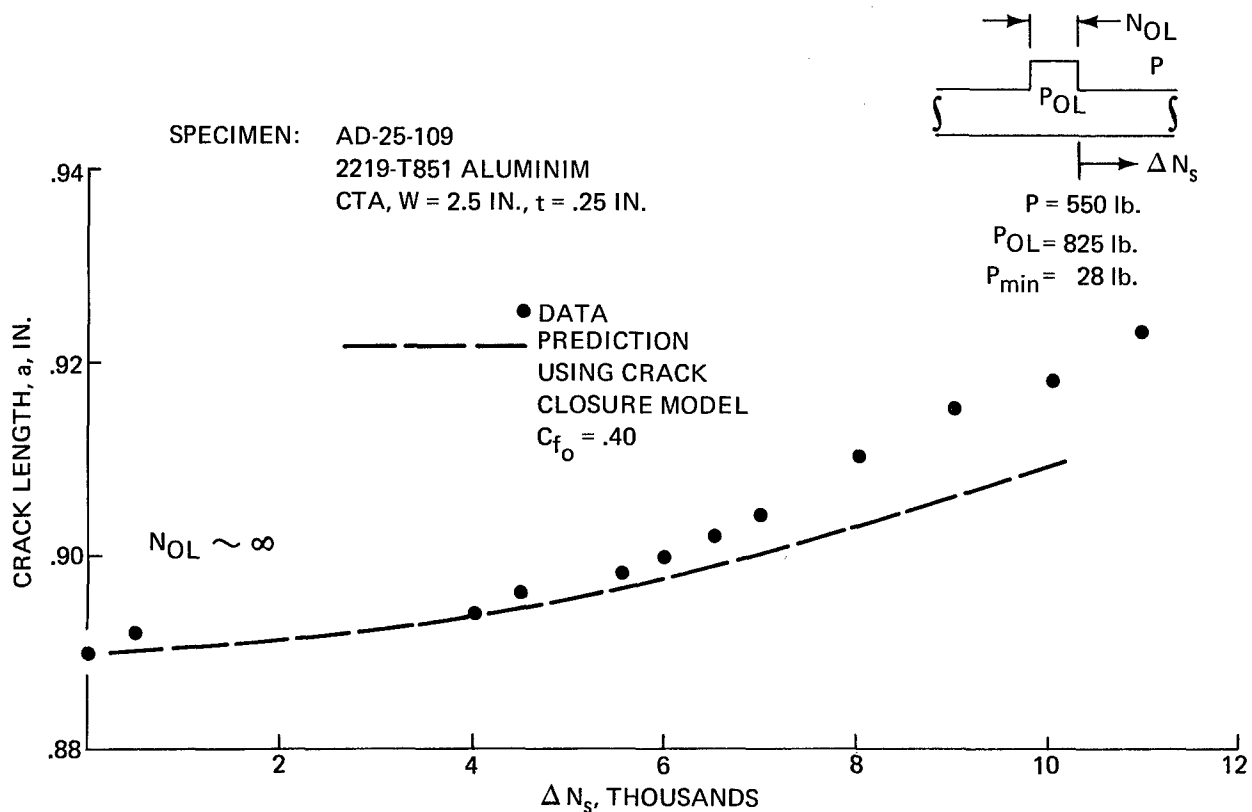


Fig. 106 Comparison of Prediction with Data for High-Low Sequence,
2219-T851 Aluminum, O/L = 1.5

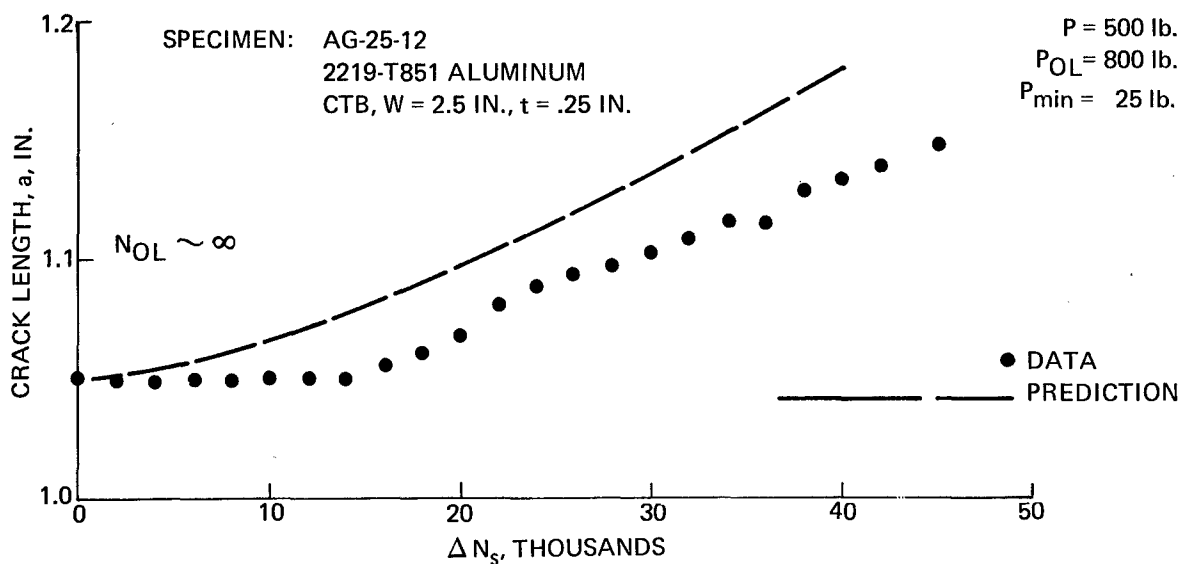


Fig. 107 Comparison of Prediction with Data for High-Low Sequence,
2219-T851 Aluminum, O/L = 1.6

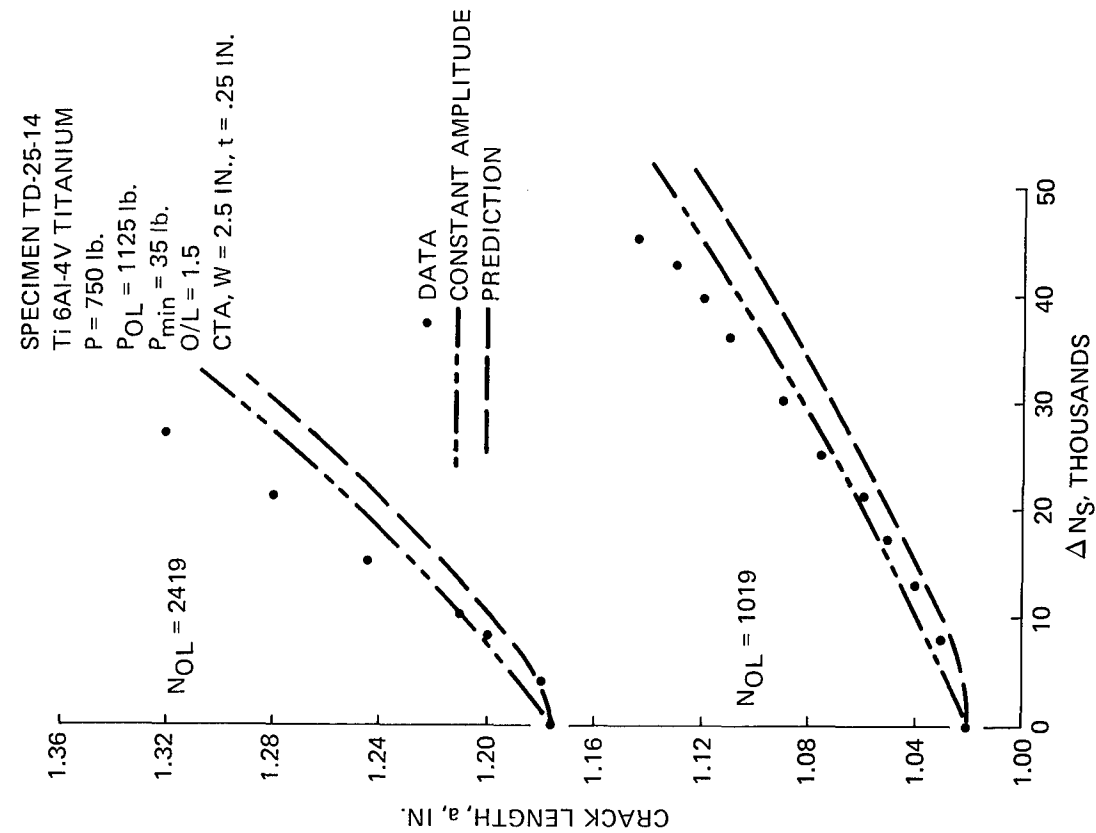


Fig. 109 Comparison of Predictions with Data for High-Low Sequence, Ti 6Al-4V Titanium, O/L = 1.5

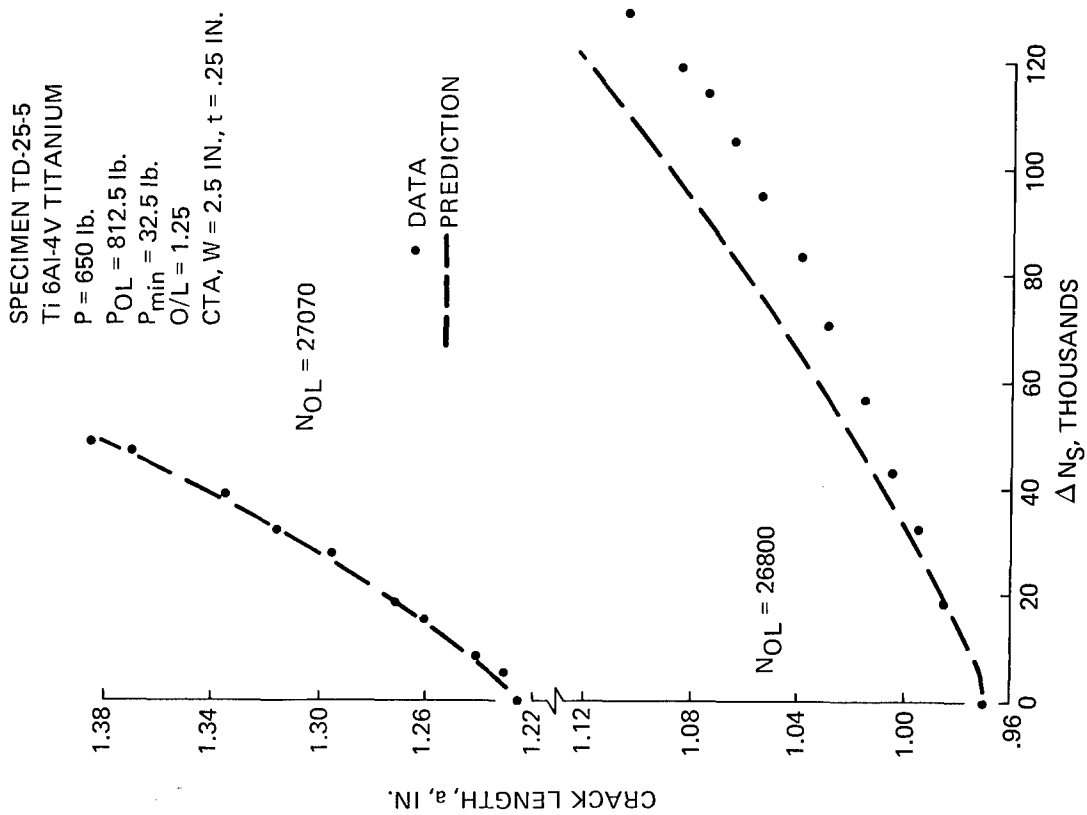


Fig. 108 Comparison of Prediction with Data for High-Low Sequence, Ti 6Al-4V Titanium, O/L = 1.25

SPECIMEN
 TG-25-2P
 Ti 6Al-4V
 CCP, W = 6 IN, t = .25

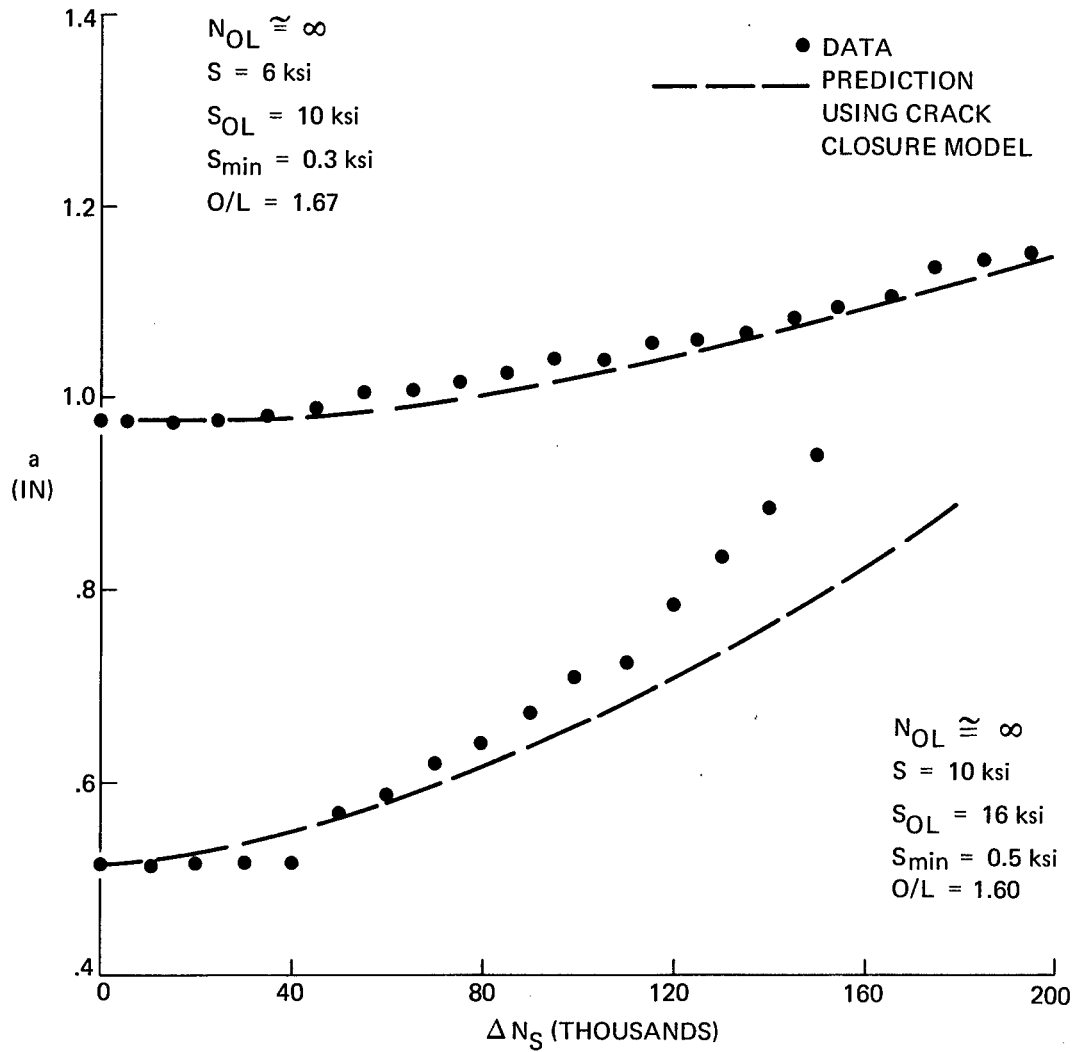


Fig. 110 Comparison of Predictions with Data for High-Low Sequence, Ti 6Al-4V Titanium
 O/L = 1.6, 1.67

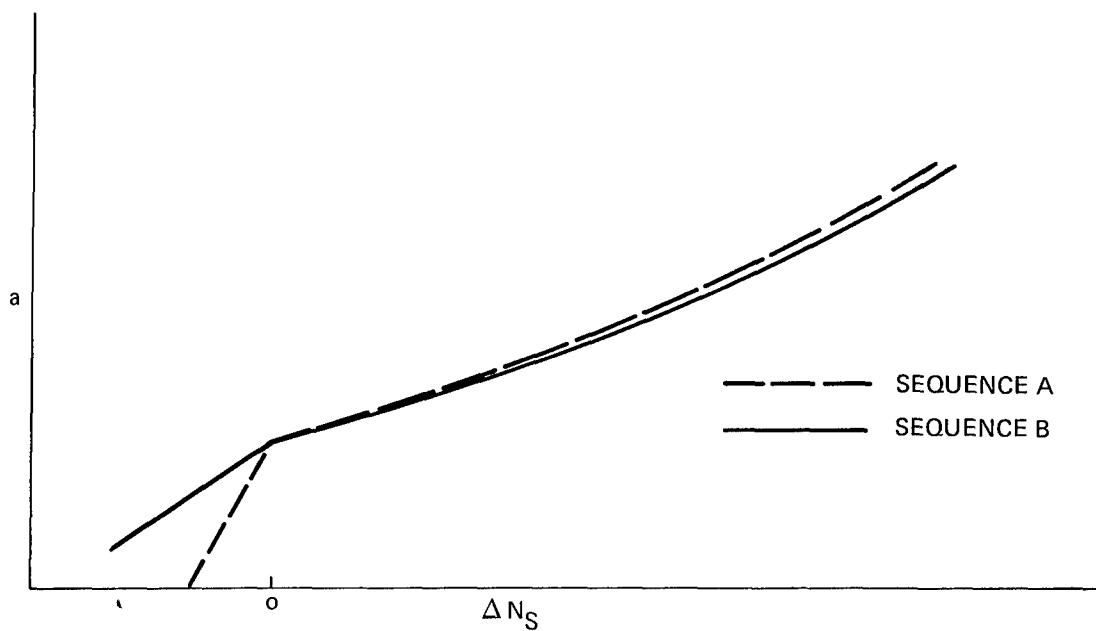
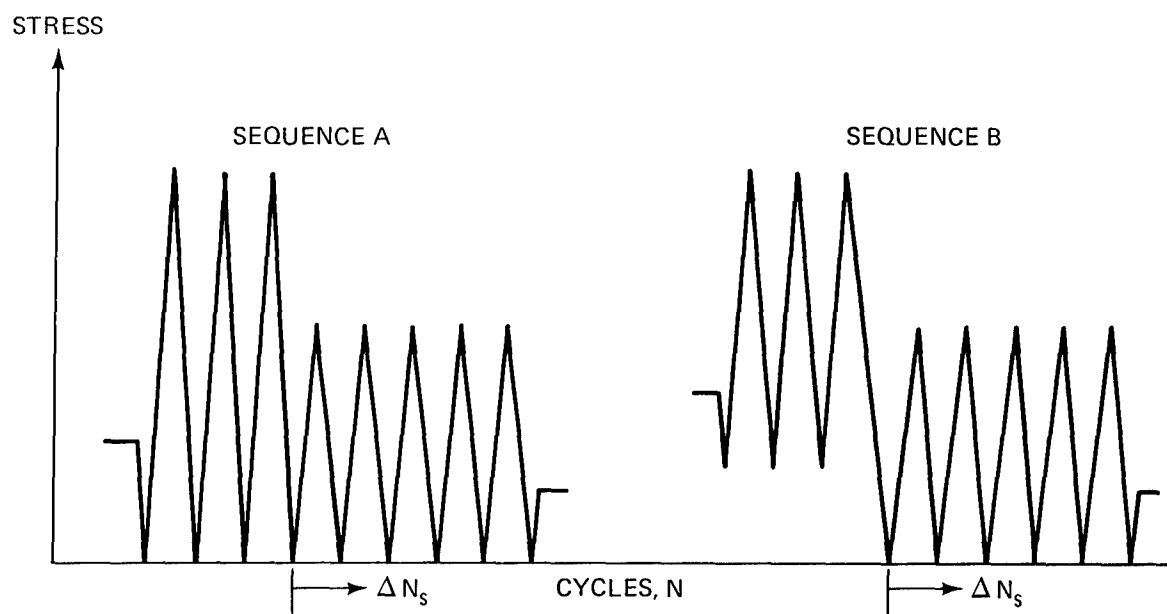


Fig. 111 Effect of Two Different Load Histories on Subsequent Crack Growth

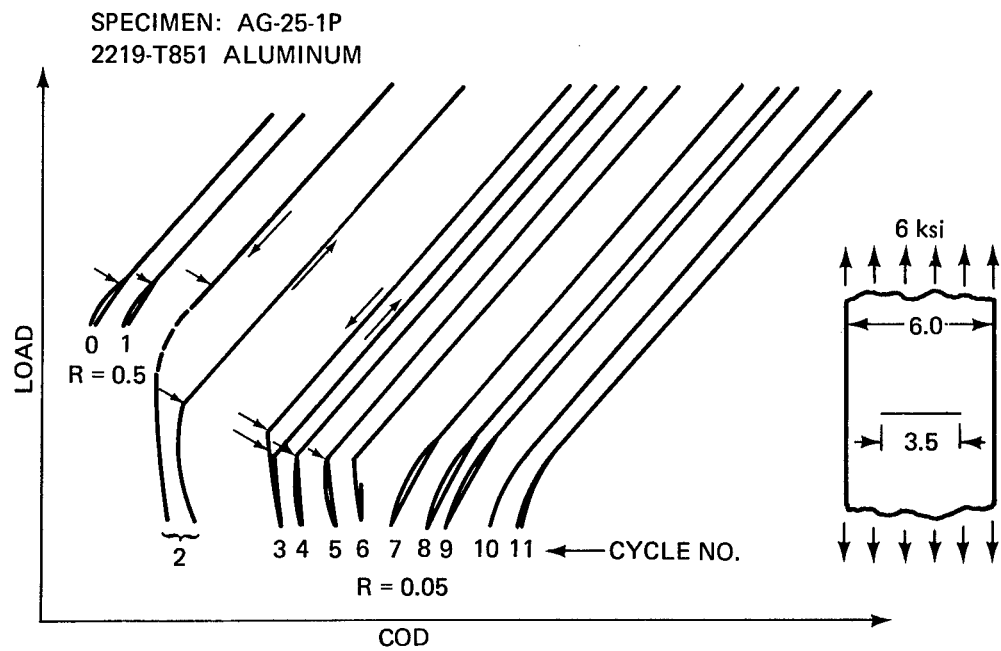


Fig. 112 Load vs COD Sequence for Two Stress Ratios, $R = .5/.05$

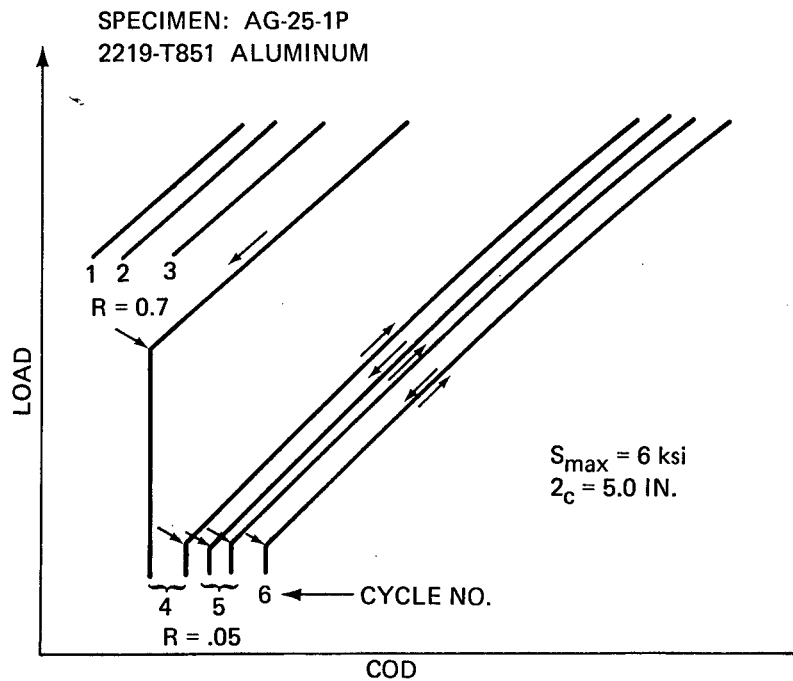


Fig. 113 Load vs COD Sequence for Two Stress Ratios, $R = .7/.05$

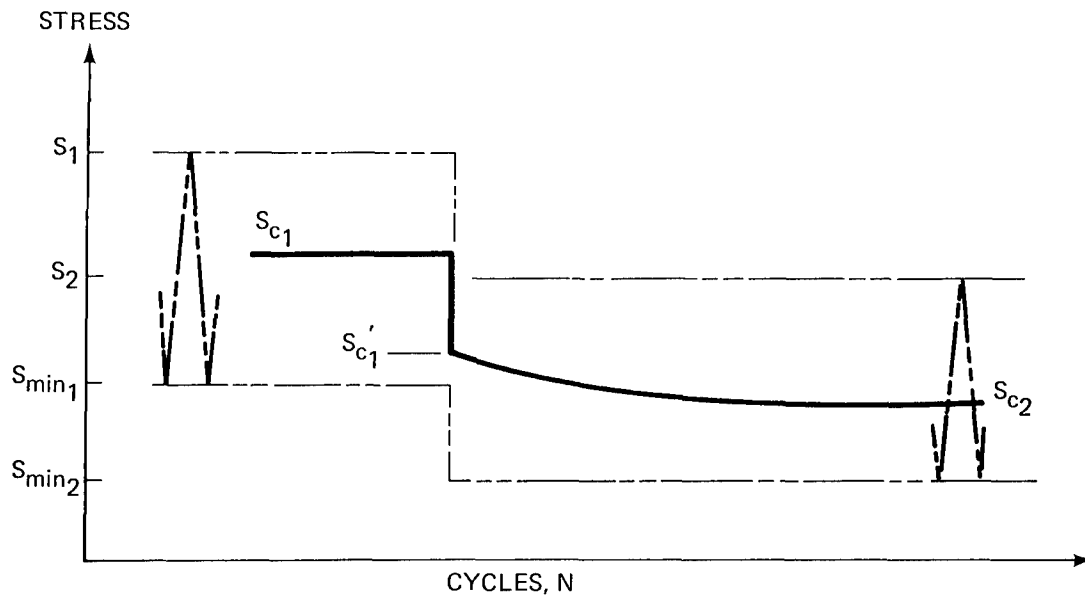


Fig. 114 Schematic of Minimum Stress Adjustment

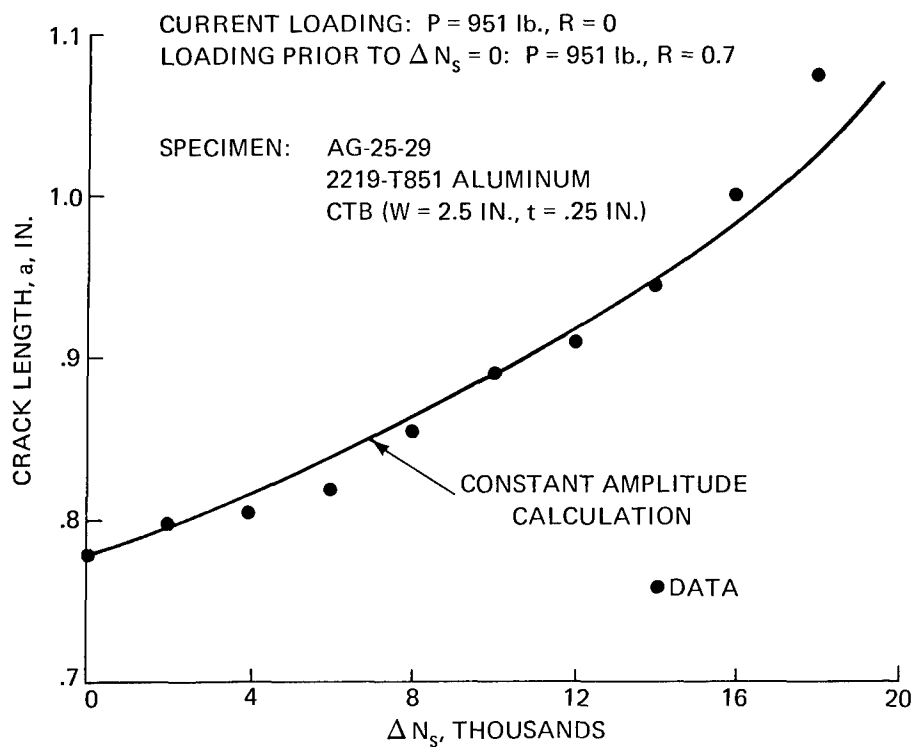


Fig. 115 Comparison of Constant Amplitude Calculation with Data For Minimum Stress Variation

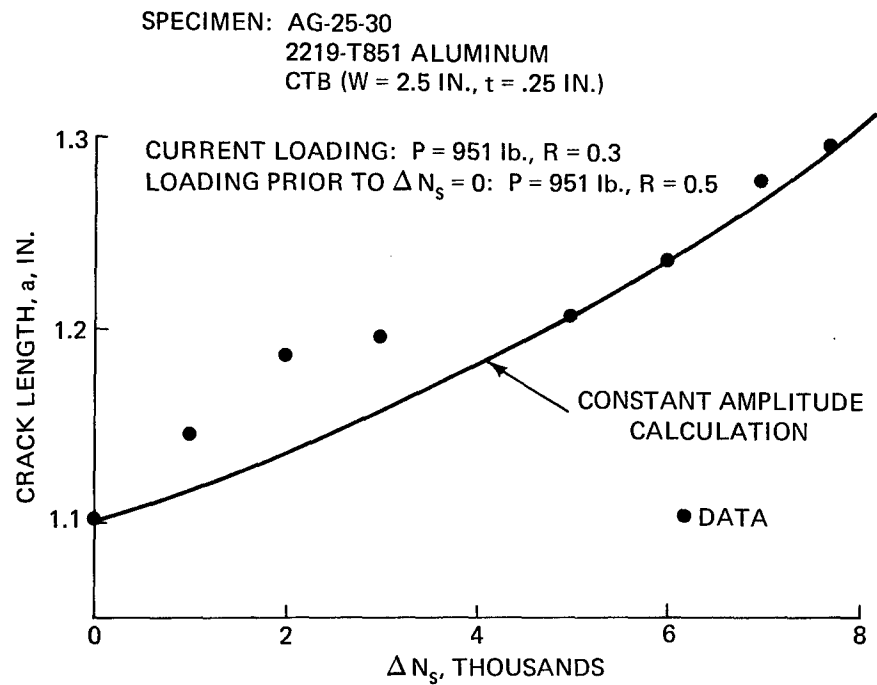


Fig. 116 Comparison of Constant Amplitude Calculation with Data for Minimum Stress Variation

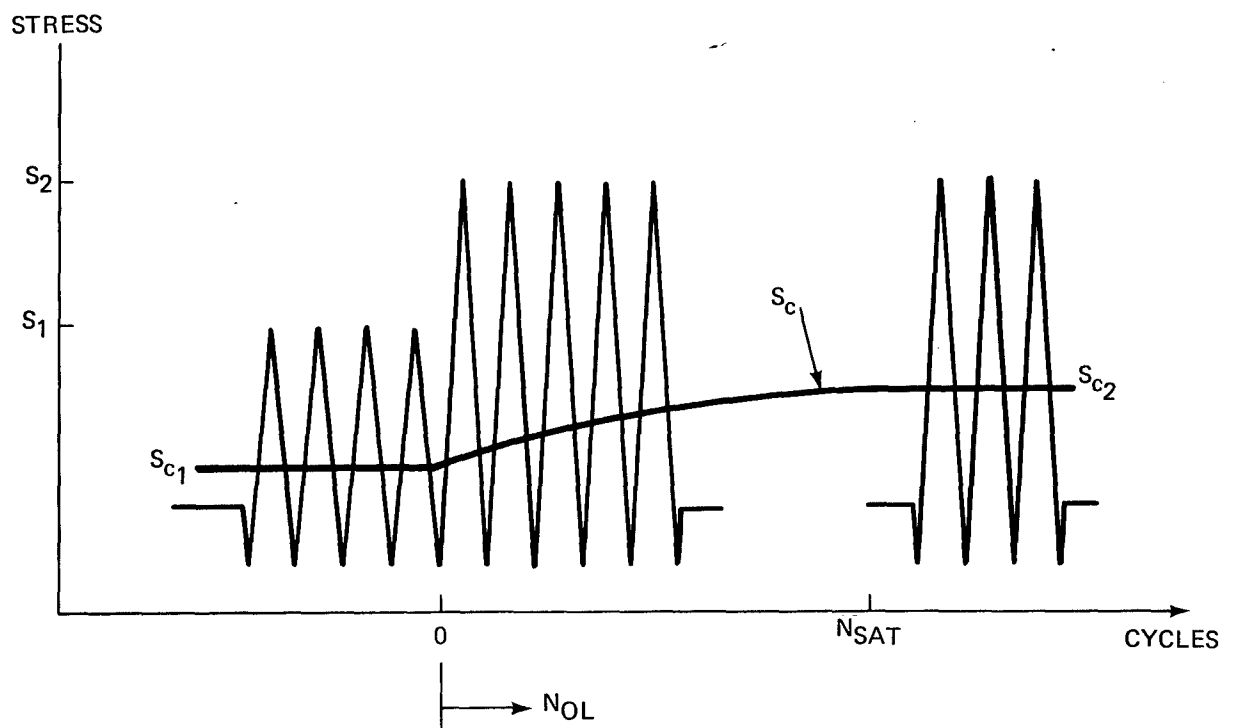


Fig. 117 Schematic of Variation of Closure Stress with Number of Overload Cycles

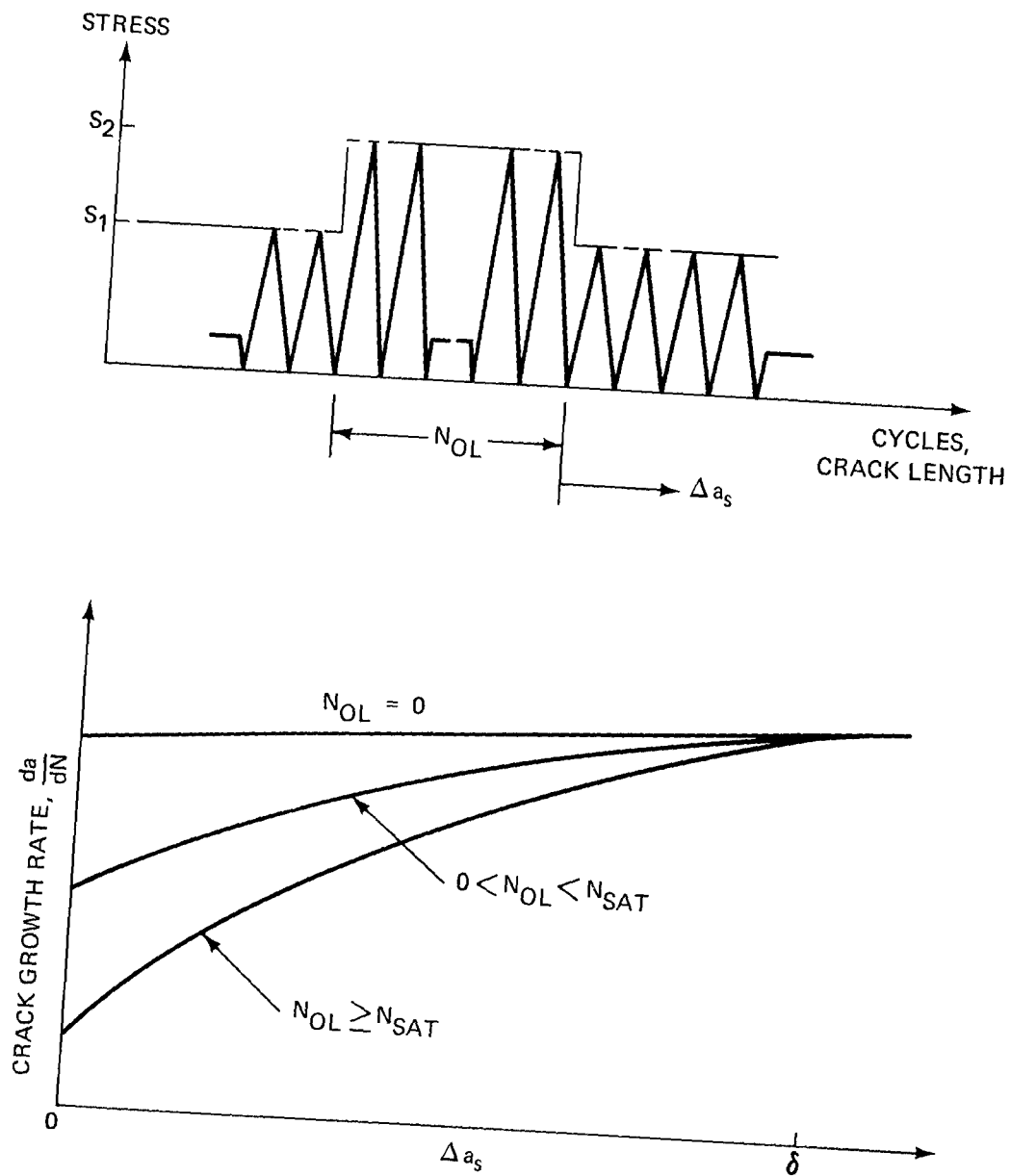


Fig. 118 Schematic of Crack Growth Rate vs Δa_s as a Function of Number of Overloads

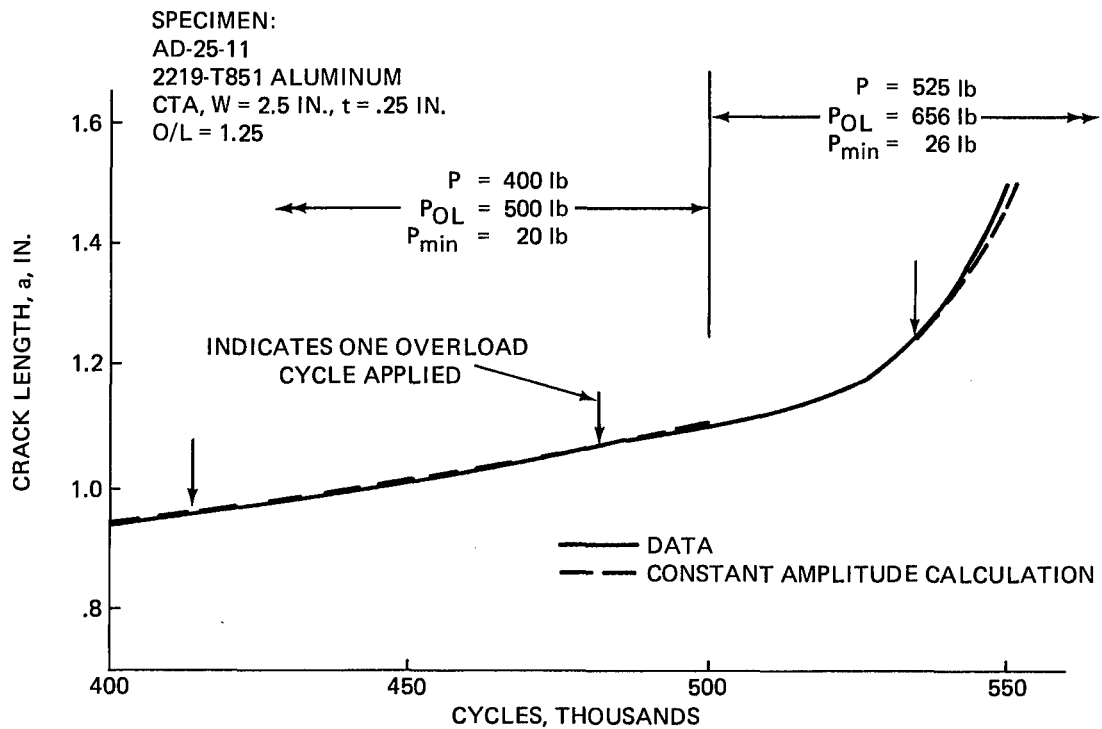


Fig. 119 Comparison of Constant Amplitude Calculation with Data, O/L = 1.25, Aluminum

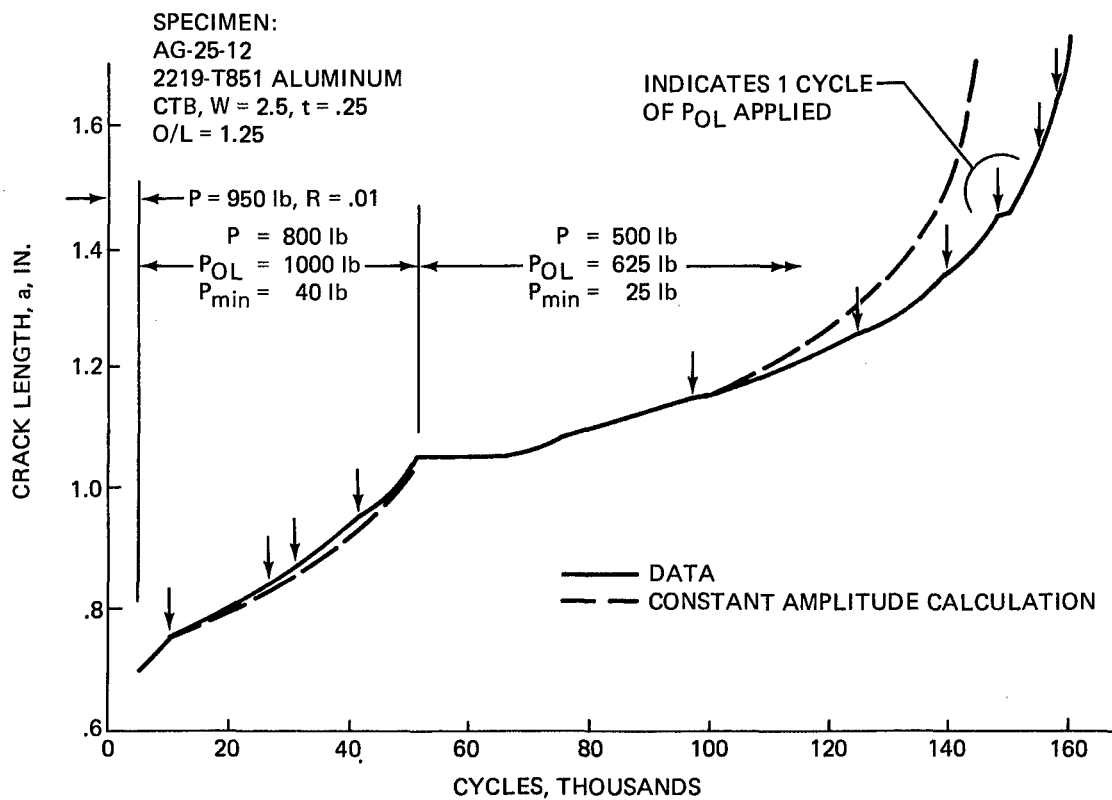


Fig. 120 Comparison of Constant Amplitude Calculation with Data, O/L = 1.25, Aluminum

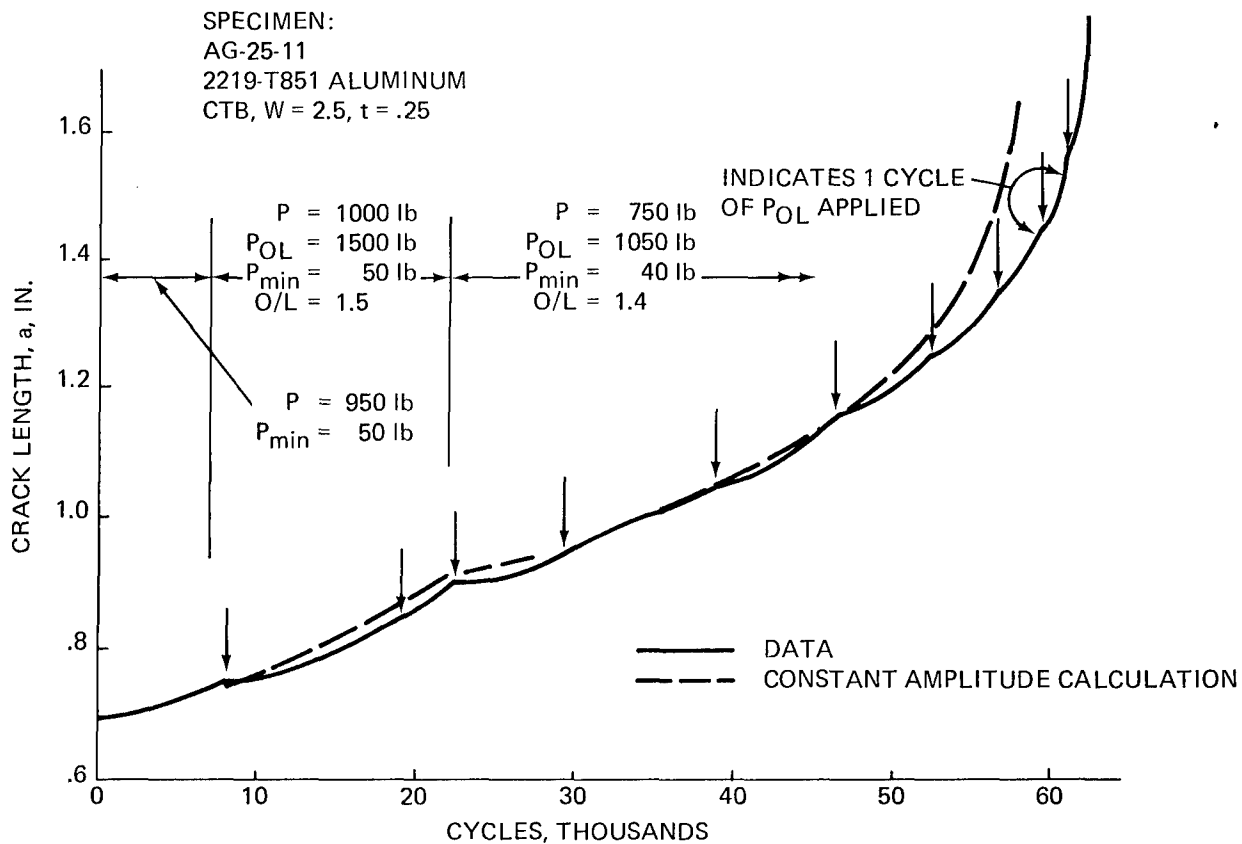


Fig. 121 Comparison of Constant Amplitude Calculation with Data, $O/L = 1.4, 1.5$, Aluminum

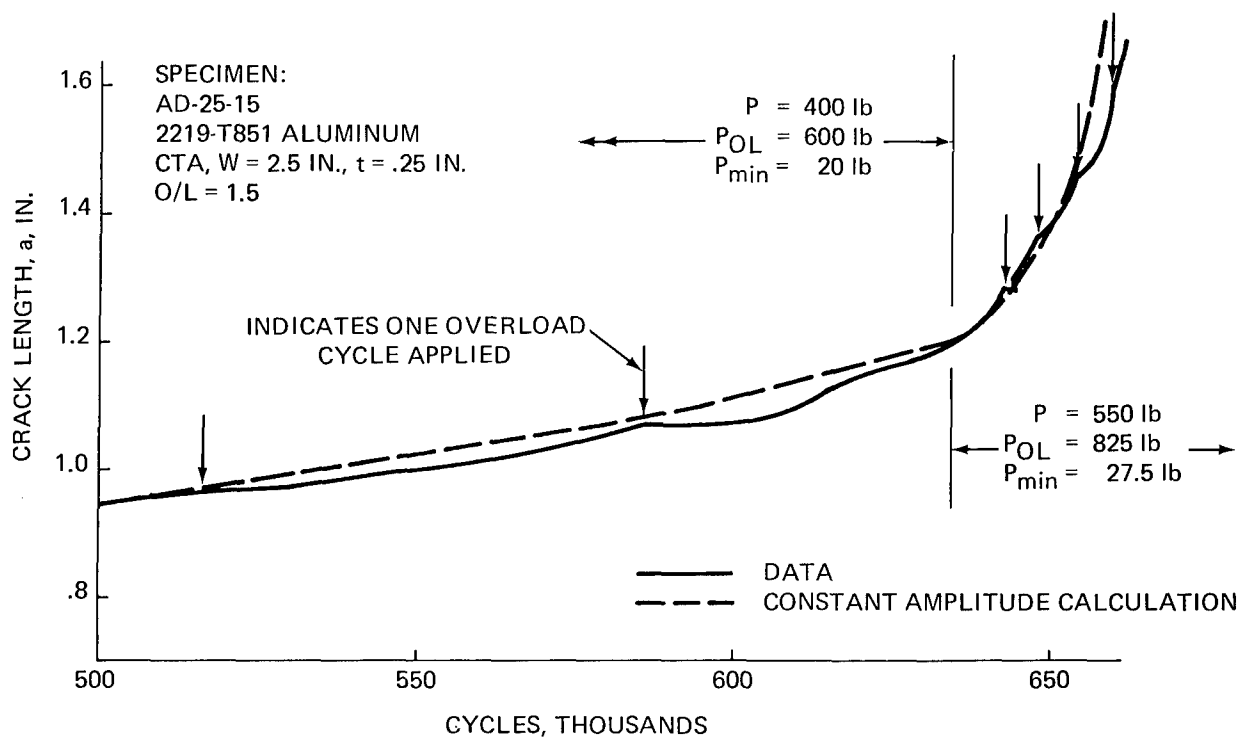


Fig. 122 Comparison of Constant Amplitude Calculation with Data, $O/L = 1.5$, Aluminum

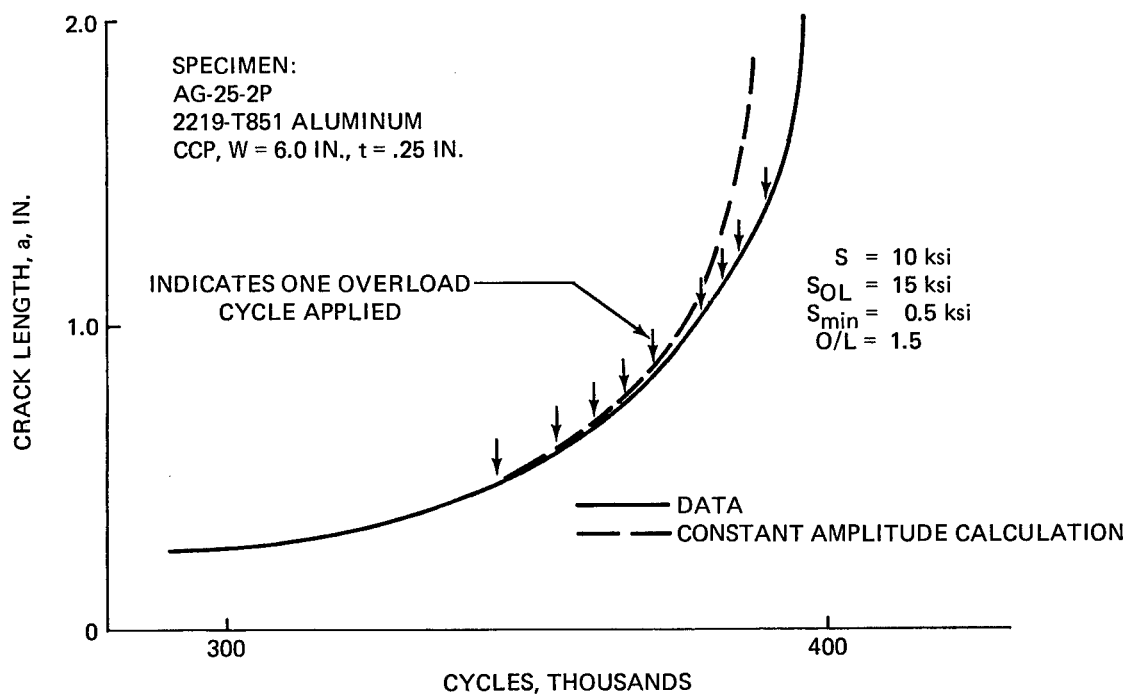


Fig. 123 Comparison of Constant Amplitude Calculation with Data, O/L = 1.5, Aluminum

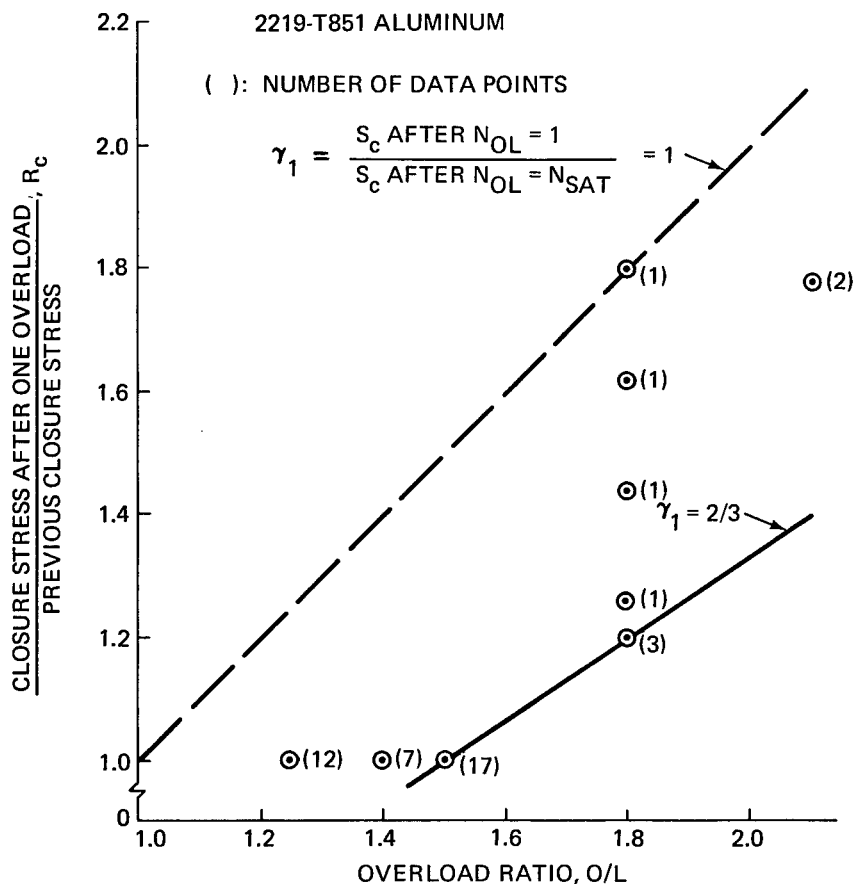


Fig. 124 Calculated Closure Stress After One Overload over Previous Closure Stress vs Overload Ratio

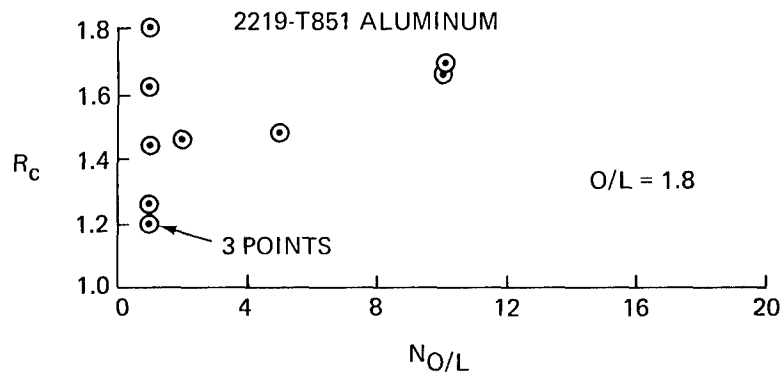


Fig. 125 R_c vs N_{OL} for $O/L = 1.8$ 2219-T851 Aluminum

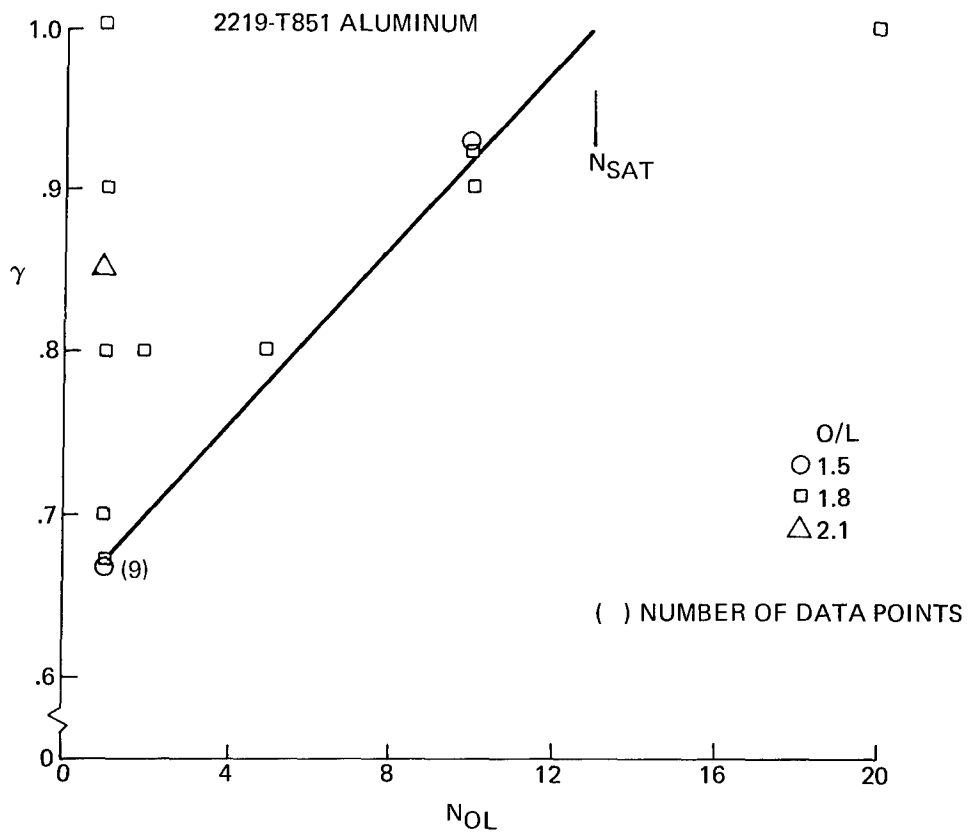


Fig. 126 Factor γ vs N_{OL} for 2219-T851 Aluminum

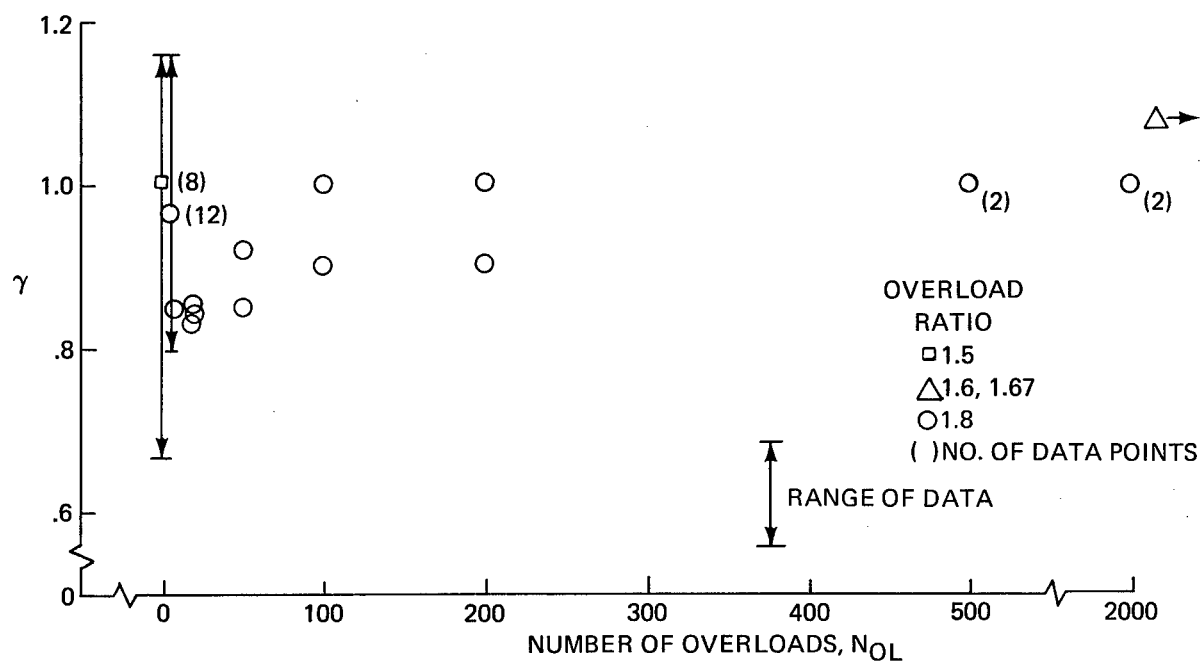


Fig. 127 Factor γ vs N_{OL} for Ti 6Al-4V Titanium

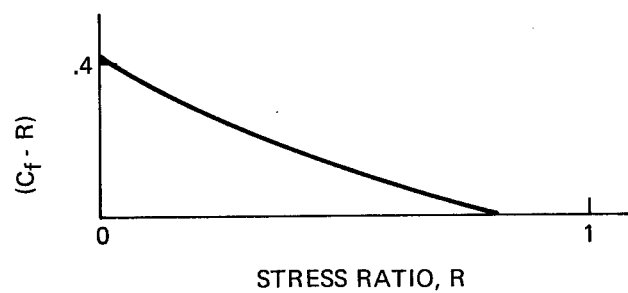


Fig. 128 Crack Tip Crushing vs. Stress Ratio, R

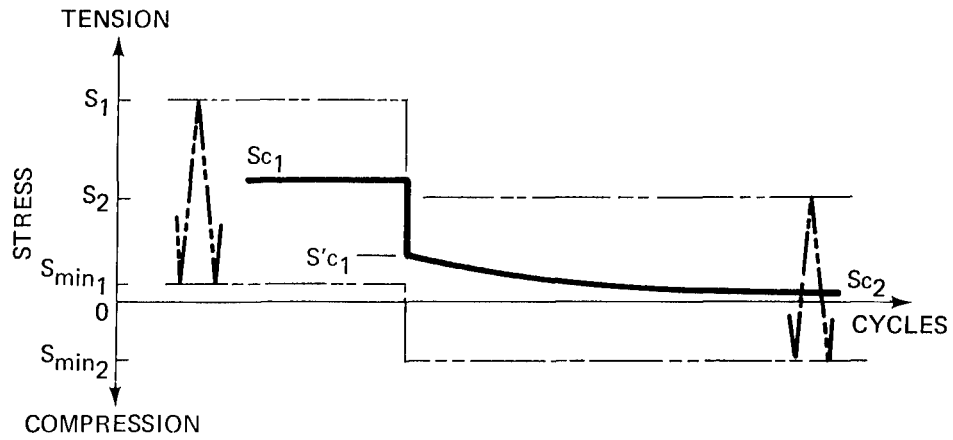


Fig. 129 Schematic of Closure Adjustment for Compression Stresses

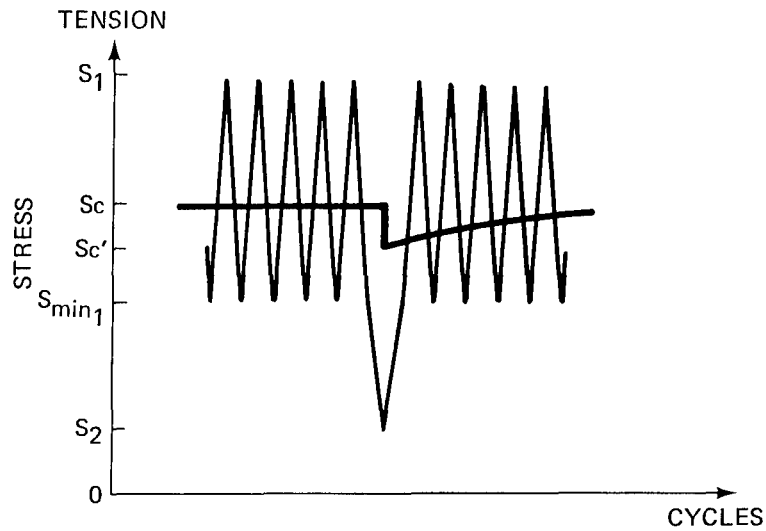


Fig. 130 Schematic of Closure Adjustment for Underload Spike

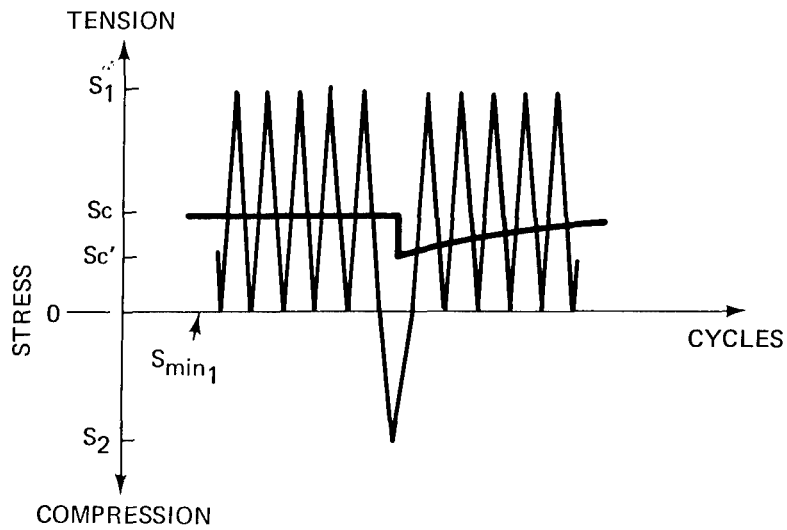


Fig. 131 Schematic of Closure Adjustment for Compression Spike

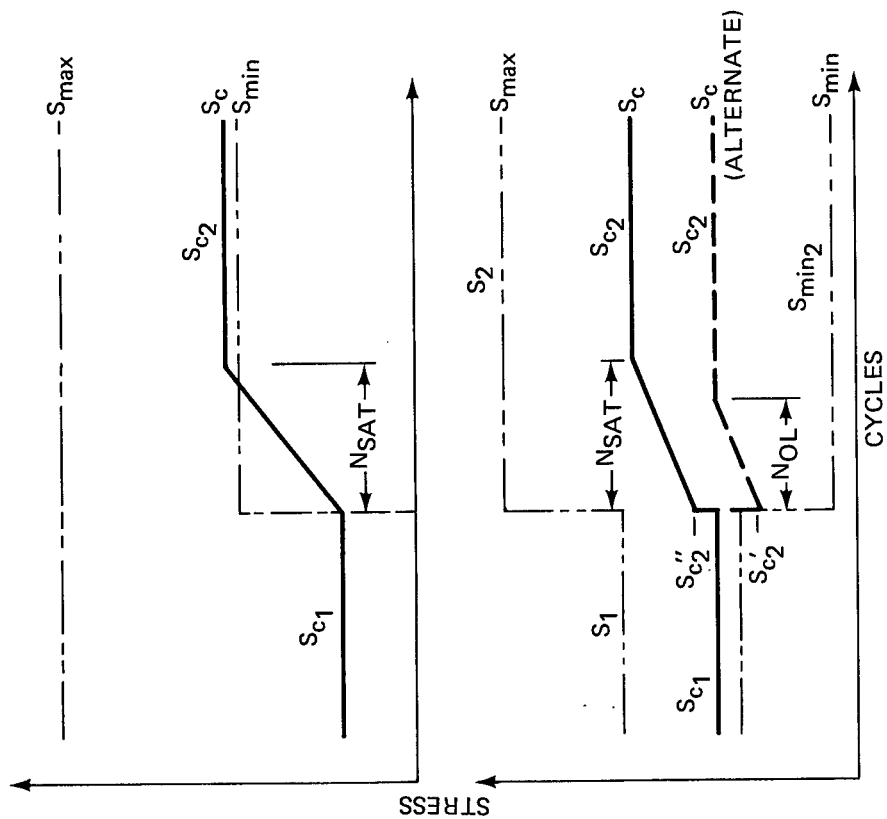


Fig. 132 Treatment of Closure Behavior
for Low-High Loading Sequence

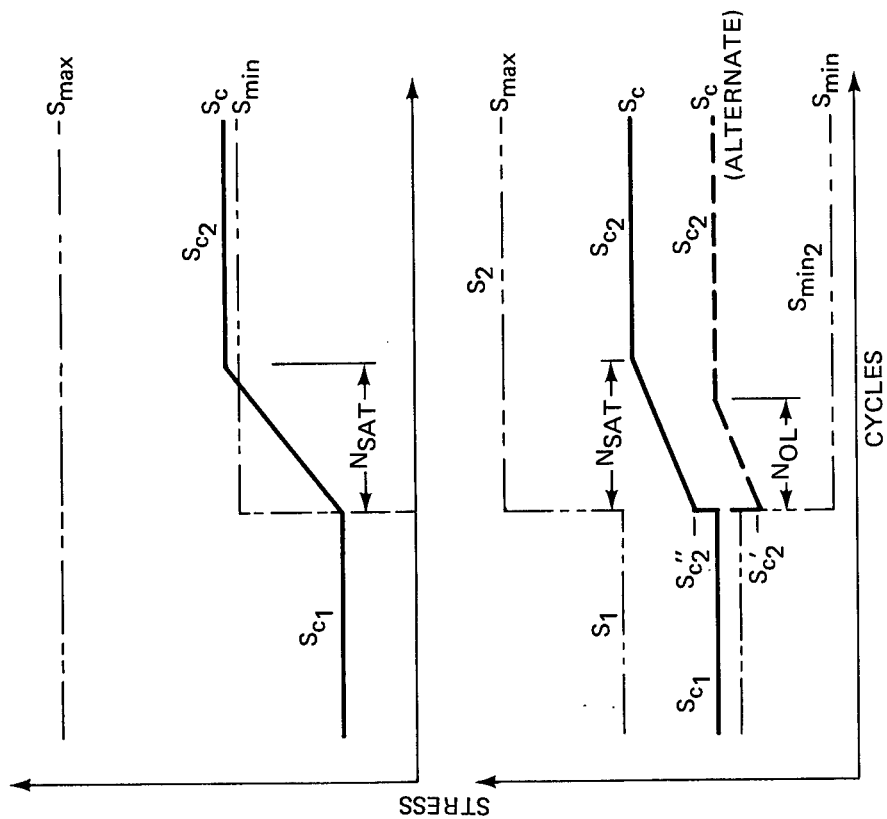


Fig. 133 Treatment of Closure Behavior for Variations
of Low-High Loading Sequence

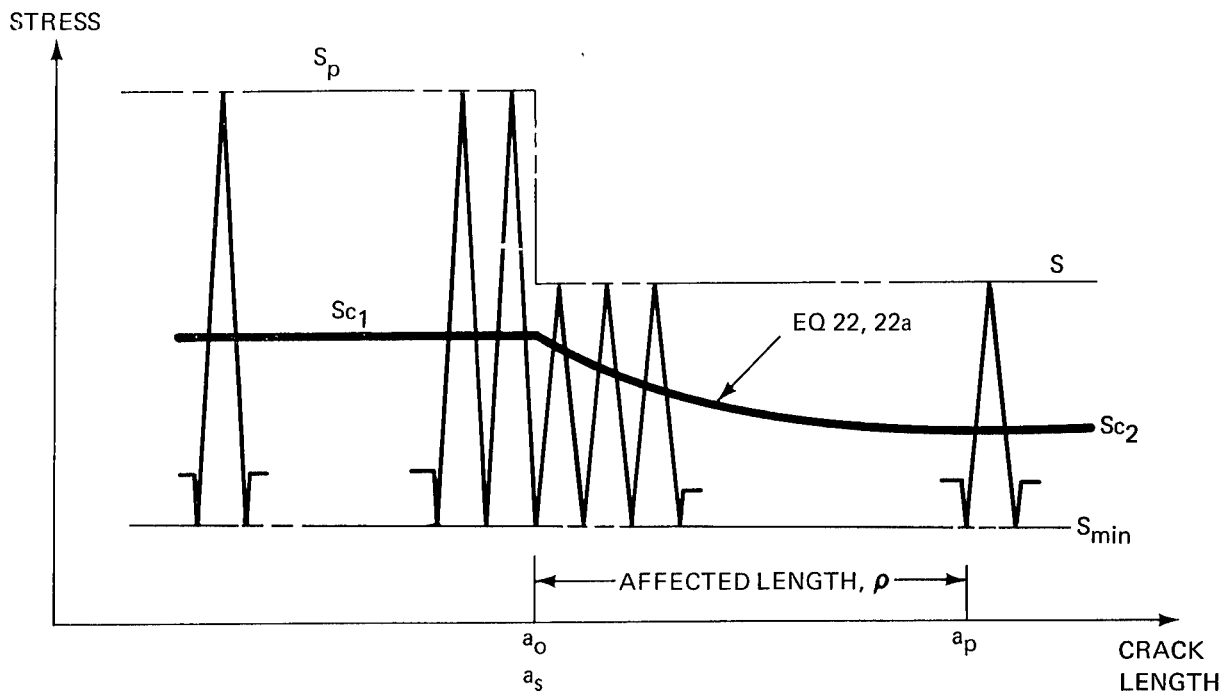


Fig. 134 Schematic of Closure Behavior for High-Low Loading Sequence — Definition of Terms

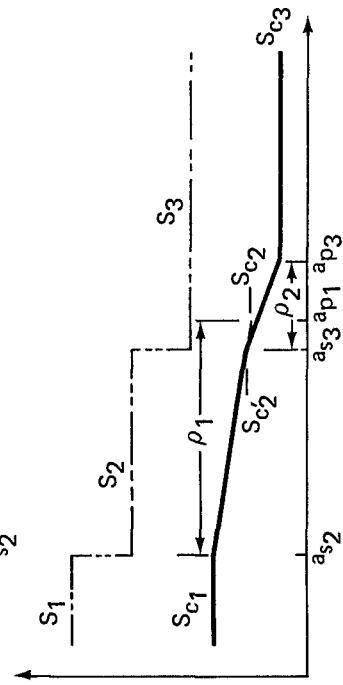
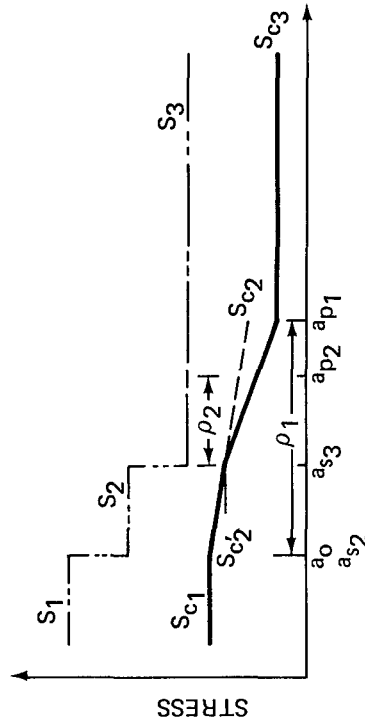
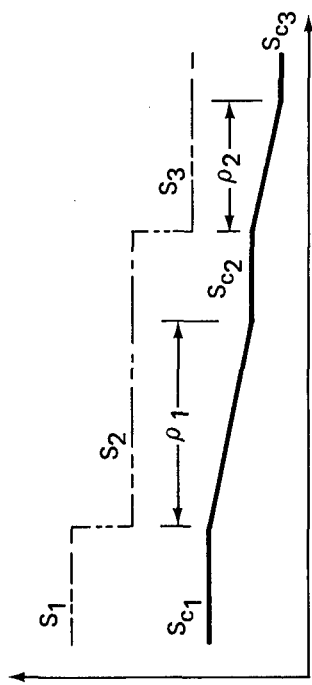


Fig. 135 Treatment of Closure Behavior during Descending Load Sequences

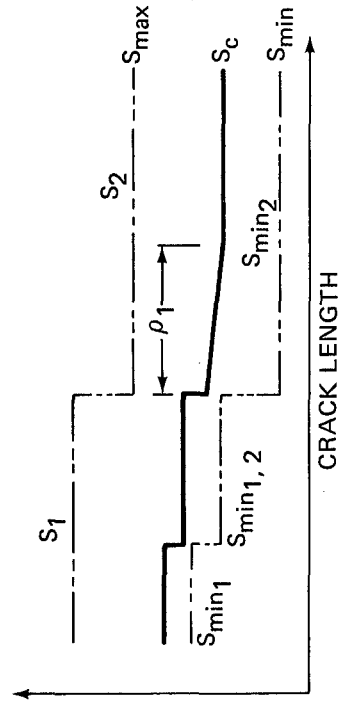
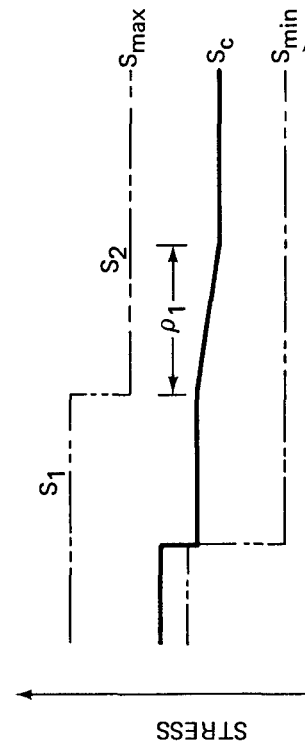
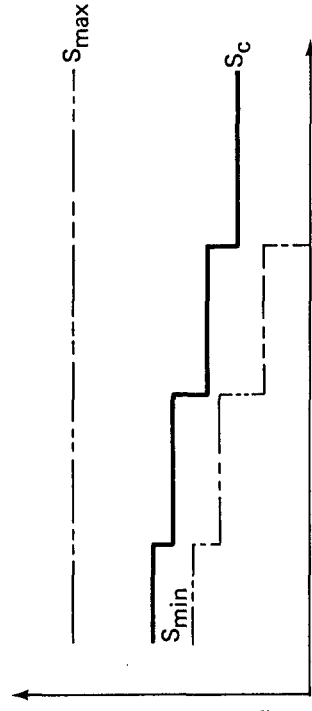


Fig. 136 Treatment of Closure Behavior during Descending Load Sequences with Minimum Stress Changes

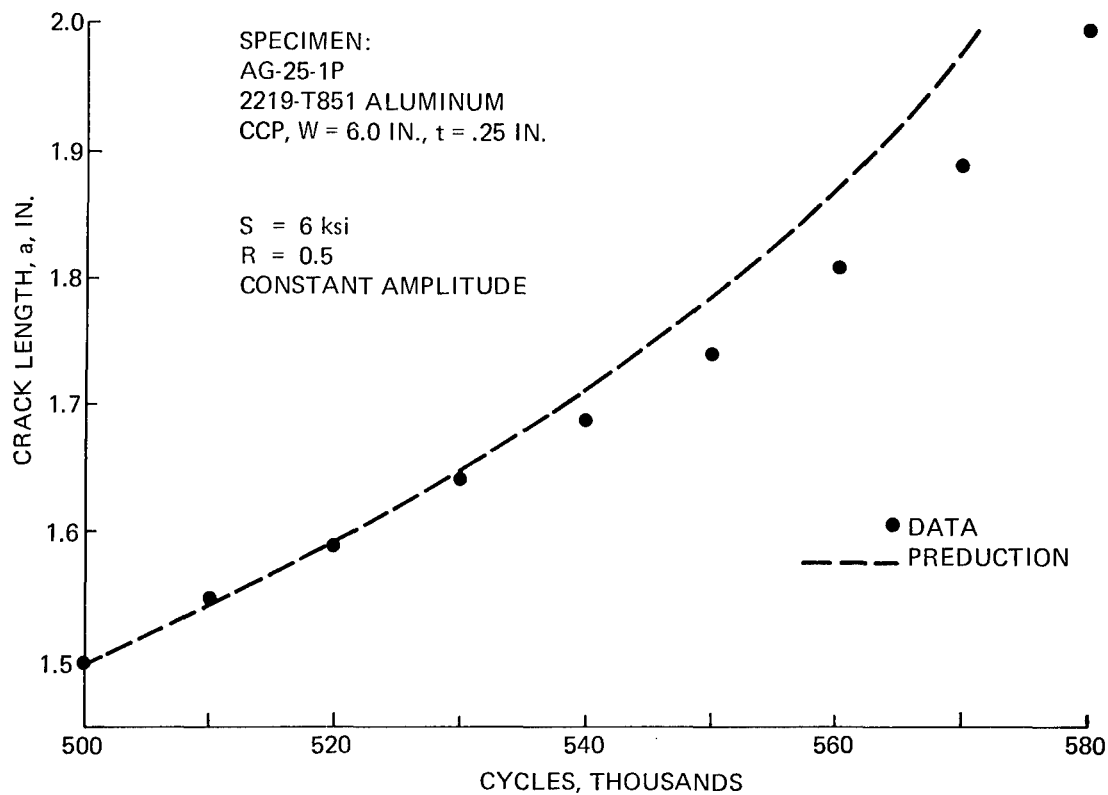


Fig. 137 Predicted a vs. N for $R = 0.5$, 2219-T851 Aluminum

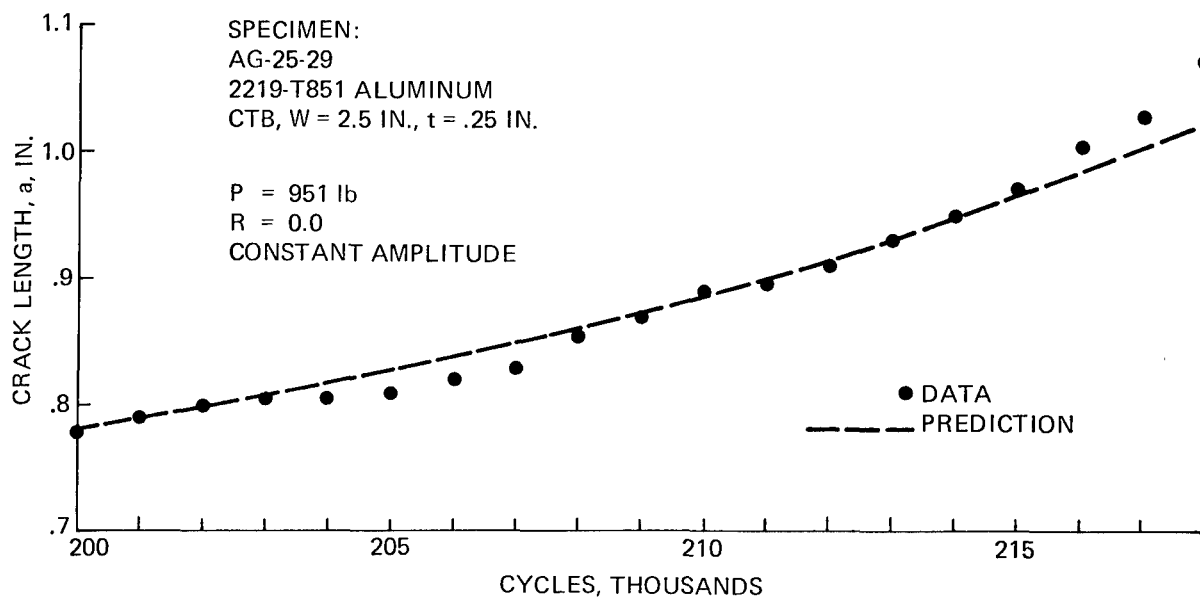


Fig. 138 Predicted a vs. N for $R = 0.$, 2219-T851 Aluminum

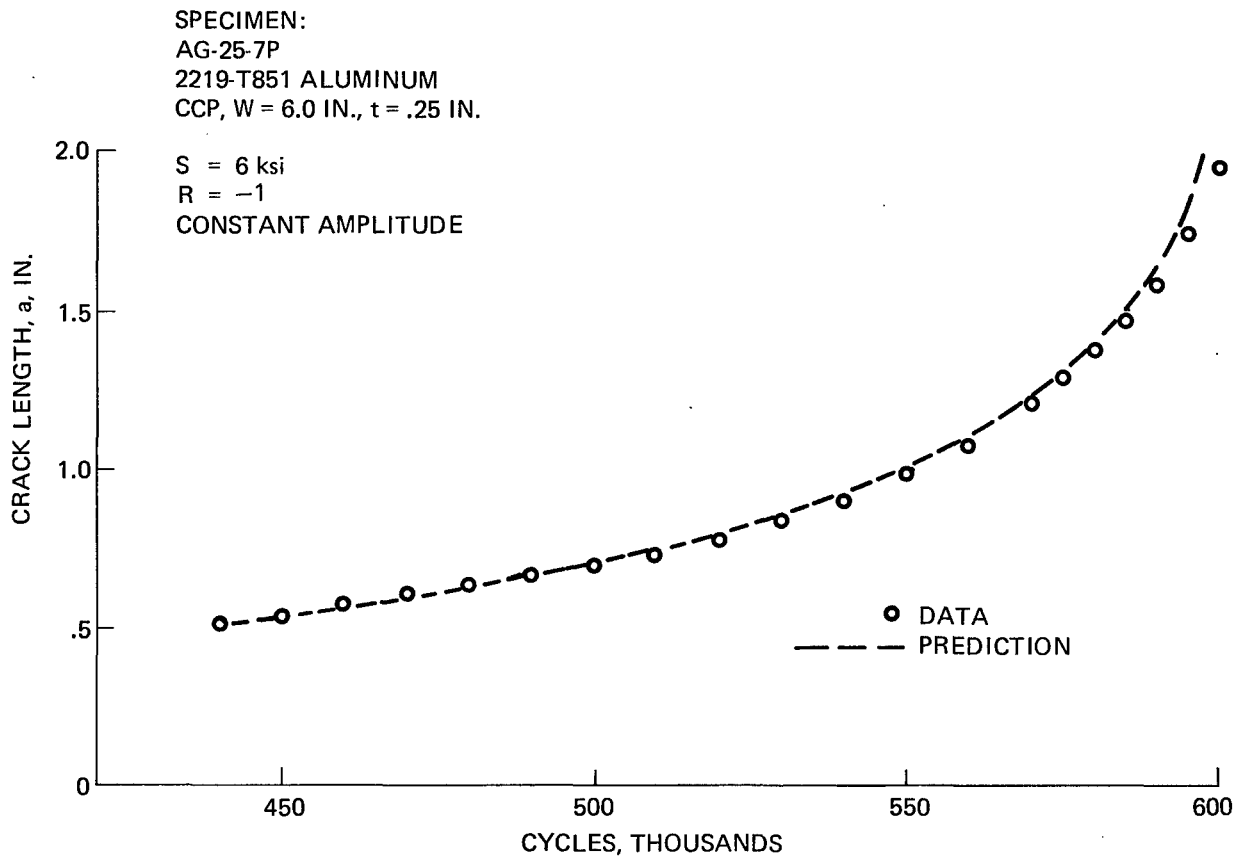


Fig. 139 Predicted a vs. N for $R = -1$, 2219-T851 Aluminum

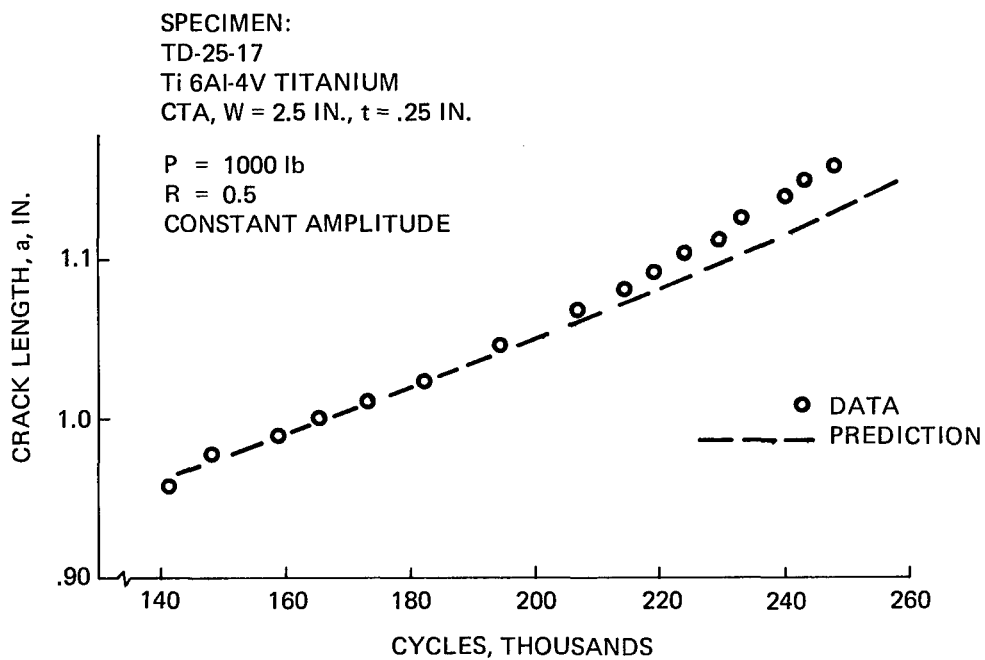


Fig. 140 Predicted a vs. N for $R = 0.5$, Ti 6Al-4V Titanium

SPECIMEN:
 TG-25-06
 Ti 6Al-4V TITANIUM
 CTA, $W = 2.5$ IN., $t = .25$

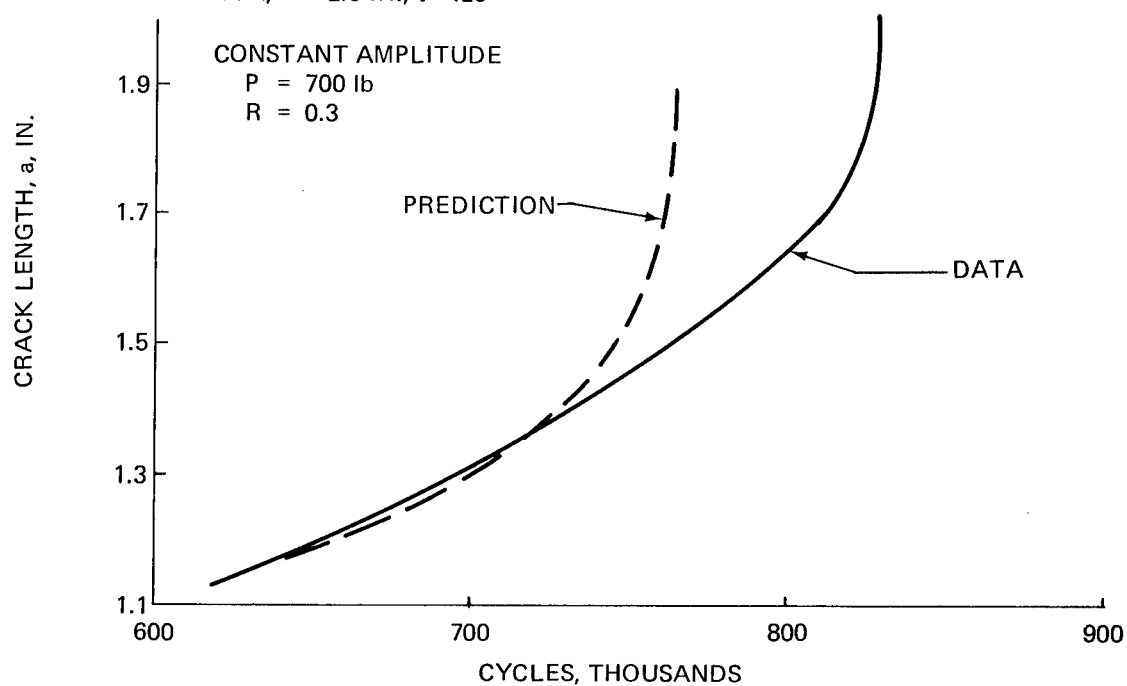


Fig. 141 Predicted a vs. N for $R = 0.3$, Ti 6Al-4V Titanium

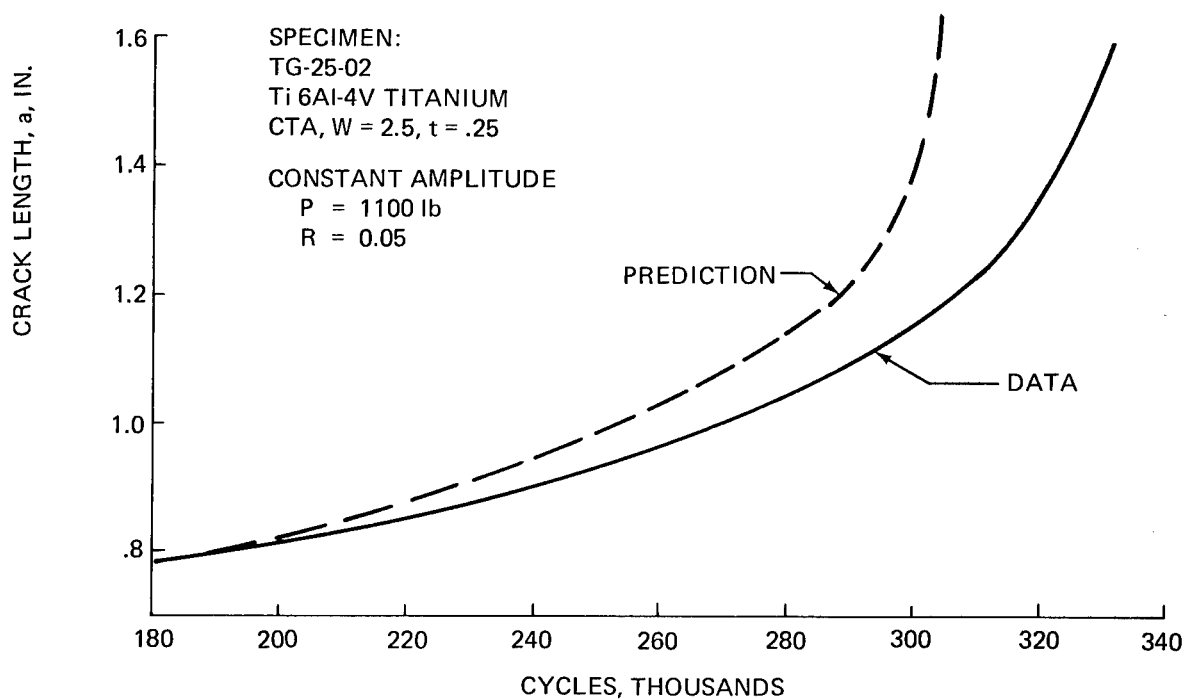


Fig. 142 Predicted a vs. N for $R = 0.05$, Ti 6Al-4V Titanium

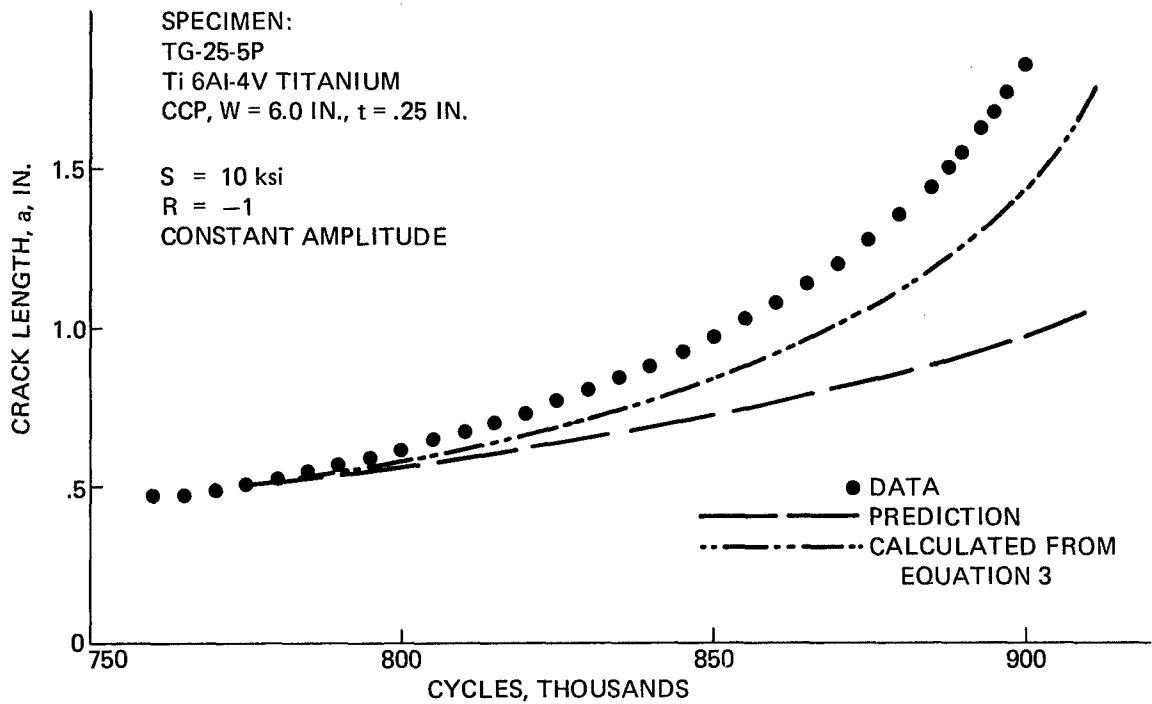


Fig. 143 Predicted a vs. N for $R = -1$, Ti 6Al-4V Titanium

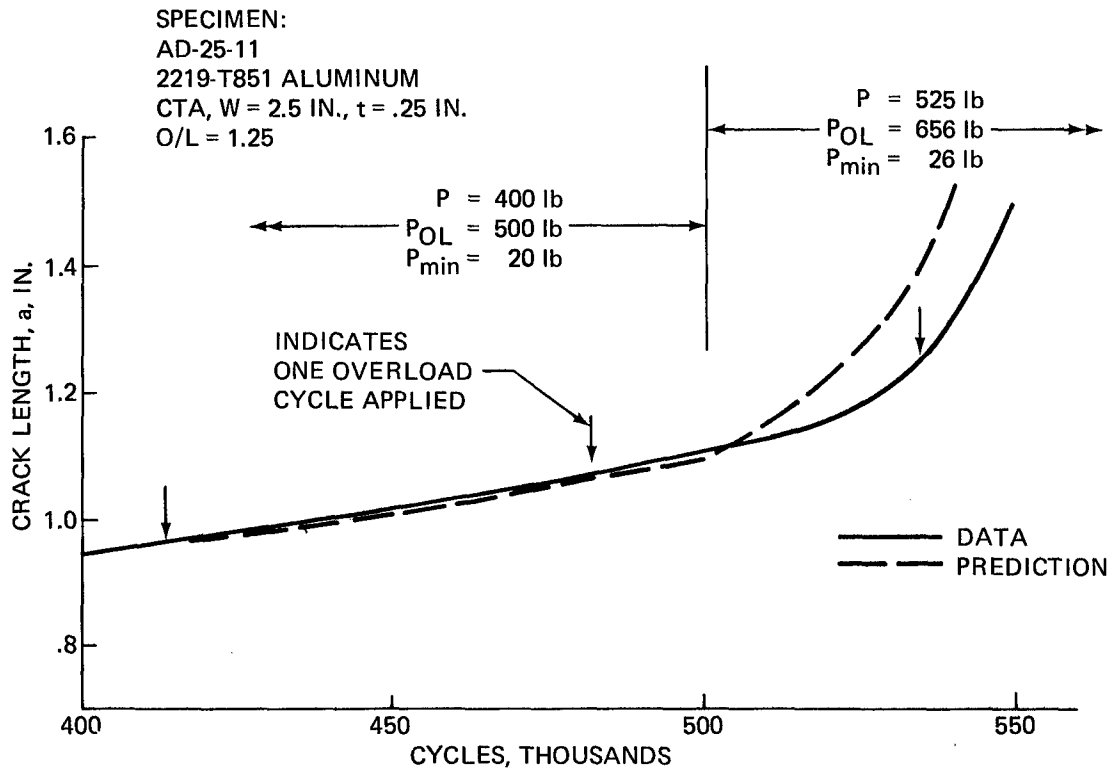


Fig. 144 Predicted a vs. N for O/L = 1.25, 2219-T851 Aluminum, Single Overload

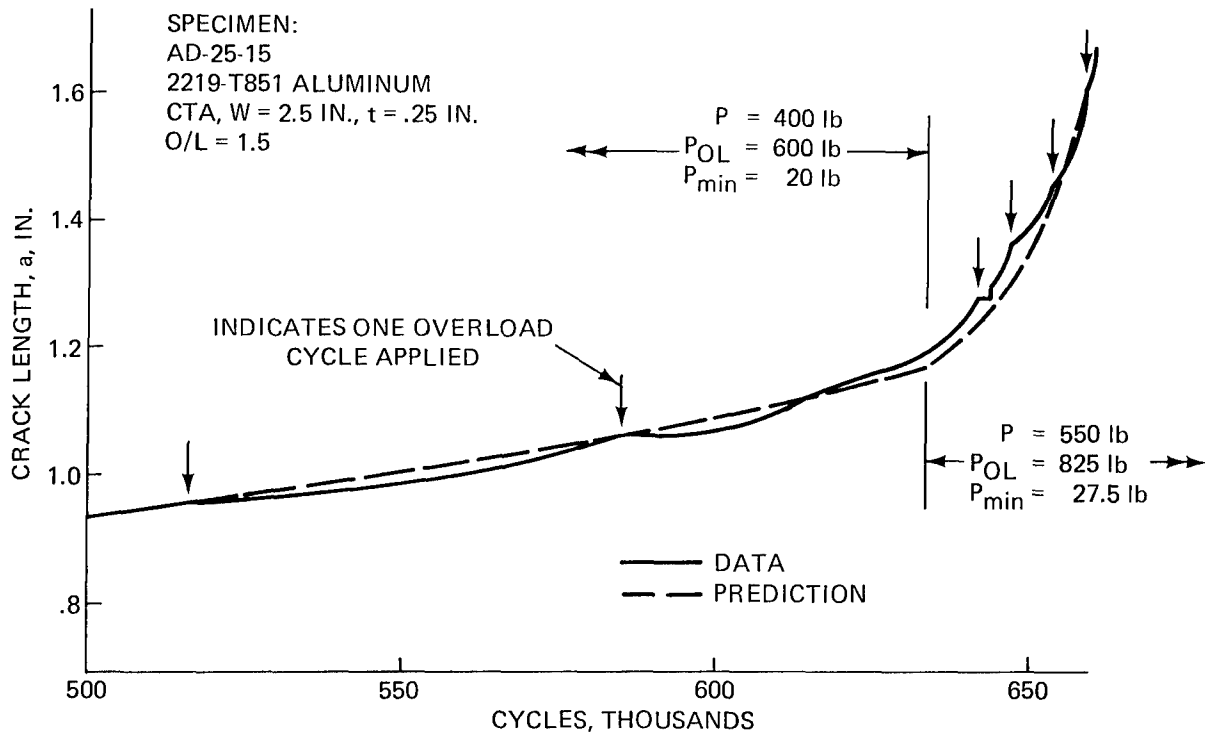


Fig. 145 Predicted a vs. N for O/L = 1.5, Single Overload, 2219-T851 Aluminum

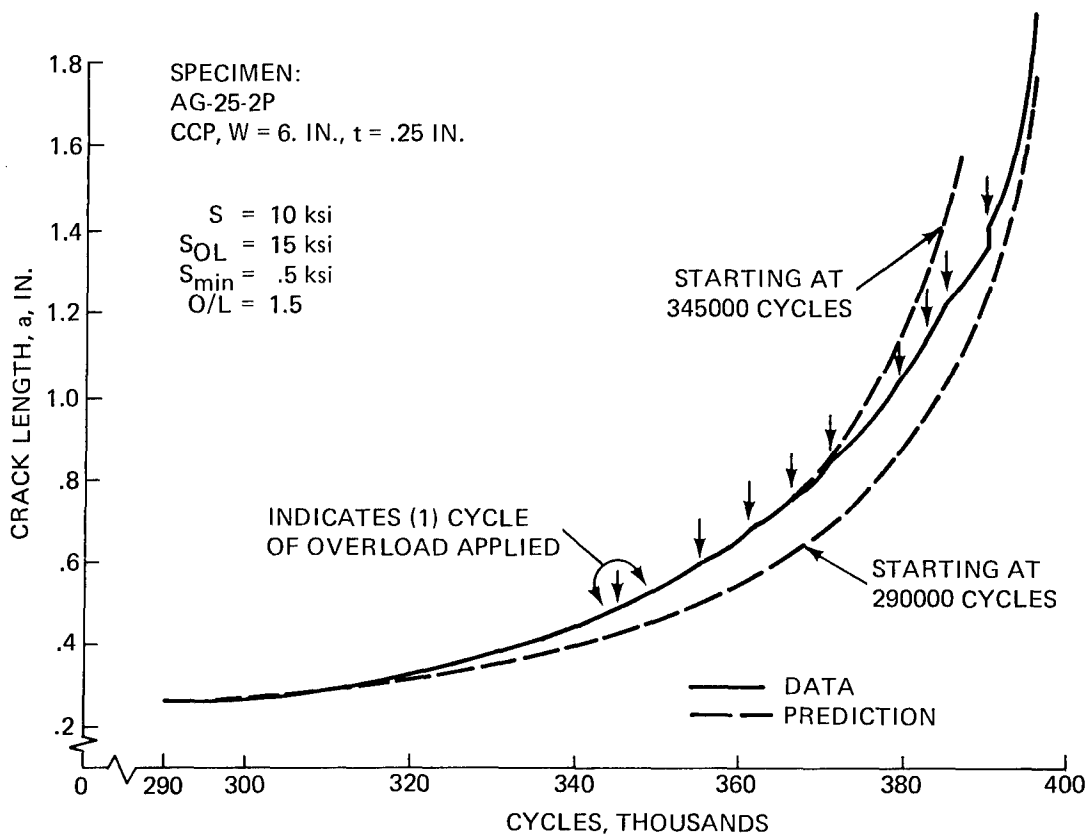


Fig. 146 Predicted a vs. N for O/L = 1.5, Single Overloads, 2219-T851 Aluminum Panel

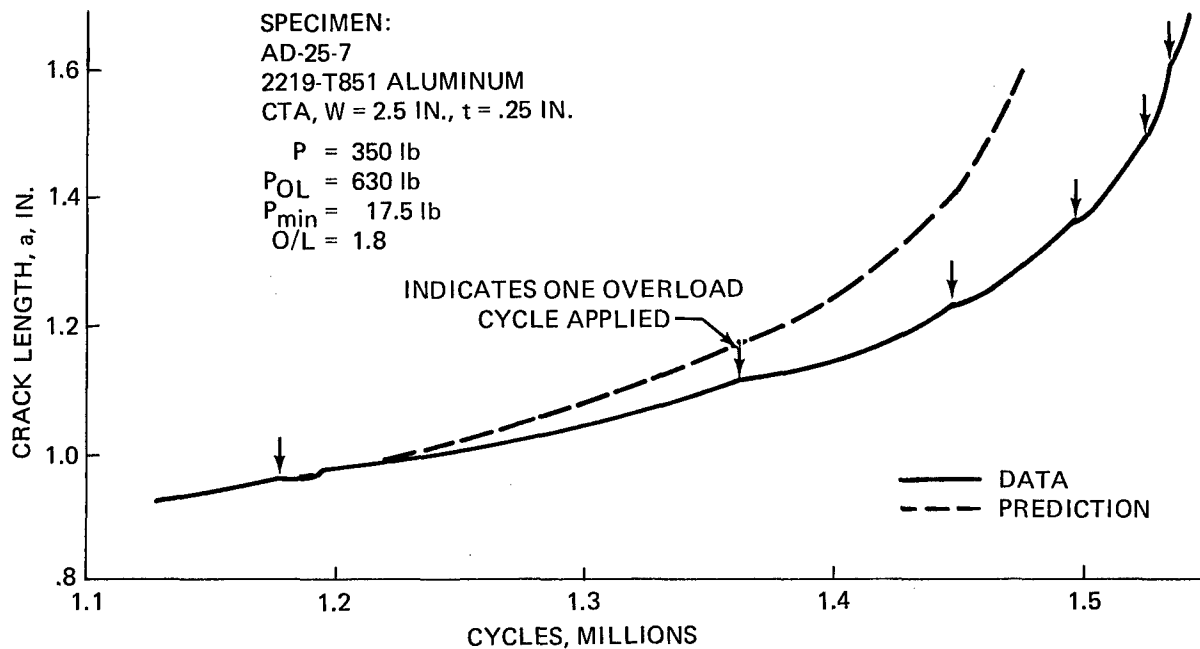


Fig. 147 Predicted a vs. N for O/L = 1.8, Single Overloads, 2219-T851 Aluminum

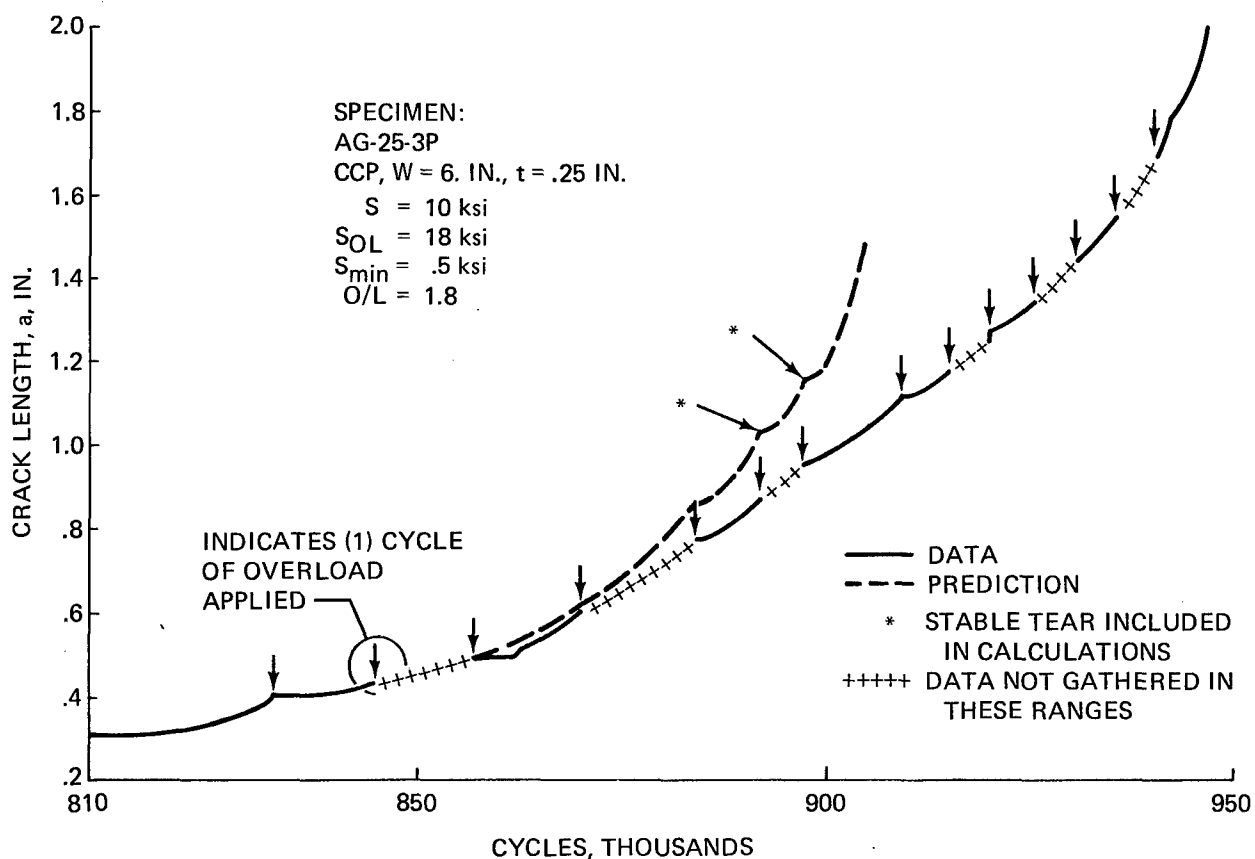


Fig. 148 Predicted a vs. N for O/L = 1.8, Single Overloads, 2219-T851 Aluminum Panel

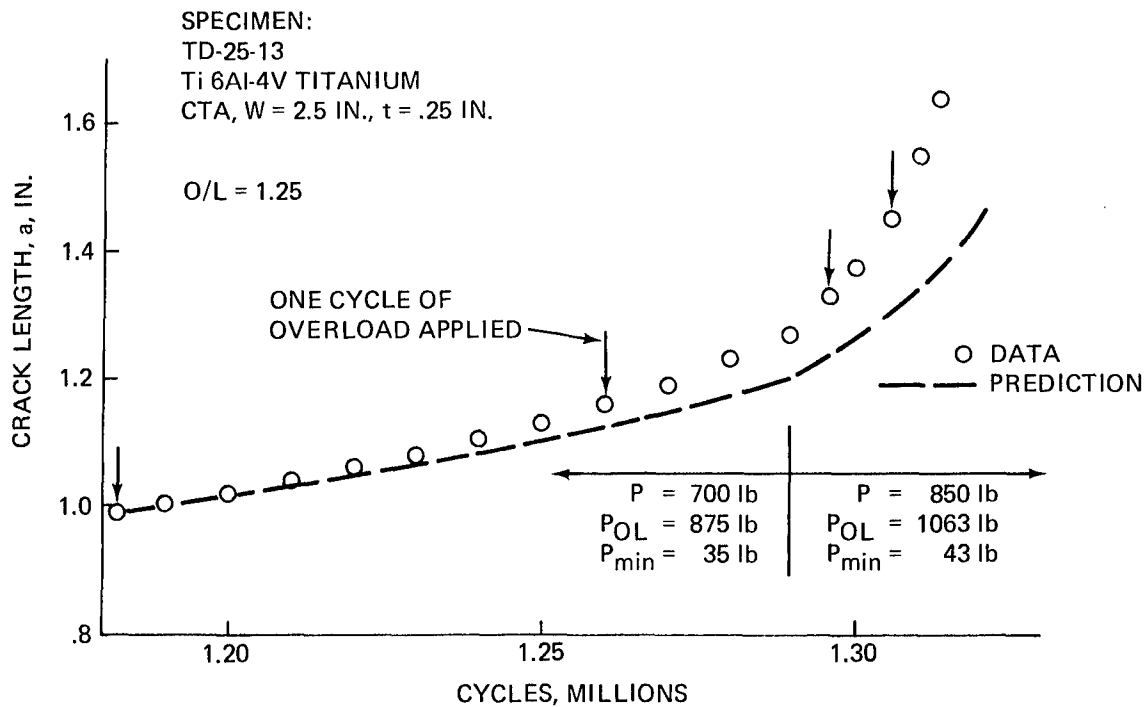


Fig. 149 Predicted a vs. N for O/L = 1.25, Single Overloads, Ti 6Al-4V Titanium

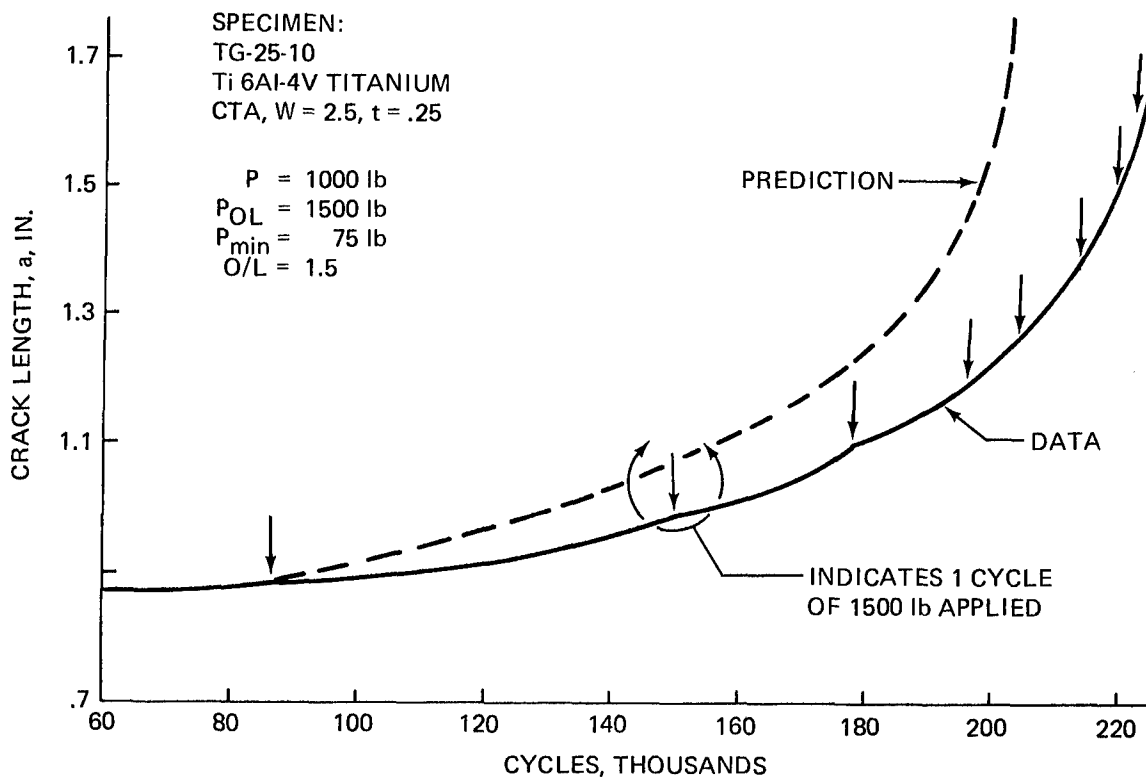


Fig. 150 Predicted a vs. N for O/L = 1.5, Single Overloads, Ti 6Al-4V Titanium

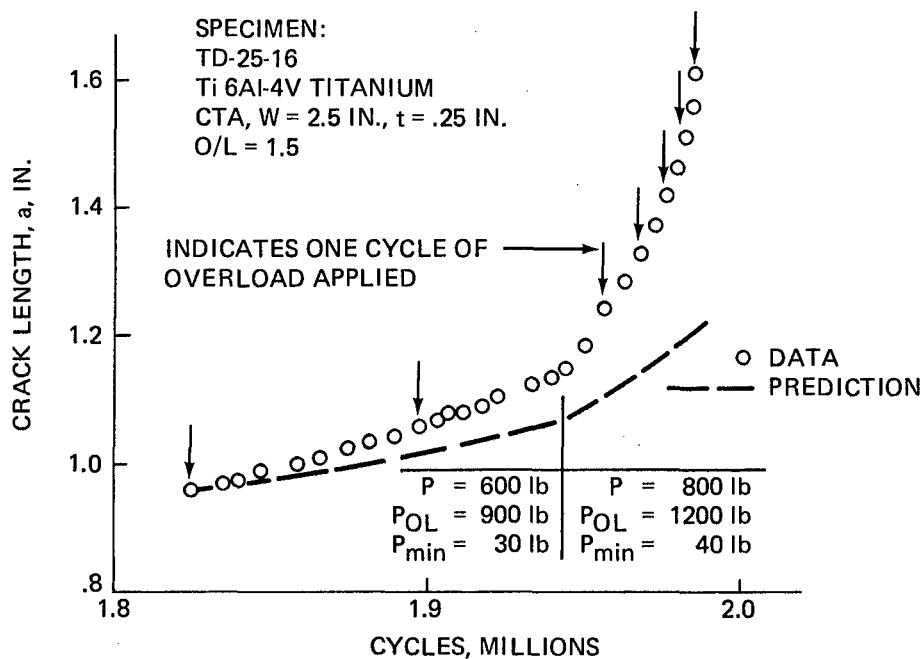


Fig. 151 Predicted a vs. N for $O/L = 1.5$, Single Overloads, Ti 6Al-4V Titanium

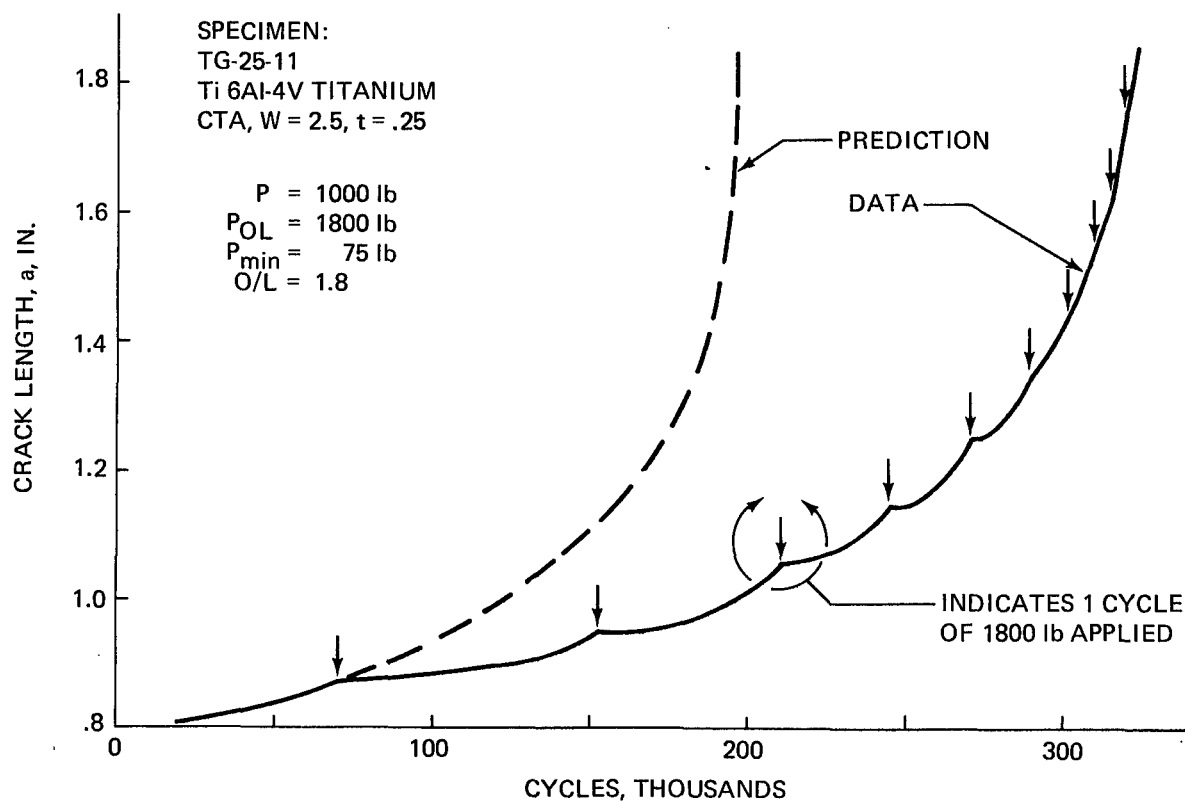


Fig. 152 Predicted a vs. N for $O/L = 1.8$, Single Overloads, Ti 6Al-4V Titanium

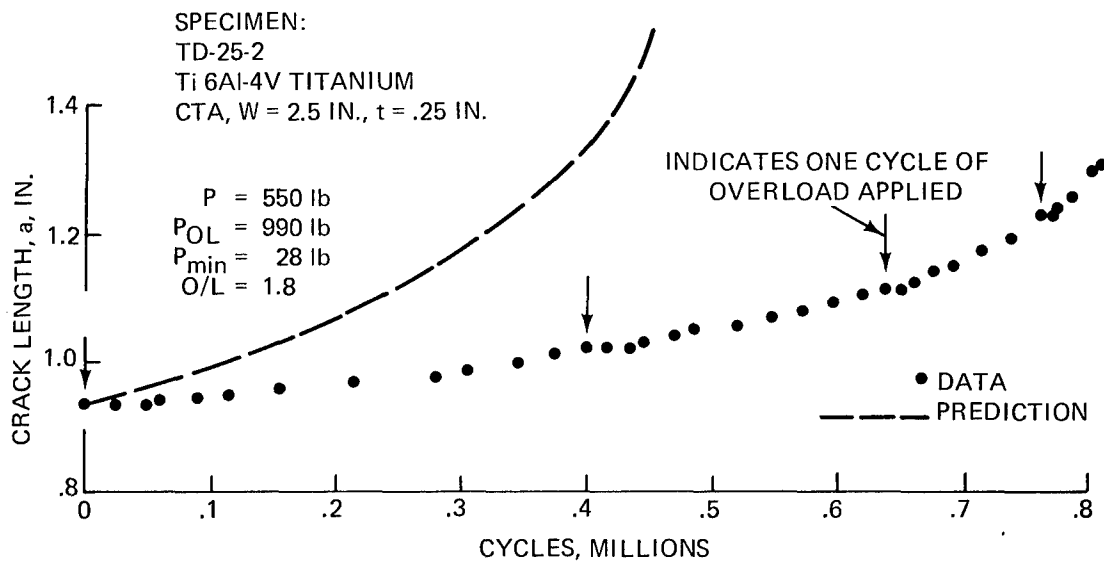


Fig. 153 Predicted a vs. N for O/L = 1.8, Single Overloads, Ti 6Al-4V Titanium

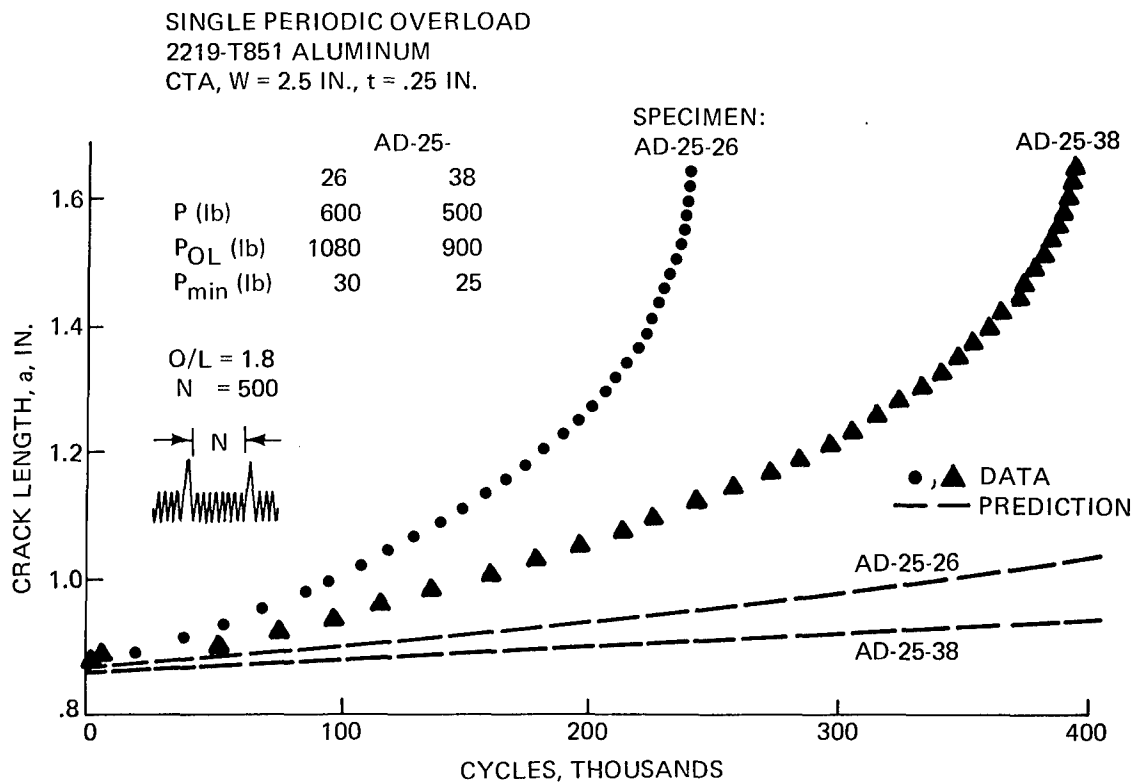


Fig. 154 Predicted a vs. N for O/L = 1.8, N = 500, Single Periodic Overloads, 2219-T851 Aluminum

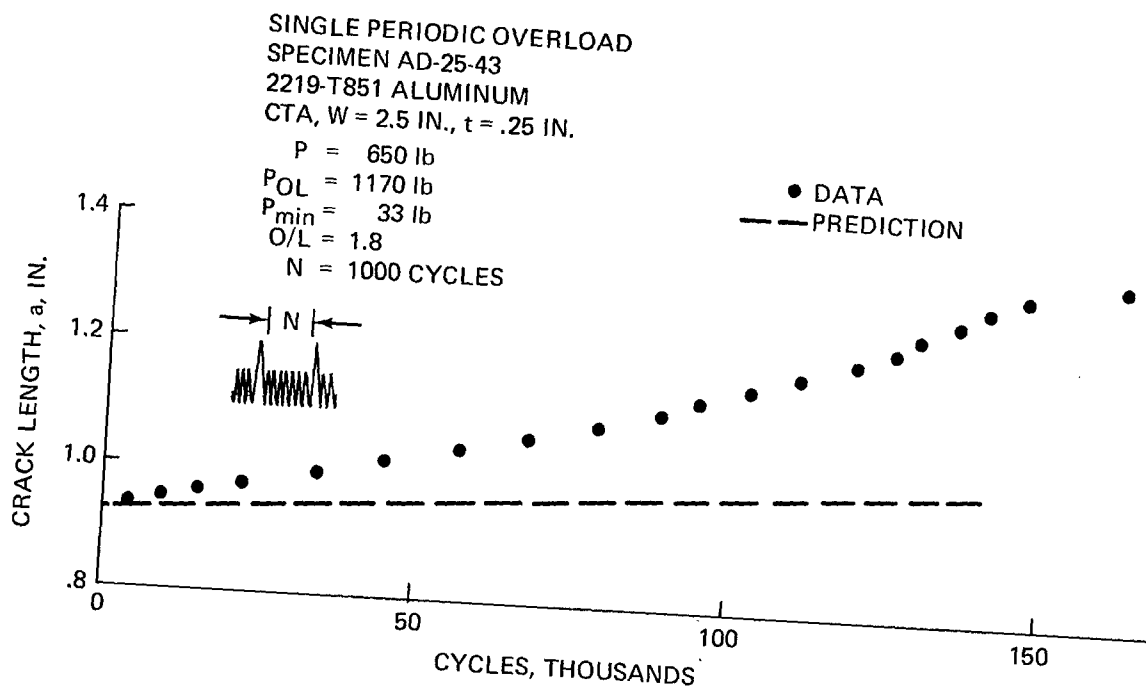


Fig. 155 Predicted a vs. N for $O/L = 1.8$, $N = 1000$, Single Periodic Overloads, 2219-T851 Aluminum

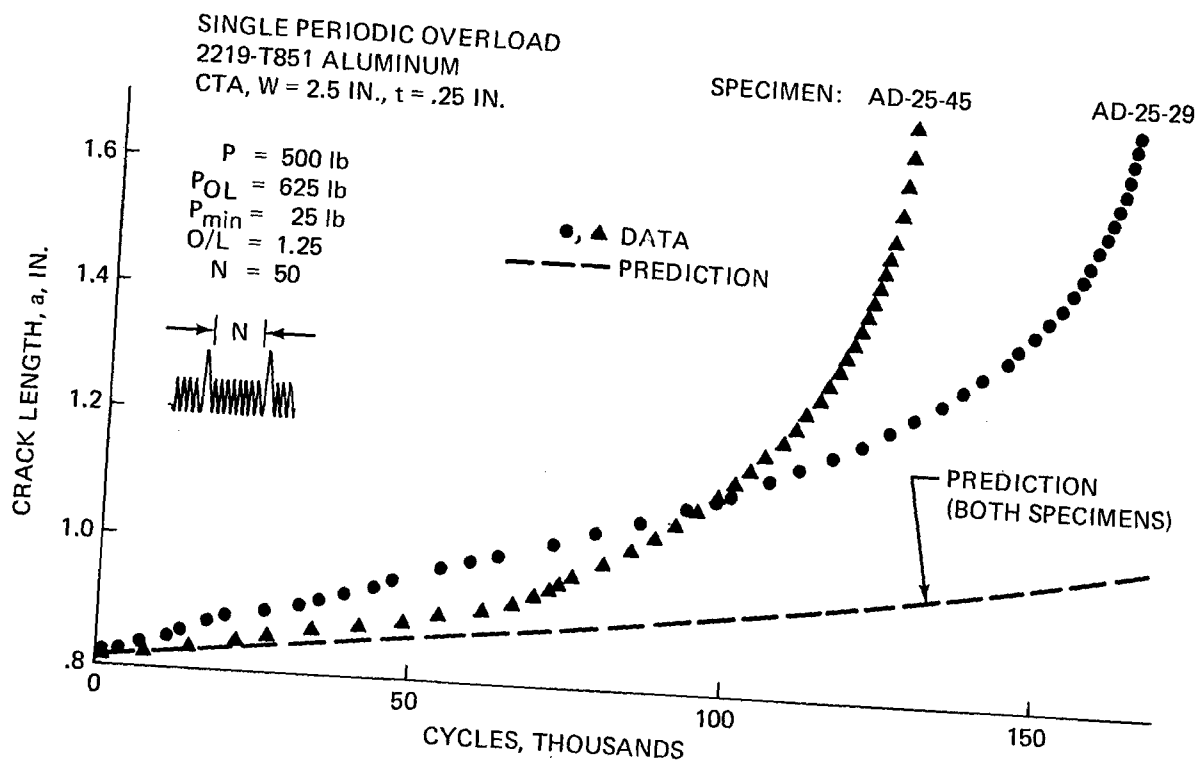


Fig. 156 Predicted a vs. N for $O/L = 1.25$, $N = 50$, Single Periodic Overloads, 2219-T851 Aluminum

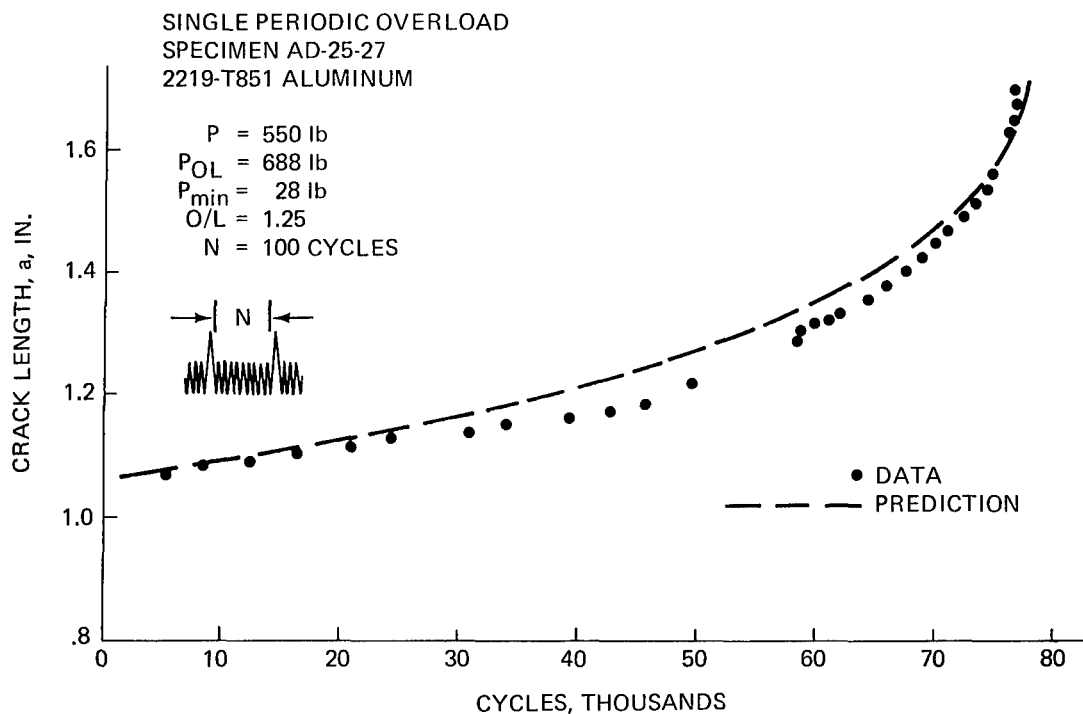


Fig. 157 Predicted a vs. N for $O/L = 1.25$, $N = 100$, Single Periodic Overloads, 2219-T851 Aluminum

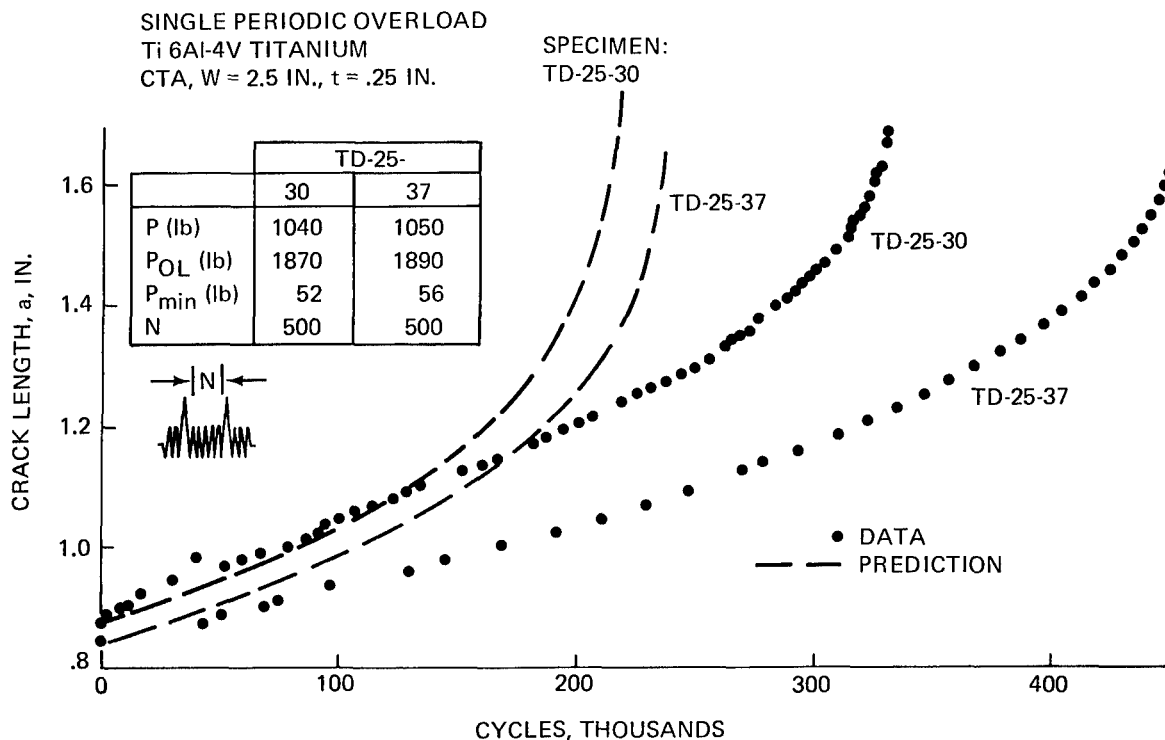


Fig. 158 Predicted a vs. N for $O/L = 1.8$, $N = 500$, Single Periodic Overloads, Ti 6Al-4V Titanium

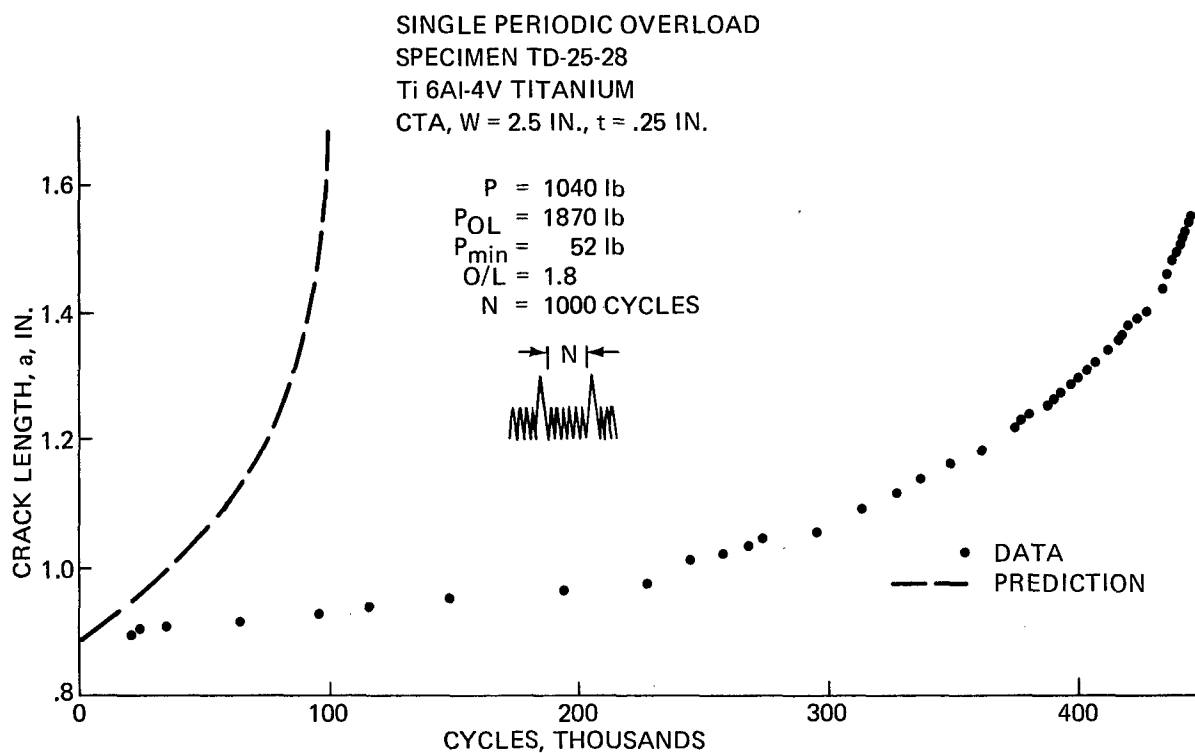


Fig. 159 Predicted a vs. N for $O/L = 1.8$, $N = 1000$, Single Periodic Overloads, Ti 6Al-4V Titanium

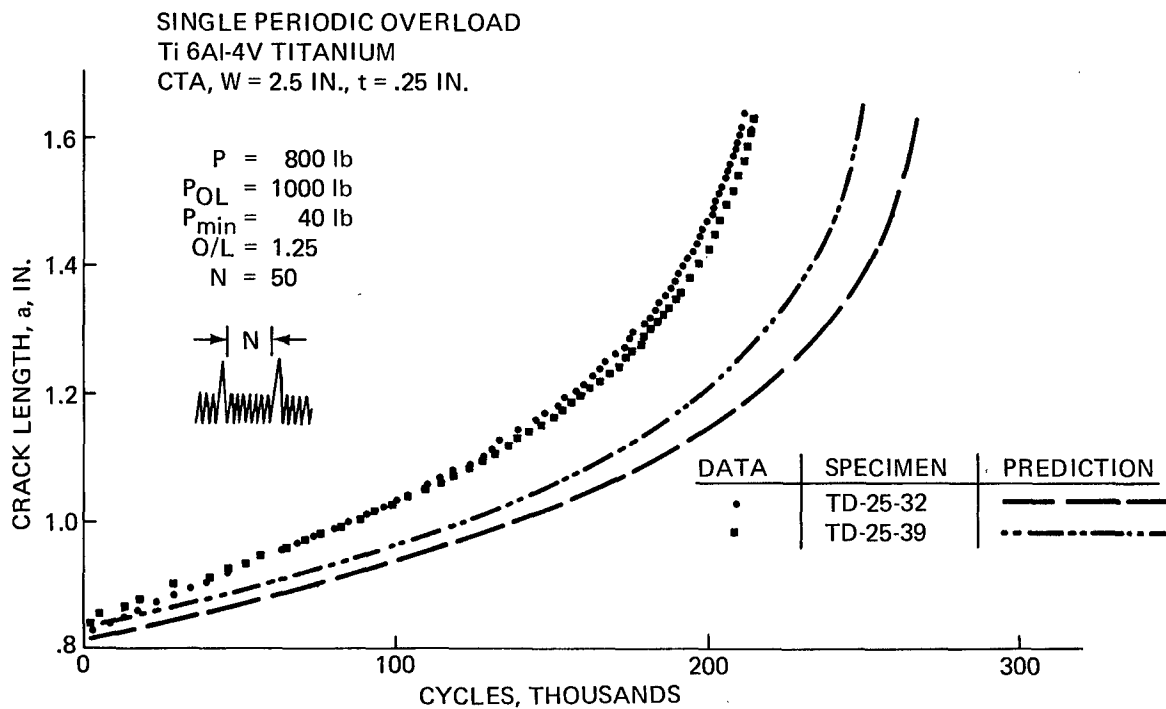


Fig. 160 Predicted a vs. N for $O/L = 1.25$, $N = 50$, Single Periodic Overloads, Ti 6Al-4V Titanium

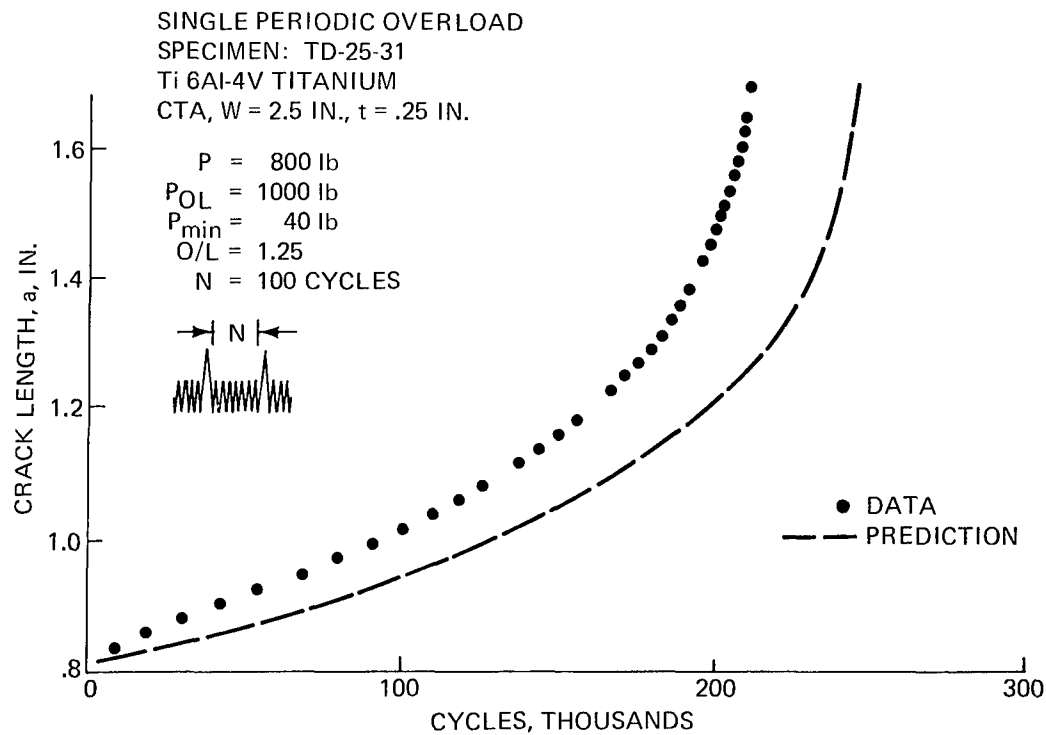


Fig. 161 Predicted a vs. N for $O/L = 1.25$, $N = 100$, Single Periodic Overloads, Ti 6Al-4V Titanium

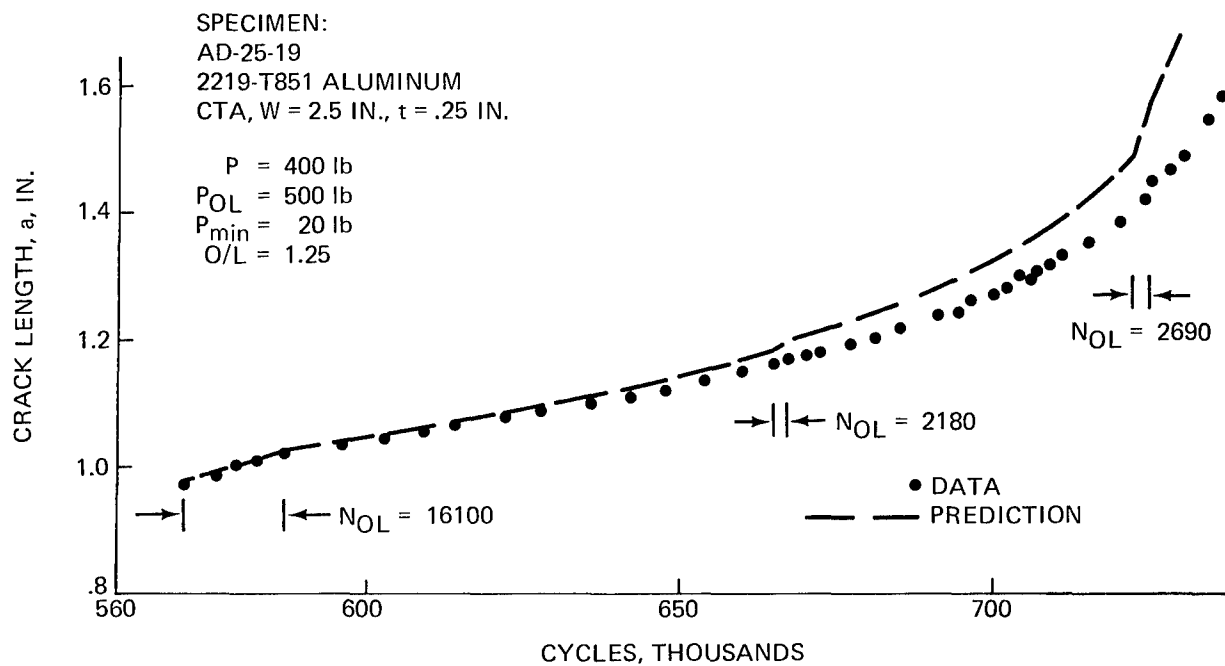


Fig. 162 Predicted a vs. N for $O/L = 1.25$, Multiple Overloads, 2219-T851 Aluminum

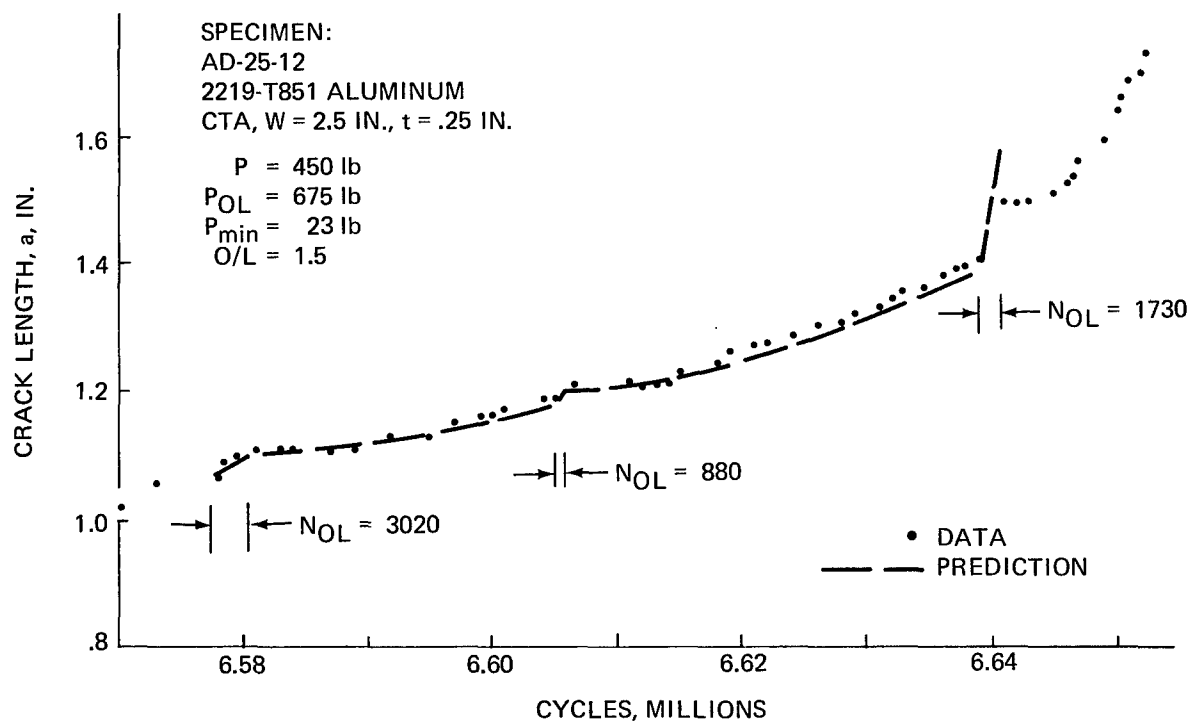


Fig. 163 Predicted a vs. N for O/L = 1.5, Multiple Overloads, 2219-T851 Aluminum

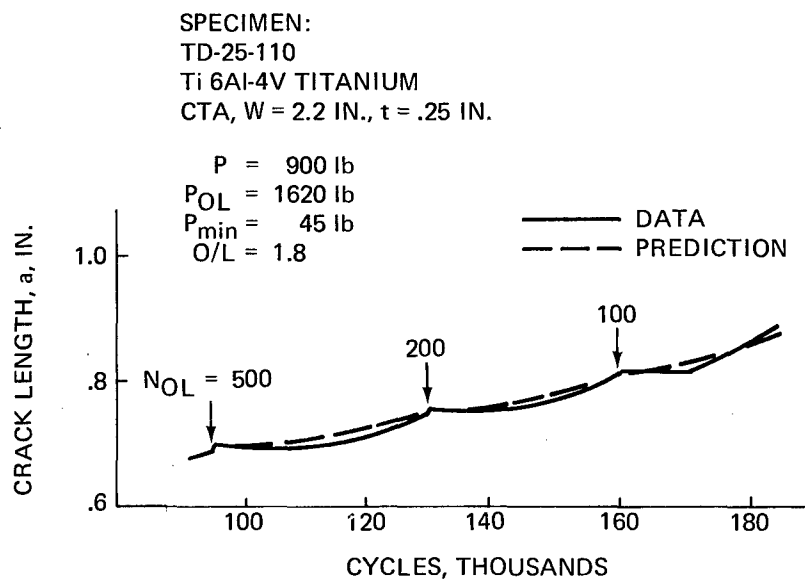


Fig. 164 Predicted a vs. N for O/L = 1.8, Multiple Overloads, Ti6Al-4V Titanium

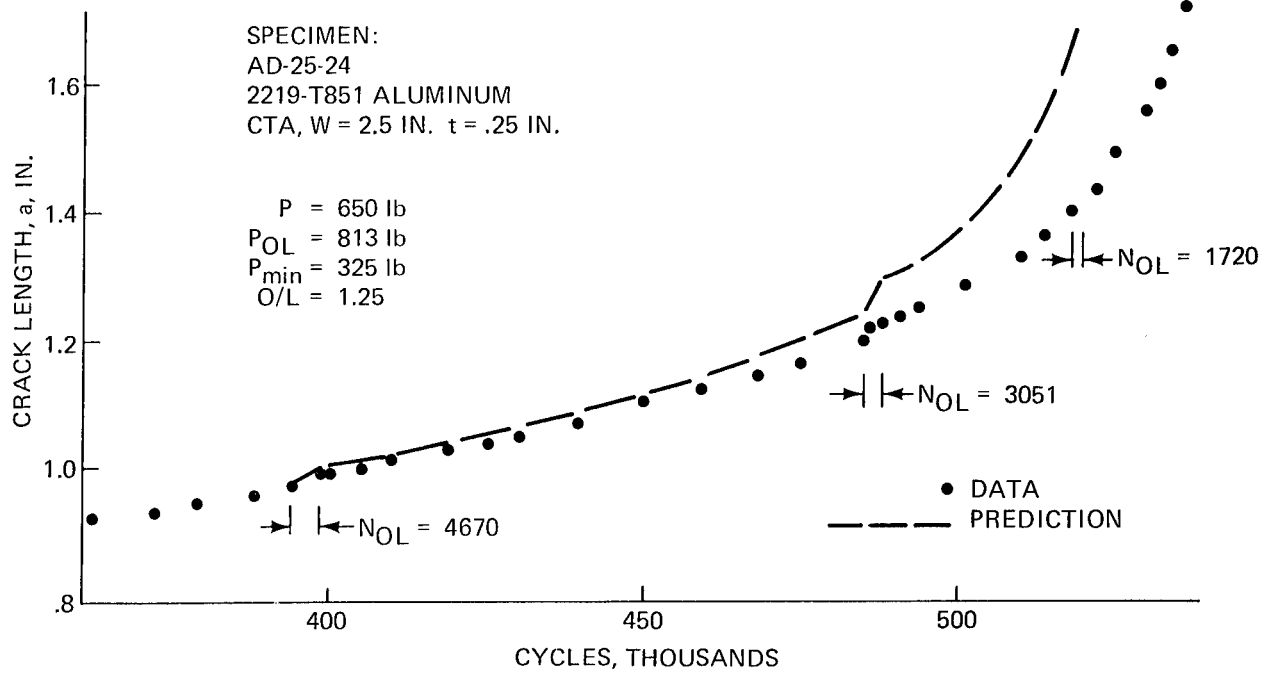


Fig. 165 Predicted a vs. N for O/L = 1.25 and R = 0.5, Multiple Overloads 2219-T851 Aluminum

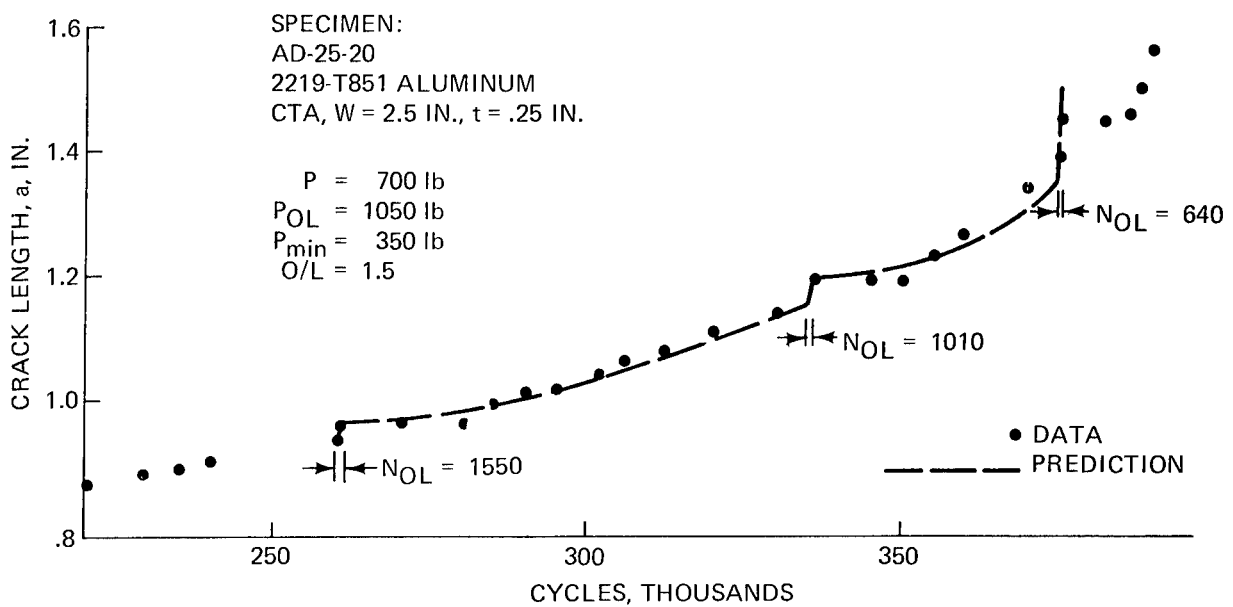


Fig. 166 Predicted a vs. N for O/L = 1.5 and R = 0.5, Multiple Overloads 2219-T851 Aluminum

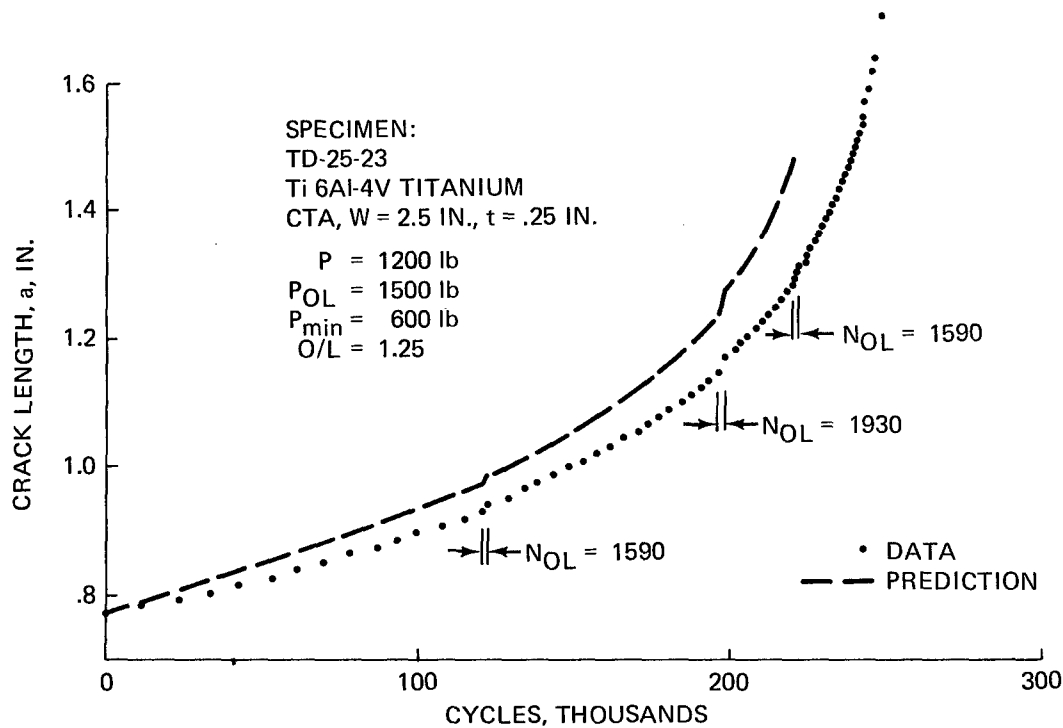


Fig. 167 Predicted a vs. N for $O/L = 1.25$ and $R = 0.5$, Multiple Overloads, Titanium

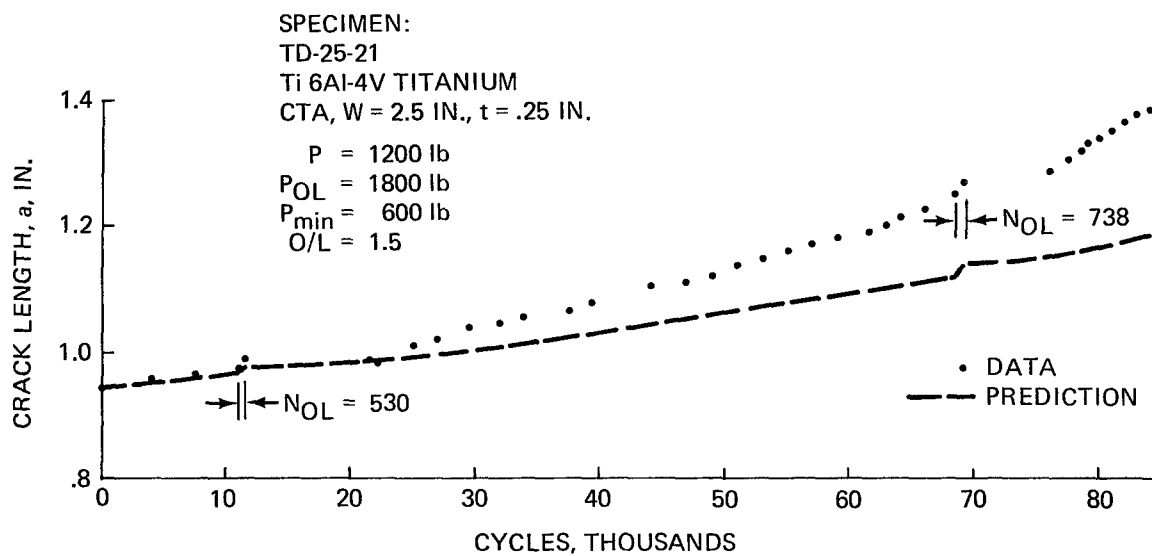


Fig. 168 Predicted a vs. N for $O/L = 1.5$ and $R = 0.5$, Multiple Overloads, Titanium

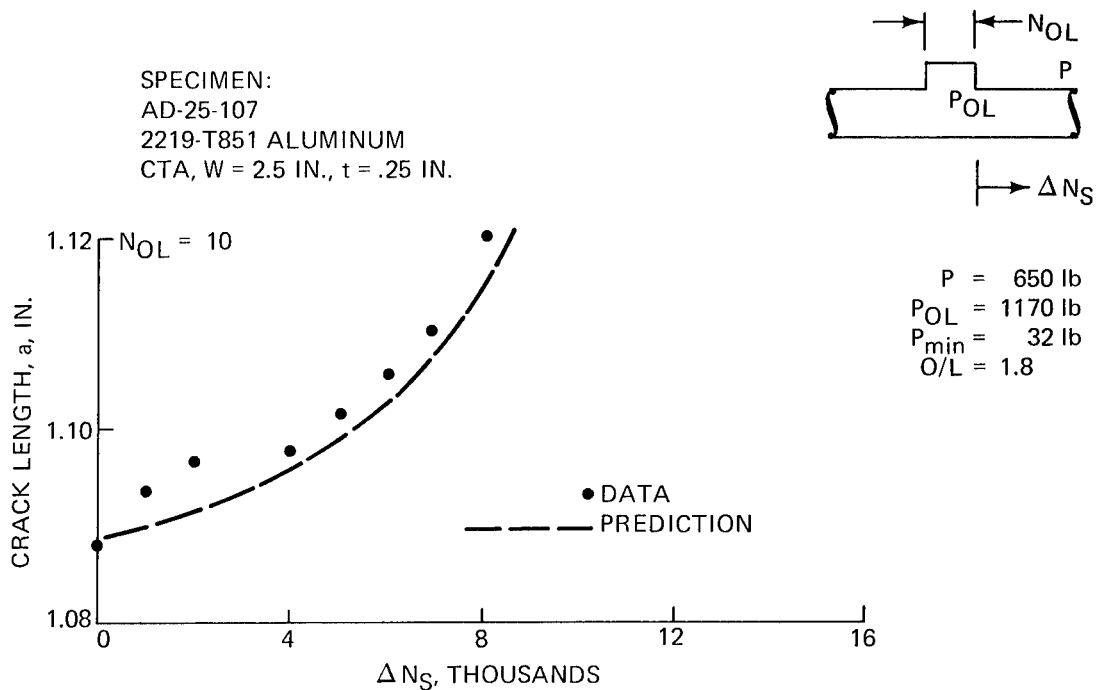


Fig. 169 Predicted a vs. ΔN_S for O/L = 1.8 and $N_{OL} = 10$, 2219-T851 Aluminum

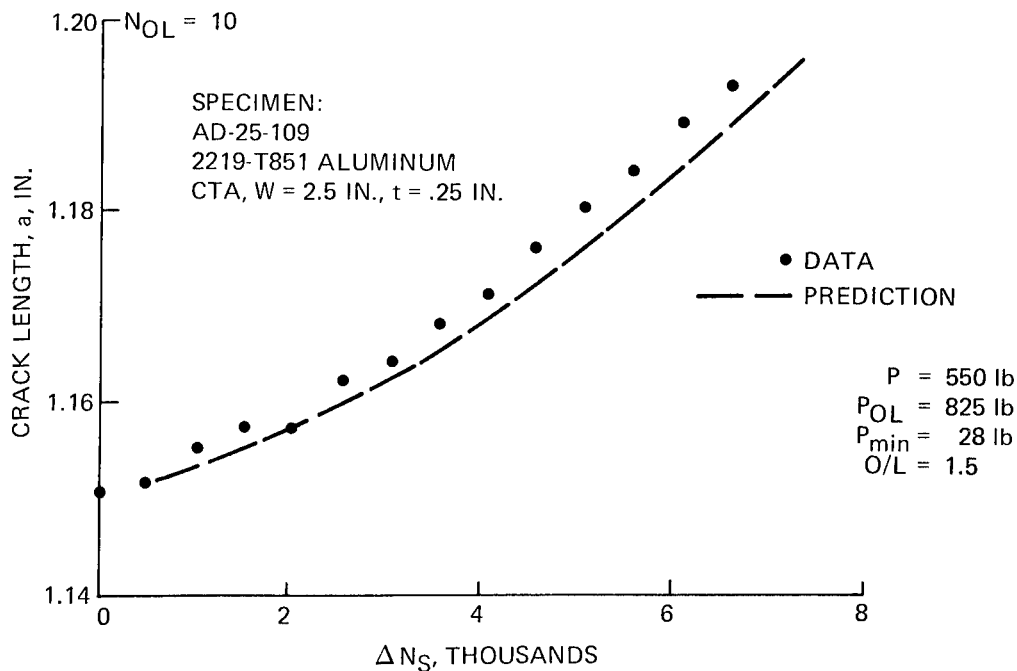


Fig. 170 Predicted a vs. ΔN_S for O/L = 1.5 and $N_{OL} = 10$, 2219-T851 Aluminum

SPECIMEN:
AD-25-110
2219-T851 ALUMINUM
CTA, W = 2.5 IN., t = .25 IN.

• DATA
— — — PREDICTION

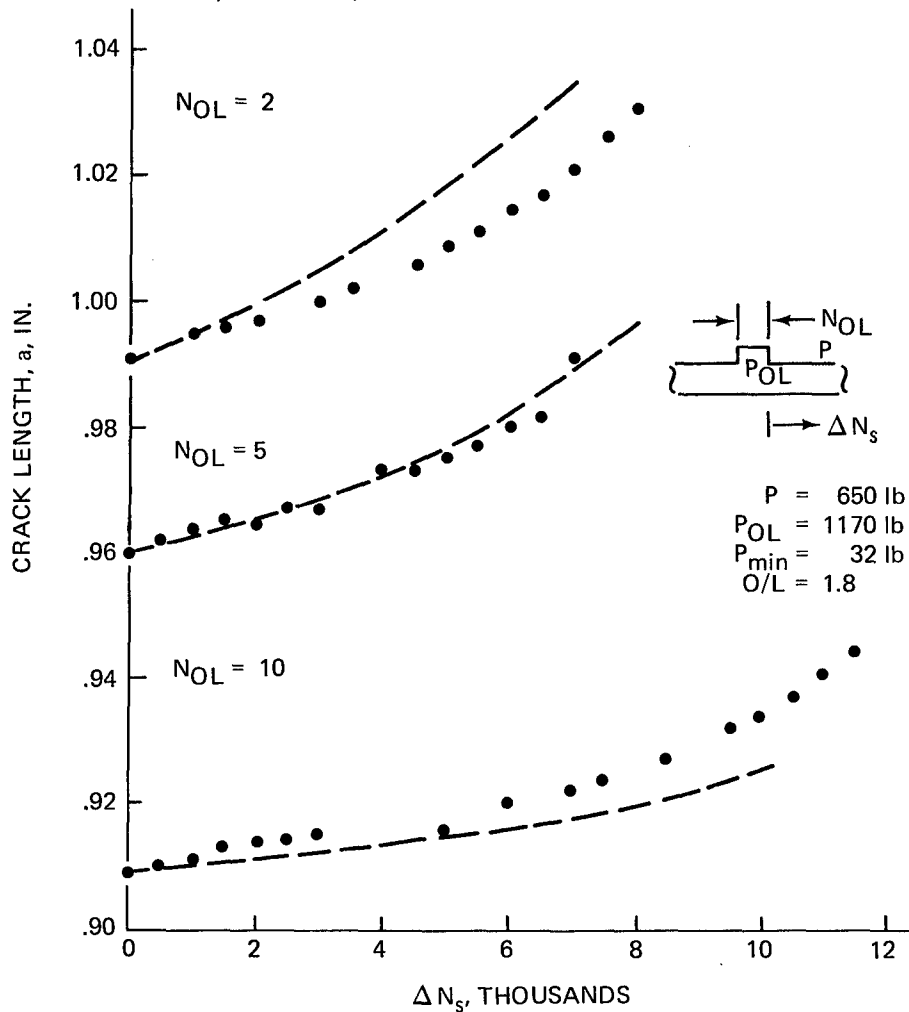


Fig. 171 Predicted a vs. ΔN_s for $O/L = 1.8$ and $N_{OL} = 2, 5 \text{ \& } 10$, 2219-T851 Aluminum

SPECIMEN:
 TD-25-110
 Ti 6Al-4V
 CTA, $W = 2.20$, $t = .251$

$P = 900$ lb
 $P_{OL} = 1620$ lb
 $P_{min} = 45$ lb
 $O/L = 1.8$

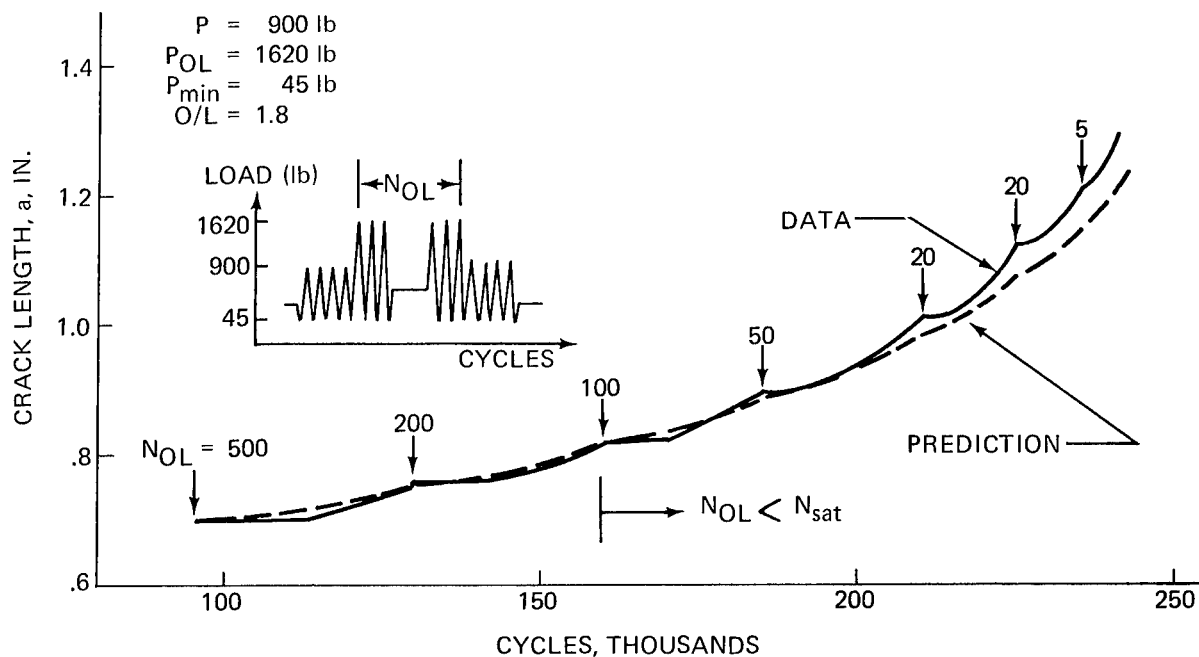


Fig. 172 Predicted a vs. N for $O/L = 1.8$ and $N_{OL} < N_{sat}$, Ti 6Al-4V Titanium

SPECIMEN:
 TD-25-111
 Ti 6Al-4V
 CTA, $W = 2.194$, $t = .250$

$P = 900$ lb
 $P_{OL} = 1620$ lb
 $P_{min} = 45$ lb

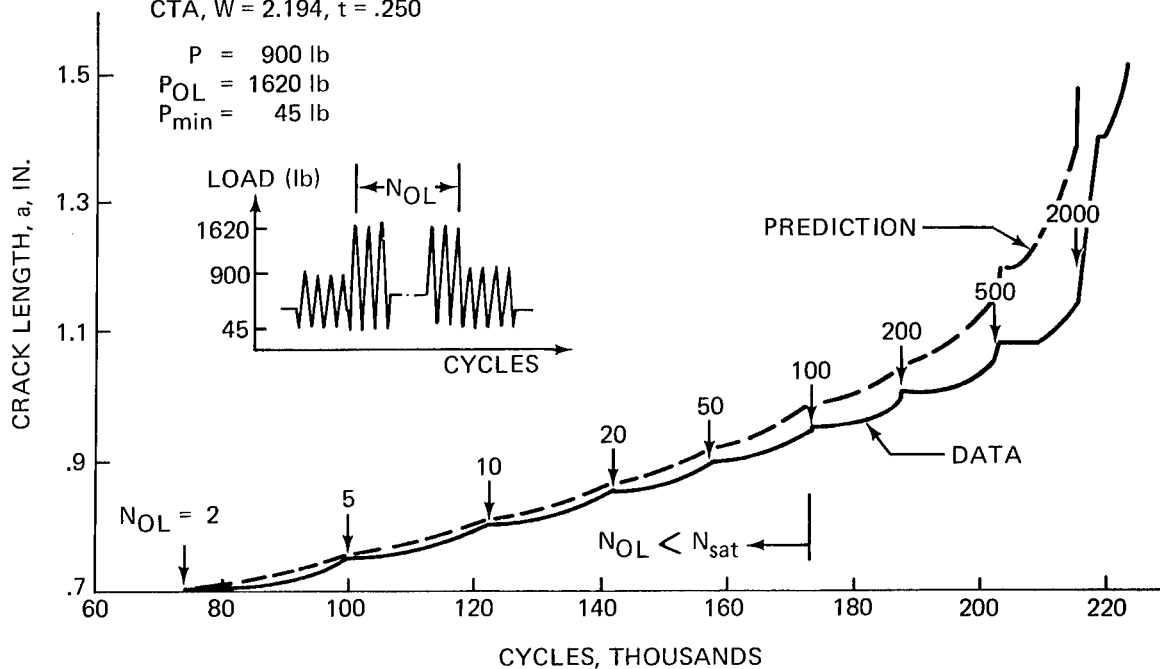


Fig. 173 Predicted a vs. N for $O/L = 1.8$ and $N_{OL} < N_{sat}$, Ti 6Al-4V Titanium

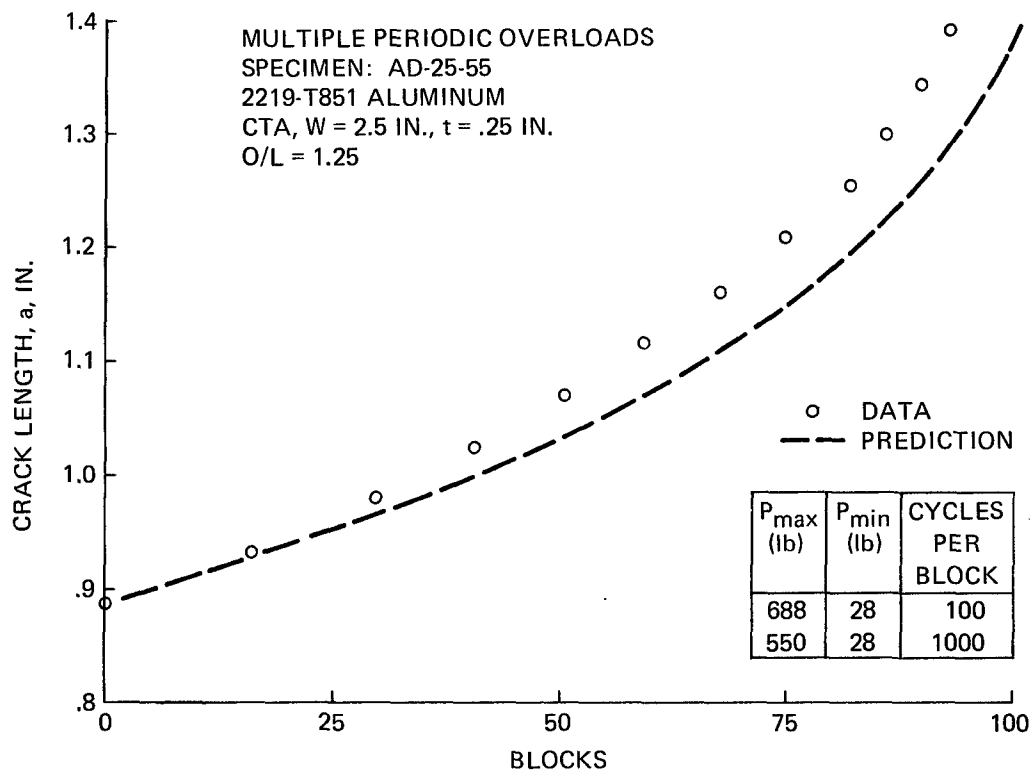


Fig. 174 Predicted B for O/L = 1.25 and $N_{OL}/N = 100/1000$,

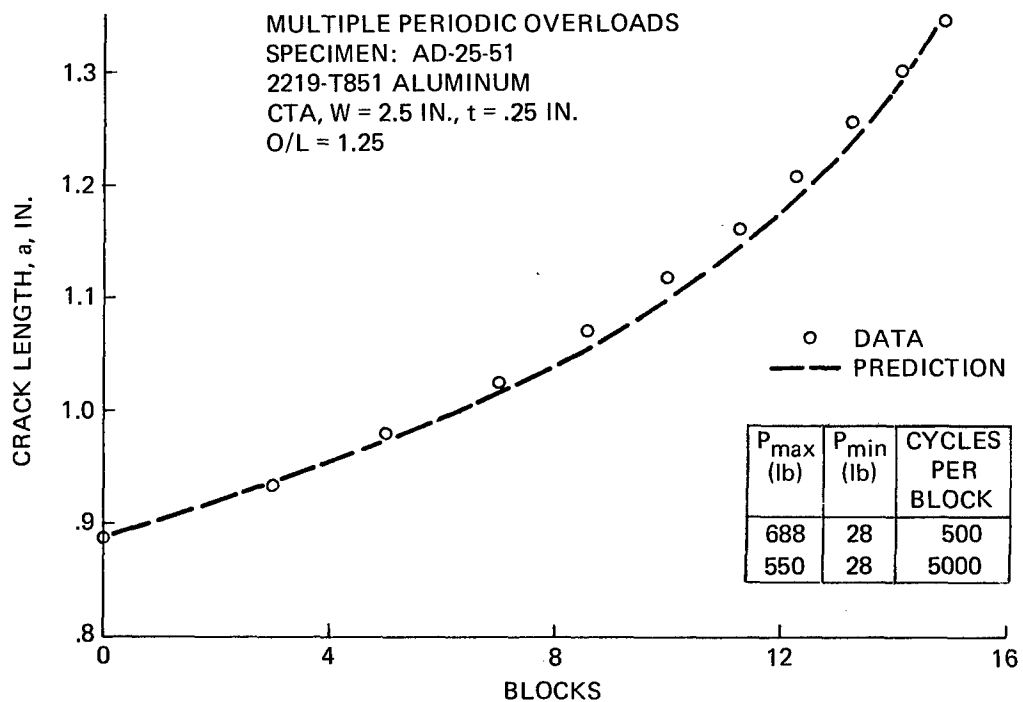


Fig. 175 Predicted a vs. B for O/L = 1.25 and $N_{OL}/N = 500/5000$,

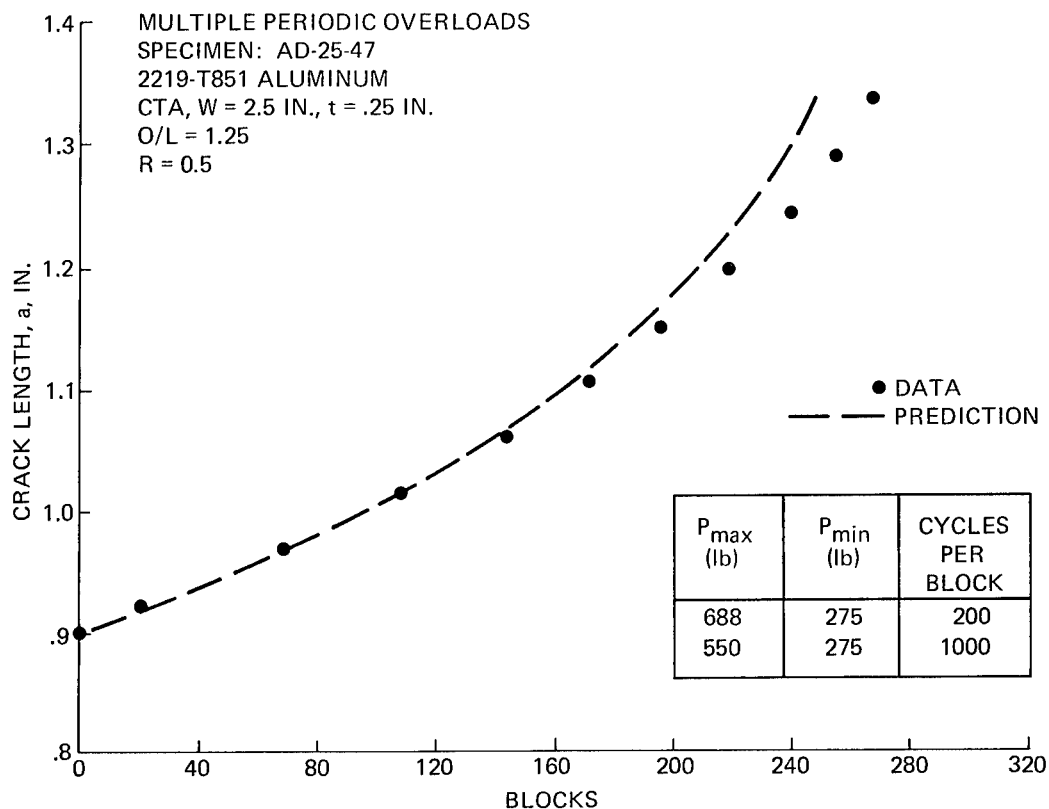


Fig. 176 Predicted a vs. B for $O/L = 1.25$ and $N_{OL}/N = 200/1000$, $R = 0.5$,
Multiple Periodic Overloads, 2219-T851 Aluminum

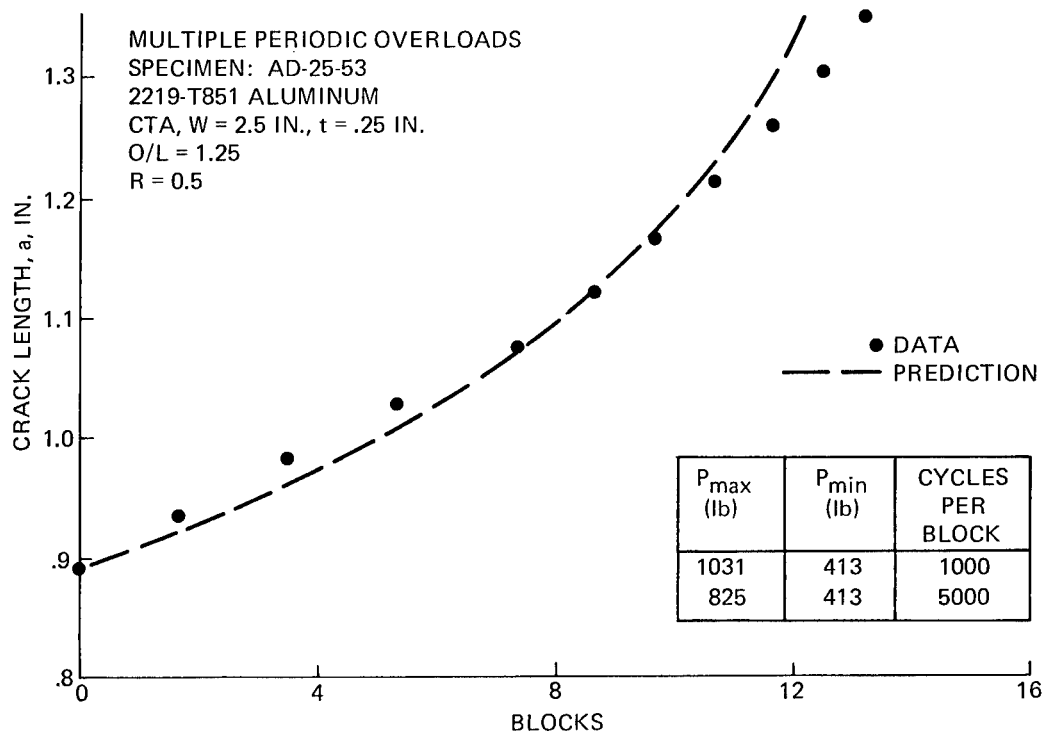


Fig. 177 Predicted a vs. B for $O/L = 1.25$ and $N_{OL}/N = 1000/5000$, $R = 0.5$,
Multiple Periodic Overloads, 2219-T851 Aluminum

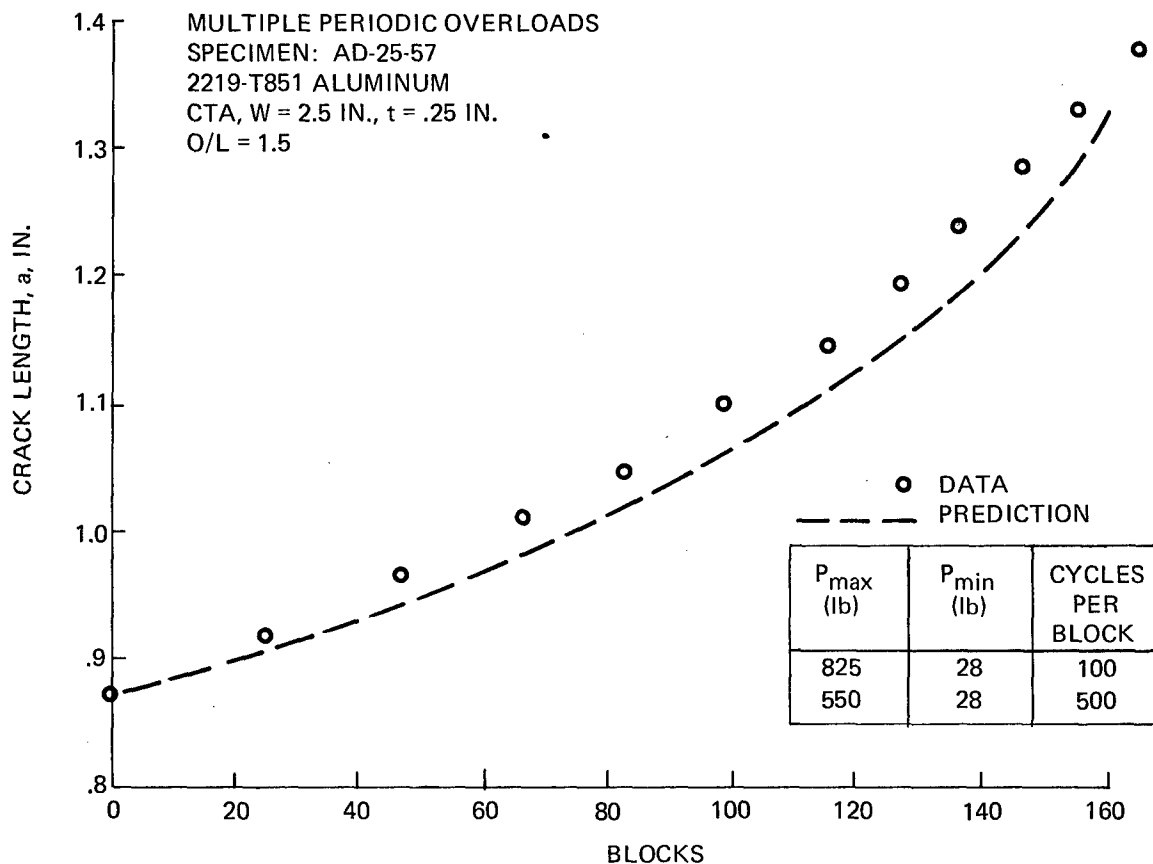


Fig. 178 Predicted a vs. B for O/L = 1.5 and $N_{OL}/N = 100/500$, Multiple Periodic Overloads, 2219-T851 Aluminum

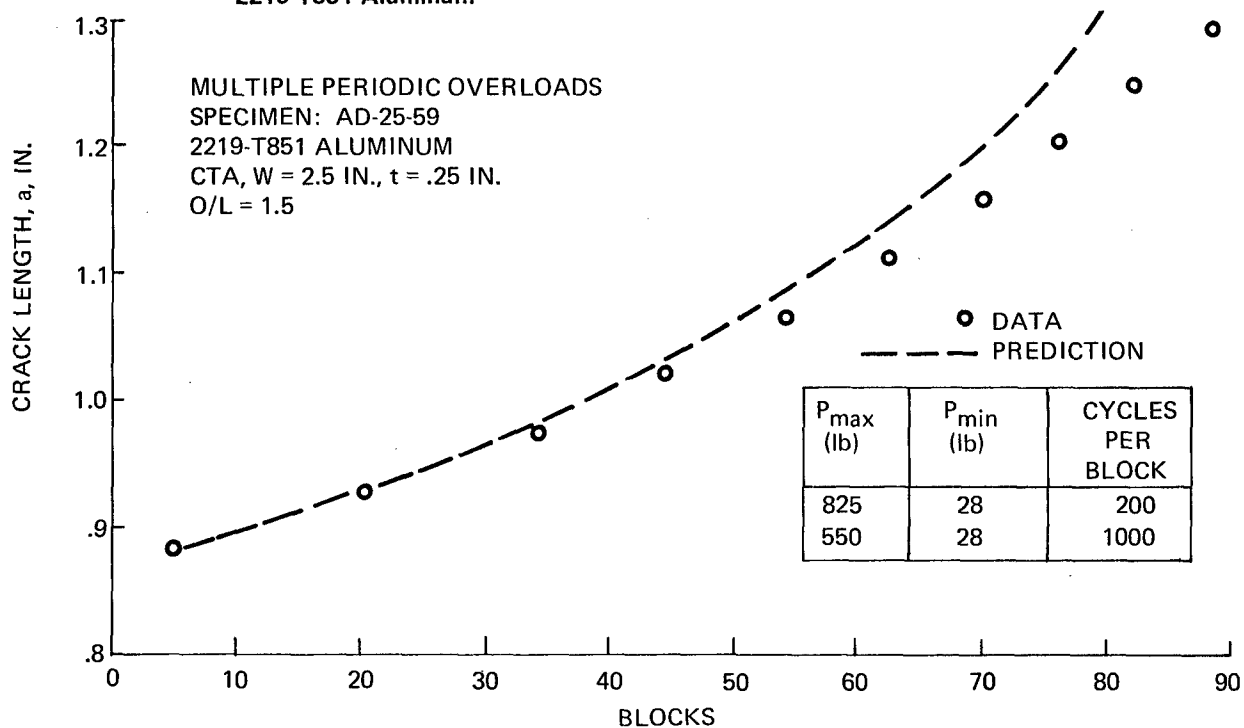


Fig. 179 Predicted a vs. B for O/L = 1.5 and $N_{OL}/N = 200/1000$, Multiple Periodic Overloads, 2219-T851 Aluminum

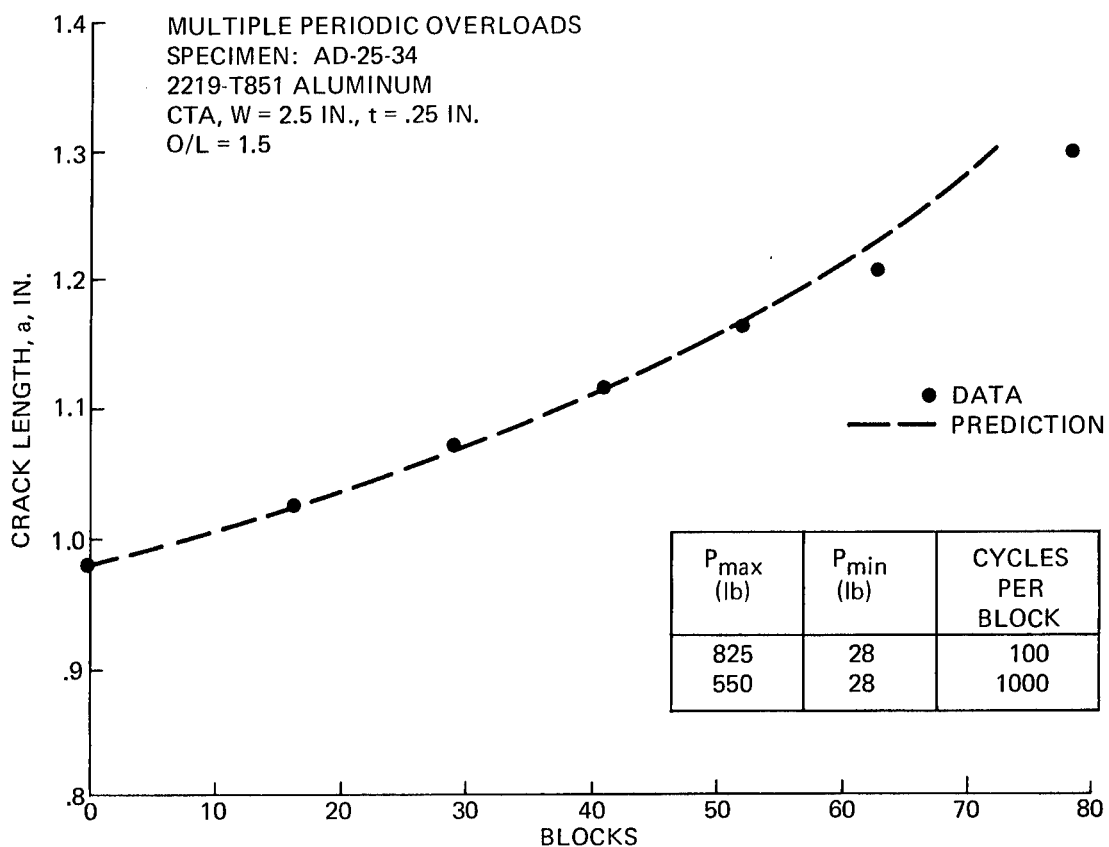


Fig. 180 Predicted a vs. B for $O/L = 1.5$ and $N_{OL}/N = 100/1000$,

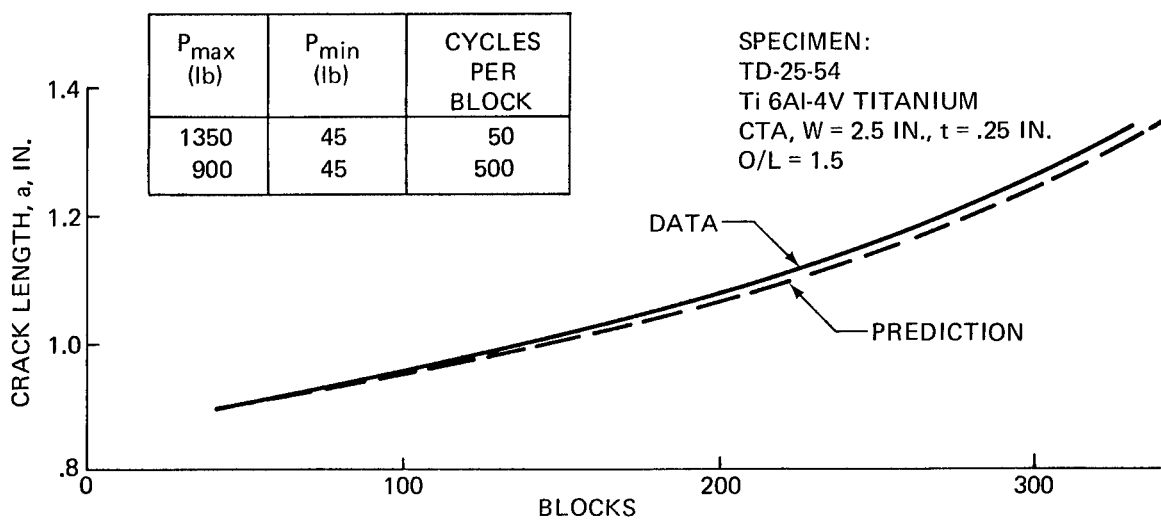


Fig. 181 Predicted a vs. B for $O/L = 1.5$ and $N_{OL}/N = 50/500$,

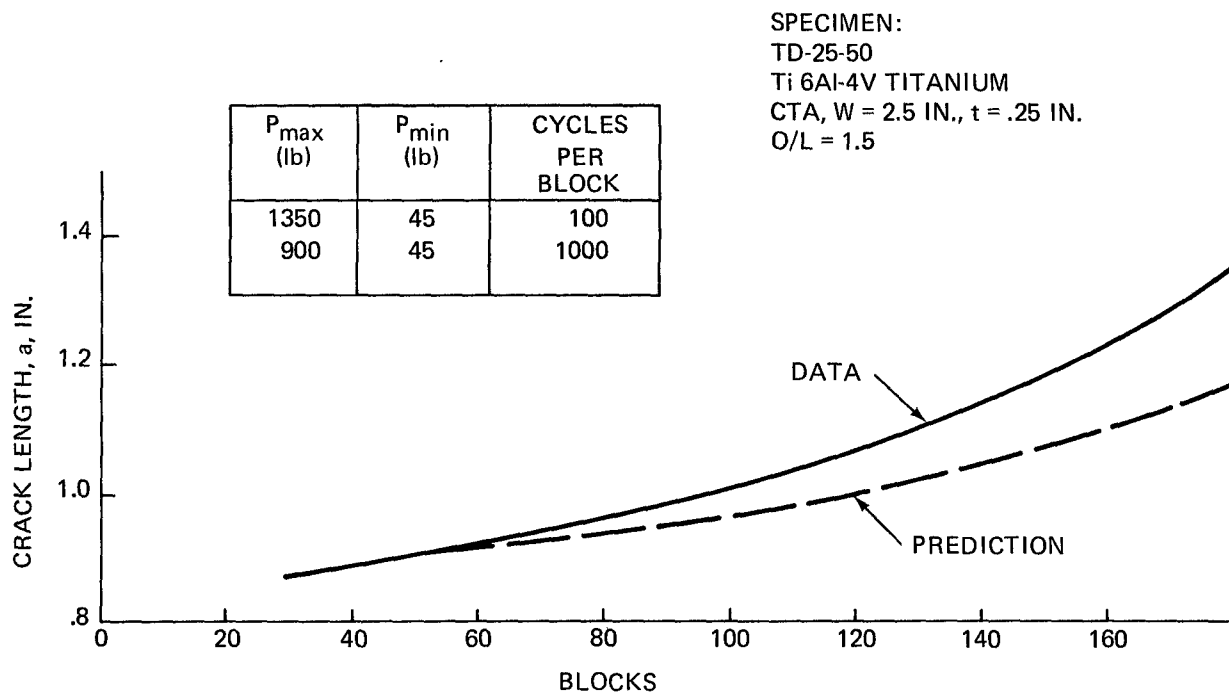


Fig. 182 Predicted a vs. B for $O/L = 1.5$ and $N_{OL}/N = 100/1000$, Multiple Periodic Overloads, Ti 6Al-4V Titanium

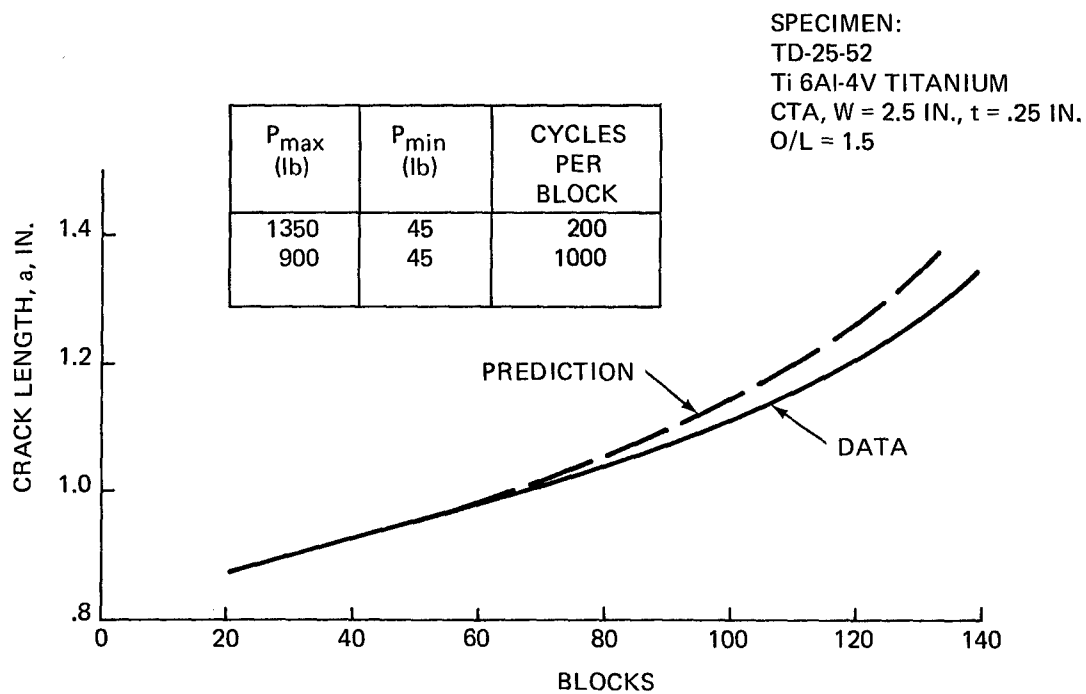


Fig. 183 Predicted a vs. B for $O/L = 1.5$ and $N_{OL}/N = 200/1000$, Multiple Periodic Overloads, Ti 6Al-4V Titanium

SPECIMEN:
 TD-25-46
 Ti 6Al-4V TITANIUM
 CTA, W = 2.5 IN., t = .25 IN.
 O/L = 1.25

P _{max} (lb)	P _{min} (lb)	CYCLES PER BLOCK
1125	45	100
900	45	1000

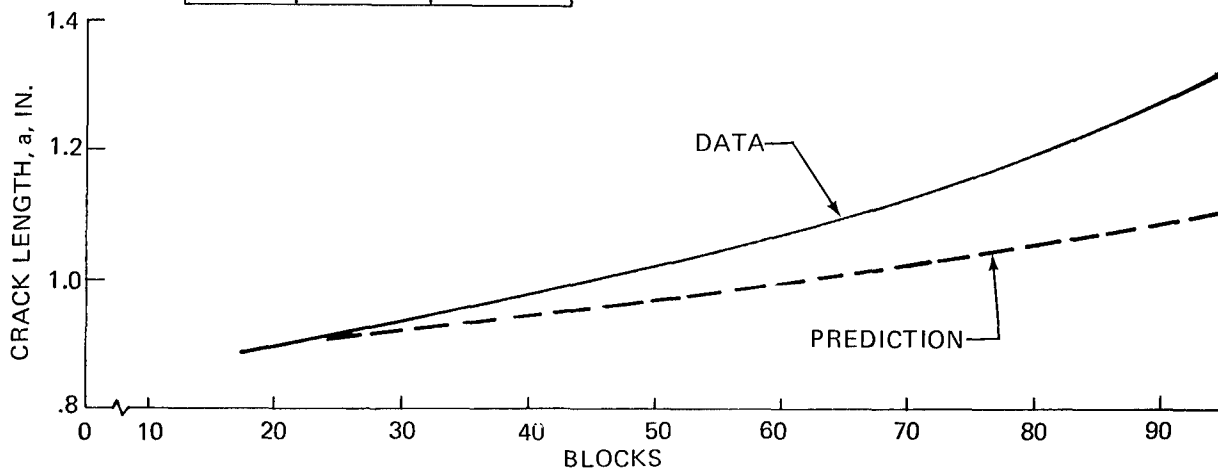


Fig. 184 Predicted a vs. B for $O/L = 1.25$ and $N_{OL}/N = 100/1000$, Multiple Periodic Overloads, Ti 6Al-4V Titanium

SPECIMEN:
 TD-25-56
 Ti 6Al-4V TITANIUM
 CTA, W = 2.5 IN., t = .25 IN.
 O/L = 1.25

P _{max} (lb)	P _{min} (lb)	CYCLES PER BLOCK
1125	45	500
900	45	5000

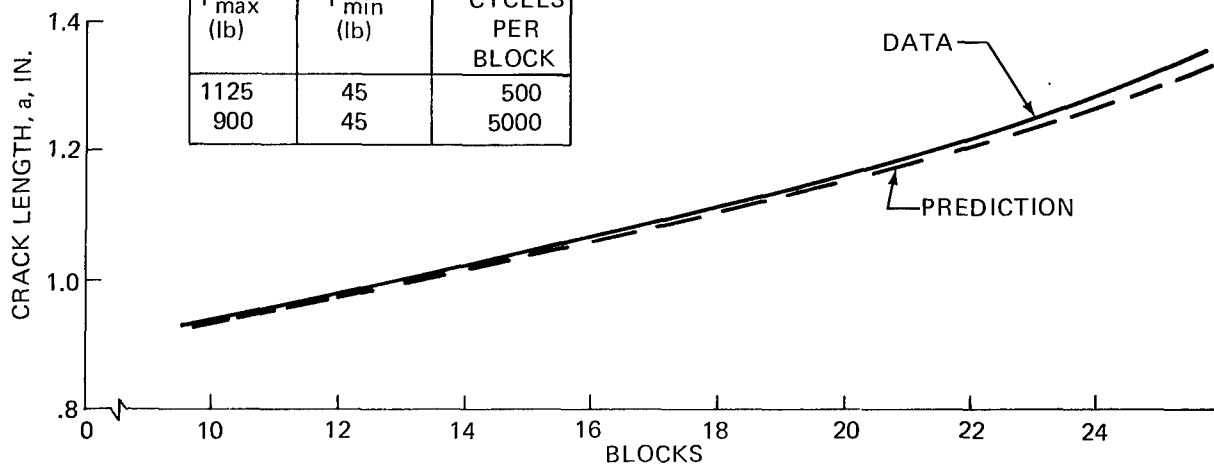


Fig. 185 Predicted a vs. B for $O/L = 1.25$ and $N_{OL}/N = 500/5000$, Multiple Periodic Overloads, Ti 6Al-4V Titanium

SPECIMEN:
 TD-25-58
 Ti 6Al-4V TITANIUM
 CTA, W = 2.5 IN., t = .25 IN.
 O/L = 1.25

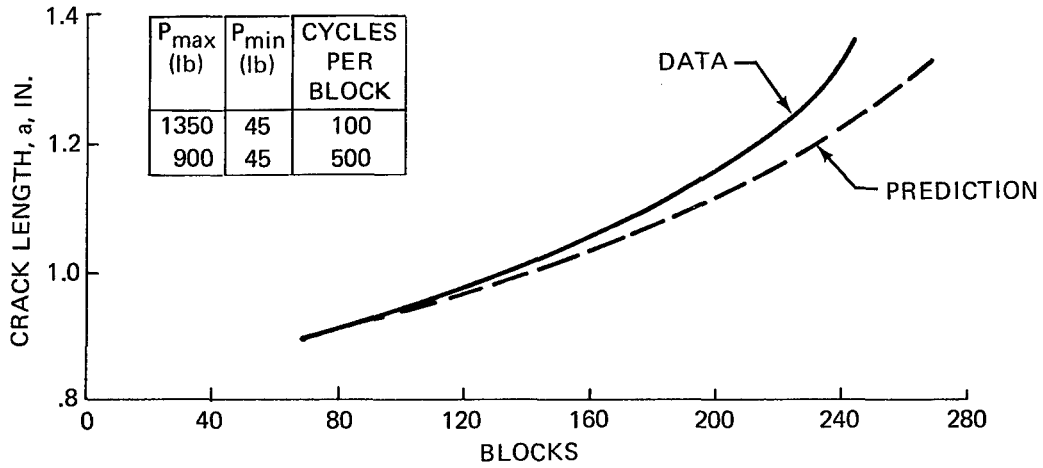


Fig. 186 Predicted a vs. B for $O/L = 1.5$ and $N_{OL}/N = 100/500$,
 Multiple Periodic Overloads, Ti 6Al-4V Titanium

SPECIMEN:
 TD-25-48
 Ti 6Al-4V TITANIUM
 CTA, W = 2.5 IN., t = .25 IN.
 O/L = 1.25
 R = .70

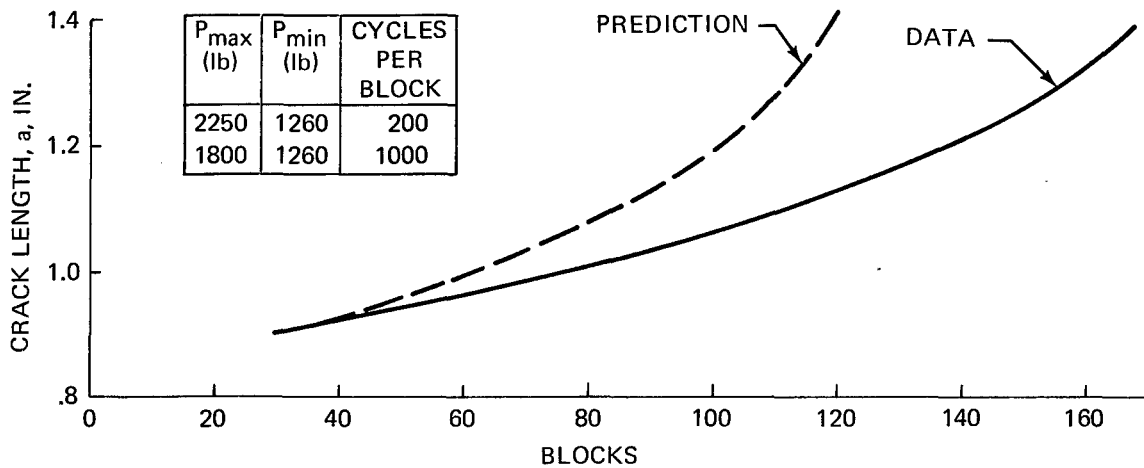


Fig. 187 Predicted a vs. B for $O/L = 1.25$ and $N_{OL}/N = 200/1000$,
 R = 0.7, Multiple Periodic Overloads, Ti 6Al-4V Titanium

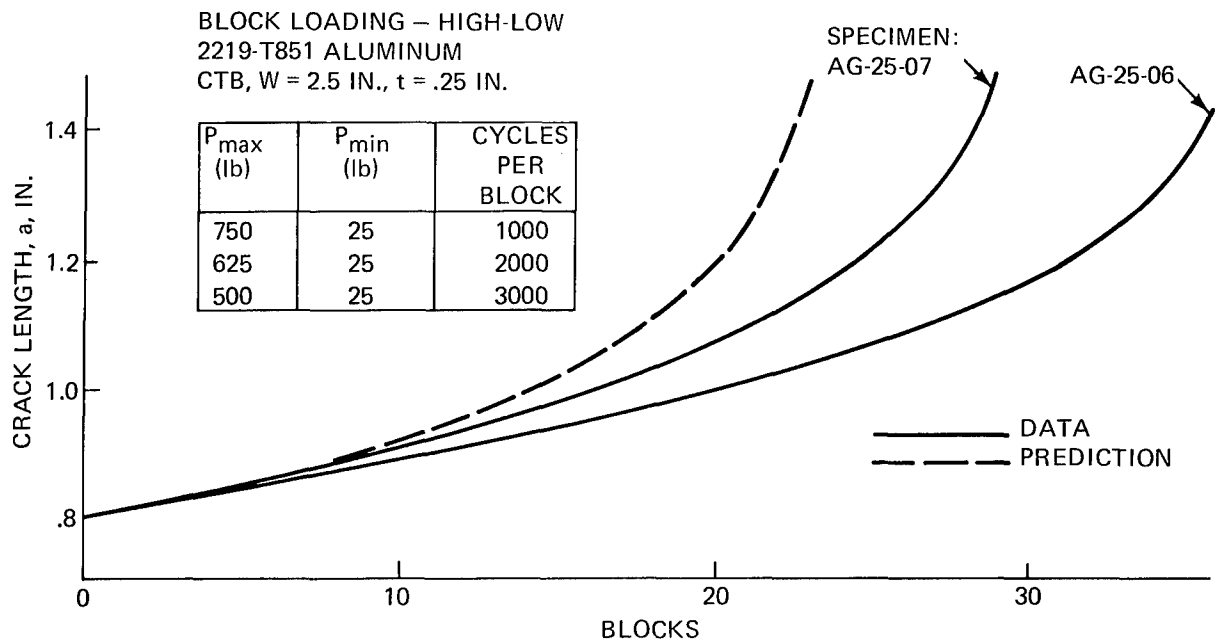


Fig. 188 Predicted a vs. B for High-Low Block Loading, 2219-T851 Aluminum

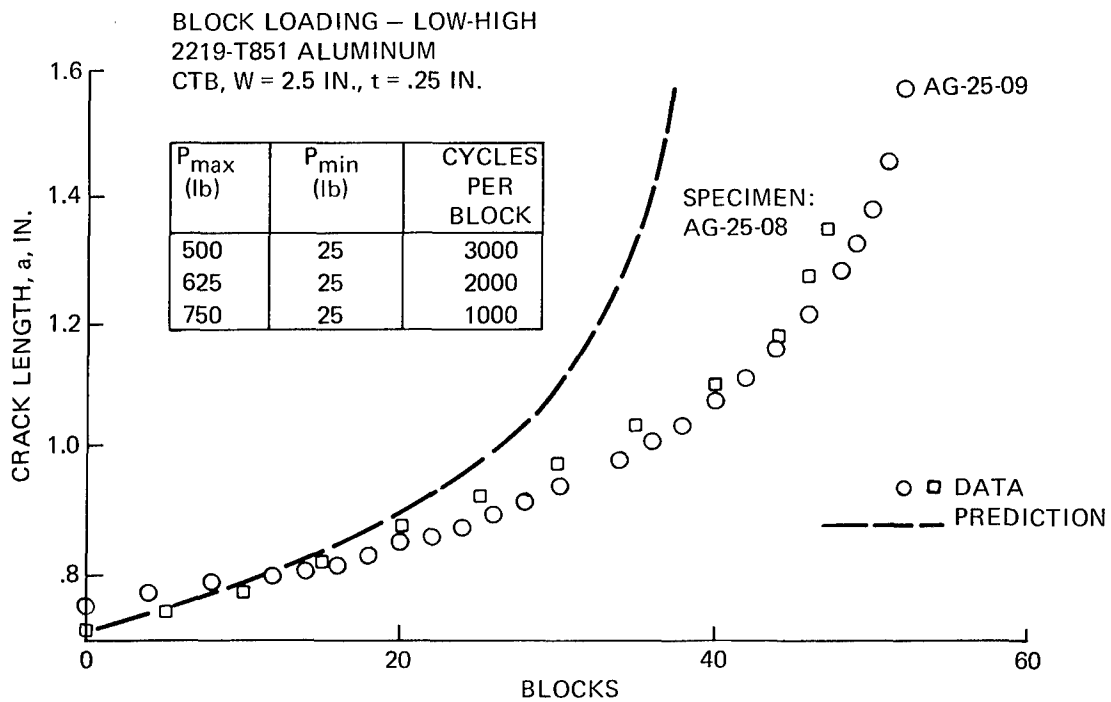


Fig. 189 Predicted a vs. B for Low-High Block Loading, 2219-T851 Aluminum

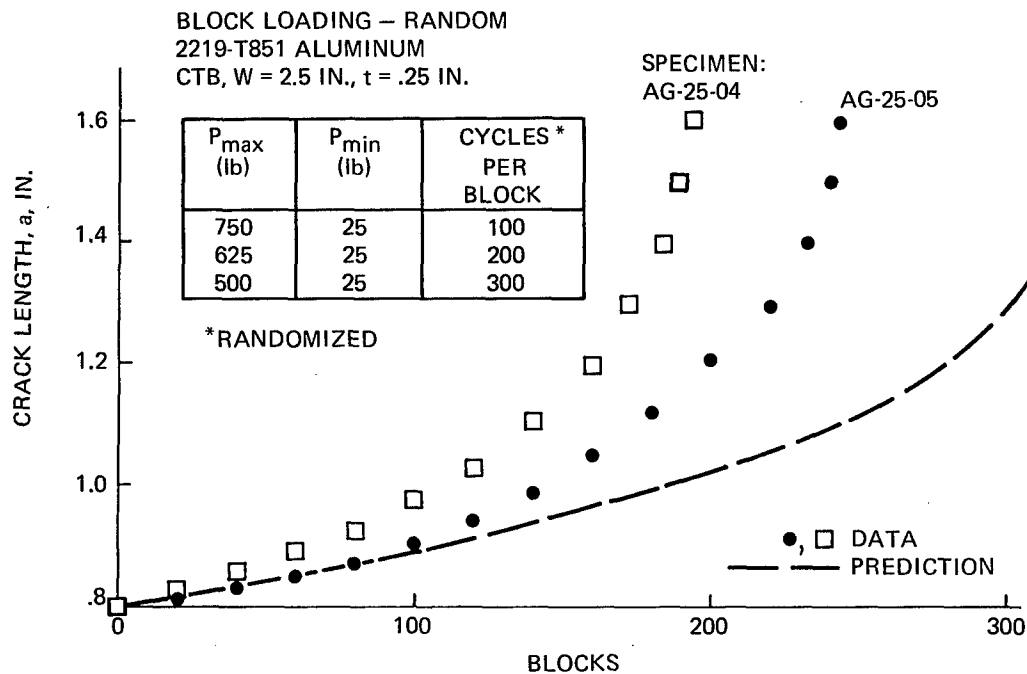


Fig. 190 Predicted a vs. B for Block Random Loading, 2219-T851 Aluminum

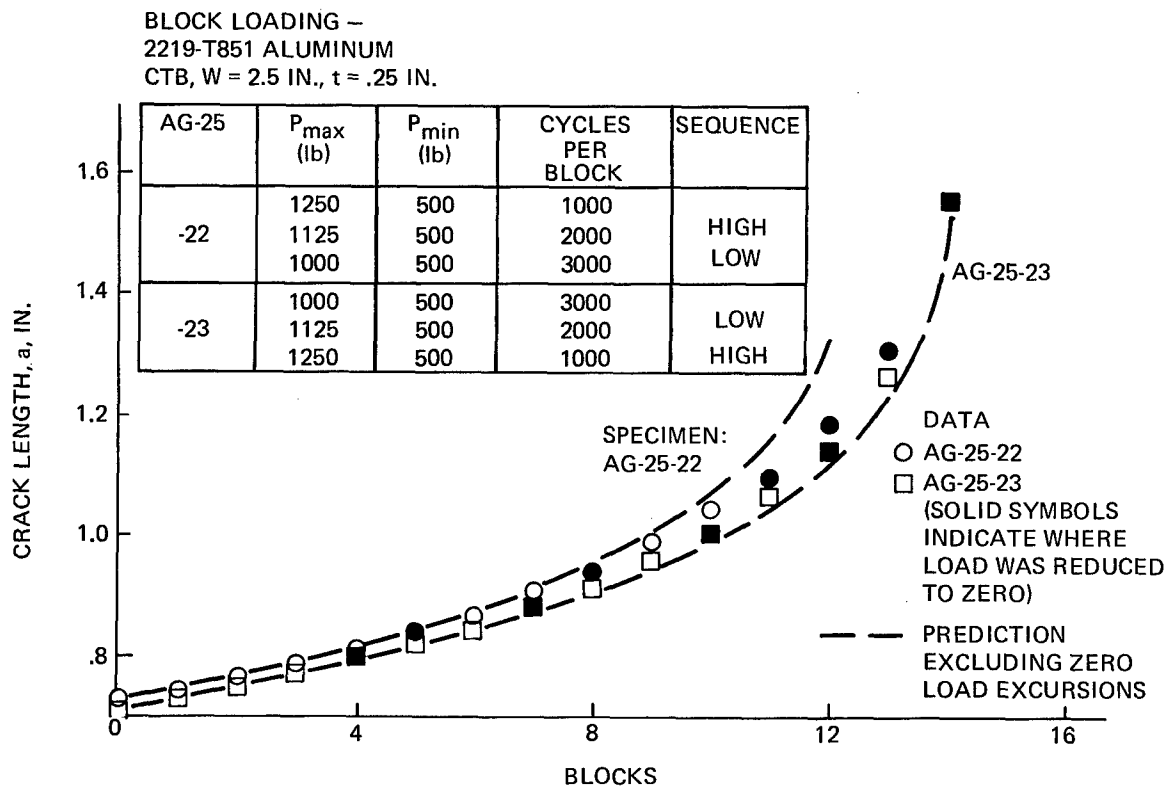


Fig. 191 Predicted a vs. B for High-Low and Low-High Block Loading, $R_{min} = 0.5$, 2219-T851 Aluminum

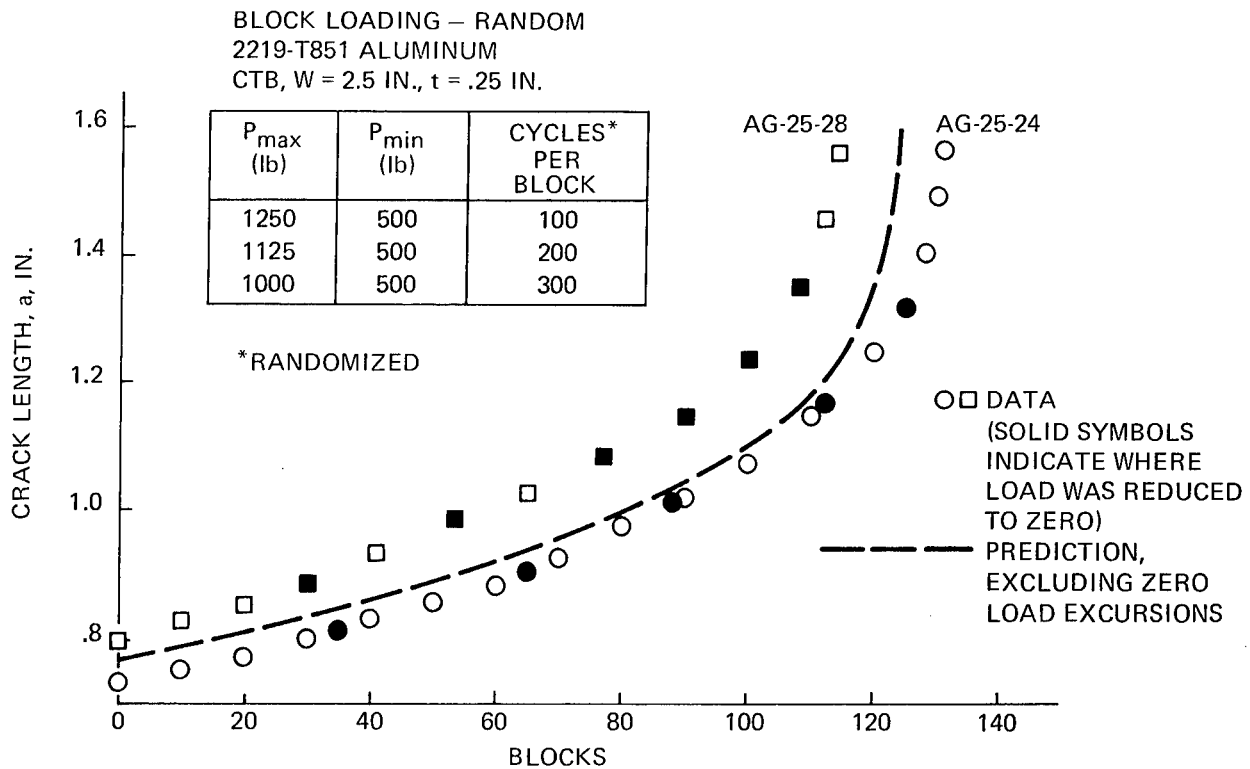


Fig. 192 Predicted a vs. B for Block Random Loading, $R_{min} = 0.5$, 2219-T851 Aluminum

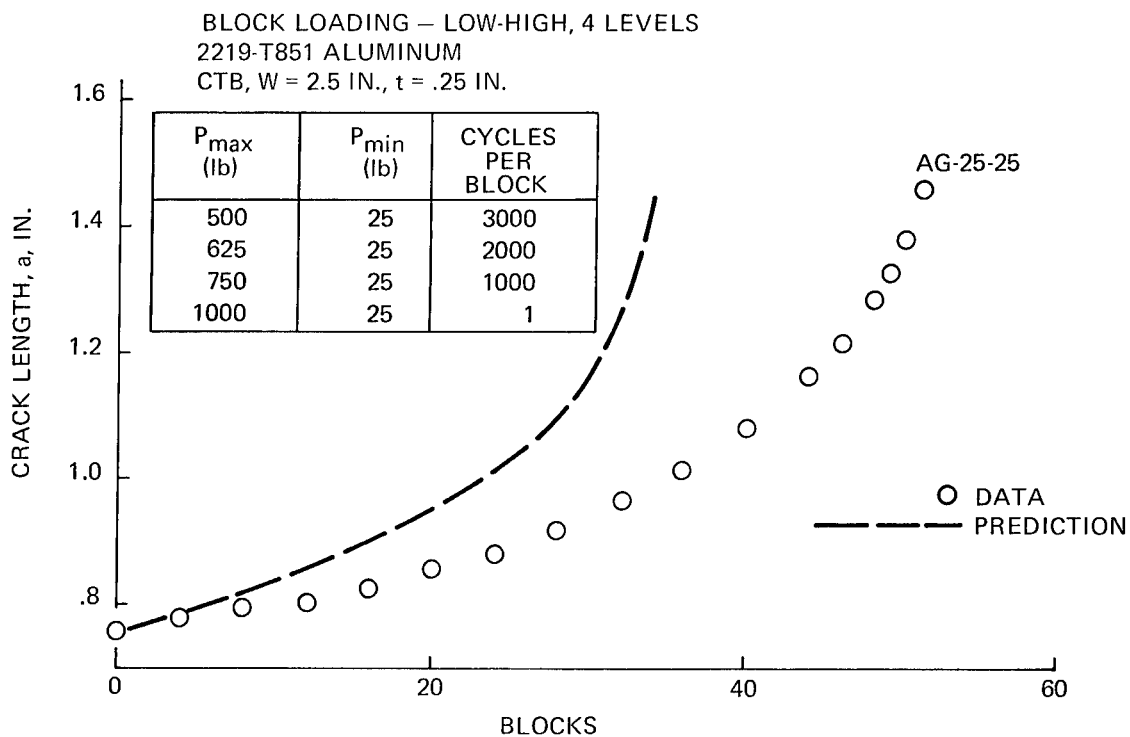


Fig. 193 Predicted a vs. B for 4 Level Low-High Block Loading, 2219-T851 Aluminum

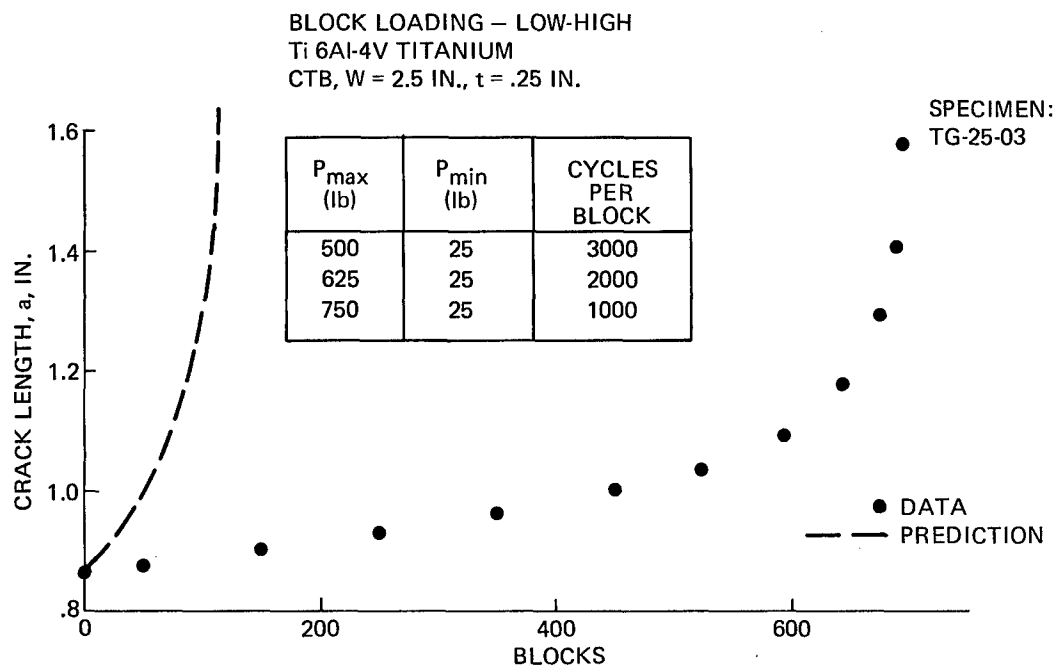


Fig. 194 Predicted a vs. B for Low-High Block Loading, Ti 6Al-4V Titanium

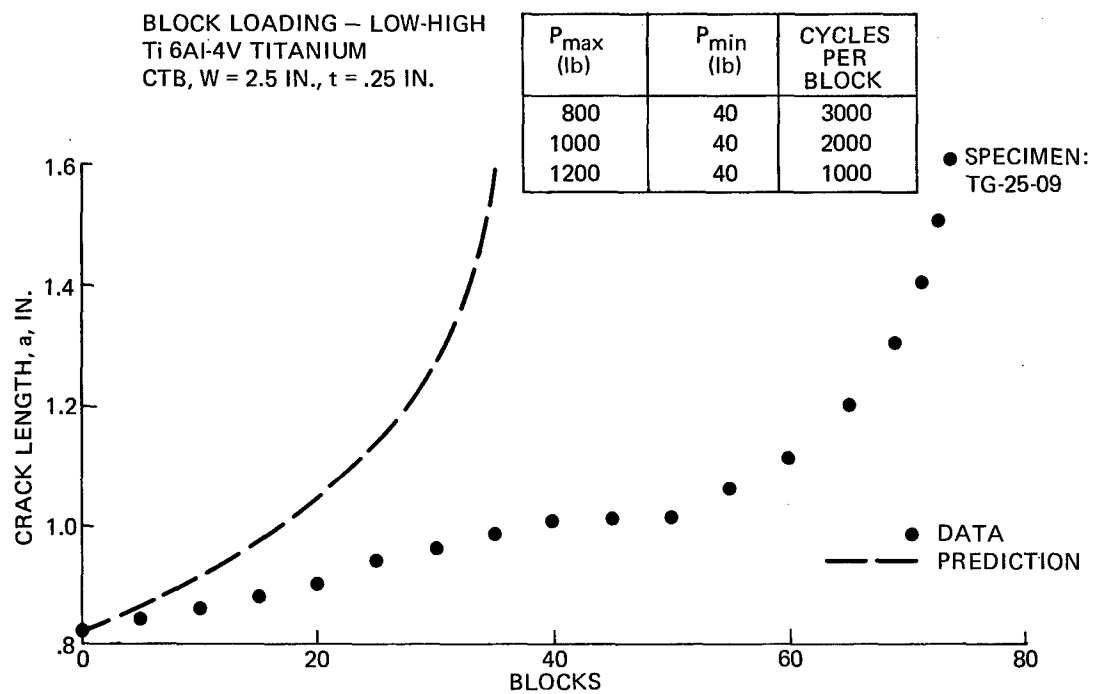


Fig. 195 Predicted a vs. B for Low-High Block Loading, Ti 6Al-4V Titanium

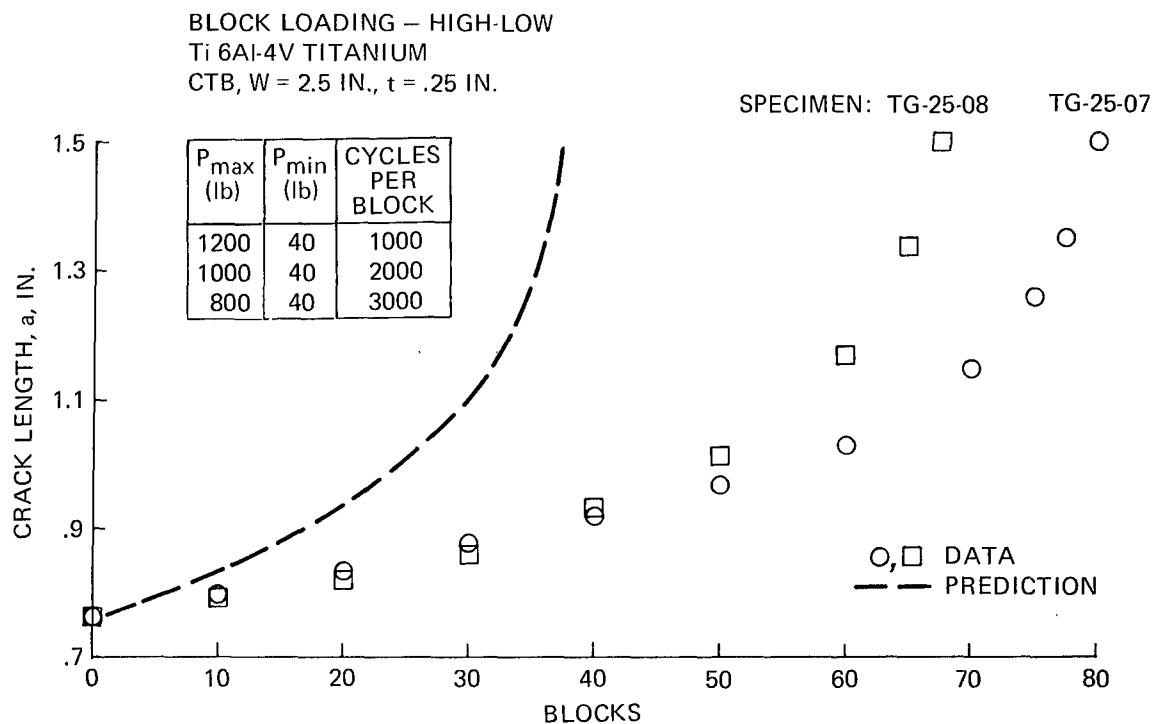


Fig. 196 Predicted a vs. B for High-Low Block Loading, Ti 6Al-4V Titanium

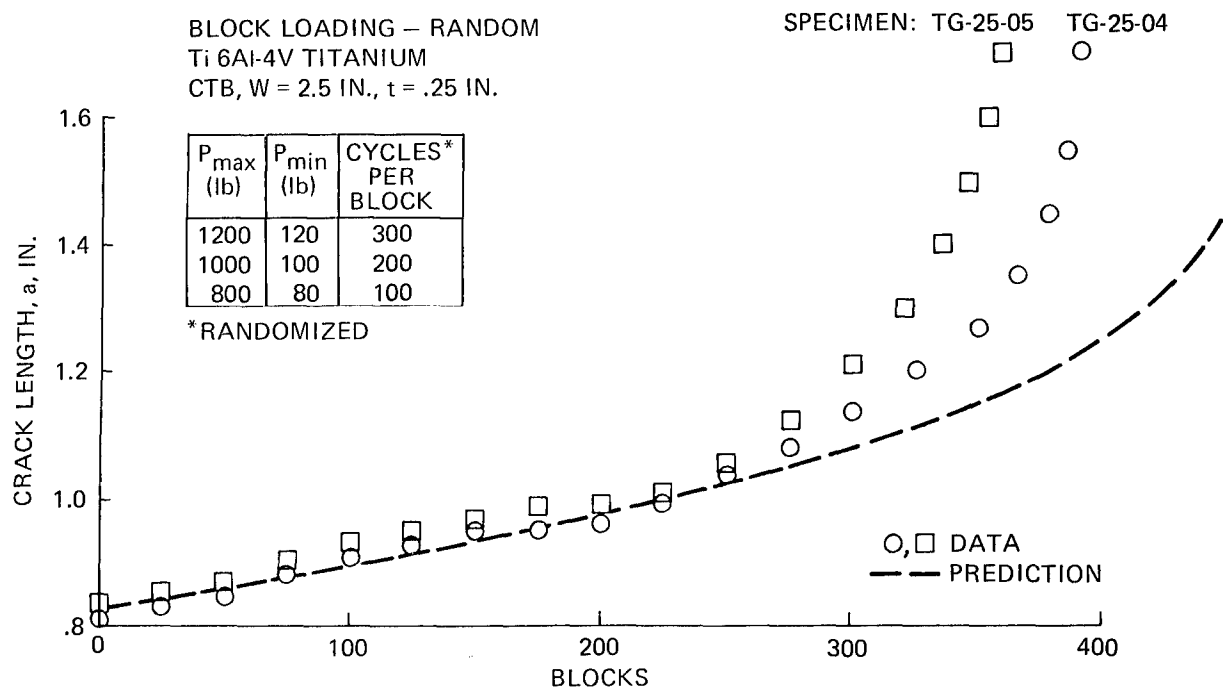


Fig. 197 Predicted a vs. B for Block Random Loading, Ti 6Al-4V Titanium

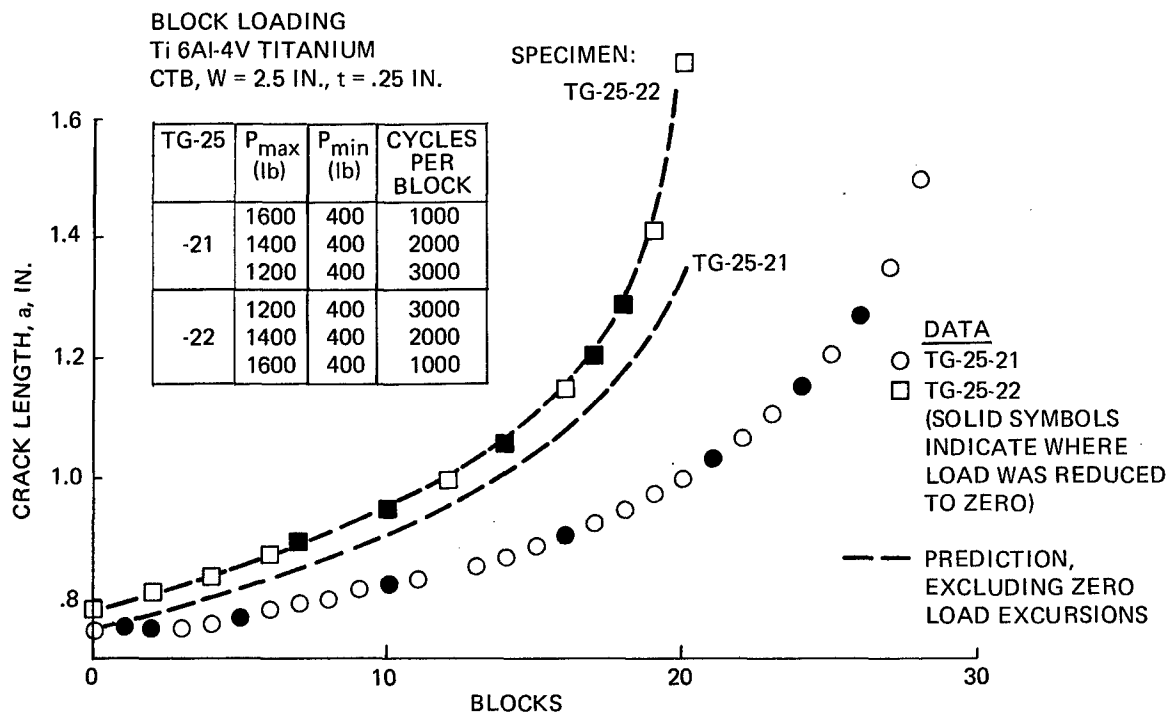


Fig. 198 Predicted a vs. B for High-Low and Low-High Block Loading, $R_{min} = 0.333$, Ti 6Al-4V Titanium

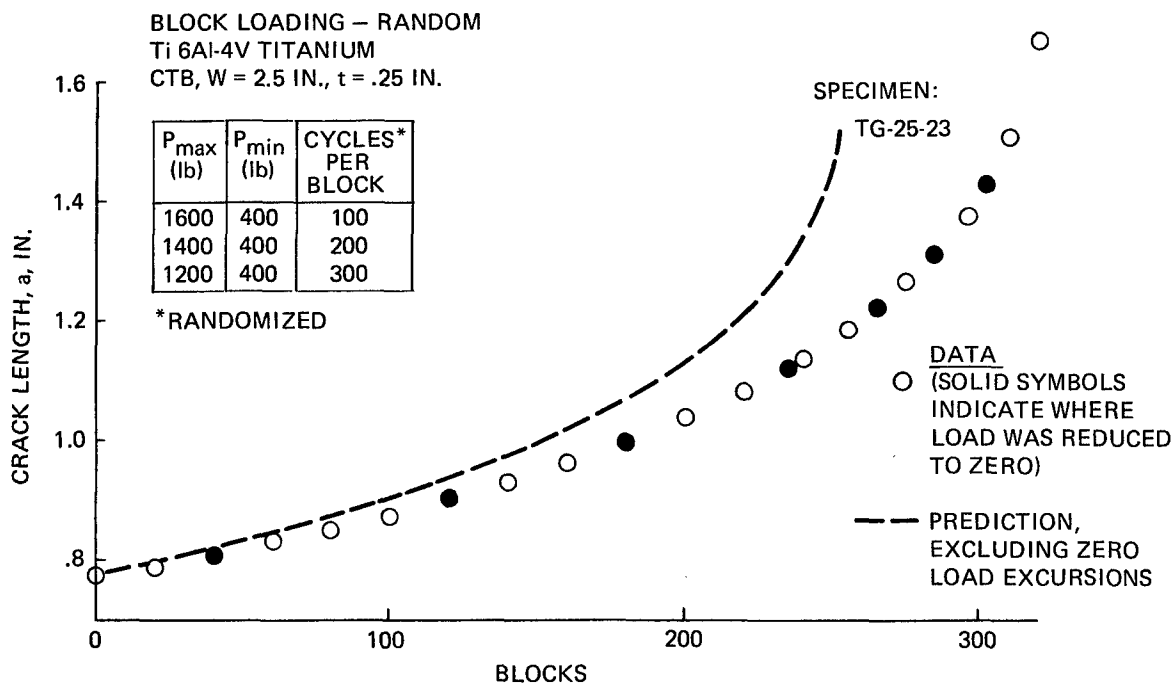


Fig. 199 Predicted a vs. B for Block Random Loading, $R_{min} = 0.333$, Ti 6Al-4V Titanium

BLOCK LOADING - 4 LEVEL
 Ti 6Al-4V TITANIUM
 CTB, W = 2.5 IN., t = .25 IN.

TG-25	P _{max} (lb)	P _{min} (lb)	CYCLES PER BLOCK
-19a	800	40	3000
	1000	40	2000
	1200	40	1000
	1600	40	1
-18	1600	40	1
	1200	40	1000
	1000	40	2000
	800	40	3000

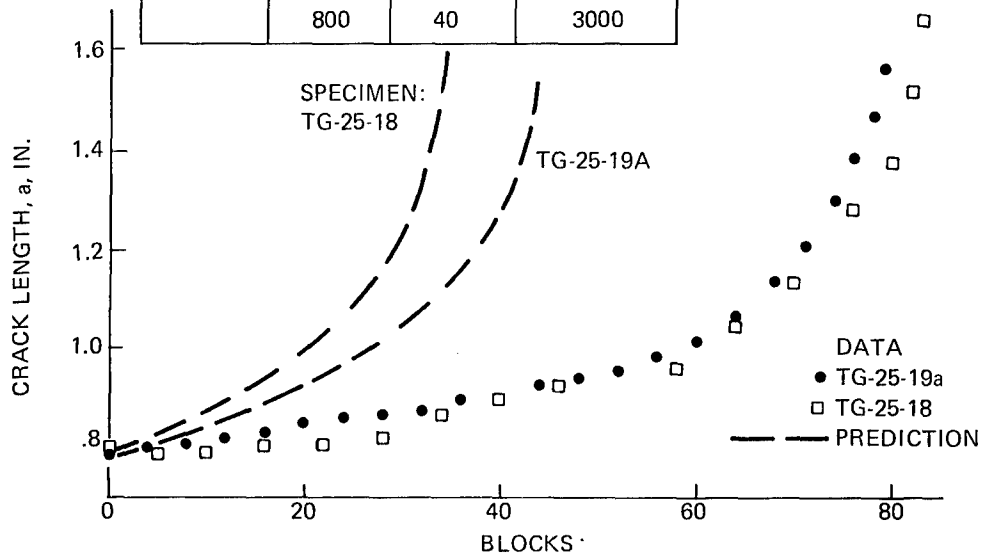


Fig. 200 Predicted a vs. B for High-Low and Low-High 4 Level Block Loading, Ti 6Al-4V Titanium

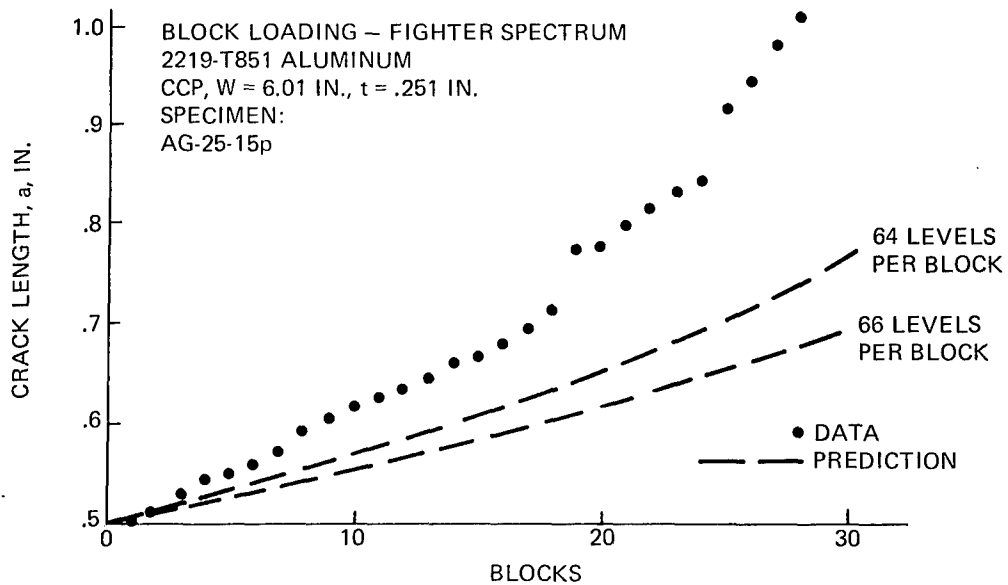


Fig. 201 Predicted a vs. B for Fighter Spectrum, 2219-T851 Aluminum

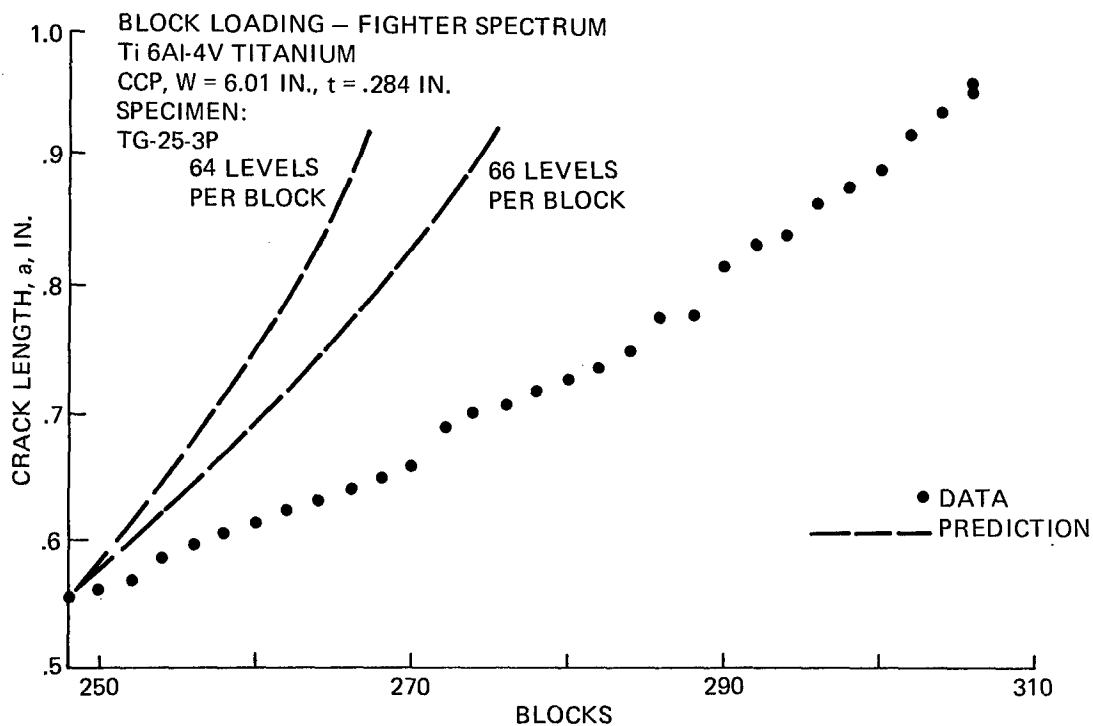


Fig. 202 Predicted a vs. B for Fighter Spectrum, Ti 6Al-4V Titanium

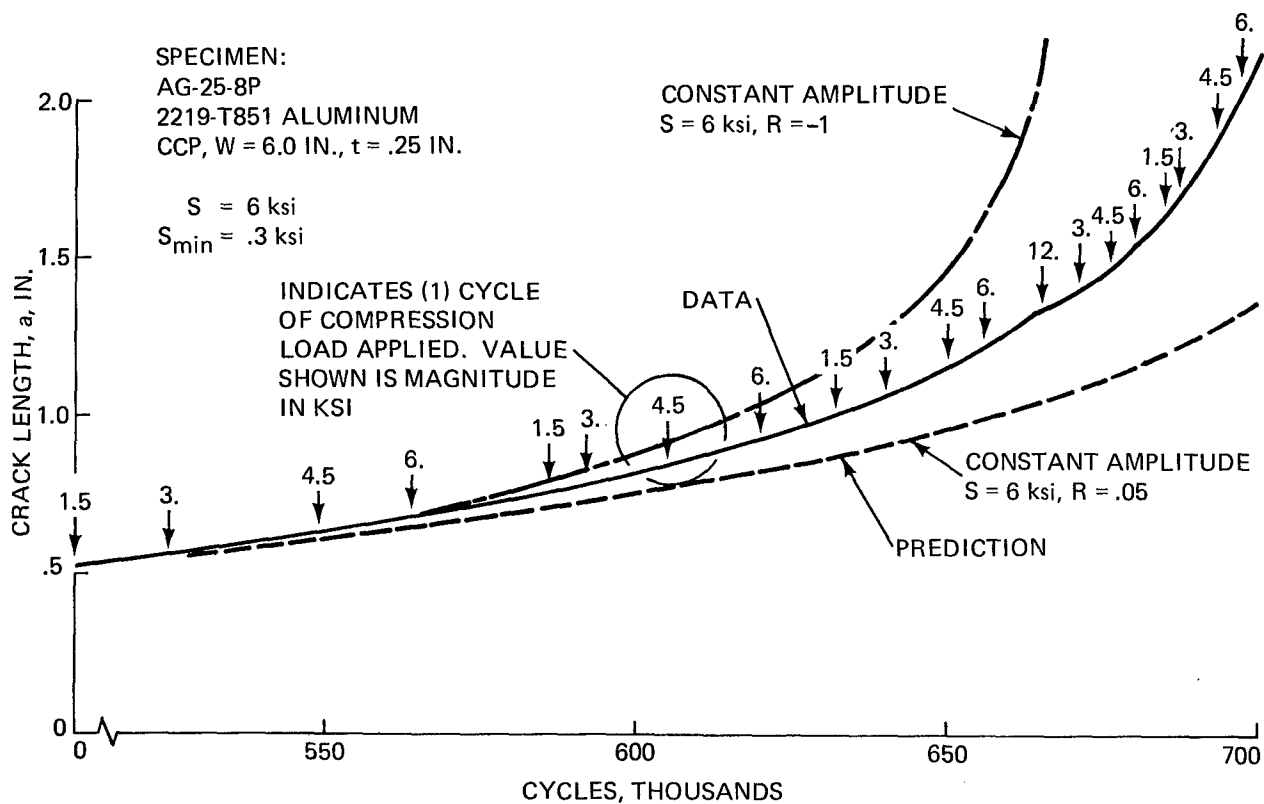


Fig. 203 Predicted a vs. N for Occasional Compression Loads, 2219-T851 Aluminum

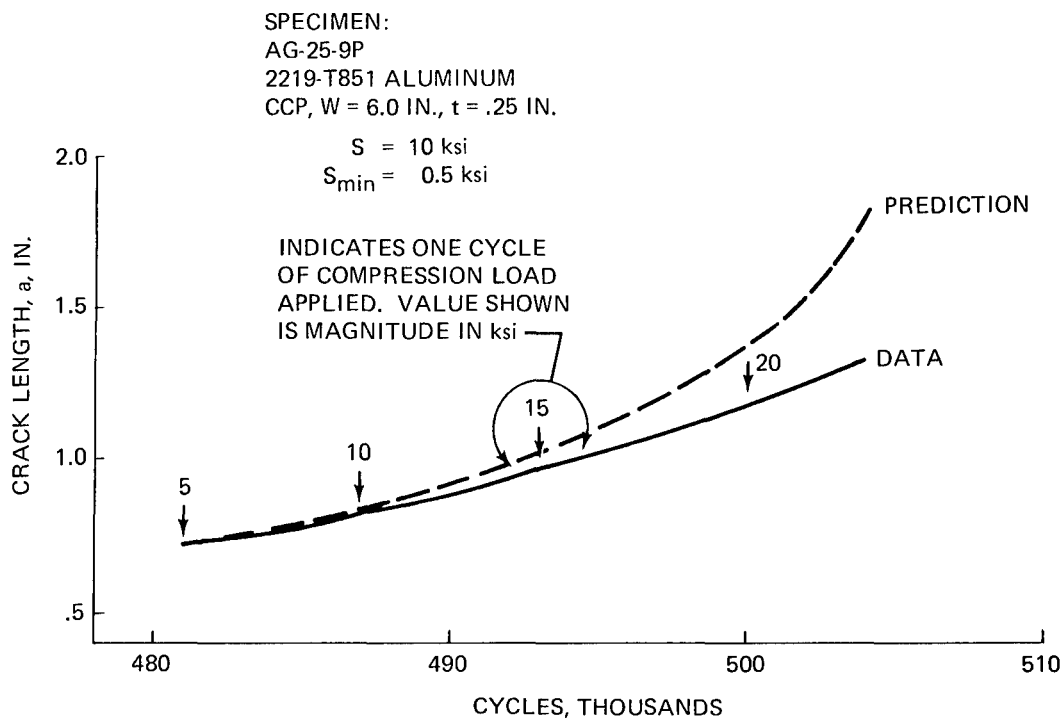


Fig. 204 Predicted a vs. N for Occasional Compression Loads, 2219-T851 Aluminum

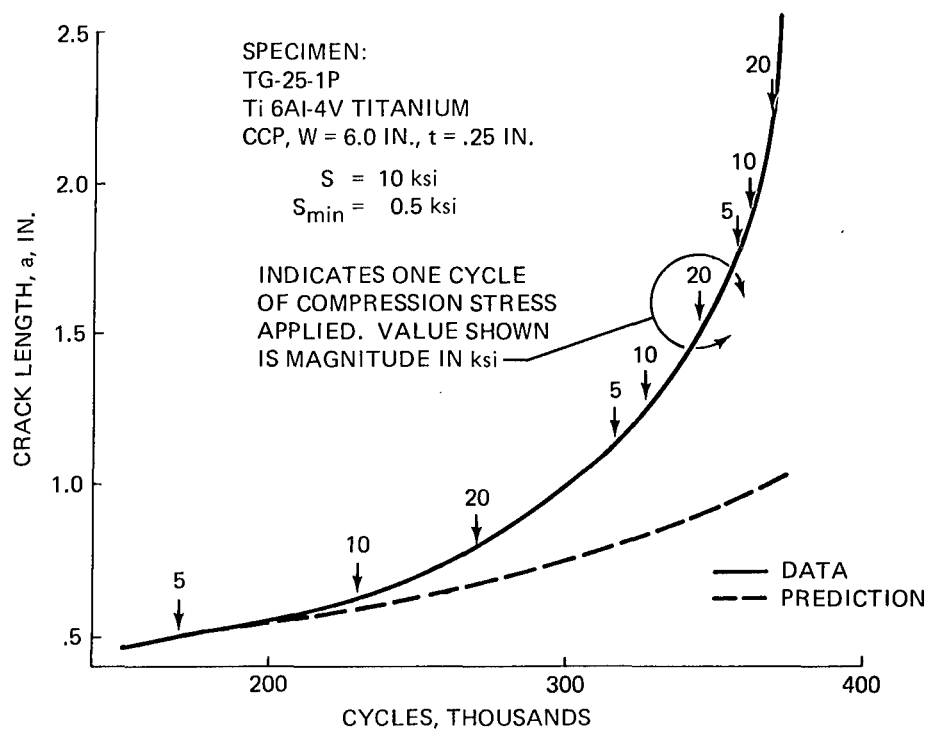


Fig. 205 Predicted a vs. N for Occasional Compression Loads, Ti 6Al-4V Titanium

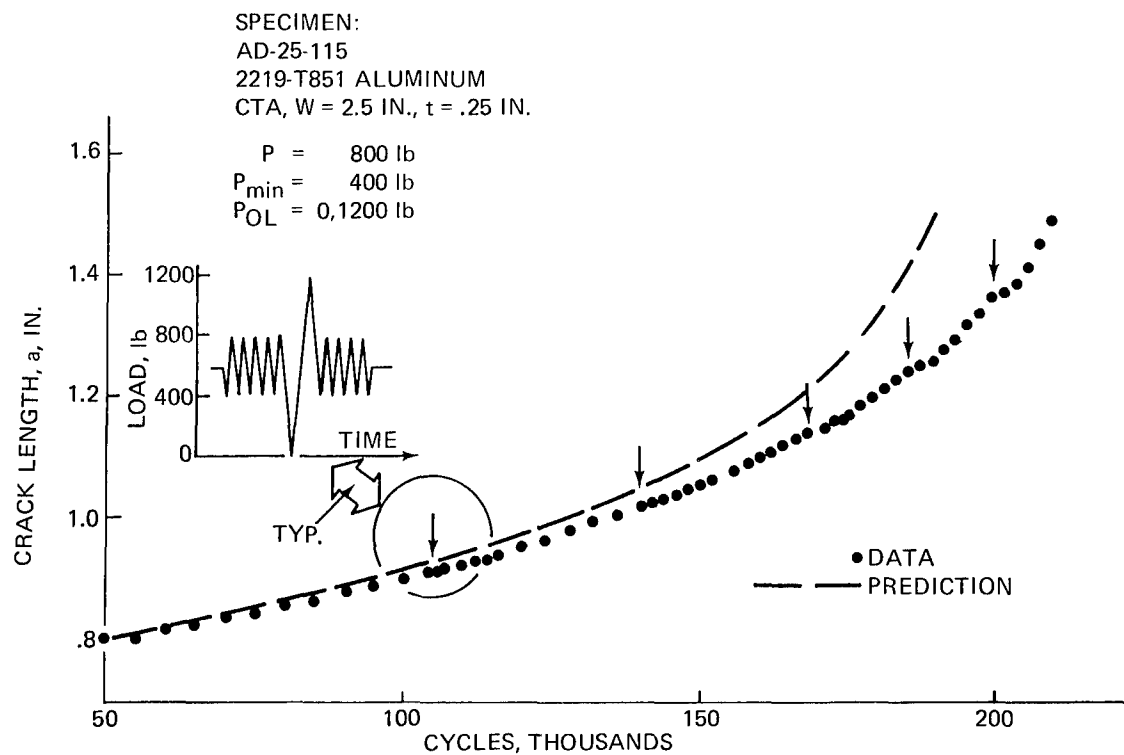


Fig. 208 Predicted a vs. N for Underload/Overload Spike Sequence, 2219-T851 Aluminum

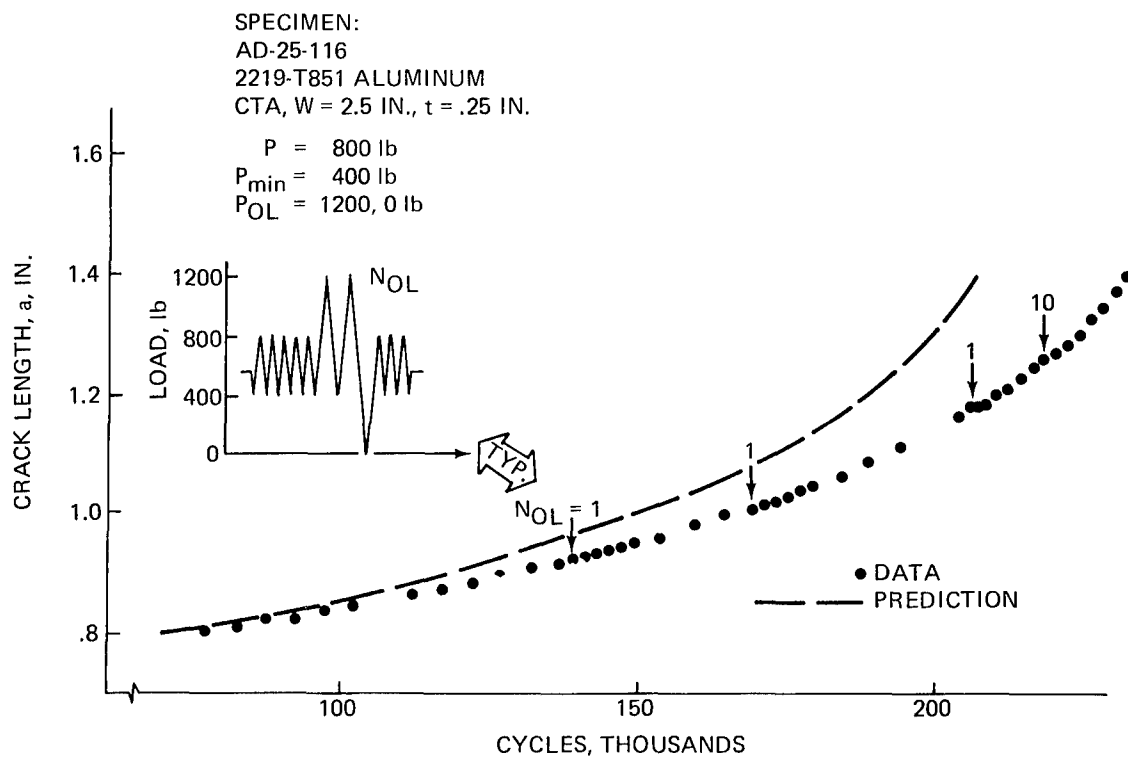


Fig. 209 Predicted a vs. N for Overload/Underload Spike Sequences, 2219-T851 Aluminum

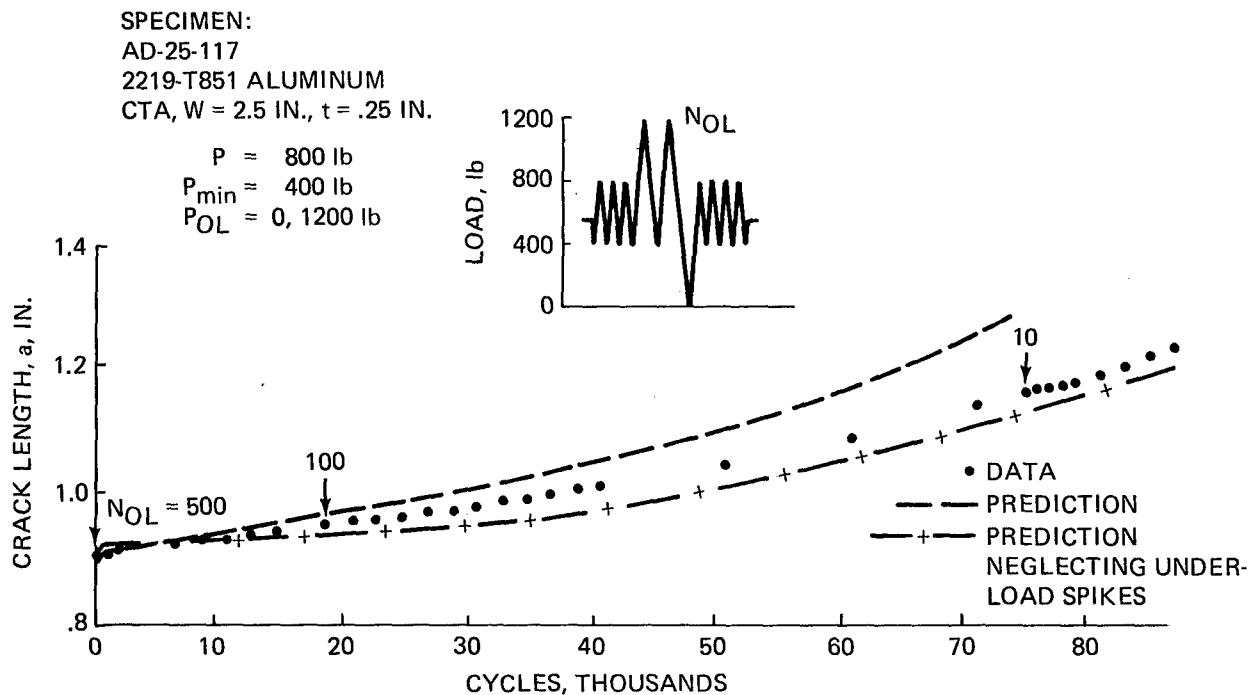


Fig. 210 Predicted a vs. N for Multiple Overload/Underload Spike Sequence, 2219-T851 Aluminum

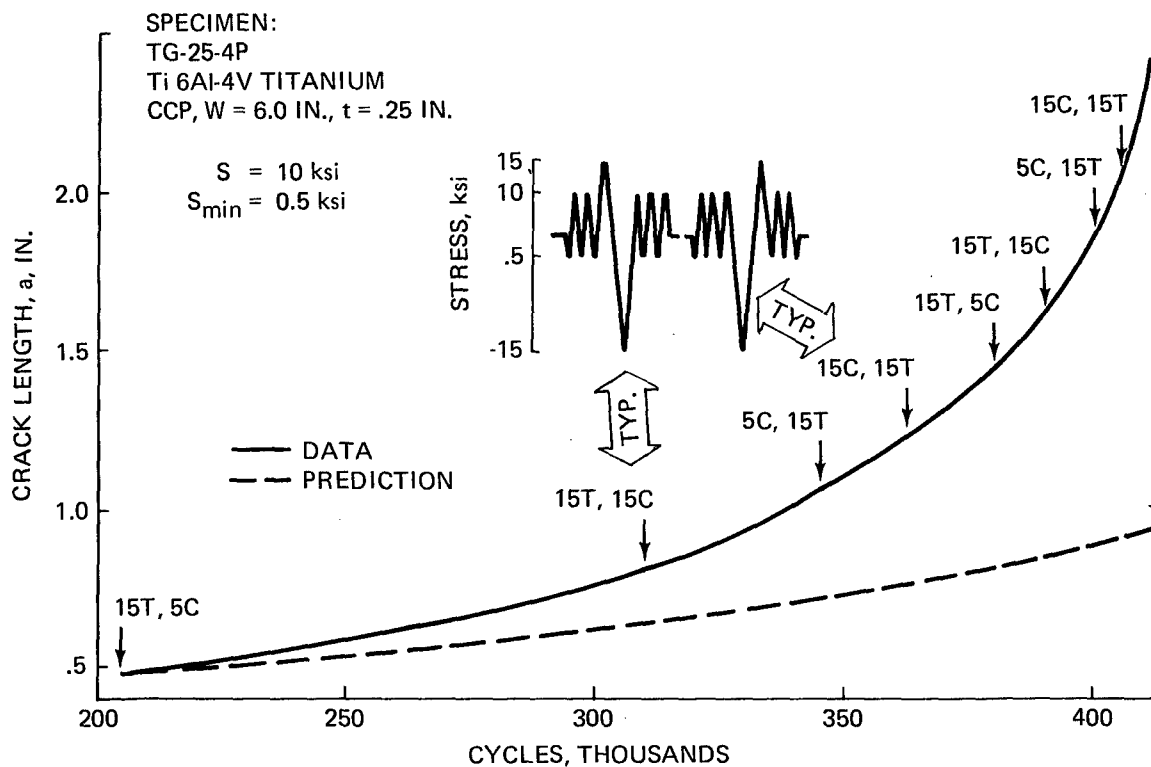


Fig. 211 Predicted a vs. N for Tension/Compression and Compression/Tension Spike Sequences, Ti 6Al-4V Titanium

SPECIMEN:
TD-25-119
Ti 6Al-4V TITANIUM

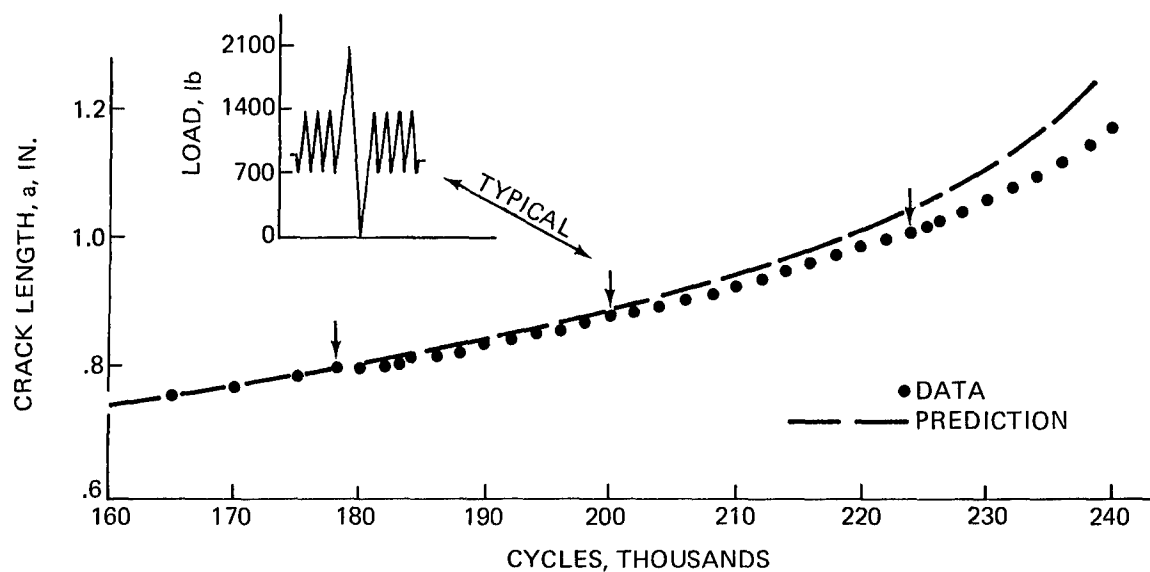


Fig. 212 Predicted a vs. N for Overload/Underload Spike Sequences, Ti 6Al-4V Titanium

SPECIMEN:
TD-25-118
Ti 6Al-4V TITANIUM
CTA, $W = 2.2$ IN., $t = .25$ IN.

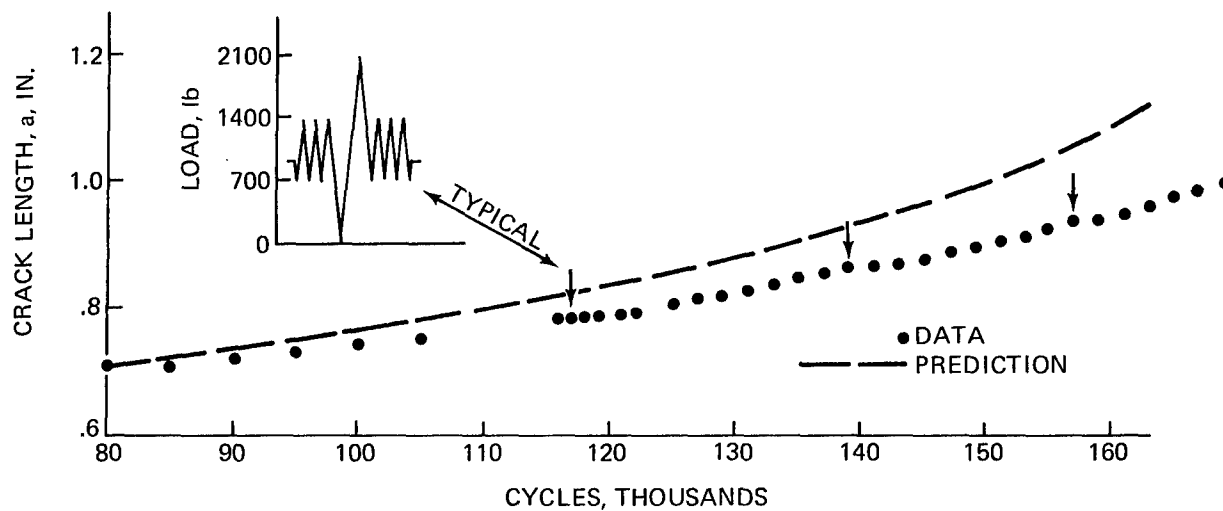


Fig. 213 Predicted a vs. N for Underload/Overload Spike Sequences, Ti 6Al-4V Titanium

SPECIMEN:
 TD-25-117
 Ti 6Al-4V TITANIUM
 CTA, W = 2.2 IN., t = .25 IN.

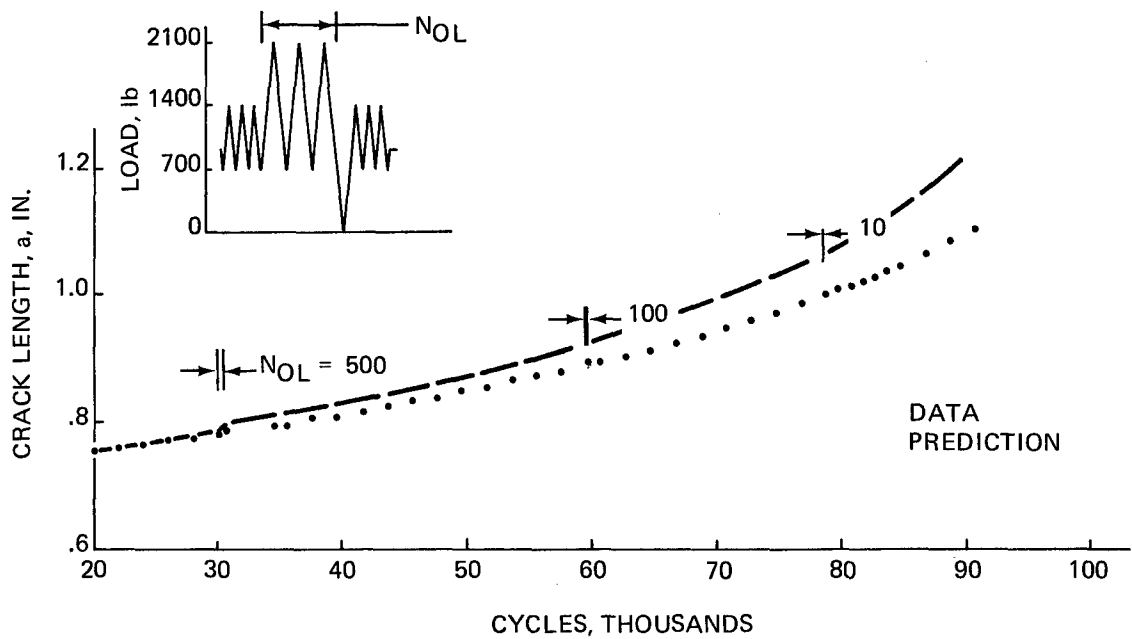


Fig. 214 Predicted a vs. N for Multiple Overload/Underload Spike Sequences, Ti 6Al-4V Titanium

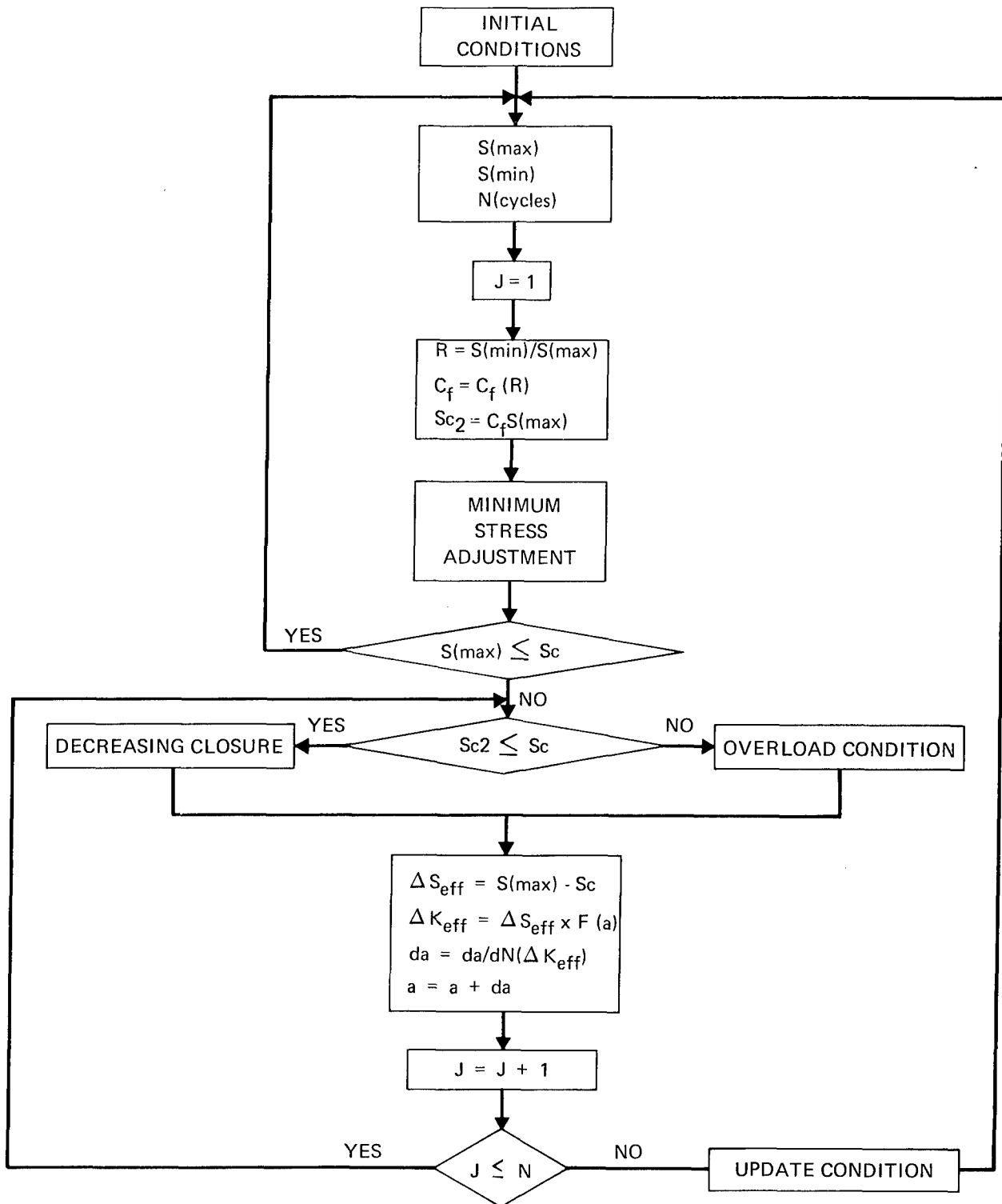


Fig. 215 Overall Logic Flow Chart

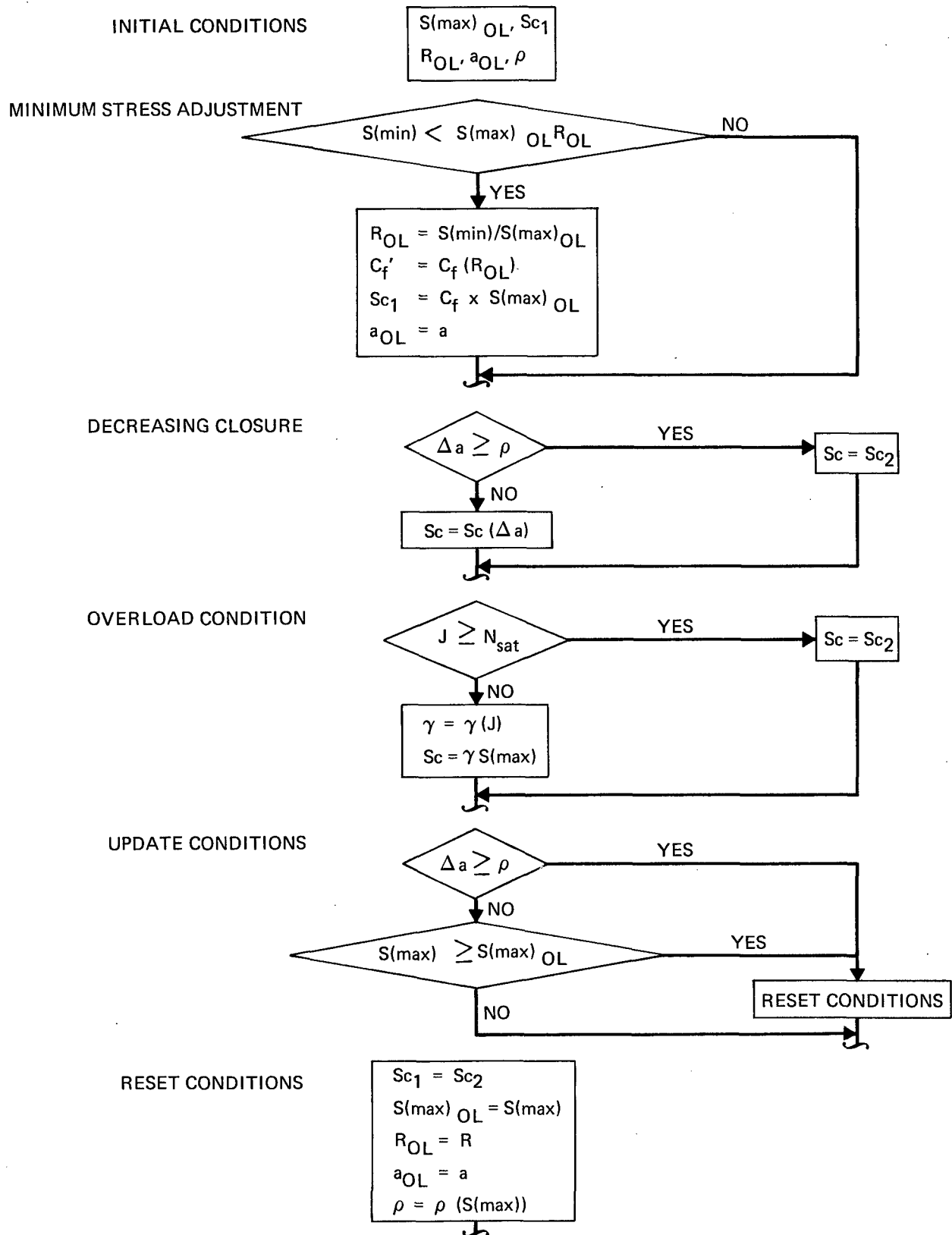


Fig. 216 Detail Logic Flow

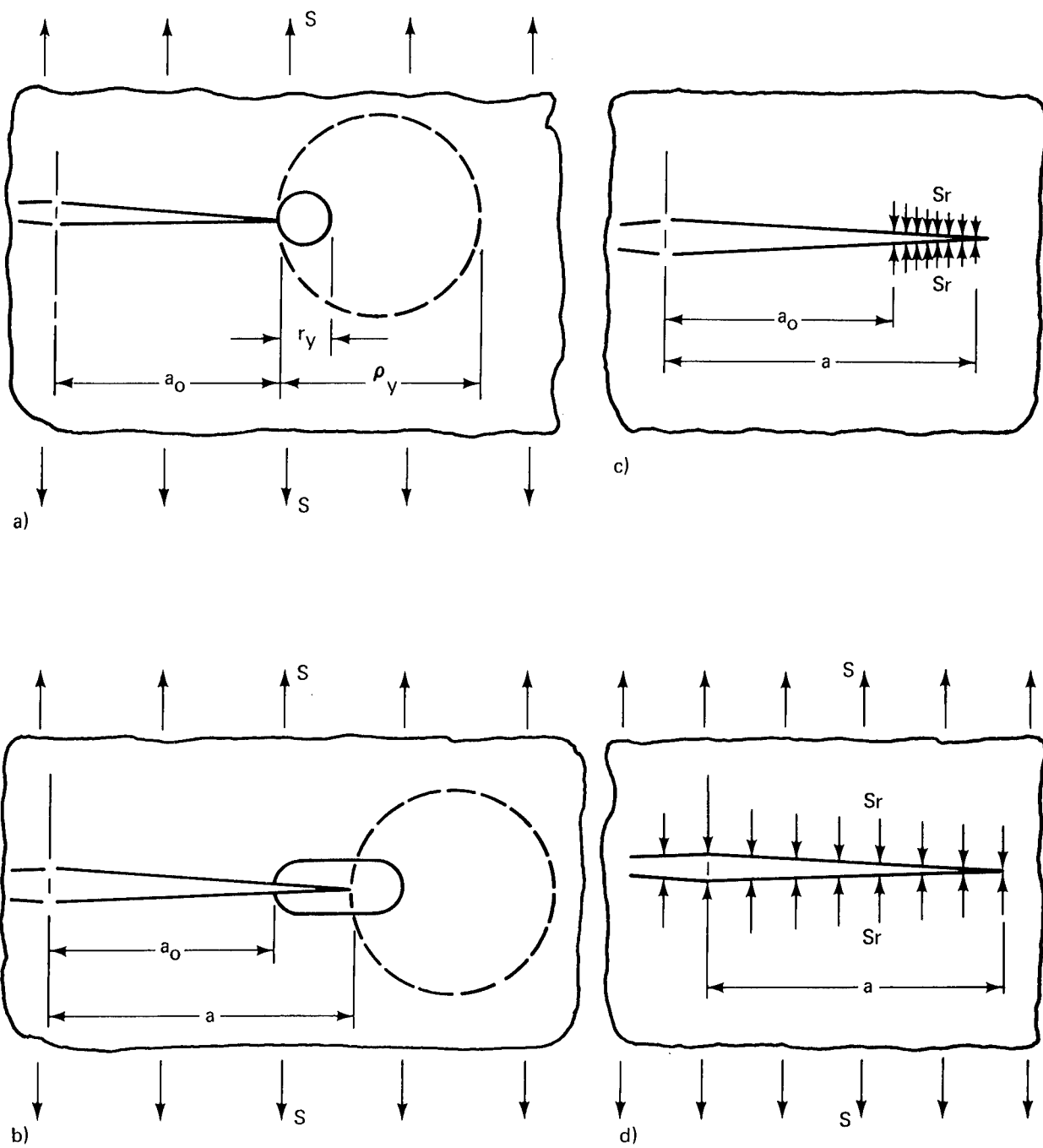


Fig. 217 Residual Stress Distributions

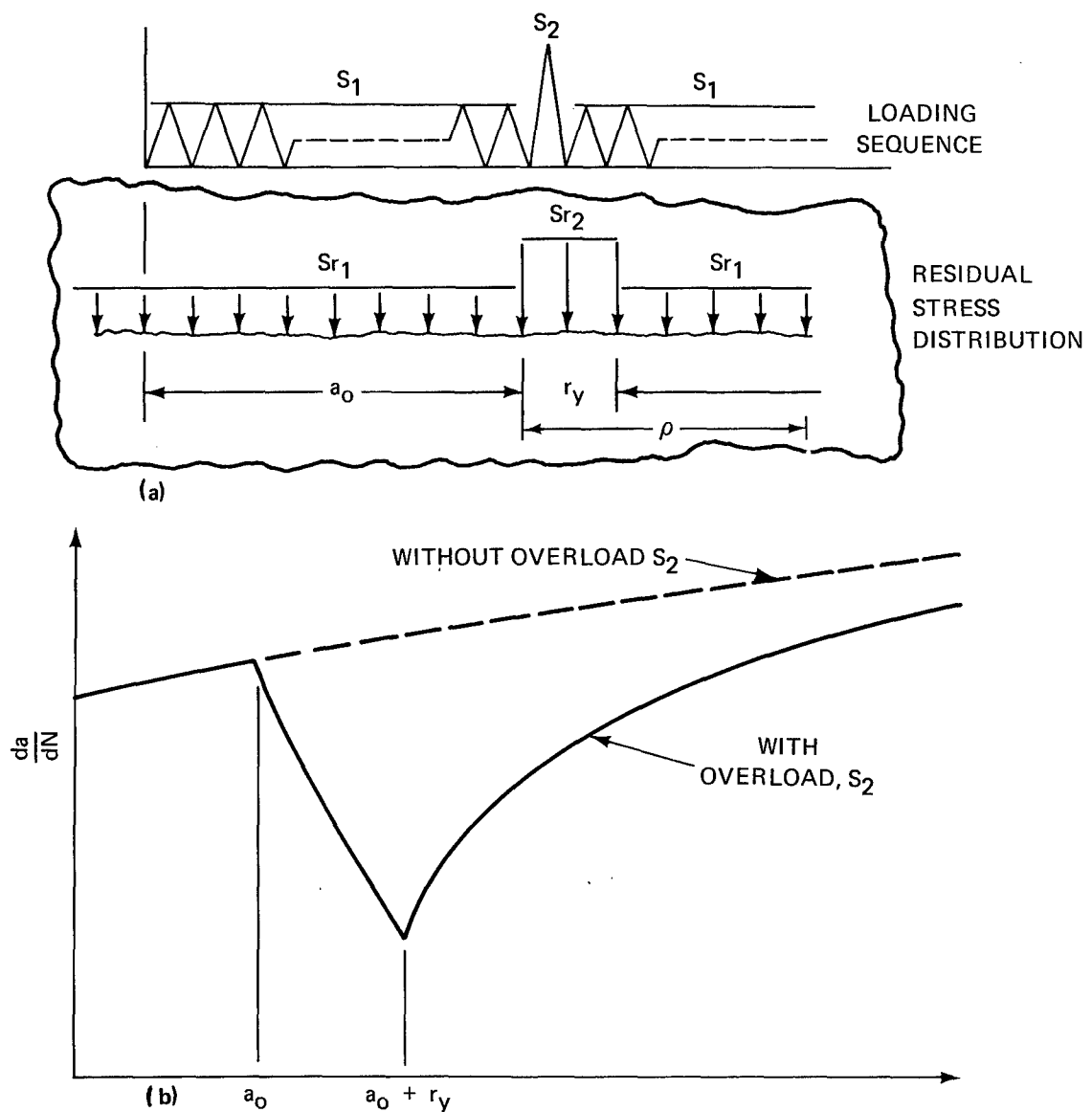


Fig. 218 Effect of a Single Overload on Residual Stresses and Subsequent Crack Growth Rate

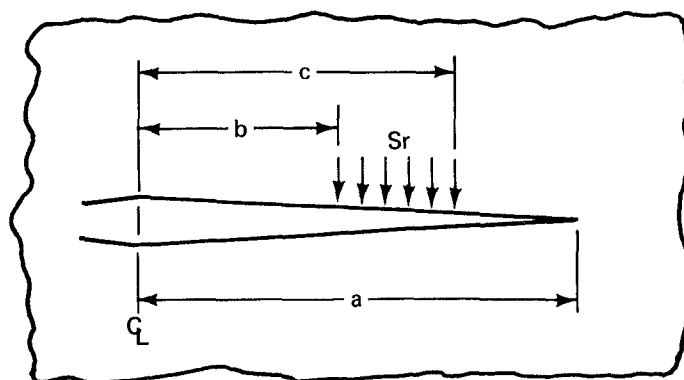


Fig. 219 Geometry for Stress on a Portion of a Crack

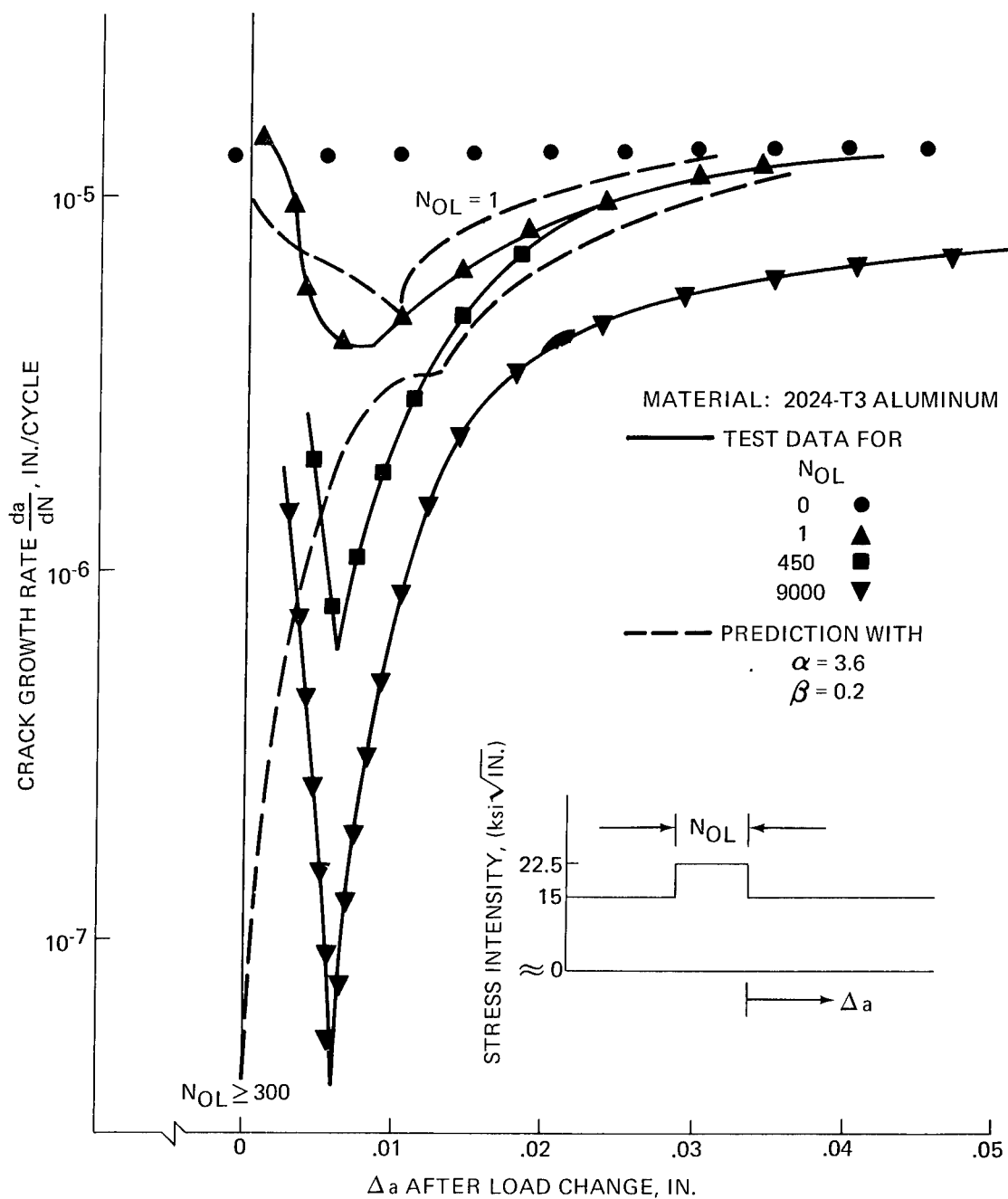


Fig. 220 Residual Force Predictions vs Data

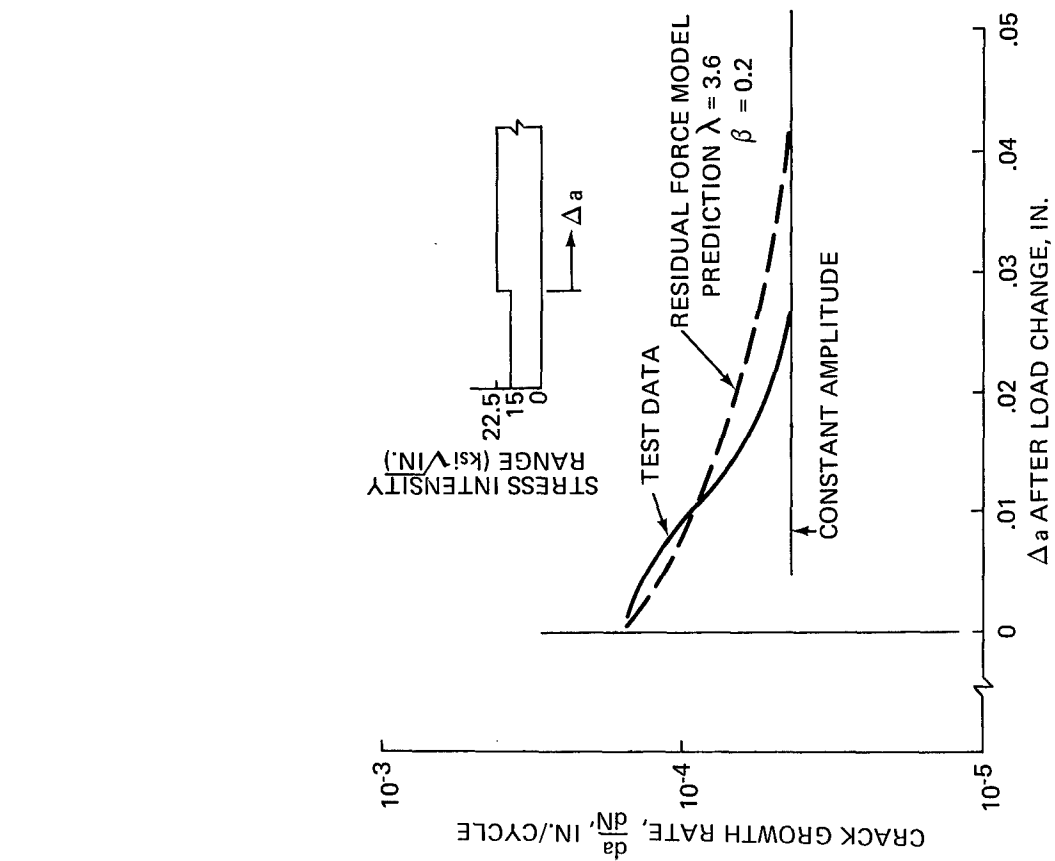
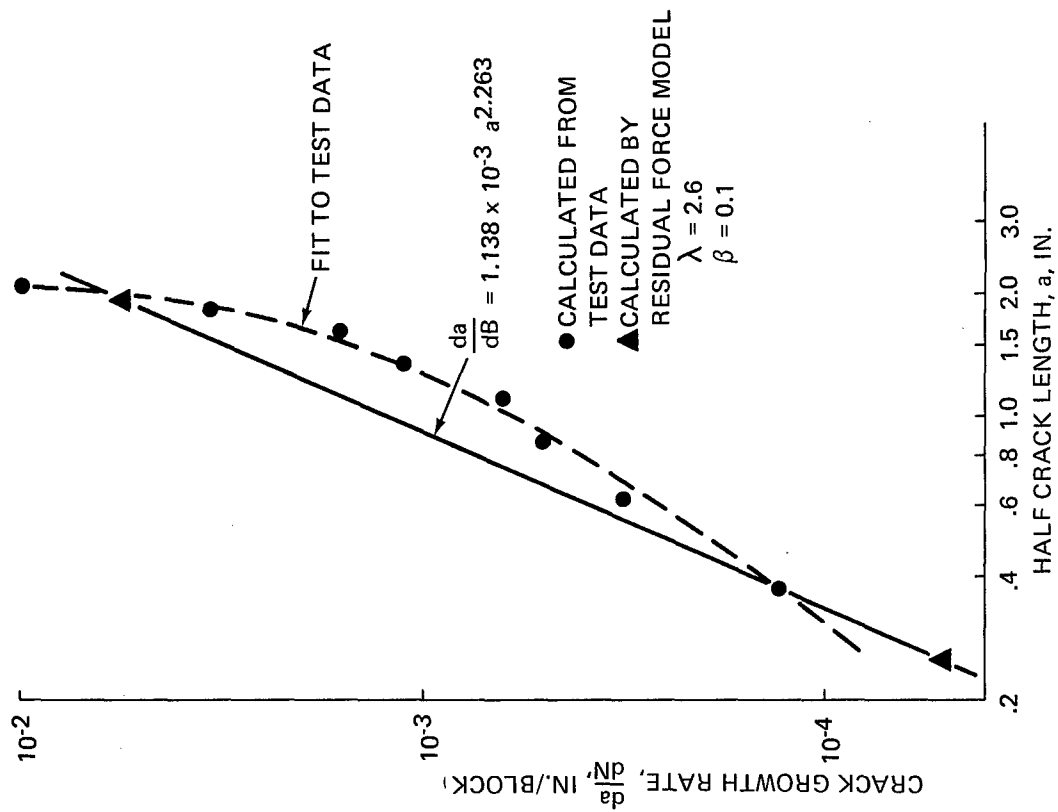


Fig. 221 Residual Force Predictions vs Data for Low-High Loading

Fig. 222 Rate vs a for Data and Residual Force Model

	x	y
1	0	50
2	50	0
3	1	50
4	3	↕
5	6	↕
6	10	↕
7	25	↕
8	50	50

Smax (ksi)	Smin (ksi)	CYCLES PER BLOCK
15	0	x
10	0	y

— TEST DATA
 - - - RESIDUAL FORCE MODEL
 PREDICTION

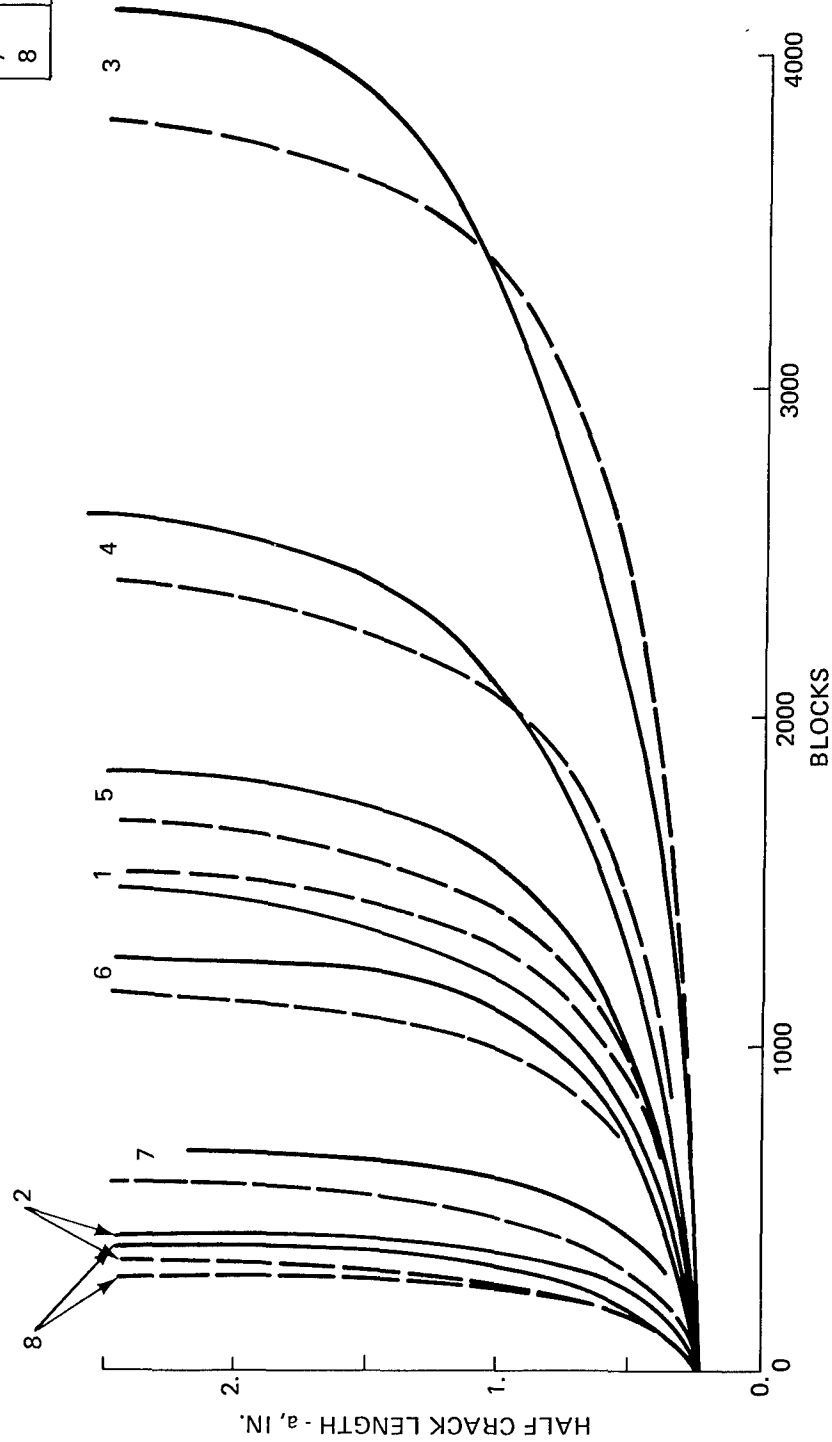


Fig. 223 Comparison of Predicted and Test Lives For 7075-T6 Aluminum Panel Specimens

TABLE 1 CONSTANT AMPLITUDE TEST PROGRAM

MATERIALS	SPEC. NO.	SPEC. TYPE	THICKNESS (INCH)	STRESS (LOAD) RATIO R	NOTES
Ti-6Al-4V Titanium	TG-25-1	CTB	.25	.05	<div> { Relative humidity= 95%, Cyclic frequency= ½ to 25 Hz. </div> <div> } S_{max} = 6 to 30 Ksi </div>
	2	CTB	.25	.05,.5	
	6	CTB	.25	.3	
	TD-25-1	CTA	.25	.05	
	3	CTA	.25	.05,.5	
	4	CTA	.25	.05	
	17	CTA	.25	.05,.5,.7	
	25	CTA	.25	.05,.3,.5	
	TG-75-1	CTB	.75	.01,.5	
	TG-25-6P	CCP	.25	0,.05,.7	
	2P	CCP	.25	.05,.5,.7	
	5P	CCP	.25	-1.	
2219-T851 Aluminum	AG-25-1	CTB	.25	-.1,-.3,.1,.3,.5,.7	<div> { Relative humidity= 95%, Cyclic frequency= ½ to 10 Hz </div> <div> } S_{max} = 6 to 16 ksi </div>
	-2a	CTB	.25	-1.	
	-20	CTB	.25	-1.	
	-21	CTB	.25	-1.	
	-27	CTB	.25	.05	
	-29	CTB	.25	0,.7	
	-30	CTB	.25	-.1,.1,.3,.5,.7	
	AD-25-6	CTA	.25	.05,.3,.5,.7,-1.	
	8	CTA	.25	.05,.3,.5,.7	
	9	CTA	.25	.05	
	10	CTA	.25	.05,.5	
	18	CTA	.25	.05,.5	
	AG-50-1	CTB	.50	.05	
	-25-1P	CCP	.25	.05,.50,.70	
	-7P	CCP	.25	-1.	
	-12P	CCP	.25	.05,.3,.4,.6	

TABLE 2 SINGLE-OVERLOAD TEST PLAN

a) Ti 6A1-4V Titanium

SPECIMEN NUMBER	SPECIMEN TYPE	OVERLOAD RATIO O/L	BASE LOAD STRESS RATIO R	CYCLES OF LOW LOAD BETWEEN OVERLOADS, N
TD-25- 2	CTA	1.8	.05	(2)
106	CTA	1.8	.05	(2)
109	CTA	1.8	.05	5000 (3)
16	CTA	1.5	.05	(2)
104	CTA	1.5	.05	(2)
105	CTA	1.5	.05	2000
13	CTA	1.25	.05	(2)
107	CTA	1.25	.05	(2)
108	CTA	1.25	.05	(3)
30	CTA	1.8	.05	500
37	CTA	1.8	.05	500
28	CTA	1.8	.05	1000
TG-25- 10	CTB	1.5	.075	(2)
TD-25- 32	CTA	1.25	.05	50
39	CTA	1.25	.05	50
31	CTA	1.25	.05	100
TG-25- 11	CTB	1.8	.075	(2)
TD-75- 3 (1)	CTA	1.8	.050	(2)

b) 2219-T851 Aluminum

AD-25- 7	CTA	1.8	.05	(2)
102	CTA	1.8	.05	(2), (3)
105	CTA	1.8	.05	(2), (3)
15	CTA	1.5	.05	(2)
106	CTA	1.5	.05	(3)
103	CTA	1.5	.05, .50	(3)
11	CTA	1.25	.05	(2)
101	CTA	1.25	.05	(2)
108	CTA	1.25	.70	(2), (3), (4)
26	CTA	1.8	.05	500
38	CTA	1.8	.05	500
43	CTA	1.8	.05	1000
AG-25- 12	CTB	1.25	.05	(2)
AD-25- 29	CTA	1.25	.05	50
45	CTA	1.25	.05	50
27	CTA	1.25	.05	100
AG-25- 11	CTB	1.5, 1.4	.05	(2)
- 2P	CCP	1.5	.05	(2)
- 3P	CCP	1.8	.05	(2)
- 4P	CCP	1.5	.05	(3)
- 6P	CCP	2.1, 1.25	.05	(2)

- (1) Thickness = .75 inch (all others .25 inch)
(2) N was large enough to prevent interaction of overloads
(3) N was selected to provide interaction of overloads
(4) Two or more consecutive overloads applied in some events

TABLE 3 OVERLOAD CRACK LENGTH,
STRESS INTENSITY AND NUMBER OF DELAY
CYCLES, N_D , FOR SPECIMEN AG-25-2P

HALF-CRACK LENGTH AT OVERLOAD, a (IN.)	K_{maxOL} (KSI $\sqrt{IN.}$)	DELAY CYCLES N_D
.490	18.6	600
.600	20.9	500
.677	22.5	600
.755	23.9	550
.842	25.7	750
1.045	29.4	800
1.222	32.8	1050
1.387	36.2	1000

TABLE 4 CALCULATED AND MEASURED PARAMETERS FOR
TITANIUM SINGLE OVERLOAD TESTS

SPECIMEN NO.	CRANK LENGTH AT OVERLOAD (INCH)	K_{maxOL} (KSI $\sqrt{IN.}$)	N_D (CYCLES)	PLANE STRESS PLASTIC ZONE RADIUS (INCH $\times 10^{-3}$)
TG-25-10	.887	22.1	21,500	4.6
	.994	25.0	4,300	5.9
	1.098	28.6	2,700	7.7
	1.189	32.2	~ 0	9.7
	1.264	35.6	~ 0	12.0
	1.383	42.5	1,100	16.9
	1.483	49.5	900	23.1
	1.581	58.5	500	32.2
TG-25-11	.873	26.1	$\sim 44,000$	6.4
	.950	27.9	27,500	7.3
	1.059	32.6	16,000	10.0
	1.147	36.6	9,000	12.5
	1.250	42.0	9,000	16.6
	1.345	48.0	4,800	21.8
	1.440	55.5	3,800	29.1
	1.550	66.5	2,500	41.6
	1.650	79.6	2,500	59.9
	1.760	100.4	2,000	94.7

TABLE 5 MULTIPLE OVERLOAD TEST PLAN

a) 2219-T851 Aluminum

SPECIMEN NO.	OVERLOAD RATIO	BASLINE STRESS RATIO	OVERLOAD STRESS RATIO	NO. OF OVERLOADS	NO. OF BASELINE LOADS
AD-25-12	1.5	.05	(1)	LARGE	(2)
-104	1.5	.05	(1)	VARIOUS	(2)
-20	1.5	.50	(1)	LARGE	(2)
-109	1.5	.05	(1)	VARIOUS	(2)
-111	1.5	.50	.67	LARGE	(2)
-112	1.5	.50	.67	LARGE	(2)
-19	1.25	.05	(1)	LARGE	(2)
-115a	1.8	.05	.77	VARIOUS	(2)
-24	1.25	.50	.40	LARGE	(2)
-114	1.25	.05	.55	VARIOUS	(2)
-110	1.8	.05	(1)	VARIOUS	(2)
-107	1.8	.05	(1)	VARIOUS	(2)
-33	1.5	.05	(1)	50	500
-34	1.5	.05	(1)	100	1000
-57	1.5	.05	(1)	100	500
-59	1.5	.05	(1)	200	1000
-55	1.25	.05	(1)	100	1000
-51	1.25	.05	(1)	500	5000
-47	1.25	.50	(1)	200	1000
-53	1.25	.50	(1)	1000	5000
AD-25-35	1.5	.05	(1)	10	500
AG-25-5P	1.5	.05	(1)	LARGE	(2)

b) Ti 6Al-4V Titanium

TD-25-14	1.5	.05	(1)	LARGE	(2)
-21	1.5	.50	(1)	LARGE	(2)
-115	1.5	.30	(1)	VARIOUS	(2)
-116	1.5	.30	(1)	VARIOUS	(2)
-112	1.5	.05	(1)	VARIOUS	(2)
-102	1.5	.05	(1)	VARIOUS	(2)
-5	1.25	.05	(1)	LARGE	(2)
-114	1.25	.05	(1)	VARIOUS	(2)
-23	1.25	.50	(1)	LARGE	(2)
-113	1.25	.30	(1)	VARIOUS	(2)
-111	1.8	.05	.55	VARIOUS	(2)
-110	1.8	.05	(1)	VARIOUS	(2)
-54	1.5	.05	(1)	50	500
-42	1.5	.05	(1)	100	500
-36	1.5	.05	(1)	50	500
-50	1.5	.05	(1)	100	1000
-40	1.5	.05	(1)	100	1000
-58	1.5	.05	(1)	100	500
-52	1.5	.05	(1)	200	1000
-44	1.5	.05	(1)	200	1000
-46	1.25	.05	(1)	100	1000
-56	1.25	.05	(1)	500	5000
-48	1.25	.70	(1)	200	1000
TD-25-103	1.25	.05	(1)	1000	5000
TD-75- 1 (3)	1.5	.05	(1)	100	1000
2 (3)	1.5	.05	(1)	VARIOUS	(2)
TD-75- 4 (3)	1.5	.05	(1)	LARGE	(2)

(1) Selected so that the minimum loads were equal for overloads and base line loads.

(2) Sufficient to reestablish constant amplitude crack growth conditions.

(3) These specimens 3/4 inch thick, all others 1/4 inch.

TABLE 6. POSSIBLE PLASTIC ZONE CALCULATIONS

$$\rho_1 = \frac{1}{2\pi} \left(\frac{K_{\max_{OL}}}{\sigma_y} \right)^2$$

$$\rho_2 = \frac{1}{2\pi} \left(\frac{K_{\max_{OL}} - K_{\min_{OL}}}{\sigma_y} \right)^2 = \frac{1}{2\pi} \left(\frac{\Delta K_{OL}}{\sigma_y} \right)^2$$

$$\rho_3 = \frac{1}{2\pi} \left(\frac{K_{\max_{OL}} - K_{\min}}{\sigma_y} \right)^2$$

$$\rho_4 = \frac{1}{2\pi} \left(\frac{K_{\max_{OL}} - K_{c_I}^*}{\sigma_y} \right)^2$$

$$\rho_5 = \frac{1}{2\pi} \left(\frac{K_{\max_{OL}} - K_{c_{II}}^{**}}{\sigma_y} \right)^2$$

* K_{c_I} calculated using $K_{\max_{OL}}$ and $K_{\min_{OL}}$

** $K_{c_{II}}$ calculated using $K_{\max_{OL}}$ and K_{\min}

**TABLE 7 COMPARISON OF MEASURED AND CALCULATED VALUES
OF r_y AFTER MULTIPLE OVERLOADS**

SPECIMEN NO.	A (IN.)	r_y (MEAS) (IN.)	$\left(\frac{K_{\max OL}}{.25 \rho_1} \right)$	$\left(\frac{\Delta K_{OL}}{.25 \rho_2} \right)$	$\left(\frac{K_{OL} - K_{\min}}{.25 \rho_3} \right)$	$\left(\frac{K_{\max OL} - K_{C_I}}{\rho_4} \right)$	$\left(\frac{K_{\max OL} - K_{C_{II}}}{\rho_5} \right)$
AD-25-109	.89	.0035	$\left(\frac{13.6}{.0025} \right)$	$\left(\frac{13.15}{.0023} \right)$	$\left(\frac{13.15}{.0023} \right)$	$\left(\frac{8.2}{.0036} \right)$	$\left(\frac{8.2}{.0036} \right)$
AD-25-110	.910	.007	$\left(\frac{19.66}{.005} \right)$	$\left(\frac{19.12}{.005} \right)$	$\left(\frac{19.12}{.005} \right)$	$\left(\frac{11.8}{.0074} \right)$	$\left(\frac{11.8}{.0074} \right)$
AD-25-110	1.156	.010	$\left(\frac{25.2}{.0085} \right)$	$\left(\frac{24.5}{.008} \right)$	$\left(\frac{24.5}{.008} \right)$	$\left(\frac{15.1}{.012} \right)$	$\left(\frac{15.1}{.012} \right)$
AD-25-111	.893	.004	$\left(\frac{13.6}{.0025} \right)$	$\left(\frac{13.15}{.0023} \right)$	$\left(\frac{13.15}{.0023} \right)$	$\left(\frac{8.2}{.0036} \right)$	$\left(\frac{8.2}{.0036} \right)$
AD-25-111	1.013	.006	$\left(\frac{22.2}{.00675} \right)$	$\left(\frac{7.4}{.00075} \right)$	$\left(\frac{14.8}{.003} \right)$	$\left(\frac{6.66}{.002} \right)$	$\left(\frac{11.1}{.007} \right)$
AD-25-111	1.097	.010	$\left(\frac{24.2}{.008} \right)$	$\left(\frac{8.1}{.0009} \right)$	$\left(\frac{16.2}{.0036} \right)$	$\left(\frac{7.3}{.0024} \right)$	$\left(\frac{12.1}{.0025} \right)$
AD-25-112	.900	.004	$\left(\frac{19.9}{.005} \right)$	$\left(\frac{6.6}{.0006} \right)$	$\left(\frac{13.3}{.0024} \right)$	$\left(\frac{6.0}{.002} \right)$	$\left(\frac{10.0}{.005} \right)$
AD-25-112	.971	.003	$\left(\frac{21.4}{.006} \right)$	$\left(\frac{7.1}{.00067} \right)$	$\left(\frac{14.2}{.0027} \right)$	$\left(\frac{6.4}{.002} \right)$	$\left(\frac{10.7}{.006} \right)$
AD-25-114	1.145	.011	$\left(\frac{25.6}{.0085} \right)$	$\left(\frac{8.5}{.001} \right)$	$\left(\frac{17.0}{.004} \right)$	$\left(\frac{7.7}{.003} \right)$	$\left(\frac{12.8}{.009} \right)$
AD-25-115	.801	.0045	$\left(\frac{17.8}{.004} \right)$	$\left(\frac{4.0}{.0002} \right)$	$\left(\frac{17.3}{.004} \right)$	$\left(\frac{3.6}{.0007} \right)$	$\left(\frac{10.7}{.006} \right)$
AD-25-20	1.205	.007	$\left(\frac{23.9}{.0076} \right)$	$\left(\frac{15.9}{.0034} \right)$	$\left(\frac{15.9}{.0034} \right)$	$\left(\frac{11.95}{.0076} \right)$	$\left(\frac{11.95}{.0076} \right)$

NOTE: Values of K are ksi $\sqrt{\text{in.}}$
Values of .25 ρ and ρ are in.

TABLE 7 (CONT'D) LOADING RELATIONSHIPS

SPECIMEN NO.	BASELINE STRESS RATIO	OVERLOAD STRESS RATIO	OVERLOAD RATIO
AD-25-109	.05	.033	1.5
110	.05	.028	1.8
111	.50	.67	1.5
112	.50	.67	1.5
114	.05	.56	1.8
115	.05	.78	1.8
20	.50	.33	1.5

TABLE 8 VARIABLE AMPLITUDE TEST

a) 2219-T851 Aluminum

SPECIMEN NO.	SPECIMEN TYPE	LOADING PROGRAM	COMMENTS
AG-25-6	CTB	AHL-3	
-7	CTB	AHL-3	
-8	CTB	ALH-3	
-9	CTB	ALH-3	
-4	CTB	AR-3	
-5	CTB	AR-3	
-2	CTB	AHL-3a	
-3	CTB	AHL-3	
-13	CTB	ALH-3	WITH OCCASSIONAL 750 lb. COMPRESSION LOADS
-14	CTB	ALH-3	WITH OCCASSIONAL 250 lb. COMPRESSION LOADS
-16	CTB	AHL-3	WITH OCCASSIONAL 750 lb. COMPRESSION LOADS
-15	CTB	AHL-3	WITH OCCASSIONAL 250 lb. COMPRESSION LOADS
-18	CTB	AR-3	WITH OCCASSIONAL 750 lb. COMPRESSION LOADS
-19	CTB	AR-3	WITH OCCASSIONAL 250 lb. COMPRESSION LOADS
-22	CTB	AHL-3b	WITH OCCASSIONAL ZERO LOADS
-23	CTB	ALH-3b	WITH OCCASSIONAL ZERO LOADS
-24	CTB	AR-3b	WITH OCCASSIONAL ZERO LOADS
-28	CTB	AR-3b	WITH OCCASSIONAL ZERO LOADS
-25	CTB	ALH-4	
-11P	CCP	AHL-3s	WITH OCCASSIONAL 2.5 AND 7.5 KSI COMPRES-
-14P	CCP	ALH-3s	SION STRESSES
-13P	CCP	AR-3s	
AG-25-15P	CCP	FIGHTER	LIMIT STRESS = 30.9 KSI (SEE TABLE 9d FOR SEQUENCE)

b) Ti 6A1-4V Titanium

TG-25-3	CTB	ALH-3	
-9	CTB	TLH-3	
-7	CTB	THL-3	
-8	CTB	THL-3	
-4	CTB	TR-3	
-5	CTB	TR-3	
-17	CTB	TLH-3	WITH OCCASSIONAL 1200 lb. COMPRESSION LOAD
-16	CTB	TLH-3	WITH OCCASSIONAL 400 lb. COMPRESSION LOAD
-15	CTB	THL-3	WITH OCCASSIONAL 1200 lb. COMPRESSION LOAD
-14	CTB	THL-3	WITH OCCASSIONAL 400 lb. COMPRESSION LOAD
-13	CTB	TR-3	WITH OCCASSIONAL 1200 lb. COMPRESSION LOAD
-12	CTB	TR-3	WITH OCCASSIONAL 400 lb. COMPRESSION LOAD
-21	CTB	THL-3b	WITH OCCASSIONAL ZERO LOADS
-22	CTB	TLH-3b	WITH OCCASSIONAL ZERO LOADS
-23	CTB	TR-3b	WITH OCCASSIONAL ZERO LOADS
-18	CTB	THL-4	
-19a	CTB	TLH-4	
-20	CTB	TR-4	
TG-25-3P	CCP	FIGHTER	LIMIT STRESS = 61.9 KSI (SEE TABLE 9d FOR SEQUENCE AND LOADS)

TABLE 9a VARIABLE AMPLITUDE LOADING PROGRAMS FOR 2219-T851 ALUMINUM

LOADING PROGRAM	LAYER	Pmax (LB)	Pmin (LB)	CYCLES PER BLOCK
AHL-3	1	750	25	100
	2	625	25	200
	3	500	25	300
ALH-3	1	500	25	3000
	2	625	25	2000
	3	750	25	1000
AR-3 ⁽¹⁾	A	500	25	300
	B	625	25	200
	C	750	25	100
AHL-3a	1	1200	120	1000
	2	1000	100	2000
	3	800	80	3000
AHL-3b	1	1250	500	1000
	2	1125	500	2000
	3	1000	500	3000
ALH-3b	1	1000	500	3000
	2	1125	500	2000
	3	1250	500	1000
AR-3b ⁽¹⁾	A	1000	500	300
	B	1125	500	200
	C	1250	500	100
ALH-4	1	500	25	3000
	2	625	25	2000
	3	750	25	1000
	4	1000	25	1

(1) Randomized block - See Table 9c for sequence

LOADING PROGRAM	LAYER	Smax (ksi)	Smin (ksi)	CYCLES PER BLOCK
AHL-3s	1	7.5	.25	1000
	2	6.25	.25	2000
	3	5.0	.25	3000
ALH-3s	1	5.0	.25	3000
	2	6.25	.25	2000
	3	7.5	.25	1000
AR-3s ⁽¹⁾	A	5.0	.25	300
	B	6.25	.25	200
	C	7.5	.25	100

(1) Randomized block - See Table 9c for sequence

TABLE 9b VARIABLE AMPLITUDE LOADING PROGRAMS FOR Ti 6A1-4V TITANIUM

LOADING PROGRAM	LAYER	Pmax (LB)	Pmin (LB)	CYCLES PER BLOCK
TLH-3	1	800	40	3000
	2	1000	40	2000
	3	1200	40	1000
THL-3	1	1200	40	1000
	2	1000	40	2000
	3	800	40	3000
TR-3a ⁽¹⁾	A	1200	40	300
	B	1000	40	200
	C	800	40	100
TR-3 ⁽¹⁾	A	800	80	300
	B	1000	100	200
	C	1200	120	100
THL-3b	1	1600	400	1000
	2	1400	400	2000
	3	1200	400	3000
TLH-3b	1	1200	400	3000
	2	1400	400	2000
	3	1600	400	1000
TR-3b ⁽¹⁾	A	1200	400	300
	B	1400	400	200
	C	1600	400	100
THL-4	1	1600	40	1
	2	1200	40	1000
	3	1000	40	2000
	4	800	40	3000
TLH-4	1	800	40	3000
	2	1000	40	2000
	3	1200	40	1000
	4	1600	40	1
TR-4 ⁽¹⁾	A	800	40	300
	B	1000	40	200
	C	1200	40	100
	D	1600	40	1 ⁽²⁾

(1) Randomized block - See Table 9c for sequence

(2) This cycle of 1600 lb. applied randomly within each 10 block group. See Table 9c for sequence of layers A, B and C.

TABLE 9c RAMODOMIZED BLOCK LOADING STEP SEQUENCE

STEP	LAYER	CYCLES	STEP	LAYER	CYCLES	STEP	LAYER	CYCLES
1	A	1	62	B	1	123	B	1
2	B	1	63	C	2	124	A	1
3	A	1	64	A	3	125	B	2
4	B	1	65	B	1	126	A	1
5	A	1	66	C	1	127	C	1
6	C	2	67	B	1	128	B	4
7	A	1	68	A	1	129	C	2
8	B	1	69	C	1	130	A	1
9	A	1	70	A	2	131	B	1
10	C	2	71	B	1	132	A	2
11	A	2	72	C	2	133	B	2
12	C	1	73	A	3	134	A	4
13	A	1	74	B	2	135	C	1
14	B	1	75	A	2	136	A	1
15	A	2	76	B	4	137	B	2
16	C	1	77	C	1	138	A	1
17	A	1	78	B	1	139	C	1
18	C	2	79	A	5	140	B	2
19	B	1	80	C	2	141	A	2
20	A	2	81	B	1	142	B	2
21	B	1	82	A	4	143	A	1
22	A	1	83	B	7	144	C	1
23	B	1	84	A	3	145	B	1
24	A	2	85	C	1	146	C	1
25	C	1	86	B	2	147	B	1
26	B	1	87	C	1	148	A	2
27	C	1	88	A	1	149	B	1
28	A	1	89	B	1	150	A	1
29	C	1	90	A	1	151	B	2
30	A	1	91	C	2	152	C	1
31	B	1	92	B	1	153	A	1
32	A	1	93	A	2	154	C	1
33	C	1	94	C	1	155	A	3
34	B	1	95	A	3	156	B	1
35	A	1	96	C	1	157	A	2
36	B	2	97	A	2	158	C	1
37	A	1	98	B	1	159	A	1
38	C	2	99	A	1	160	B	1
39	A	2	100	B	1	161	A	2
40	C	1	101	C	1	162	B	1
41	B	2	102	B	1	163	A	7
42	C	1	103	A	1	164	B	1
43	A	1	104	B	2	165	A	1
44	C	1	105	A	3	166	C	1
45	B	1	106	B	1	167	B	1
46	A	4	107	A	5	168	A	1
47	B	1	108	B	1	169	B	1
48	A	2	109	A	1	170	A	2
49	B	1	110	B	1	171	B	2
50	A	1	111	A	6	172	A	1
51	C	1	112	C	2	173	C	1
52	B	1	113	B	1	174	A	2
53	A	3	114	C	1	175	C	1
54	C	1	115	A	6	176	B	1
55	B	3	116	B	1	177	A	1
56	C	1	117	A	2	178	C	1
57	B	1	118	B	1	179	A	2
58	A	6	119	C	2	180	B	1
59	C	2	120	A	4	181	C	1
60	B	2	121	B	1	182	B	1
61	A	3	122	A	3	183	A	2

TABLE 9c (CONTINUED)

STEP	LAYER	CYCLES	STEP	LAYER	CYCLES	STEP	LAYER	CYCLES
184	B	1	245	B	1	306	A	7
185	A	1	246	A	1	307	B	1
186	C	1	247	B	2	308	A	3
187	A	1	248	C	1	309	B	1
188	C	1	249	B	2	310	C	1
189	B	1	250	C	1	311	A	1
190	C	2	251	B	3	312	B	1
191	A	1	252	A	2	313	A	3
192	C	3	253	C	1	314	B	1
193	A	1	254	A	3	315	C	1
194	B	1	255	B	1	316	B	1
195	A	2	256	A	1	317	A	1
196	B	1	257	B	1	318	B	2
197	A	1	258	A	1	319	C	1
198	C	2	259	B	1	320	A	3
199	A	1	260	C	2	321	B	1
200	B	7	261	B	2	322	C	1
201	A	2	262	A	2	323	A	1
202	B	3	263	B	1	324	B	1
203	A	3	264	A	3	325	C	1
204	C	2	265	B	2	326	A	2
205	A	4	266	A	1	327	B	2
206	B	1	267	B	2	328	A	1
207	A	2	268	A	3	329	B	1
208	B	2	269	B	1	330	A	1
209	A	1	270	C	1	331	C	2
210	B	1	271	B	2	332	A	1
211	A	4	272	A	6	333	B	2
212	B	1	273	C	1	334	A	1
213	C	2	274	A	2	335	B	1
214	B	1	275	B	1	336	A	1
215	A	5	276	A	3	337	B	1
216	C	2	277	C	1	338	A	6
217	A	3	278	A	1	339	C	1
218	C	1	279	C	1	340	B	2
219	B	4	280	A	2	341	A	3
220	A	1	281	B	1	342	B	1
221	B	1	282	A	2	343	A	1
222	A	2	283	B	1	344	B	2
223	B	2	284	A	1	345	A	1
224	C	1	285	C	1	346	B	2
225	A	1	286	B	1	347	A	1
226	B	1	287	A	1	348	B	2
227	A	1	288	B	1	349	A	1
228	B	1	289	A	2	350	B	2
229	A	5	290	B	1	351	A	1
230	B	1	291	A	5	352	B	1
231	A	1	292	B	1	353	A	1
232	C	1	293	A	2	354	B	1
233	B	1	294	B	1	355	A	1
234	A	1	295	A	4	356	B	6
235	B	1	296	B	3			
236	C	1	297	C	1			
237	B	1	298	B	1			
238	C	1	299	C	1			
239	A	2	300	A	1			
240	B	2	301	B	1			
241	C	2	302	A	3			
242	A	5	303	B	2			
243	B	1	304	A	2			
244	A	1	305	B	2			

TABLE 9d FIGHTER SPECTRUM

STEP	LOAD (% LIMIT)		CYCLES PER MISSION	STEP	LOAD (% LIMIT)		CYCLES PER MISSION
	MAX.	MIN.			MAX.	MIN.	
1	63.2	17.5	10	34	103.1	5.8	1
2	55.3	17.5	9	35	70.8	3.4	5
3	70.8	3.4	1	36	47.0	16.4	4
4	28.9	13.2	13	37	46.5	-18.9	1
5	70.8	3.4	1	38	37.5	17.5	5
6	37.5	17.5	39	39	63.2	17.5	1
7	70.8	3.4	1	40	28.9	13.2	1
8	84.8	7.0	1	41	47.0	16.4	16
9	47.0	16.4	18	42	70.8	3.4	3
10	37.5	17.5	39	43	55.3	17.5	13
11	28.9	13.2	26	44	37.5	17.5	39
12	76.4	4.6	1	45	28.9	13.2	13
13	47.0	16.4	18	46	47.0	16.4	18
14	28.9	13.2	13	47	63.2	17.5	5
15	47.0	16.4	19	48	28.9	13.2	13
16	76.4	4.6	1	49	70.8	3.4	1
17	55.3	17.5	28	50	47.0	16.4	19
18	37.5	17.5	39	51	37.5	17.5	39
19	63.2	17.5	5	52	55.3	17.5	9
20	47.0	16.4	19	53	28.9	13.2	13
21	37.5	17.5	39	54	37.5	17.5	39
22	70.8	3.4	1	55	28.9	13.2	13
23	63.2	17.5	4	56	63.2	17.5	5
24	76.4	4.6	1	57	76.4	4.6	1
25	94.4	14.7	5	58	37.5	17.5	39
26	37.5	17.5	12	59	55.3	17.5	9
27	63.2	17.5	2	60	47.0	16.4	36
28	76.4	4.6	2	61	55.3	17.5	9
29	66.4	22.2	7	62	70.8	3.4	3
30	63.2	17.5	10	63	84.8	7.0	1
31	66.4	22.2	4	64	63.2	17.5	10
32	55.3	17.5	30	65	118.1	4.1	1 EVERY 6 STARTING WITH 6TH MISSION
33	47.0	16.4	7	66	120.4	-14.2	1 EVERY 18 STARTING WITH 18TH MISSION

TABLE 10 UNDERLOAD AND COMPRESSION SPIKE TEST PLAN

SPECIMEN NO.	COMPR / ONLY	TENS / COMPR	COMPR / TENS	OVER / UNDER	UNDER / OVER
AD-25-115					X
AD-25-116				X	
AD-25-117				X ⁽¹⁾	
TD-25-117				X ⁽¹⁾	
TD-25-118					X
TD-25-119				X	
AG-25- 8P	X				
AG-25- 9P	X	X			
AG-25-10P		X	X		
TG-25- 1P	X				
TG-25- 4P		X	X		

(1) Multiple Overloads before Underload

TABLE 11 MEASURED AND CALCULATED STABLE TEAR, SPECIMEN AG-25-6P

SURFACE CRACK LENGTH AFTER OVERLOAD (IN.)	$K_{\max OL}$ (KSI $\sqrt{IN.}$)	MEASURED (ON FRACTURE SURFACE)	FROM RESISTANCE CURVE
.633	30.4	.003	.00
.852	36.3	.007	.008
1.045	41.4	.020	.023
1.282	47.9	.044	.052
1.532	55.5	.095	.105

TABLE 12 MECHANICAL PROPERTY RESULTS

MATERIAL	2219-T851 ALUMINUM	Ti 6Al - 4V TITANIUM	
THICKNESS (INCH)	1/4	1/4	3/4
TENSILE ULTIMATE (KSI)	66.9	132.6	137.6
TENSILE YIELD (KSI)	54.7	130.0	135.3
*ELONGATION AT FAILURE (%)	10.3	17.8	12.6
NUMBER OF TESTS	6	4	4

* Gage length = 2 inches

TABLE 13 COMPARISON OF CRACK GROWTH RATES
AS A FUNCTION OF R FOR 2219-T851 ALUMINUM

STRESS RATIO R	CRACK GROWTH RATE, da/dN (IN./CYCLE) @ K = 15 KSI√IN*			
	EQ 19a EQ 21	EQ 1a	EQ 1b	EQ 2
-1	2.18×10^{-6}			2.18×10^{-6}
0	1.66×10^{-5}	1.66×10^{-5}		
.2	2.52×10^{-5}	2.43×10^{-5}		
.4	3.57×10^{-5}	3.41×10^{-5}		
.5	4.00×10^{-5}	4.0×10^{-5}		
.6	4.08×10^{-5}		4.0×10^{-5}	
.7	3.38×10^{-5}		4.0×10^{-5}	

* $K_{MAX} = \frac{15 \text{ ksi } \sqrt{\text{in}}}{1-R}$ FOR ALL VALUES OF $R \geq -1$

TABLE 14 COMPARISON OF CRACK GROWTH RATES AS
A FUNCTION OF R FOR Ti 6Al-4V TITANIUM

STRESS RATIO R	CRACK GROWTH RATE, da/dN (IN./CYCLE) @ K = 15 KSI√IN*		
	EQ 19a EQ 21	EQ 1c	EQ 3
-1	3.44×10^{-6}		4.65×10^{-6}
0	2.47×10^{-6}	2.47×10^{-6}	
.3	4.37×10^{-6}	4.45×10^{-6}	
.5	6.26×10^{-6}	6.23×10^{-6}	
.7	8.62×10^{-6}	8.45×10^{-6}	

* $K_{max} = \frac{15 \text{ ksi } \sqrt{\text{in}}}{1-R}$ for all values of $R \geq -1$

**TABLE 15 COMPARISON OF TEST AND PREDICTED LIVES FOR
SINGLE PERIODIC OVERLOAD TESTS**

MATERIAL	SPECIMEN NO.	OVERLOAD RATIO, O/L	CYCLES OF LOW LOAD BETWEEN OVERLOADS	CYCLES REQUIRED TO REACH $a = 1.6$ IN		PREDICTED LIFE TEST LIFE (AT $a = 1.6$ INCHES)
				TEST	PREDICTION	
2219-T851 ALUMINUM	AD-25-26	1.8	500	238,000	(2)	
	-38	1.8	500	390,000	1,500,000	3.98
	-43	1.8	1000	142,000 (1)	430,400	3.04
	-29	1.25	50	160,000	(2)	
	-45	1.25	50	126,000	290,000	2.30
	-27	1.25	100	75,500	75,500	1.00
Ti 6Al-4V TITANIUM	TD-25-30	1.8	500	323,000	212,000	.66
	-37	1.8	500	445,000	235,000	.53
	-28	1.8	1000	~900,000	195,000	.22
	-32	1.25	50	210,000	265,000	1.26
	-39	1.25	50	214,000	248,000	1.16
	-31	1.25	100	207,000	241,000	1.16

(1) $a_{\text{final}} = 1.3$ in.

(2) Prediction terminated

**Table 16 - Values of C' and n' used in Equation 39 for Predictions
in Figure 223 when $\alpha = 2.6$ and $\beta = 0.10$**

CASE	REF. FIGURE 223		FOR EQUATION (39)	
	x	y	C'	n'
1	0	50	2.571×10^{-3}	2.119
2	50	0	1.223×10^{-2}	2.102
3	1	50	1.138×10^{-3}	2.263
4	3	50	1.563×10^{-3}	2.066
5	6	50	2.249×10^{-3}	2.063
6	10	50	3.289×10^{-3}	2.088
7	25	50	6.962×10^{-3}	2.096
8	50	50	1.321×10^{-2}	2.105

APPENDIX A - EQUATIONS

The equations which are referred to most frequently in the text are presented here for reference.

$$\frac{da}{dN} = 1.96 \times 10^{-9} [(1 + .6R)\Delta K]^{3.34} \quad 0 \leq R \leq 0.5 \quad (1a)$$

$$= 1.96 \times 10^{-9} [1.3\Delta K]^{3.34} \quad R > 0.5 \quad (1b)$$

$$= 5.9 \times 10^{-10} [(1 + .7R)\Delta K]^{3.08} \quad 0 < R < 0.7 \quad (1c)$$

$$= 2.6 \times 10^{-9} [K_{max}]^{3.34} \quad R = -1 \quad (2)$$

$$= 1.11 \times 10^{-9} [K_{max}]^{3.08} \quad R = -1 \quad (3)$$

$$C_f(R) = \frac{K_{max_2} - K_{max_1}}{O/L \cdot K_{max_2} - K_{max_1}} \quad (7)$$

where:

$$R = \frac{P_{min_1}}{P_{max_1}} = \frac{P_{min_2}}{O/L \cdot P_{max_2}}$$

$$\Delta S_{eff} = S_{max} - S_c = S_{max} (1 - C_f) \quad (15)$$

$$C_f = \frac{S_c}{S_{max}} \quad (16)$$

$$\frac{da}{dN} = C \left[\frac{S_{\max} - S_c}{1 - C_{f_o}} \sqrt{\pi \alpha} \right]^n \quad (19)$$

$$C_f = C_{f_{-1}} + (C_{f_o} - C_{f_{-1}}) (1 + R)^p \quad (21)$$

where for:

	2219-T851 Aluminum	Ti 6Al-4V Titanium
C_{f_o}	.40	.40
$C_{f_{-1}}$.347	.332
p	3.93	3.33

$$S_c = S_{c_1} - (S_{c_1} - S_{c_2}) \left(\frac{\Delta \alpha}{\rho} \right)^B \quad (22)$$

$$\gamma = \gamma_1 + (1 - \gamma_1) \left(\frac{N_{OL} - 1}{N_{sat} - 1} \right) \quad (26)$$

where for:

	2219-T851 Aluminum	Ti 6Al-4V Titanium
γ_1	.67	.80
N_{sat}	13	100

$$\Delta K_{eff} = (S - S_r) \sqrt{\pi \alpha} \quad (30)$$

$$S_r = \alpha \cdot S \quad (32)$$

$$\frac{da}{dN} = C \left\{ \frac{S \sqrt{\pi a} - \sum_{a-\rho_y}^a \left\{ S_{ri} \sqrt{\frac{a}{\pi}} \left[\sin^{-1} \left(\frac{c_i}{a} \right) - \sin^{-1} \left(\frac{b_i}{a} \right) - \sqrt{1 - \left(\frac{c_i}{a} \right)^2} + \sqrt{1 - \left(\frac{b_i}{a} \right)^2} \right] \right\}}{1 - \frac{\alpha}{\pi} \left[\frac{\pi}{2} - \sin^{-1} \left(\frac{a - \rho_y}{a} \right) + \sqrt{1 - \left(\frac{a - \rho_y}{a} \right)^2} \right]} \right\}^n \quad (37)$$

APPENDIX B - COMPUTER PROGRAM

The Crack Closure Model developed during this program, called subroutine CLOSUR, was mated to the CRACKS 2 computer program. The combined programs have been checked out on both IBM and CDC facilities although only the CDC program is available for general usage. The CRACKS 2 CDC computer program was converted to run on the IBM system 360/70 computer. In order to perform this conversion, the following changes were required:

- All A10 formats became 2A4, A2. Whenever this was required, the necessary redimensioning was included. A result of this operation was that DATA statements defining those variables were replaced with REAL type statements which included the appropriate dimensioning. In addition, where the original program tested against a single variable, now a three-part logical IF statement is required.
- All variable and program names exceeding six characters were contracted to six characters. The equivalences between the original and contracted names are tabulated as comments at the beginning of each program.

These changes were retained when the composite program was re-converted to CDC.

B-1 MODIFICATIONS TO CRACKS 2

The addition of the Crack Closure Model was achieved in as straightforward a manner as possible and can be considered to be a comparatively independent subroutine. It does interface with the CRACKS 2 program at appropriate locations. These include the following subroutine programs:

<u>Name</u>	<u>Type</u>
MAIN	-
INPUT	Subroutine
OUTPUT	Subroutine
GRWCRK (GROWCRK)	Subroutine
BETAS	Subroutine
RY	Real function

NOTE: Names in () shortened to six characters for IBM 360.

A flow chart showing the overall path through the program is presented in Figure B-1. Links between original CRACKS 2 subroutines or subroutines called by CLOSUR are not shown.

Changes to the original program in order to implement CLOSURE were minimal. These are described below.

MAIN - No changes.

INPUT - Added:

1. Common blocks CLOS and CLOSIC. Also REAL NSAT.
2. Initial conditions immediately following common information.
3. The CLOSUR option was defined as model three. Subsequent to statement 523, READ/WRITE statements introduced to read additional input required and print out appropriate information. The READ statement uses existing format 1020. Format statements 2107 and 2108 were added for output.
4. Appropriate READ/WRITE statements following statements 537 and 538 to read BETA factors 7 and 8. These are described under BETAS. Formats 2206 and 2207 were added for new BETA functions.
5. The Crack Closure Model accepts negative loads. Therefore, appropriate statements were introduced between statements 600 and 650 to circumvent instructions setting negative stresses equal to zero whenever MODEL = 3.

OUTPUT - No changes.

GRWCRK - Immediately following statement 130, added: CALL CLOSUR (CYC, A, DN)

BETAS - These two new stress intensity solutions for compact tension specimens were added. Type 7 is the ASTM standard geometry compact specimen. The stress intensity expression was taken from Equation 12 of Reference B-1. Type 8 is for the Grumman compact tension specimen geometry used in this program. The stress intensity solution is described in Appendix C.

RY - No changes.

B-2 ADDITIONAL INPUT DATA REQUIREMENTS

No changes were made to the basic input data format. Additions were required. The following descriptions refer to the tables of Reference B-2. Table 3 - If CON1 (Model) on RETARD card is 3., one additional input card is required. This card immediately follows the RETARD card. All other variables on the RETARD card remain the same. The new card contains the following variables and a description of their relationship to equations within this report, Section 4. The format is number 1020 in INPUT, 8E10.0.

The card contains: CF, CCOEF, CFEXP, B, BOL, NSAT

<u>Program Name</u>	<u>Equivalent Name</u>	<u>Description</u>
CF	C_{f_0}	Equation 21
CCOEF	$C_{f_{-1}}$	Equation 21
CFEXP	p	Equation 21
B	B	Equation 22
BOL	γ_1	Equation 26
NSAT	N_{sat}	Equation 26

Description of BETA following Table 3 - There, type 7 and 8 BETA functions were added. The type 7 factor is for the ASTM standard geometry while the type 8 factor is for the Grumman compact tension geometry used in the test program. The format remains the same as for type 1 for example, with the following definitions:

CON 1 - Specimen type (7. or 8.)

CON 2 - Specimen width - reference Figure 2 of this report

CON 3 - Specimen thickness

CON 4 - a_i }
 CON 5 - a_f } Same as existing definitions

Whenever these BETA factors are employed, the input stresses are replaced by loads. That is, simply assume the equivalence $S = P$. The loads are either in pounds or kips to be compatible with the crack growth equation parameters selected.

B-3 DESCRIPTION OF SUBROUTINE CLOSUR

The CLOSUR subroutine contains its own integration and crack growth rate calculation routines.

The integration routine is implemented only if the closure level is decreasing (retarded growth) or constant (constant amplitude growth) and the number of cycles in the current layer is greater than or equal to 20. The

routine only applies to the current layer and does not integrate overall flight growth. It assumes that, for small increments of crack extension (arbitrarily selected as 10% of the current crack length), the crack growth rate follows the law:

$$\frac{da}{dN} = C \cdot a^n \quad (B-1)$$

within a given load layer. The parameters C and n are evaluated by calculating the crack growth rates at crack lengths a_i and a_f . There, a_i is the current crack length and a_f is either $1.1 a_i$ or a_p , whichever is less. As described in Section 4 of this report, a_p is the location of the elastic-plastic interface. Then, given C and n, Equation B-1 is integrated to obtain ΔN :

$$\Delta N = \frac{1}{C (1 - n)} \left[a_f^{(1 - n)} - a_i^{(1 - n)} \right] \quad (B-2)$$

The value of ΔN is the number of cycles required for the crack to propagate from a_i to a_f . If ΔN is less than N, the number of cycles in the current layer, a_i , is set equal to a_f and the process is repeated. When the accumulation of ΔN s exceeds N, Equation B-2 is evaluated for a_f in the last definition so that $\Sigma \Delta N = N$. Control is then returned to GRWCRK.

The Crack Closure Model intrinsically contains a stress ratio effect on crack growth rates. As a result, only the bi-linear Paris and tabular da/dN vs. ΔK input formats are accepted and used by CLOSUR. If either the Walker or Forman equations are called with CLOSUR, a diagnostic message is printed and execution of the problem is terminated. As a convenience, the subroutine RATE is not called by CLOSUR and the crack growth rates are calculated within CLOSUR. CLOSUR calls BETAS and RY as required.

An overall flow chart for CLOSUR is presented in Figure B-2 while the computer listing is presented in Table B-1.

REFERENCES

- B-1 Newman, Jr., J. C., "Stress Analysis of the Compact Specimen Including the Effects of Pin Loading", Presented at the ASTM Seventh National Symposium on Fracture Mechanics, College Park, Maryland, August 1973.
- B-2 Engle, R. M., "CRACKS II Input Instructions", 13 November 1973.

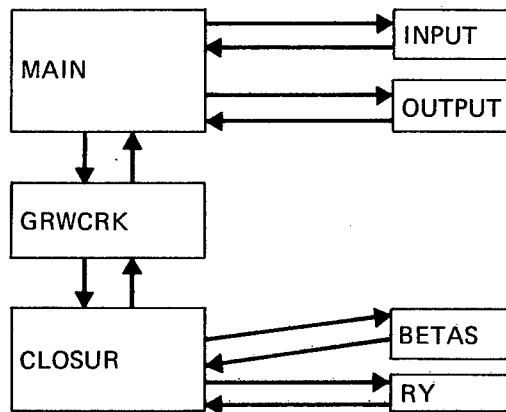


Fig. B-1 Overall Flow Chart of Modified CRACKS 2 Program

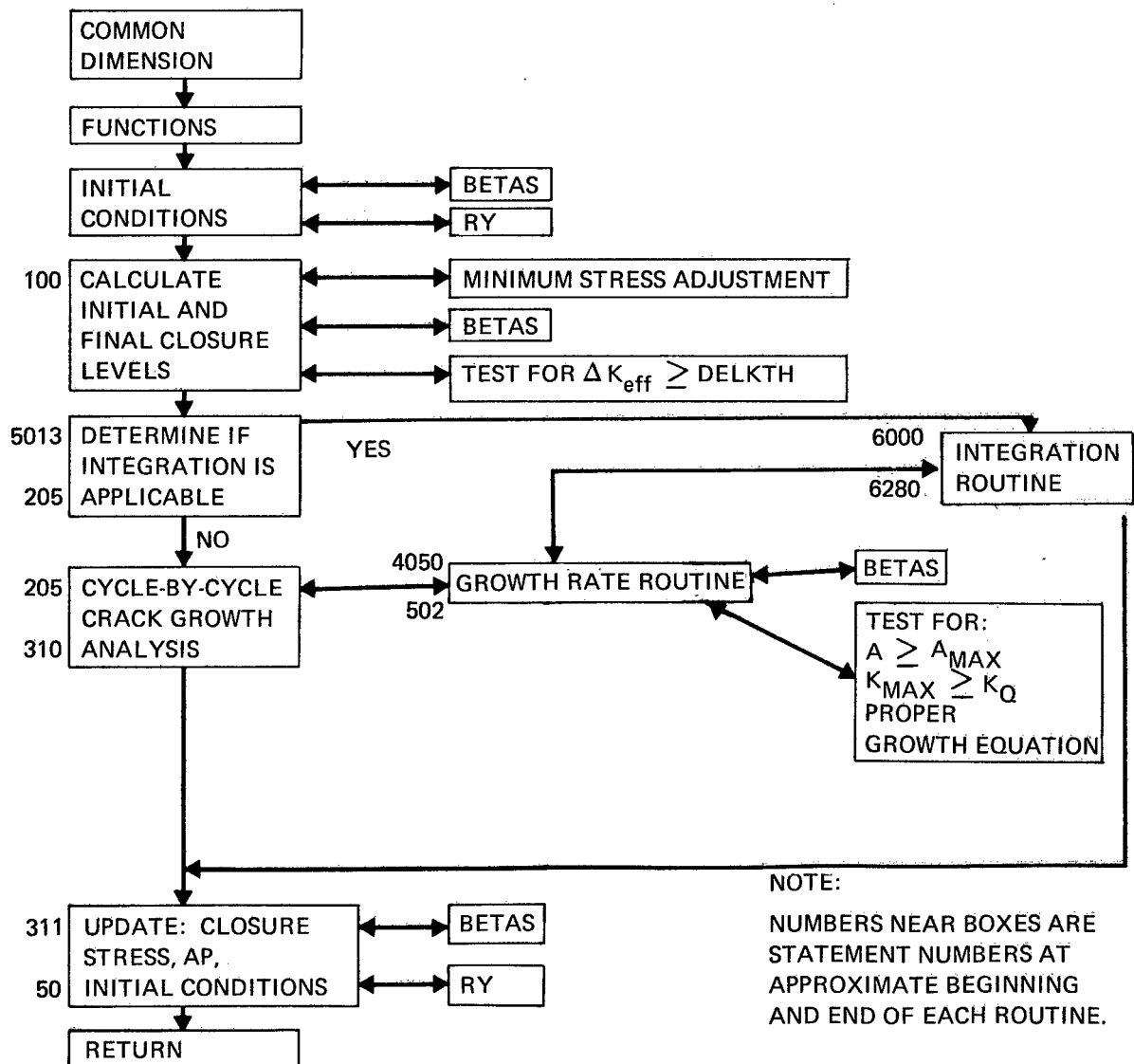


Fig. B-2 Subroutine CLOSUR Flow Chart

TABLE B-1 CLOSUR SUBROUTINE, SHEET 1 OF 8

SURROUTINE CLOSUR(CYC,A1,DN)

INCLUDES MODIFICATION 4 OF SMALL
SEPT 4, 1974

EQUIVALENCE BETWEEN CRACKS 2 AND CLOSUR

CRACKS 2	CLOSUR
ASUBP	AP
SMAX	S
CYCLES	CYCLS
ISEG	I
J4	K
SMALLN	AN (NOT USED AS SMALLN ANYWAY)
KSURQ	AKC
DELKTH	KTH
A	A1
AMAX	AF

```

COMMON/DATA/ EQN,NASA,J1PRT,J2PRT,J3PRT,J4PRT,AZERO,AF,NZERO
INTEGER EQN
REAL NZERO
COMMON/RDATA/ MODEL,RETARD,PLSTRN,OVLD,SIGMAX,SIGMIN,AP,SMALLM
INTEGER RETARD,PLSTRN
COMMON/MDATA/ MATID(20),C,AN,CARRAY(100),SNARAY(100),KSURC,
/ AKC,SIGMAY, KTH,RMULT,RCUT,OLMAX
REAL KSURC
COMMON/LDATA/ S(100,50),SMIN(100,50),CYCLS(100,50),NLYRS(50),
/ NRLKS,IBLKS(1000),ISEGS(1000),NSEGS
COMMON/STEPS/ K,J1,J2,J3,I,ISTOP,IRSTRT,NORTRD
COMMON/CORFAC/ ISURF,RATIO,PHI,THICK,IBETA(10),BETA(10),NPTS,
/ AOVERB(100),BTABLE(100),NPTS2,AOVRB2(100),
/ BTABL2(100),ASTART(10),ASTOP(10)
COMMON/PARIS/C1,SN1,DKCOM,C2,SN2
COMMON /DIRECT/ NCADN
COMMON/OUTPOT/XK,XKA,XKEFFN
REAL KMAX,KMAXA
COMMON/CLOS/CF,CCOEF,CFEXP,B,BOL,NSAT
COMMON/CLOSIC/SC,SPEAK,PRVMX,APEAK,SC1,SC2,SC3,PRVMN
DATA PI/3.14159265/
REAL ISUM,KTHSG,KCOEF,KEXP,NOL,NSAT,NPR,NPREV,KTH
DIMENSION Q(6),QQ(2)

```

CLOSURE FUNCTION

CLOSE(G1,G2) = G1*(CCOEF + (CF - CCOEF)*(1. + G2)**CFEXP)

FUNCTION FOR SC LT OR EQ SC INITIAL

DOWN(Z1,Z2,Z3) = Z1 - (Z1-SC3)*(Z2/Z3)**B

TABLE B-1 CLOSUR SUBROUTINE, SHEET 2 OF 8

```

C
C      FUNCTIONS FOR SC  GT  SC INITIAL
SCONE(SC3) = SC3*BOL
C
C      FUNCTION FOR INCREASING CLOSURE STRESS
NPREV(SC,SC3,SC11) = 1.+(NSAT-1.)*(SC-SC11)/(SC3-SC11)
C
C
C INITIALIZE PARAMETERS
      IGROW = 0
      MODE = 0
      ITEM = 1
      IGROW = 1
      CYSUM = CYCLS(I,K)
      NOL = 0.
      ASTRT = A1
      KLU = 1
      R = 0.
      IF ( S(I,K) .NE. 0. ) R = SMIN(I,K)/S(I,K)
      SMNGR = SMIN(I,K)
      IF ( SPEAK .NE. 0. ) GO TO 30
      SINITL = S(I,K)
      IF ( SINITL .LE. 0. ) SINITL = 0.05*SIGMAY
      R = SMIN(I,K)/SINITL
      CALL BETAS(S(I,K),A1,ALP,QE)
      XK = SINITL*SQRT(PI*A1)*ALP
      G1 = SINITL
      G2 = R
      IF ( G2 .LT. -1. ) G2 = -1.
      SC = CLOSE(G1,G2)
      SC1 = SC
      SC2 = SC
      SC3 = SC
      SPEAK = SINITL
      PRVMX = SINITL
      PRVMN = SMIN(I,K)
      APEAK = A1
      AP = A1 + RY(XK,PLSTRN)
      OMGA2 = AP

      30 CONTINUE
C
C
C START ANALYSIS
100      ISUM = 0.
C
C
      G1 = S(I,K)
      G2 = R
      IF ( G2 + 1. ) 104,105,105
104      G2 = -1.
105      SC3 = CLOSE(G1,G2)
      IF(SMIN(I,K) - PRVMN) 5003,60,60
C      MINIMUM STRESS ADJUSTMENT
5003 CONTINUE
      PRVMN = SMIN(I,K)

```

TABLE B-1 CLOSUR SUBROUTINE, SHEET 3 OF 8

```

      G1 = SPEAK
      G2 = SMIN(I,K)/SPEAK
      IF (G2 + 1.) 5005,5006,5006
5005   G2 = -1.
5006   SC1 = CLOSE(G1,G2)
      G1 = PRVMX
      G2 = SMIN(I,K)/PRVMX
      IF (G2 + 1.) 57,58,58
57     G2 = -1.
58     SC3 = CLOSE(G1,G2)
      G3 = ASTR - APEAK
      G4 = AP - APEAK
      SC2T = DOWN(SC1,G3,G4)
      IF(SC2T - SC2) 59,60,60
59     SC2 = SC2T
60     SC = SC2
      IF(S(I,K)-SC2) 450,450,5009
5009   SMNGR = SC2
      IF (SMIN(I,K)-SC2) 5010,5011,5011
5010   SMNGR = SC2
5011 CALL BETAS(S(I,K),A1,ALP,QE)
      XKEFF=(S(I,K)-SMNGR)*SQRT(PI*A1)*ALP
      IF((XKEFF/(1.-RMULT*R)/(1.-CF))-KTH) 450,450,5012
5012   G1 = S(I,K)
      G2 = R
      IF (G2 + 1.) 93,94,94
93     G2 = -1.
94     SC3 = CLOSE(G1,G2)
      IF ( S(I,K) - SC3 ) 95,96,96
95     SC3 = S(I,K)
96 CONTINUE
      IF(S(I,K) - SPEAK) 90,5013,5013
5013   KLU = 3
C
C     INITIALIZATION FOR INTEGRATION ROUTINE
C
C     MODE = 1   IF  CYCLS(I,K) .LT. 20 AND SC3 .LE. SC
C     MODE = 2   IF  CYCLS(I,K) .LT. 20 AND SC3 .GT. SC
C     MODE = 3   IF  CYCLS(I,K) .GE. 20, SC3.GT.SC AND N.LT.NSAT
C     MODE = 4   IF  CYCLS(I,K) .GE. 20 AND SC3 .LT. SC
C     MODE = 5   IF  CYCLS(I,K) .GE. 20 AND SC3 = SC
C     INTEGRATION PERFORMED FOR MODE = 4 AND 5
90     MODE = 5
      IF ( CYCLS(I,K) - 20. ) 201,203,203
201     MODE = 1
      IF ( SC - SC3 ) 202,205,205
202     MODE = 2
      GO TO 205
203     IF ( SC .EQ. SC3 ) GO TO 205
      MODE = 3
      IF ( SC3 - SC ) 204,205,205
204     MODE = 4
205 CONTINUE
C
C
      DCYC = CYCLS(I,K)/30000.

```

TABLE B-1 CLOSUR SUBROUTINE, SHEET 4 OF 8

```

C
C
C
      IF ( DCYC .LT. 1.0 ) DCYC = 1.0
      NNCYC = CYCLS(I,K)/DCYC

      START CYCLE - BY - CYCLE ANALYSIS

      DO 310 J = 1,NNCYC
        IF ( MODE - 3 ) 210,210,6000
        210 IF (SC3 - SC) 92,92,111
        92 GO TO (101,160,101,101),KLU
        101 IF (OMGA1) 5014,5015,5015
        5014 OMGA1 = 0.
        5015 IF (OMGA1/OMGA2 - 1.) 5017,5017,5016
        5016 OMGA1 = OMGA2
        5017 SC = DOWN(SC2,OMGA1,OMGA2)
        111 IF (SMIN(I,K) - SC) 5023,160,160
        5023 SMNGR = SC
        160 CONTINUE
        GO TO 4050
      4051 CONTINUE
        ISUM = ISUM + DCYC
        CYC = CYC + DCYC
        CYSUM = CYSUM - DCYC
        DN = CYSUM
        GO TO (138,501,501,501),ITEM
      138 CONTINUE
        IF ( MODE - 2 ) 143,144,144
        143 OMGA1 = A1 - ASTRT
        IF (A1 - AP) 300,141,141
        141 KLU = 2
        SC = SC3
        AP = A1
        GO TO 300
        144 SC11 = SCONE(SC3)
        NPR = NPREV(SC,SC3,SC11)
        IF ( NPR ) 145,146,146
        145 NPR = 0.
        146 NOL = NPR + DCYC
        SC = SC11 + (SC3-SC11)*(NOL-1.)/(NSAT-1.)
        IF ( SC3 - SC ) 147,147,300
        147 SC = SC3
        IF ( MODE - 2 ) 300,300,148
        148 MODE = 5
        300 CONTINUE
        310 CONTINUE
        311 CONTINUE
        PRVMX = S(I,K)
        SC2 = SC
        GO TO (501,400,400,400),KLU
      400 CALL BETAS(S(I,K),A1,ALP,QE)
        XK = S(I,K)*SQRT(P1*A1)*ALP
        AP = A1 + RY(XK,PLSTRN)
        APEAK = A1
        SPEAK = S(I,K)
        PRVMN = SMIN(I,K)
        IF (SC3 - SC) 420,420,430
        420 SC1 = SC3
        GO TO 501

```

TABLE B-1 CLOSUR SUBROUTINE, SHEET 5 OF 8

```

430     SC1 = SC
      GO TO 501
450     ISUM = ISUM + CYCLS(I,K)
      CYC = CYC + CYCLS(I,K)
      DN = 0.
501 CONTINUE
C
      GO TO(500,600,620,503),ITEM
503     ISTOP = 2
      A1 = ATRANS/(2.*RATIO)
      WRITE(6,1) A1,CYC
1  FORMAT(1H0,120(1H*)/25X,55HTRANSITIONTFO A THRU CRACK OF EFFECTIVE
1  LENGTH, AEFF = ,F9.5,4H AT ,F12.2,7H CYCLES /,1X,120(1H*))
      GO TO 50
C
C
C     END OF CYCLE BY CYCLE ROUTINE
C
500 CONTINUE
      GO TO 50
C     A1 EXCEEDED AF (AMAX)
600     ISTOP = 1
      GO TO 50
620     ISTOP = 1
      WRITE(6,7)
7  FORMAT(1H0,120(1H*)/25X,46HKMAX APPLIED EXCEEDS KSUBQ. PROBLEM TER
1MINATED/1X,120(1H*)/1H0,24X,26HLAST CALCULATED VALUES ARE///)
      DELTAK = XK*(1.-R)
      WRITE(6,8) J1,J2,I,J3,K,CYC,A1,XK,XKEFF,DELTAK,DADN
8  FORMAT(25X,18HBLOCK IN SPECTRUM ,I4/
/      25X,18HFLIGHT NUMBER ,I4/
/      25X,18HMISSION NUMBER ,I4/
/      25X,18HPASS OF MISSION ,I4/
/      25X,18HLAYER IN MISSION ,I4/
5      25X,18HACCUMULATED CYCLES,E16.8/
6      25X,18HCRACK LENGTH ,E16.8/
7      25X,18HKMAX APPLIED ,E16.8/
8      25X,18HKMAX EFFECTIVE ,E16.8/
9      25X,18HDELTA K ,E16.8/
/      25X,18HDA/DN ,E16.8)
C
C
50 CONTINUE
      XKA = XK
      RETURN
C
C
C     GROWTH CALCULATIONS
4050 CONTINUE
C     CHECK FOR XK (KMAXA) .GE. AKC (KSUBQ)
      CALL BETAS(S(I,K),A1,ALP,QE)
      XK = S(I,K) *SQRT(PI*A1)*ALP
      IF(XK - AKC) 4062,4060,4060
4060     ITEM = 3
      DADN = 0.
      GO TO (502,502,502,4062,4062),MODE
4062     XKEFF = (S(I,K) - SMNGR)*SQRT(PI*A1)*ALP

```

TABLE B-1 CLOSUR SUBROUTINE, SHEET 6 OF 8

```

      XKEFFN = XKEFF/(1.-CF)
      IF ( EQN .EQ. 1 ) GO TO 9000
      IF ( EQN .EQ. 4 ) GO TO 9010
      IF ( EQN = 2 ) 8000,8000,8010
8000 CONTINUE
C      BI-LINEAR PARIS EQUATION
      C = C1
      AN = SN1
      IF ( XKEFFN .GE. DKCOM ) C = C2
      IF ( XKEFFN .GE. DKCOM ) AN = SN2
      DADN = C*XKEFFN**AN
      GO TO 8020

C
8010 CONTINUE
C      TABULAR RATE VALUES
      DADN = TBLKUP(CARRAY,SNARRAY,NDADN,100,XKEFFN)
      DADN = 10.**DADN
8020 CONTINUE
      A1 = A1 + DADN*DCYC
      IF (A1 - AF)4064,4063,4063
4063      ITEM = 2
      GO TO 502
4064      IF ( ISURF .EQ. 0 ) GO TO 502
      ATRANS = THICK - (((XK/SIGMAY)**2.)/(2.*PI))
      IF ( A1 .LT. ATRANS ) GO TO 502
      ITEM = 4
502      GO TO (4051,6060),IGROW

C
C
C      END OF CRACK GROWTH CALCULATIONS
C
C
C      INTEGRATION ROUTINE
6000 CONTINUE
      IF ( MODE = 4 ) 6010,6010,6020
6010      Q(1) = A1
      Q(2) = AP
      Z2 = A1 - ASTRT
      Z3 = AP - ASTRT
      QQ(1) = DOWN(SC2,Z2,Z3)
      QQ(2) = SC3
      IF ( ISURF .EQ. 0 ) GO TO 6030
      IF ( Q(2) .LT. THICK ) GO TO 6030
      Q(2) = THICK
      Z2 = THICK - ASTRT
      QQ(2) = DOWN(SC2,Z2,Z3)
      ISTOP = 2
      GO TO 6030
6020      Q(1) = A1
      Q(2) = 1.10*A1
      QQ(1) = SC3
      QQ(2) = SC3

```

TABLE B-1 CLOSUR SUBROUTINE, SHEET 7 OF 8

```

      IF ( ISURF .EQ. 0 ) GO TO 6030
      IF ( Q(2) .LT. THICK ) GO TO 6030
      Q(2) = THICK
      ISTOP = 2
6030 CONTINUE
      SC = QQ(1)
      DO 6100 KK = 1,2
      A1 = Q(KK)
      SMNGR = SMIN(I,K)
      IF ( SMIN(I,K) - QQ(KK) ) 6045,6050,6050
6045 SMNGR = QQ(KK)
6050 IGROW = 2
      GO TO 4050
6060 GO TO (6070,6065,6065,6065),ITEM
6065 GO TO (501,6068),KK
6068 ITEM = 1
      ISTOP = 0
6070 KKK = KK + 2
      KKKK = KK + 4
      Q(KKK) = XKEFF
      Q(KKKK) = DADN
6100 CONTINUE
      Q2 = (Q(3)-Q(4))/(Q(1)-Q(2))
      Q1 = Q(3) - Q2*Q(1)
      Q4 = (ALOG(Q(5)/Q(6)))/(ALOG(Q(3)/Q(4)))
      Q3 = Q(5)/(Q(3)**Q4)
      Q5 = 1. - Q4
      DELTN = (Q(4)**Q5 - Q(3)**Q5)/(Q2*Q3*Q5)
      IF ( DELTN - CYSUM ) 6200,6150,6250
6150 CONTINUE
6200 A1 = Q(2)
      IF ( AP - A1 ) 6210,6210,6220
6210 AP = A1
      KLU = 2
      MODE = 5
6220 ISUM = ISUM + DELTN
      CYC = CYC + DELTN
      CYSUM = CYSUM - DELTN
      DN = CYSUM
      IF ( CYSUM - .01 ) 6260,6240,6240
6240 IF ( MODE - 4 ) 6010,6010,6020
6250 Q(4) = (Q(3)**Q5+CYSUM*Q2*Q3*Q5)**(1./Q5)
      Q(2) = (Q(4) -Q1)/Q2
      DELTN = CYSUM
      ISTOP = 0
      GO TO 6150
6260 SC = SC3
      IF ( KLU - 2 ) 6270,6280,6280
6270 Z2 = A1 - ASTRT
      Z3 = AP - ASTRT
      IF (Z3 .LE. 0. ) Z3 = Z2
      SC = DOWN(SC2,Z2,Z3)
6280 GO TO 311
C
C
C
      END OF INTEGRATION ROUTINE

```

TABLE B-1 CLOSUR SUBROUTINE, SHEET 8 OF 8

```
C
C
C      DIAGNOSTICS FOR IMPROPER EQN
9000 WRITE(6,9005)
9005 FORMAT(1H0,24X,44HCLOSURE MODEL CAN NOT ACCEPT FORMAN EQUATION /
1      40X,20HEXECUTION SUPPRESSED )
      GO TO 9020
9010 WRITE(6,9015)
9015 FORMAT(1H0,24X,44HCLOSURE MODEL CAN NOT ACCEPT WALKER EQUATION /
1      40X,20HEXECUTION SUPPRESSED )
9020      ISTOP = 1
      XKA = XK
      RETURN
C
C
      END
```

APPENDIX C - STRESS INTENSITY FACTOR FOR CTB SPECIMEN

The compact tension specimen used by Grumman (CTB) was longer in the loading direction than its ASTM shaped counterpart, CTA. Referring to Figure 2, the values of H/W and d/W were 0.95 and 0.60 respectively. An analytical solution for this geometry was interpolated from Table 3 of Reference C-1, using W = 2.5 inches. In addition, two aluminum specimens were equipped with clip gages and the stress intensity factors were determined using the method of Reference C-2. The results, shown in Figure C-1, were fitted to the equation:

$$\frac{Kt}{P} = .1229 + 16.4098 \left(\frac{a}{w}\right) - 37.395 \left(\frac{a}{w}\right)^2 + 54.7667 \left(\frac{a}{w}\right)^3 \quad (C-1a)$$

$$\text{for } .2 \leq \frac{a}{w} \leq .5$$

$$\frac{Kt}{P} = 114.054 - 830.132 \left(\frac{a}{w}\right) + 2327.177 \left(\frac{a}{w}\right)^2 - 2890.811 \left(\frac{a}{w}\right)^3 + 1382.306 \left(\frac{a}{w}\right)^4$$

$$\text{for } .5 \leq \frac{a}{w} \leq .8 \quad (C-1b)$$

where:

K = stress intensity
t = specimen thickness
P = applied load

REFERENCES

- C-1 Srawley, J.E. and Gross, B., "Stress Intensity Factors for Bend and Compact Specimens", Engineering Fracture Mechanics, Vol. 4, Compendium, 1972.
- C-2 Paris, P. C. and Sih, G. C. M., "Stress Analysis of Cracks", ASTM STP 381, 1965.

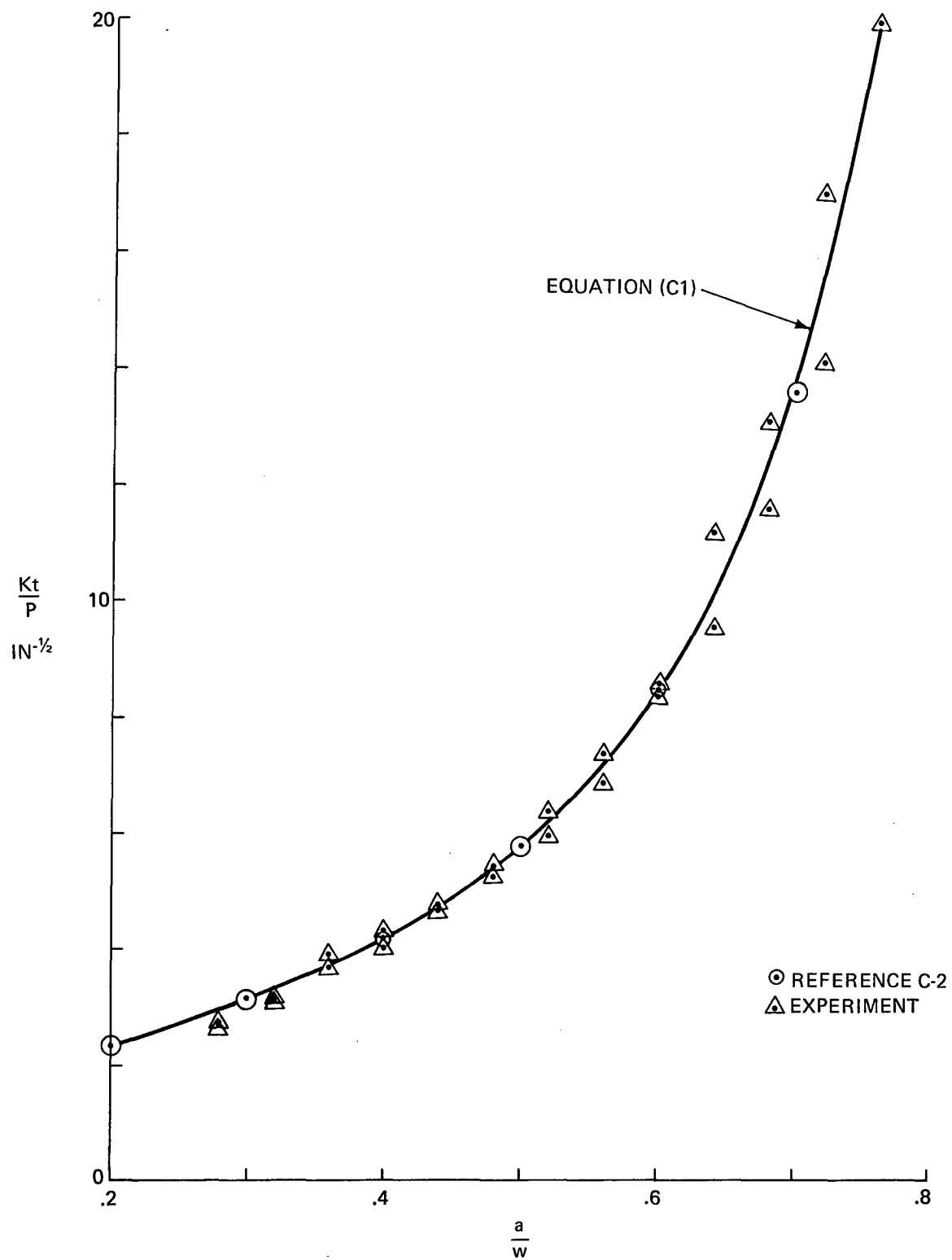


Fig. C-1 Stress Intensity Factor For CTB Specimen